



The PRODATA Thermochemical database. A database applied for uranium mining operations

Pascal E. Reiller

► To cite this version:

Pascal E. Reiller. The PRODATA Thermochemical database. A database applied for uranium mining operations. [Technical Report] CEA-R-6573, Commissariat à l'énergie atomique et aux énergies alternatives. 2022. cea-03757400

HAL Id: cea-03757400

<https://cea.hal.science/cea-03757400>

Submitted on 22 Aug 2022

HAL is a multi-disciplinary open access archive for the deposit and dissemination of scientific research documents, whether they are published or not. The documents may come from teaching and research institutions in France or abroad, or from public or private research centers.

L'archive ouverte pluridisciplinaire **HAL**, est destinée au dépôt et à la diffusion de documents scientifiques de niveau recherche, publiés ou non, émanant des établissements d'enseignement et de recherche français ou étrangers, des laboratoires publics ou privés.



COMMISSARIAT À L'ÉNERGIE ATOMIQUE
ET AUX ÉNERGIES ALTERNATIVES

DIRECTION DES ÉNERGIES NUCLÉAIRES

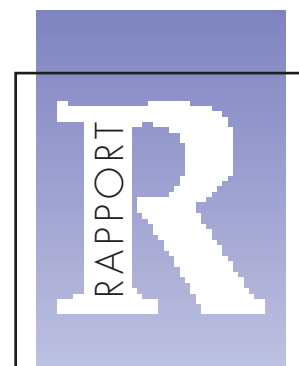
2022

**THE PRODATA THERMOCHEMICAL DATABASE
A DATABASE APPLIED FOR URANIUM MINING OPERATIONS**

par

Pascal REILLER

CENTRE D'ÉTUDES NUCLÉAIRES DE SACLAY
DIRECTION DES ÉNERGIES
INSTITUT DES SCIENCES APPLIQUÉES ET DE LA
SIMULATION POUR LES ÉNERGIES BAS CARBONE
DÉPARTEMENT DE PHYSICO-CHIMIE
SERVICE D'ÉTUDES ANALYTIQUE ET RÉACTIVITÉ
DES SURFACES



DIRECTION DES SYSTÈMES
D'INFORMATION

CEA / PARIS SACLAY 91191 Gif-sur-Yvette CEDEX FRANCE

**RAPPORT
CEA-R-6573**

- Rapport CEA-R-6573 -

Centre d'Études Nucléaires de Saclay
Direction des Énergies
Institut des Sciences Appliquées et de la Simulation pour les énergies bas carbone
Département de Physico-Chimie
Service d'Études Analytique et Réactivité des Surfaces

THE PRODATA THERMOCHEMICAL DATABASE
A DATABASE APPLIED FOR URANIUM MINING OPERATIONS

par

Pascal REILLER

– Juillet 2022 –

RAPPORT CEA-R-6573 – Pascal REILLER

«La base de données thermochimique PRODATA. Une base de données dédiée aux opérations minières pour l'uranium.»

Résumé - Ce document présente les données thermochimiques, constants et fonctions, incluses dans la base de données PRODATA, développée pour répondre aux besoins d'ORANO Mining en terme d'exploration, d'exploitation et de remédiation des activités minières pour l'uranium. Les réactions de complexation, dissolution-précipitation de phases solides et de gaz peuvent être exportées sous forme de fichiers qui peuvent être utilisés par chacun des trois logiciels PHREEQC, CHESS, et Geochemist's WorkBench (GWB). La base PRODATA inclut les données pour l'uranium et le radium, ainsi que pour les éléments nécessaires à la simulation de leur comportement dans différents contextes pour un total de 38 éléments. La sélection des données est fondée sur celles de CODATA et de la base de l'OCDE-AEN. La cohérence et la traçabilité sont vérifiées autant que possible. La correction de force ionique est faite soit par l'équation de Davies, soit par la théorie de l'interaction spécifique (SIT). Des applications des fichiers d'extraction sont proposées pour des solutions contenant les 38 éléments inclus dans PRODATA. Des diagrammes de Pourbaix en fonction de la pression partielle d' $O_2(g)$, et des diagrammes de spéciations à pression atmosphérique d' $O_2(g)$ et à 1 atm d' $H_2(g)$ sont proposés afin de tester les performances de la base de données.

2022 – Commissariat à l'Énergie Atomique et aux Énergies Alternatives – France

RAPPORT CEA-R-6573 – Pascal REILLER

« The PRODATA Thermochemical Database A Database Applied for Uranium Mining Operations »

Abstract - This document presents the thermochemical data, i.e. constants and functions, that are included in the database PRODATA, which is developed to answer the needs of ORANO Mining in terms of exploration, exploitation, and remediation of uranium mining facilities. The reactions for complexation, dissolution-precipitation and gas solubility can be exported in three database files that can be used by either software packages PHREEQC, CHESS, and Geochemist's WorkBench (GWB). The PRODATA database includes data for uranium and radium, and all elements that are necessary to model their comportment in the different contexts for a total of 38 elements. The data selection is based on CODATA and NEA-OECD selections. The coherency and traceability are checked whenever possible. The ionic strength correction is done through either the Davies equation or the specific ion interaction theory (SIT). Application of the database files is proposed for a solution that is containing the 38 elements included in PRODATA. Pourbaix diagrams at varying $O_2(g)$ fugacity, and speciations at atmospheric $O_2(g)$ and 1 atm $H_2(g)$, are proposed to exemplify the performance of the database.

2022 – Commissariat à l'Énergie Atomique et aux Énergies Alternatives – France

Centre d'Études Nucléaires de Saclay
Direction des Énergies
Institut des Sciences Appliquées et de la Simulation pour les énergies bas carbone
Département de Physico-Chimie
Service d'Études Analytique et Réactivité des Surfaces

The PRODATA Thermochemical Database

A Database Applied for Uranium Mining Operations

Pascal E. Reiller

Table of Content

1. Context.....	1
2. General Considerations.....	5
2.1. <i>Definition of Species</i>	5
2.2. <i>Variation With Temperature</i>	6
2.3. <i>Choice of the Master Species</i>	8
2.4. <i>Expressions of Redox Equilibria</i>	9
2.5. <i>Swap Between Master and Redox Species</i>	10
2.6. <i>Correction of Ionic Strength Effect</i>	10
2.6.1. Debye-Hückel	10
2.6.2. Equations from Cecil W. Davies	11
2.6.3. Specific ion Interaction Theory (SIT)	11
2.6.3.1. <i>General Description</i>	11
2.6.3.2. <i>Particular Cases</i>	12
2.6.3.3. <i>Estimation of Missing Specific Ion Interaction Coefficients</i>	13
2.6.3.4. <i>Rationale on Specific Ion Interaction Coefficients</i>	15
3. Selection of Data.....	17
3.1. <i>Oxygen-Hydrogen-Water</i>	17
3.2. <i>Group 17</i>	17
3.3. <i>Group 16</i>	19
3.3.1. Sulphur	19
3.3.2. Selenium	22
3.4. <i>Group 15</i>	24
3.4.1. Nitrogen	24
3.4.2. Phosphor	25
3.4.3. Arsenic	27
3.4.3.1. <i>Inorganic Compounds</i>	27
3.4.3.2. <i>Organic Compounds</i>	30
3.5. <i>Carbon</i>	30
3.6. <i>Metalloids</i>	32
3.6.1. Silicon	32
3.6.1.1. <i>Native Silicon and Silicic Acid</i>	32
3.6.1.2. <i>Allotropic Forms of Solid SiO₂</i>	33
3.6.1.3. <i>Silicate Ions</i>	34
3.6.2. Lead	34
3.6.2.1. <i>Native Metal and Free Ion</i>	34
3.6.2.2. <i>Oxo and Hydroxo Compounds</i>	35
3.6.2.3. <i>Halide Compounds</i>	35
3.6.2.4. <i>Sulphur and Selenium Compounds</i>	36
3.6.2.5. <i>Phosphor and Arsenic Compounds</i>	36
3.6.2.6. <i>Carbon compounds</i>	37
3.6.2.7. <i>Silicate Compounds</i>	37
3.6.2.8. <i>Tables of Thermodynamic Constants, Functions, and Specific Ion Interaction Coefficients for Pb</i>	37
3.6.3. Aluminium	42
3.6.3.1. <i>Native Metal and Free ion</i>	42
3.6.3.2. <i>Oxo and Hydroxo Compounds</i>	43
3.6.3.3. <i>Halogen Compounds</i>	46
3.6.3.4. <i>Sulphur Compounds</i>	46
3.6.3.5. <i>Group 15 Compounds</i>	49
3.6.3.6. <i>Silicate Compounds</i>	49
3.6.3.7. <i>Thermodynamic Constants, Functions, and Specific Ion Interaction Coefficients for Al.</i>	49
3.7. <i>d-Transition Metals Series</i>	51
3.7.1. Zinc	51
3.7.1.1. <i>Native Metal and Free Ion</i>	51
3.7.1.2. <i>Oxo and Hydroxo Compounds</i>	52
3.7.1.3. <i>Chloro Compounds</i>	52
3.7.1.4. <i>Sulphur and Selenium Compounds</i>	52
3.7.1.5. <i>Phosphor and Arsenic Compounds</i>	53
3.7.1.6. <i>Carbon and Silicium Compounds</i>	54
3.7.1.7. <i>Thermodynamic Constants and Functions, and Specific Ion Interaction Coefficients for Zn</i>	54
3.7.2. Cadmium	57
3.7.2.1. <i>Native Metal and Free Ion</i>	57

Table of Content

3.7.2.2.	<i>Oxo and Hydroxo Compounds</i>	57
3.7.2.3.	<i>Chloro Complexes</i>	58
3.7.2.4.	<i>Sulphur and Selenium Compounds</i>	58
3.7.2.5.	<i>Phosphor Compounds</i>	59
3.7.2.6.	<i>Carbon Compounds</i>	60
3.7.2.7.	<i>Tables of Thermodynamic Constants and Functions, and Specific Ion Interaction Coefficients for Cd</i>	60
3.7.3.	Mercury	62
3.7.3.1.	<i>Native Metal and Free Ions</i>	62
3.7.3.2.	<i>Oxo and Hydroxo Compounds</i>	62
3.7.3.3.	<i>Halogeno Compounds</i>	63
3.7.3.4.	<i>Group 16 Compounds</i>	63
3.7.3.5.	<i>Phosphor Compounds</i>	65
3.7.3.6.	<i>Carbon Compounds</i>	67
3.7.3.7.	<i>Tables of Thermodynamic Constants and Functions, and Specific Ion Interaction Coefficients for Hg</i>	67
3.7.4.	Copper	69
3.7.4.1.	<i>Native Metal and free Ions</i>	69
3.7.4.2.	<i>Hydroxo Compounds</i>	69
3.7.4.3.	<i>Halogen Compounds</i>	70
3.7.4.4.	<i>Sulphur Compounds</i>	70
3.7.4.5.	<i>Selenium Compounds</i>	70
3.7.4.6.	<i>Phosphor Compounds</i>	70
3.7.4.7.	<i>Arsenic Compounds</i>	71
3.7.4.8.	<i>Carbon Compounds</i>	71
3.7.4.9.	<i>Thermodynamic Constants and Functions, and Specific Ion Interaction Coefficients for Cu</i>	72
3.7.5.	Silver	76
3.7.5.1.	<i>Native Metal and Free Ions</i>	76
3.7.5.2.	<i>Oxo and Hydroxo Compounds</i>	77
3.7.5.3.	<i>Halogen Compounds</i>	77
3.7.5.4.	<i>Group 16 Compounds</i>	77
3.7.5.5.	<i>Group 15 Compounds</i>	78
3.7.5.6.	<i>Carbon Compounds</i>	80
3.7.5.7.	<i>Thermodynamic Constants and Functions for Ag</i>	80
3.7.6.	Nickel	81
3.7.6.1.	<i>General Data</i>	81
3.7.6.2.	<i>Complementary Data</i>	81
3.7.6.3.	<i>Additional Thermodynamic Constants and Functions for Ni</i>	84
3.7.7.	Cobalt	86
3.7.7.1.	<i>Native Metal and Free Ions</i>	86
3.7.7.2.	<i>Oxo and Hydroxo Compounds</i>	87
3.7.7.3.	<i>Halogeno Compounds</i>	88
3.7.7.4.	<i>Group 16 Compounds</i>	88
3.7.7.5.	<i>Group 15 Compounds</i>	89
3.7.7.6.	<i>Carbon Compounds</i>	91
3.7.7.7.	<i>Silicate Compounds</i>	91
3.7.7.8.	<i>Thermodynamic Constants and Functions, and Estimation of Specific Ion Interaction Coefficients for Co</i>	91
3.7.8.	Iron	95
3.7.8.1.	<i>Free Ion and Hydroxo Compound</i>	95
3.7.8.2.	<i>Sulphate Compounds</i>	96
3.7.8.3.	<i>Phosphor Compounds</i>	96
3.7.8.4.	<i>Arsenousulphide</i>	96
3.7.8.5.	<i>Thermodynamic Functions and Constants for Compounds of Fe</i>	96
3.7.9.	Manganese	100
3.7.9.1.	<i>Native Metal and Free Ions</i>	100
3.7.9.2.	<i>Hydroxo Compounds</i>	101
3.7.9.3.	<i>Halogen Compounds</i>	102
3.7.9.4.	<i>Group 16 Compounds</i>	102
3.7.9.5.	<i>Group 15 Compounds</i>	102
3.7.9.6.	<i>Carbonate Compounds</i>	103
3.7.9.7.	<i>Silicate Compounds</i>	103
3.7.9.8.	<i>Zinc Phase</i>	103
3.7.9.9.	<i>Thermodynamic Functions and Constants, and Specific Ion Interaction Coefficients for Mn</i>	104
3.7.10.	Molybdenum	107
3.7.10.1.	<i>Native Element and Free Ions</i>	107
3.7.10.2.	<i>Oxides and Molybdates</i>	107
3.7.10.3.	<i>Sulphur Compounds</i>	108
3.7.10.4.	<i>Thermodynamic Functions and Constants for Mo</i>	108
3.7.11.	Vanadium	109
3.7.11.1.	<i>Native Element and Free Ions</i>	109
3.7.11.2.	<i>Oxo, Hydroxo, Chloride and Sulphate Compounds</i>	111

3.7.12.	Titanium	119
3.7.12.1.	<i>Native Element and Free Ions</i>	119
3.7.12.2.	<i>Oxo and Hydroxo Compounds</i>	119
3.7.12.3.	<i>Multiple Oxides</i>	119
3.7.12.4.	<i>Halogen Compounds</i>	120
3.7.12.5.	<i>Sulphur Compounds</i>	120
3.7.12.6.	<i>Thermodynamic Functions and Constants for Ti</i>	120
3.7.13.	Zirconium	121
3.8.	<i>Actinides</i>	122
3.8.1.	Uranium	122
3.8.1.1.	<i>Free Ions</i>	123
3.8.1.2.	<i>Oxo and Hydroxo Compounds</i>	123
3.8.1.3.	<i>Group 17 Compounds</i>	124
3.8.1.4.	<i>Group 16 Compounds</i>	124
3.8.1.5.	<i>Group 15 Compounds</i>	125
3.8.1.6.	<i>Carbonate Compounds</i>	128
3.8.1.7.	<i>Silicate Compounds</i>	135
3.8.1.8.	<i>d-Transition Series Compounds</i>	136
3.8.1.9.	<i>Alkaline Earth Compounds</i>	138
3.8.1.10.	<i>Alkaline Compounds</i>	139
3.8.2.	Thorium	139
3.8.2.1.	<i>Hydroxo Compounds</i>	139
3.8.2.2.	<i>Phosphate Complexes</i>	140
3.9.	<i>Alkaline Earth Metals</i>	140
3.9.1.	Native Metals and Free Ions	140
3.9.2.	Oxo and Hydroxo Compounds	141
3.9.3.	Halogen Compounds	142
3.9.4.	Sulphur Compounds	144
3.9.5.	Selenium Compounds	144
3.9.6.	Nitrate Compounds	145
3.9.7.	Phosphate Compounds	145
3.9.7.1.	<i>Magnesium solids</i>	145
3.9.7.2.	<i>Calcium solids</i>	145
3.9.7.3.	<i>Strontium solid</i>	147
3.9.7.4.	<i>Phosphate complexes</i>	147
3.9.8.	Arsenic Compounds	148
3.9.9.	Carbonato Compounds	149
3.9.9.1.	<i>Solids</i>	149
3.9.9.2.	<i>Complexes</i>	149
3.9.10.	Silicate Compounds	152
3.9.11.	Estimation of Specific Ion Interaction Parameters	153
3.10.	<i>Alkali Metals</i>	155
3.10.1.	Native Metals and Free Ions	155
3.10.2.	Oxide and Hydroxide Compounds	155
3.10.3.	Halogen Compounds	155
3.10.4.	Sulphur Compounds	155
3.10.5.	Group 15	155
3.10.6.	Carbon Compounds	155
3.10.7.	Silicate Compounds	155
3.10.8.	Estimation of Specific Interaction Theory for Cs ⁺	156
3.11.	<i>Aluminosilicate Compounds</i>	156
3.11.1.	Ortho and Ring Structure, and Chain and Band Structure Silicate Minerals	156
3.11.2.	Framework Structure Silicate Minerals	156
3.11.3.	Sheet Structure Silicate Minerals	157
3.12.	<i>Rationale on the Choice of Data</i>	158
4.	<i>Speciation</i>	159
4.1.	<i>General Conditions</i>	159
4.2.	<i>Pourbaix Diagrams</i>	159
4.2.1.	Complete Database	160
4.2.1.1.	<i>Halogens</i>	160
4.2.1.2.	<i>Non-metals</i>	160
4.2.1.3.	<i>Metalloids</i>	160
4.2.1.4.	<i>d-transition metal series</i>	160
4.2.1.5.	<i>Actinides</i>	166
4.2.1.6.	<i>Alkaline earth metals</i>	167

Table of Content

4.2.1.7.	<i>Akaline metals</i>	169
4.2.2.	Pourbaix Diagrams Excluding Ca ₂ ZrSi ₃ O ₁₂ (cr)	170
4.2.2.1.	<i>Halogens</i>	170
4.2.2.2.	<i>Non-metals</i>	171
4.2.2.3.	<i>Metalloids</i>	171
4.2.2.4.	<i>d-transition metals</i>	171
4.2.2.5.	<i>Actinides</i>	177
4.2.2.6.	<i>Alkaline earth metals</i>	177
4.2.2.7.	<i>Alkaline metals</i>	178
4.3.	<i>Species Repartitions Under Atmospheric Oxygen</i>	179
4.3.1.	Complete Database	179
4.3.1.1.	<i>Halogens</i>	179
4.3.1.2.	<i>Non-metals</i>	179
4.3.1.3.	<i>Metalloids</i>	180
4.3.1.4.	<i>d-transition metal series</i>	183
4.3.1.5.	<i>Actinides</i>	186
4.3.1.6.	<i>Alkaline earth metals</i>	187
4.3.1.7.	<i>Alkaline metals</i>	187
4.3.2.	Species Repartition Excluding Ca ₂ ZrSi ₃ O ₁₂ (cr)	189
4.3.2.1.	<i>Halogens</i>	189
4.3.2.2.	<i>Non-metals</i>	190
4.3.2.3.	<i>Metalloids</i>	191
4.3.2.4.	<i>d-transitions metals</i>	192
4.3.2.5.	<i>Actinides</i>	195
4.3.2.6.	<i>Alkaline earth metals</i>	196
4.3.2.7.	<i>Alkaline metals</i>	196
4.4.	<i>Species Repartition at 1 atm Hydrogen</i>	197
4.4.1.	Complete Database	197
4.4.1.1.	<i>Halogens</i>	197
4.4.1.2.	<i>Non-metals</i>	198
4.4.1.3.	<i>Metalloids</i>	199
4.4.1.4.	<i>d-transition metal series</i>	200
4.4.1.5.	<i>Actinides</i>	203
4.4.1.6.	<i>Alkaline earth metals</i>	204
4.4.1.7.	<i>Alkaline metals</i>	204
4.4.2.	Species Repartition Excluding Ca ₂ ZrSi ₃ O ₁₂ (cr)	205
4.4.2.1.	<i>Halogens</i>	205
4.4.2.2.	<i>Non-metals</i>	205
4.4.2.3.	<i>Metalloids</i>	206
4.4.2.4.	<i>d-transition metals</i>	207
4.4.2.5.	<i>Actinides</i>	210
4.4.2.6.	<i>Alkaline earth metals</i>	210
4.4.2.7.	<i>Alkaline metals</i>	211
4.5.	<i>Predominance in Sulphate-Carbonate media</i>	212
4.5.1.	Lead and Iron	212
4.5.2.	Uranium	214
4.5.3.	Barium and Radium	216
4.6.	<i>Predominance of Uranium in Na-Mg-Ca-OH-HCO₃-H domains</i>	217
4.6.1.	Mg-Ca-HCO ₃ -H domain	217
4.6.2.	Na-Cl influence	218
4.7.	<i>Rationale on the Speciation Exercise</i>	219
5.	References.....	220

List of Figures

Figure 2.2-1. Variations of $\log_{10}K^\circ(T)$ for the formation of MgAcetate ⁺ complex using thermodynamic functions in Shock and Koretsky [1993SHO/KOR]: blue line Equation (4), and orange dashed line Equation (5).....	7
Figure 2.6-1. Evolutions of the specific ion interaction coefficients for the divalent free ions in (a) Cl ⁻ , (b) ClO ₄ ⁻ , and (c) NO ₃ ⁻	14
Figure 2.6-2. Evolutions of the activity coefficient of Pb ²⁺ in Cl ⁻ media using various values for $\epsilon(Pb^{2+},Cl^-)$: (a) not implementing a value — <i>i.e.</i> $\epsilon = 0$ (plain line); (b) using $\epsilon(Pb^{2+},ClO_4^-) = -0.18 \text{ kg}_w \text{ mol}^{-1}$ (dotted line) from the regression $1/r = f(\epsilon)$ in Figure 2.6-1a; (c) using the close value of $1/r$ between Pb ²⁺ and Ba ²⁺ (dashed line); and (c) using the $\epsilon(Pb^{2+},ClO_4^-) = 0.15 \text{ kg}_w \text{ mol}^{-1}$ value for $\epsilon(Pb^{2+},Cl^-)$	14
Figure 2.6-3. Frequency distribution of $\epsilon(X^{2+},ClO_4^-)$ [1980CIA; 1983SPA; 1995SIL/BID; 2001LEM/FUG; 2003GUI/FAN; 2005BRO/CUR; 2005GAM/BUG; 2009RAN/FUG; 2012GAM/GAJ; 2013LEM/BER; 2016BRO/EKB; 2018JOR/DEM; 2020LEM/PAL].....	15
Figure 3.2-1. Pourbaix diagram of $10^{-4} \text{ mol kg}_w^{-1}$ I using PHREEPLOT (a), CHESS (b), and GWB (c) in a $0.1 \text{ mol kg}_w^{-1}$ hypothetical indifferent electrolyte solution.....	19
Figure 3.3-1. Specific ion interaction coefficients for sulphur ions.....	21
Figure 3.3-2. Pourbaix diagram of $10^{-4} \text{ mol kg}_w^{-1}$ S in a $0.1 \text{ mol kg}_w^{-1}$ NaClO ₄ solution, obtained using PHREEPLOT (a), CHESS (b), and GWB (c) — no gas is allowed to equilibrate.....	22
Figure 3.3-3. Pourbaix diagram of $10^{-4} \text{ mol kg}_w^{-1}$ Se in a $0.1 \text{ mol kg}_w^{-1}$ NaCl solution PHREEPLOT (a), CHESS (b), and GWB (c), with the common master species SeO ₄ ²⁻ ; all solid phases are allowed to precipitate.....	23
Figure 3.4-1. Pourbaix diagram of $10^{-4} \text{ mol kg}_w^{-1}$ N in a $0.1 \text{ mol kg}_w^{-1}$ NaCl solution (PHREEPLOT) including (a) and not including (b) N(0), NO ₂ ⁻ , and N ₃ ⁻	25
Figure 3.4-2. Pourbaix diagram of $10^{-4} \text{ mol kg}_w^{-1}$ P in a hypothetical indifferent $0.1 \text{ mol kg}_w^{-1}$ electrolyte solution (PHREEPLOT).	26
Figure 3.4-3. Pourbaix diagram of $10^{-4} \text{ mol kg}_w^{-1}$ As in a hypothetical indifferent $0.1 \text{ mol kg}_w^{-1}$ electrolyte solution using PHREEPLOT (a), CHESS (b), and GWB (c). All solid phases are allowed to precipitate.....	28
Figure 3.4-4. Pourbaix diagram of $10^{-4} \text{ mol kg}_w^{-1}$ As and S in a hypothetical indifferent $0.1 \text{ mol kg}_w^{-1}$ electrolyte solution using GWB. All solid phases are allowed to precipitate.....	29
Figure 3.5-1. Pourbaix diagram of carbon $10^{-2} \text{ mol kg}_w^{-1}$ using PHREEPLOT and the thermodynamic constants calculated from thermodynamic functions for carbon species up to C ₁₂ in Shock and Helgeson [1990SHO/HEL].....	31
Figure 3.6-1. Thermodynamic functions and constants for silicate ions [1982WAG/EVA; 1992GRE/FUG; 2003GUI/FAN; 2020GRE/GAO].	34
Figure 3.6-2. Specific ion interaction coefficients for silicate ions.....	34
Figure 3.6-3. Re-estimation of $\log_{10}\beta_3$ and $\epsilon(Pb(OH)_3^-,Na^+)$ using selected data from Brown and Ekberg [2016BRO/EKB] (plain line), and estimation in Brown and Ekberg [2016BRO/EKB] (dashed line).	35
Figure 3.6-4. Pourbaix diagram of $10^{-6} \text{ mol kg}_w^{-1}$ Pb in a hypothetical indifferent $0.1 \text{ mol kg}_w^{-1}$ electrolyte solution using PHREEPLOT (a) and GWB (b). All solid phases are allowed to precipitate.....	38
Figure 3.6-5. Pourbaix diagram of $10^{-6} \text{ mol kg}_w^{-1}$ Pb in a hypothetical $0.1 \text{ mol kg}_w^{-1}$ indifferent electrolyte solution containing $10^{-4} \text{ mol kg}_w^{-1}$ of S using GWB. All solid phases are allowed to precipitate.....	40
Figure 3.6-6. Pourbaix diagram of $10^{-6} \text{ mol kg}_w^{-1}$ Pb in a hypothetical indifferent $0.1 \text{ mol kg}_w^{-1}$ electrolyte solution containing $10^{-4} \text{ mol kg}_w^{-1}$ of P using GWB. All solid phases are allowed to precipitate.....	41
Figure 3.6-7. Pourbaix diagram of $10^{-6} \text{ mol kg}_w^{-1}$ Pb in a hypothetical indifferent $0.1 \text{ mol kg}_w^{-1}$ electrolyte solution in equilibrium with $P(CO_2) = 10^{-2} \text{ atm}$, using GWB; all solid phases are allowed to precipitate.....	42
Figure 3.6-8. Solubility of aluminium oxides and hydroxide, using PHREEPLOT: $\gamma\text{-Al}_2\text{O}_3$ (a), corundum ($\alpha\text{-Al}_2\text{O}_3$) (b), bayerite ($\beta\text{-Al(OH)}_3$) (c), boehmite (AlOOH) (d), gibbsite (Al(OH) ₃) (e), and diasporite (AlOOH) (f).....	45
Figure 3.6-9. Pourbaix diagram of $10^{-6} \text{ mol kg}_w^{-1}$ Al in a hypothetical $0.1 \text{ mol kg}_w^{-1}$ indifferent electrolyte using GWB; all phases are allowed to precipitate.....	46

List of Figures

Figure 3.6-10. Extrapolation of solubility constant for $\text{Al}_4(\text{OH})_{10}\text{SO}_4$ from original data in Adams and Rawajfih [1977ADA/RAW].....	47
Figure 3.6-11. Extrapolation of solubility constant for $\text{NaAl}_3(\text{OH})_6(\text{SO}_4)_2$ from original data [1977ADA/RAW].....	48
Figure 3.6-12. Extrapolation of solubility constant for $\text{KAl}_3(\text{OH})_6(\text{SO}_4)_2$ and average activity product from original data [1977ADA/RAW].....	48
Figure 3.7-1. (a) Solubility of Zn (PHREEPLOT) in a hypothetical indifferent electrolyte at $0.1 \text{ mol kg}_w^{-1}$; all phases are allowed to precipitate; (b) Pourbaix diagram (GWB) of Zn under the same conditions.....	52
Figure 3.7-2. Pourbaix diagram of $10^{-6} \text{ mol kg}_w^{-1}$ Zn (GWB) in a hypothetical indifferent electrolyte $0.1 \text{ mol kg}_w^{-1}$, in presence of $10^{-4} \text{ mol kg}_w^{-1}$ of S (a) and Se (b).....	53
Figure 3.7-3. Pourbaix diagram of $10^{-6} \text{ mol kg}_w^{-1}$ Zn (GWB) in a hypothetical indifferent electrolyte $0.1 \text{ mol kg}_w^{-1}$, in presence of $10^{-4} \text{ mol kg}_w^{-1}$ of P (a) and As (b)	53
Figure 3.7-4. Values of $\varepsilon(\text{M}^{2+},\text{ClO}_4^-)$ (a) and $\varepsilon(\text{M}^{2+},\text{Cl}^-)$ for transition metals vs. $1/r$ [1976SHA].....	57
Figure 3.7-5. (a) Solubility of Cd in a hypothetical indifferent electrolyte at $0.1 \text{ mol kg}_w^{-1}$ using PHREEPLOT; all phases are allowed to precipitate; (b) Pourbaix diagram of Cd in the same conditions using GWB.	58
Figure 3.7-6. Pourbaix diagram (GWB) of $10^{-6} \text{ mol kg}_w^{-1}$ Cd in a hypothetic indifferent $0.1 \text{ mol kg}_w^{-1}$ electrolyte solution containing $10^{-4} \text{ mol kg}_w^{-1}$ of S (a) and Se (b). All solid phases are allowed to precipitate.....	59
Figure 3.7-7. Pourbaix diagram (GWB) of $10^{-6} \text{ mol kg}_w^{-1}$ Cd in a hypothetic indifferent $0.1 \text{ mol kg}_w^{-1}$ electrolyte solution containing $10^{-4} \text{ mol kg}_w^{-1}$ P. All solid phases are allowed to precipitate.....	60
Figure 3.7-8. Pourbaix diagram (GWB) of $10^{-6} \text{ mol kg}_w^{-1}$ Cd in a hypothetic indifferent $0.1 \text{ mol kg}_w^{-1}$ electrolyte solution containing $10^{-4} \text{ mol kg}_w^{-1}$ C. All solid phases are allowed to precipitate.....	60
Figure 3.7-9. Pourbaix diagram (PHREEPLOT) of $10^{-6} \text{ mol kg}_w^{-1}$ Hg in a hypothetic indifferent $0.1 \text{ mol kg}_w^{-1}$ electrolyte solution; all solid phases are allowed to precipitate.	63
Figure 3.7-10. Pourbaix diagram (GWB) of $10^{-6} \text{ mol kg}_w^{-1}$ Hg in a hypothetic indifferent $0.1 \text{ mol kg}_w^{-1}$ electrolyte solution containing $10^{-4} \text{ mol kg}_w^{-1}$ Cl. All solid phases are allowed to precipitate.....	63
Figure 3.7-11. Pourbaix diagram (GWB) of $10^{-6} \text{ mol kg}_w^{-1}$ Hg in a hypothetic indifferent $0.1 \text{ mol kg}_w^{-1}$ electrolyte solution containing $10^{-4} \text{ mol kg}_w^{-1}$ S. All solid phases are allowed to precipitate.	65
Figure 3.7-12. Pourbaix diagram (GWB) of $10^{-6} \text{ mol kg}_w^{-1}$ Hg in a hypothetic indifferent $0.1 \text{ mol kg}_w^{-1}$ electrolyte solution containing $10^{-4} \text{ mol kg}_w^{-1}$ Se. All solid phases are allowed to precipitate.	65
Figure 3.7-13. Pourbaix diagram (GWB) of $10^{-6} \text{ mol kg}_w^{-1}$ Hg in a hypothetic indifferent $0.1 \text{ mol kg}_w^{-1}$ electrolyte solution containing $10^{-4} \text{ mol kg}_w^{-1}$ P. All solid phases are allowed to precipitate.	67
Figure 3.7-14. Evolution of the $\ln K$ values vs. $1/T$ (blue circles) for the dissolution of enargite (Cu_3AsS_4) in the SOLTHERM-XPT database [2015PAL; 2016REE/SPY], and estimation of the formation functions by the Van't Hoff relationship (orange plain line).	71
Figure 3.7-15. Pourbaix diagram of $10^{-6} \text{ mol kg}_w^{-1}$ Cu (PHREEPLOT) (a) and with $10^{-2} \text{ mol kg}_w^{-1}$ of Cl (GWB) (b) in a hypothetic indifferent $0.1 \text{ mol kg}_w^{-1}$ electrolyte solution; all solid phases are allowed to precipitate.	73
Figure 3.7-16. Pourbaix diagram (GWB) of $10^{-6} \text{ mol kg}_w^{-1}$ Cu in a hypothetic indifferent $0.1 \text{ mol kg}_w^{-1}$ electrolyte solution containing $10^{-4} \text{ mol kg}_w^{-1}$ of S (a) and Se (b); all solid phases are allowed to precipitate.....	74
Figure 3.7-17. Pourbaix diagram (GWB) of $10^{-6} \text{ mol kg}_w^{-1}$ Ag.	77
Figure 3.7-18. Pourbaix diagram (GWB) of $10^{-6} \text{ mol kg}_w^{-1}$ Ag and $10^{-4} \text{ mol kg}_w^{-1}$ S (a) and Se (b).	78
Figure 3.7-19. Evolution of the $\ln K$ values vs. $1/T$ (blue circles) for the dissolution of proustite (Ag_3AsS_3) in Spycher and Reed [1989SPY/REE], and estimation of the formation functions by the Van't Hoff relationship (orange plain line).	79
Figure 3.7-20. Pourbaix diagram (GWB) of $10^{-6} \text{ mol kg}_w^{-1}$ Ag and $10^{-4} \text{ mol kg}_w^{-1}$ S and As.	79
Figure 3.7-21. (a) Solubility of Ni in a hypothetical indifferent electrolyte at $0.1 \text{ mol kg}_w^{-1}$ (PHREEPLOT); all phases are allowed to precipitate; (b) Pourbaix diagram of Ni in the same conditions (GWB).	82
Figure 3.7-22. Evolution of the $\ln K$ values vs. $1/T$ (blue circles) for the dissolution of gersdorffite (NiAsS) in the SOLTHERM-XPT database [2015PAL; 2016REE/SPY], and estimation of the formation functions by the Van't Hoff relationship (orange line).	83

Figure 3.7-23. Evolutions of the $\log_{10}K_s$ of NiAsS(cr) with functions of formation from Table 3.7-27.	84
Figure 3.7-24. Pourbaix diagram using GWB of 10^{-6} mol kg $^{-1}$ Cd in a hypothetic indifferent 0.1 mol kg $^{-1}$ electrolyte solution containing 10^{-4} mol kg $^{-1}$ S (a) and Se (b), 10^{-4} mol kg $^{-1}$ As (c), 10^{-3} mol kg $^{-1}$ C (d), at equilibrium with quartz (SiO ₂) (e), and 10^{-4} mol kg $^{-1}$ S and As (f); all solid phases are allowed to precipitate.	85
Figure 3.7-25. Comparison of the $E^\circ_h(\text{Co}^{2+}/\text{Co})$ calculated from different origin of $\Delta_fG^\circ_m$	86
Figure 3.7-26. Evolution of the $\ln K$ vs. $1/T$ values (blue circles) for the dissolution of CoAsS phases in the SOLTHERM-XPT database [2015PAL; 2016REE/SPY], and estimation of the formation functions by the Van't Hoff relationship (orange line).	90
Figure 3.7-27. Evolutions of the $\log_{10}K_s$ vs. t (°C) of CoAsS(cr) with formation functions from Table 3.7-29.	90
Figure 3.7-28. Pourbaix diagram (PHREEPLOT) of 10^{-6} mol kg $^{-1}$ Co in a hypothetic indifferent 0.1 mol kg $^{-1}$ electrolyte solution; all solid phases are allowed to precipitate.	92
Figure 3.7-29. Pourbaix diagram (GWB) of 10^{-6} mol kg $^{-1}$ Co and 10^{-4} mol kg $^{-1}$ S (a) and Se(b) in a hypothetic indifferent 0.1 mol kg $^{-1}$ electrolyte solution; all solid phases are allowed to precipitate.	93
Figure 3.7-30. Pourbaix diagram (GWB) of 10^{-6} mol kg $^{-1}$ Co and 10^{-4} mol kg $^{-1}$ of As in a hypothetic indifferent 0.1 mol kg $^{-1}$ electrolyte solution; all solid phases are allowed to precipitate.	94
Figure 3.7-31. Pourbaix diagram (GWB) of 10^{-6} mol kg $^{-1}$ Co and 10^{-3} mol kg $^{-1}$ C (a), and in equilibrium with quartz (SiO ₂) (b); all phases are allowed to precipitate.	95
Figure 3.7-32. Pourbaix diagram (PHREEPLOT) of 10^{-6} mol kg $^{-1}$ Fe in a 0.1 mol kg $^{-1}$ solution; all solid phases are allowed to precipitate.	97
Figure 3.7-33. Pourbaix diagram (GWB) of 10^{-6} mol kg $^{-1}$ Fe with 10^{-4} mol kg $^{-1}$ S (a) and Se (b); all phases are allowed to precipitate.	98
Figure 3.7-34. Pourbaix diagram (GWB) of 10^{-6} mol kg $^{-1}$ Fe and 10^{-4} mol kg $^{-1}$ P (a), As (b), and As and S (c); all phases are allowed to precipitate.	99
Figure 3.7-35. Pourbaix diagram (GWB) of 10^{-6} mol kg $^{-1}$ Fe at equilibrium with quartz (SiO ₂); all phases are allowed to precipitate.	100
Figure 3.7-36. Values of $\varepsilon(M^{2+}, \text{NO}_3^-)$ for d-transition element series, and estimation of $\varepsilon(\text{Mn}^{2+}, \text{NO}_3^-)$	101
Figure 3.7-37. Dependence of $\log_{10}\beta_1$ of Mn(OH) $^+$ on ionic strength in potassium nitrate media: the dashed line is obtained using the interaction coefficients and stability constant at zero ionic strength from Brown and Ekberg [2016BRO/EKB], and solid line represents the linear fitting.	102
Figure 3.7-38. Pourbaix diagram (PHREEPLOT) of 10^{-6} mol kg $^{-1}$ Mn in a 0.1 mol kg $^{-1}$ solution; all solid phases are allowed to precipitate.	105
Figure 3.7-39. Pourbaix diagram (GWB) of 10^{-6} mol kg $^{-1}$ Mn and 10^{-4} mol kg $^{-1}$ S; all phases are allowed to precipitate.	106
Figure 3.7-40. Pourbaix diagram (GWB) of 10^{-6} mol kg $^{-1}$ Mn and 10^{-4} mol kg $^{-1}$ P (a), 10^{-3} mol kg $^{-1}$ C (b), and at equilibrium with quartz (SiO ₂) (c).	107
Figure 3.7-41. Pourbaix diagram of 10^{-6} mol kg $^{-1}$ Mo in a hypothetic indifferent 0.1 mol kg $^{-1}$ electrolyte solution using PHREEPLOT (a), and with 10^{-4} mol kg $^{-1}$ S using GWB (b); all solid phases are allowed to precipitate.	109
Figure 3.7-42. Latimer diagram for vanadium native metal and free ions [1985BAR/PAR].	111
Figure 3.7-43. Dependence of (a) $\log_{10}K_3^\circ$ of VO ₂ (OH) ₃ $^{2-}$ (HVO ₄ $^{2-}$) and (b) $\log_{10}K_4^\circ$ of VO ₂ (OH) ₄ $^{3-}$ (VO ₄ $^{3-}$) vs. ionic strength in NaCl/NaClO ₄ : the dashed line is obtained using the interaction coefficients and stability constants at zero ionic strength from Brown and Ekberg [2016BRO/EKB], and solid line represents the linear fittings.	112
Figure 3.7-44. Dependence of $\log_{10}K_D^\circ$ of (a) (VO ₂) ₂ (OH) ₆ $^{4-}$ (V ₂ O ₇ $^{4-}$) and (b) (VO ₂) ₂ (OH) ₄ $^{2-}$ (V ₂ O ₆ $^{2-}$) on ionic strength in NaCl (circles) and NaClO ₄ (squares): the dashed line is obtained using the interaction coefficients and stability constants at zero ionic strength from Brown and Ekberg [2016BRO/EKB], and solid line represents the linear fittings.	113

List of Figures

Figure 3.7-45. Dependence of $\log_{10}K^\circ$ of $(\text{VO}_2)_2(\text{OH})_5^{3-}$ ($\text{HV}_2\text{O}_7^{3-}$) on ionic strength in NaCl (circles) and NaClO ₄ (squares): the dashed line is obtained using the interaction coefficients and stability constants at zero ionic strength from Brown and Ekberg [2016BRO/EKB] (Eq. 21), and solid line represents the linear fittings (Eq. 18).	113
Figure 3.7-46. Dependence of $\log_{10}K^\circ$ of (a) $(\text{VO}_2)_4(\text{OH})_8^{4-}$ ($\text{V}_4\text{O}_{12}^{4-}$), (b) $(\text{VO}_2)_4(\text{OH})_9^{5-}$ ($\text{HV}_4\text{O}_{13}^{5-}$), (c) $(\text{VO}_2)_4(\text{OH})_{10}^{6-}$ ($\text{V}_4\text{O}_{13}^{6-}$), and (d) $(\text{VO}_2)_5(\text{OH})_{10}^{5-}$ ($\text{V}_5\text{O}_{15}^{5-}$) on ionic strength in NaCl (circles) and NaClO ₄ (squares): the dashed line is obtained using the interaction coefficients and stability constants at zero ionic strength from Brown and Ekberg [2016BRO/EKB] (Eq. 21), and solid lines represent the linear fittings (Eq. 18) — the linear fitting on NaCl only are plotted in dotted line.	114
Figure 3.7-47. Dependence of $\log_{10}K^\circ$ of (a) $(\text{VO}_2)_{10}(\text{OH})_{14}^{4-}$ ($\text{V}_{10}\text{O}_{27}^{4-}$), (b) $(\text{VO}_2)_{10}(\text{OH})_{15}^{5-}$ ($\text{HV}_{10}\text{O}_{28}^{5-}$), and (c) $(\text{VO}_2)_{10}(\text{OH})_{16}^{6-}$ ($\text{V}_{10}\text{O}_{28}^{6-}$) on ionic strength in NaCl (circles) and NaClO ₄ (squares): the dashed line is obtained using the interaction coefficients and stability constants at zero ionic strength from Brown and Ekberg [2016BRO/EKB] (Eq. 21), and solid line represents the linear fittings (Eq. 18).	115
Figure 3.7-48. Pourbaix diagram of 10^{-6} mol kg _w ⁻¹ vanadium in a 0.1 mol kg _w ⁻¹ solution using PHREEPLOT; all solid phases are allowed to precipitate.	117
Figure 3.8-1. Pourbaix diagram of 10^{-6} mol kg _w ⁻¹ U in a hypothetical indifferent 0.1 mol kg _w ⁻¹ electrolyte solution using PHREEPLOT; all solid phases are allowed to precipitate.	124
Figure 3.8-2. Pourbaix diagram of 10^{-6} mol kg _w ⁻¹ U with 10^{-4} mol kg _w ⁻¹ P using GWB.	127
Figure 3.8-3. Pourbaix diagram using GWB of 10^{-6} mol kg _w ⁻¹ U and 10^{-3} mol kg _w ⁻¹ C (a), and in equilibrium with $P(\text{CO}_2) = 10^{-3.5}$ atm (b).	129
Figure 3.8-4. Speciation of uranium(VI) at equilibrium with $P(\text{CO}_2(\text{g})) = 10^{-3.5}$ atm at ionic strength $I_m = 0.1$ mol kg _w ⁻¹ NaCl with $[\text{Ca}]_{\text{total}} = 1$ mmol kg _w ⁻¹ (a,b), and $I_m = 0.5$ mol kg ⁻¹ with $[\text{Ca}]_{\text{total}} = 10$ mmol kg _w ⁻¹ (c,d) using thermodynamic constants and specific ion interaction coefficients from Shang and Reiller [2020aSHA/REI] (a,c), and constants and $\varepsilon = 0$ from NEA-OECD [2020GRE/GAO] (b,d); pH fixed by NaOH, PHREEQC extraction for SIT calculation.	132
Figure 3.8-5. Comparision of thermodynamic functions $\Delta_rH^\circ_m$ and $-\text{T}\Delta_rS^\circ_m$ for the stepwise formation of $\text{CaUO}_2(\text{CO}_3)_3^{2-}$ and $\text{Ca}_2\text{UO}_2(\text{CO}_3)_3(\text{aq})$	133
Figure 3.8-6. Speciation of uranium(VI) at equilibrium with $P(\text{CO}_2(\text{g})) = 10^{-3.5}$ atm at ionic strength $I_m = 0.1$ mol kg _w ⁻¹ NaCl with $[\text{Mg}]_{\text{total}} = 1$ mmol kg _w ⁻¹ (a,b), and $I_m = 0.5$ mol kg ⁻¹ with $[\text{Mg}]_{\text{total}} = 10$ mmol kg _w ⁻¹ (c,d) using thermodynamic constants and specific ion interaction coefficients from Shang and Reiller [2021aSHA/REI] (a,c), and constants and $\varepsilon = 0$ from NEA-OECD [2020GRE/GAO] (b,d); pH fixed by NaOH, PHREEQC extraction for SIT calculation.	134
Figure 3.8-7. Pourbaix diagram using GWB of 10^{-6} mol kg _w ⁻¹ U in the presence of 10^{-3} mol kg _w ⁻¹ V.	137
Figure 3.8-8. Activity products of billietite $(\text{Ba}(\text{UO}_2)_6\text{O}_4(\text{OH})_{10}:4\text{H}_2\text{O})$ from the solubility data in Vochten and Van Haverbeke [1990VOC/HAV] calculated using PHREEQC and PRODATA.	139
Figure 3.9-1. Speciation of Mg-CO ₃ with increasing concentration of carbonate plotted as percentage of species vs. equivalent P(CO ₂) in equilibrium using the data from Königsberger <i>et al.</i> [1999KÖN/KÖN]: $C_{\text{Mg}} = 0.1$ mmol kg _w ⁻¹ , pH = 8, $[\text{NaClO}_4] = 0.1$ mol kg _w ⁻¹	150
Figure 3.9-2. Dependence of $\varepsilon(\text{M}^{2+}, \text{Cl}^-)$ (a), $\varepsilon(\text{M}^{2+}, \text{NO}_3^-)$ (b), and $\varepsilon(\text{M}^{2+}, \text{ClO}_4^-)$ (c) for the alkaline earth metals from Guillaumont <i>et al.</i> [2003GUI/FAN] with the 1/IR value from Shannon [1976SHA]: linear regression (plain line) is calculated as $1/\text{IR} = f(\varepsilon)$ even plotted otherwise in a typical manner; the dashed lines represent the 95% confidence interval; dotted line represents the $\varepsilon(\text{Sr}^{2+}, \text{X}^-)$ calculated values; the short dotted line represent the $\varepsilon(\text{Ra}^{2+}, \text{X}^-)$ values.	154
Figure 3.10-1. Dependence of $\varepsilon(\text{M}^+, \text{Cl}^-)$ for the alkaline metals from Guillaumont <i>et al.</i> [2003GUI/FAN] (diamonds) with the 1/IR value from Shannon [1976SHA]: linear regression (plain line) is calculated as $1/\text{IR} = f(\varepsilon)$ even plotted otherwise in a typical manner; the dashed lines represent the 95% confidence interval; the short dotted line represent the $\varepsilon(\text{Cs}^+, \text{Cl}^-)$ value; the value estimated in Spahiu [2002SPA] is shown as a circle.	156
Figure 4.1-1. Potential (dashed lines) and ionic strength (plain lines) evolution during speciation at $P(\text{O}_2) = 0.21$ atm (blue lines) and $P(\text{H}_2) = 1$ atm (orange lines) in a solution containing all elements included in PRODATA at 10^{-4} mol kg _w ⁻¹ ; the ionic strength is maintained at 0.1 mol kg _w ⁻¹ by a solution containing a hypothetical indifferent Cation/Anion electrolyte; all possible phases are allowed to precipitate; the Davies extraction of the database is used.	159

Figure 4.2-1. Pourbaix diagrams (PHREEPLOT) of halogens — F(a), Cl (b), Br (c), and I(d) — in a solution containing all elements included in PRODATA at 10^{-4} mol kg _w ⁻¹ ; the ionic strength is maintained at 0.1 mol kg _w ⁻¹ by a solution containing a hypothetic indifferent Cation/Anion electrolyte; all possible phases are allowed to precipitate; the Davies PHREEQC extraction of the database is used.....	161
Figure 4.2-2. Pourbaix diagrams (PHREEPLOT) of non-metals — S (a), Se (b), N (c), P (d), As (e), and C (f) — in a solution containing all elements included in PRODATA at 10^{-4} mol kg _w ⁻¹ ; the ionic strength is maintained at 0.1 mol kg _w ⁻¹ by a solution containing a hypothetic indifferent Cation/Anion electrolyte; all possible phases are allowed to precipitate; the Davies PHREEQC extraction of the database is used.....	162
Figure 4.2-3. Pourbaix diagrams (PHREEPLOT) of metalloids — Si (a), Pb (b), and Al (c) — in a solution containing all elements included in PRODATA at 10^{-4} mol kg _w ⁻¹ ; the ionic strength is maintained at 0.1 mol kg _w ⁻¹ by a solution containing a hypothetic indifferent Cation/Anion electrolyte; all possible phases are allowed to precipitate; the Davies PHREEQC extraction of the database is used.....	163
Figure 4.2-4. Pourbaix diagrams (PHREEPLOT) of d-transition metal series — Zn (a), Cd (b), Hg (c), Cu (d), and Ag (e) — in a solution containing all elements included in PRODATA at 10^{-4} mol kg _w ⁻¹ ; the ionic strength is maintained at 0.1 mol kg _w ⁻¹ by a solution containing a hypothetic indifferent Cation/Anion electrolyte; all possible phases are allowed to precipitate; the Davies PHREEQC extraction of the database is used.....	164
Figure 4.2-5. Pourbaix diagrams (PHREEPLOT) of d-transition metal series — Ni (a), Co (b), Fe (c), and Mn (d) — in a solution containing all elements included in PRODATA at 10^{-4} mol kg _w ⁻¹ ; the ionic strength is maintained at 0.1 mol kg _w ⁻¹ by a solution containing a hypothetic indifferent Cation/Anion electrolyte; all possible phases are allowed to precipitate; the Davies PHREEQC extraction of the database is used.....	165
Figure 4.2-6. Pourbaix diagrams (PHREEPLOT) of d-transition metal series — Mo (a), V (b), Ti (c), and Zr (d) — in a solution containing all elements included in PRODATA at 10^{-4} mol kg _w ⁻¹ ; the ionic strength is maintained at 0.1 mol kg _w ⁻¹ by a solution containing a hypothetic indifferent Cation/Anion electrolyte; all possible phases are allowed to precipitate; the Davies PHREEQC extraction of the database is used.....	166
Figure 4.2-7. Pourbaix diagrams (PHREEPLOT) of actinides — U (a), and Th (b) — in a solution containing all elements included in PRODATA at 10^{-4} mol kg _w ⁻¹ ; the ionic strength is maintained at 0.1 mol kg _w ⁻¹ by a solution containing a hypothetic indifferent Cation/Anion electrolyte; all possible phases are allowed to precipitate; the Davies PHREEQC extraction of the database is used.....	167
Figure 4.2-8. Pourbaix diagrams (PHREEPLOT) of alkaline earth metals — Mg (a), Ca (b), Sr (c), Ba (d), and Ra (e) — in a solution containing all elements included in PRODATA at 10^{-4} mol kg _w ⁻¹ ; the ionic strength is maintained at 0.1 mol kg _w ⁻¹ by a solution containing a hypothetic indifferent Cation/Anion electrolyte; all possible phases are allowed to precipitate; the Davies PHREEQC extraction of the database is used.....	168
Figure 4.2-9. Pourbaix diagrams (PHREEPLOT) of alkaline metals — Li (a), Na (b), K (c), Rb (d), and Cs (e) — in a solution containing all elements included in PRODATA at 10^{-4} mol kg _w ⁻¹ ; the ionic strength is maintained at 0.1 mol kg _w ⁻¹ by a solution containing a hypothetic indifferent Cation/Anion electrolyte; all possible phases are allowed to precipitate; the Davies PHREEQC extraction of the database is used.....	169
Figure 4.2-10. Pourbaix diagrams (PHREEPLOT) of halogens — F (a), Cl (b), Br (c), and I (d) — in a solution containing all elements included in PRODATA at 10^{-4} mol kg _w ⁻¹ ; the ionic strength is maintained at 0.1 mol kg _w ⁻¹ by a solution containing a hypothetic indifferent Cation/Anion electrolyte; all possible phases are allowed to precipitate; the Davies PHREEQC extraction of the database is used, excluding Ca ₂ ZrSi ₃ O ₁₂ (cr) in the input file.....	170
Figure 4.2-11. Pourbaix diagrams (PHREEPLOT) of non-metals — S (a), Se (b), N (c), P (d), As (e), and C (f) — in a solution containing all elements included in PRODATA at 10^{-4} mol kg _w ⁻¹ ; the ionic strength is maintained at 0.1 mol kg _w ⁻¹ by a solution containing a hypothetic indifferent Cation/Anion electrolyte; all possible phases are allowed to precipitate; the Davies PHREEQC extraction of the database is used, excluding Ca ₂ ZrSi ₃ O ₁₂ (cr) in the input file.....	172
Figure 4.2-12. Pourbaix diagrams (PHREEPLOT) of metalloids — Si (a), Pb (b), and Al (c) — in a solution containing all elements included in PRODATA at 10^{-4} mol kg _w ⁻¹ ; the ionic strength is maintained at 0.1 mol kg _w ⁻¹ by a solution containing a hypothetic indifferent Cation/Anion electrolyte; all possible phases are allowed to precipitate; the Davies PHREEQC extraction of the database is used, excluding Ca ₂ ZrSi ₃ O ₁₂ (cr) in the input file.....	173

List of Figures

Figure 4.2-13. Pourbaix diagrams (PHREEPLOT) of d-transition metals — Zn (a), Cd (b), Hg (c), Cu(d), and Ag(e) — in a solution containing all elements included in PRODATA at 10^{-4} mol kg $_{w^{-1}}$; the ionic strength is maintained at 0.1 mol kg $_{w^{-1}}$ by a solution containing a hypothetic indifferent Cation/Anion electrolyte; all possible phases are allowed to precipitate; the Davies PHREEQC extraction of the database is used, excluding Ca ₂ ZrSi ₃ O ₁₂ (cr) in the input file.....	174
Figure 4.2-14. Pourbaix diagrams (PHREEPLOT) of d-transition metals — Ni (a), Co (b), Fe (c), and Mn(d) — in a solution containing all elements included in PRODATA at 10^{-4} mol kg $_{w^{-1}}$; the ionic strength is maintained at 0.1 mol kg $_{w^{-1}}$ by a solution containing a hypothetic indifferent Cation/Anion electrolyte; all possible phases are allowed to precipitate; the Davies PHREEQC extraction of the database is used, excluding Ca ₂ ZrSi ₃ O ₁₂ (cr) in the input file.....	175
Figure 4.2-15. Pourbaix diagrams (PHREEPLOT) of d-transition metals — Mo (a), V (b), Ti (c), and Zr (d) — in a solution containing all elements included in PRODATA at 10^{-4} mol kg $_{w^{-1}}$; the ionic strength is maintained at 0.1 mol kg $_{w^{-1}}$ by a solution containing a hypothetic indifferent Cation/Anion electrolyte; all possible phases are allowed to precipitate; the Davies PHREEQC extraction of the database is used, excluding Ca ₂ ZrSi ₃ O ₁₂ (cr) in the input file.....	176
Figure 4.2-16. Pourbaix diagrams (PHREEPLOT) of actinides — U (a), and Th (b) — in a solution containing all elements included in PRODATA at 10^{-4} mol kg $_{w^{-1}}$; the ionic strength is maintained at 0.1 mol kg $_{w^{-1}}$ by a solution containing a hypothetic indifferent Cation/Anion electrolyte; all possible phases are allowed to precipitate; the Davies PHREEQC extraction of the database is used, excluding Ca ₂ ZrSi ₃ O ₁₂ (cr) in the input file.....	177
Figure 4.2-17. Pourbaix diagrams (PHREEPLOT) of alkaline earth metals — Mg (a), Ca (b), Sr (c), Ba (d), and Ra (e) — in a solution containing all elements included in PRODATA at 10^{-4} mol kg $_{w^{-1}}$; the ionic strength is maintained at 0.1 mol kg $_{w^{-1}}$ by a solution containing a hypothetic indifferent Cation/Anion electrolyte; all possible phases are allowed to precipitate; the Davies PHREEQC extraction of the database is used, excluding Ca ₂ ZrSi ₃ O ₁₂ (cr) in the input file.....	178
Figure 4.3-1. Speciation at P(O ₂) = 0.21 atm (PHREEPLOT) of halogens — F (a), Cl (b), Br (c), and I (d) — in a solution containing all elements included in PRODATA at 10^{-4} mol kg $_{w^{-1}}$; the ionic strength is maintained at 0.1 mol kg $_{w^{-1}}$ by a solution containing a hypothetic indifferent Cation/Anion electrolyte; all possible phases are allowed to precipitate; species less than 2% are not plotted; the Davies PHREEQC extraction of the database is used.....	180
Figure 4.3-2. Speciation at P(O ₂) = 0.21 atm (PHREEPLOT) of non-metals — S (a), Se (b), N (c), P(d), As (e), and C (f) — in a solution containing all elements included in PRODATA at 10^{-4} mol kg $_{w^{-1}}$; the ionic strength is maintained at 0.1 mol kg $_{w^{-1}}$ by a solution containing a hypothetic indifferent Cation/Anion electrolyte; all possible phases are allowed to precipitate; species less than 2% are not plotted; the Davies PHREEQC extraction of the database is used.....	181
Figure 4.3-3. Speciation at P(O ₂) = 0.21 atm (PHREEPLOT) of Si (a), Pb (b), and Al (c) in a solution containing all elements included in PRODATA at 10^{-4} mol kg $_{w^{-1}}$; the ionic strength is maintained at 0.1 mol kg $_{w^{-1}}$ by a solution containing a hypothetic indifferent Cation/Anion electrolyte; all possible phases are allowed to precipitate; species less than 2% are not plotted; the Davies PHREEQC extraction of the database is used.....	182
Figure 4.3-4. Speciation at P(O ₂) = 0.21 atm of Pb in a solution containing all elements included in PRODATA at 10^{-4} mol kg $_{w^{-1}}$; the ionic strength is maintained at 0.1 mol kg $_{w^{-1}}$ by a solution containing a hypothetic indifferent Cation/Anion electrolyte; all possible phases are allowed to precipitate; species less than 2% are not plotted; the CHESS (a) and GWB (b) extraction of the database is used.....	182
Figure 4.3-5. Speciation at P(O ₂) = 0.21 atm (PHREEPLOT) of d-series elements Zn (a), Cd (b), Hg (c), Cu (d), and Ag (e) in a solution containing all elements included in PRODATA at 10^{-4} mol kg $_{w^{-1}}$; the ionic strength is maintained at 0.1 mol kg $_{w^{-1}}$ by a solution containing a hypothetic indifferent Cation/Anion electrolyte; all possible phases are allowed to precipitate; species less than 2% are not plotted; the Davies PHREEQC extraction of the database is used.....	184
Figure 4.3-6. Speciation at P(O ₂) = 0.21 atm (PHREEPLOT) of d-series elements Ni (a), Co (b), Fe (c), and Mn (d) in a solution containing all elements included in PRODATA at 10^{-4} mol kg $_{w^{-1}}$; the ionic strength is maintained at 0.1 mol kg $_{w^{-1}}$ by a solution containing a hypothetic indifferent Cation/Anion electrolyte; all possible phases are allowed to precipitate; species less than 2% are not plotted; the Davies PHREEQC extraction of the database is used.....	185

Figure 4.3-7. Speciation at $P(O_2) = 0.21 \text{ atm}$ (PHREEPLOT) of d-series elements Mo (a), V (b), Ti (c), and Zr (d) in a solution containing all elements included in PRODATA at $10^{-4} \text{ mol kg}_w^{-1}$; the ionic strength is maintained at $0.1 \text{ mol kg}_w^{-1}$ by a solution containing a hypothetic indifferent Cation/Anion electrolyte; all possible phases are allowed to precipitate; species less than 2% are not plotted; the Davies PHREEQC extraction of the database is used.....	186
Figure 4.3-8. Speciation at $P(O_2) = 0.21 \text{ atm}$ (PHREEPLOT) of actinides U (a) and Th (b) in a solution containing all elements included in PRODATA at $10^{-4} \text{ mol kg}_w^{-1}$; the ionic strength is maintained at $0.1 \text{ mol kg}_w^{-1}$ by a solution containing a hypothetic indifferent Cation/Anion electrolyte; all possible phases are allowed to precipitate; species less than 2% are not plotted; the Davies PHREEQC extraction of the database is used.....	187
Figure 4.3-9. Speciation at $P(O_2) = 0.21 \text{ atm}$ (PHREEPLOT) of alkaline earth metals Mg (a), Ca (b), Sr (c), Ba (d), and Ra (e) in a solution containing all elements included in PRODATA at $10^{-4} \text{ mol kg}_w^{-1}$; the ionic strength is maintained at $0.1 \text{ mol kg}_w^{-1}$ by a solution containing a hypothetic indifferent Cation/Anion electrolyte; all possible phases are allowed to precipitate; species less than 2% are not plotted; the Davies PHREEQC extraction of the database is used.....	188
Figure 4.3-10. Speciation at $P(O_2) = 0.21 \text{ atm}$ (PHREEPLOT) of alkaline metals Li (a), Na (b), K (c), Rb (d) and Cd (e) in a solution containing all elements included in PRODATA at $10^{-4} \text{ mol kg}_w^{-1}$; the ionic strength is maintained at $0.1 \text{ mol kg}_w^{-1}$ by a solution containing a hypothetic indifferent Cation/Anion electrolyte; all possible phases are allowed to precipitate; species less than 2% are not plotted; the Davies PHREEQC extraction of the database is used.....	189
Figure 4.3-11. Speciation at $P(O_2) = 0.21 \text{ atm}$ (PHREEPLOT) of halogens — F (a), Cl (b), Br (c), and I (d) — in a solution containing all elements included in PRODATA at $10^{-4} \text{ mol kg}_w^{-1}$; the ionic strength is maintained at $0.1 \text{ mol kg}_w^{-1}$ by a solution containing a hypothetic indifferent Cation/Anion electrolyte; all possible phases are allowed to precipitate; species less than 2% are not plotted; the Davies PHREEQC extraction of the database is used, excluding $\text{Ca}_2\text{ZrSi}_3\text{O}_{12}(\text{cr})$ in the input file.....	190
Figure 4.3-12. Speciation at $P(O_2) = 0.21 \text{ atm}$ (PHREEPLOT) of non-metals — S (a), Se (b), N (c), P (d), As (e), and C (f) — in a solution containing all the elements included in PRODATA at $10^{-4} \text{ mol kg}_w^{-1}$; the ionic strength is maintained at $0.1 \text{ mol kg}_w^{-1}$ by a solution containing a hypothetic indifferent Cation/Anion electrolyte; all possible phases are allowed to precipitate; species less than 2% are not plotted; the Davies PHREEQC extraction of the database is used, excluding $\text{Ca}_2\text{ZrSi}_3\text{O}_{12}(\text{cr})$ in the input file.....	191
Figure 4.3-13. Speciation at $P(O_2) = 0.21 \text{ atm}$ (PHREEPLOT) of metalloids — Si (a), Pb (b), and Al (c) — in a solution containing all elements included in PRODATA at $10^{-4} \text{ mol kg}_w^{-1}$; the ionic strength is maintained at $0.1 \text{ mol kg}_w^{-1}$ by a solution containing a hypothetic indifferent Cation/Anion electrolyte; all possible phases are allowed to precipitate; species less than 2% are not plotted; the Davies PHREEQC extraction of the database is used, excluding $\text{Ca}_2\text{ZrSi}_3\text{O}_{12}(\text{cr})$ in the input file.....	192
Figure 4.3-14. Speciation at $P(O_2) = 0.21 \text{ atm}$ (PHREEPLOT) of d-transition metals — Zn (a), Cd (b), Hg (c), Cu (d), and Ag (e) — in a solution containing all elements included in PRODATA at $10^{-4} \text{ mol kg}_w^{-1}$; the ionic strength is maintained at $0.1 \text{ mol kg}_w^{-1}$ by a solution containing a hypothetic indifferent Cation/Anion electrolyte; all possible phases are allowed to precipitate; species less than 2% are not plotted; the Davies PHREEQC extraction of the database is used, excluding $\text{Ca}_2\text{ZrSi}_3\text{O}_{12}(\text{cr})$ in the input file.....	193
Figure 4.3-15. Speciation at $P(O_2) = 0.21 \text{ atm}$ (PHREEPLOT) of d-transition metals — Ni (a), Co (b), Fe (c), and Mn (d) — in a solution containing all elements included in PRODATA at $10^{-4} \text{ mol kg}_w^{-1}$; the ionic strength is maintained at $0.1 \text{ mol kg}_w^{-1}$ by a solution containing a hypothetic indifferent Cation/Anion electrolyte; all possible phases are allowed to precipitate; species less than 2% are not plotted; the Davies PHREEQC extraction of the database is used, excluding $\text{Ca}_2\text{ZrSi}_3\text{O}_{12}(\text{cr})$ in the input file.....	194
Figure 4.3-16. Speciation at $P(O_2) = 0.21 \text{ atm}$ (PHREEPLOT) of d-transition metals — Mo (a), V (b), Ti (c), and Zr (d) — in a solution containing all elements included in PRODATA at $10^{-4} \text{ mol kg}_w^{-1}$; the ionic strength is maintained at $0.1 \text{ mol kg}_w^{-1}$ by a solution containing a hypothetic indifferent Cation/Anion electrolyte; all possible phases are allowed to precipitate; species less than 2% are not plotted; the Davies PHREEQC extraction of the database is used, excluding $\text{Ca}_2\text{ZrSi}_3\text{O}_{12}(\text{cr})$ in the input file.....	195
Figure 4.3-17. Speciation at $P(O_2) = 0.21 \text{ atm}$ (PHREEPLOT) of actinides — U (a), and Th (b) — in a solution containing all elements included in PRODATA at $10^{-4} \text{ mol kg}_w^{-1}$; the ionic strength is maintained at $0.1 \text{ mol kg}_w^{-1}$ by a solution containing a hypothetic indifferent Cation/Anion electrolyte; all possible phases are allowed to precipitate; species less than 2% are not plotted; the Davies PHREEQC extraction of the database is used, excluding $\text{Ca}_2\text{ZrSi}_3\text{O}_{12}(\text{cr})$ in the input file.....	195

List of Figures

Figure 4.3-18. Speciation at $P(O_2) = 0.21 \text{ atm}$ (PHREEPLOT) of alkaline earth metals — Mg (a), Ca (b), Sr (c), Ba (d), and Ra (e) — in a solution containing all elements included in PRODATA at $10^{-4} \text{ mol kg}^{-1}$; the ionic strength is maintained at 0.1 mol kg^{-1} by a solution containing a hypothetic indifferent Cation/Anion electrolyte; all possible phases are allowed to precipitate; species less than 2% are not plotted; the Davies PHREEQC extraction of the database is used, excluding $\text{Ca}_2\text{ZrSi}_3\text{O}_{12}(\text{cr})$ in the input file.....	196
Figure 4.3-19. Speciation at $P(O_2) = 0.21 \text{ atm}$ (PHREEPLOT) of K in a solution containing all elements included in PRODATA at $10^{-4} \text{ mol kg}^{-1}$; the ionic strength is maintained at 0.1 mol kg^{-1} by a solution containing a hypothetic indifferent Cation/Anion electrolyte; all possible phases are allowed to precipitate; species less than 2% are not plotted; the Davies PHREEQC extraction of the database is used, excluding $\text{Ca}_2\text{ZrSi}_3\text{O}_{12}(\text{cr})$ in the input file.....	197
Figure 4.4-1. Speciation at $P(H_2) = 1 \text{ atm}$ (PHREEPLOT) of halogens — F(a), Cl (b), Br (c), and I(d) — in a solution containing all elements included in PRODATA at $10^{-4} \text{ mol kg}^{-1}$; the ionic strength is maintained at 0.1 mol kg^{-1} by a solution containing a hypothetic indifferent Cation/Anion electrolyte; all possible phases are allowed to precipitate; species less than 2% are not plotted; the Davies PHREEQC extraction of the database is used.....	198
Figure 4.4-2. Speciation at $P(H_2) = 1 \text{ atm}$ (PHREEPLOT) of non-metals S (a), Se (b), N (c), P(d), As (e), and C (f) in a solution containing all elements included in PRODATA at $10^{-4} \text{ mol kg}^{-1}$; the ionic strength is maintained at 0.1 mol kg^{-1} by a solution containing a hypothetic indifferent Cation/Anion electrolyte; all possible phases are allowed to precipitate; species less than 2% are not plotted; the Davies PHREEQC extraction of the database is used.....	199
Figure 4.4-3. Speciation at $P(H_2) = 1 \text{ atm}$ (PHREEPLOT) of Si (a), Pb (b), and Al (c) in a solution containing all elements included in PRODATA at $10^{-4} \text{ mol kg}^{-1}$; the ionic strength is maintained at 0.1 mol kg^{-1} by a solution containing a hypothetic indifferent Cation/Anion electrolyte; all possible phases are allowed to precipitate; species less than 2% are not plotted; the Davies PHREEQC extraction of the database is used.....	200
Figure 4.4-4. Speciation at $P(H_2) = 1 \text{ atm}$ (PHREEPLOT) of d-series elements Zn (a), Cd(b), (c), Cu (d), and Ag (e) in a solution containing all elements included in PRODATA at $10^{-4} \text{ mol kg}^{-1}$; the ionic strength is maintained at 0.1 mol kg^{-1} by a solution containing a hypothetic indifferent Cation/Anion electrolyte; all possible phases are allowed to precipitate; species less than 2% are not plotted; the Davies PHREEQC extraction of the database is used.....	201
Figure 4.4-5. Speciation at $P(H_2) = 1 \text{ atm}$ (PHREEPLOT) of d-series elements Ni (a), Co(b), Fe(c), and Mn (d) in a solution containing all elements included in PRODATA at $10^{-4} \text{ mol kg}^{-1}$; the ionic strength is maintained at 0.1 mol kg^{-1} by a solution containing a hypothetic indifferent Cation/Anion electrolyte; all possible phases are allowed to precipitate; species less than 2% are not plotted; the Davies PHREEQC extraction of the database is used.....	202
Figure 4.4-6. Speciation at $P(H_2) = 1 \text{ atm}$ (PHREEPLOT) of d-series elements Mo (a), V (b), Ti (c), and Zr (d) in a solution containing all elements included in PRODATA at $10^{-4} \text{ mol kg}^{-1}$; the ionic strength is maintained at 0.1 mol kg^{-1} by a solution containing a hypothetic indifferent Cation/Anion electrolyte; all possible phases are allowed to precipitate; species less than 2% are not plotted; the Davies PHREEQC extraction of the database is used.....	203
Figure 4.4-7. Speciation at $P(H_2) = 1 \text{ atm}$ (PHREEPLOT) of U in a solution containing all elements included in PRODATA at $10^{-4} \text{ mol kg}^{-1}$; the ionic strength is maintained at 0.1 mol kg^{-1} by a solution containing a hypothetic indifferent Cation/Anion electrolyte; all possible phases are allowed to precipitate; species less than 2% are not plotted; the Davies PHREEQC extraction of the database is used.	203
Figure 4.4-8. Speciation at $P(H_2) = 1 \text{ atm}$ (PHREEPLOT) of alkaline earth metals in a solution containing all elements included in PRODATA at $10^{-4} \text{ mol kg}^{-1}$; the ionic strength is maintained at 0.1 mol kg^{-1} by a solution containing a hypothetic indifferent Cation/Anion electrolyte; all possible phases are allowed to precipitate; species less than 1% are not plotted; the Davies PHREEQC extraction of the database is used.....	204
Figure 4.4-9. Speciation at $P(H_2) = 1 \text{ atm}$ (PHREEPLOT) of halogens — F (a), Cl (b), Br (c), and I (d) — in a solution containing all elements included in PRODATA at $10^{-4} \text{ mol kg}^{-1}$; the ionic strength is maintained at 0.1 mol kg^{-1} by a solution containing a hypothetic indifferent Cation/Anion electrolyte; all possible phases are allowed to precipitate; species less than 2% are not plotted; the Davies PHREEQC extraction of the database is used, excluding $\text{Ca}_2\text{ZrSi}_3\text{O}_{12}(\text{cr})$ in the input file.	205

Figure 4.4-10. Speciation at $P(H_2) = 1 \text{ atm}$ (PHREEPLOT) of non-metals S (a), Se (b), N (c), P(d), As (e), and C (f) in a solution containing all elements included in PRODATA at $10^{-4} \text{ mol kg}_w^{-1}$; the ionic strength is maintained at $0.1 \text{ mol kg}_w^{-1}$ by a solution containing a hypothetic indifferent Cation/Anion electrolyte; all possible phases are allowed to precipitate; species less than 2% are not plotted; the Davies PHREEQC extraction of the database is used excluding $\text{Ca}_2\text{ZrSi}_3\text{O}_{12}(\text{cr})$	206
Figure 4.4-11. Speciation at $P(H_2) = 1 \text{ atm}$ (PHREEPLOT) of metalloids — Si (a), Pb (b), and Al (c) — in a solution containing all elements included in PRODATA at $10^{-4} \text{ mol kg}_w^{-1}$; the ionic strength is maintained at $0.1 \text{ mol kg}_w^{-1}$ by a solution containing a hypothetic indifferent Cation/Anion electrolyte; all possible phases are allowed to precipitate; species less than 2% are not plotted; the Davies PHREEQC extraction of the database is used, excluding $\text{Ca}_2\text{ZrSi}_3\text{O}_{12}(\text{cr})$ in the input file.	207
Figure 4.4-12. Speciation at $P(H_2) = 1 \text{ atm}$ (PHREEPLOT) of d-transition metals Zn (a), Cd (b), Hg (c), Cu(d), and Ag (e) in a solution containing all elements included in PRODATA at $10^{-4} \text{ mol kg}_w^{-1}$; the ionic strength is maintained at $0.1 \text{ mol kg}_w^{-1}$ by a solution containing a hypothetic indifferent Cation/Anion electrolyte; all possible phases are allowed to precipitate; species less than 2% are not plotted; the Davies PHREEQC extraction of the database is used excluding $\text{Ca}_2\text{ZrSi}_3\text{O}_{12}(\text{cr})$	208
Figure 4.4-13. Speciation at $P(H_2) = 1 \text{ atm}$ (PHREEPLOT) of d-transition metals Ni (a), Co (b), Fe (c), and Mn (d) in a solution containing all elements included in PRODATA at $10^{-4} \text{ mol kg}_w^{-1}$; the ionic strength is maintained at $0.1 \text{ mol kg}_w^{-1}$ by a solution containing a hypothetic indifferent Cation/Anion electrolyte; all possible phases are allowed to precipitate; species less than 2% are not plotted; the Davies PHREEQC extraction of the database is used excluding $\text{Ca}_2\text{ZrSi}_3\text{O}_{12}(\text{cr})$	209
Figure 4.4-14. Speciation at $P(H_2) = 1 \text{ atm}$ (PHREEPLOT) of d-transition metals Mo (a), V (b), Ti (c), and Zr (d) in a solution containing all elements included in PRODATA at $10^{-4} \text{ mol kg}_w^{-1}$; the ionic strength is maintained at $0.1 \text{ mol kg}_w^{-1}$ by a solution containing a hypothetic indifferent Cation/Anion electrolyte; all possible phases are allowed to precipitate; species less than 2% are not plotted; the Davies PHREEQC extraction of the database is used excluding $\text{Ca}_2\text{ZrSi}_3\text{O}_{12}(\text{cr})$	210
Figure 4.4-15. Speciation at $P(H_2) = 1 \text{ atm}$ (PHREEPLOT) of alkaline earth metals Mg (a), Ca (b), Sr (c), Ba (d), and Ra (e) in a solution containing all elements included in PRODATA at $10^{-4} \text{ mol kg}_w^{-1}$; the ionic strength is maintained at $0.1 \text{ mol kg}_w^{-1}$ by a solution containing a hypothetic indifferent Cation/Anion electrolyte; all possible phases are allowed to precipitate; species less than 2% are not plotted; the Davies PHREEQC extraction of the database is used excluding $\text{Ca}_2\text{ZrSi}_3\text{O}_{12}(\text{cr})$	211
Figure 4.4-16. Speciation at $P(H_2) = 1 \text{ atm}$ (PHREEPLOT) of K in a solution containing all elements included in PRODATA at $10^{-4} \text{ mol kg}_w^{-1}$; the ionic strength is maintained at $0.1 \text{ mol kg}_w^{-1}$ by a solution containing a hypothetic indifferent Cation/Anion electrolyte; all possible phases are allowed to precipitate; species less than 2% are not plotted; the Davies PHREEQC extraction of the database is used excluding $\text{Ca}_2\text{ZrSi}_3\text{O}_{12}(\text{cr})$	212
Figure 4.5-1. Predominance plot (PHREEPLOT) of $1 \mu\text{mol kg}_w^{-1}$ Pb, in a $0.1 \text{ mol kg}_w^{-1}$ HClO_4 solution with increasing $a(\text{SO}_4^{2-})$ and pH, and fixed total carbonate defined in Reiller and Descostes [2020REI/DES]: $p\text{CO}_2 = 2.6$ (a), 2.4 (b), and 1.8 (c) ; the SIT PHREEQC extraction of the database is used.	213
Figure 4.5-2. Predominance plot (PHREEPLOT) of $1 \mu\text{mol kg}_w^{-1}$ Fe at $P(\text{O}_2) = 0.21 \text{ atm}$, in a $0.1 \text{ mol kg}_w^{-1}$ HClO_4 solution with increasing $a(\text{SO}_4^{2-})$ and pH, and fixed total carbonate defined in Reiller and Descostes [2020REI/DES]: $p\text{CO}_2 = 2.6$ (a), 2.4 (b), and 1.8 (c) ; the SIT PHREEQC extraction of the database is used.	214
Figure 4.5-3. Predominance plot (PHREEPLOT) of $10^{-6} \text{ mol kg}_w^{-1}$ U at $P(\text{O}_2) = 0.2095 \text{ atm}$ in a $0.1 \text{ mol kg}_w^{-1}$ HClO_4 solution with increasing $a(\text{SO}_4^{2-})$ and pH, and fixed total concentration of Ca, Mg, and total carbonate defined in Reiller and Descostes [2020REI/DES]: $p\text{Ca} = p\text{Mg} = 3.2$, $p\text{CO}_2 = 2.6$ (a); $p\text{Ca} = p\text{Mg} = 2.8$, $p\text{CO}_2 = 2.4$ (b); and $p\text{Ca} = 2.0$, $p\text{Mg} = 2.2$, $p\text{CO}_2 = 1.8$ (c); no phases were allowed to precipitate; the SIT PHREEQC extraction of the database is used.....	215
Figure 4.5-4. Activity predominance plot (PHREEPLOT) of $10^{-7} \text{ mol kg}_w^{-1}$ Ba, in a $0.1 \text{ mol kg}_w^{-1}$ HClO_4 solution with increasing $a(\text{SO}_4^{2-})$ and pH, and fixed total carbonate defined in Reiller and Descostes [2020REI/DES]: $p\text{CO}_2 = 2.6$ (a), 2.4 (b), and 2.6 (c); the Davies PHREEQC extraction of the database is used.	216
Figure 4.5-5. Predominance plot (PHREEPLOT) of $10^{-10} \text{ mol kg}_w^{-1}$ Ra, in a $0.1 \text{ mol kg}_w^{-1}$ HClO_4 solution with increasing $a(\text{SO}_4^{2-})$ and pH, and fixed total carbonate defined in Reiller and Descostes [2020REI/DES]: $p\text{CO}_2 = 2.6$ (a), 2.4 (b) and 1.8 (c); the Davies PHREEQC extraction of the database is used.	217
Figure 4.6-1. Activity predominance plots (PHREEPLOT) of $10^{-6} \text{ mol kg}_w^{-1}$ U at $P(\text{O}_2) = 0.21 \text{ atm}$ and $[\text{NaCl}] = 0.5 \text{ mol kg}_w^{-1}$; the SIT PHREEQC extraction of the database is used.	218

List of Figures

Figure 4.6-2. Activity predominance plots (PHREEPLOT) of 10^{-6} mol kg_w⁻¹ U at P(O₂) = 0.21 atm, log₁₀a(HCO₃⁻) + log₁₀a(H⁺) values of -12 (a), -10 (b), and -8 (c); the SIT PHREEQC extraction of the database is used..... 219

List of Tables

Table 3.1-1. Thermodynamic functions for the O ₂ -H ₂ -H ₂ O system from Wagman <i>et al.</i> [1982WAG/EVA], and calculated constants.....	17
Table 3.1-2. Specific ion interaction coefficients for H ⁺ and OH ⁻	17
Table 3.2-1. Thermodynamic functions and calculated constants for halogens.....	18
Table 3.2-2. Specific ion interaction coefficients for halogen ions	18
Table 3.3-1. Functions of reaction, redox reaction constants, and potentials for the reduction of SO ₄ ²⁻ to HS ⁻ using different sources of data.....	20
Table 3.3-2. Thermodynamic functions from Chivot [2004CHI], and constants calculated for the S species.	21
Table 3.3-3. Comparison of thermodynamic functions and constants for the formation of HSe ⁻ and Se ²⁻ from Se(cr) in Olin <i>et al.</i> [2005OLI/NOL], Wagman <i>et al.</i> [1982WAG/EVA], and Naumov <i>et al.</i> [1974NAU/RYZ].....	23
Table 3.3-4. Specific ion interaction coefficients for selenium ions	24
Table 3.4-1. Thermodynamic functions and constants for nitrogen species from Wagman <i>et al.</i> [1982WAG/EVA].....	24
Table 3.4-2. Specific ion interaction coefficients for nitrogen ions	24
Table 3.4-3. Thermodynamic constants and functions for the phosphate system with $\sigma(\Delta_f G^\circ_m)$ recalculated from the selected constants in NEA-OECD reviews [2003GUI/FAN; 2020GRE/GAO].	26
Table 3.4-4. Thermodynamic functions and constants of P(-III) calculated from Wagman <i>et al.</i> [1982WAG/EVA].....	27
Table 3.4-5. Specific ion interaction coefficients for phosphate ions.....	27
Table 3.4-6. Specific ion interaction coefficients for arsenic ions.....	27
Table 3.4-7. Thermodynamic functions and constants for As(-III).	27
Table 3.4-8. Thermodynamic functions of arsensosulphide from native elements in Robie and Hemingway [1995ROB/HEM], and calculated dissolution to oxoanions from NEA-OECD review [2005OLI/NOL].....	30
Table 3.5-1. Thermodynamic functions and constants for C(-IV) and C(IV) [1982WAG/EVA; 1992GRE/FUG; 2003GUI/FAN; 2020GRE/GAO].	32
Table 3.5-2. Specific ion interaction coefficients for carbonate ions	32
Table 3.6-1. Thermodynamic functions and solubility constants of silica allotropic forms.	33
Table 3.6-2. Thermodynamic functions and constants for free ion, oxo, and hydroxo compounds of Pb.....	37
Table 3.6-3. Thermodynamic functions and constants for halogen compounds of Pb.....	39
Table 3.6-4. Thermodynamic function and constants for S and Se compounds of Pb.	39
Table 3.6-5. Thermodynamic function and constants for N, P, and As compounds of Pb.	40
Table 3.6-6. Thermodynamic function and constants for C compounds of Pb.....	41
Table 3.6-7. Specific ion interaction coefficients for Pb complexes in PRODATA.....	42
Table 3.6-8. Thermodynamic functions and constants for native metal, free ion, and oxo and hydroxo compounds of Al.....	49
Table 3.6-9. Thermodynamic functions and constants for halogen compounds of Al.....	50
Table 3.6-10. Thermodynamic functions and constants for S compounds of Al.	50
Table 3.6-11. Thermodynamic functions and constants for P, As, and Si compounds of Al.....	51
Table 3.6-12. Specific ion interaction coefficients for Al species.	51
Table 3.7-1. Thermodynamic constants and functions for native metal, free ion, oxo, hydroxo-, and chloro-compounds of Zn.....	54
Table 3.7-2. Thermodynamic constants and functions of S and Se compounds of Zn.....	55
Table 3.7-3. Thermodynamic constants and functions of P and As compounds of zinc.	55

List of Tables

Table 3.7-4. Thermodynamic constants and functions of C and Si compounds of zinc.....	56
Table 3.7-5. Specific ion interaction coefficient for Zn(II) complexes.....	56
Table 3.7-6. Thermodynamic functions and constants for the CdS solids.....	58
Table 3.7-7. Thermodynamic constants and functions for the native element, free ion, and oxo and hydroxo compounds of Cd.....	60
Table 3.7-8. Thermodynamic constants and functions for the Cl, S, Se, P, and C compounds of Cd.....	61
Table 3.7-9. Specific ion interaction coefficients for the Cd complexes.....	61
Table 3.7-10. Gibbs energies of reaction for the solubility of mercury sulphide phases from different sources.....	64
Table 3.7-11. Acidity constants and variation of specific ion interaction coefficients for the phosphate system selected in Powell <i>et al.</i> [2005POW/BRO] and Guillaumont <i>et al.</i> [2003GUI/FAN].	66
Table 3.7-12. Thermodynamic constants and functions for native element, free ions, and oxo and hydroxo compounds of Hg.....	67
Table 3.7-13. Thermodynamic constants and functions for S and Se compounds of Hg.....	68
Table 3.7-14. Thermodynamic constants and functions for P and C compounds of Hg.....	68
Table 3.7-15. Specific ion interaction coefficients for Hg soluble species.....	69
Table 3.7-16. Thermodynamic constants and functions for free ions, oxo, and hydroxo Cu compounds.....	72
Table 3.7-17. Thermodynamic constants and functions for halogen compounds of Cu.....	73
Table 3.7-18. Thermodynamic constants and functions for S and Se compounds of Cu.....	73
Table 3.7-19. Thermodynamic constants and functions for N, P, and As compounds of Cu.....	75
Table 3.7-20. Thermodynamic constants and functions for C compounds of Cu.....	76
Table 3.7-21. Specific ion interaction coefficients for Cu species	76
Table 3.7-22. Thermodynamic functions and constants for proustite and xanthoconite (Ag_3AsS_3).....	79
Table 3.7-23. Thermodynamic constants and functions for native element, free ions, and oxo and hydroxo compounds of Ag.....	80
Table 3.7-24. Thermodynamic constants and functions for halogen compounds of Ag.....	80
Table 3.7-25. Thermodynamic constants and functions for S, Se, N, and C compounds of Ag.....	80
Table 3.7-26. Specific ion interaction coefficients for Ag aqueous species.....	81
Table 3.7-27. Thermodynamic functions and constants estimated for gersdorffite (NiAsS) in the SOLTHERM-XPT database [2015PAL; 2016REE/SPY].	83
Table 3.7-28. Thermodynamic functions and constants for hydroxide, Si, and AsS compounds of Ni	84
Table 3.7-29. Thermodynamic functions and constants estimated for the CoAsS phases in the SOLTHERM-XPT database [2015PAL; 2016REE/SPY].	90
Table 3.7-30. Thermodynamic constants and functions for native metals, free metals, oxo and hydroxo compounds of Co.....	91
Table 3.7-31. Thermodynamic constants and functions for halogen compounds of Co.....	92
Table 3.7-32. Thermodynamic constants and functions for the S and Se compounds of Co.....	92
Table 3.7-33. Thermodynamic constants and functions for the P and As compounds of Co.....	93
Table 3.7-34. Thermodynamic constants and functions for the C and Si compounds of Co.....	94
Table 3.7-35. Specific ion interaction coefficients for Co aqueous species and complexes.....	95
Table 3.7-36. Thermodynamic constants and functions for hydroxo compounds of Fe.	96
Table 3.7-37. Thermodynamic constants and functions for halogen compounds of Fe.	97
Table 3.7-38. Thermodynamic constants and functions for complementary P and As compounds of Fe.....	98
Table 3.7-39. Thermodynamic constants and functions for C and Si compounds of Fe.	100

Table 3.7-40. Thermodynamic functions and constants for native metal, free ions, and oxo and hydroxo compounds of Mn	104
Table 3.7-41. Thermodynamic functions and constants for halogen, S, and Se compounds of Mn	105
Table 3.7-42. Thermodynamic functions and constants for As, P, C and Si compounds of Mn.....	106
Table 3.7-43. Thermodynamic functions and constants of Mo compounds.....	108
Table 3.7-44. Comparison of the Gibbs energies of reaction, $\log_{10}\beta^\circ$ and E°_h calculated from Shock <i>et al.</i> [1997aSHO/SAS] — H ₂ O from Helgeson and Kirkham [1974aHEL/KIR] — and Brown and Ekberg [2016BRO/EKB] for vanadium free ions.....	110
Table 3.7-45. Thermodynamic constants and functions for native, free ions of vanadium, and dihydrogenovanadate ion.....	116
Table 3.7-46. Thermodynamic functions and constants for oxides of V.....	117
Table 3.7-47. Thermodynamic functions and constants for hydroxide complexes of V [2016BRO/EKB]......	117
Table 3.7-48. Thermodynamic functions and constants for Cl and S compounds of V.....	119
Table 3.7-49. Thermodynamic functions and constants of Ti.	120
Table 3.7-50. Thermodynamic functions and constants of native, free metal and oxo and hydroxo compounds of Zr from Brown <i>et al.</i> [2005BRO/CUR].....	121
Table 3.7-51. Thermodynamic functions and constants of halogeno compounds of Zr from Brown <i>et al.</i> [2005BRO/CUR].....	122
Table 3.7-52. Thermodynamic functions and constants of S compounds of Zr from Brown <i>et al.</i> [2005BRO/CUR].....	122
Table 3.8-1. Thermodynamic function of reaction for the hydroxouranyl(VI) complexes calculated from the thermodynamic function of formation estimated in Shock <i>et al.</i> [1997bSHO/SAS].....	124
Table 3.8-2. Reinterpretation of the solubility data of chernikovite and meta-ankoleite from Van Haverbeke <i>et al.</i> [1996HAV/VOC] using U(VI) and P(V) chemistry from NEA-OECD reviews	126
Table 3.8-3. Thermodynamic constants and functions of reaction for the uranyl(VI)phosphate phases, and functions of formation calculated relative to Guillaumont <i>et al.</i> [2003GUI/FAN].....	127
Table 3.8-4. Thermodynamic constants and functions of reaction for the As(V) phases of U(VI).	128
Table 3.8-5. Comparision of thermodynamic functions $\Delta_rH^\circ_m$ and $T\Delta_rS^\circ_m$ for the stepwise and cumulative formation of CaUO ₂ (CO ₃) ₃ ²⁻ and Ca ₂ UO ₂ (CO ₃) ₃ (aq).....	132
Table 3.8-6. Thermodynamic constants and functions for the alkaline earth(II)triscarbonatouranyl(VI) complexes.....	135
Table 3.8-7. Thermodynamic constants and thermodynamic functions of Si phases of U.	136
Table 3.8-8. Thermodynamic functions and constants for the solubility of U(VI) vanadate phases.	136
Table 3.8-9. Thermodynamic functions and constants for the solubility of U(VI) vanadate phases of the first transition elements series discussed but not selected in Grenthe <i>et al.</i> [2020GRE/GAO].....	137
Table 3.8-10. Thermodynamic functions and constants for the solubility of uranyl(VI) oxides of alkaline metals phases from Gorman-Lewis <i>et al.</i> [2008GOR/FEI].	139
Table 3.9-1. Thermodynamic functions of reactions and constants for the native metal oxidation for alkaline earths.	141
Table 3.9-2. Thermodynamic functions and constants for the oxo and hydroxo-alkaline earth compounds.....	142
Table 3.9-3. Thermodynamic functions and constants for the halogeno compounds of alkaline earth(II).	143
Table 3.9-4. Thermodynamic functions and constants for the S and Se compounds of alkaline earth(II).	144
Table 3.9-5. Thermodynamic functions and constants for the N compounds of alkaline earth(II) calculated from Wagman <i>et al.</i> [1982WAG/EVA].....	145
Table 3.9-6. Thermodynamic constants and Gibbs energies of reaction of P(V) compounds of Mg(II) and Ca(II), and Gibbs energies of formation using Guillaumont <i>et al.</i> [2003GUI/FAN].....	148
Table 3.9-7. Thermodynamic functions and constants for the C compounds of alkaline earth(II).	151

List of Tables

Table 3.9-8. Thermodynamic functions and constants for Si compounds of alkaline earth(II) metals.	152
Table 3.9-9. Specific ion interaction coefficients between alkaline earth metals (Mg^{2+} , Ca^{2+} , and Ba^{2+}) and anions (Cl^- , ClO_4^- , and NO_3^-) from NEA-OECD reviews and values for Sr^{2+} and Ra^{2+} obtained after regression 1/IR vs. $\epsilon(M^{2+}, X^-)$	154

1. Context

The general objectives and context of this database have been exposed in details in Reiller and Descostes [2020REI/DES]. The PRODATA database was developed to provide a tool that can export database files for three different software packages that allow calculating equilibrium distribution of species in different types of chemical and geochemical contexts.

Evaluation of environmental impact of anthropic activities, particularly of mining activities, must be considered before any industrial project development. One of the approaches currently developed relies on predictive reactive transport modelling. Such strategy requires, on the one hand, a thorough description of the physico-chemical reactions that govern the mobility of contaminants of concern and, on the other hand, their couplings in order to better constrain the studied system. These approaches allow testing several evolution scenarii on space and time scales beyond the ones probed by laboratory and field experiments [2015STE/APP]. This is particularly true for: (i) mining and nuclear industries [2001ZHU/HU; 2006CUR/DAV] including the management of legacy sites [2016DZO/LEE; 2019HUS/LEE]; (ii) uranium in the framework of long-term safety assessment of radioactive waste repositories [2003LEE/WIN; 2007MON/MÜG; 2018CLA/MAR; 2019MUR/WAG]; (iii) management of polluted soils and aquifers inherited from the use of depleted uranium from armor-piercing ammunition [2002CHEN/YIA; 2003MIT/ELE]; (iv) assessment of the ecotoxicological impact of uranium [2016PAR/AVA; 2018PAR/AVA; 2019HUS/LEE; 2020LAR/CHA]. One may also use such an approach for mining exploration, optimizing mining operations — especially in the case of In Situ Leaching or In Situ Recovery (ISR) mines [2007DAV/CUR; 2016JOH/TUT; 2019LAG/REG] —, and remediation [2007YAB/FAN].

Uranium is considered as a trace element that is showing a complex aqueous chemistry, especially in natural environments. Its mobility is generally governed by pH and redox, the presence of inorganic — *e.g.*, CO_3^{2-} , SO_4^{2-} , PO_4^{3-} , $\text{Si}(\text{OH})_4(\text{aq})$ — [1992GRE/FUG; 2003GUI/FAN; 2020GRE/GAO] and organic ligands [2005HUM/AND; 2008BON/COT], but also adsorption reactions at the mineral water interfaces [2003ZHE/TOK; 2008BAC/PLA; 2009MEL/AZE; 2010STE/MAY; 2011BRA/BAE; 2011JOS/SCH; 2015MAR/VER; 2015SMI/BRY; 2016AMA/FRO; 2018TRA/TEU; 2019TRA/TEU]. Hence, assessing and understanding the geochemical mechanisms controlling the mobility of uranium in the environment requires also the consideration of the other major elements chemical properties that are often observed at higher significant concentrations.

The environmental footprint of uranium mines is driven, on the one hand, by the mining extraction process, and, on the other hand, by the composition of the treated ore. The extraction processes generally involve highly concentrated and oxidizing solutions — in sulphuric acid or under alkaline conditions — in order to increase uranium solubility. In addition to ^{226}Ra — one of the main radioactive decay products of ^{238}U —, the ores are generally associated to other metals (*e.g.*, Pb, Cu, Ni, Fe, Mo...) and elements (*e.g.*, As, Se...). These elements are showing different geochemical behaviours than U, and may become in turn (secondary) contaminants.

The geochemical behaviour of ^{226}Ra is particular. Through its radioactive half-life (1 600 years) and its high specific activity (36.6 GBq g⁻¹), ^{226}Ra is always observed at elementary concentrations drastically lower than uranium. As an illustration, for a uranium ore older than 1 My, with an average U content of 1‰ (ca. 12 500 Bq kg⁻¹), the secular equilibrium will lead to a hypothetical ^{226}Ra concentration of 342 ppt. The migration of ^{226}Ra in the environment is mainly governed by adsorption reactions — see *e.g.* [2014SAJ/BRY; 2016REI/LY;

Context

2017ROB/TER; 2018BOR/BEA] —, coprecipitation through solid solution formation with other alkaline earth sulphate minerals [2010CUR/FUJ; 2019LES/BEA], and carbonate bearing minerals [2011JON/BUT].

The description of the physico-chemical reactions involved, directly or indirectly, in the fate of contaminants is usually gathered in a thermodynamic database. It includes redox and aqueous complexation formation equilibria, dissolution or formation of solid or gaseous phases; sometimes, coprecipitation or adsorption reactions are also included. To perform the calculation on these intricate systems, several modelling codes are available, from aqueous speciation calculation to reactive transport, even if this approach has inherent limitations [1996NOR], particularly concerning uncertainties [1999EMR/ART; 2011EKB/ODE; 2011MAY/FIL]

Currently, ORANO Mining, the historic French uranium mining company (former AREVA Mines and Cogema, <https://www.orano.group/en/expertise/from-exploration-to-recycling/leading-uranium-producer>), has to answer to different national regulators and nuclear safety agencies for the exploration, exploitation, and remediation of its sites. This includes the building of Safety Cases, applying Safety Assessment processes, which require evaluation of the chemistry of uranium, radium, and other eventual secondary pollutants, in different contexts, including speciation and transport. Different software packages are usually needed to attain these objectives, which provided databases are generally not built around the same core of data. To provide robust cases, there is a need to have a common database for the different software packages used to perform the calculations. ORANO Mining is using widely available speciation codes, i.e. PHREEQC* [1999PAR/APP; 2013PAR/APP], CHESS,[†] and the Geochemists' WorkBench (GWB),[‡] with which thermodynamic database files are provided. However, a thermodynamic database that can be used with several codes, and can be exploited in monitoring of mining activities, is seldom found. Besides, thermodynamic databases provided with the different modelling codes do not systematically share either the same thermodynamic data, the same traceability, or the same completeness [2019HUM/FIL]. Direct comparison between modelling codes' results, but also between studied cases, may therefore be limited.

Uranium is the central element of the nuclear fuel cycle. Its thermodynamic properties have been the subject of a large body of work. The data selections that are subject of the largest consensus have been commissioned by the Thermochemical DataBase (TDB) project from the Nuclear Energy Agency (NEA) within the Organization for the Economic Co-operation and Development (OECD) [1988WAN; 2003MON/WAN; 2015RAG/BRA].[§] The selection is including inorganic [1992GRE/FUG; 2003GUI/FAN] and selected organic complexes [2005HUM/AND] — a PHREEQC database file has been made available recently [2019MAR/SAN]. The selection criteria being rather strict, it is inevitable that some data are rejected, and the selected data cannot be used as is to perform calculations in relevant media for mining activities and environmental monitoring. A recent study suggests that database files that are sit on the NEA-OECD database selection can be more likely recommended to estimate uranium speciation [2019WAN/SHI], but effectively needed some implementations from other sources, even if traceability issues may appear [2019HUM/FIL].

Despite of the great interest in the monitoring of mining activities, radium has not been the subject of the same attention. Nevertheless, some data are available, and have sometimes been included in databases. To perform relevant speciation calculation in actual situations, the database used should be containing the relevant chemical

* <https://www.usgs.gov/software/phreeqc-version-3>

[†] http://chess.geosciences.mines-paristech.fr/?set_language=en

[‡] <http://www.gwb.com>

[§] https://www.oecd-nea.org/jcms/pl_22166/thermochemical-database-tdb-project

equilibria and species predominant in the system to describe the geochemistry of the site, and should also be as consistent as possible. In addition to uranium, the TDB project from NEA-OECD has commissioned reviews on elements relevant for the management of radioactive wastes that can be directly implemented in a database — *e.g.* [2005BRO/CUR; 2005GAM/BUG; 2005OLI/NOL; 2009RAN/FUG; 2013LEM/BER]. From the strict definition of the selection criteria of the NEA-OECD selection, it can be understood that complementary data must be implemented either on already reviewed elements, or on elements that are necessary for natural or mining systems, such as *e.g.*, Ca, Mg, Si, Al, or Fe.

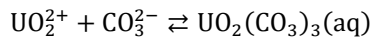
Some thermodynamic database files provided with software packages are containing a large body of data on several complexes and phases. But the data within these database files are not always easy to trace, as they are necessarily in the NEA-OECD reviews. There is a pressing demand from nuclear safety authorities to provide evidence that the data used to evaluate a speciation calculation are traceable and retrievable, which if achieved provides a further confidence in the evaluation of a safety case.

From these constraints and legal obligations, there is a need for the building of a thermodynamic database dedicated to uranium mining activities from exploration to remediation: the PRODATA database. This database was thought as a tool in which thermodynamic data (constants and functions) relevant for mining activities and environmental monitoring can be compiled, and database files for the different speciation codes can be exported on demand.

2. General Considerations

2.1. Definition of Species

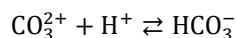
From the start of the project, it was decided that the tool used to handle the database should allow to export the reaction constants and that the reactions could be written in different ways, but in consistent manner. As an example, the carbonation reaction uranium could be written as well as relative to CO_3^{2-} ion,



and as relative to HCO_3^- ion.



These two ways of writing the same equilibrium are giving different values of $\log_{10} K^\circ$ that are differing from the protonation equilibrium of CO_3^{2-} to HCO_3^- .



The simplest way to handle the situation is to develop a database of thermodynamic functions of formation — *i.e.*, Gibbs energy ($\Delta_f G_m^\circ$), enthalpy ($\Delta_f H_m^\circ$), and entropy ($S_{f,m}^\circ$) — that would allow calculating the thermodynamic functions of reaction — *i.e.*, Gibbs energy ($\Delta_r G_m^\circ$), enthalpy ($\Delta_r H_m^\circ$), and entropy ($\Delta_r S_m^\circ$) — that would be used to calculate the thermodynamic constants of reaction.

In the preceding example, the Gibbs energy of reaction of the first reaction could be written as follows.

$$\Delta_r G_m^\circ = \Delta_f G_m^\circ(\text{UO}_2(\text{CO}_3)_3(\text{aq})) - \Delta_f G_m^\circ(\text{UO}_2^{2+}) - \Delta_f G_m^\circ(\text{CO}_3^{2-})$$

The second expression of the same formation is written as follows.

$$\Delta_r G_m^\circ' = \Delta_f G_m^\circ(\text{UO}_2(\text{CO}_3)_3(\text{aq})) + \Delta_f G_m^\circ(\text{H}^+) - \Delta_f G_m^\circ(\text{UO}_2^{2+}) - \Delta_f G_m^\circ(\text{HCO}_3^-)$$

Under standard conditions, the thermodynamic constants of reaction are then calculated.

$$\log_{10} K^\circ = -\frac{\Delta_r G_m^\circ}{RT \ln 10}$$

Using tabulated and recommended values of thermodynamic functions of formation of the preceding reactions, allows calculating the $\log_{10} K^\circ$ values as follows.

$$\Delta_r G_m^\circ = \Delta_f G_m^\circ(\text{UO}_2(\text{CO}_3)_3(\text{aq})) - \Delta_f G_m^\circ(\text{UO}_2^{2+}) - \Delta_f G_m^\circ(\text{CO}_3^{2-}) = -1537.188 - (-952.551) - (-527.900)$$

$$\Delta_r G_m^\circ = -56.737 \text{ kJ mol}^{-1}$$

$$\log_{10} K^\circ = 9.94$$

$$\Delta_r G_m^\circ' = \Delta_f G_m^\circ(\text{UO}_2(\text{CO}_3)_3(\text{aq})) + \Delta_f G_m^\circ(\text{H}^+) - \Delta_f G_m^\circ(\text{UO}_2^{2+}) - \Delta_f G_m^\circ(\text{HCO}_3^-)$$

$$\Delta_r G_m^\circ' = 2.209 \text{ kJ mol}^{-1}$$

$$\log_{10} K^\circ' = -0.39$$

These constants are given in different ways using the different software packages:

- PHREEQC is requiring the equilibrium definition and the definition of the thermodynamic constant under standard conditions (25 °C, 1 bar) of this equilibrium constant, eventually the $\Delta_r H_m^\circ$ of the

equilibrium to calculate $\log_{10} K(T)$ using the Van't Hoff relationship. An analytical expression of the $\log_{10} K^\circ = f(T)$ is possible.

- CHESS and GWB are requiring individual $\log_{10} K(T)$ at fixed temperature values. It is the responsibility of the database developer to calculate the $\log_{10} K(T)$ values with the desired relationship.

Having the functions of formation being developed, it is then necessary to develop databases of reactions.

- A database of formation of complexes in solution;
- A database for the dissolution of phases;
- A database for the dissolution of gases.

Using the stoichiometric coefficients for the different reactions, the functions of formation of the different species can then be used to calculate the functions of reactions, and finally the $\log_{10} K^\circ$, $\Delta_r H_m^\circ$ or $\log_{10} K(T)$ needed for each software package extraction. The different ways to write the reactions can then be implemented in order to be able to change the type of species, and calculate the constants and functions of reaction in a consistently.

2.2. Variation With Temperature

The general dependence of the thermodynamic constants are described in details in Puigdomènech *et al.* [1997PUI/PLY]. When the $\Delta_f H_m^\circ(T^\circ)$ values of the different species are known, the general dependence can be written as follows,

$$\begin{aligned} \log_{10} K^\circ(T) = & \log_{10} K^\circ(T^\circ) - \frac{\Delta_r H_m^\circ(T^\circ)}{R \ln(10)} \left(\frac{1}{T} - \frac{1}{T^\circ} \right) \\ & - \frac{1}{RT \ln(10)} \int_{T^\circ}^T \Delta_r C_{p,m}^\circ \cdot dT + \frac{1}{R \ln(10)} \int_{T^\circ}^T \frac{\Delta_r C_{p,m}^\circ}{T} \cdot dT \end{aligned} \quad (1)$$

or equivalently as follows.

$$\Delta_r G_m^\circ = \sum_i v \left(\Delta_f G_m^\circ(i, T^\circ) - (T - T^\circ) S_m^\circ(i, T^\circ) + \int_{T^\circ}^T C_{p,m}^\circ(i, T) dT - T \int_{T^\circ}^T \frac{C_{p,m}^\circ}{T} dT \right) \quad (2)$$

The variation of the $C_{p,m}^\circ$ values for any species in solution can be expressed as follows.

$$C_{p,m}^\circ(T) = a + bT + cT^2 + \frac{d}{T} + \frac{e}{T^2} + f \ln(T) + gT \ln(T) + h\sqrt{T} + \frac{i}{\sqrt{T}} + jT^3 + \frac{k}{T^3} \quad (3)$$

The variation of the acetate complexes of alkaline earth metals defined in Shock and Koretsky [1993SHO/KOR] could be drawn under two hypotheses:

- $\Delta_r C_{p,m}^\circ$ is assumed to be nill;
- $\Delta_r C_{p,m}^\circ$ is known, and the temperature interval is small enough for $\Delta_r C_{p,m}^\circ$ to be considered constant.

In the first hypothesis equation (1) is altered to the following,

$$\log_{10}K^\circ(T) = \log_{10}K^\circ(T^\circ) - \frac{\Delta_r H_m^\circ(T^\circ)}{R \ln(10)} \left(\frac{1}{T} - \frac{1}{T^\circ} \right) \quad (4)$$

which is represented as the plain line in Figure 2.2-1.

In the second hypothesis, $C_{p,m}^\circ(T) = a$, and equation (1) is altered to the following,

$$\log_{10}K^\circ(T) = \log_{10}K^\circ(T^\circ) - \frac{\Delta_r H_m^\circ(T^\circ)}{R \ln(10)} \left(\frac{1}{T} - \frac{1}{T^\circ} \right) - \frac{\Delta_r C_{p,m}^\circ}{RT \ln(10)} (T - T^\circ) + \Delta_r C_{p,m}^\circ \ln\left(\frac{T}{T^\circ}\right) \quad (5)$$

which is represented as the dashed line in Figure 2.2-1.

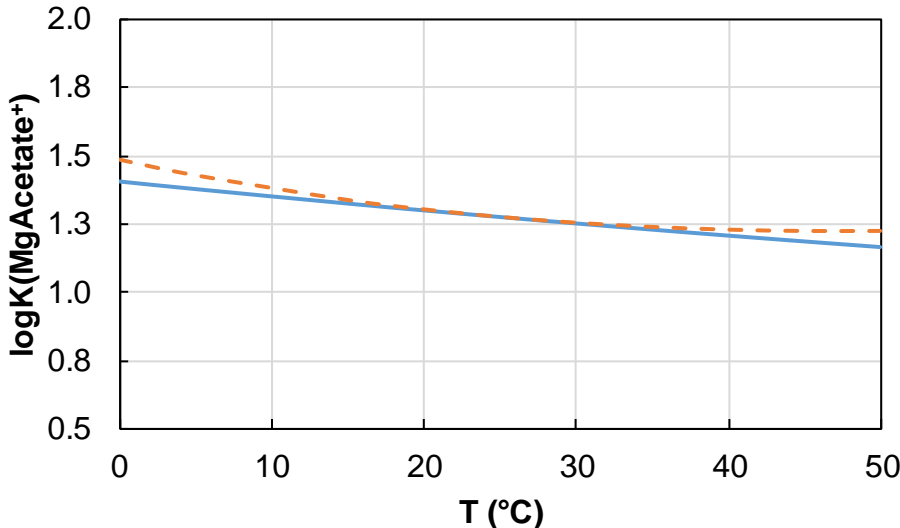


Figure 2.2-1. Variations of $\log_{10}K^\circ(T)$ for the formation of MgAcetate⁺ complex using thermodynamic functions in Shock and Koretsky [1993SHO/KOR]: blue line Equation (4), and orange dashed line Equation (5).

Chess and GWB both require the explicit calculation of $\log_{10}K^\circ(T)$, which can be automated easily. Conversely, PHREEQC offers the possibility to define the $\Delta_r H_m^\circ(T^\circ)$ via the `-delta_h` keyword, and/or to define an analytical expression of $\log_{10}K^\circ(T)$ via the `-analytic` or `-a_e` keyword,

$$\log_{10}K^\circ(T) = A_1 + A_2 T + \frac{A_3}{T} + A_4 \log_{10}(T) + \frac{A_5}{T^2} + A_6 T^2 \quad (6)$$

where T is in Kelvin.

Considering that $C_{p,m}^\circ$ is not known, Eq. 4 is then rewritten as follows,

$$\log_{10}K^\circ(T) = \log_{10}K^\circ(T^\circ) + \frac{\Delta_r H_m^\circ(T^\circ)}{R \ln(10)} \left(\frac{1}{T^\circ} \right) - \frac{\Delta_r H_m^\circ(T^\circ)}{R \ln(10)} \left(\frac{1}{T} \right) \quad (7)$$

where $A_2 = A_4 = A_5 = A_6 = 0$, and

$$A_1 = \log_{10}K^\circ(T^\circ) + \frac{\Delta_r H_m^\circ(T^\circ)}{R \ln(10)} \left(\frac{1}{T^\circ} \right)$$

$$A_3 = -\frac{\Delta_r H_m^\circ(T^\circ)}{R \ln(10)}$$

Defining the A_i values is then useless as PHREEQC is using the Van't Hoff equation to calculate $\log_{10}K^\circ(T)$.

Considering that $\Delta_r C_{p,m}^\circ$ is constant in the temperature interval then

$$\log_{10} K^\circ(T) = \log_{10} K^\circ(T^\circ) + \frac{\Delta_r H_m^\circ(T^\circ)}{R \ln(10)} \frac{1}{T^\circ} + \frac{\Delta_r C_{p,m}^\circ}{RT \ln(10)} T^\circ - \Delta_r C_{p,m}^\circ \ln T^\circ - \frac{\Delta_r C_{p,m}^\circ}{RT \ln(10)} T - \frac{\Delta_r H_m^\circ(T^\circ)}{R \ln(10)} \frac{1}{T} + \Delta_r C_{p,m}^\circ \ln T \quad (8)$$

where $A_5 = A_6 = 0$, and

$$A_1 = \log_{10} K^\circ(T^\circ) + \frac{\Delta_r H_m^\circ(T^\circ)}{R \ln(10)} \frac{1}{T^\circ} + \frac{\Delta_r C_{p,m}^\circ}{RT \ln(10)} T^\circ - \Delta_r C_{p,m}^\circ \ln T^\circ$$

$$A_2 = -\frac{\Delta_r C_{p,m}^\circ}{RT \ln(10)}$$

$$A_3 = -\frac{\Delta_r H_m^\circ(T^\circ)}{R \ln(10)}$$

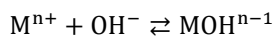
$$A_4 = \ln(10) \cdot \Delta_r C_{p,m}^\circ$$

A large number of species do not show a recommended value at least for $C_{p,m}^\circ$ in the NEA-OECD commissioned compilation of thermochemical data, when the majority does show a value of $\Delta_f H_m^\circ$ or $\Delta_r H_m^\circ$. Hence, the different coefficients in equation (6) cannot be calculated in a coherent way for every reactions for PHREEQC, and it could be for neither CHESS nor GWB. Nevertheless, the difference in calculated $\log_{10} K^\circ(T)$ could be significant as shown in Figure 2.2-1.

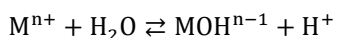
In view of the limited temperature range to which the database will be applied, and of the limited number of instances where the $C_{p,m}^\circ$ values are available for aqueous species, it was chosen to use only the Van't Hoff equation to calculate the $\log_{10} K^\circ(T)$ values in a first approximation. Hence, the use of PRODATA will not be recommended to estimate the aqueous speciation and transformation of phases at temperature higher than 80°C.

2.3. Choice of the Master Species

As already stressed in Reiller and Descostes [2020REI/DES], each software package has its own requirements concerning the formatting of its database file. The definitions of species in PHREEQC relies on the definition of a master species in solution (`SOLUTION_MASTER_SPECIES`), which can undergo reactions, which species are formed in solution (`SOLUTION_SPECIES`) from eventual redox species to complexes. The species in solution can be in equilibrium with solid phases or gases (`PHASES`). From the definition of the redox species, all reactions can be defined either from the `SOLUTION_MASTER_SPECIES`, or from another `SOLUTION_SPECIES`. As an example, the formation of a hydroxo complex of a metal ion M^{n+} can either be defined as the complexation with OH^- ,



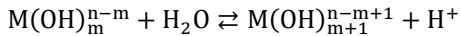
from the hydrolysis of a water molecule.



The successive hydrolysis can be defined as successive reactions,



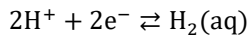
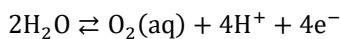
or as stepwise reactions.



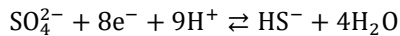
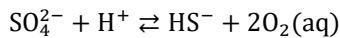
CHESS and GWB do not support the definition of stepwise reactions. They both require that an equilibrium be defined relative to the equivalent of either the `SOLUTION_MASTER_SPECIES` — *i.e.*, basis-species for CHESS and basis species for GWB — or the redox `SOLUTION_SPECIES` defined species — *i.e.*, redox-couples for CHESS and redox couples for GWB. Choices of master species must be made for the definition of the reaction database in order to ease the process of exporting the database files.

2.4. Expressions of Redox Equilibria

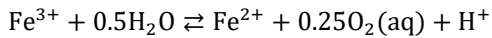
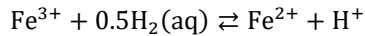
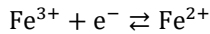
The first choice that is to be done is the expression of redox couples. PHREEQC is imposing the definition of the oxidation of H_2O and reduction of H^+ .



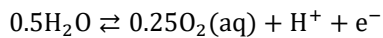
The other redox couples can be defined relative to either e^- , or $\text{O}_2(\text{aq})$,



or even $\text{H}_2(\text{aq})$.



In CHESS and GWB it is required that the definition of the redox-couples be given relative to $\text{O}_2(\text{aq})$. In GWB the `free electron` keyword is linking the oxidation of water.



Hence, the database of reaction is fixed to the more stringent definition relative to $\text{O}_2(\text{aq})$ for the sake of easing the export of the database files.

It can be noted that PHREEQC does not require the definition of the redox potential of a solution, but rather the `pe` value calculated as follows.

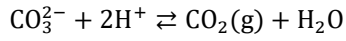
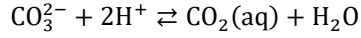
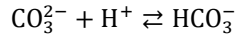
$$\text{pe} = \frac{FE}{RT \ln 10} \quad (9)$$

From a general point of view, the relationship between the Nernst potential E_h° of a redox reaction and its equilibrium constant, or Gibbs energy of reaction, can be usefully recalled.

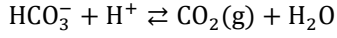
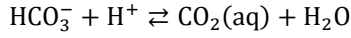
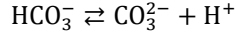
$$E_h^\circ = \frac{RT \cdot \ln 10 \cdot \log_{10} K^\circ}{nF} = -\frac{\Delta_r G^\circ}{nF} \quad (10)$$

2.5. Swap Between Master and Redox Species

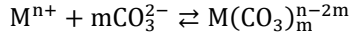
In some instances, it can be useful to export particular databases using different master or redox species. The simplest example is the swap between ions of the carbonate system, which can be defined either relative to CO_3^{2-} ,



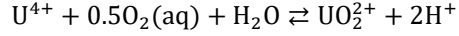
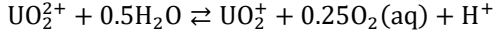
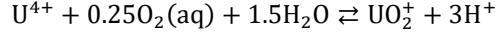
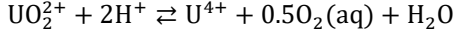
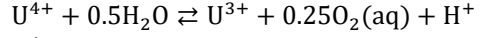
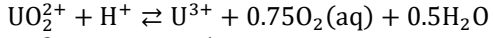
or relative to HCO_3^- .



This choice implies the definition of different equilibria for the carbonation of metal ions for CHESS and GWB as explained in § 2.1.



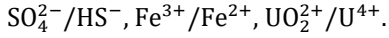
The same is true for the swap between redox species, *e.g.*, in the case of uranium.



This implementation is defined as multiple choices for ligands



and also for some redox couples.



2.6. Correction of Ionic Strength Effect

2.6.1. Debye-Hückel

In completely dissociated and diluted electrolyte solution, the Debye-Hückel [1923DEB/HÜC] theory describes the deviation from ideality from a coulombic point of view. The activity coefficient of an ion is written as follows.

$$\log_{10} \gamma_i = - \frac{A z_i^2 \sqrt{I_m}}{1 + B a_i^\circ \sqrt{I_m}} \quad (11)$$

where A and B are calculated at each temperature [1974bHEL/KIR].

$$A = \frac{\log e \sqrt{2} e F^2}{8\pi(\varepsilon_0 \varepsilon R T)^{3/2}} \quad (12)$$

$$B = \frac{\sqrt{2} F}{(\varepsilon_0 \varepsilon R T)^{1/2}} \quad (13)$$

In more concentrated solution, the WATEQ Debye-Hückel equation, or so-called b-dot equation is written as follows.

$$\log_{10} \gamma_i = - \frac{A z_i^2 \sqrt{I_m}}{1 + B a_i^\circ \sqrt{I_m}} + b I_m \quad (14)$$

The radius of closest approach for the hydrated ion I , a_i° , and b parameter are taken from Kielland [1937KIE].

CHESS and GWB are using Equation 11 or 14, with a_i° and b values given in the database file. PHREEQC can use Equation 14.

In these definitions, the a_i° and b couples of parameter depend on the ion couples. They are thus difficult to use in the case of mixtures of electrolytes or mixtures of ions.

2.6.2. Equations from Cecil W. Davies

Davies [1938DAV] proposed an empirical equation for the mean activity coefficient derived from the Debye-Hückel [1923DEB/HÜC] theory, which is valid up to 0.1 M.

$$\log_{10} \gamma_\pm = -A |z^+ z^-| \left(\frac{\sqrt{I_m}}{1 + \sqrt{I_m}} + 0.2 I_m \right) \quad (15)$$

Twenty four years later Davies [1962DAV] extended the validity of the expression to 0.3 M.

$$\log_{10} \gamma_\pm = -A |z^+ z^-| \left(\frac{\sqrt{I_m}}{1 + \sqrt{I_m}} + 0.3 I_m \right) \quad (16)$$

This latter expression is used by default in PHREEQC for ionic species. The extended Debye-Hückel expression (Equation 14) is also possible. For uncharged species the extended Debye-Hückel expression is reduced to the Setschenow equation [1889SET],

$$\log_{10} \gamma_i = b I_m \quad (17)$$

where b_i is assumed to be 0.1 for all uncharged species.

2.6.3. Specific ion Interaction Theory (SIT)

In some instances of the monitoring of mining operation, the total concentration of ions can be important, e.g. for ISR processes.

2.6.3.1. General Description

From Equation 14, it can be seen that several couples of values can satisfy a possible fit for $\log_{10} \gamma_i$ vs. I_m . Fixing the value of $B a_i^\circ$ to a unique value for all salts allows the variation for each salt to be represented by the b parameter. This was proposed using the Specific ion Interaction Theory (SIT) by adopting $B a_i^\circ = 1.5 \text{ kg}_w^{0.5} \text{ mol}^{-0.5}$ — see NEA-OECD reviews for details [1992GRE/FUG; 2003GUI/FAN; 2020GRE/GAO].

The account of the ionic strength effect is written as follows.

$$\begin{aligned} \log_{10} \gamma_j &= -z_j^2 \frac{A \sqrt{I_m}}{1 + 1.5 \sqrt{I_m}} + \sum_k \varepsilon(j, k, I_m) m_k \\ \text{mM}^{n+} + p\text{L}^{q-} + h\text{H}_2\text{O} &\rightleftharpoons \text{M}_m \text{L}_p (\text{OH})_h^{mn-pq} + h\text{H}^+ \\ \log_{10} {}^*\beta &= \log_{10} {}^*\beta^\circ + \Delta z^2 \frac{A \sqrt{I_m}}{1 + 1.5 \sqrt{I_m}} - \Delta \varepsilon I_m + n \log_{10} a_{\text{H}_2\text{O}} \\ \Delta \varepsilon &= \varepsilon(\text{M}_n \text{L}_q (\text{OH})_n, \text{N or X}) - q \varepsilon(\text{N}, \text{L}) - m \varepsilon(\text{M}, \text{X}) \end{aligned} \quad (18)$$

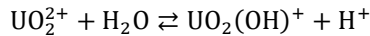
The water activity in an NX electrolyte is calculated from the osmotic coefficient Φ ,

$$\log_{10} a_{H_2O} = \frac{-\Phi \sum_n m_k}{\ln(10) \cdot 55.51} \quad (19)$$

$$1 - \Phi = \frac{A \ln(10) |z_+ z_-|}{I_m (B a_i^\circ)^3} \left[1 + B a_i^\circ \sqrt{I_m} - 2 \ln(1 + B a_i^\circ \sqrt{I_m}) - \frac{1}{1 - B a_i^\circ \sqrt{I_m}} \right] \\ - \ln(10) \varepsilon(N^+, X^-) m_{NX} \left(\frac{\nu_+ \cdot \nu_-}{\nu_+ + \nu_-} \right) \quad (20)$$

It is to be reminded that in the above equation $B a_i^\circ = 1.5$ for SIT.

As an example, the first hydrolysis of uranium(VI) in an NaCl media can be written as follows.



The dependence of $\log_{10} \beta$ with ionic strength at 25°C and 1 bar is written as follows.

$$\log_{10} * \beta = \log_{10} * \beta^\circ - 2 \frac{0.509 \sqrt{I_m}}{1 + 1.5 \sqrt{I_m}} - \Delta \varepsilon I_m + \log_{10} a_{H_2O}$$

The $\Delta \varepsilon$ value is then written as follows

$$\Delta \varepsilon = \varepsilon(UO_2(OH)^+, Cl^-) + \varepsilon(H^+, Cl^-) - \varepsilon(UO_2^{2+}, Cl^-)$$

2.6.3.2. Particular Cases

Some cases where the linear representation does not satisfactorily fits the ionic strength comportment, and a variation of ε can be used. Ciavatta [1980CIA] proposed the relationship,

$$\varepsilon = \varepsilon_1 + \varepsilon_2 \log_{10} I_m \quad (21)$$

where the term $\Delta \varepsilon I_m$ is approaching 0 when $I_m \rightarrow 0$.

Other relationships have been proposed, such as the one from Spahiu [2002SPA].

$$\varepsilon(j, k, I_m) = \varepsilon_j I^{-\varepsilon_k} \quad (22)$$

Bretti et al. [2004BRE/FOT; 2006BRE/FOT] who added a term, which takes into account the formation of weak ion pairs,

$$\varepsilon(j, k, I_m) = \varepsilon_\infty + \frac{\varepsilon_0 - \varepsilon_\infty}{I_m + 1} \quad (23)$$

where ε_0 and ε_∞ are parameters at $I_m \rightarrow 0$ and $I_m \rightarrow \infty$, respectively.

Crea et al. [2004CRE/ROB] proposed the following relationship,

$$\log_{10} K = \log_{10} K^\circ + \Delta z^2 \frac{A \sqrt{I_m}}{1 + 1.5 \sqrt{I_m}} + \varepsilon_1 I_m + \varepsilon_2 I_m^{3/2} + \varepsilon_3 I_m^2 \quad (24)$$

from which [2017BRE/CIG] proposed a restricted version

$$\log_{10} K = \log_{10} K^\circ + \Delta z^2 \frac{A \sqrt{I_m}}{1 + 1.5 \sqrt{I_m}} + \varepsilon_1 I_m + \varepsilon_2 I_m^{3/2} \quad (25)$$

These case will not be represented in PRODATA.

2.6.3.3. Estimation of Missing Specific Ion Interaction Coefficients

A large number of values for the specific ion interaction are available in literature. Nevertheless, a consistent number of values are not available, yet. This is leading to two situations:

1. The value of ε is not known and not defined, which means that during an SIT calculation $\varepsilon = 0$;
2. The value of ε can be approximated by analogy, the most common being the like-charged analogy frequently used in the NEA-OECD reviews;
3. The value of ε can be evaluated from the evolution *vs.* a physical property, such as the ionic radius, or charge over ionic radius ratio.

2.6.3.3.1 Charge over radius (z_i/r) evolutions for free ions

The variations of $\varepsilon(M^{2+}, X^-)$ *vs.* $1/r$ for Cl^- , ClO_4^- , and NO_3^- (ref) are shown in Figure 2.6-1. There are tendencies that could eventually be proposed. However, it can also be seen that reliable correlations would be difficult to establish. Particularly the case of Be^{2+} in ClO_4^- is clearly out of the general trend.

Linear correlation could be proposed as $1/r = f(\varepsilon)$ (dashed grey lines), but are more relevant when calculated as $\varepsilon = f(1/r)$ (plain lines, but plotted in the same graph), which allow calculating the 95% uncertainties hyperboles (dotted lines). These tentative correlations are leading to high uncertainties on the estimated $\varepsilon(M^{2+}, X^-)$ values, particularly in the case of Cl^- .

As an example, no value has been proposed up to now for $\varepsilon(Pb^{2+}, Cl^-)$, when $\varepsilon(Pb^{2+}, ClO_4^-)$ and $\varepsilon(Pb^{2+}, NO_3^-)$ are available in Grenthe *et al.* [1992GRE/FUG]. Using the regression in Figure 2.6-1a ($r = 1.2 \text{ \AA}$, $1/r = 0.83 \text{ \AA}^{-1}$) gives $\varepsilon(Pb^{2+}, Cl^-) = -0.18 \pm 0.33$. The impact on the $\log_{10} \gamma_{Pb^{2+}}$ is shown in Figure 2.6-2 (dotted line). It can also be noted that in ClO_4^- and NO_3^- , $\varepsilon(M^{2+}, X^-)$ are mostly the same for Pb^{2+} and Ba^{2+} , and that their $1/r$ values are close. Then using the analogy $\varepsilon(Pb^{2+}, Cl^-) \approx \varepsilon(Ba^{2+}, Cl^-) = 0.07 \text{ kg}_w \text{ mol}^{-1}$ the evolution of $\log_{10} \gamma_{Pb^{2+}}$ is shown in dotted line. Finally, the equivalence $\varepsilon(M^{2+}, Cl^-) = \varepsilon(M^{2+}, ClO_4^-)$ is often used to avoid a nil value. The obtained $\log_{10} \gamma_{Pb^{2+}}$ variation with I_m is reported in Figure 2.6-2 (dash-dotted line). The global impact on the speciation of the cation will follow the variation of the $\log_{10} \gamma_{Pb^{2+}}$

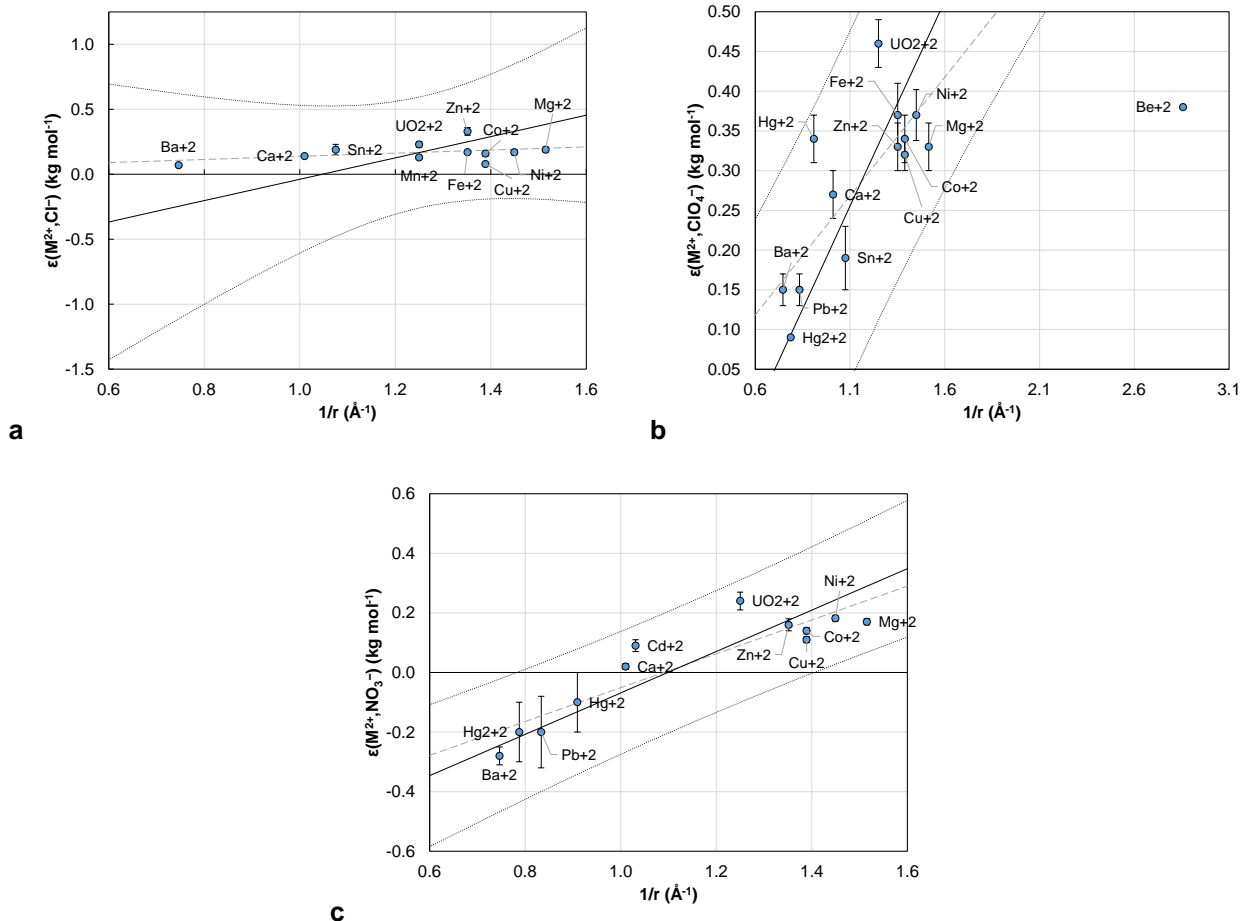


Figure 2.6-1. Evolutions of the specific ion interaction coefficients for the divalent free ions in (a) Cl^- , (b) ClO_4^- , and (c) NO_3^- .

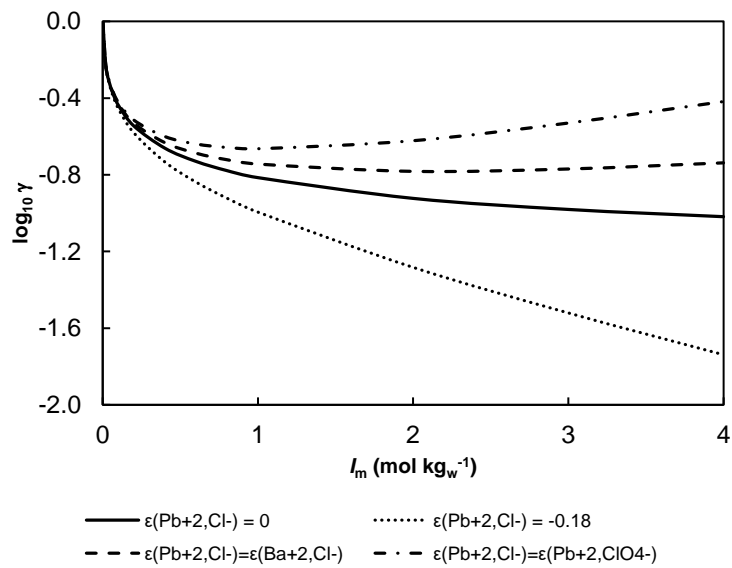


Figure 2.6-2. Evolutions of the activity coefficient of Pb^{2+} in Cl^- media using various values for $\epsilon(\text{Pb}^{2+}, \text{Cl}^-)$: (a) not implementing a value — i.e. $\epsilon = 0$ (plain line); (b) using $\epsilon(\text{Pb}^{2+}, \text{ClO}_4^-) = -0.18 \text{ kg}_w \text{ mol}^{-1}$ (dotted line) from the regression $1/r = f(\epsilon)$ in Figure 2.6-1a; (c) using the close value of $1/r$ between Pb^{2+} and Ba^{2+} (dashed line); and (d) using the $\epsilon(\text{Pb}^{2+}, \text{ClO}_4^-) = 0.15 \text{ kg}_w \text{ mol}^{-1}$ value for $\epsilon(\text{Pb}^{2+}, \text{Cl}^-)$

2.6.3.3.2 Frequency distribution of ε values

It is difficult to estimate *a priori* an $\varepsilon(X, Y)$ value to extrapolate the formation constant to infinite dilution. Values for +2 cations are ranging from $\varepsilon((UO_2)_3(OH)_4^{2+}, Na^+) = 0.89 \pm 0.23 \text{ kg}_w \text{ mol}^{-1}$ [2003GUI/FAN] to $\varepsilon(Sn_3(OH)_4^{2+}, Na^+) = -0.02 \pm 0.16 \text{ kg}_w \text{ mol}^{-1}$ [2012GAM/GAJ], the majority of them being *ca.* $0.4 \text{ kg}_w \text{ mol}^{-1}$ — see Figure 2.6-3. When no other argument can be done this value can eventually be used.

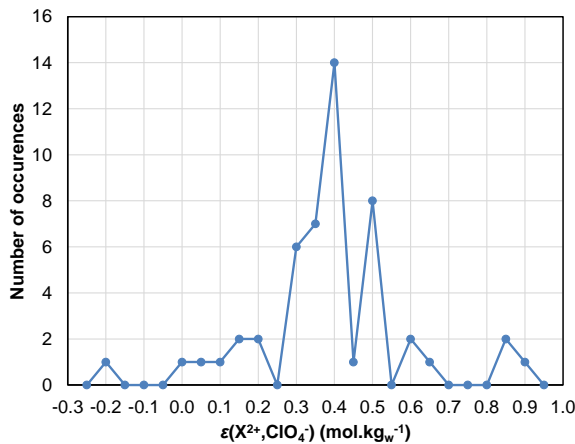


Figure 2.6-3. Frequency distribution of $\varepsilon(X^{2+}, ClO_4^-)$ [1980CIA; 1983SPA; 1995SIL/BID; 2001LEM/FUG; 2003GUI/FAN; 2005BRO/CUR; 2005GAM/BUG; 2009RAN/FUG; 2012GAM/GAJ; 2013LEM/BER; 2016BRO/EKB; 2018JOR/DEM; 2020LEM/PAL].

2.6.3.3.3 Estimation for complexes

In some instances, the specific ion interaction coefficients are not determined due to insufficiently available data vs. ionic strength. The aforementioned hypotheses can be also used here. Nevertheless, it has been shown that such hypotheses may not be justified [2020aSHA/REI].

Ciavatta [1990CIA] proposed different empirical expressions for estimating missing specific ion interaction coefficients of complexes. For an ML complex in an XY background electrolyte, he proposes

$$\varepsilon(ML, XY) = \frac{\varepsilon(M, Y) + \varepsilon(L, X)}{2} \quad (26)$$

and for the formation of an ML_2 complex from M and 2Ls, the proposed expression is the following.

$$\varepsilon(ML_2, XY) = \frac{\varepsilon(M, Y) + 2\varepsilon(L, X)}{3} \quad (27)$$

As useful as they can be, these hypotheses are also to be used with care [2020aSHA/REI].

2.6.3.3.4 Estimation from charges

Thoenen *et al.* [2014THO/HUM] provided a detailed analysis of the charge evolution of $\varepsilon(M^{n+}, Cl^-/ClO_4^-)$, and $\varepsilon(X^{n-}, Na^+)$. These estimations will be used in PRODATA in cases where no other estimation is possible.

2.6.3.4. Rationale on Specific Ion Interaction Coefficients

In some instances, the speciation that will be done using PRODATA could occur in relatively high ionic strength media [2020REI/DES], particularly in the ISR framework. The reliability of the output of the speciation calculation would then be impacted by the account of ionic strength, and by the presence and value of the specific ion

interaction coefficients implemented in the database file for *e.g.* PHREEQC. Other relationships have been proposed, such as the Pitzer model [1991PIT]. Discussion on different models can be found in Grenthe *et al.* [1997GRE/PLY]. For the sake of consistency with the approach in the NEA-OECD approach [1992GRE/FUG; 2003GUI/FAN; 2020GRE/GAO], only SIT model will be used.

3. Selection of Data

3.1. Oxygen-Hydrogen-Water

The definition of the common master species is imposed to liquid H₂O, and H⁺ for oxygen and hydrogen in solution. The functions of formation from the NEA-OECD reviews [1992GRE/FUG; 2003GUI/FAN; 2020GRE/GAO] from CODATA recommended values [1989COX/WAG] are included. The specific ion interaction coefficients for $\varepsilon(H^+, X^-)$ and $\varepsilon(M^+, OH^-) — M^+ = \{Li^+; Na^+; K^+\}$, and $X^- = \{Cl^-; ClO_4^-; NO_3^-\}$ — are taken from the NEA-OECD reviews [1992GRE/FUG; 2003GUI/FAN; 2020GRE/GAO].

Gaseous dioxygen (O₂(g)) and dihydrogen (H₂(g)) are selected in NEA-OECD reviews [1992GRE/FUG; 2003GUI/FAN; 2020GRE/GAO] from CODATA recommended values [1989COX/WAG]. Unfortunately, the dissolution of dioxygen and dihydrogen in water (O₂(aq), H₂(aq)) are not apparent in the auxiliary data in the NEA commissioned selection from Grenthe *et al.* [1992GRE/FUG] to the latter Grenthe *et al.* [2020GRE/GAO]. As these values are mandatory for the definition of the thermodynamic database files for software packages, they are selected from the compilation from the National Bureau of Standard [1982WAG/EVA]. It can be noticed that Shock *et al.* [1989SHO/HEL] — and later Schulte *et al.* [2001SCH/SHO] — proposed estimations of functions of formations of O₂(aq) based on the log₁₀ K° values calculated from the function of formations in Wagman *et al.* [1982WAG/EVA]. The values in PRODATA will then be taken directly from the functions of reaction calculated from Wagman *et al.* [1982WAG/EVA].

Table 3.1-1. Thermodynamic functions for the O₂-H₂-H₂O system from Wagman *et al.* [1982WAG/EVA], and calculated constants.

Reaction	$\Delta_r G_m^\circ$ *	$\log_{10} K^\circ$	$\Delta_f G_m^\circ$ †	$\Delta_r H_m^\circ$ *	$\Delta_f H_m^\circ$ †
	(kJ mol ⁻¹)		(kJ mol ⁻¹)	(kJ mol ⁻¹)	(kJ mol ⁻¹)
2H ₂ O ⇌ O ₂ (aq) + 4e ⁻ + 4H ⁺	490.658 ± 0.892	-85.96 ± 0.16	16.378 ± 0.895	559.96 ± 0.90	-11.70 ± 0.89
2H ⁺ + 2e ⁻ ⇌ H ₂ (aq)	17.6 ± 4.8	-3.08 ± 0.84	17.6 ± 4.8	-4.2 ± 1.6	-4.2 ± 1.6
O ₂ (g) ⇌ O ₂ (aq)	16.4 ± 3.2	-2.87 ± 0.55		-11.7 ± 5.6	
H ₂ (g) ⇌ H ₂ (aq)	17.6 ± 4.8	-3.08 ± 0.84		-4.2 ± 1.6	

* calculated from $\Delta_f G_m^\circ$ and $\Delta_f H_m^\circ$ from [1982WAG/EVA]; † calculated from $\log_{10} K^\circ$, and $\Delta_f G_m^\circ$ and $\Delta_f H_m^\circ$ from [2003GUI/FAN].

Table 3.1-2. Specific ion interaction coefficients for H⁺ and OH⁻.

Specific ion interaction coefficient	Value ± σ	Reference
$\varepsilon(H^+, Cl^-)$	0.12 ± 0.01	[1992GRE/FUG]
$\varepsilon(H^+, ClO_4^-)$	0.14 ± 0.01	
$\varepsilon(H^+, NO_3^-)$	0.07 ± 0.01	
$\varepsilon(Li^+, OH^-)$	-0.02 ± 0.03	
$\varepsilon(Na^+, OH^-)$	0.04 ± 0.01	
$\varepsilon(K^+, OH^-)$	0.09 ± 0.01	

3.2. Group 17

The thermodynamic functions and constants in NEA-OECD reviews [1992GRE/FUG; 2003GUI/FAN; 2005OLI/NOL; 2020GRE/GAO] for F(-I), F(0), Cl(-I), Cl(III), Cl(V), Cl(VII), Br(-I), Br(0), Br(I), Br(V), I(-I), I(0), and I(V) are accepted. The definition of the common master species is F⁻, Cl⁻, Br⁻, and I⁻. The specific ion interaction coefficients for the halide ions are taken from the NEA-OECD reviews [1992GRE/FUG; 2003GUI/FAN; 2020GRE/GAO].

The dissolution of $\text{Cl}_2(\text{g})$ to $\text{Cl}_2(\text{aq})$ is taken from Wagman *et al.* [1982WAG/EVA], the dissolution of $\text{I}_2(\text{g})$ to $\text{I}_2(\text{aq})$ is taken from Wagman *et al.* [1982WAG/EVA].

The formation of I_3^- is recalculated from Ramette and Sandford [1965RAM/SAN].

Table 3.2-1. Thermodynamic functions and calculated constants for halogens.

Reaction	$\Delta_r G_m^\circ$ (kJ mol ⁻¹)	$\log_{10} K^\circ$	$\Delta_f G_m^\circ$ * (kJ mol ⁻¹)	$\Delta_r H_m^\circ$ (kJ mol ⁻¹)	$\Delta_f H_m^\circ$ * (kJ mol ⁻¹)
$2\text{Cl}^- + 0.5\text{O}_2(\text{g}) + 2\text{H}^+ \rightleftharpoons \text{Cl}_2(\text{aq}) + \text{H}_2\text{O}$	$32.267 \pm 0.216^{\text{a}}$	-5.65 ± 0.04	6.973 ± 0.080	$24.930 \pm 3.206^{\text{a}}$	-23.400 ± 3.200
$2\text{Cl}^- + 0.5\text{O}_2(\text{aq}) + 2\text{H}^+ \rightleftharpoons \text{Cl}_2(\text{aq}) + \text{H}_2\text{O}$	$24.078 \pm 0.497^{\text{a}}$	-4.22 ± 0.09		$30.780 \pm 3.238^{\text{a}}$	
$2\text{I}^- + 0.5\text{O}_2(\text{g}) + 2\text{H}^+ \rightleftharpoons \text{I}_2(\text{aq}) + \text{H}_2\text{O}$	$-117.589 \pm 3.134^{\text{a}}$	20.60 ± 0.55	16.103 ± 3.142	$-152.850 \pm 4.126^{\text{a}}$	19.420 ± 4.125
$2\text{I}^- + 0.5\text{O}_2(\text{aq}) + 2\text{H}^+ \rightleftharpoons \text{I}_2(\text{aq}) + \text{H}_2\text{O}$	$-125.778 \pm 3.102^{\text{a}}$	22.04 ± 0.54		$-147.000 \pm 4.150^{\text{a}}$	
$\text{I}^- + \text{I}_2(\text{aq}) \rightleftharpoons \text{I}_3^-$	$-16.401 \pm 0.395^{\text{b}}$	2.87 ± 0.07	-52.003 ± 3.235	$-17.019 \pm 0.280^{\text{b}}$	-54.379 ± 4.134

a [1982WAG/EVA]; b calculated from $\log_{10} K^\circ = f(1/T)$ in [1965RAM/SAN]

* calculated from $\Delta_f G_m^\circ$ or $\Delta_f H_m^\circ$ of [2003GUI/FAN].

Table 3.2-2. Specific ion interaction coefficients for halogen ions

Specific ion interaction coefficient	Value $\pm \sigma$	Reference
$\varepsilon(\text{Na}^+, \text{F}^-)$	0.02 ± 0.02	[1992GRE/FUG]
$\varepsilon(\text{K}^+, \text{F}^-)$	0.03 ± 0.02	
$\varepsilon(\text{Li}^+, \text{Cl}^-)$	0.10 ± 0.03	
$\varepsilon(\text{Li}^+, \text{ClO}_4^-)$	0.15 ± 0.01	
$\varepsilon(\text{Na}^+, \text{Cl}^-)$	0.03 ± 0.01	
$\varepsilon(\text{Na}^+, \text{ClO}_4^-)$	0.01 ± 0.01	
$\varepsilon(\text{K}^+, \text{Cl}^-)$	0.00 ± 0.01	
$\varepsilon(\text{Cs}^+, \text{Cl}^-)$	-0.05 ± 0.02	[2002SPA]
$\varepsilon(\text{Li}^+, \text{Br}^-)$	0.13 ± 0.02	[1992GRE/FUG]
$\varepsilon(\text{Na}^+, \text{Br}^-)$	0.05 ± 0.01	
$\varepsilon(\text{K}^+, \text{Br}^-)$	0.01 ± 0.02	
$\varepsilon(\text{Li}^+, \text{I}^-)$	0.16 ± 0.01	
$\varepsilon(\text{Na}^+, \text{I}^-)$	0.08 ± 0.02	
$\varepsilon(\text{Na}^+, \text{IO}_3^-)$	-0.06 ± 0.02	
$\varepsilon(\text{K}^+, \text{I}^-)$	0.02 ± 0.02	

Only Cl^- and Br^- are stable in water. The perchlorate ion ClO_4^- is defined as a named species Perchlorate- to which all $\varepsilon(\text{M}^{n+}, \text{ClO}_4^-)$ are referred as $\varepsilon(\text{M}^{n+}, \text{Perchlorate}^-)$

The Pourbaix diagrams of iodine are plotted in Figure 3.2-1.

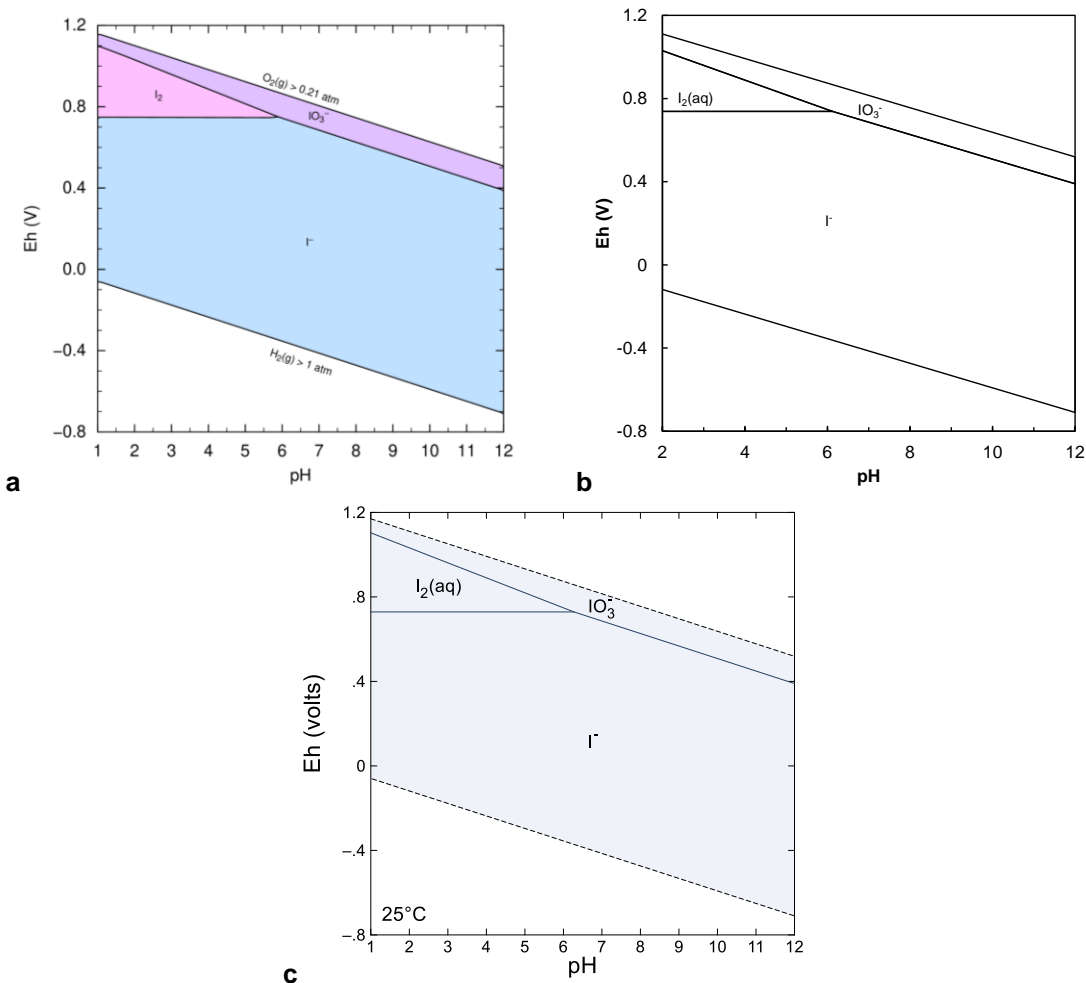


Figure 3.2-1. Pourbaix diagram of 10^{-4} mol $\text{kg}_{\text{w}}^{-1}$ I using PHREEPLOT (a), CHESS (b), and GWB (c) in a 0.1 mol $\text{kg}_{\text{w}}^{-1}$ hypothetical indifferent electrolyte solution.

3.3. Group 16

3.3.1. Sulphur

The thermodynamic functions and constants, and specific ion interaction coefficients in Guillaumont *et al.* [2003GUI/FAN] for S(VI), S(IV), S(II), S(0), and S(-II) are accepted in PRODATA — *i.e.* SO₄²⁻, HSO₄⁻, SO₃²⁻, HSO₃²⁻, SO₂(g), H₂SO₃(aq), S₂O₃²⁻, HS₂O₃⁻, S(cr), S₂(g), H₂S(g), H₂S(aq), HS⁻, and S²⁻. The definition of the common master species could be either HS⁻ or SO₄²⁻. The specific ion interaction coefficients are taken from the NEA-OECD reviews [1992GRE/FUG; 2003GUI/FAN; 2020GRE/GAO] — it is noteworthy that no $\varepsilon(\text{HS}^-, \text{M}^+)$ value has been selected.

As there is a large difference in the thermodynamic functions of the S(-II) species between Robie and Hemingway [1995ROB/HEM] and NEA-OECD [1992GRE/FUG; 2003GUI/FAN; 2020GRE/GAO], and also with Wagman *et al.* [1982WAG/EVA], Shock and Helgeson [1988SHO/HEL], or Chivot [2004CHI] — *e.g.*, $\Delta_f G^\circ(\text{HS}^-)$ is (44.8 ± 0.3) kJ mol⁻¹ [1995ROB/HEM], (12.243 ± 2.115) kJ mol⁻¹ [2003GUI/FAN], (12.08 ± 0.64) kJ mol⁻¹ [1982WAG/EVA], 11.966 kJ mol⁻¹ [1988SHO/HEL], and 12.2 kJ mol⁻¹ [2004CHI].

Hence, as an example the redox equilibrium between HS⁻ and SO₄²⁻ is written for the different sources in Table 3.3-1. When writing the equilibrium relative to e⁻ or O₂(g) evidences the commonalities and differences in Gibbs energies of formation, formation constants, and Nernst potentials. The Gibbs energies from Guillaumont *et al.* [2003GUI/FAN] and Wagman *et al.* [1982WAG/EVA] are giving coherent $\Delta_r G^\circ$, $\log_{10} K^\circ$, and E° values, when

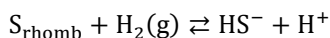
there is large discrepancy with the values of Robie and Hemingway [1995ROB/HEM]. A problem can be seen in the enthalpy of formation values, where $\Delta_f H_m^\circ(\text{HS}^-)$ is $-(16.3 \pm 1.5) \text{ kJ mol}^{-1}$ [2003GUI/FAN], $+(16.3 \pm 0.2) \text{ kJ mol}^{-1}$ [1995ROB/HEM], and $-(17.6 \pm 4.8) \text{ kJ mol}^{-1}$ [1982WAG/EVA]. The simplest reason could be a misprint, as the absolute values are coherent between the three sources. It can be noted that this misprint was not apparent in Robie *et al.* [1979ROB/HEM]. It can be also be noted that in Robie and Hemingway [1995ROB/HEM], as well as in Robie *et al.* [1979ROB/HEM], S-orthorhombic(cr) is the reference state.

Table 3.3-1. Functions of reaction, redox reaction constants, and potentials for the reduction of SO_4^{2-} to HS^- using different sources of data.

Reaction	$\Delta_r G^\circ$ (kJ mol ⁻¹)	$\log_{10} K^\circ$	E° (mV)	$\Delta_r H^\circ$ (kJ mol ⁻¹)	Reference
$\text{SO}_4^{2-} + 8\text{e}^- + 9\text{H}^+ \rightleftharpoons \text{HS}^- + 4\text{H}_2\text{O}$	-192.313 ± 2.080	33.69 ± 0.36	249.1 ± 2.7	-250.28 ± 1.455	[2003GUI/FAN]
	-159.6 ± 0.2	27.96 ± 0.04	206.8 ± 0.3	-217.6 ± 0.2^a	[1995ROB/HEM]
	-191.906 ± 0.597	33.62 ± 0.10	248.6 ± 0.7	-250.2 ± 0.2^b	[1982WAG/EVA]
$\text{SO}_4^{2-} + \text{H}^+ \rightleftharpoons \text{HS}^- + \text{O}_2(\text{aq})$	789.41 ± 3.255	-138.30 ± 0.57			[1982WAG/EVA]
$\text{SO}_4^{2-} + \text{H}^+ \rightleftharpoons \text{HS}^- + \text{O}_2(\text{g})$	756.247 ± 2.073	-132.49 ± 0.36			[2003GUI/FAN]
	788.8 ± 0.3	-138.19 ± 0.05			[1995ROB/HEM]
	756.61 ± 0.59	-132.55 ± 0.10			[1982WAG/EVA]
$\text{HS}^- + \text{H}^+ \rightleftharpoons \text{H}_2\text{S(g)}$	-45.686 ± 2.055	8.00 ± 0.36			[2003GUI/FAN]
	-78.2 ± 0.5	13.70 ± 0.09			[1995ROB/HEM]
	-45.64 ± 0.42	8.00 ± 0.07			[1982WAG/EVA]

a using $\Delta_f H^\circ(\text{HS}^-)$ in [1995ROB/HEM]; b using corrected $-\Delta_r H^\circ(\text{HS}^-)$ in [1995ROB/HEM]

It is interesting to recalculate the $\Delta_f G_m^\circ(\text{HS}^-)$ value from the $\Delta_f H_m^\circ$ and $S_{f,m}^\circ$ values for the reductive dissolution of S_{orthorhombic} using the three sources as follows.



Then the $\Delta_f G_m^\circ(\text{HS}^-) = \Delta_r G^\circ$ as all the other $\Delta_f G_m^\circ$ values are nil.

Using the $\Delta_f H_m^\circ$ and $S_{f,m}^\circ$ in the three references one can obtain the following values.

$$\Delta_r H^\circ = -16.3 \text{ kJ mol}^{-1} \quad \Delta_r S^\circ = -95.734 \text{ J mol}^{-1} \text{ K}^{-1} \quad \Delta_r G^\circ = 12.243 \text{ kJ mol}^{-1} \quad [2003GUI/FAN]$$

$$\Delta_r H^\circ = -17.6 \text{ kJ mol}^{-1} \quad \Delta_r S^\circ = -99.684 \text{ J mol}^{-1} \text{ K}^{-1} \quad \Delta_r G^\circ = 12.421 \text{ kJ mol}^{-1} \quad [1982WAG/EVA]$$

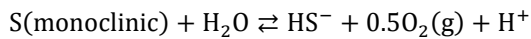
$$\Delta_r H^\circ = 16.3 \text{ kJ mol}^{-1} \quad \Delta_r S^\circ = -95.73 \text{ J mol}^{-1} \text{ K}^{-1} \quad \Delta_r G^\circ = 44.84 \text{ kJ mol}^{-1} \quad [1995ROB/HEM]$$

It is worthy to notice that the apparent error in the sign of $\Delta_f H_m^\circ(\text{HS}^-)$ seems to be at the origin of the erroneous value of $\Delta_f G_m^\circ(\text{HS}^-)$. When using the opposite value of $\Delta_f H_m^\circ(\text{HS}^-)$ in Robie and Hemingway [1995ROB/HEM] then the correct $\Delta_r G^\circ = \Delta_f G_m^\circ(\text{HS}^-)$ value is obtained.

$$\Delta_r H^\circ = -16.3 \pm 0.2 \text{ kJ mol}^{-1} \quad \Delta_r S^\circ = -95.73 \pm 0.90 \text{ J mol}^{-1} \text{ K}^{-1} \quad \Delta_r G^\circ = \Delta_f G_m^\circ(\text{HS}^-) = 12.2 \pm 0.2 \text{ kJ mol}^{-1}$$

Robie and Hemingway [1995ROB/HEM] selected the monoclinic form of elemental sulphur, which differs in terms of $\Delta_f H^\circ(\text{S}_{\text{mono}}) = (0.3 \pm 0.1) \text{ kJ mol}^{-1}$ and $S_{f,m}^\circ(\text{S}_{\text{mono}}) = (33.03 \pm 0.05) \text{ J mol}^{-1} \text{ K}^{-1}$, from the orthorhombic form — $\Delta_f G^\circ(\text{S}_{\text{orthorhombic}}) = \Delta_f H^\circ(\text{S}_{\text{orthorhombic}}) = 0$, $S_f^\circ(\text{S}_{\text{orthorhombic}}) = (32.05 \pm 0.05) \text{ J mol}^{-1} \text{ K}^{-1}$. Only the $\Delta_f H^\circ(\text{S}_{\text{monoclinic}}) = (0.33 \pm 0.24) \text{ kJ mol}^{-1}$ value were selected in Wagman *et al.* [1982WAG/EVA].

From the problems encountered for $\Delta_f G^\circ(\text{HS}^-)$, it is difficult to ascertain the $\log_{10} K_s(\text{S}(\text{monoclinic}))$ that would be obtained is consistent. Nevertheless, the values are added for scoping calculation.



$$\Delta_r G_m^\circ = (249.3 \pm 0.17) \text{ kJ mol}^{-1}$$

$$\Delta_r H_m^\circ = (269.2 \pm 0.14) \text{ kJ mol}^{-1}$$

$$\Delta_r S_m^\circ = (-36.03 \pm 0.893) \text{ kJ mol}^{-1}$$

$$\log_{10} K_s^\circ = -43.68 \pm 0.03$$

For the sake of completeness, S(VIII), S(VI), S(V), S(IV), S(III), S(II), S(-I) and polysulfide data from Chivot [2004CHI] are included. This latter compilation of thermodynamic functions, is referring to the CODATA values [1989COX/WAG] as those of Guillaumont *et al.* [2003GUI/FAN], which assures a maximum of consistency.

Table 3.3-2. Thermodynamic functions from Chivot [2004CHI], and constants calculated for the S species.

Reaction	$\Delta_f G_m^\circ$ kJ mol ⁻¹	$\Delta_f G_m^\circ$ kJ mol ⁻¹	$\log_{10} K^\circ$	$\Delta_f H_m^\circ$ kJ mol ⁻¹	$\Delta_f H_m^\circ$ kJ mol ⁻¹
$2\text{SO}_4^{2-} + 0.5\text{O}_2(\text{aq}) \rightleftharpoons \text{S}_2\text{O}_8^{2-} + \text{H}_2\text{O}$	-1 115.036	127.643	-22.36	-1 344.77	193.930
$\text{SO}_4^{2-} + 2\text{H}^+ \rightleftharpoons \text{HSO}_4(\text{aq})$	-744.41	-0.406	0.07	-909.27	0.07
$2\text{SO}_4^{2-} + 2\text{H}^+ \rightleftharpoons \text{S}_2\text{O}_6^{2-} + 0.5\text{O}_2(\text{aq}) + \text{H}_2\text{O}$	-966.504	292.553	-51.25	-1 173.19	353.81
$2\text{SO}_3^{2-} + 2\text{H}^+ \rightleftharpoons \text{S}_2\text{O}_5^{2-} + \text{H}_2\text{O}$	-808.61 ± 0.94	-70.806 ± 7.985	12.40 ± 1.40	-973.6 ± 4.1	2.69 ± 4.02
$\text{SO}_3^{2-} + 2\text{H}^+ \rightleftharpoons \text{SO}_2(\text{aq}) + \text{H}_2\text{O}$	-300.60 ± 0.23	-50.268 ± 4.013	8.81 ± 0.70	-323.78 ± 0.32	21.45 ± 0.24
$2\text{SO}_4^{2-} + 2\text{H}^+ \rightleftharpoons \text{S}_2\text{O}_4^{2-} + 1.5\text{O}_2(\text{aq}) + \text{H}_2\text{O}$	-600.40	675.027	-118.26	-753.540	761.76
$\text{S}_2\text{O}_4^{2-} + \text{H}^+ \rightleftharpoons \text{HS}_2\text{O}_4^-$	-614.63	-14.222	2.49	-749.35	4.19
$\text{S}_2\text{O}_4^{2-} + 2\text{H}^+ \rightleftharpoons \text{H}_2\text{S}_2\text{O}_4(\text{aq})$	-616.72	-16.312	2.86	-733.46	20.08
$3\text{SO}_4^{2-} + 4\text{H}^+ \rightleftharpoons \text{S}_3\text{O}_6^{2-} + 2\text{O}_2(\text{aq}) + 2\text{H}_2\text{O}$	-958.14	832.348	-145.82	-1 167.34	965.62
$4\text{SO}_4^{2-} + 6\text{H}^+ \rightleftharpoons \text{S}_4\text{O}_6^{2-} + 3.5\text{O}_2(\text{aq}) + 3\text{H}_2\text{O}$	-1 040.56	1 281.359	-224.48	-1 224.24	1 514.680
$5\text{SO}_4^{2-} + 8\text{H}^+ \rightleftharpoons \text{S}_5\text{O}_6^{2-} + 5\text{O}_2(\text{aq}) + 4\text{H}_2\text{O}$	-958.14	1 895.210	-332.02	-1 175.7	2 169.18
$2\text{SO}_4^{2-} + 2\text{H}^+ \rightleftharpoons \text{S}_2^{2-} + 3.5\text{O}_2(\text{aq}) + \text{H}_2\text{O}$	84.706	1 392.897	-244.02	35.041	1 526.941
$2\text{SO}_4^{2-} + 14\text{e}^- + 2\text{H}^+ \rightleftharpoons \text{S}_2^{2-} + 8\text{H}_2\text{O}$		-324.406	56.833		-432.92
$1.5\text{S}_2^{2-} + 0.25\text{O}_2(\text{aq}) + \text{H}^+ \rightleftharpoons \text{S}_3^{2-} + 0.5\text{H}_2\text{O}$	83.593	-166.131	29.10	45.225	-147.327
$2\text{S}_2^{2-} + 0.5\text{O}_2(\text{aq}) + 2\text{H}^+ \rightleftharpoons \text{S}_4^{2-} + \text{H}_2\text{O}$	66.583	-348.158	60.99	39.306	-310.756
$2.5\text{S}_2^{2-} + 0.75\text{O}_2(\text{aq}) + 3\text{H}^+ \rightleftharpoons \text{S}_5^{2-} + 1.5\text{H}_2\text{O}$	65.955	-513.804	90.01	37.632	-469.941
$3\text{S}_2^{2-} + \text{O}_2(\text{aq}) + 4\text{H}^+ \rightleftharpoons \text{S}_6^{2-} + 2\text{H}_2\text{O}$	67.154	-677.622	118.714	62	-603.083

Figure 3.3-1. Specific ion interaction coefficients for sulphur ions

Specific ion interaction coefficient	Value ± σ	Reference
$\varepsilon(\text{Li}^+, \text{SO}_4^{2-})$	-0.03 ± 0.04	[1992GRE/FUG]
$\varepsilon(\text{Na}^+, \text{SO}_4^{2-})$	-0.12 ± 0.06	
$\varepsilon(\text{K}^+, \text{SO}_4^{2-})$	-0.06 ± 0.02	
$\varepsilon(\text{H}^+, \text{HSO}_4^-)$	0.14 ± 0.05	[2013LEM/BER], Footnote p. 476
$\varepsilon(\text{Na}^+, \text{HSO}_4^-)$	-0.01 ± 0.02	[1992GRE/FUG]
$\varepsilon(\text{Na}^+, \text{SO}_3^{2-})$	-0.08 ± 0.05	
$\varepsilon(\text{Na}^+, \text{S}_2\text{O}_3^{2-})$	-0.08 ± 0.06	

The Pourbaix diagram of 10^{-4} mol kg_w⁻¹ sulphur in a hypothetical indifferent electrolyte at 0.1 mol kg_w⁻¹ is drawn in Figure 3.3-2 for PHREEPLOT, CHESS, and GWB. There are slight differences in the limits of acidity couples, and area of S(cr). The limits of the acidity couples can be attributed to the particular mode of calculation for PHREEPLOT — see Kinniburgh and Cooper [2004KIN/COO] and Kinniburgh and Cooper [2011KIN/COO] for details — compared to calculation in activity for CHESS and GWB.

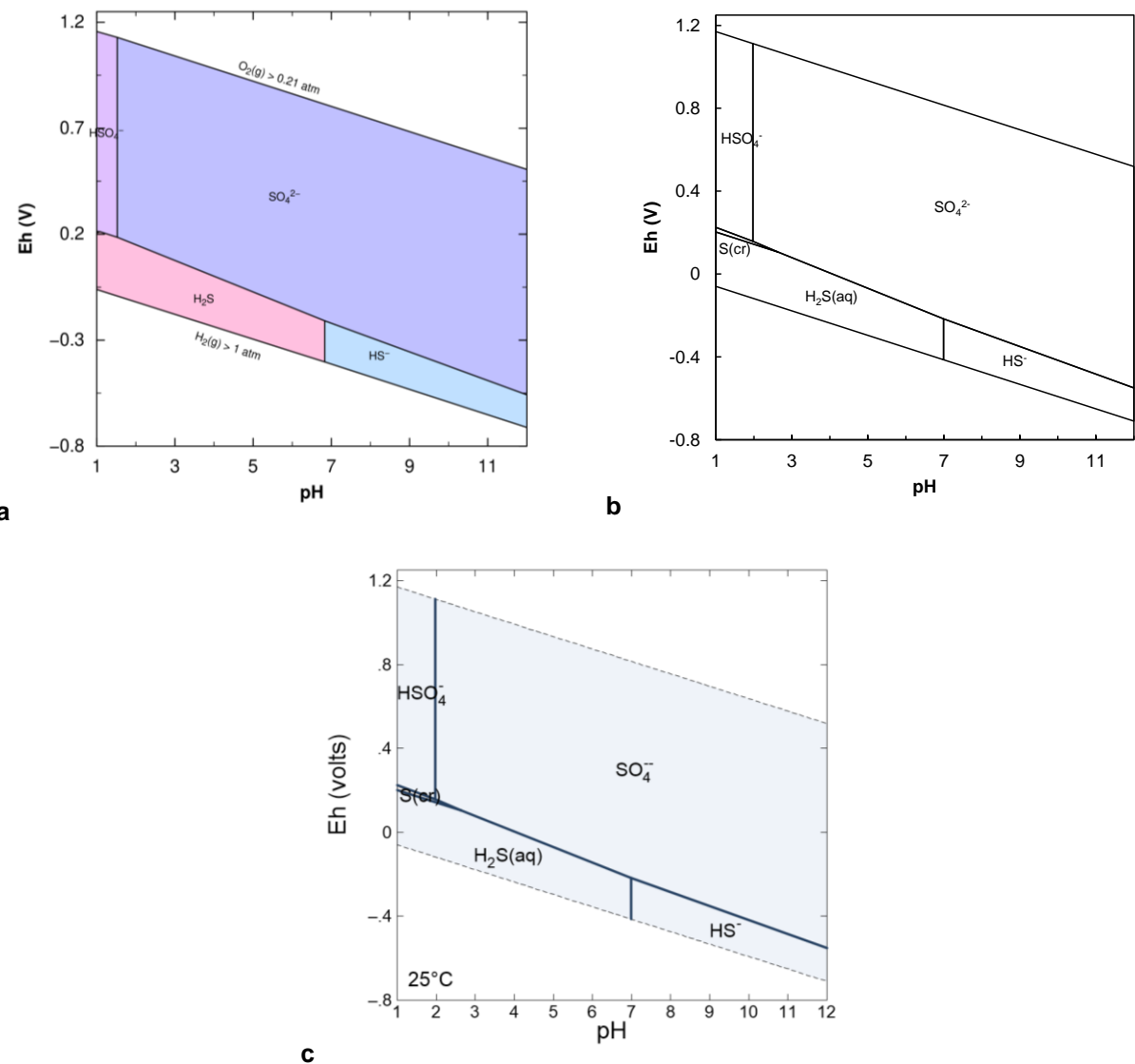


Figure 3.3-2. Pourbaix diagram of 10^{-4} mol kg $^{-1}$ S in a 0.1 mol kg $^{-1}$ NaClO $_4$ solution, obtained using PHREEPLOT (a), CHESS (b), and GWB (c) — no gas is allowed to equilibrate.

3.3.2. Selenium

The thermodynamic functions, constants, and specific ion interaction coefficients in Olin *et al.* [2005OLI/NOL] are accepted. The choice of the common master species could be done between either SeO_4^{2-} , SeO_3^{2-} , Se_2^{2-} , or one of the Se(-II) aqueous species.

For Se(-II) aqueous species, the $\Delta_f H_m^\circ$ or S_m° values have only been selected for $\text{H}_2\text{Se(aq)}$. No $\Delta_f H_m^\circ$ or S_m° values for HSe^- or Se^{2-} are selected in Olin *et al.* [2005OLI/NOL]. It is then tempting to choose $\text{H}_2\text{Se(aq)}$ as a common master species, otherwise no $\Delta_r H_m^\circ$ or $\log_{10} \beta(T)$ could be included.

The $\Delta_f H^\circ(\text{HSe}^-)$, and $S_f^\circ(\text{HSe}^-)$ values are proposed in Wagman *et al.* [1982WAG/EVA] and Naumov *et al.* [1974NAU/RYZ]. The coherent obtained Gibbs energies of reaction and $\log_{10} K_s^\circ$ values can be compared in Table 3.3-3. In view of the coherent values obtained, the enthalpy of formation from Wagman *et al.* [1982WAG/EVA] is added in PRODATA. The S° variation could also be compared favourably between Wagman *et al.* [1982WAG/EVA] and Naumov *et al.* [1974NAU/RYZ].

Naumov *et al.* [1974NAU/RYZ] also proposed a value for $\Delta_f H^\circ(\text{HSe}^-)$, with which the values from Wagman *et al.* [1982WAG/EVA] and [2005OLI/NOL] are coherent (c.f. Table 3.3-3). Naumov *et al.* [1974NAU/RYZ] also proposed a value for $\Delta_f H^\circ(\text{Se}^{2-})$, which is included in PRODATA.

The Pourbaix diagram obtained with PHREEPLOT, CHESS, and GWB extraction of the database are plotted in Figure 3.3-3. There are slight differences between the limits of the acidity couples, and the $\text{Se}(\text{cr})/\text{H}_2\text{Se}(\text{aq})$ limit given a greater area in the decreasing order GWB, PHREEPLOT, and CHESS.

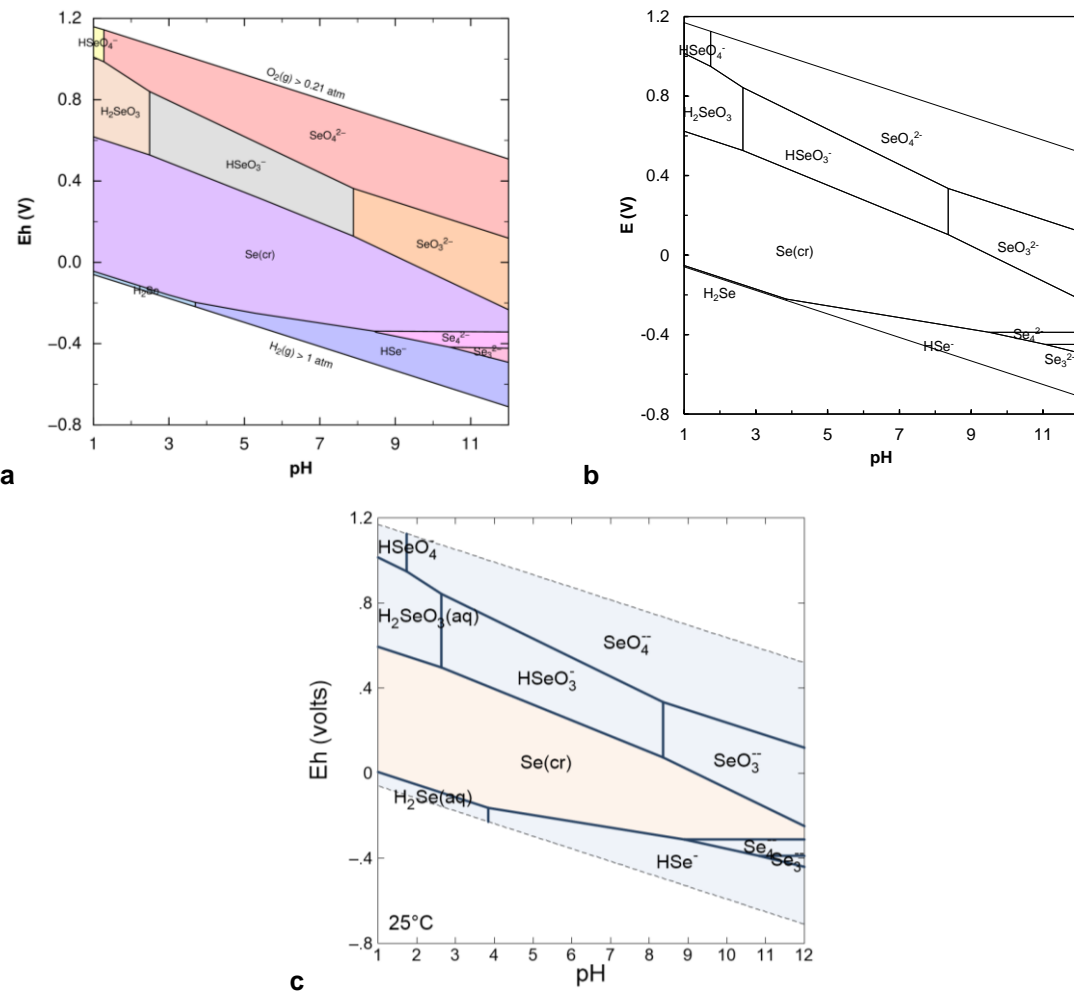


Figure 3.3-3. Pourbaix diagram of 10^{-4} mol $\text{kg}_{\text{w}}^{-1}$ Se in a 0.1 mol $\text{kg}_{\text{w}}^{-1}$ NaCl solution PHREEPLOT (a), CHESS (b), and GWB (c), with the common master species SeO_4^{2-} ; all solid phases are allowed to precipitate.

Table 3.3-3. Comparison of thermodynamic functions and constants for the formation of HSe^- and Se^{2-} from $\text{Se}(\text{cr})$ in Olin *et al.* [2005OLI/NOL], Wagman *et al.* [1982WAG/EVA], and Naumov *et al.* [1974NAU/RYZ].

Reaction	$\Delta_r G_m^\circ$ kJ mol ⁻¹	$\log_{10} K_s$	$\Delta_r G_m^\circ$ kJ mol ⁻¹	$\log_{10} K_s$	$\Delta_r H_m^\circ$ kJ mol ⁻¹
$\text{Se}(\text{cr}) + \text{H}^+ + 2\text{e}^- \rightleftharpoons \text{HSe}^-$	$43.471 \pm 2.024^{\text{a}}$	-7.62 ± 0.39	$44.0 \pm 0.8^{\text{b}}$	-7.71 ± 0.14	$15.9 \pm 7.2^{\text{b}}$
			$43.9 \pm 8.4^{\text{c}}$	-7.69 ± 1.47	$15.9 \pm 8.4^{\text{c}}$
$\text{Se}(\text{cr}) + 2\text{e}^- \rightleftharpoons \text{Se}^{2-}$	$112.670 \pm 6.294^{\text{a}}$	-19.74 ± 1.10	$129.3 \pm 8.4^{\text{c}}$	-19.78 ± 1.29	$64.0 \pm 8.4^{\text{c}}$

a [2005OLI/NOL]; b [1982WAG/EVA]; c [1974NAU/RYZ].

Table 3.3-4. Specific ion interaction coefficients for selenium ions

Specific ion interaction coefficient	Value	Reference
$\varepsilon(\text{Na}^+, \text{SeO}_4^{2-})$	-0.12	Analogy S(VI)
$\varepsilon(\text{Na}^+, \text{HSeO}_4^-)$	-0.01	
$\varepsilon(\text{Na}^+, \text{SeO}_3^{2-})$	-0.08	Analogy S(IV)
$\varepsilon(\text{Na}^+, \text{HSeO}_3^-)$	0.02	

3.4. Group 15

3.4.1. Nitrogen

The thermodynamic functions and constants in NEA-OECD reviews [1992GRE/FUG; 2003GUI/FAN; 2020GRE/GAO] for N(-III), N(0), azide, and N(V) are accepted — *i.e.*, $\text{NH}_3(\text{g})$, $\text{NH}_3(\text{aq})$, NH_4^+ , $\text{N}_2(\text{g})$, N_3^- , $\text{HN}_3(\text{aq})$, NO_3^- . The $\log_{10}K$ for the acidity of N(III) is selected in Guillaumont *et al.* [2003GUI/FAN], whereas no thermodynamic functions are selected for either N(III) species.



The $\Delta_r G_m^\circ(\text{NO}_2^-)$ is chosen from Wagman *et al.* [1982WAG/EVA].

Nitrogen phases $\text{N}_2\text{O}_5(\text{cr})$, and $\text{NH}_4\text{NO}_3(\text{cr})$ are added to PRODATA from Wagman *et al.* [1982WAG/EVA] and Robie and Hemingway [1995ROB/HEM], respectively. For $\text{N}_2\text{O}_5(\text{cr})$ thermodynamic functions are recalculated from Wagman *et al.* [1982WAG/EVA] in coherence with NEA-OECD reviews [2003GUI/FAN; 2020GRE/GAO].

The functions of formation of $\text{N}_2(\text{g})$ are taken from the NEA-OECD [2003GUI/FAN]. The dissolution of $\text{N}_2(\text{aq})$ is taken from the Henry's constant in Sander [2016SAN].

The redox chemistry of nitrogen in water is rather complicated and often mediated by bacteria — *e.g.*, $\text{NO}_3^-/\text{NO}_2^-$, $\text{NO}_2^-/\text{NH}_4^+$, and $\text{NO}_3^-/\text{N}_2(\text{aq})$. The NO_2^- and $\text{N}_2(\text{aq})$ species are not included by default in PRODATA, but can be added on demand.

The specific ion interaction coefficients are taken from the NEA-OECD reviews [1992GRE/FUG; 2003GUI/FAN; 2020GRE/GAO].

Table 3.4-1. Thermodynamic functions and constants for nitrogen species from Wagman *et al.* [1982WAG/EVA].

Reaction	$\Delta_r G_m^\circ$ *	$\log_{10} K^\circ$	$\Delta_f G_m^\circ$ †	$\Delta_r H_m^\circ$ *	$\Delta_f H_m^\circ$ †
	kJ mol^{-1}		kJ mol^{-1}	kJ mol^{-1}	kJ mol^{-1}
$\text{NO}_2^- + 0.5\text{O}_2(\text{g}) \rightleftharpoons \text{NO}_3^-$	76.540 ± 1.545	-13.41 ± 0.27	-34.254 ± 1.600	100.400 ± 4.817	-106.45 ± 4.80
$\text{NH}_4\text{NO}_3(\text{cr}) \rightleftharpoons \text{NH}_4^+ + \text{NO}_3^-$	-6.39 ± 0.75	1.12 ± 0.13	-183.8 ± 0.9	25.490 ± 0.646	-365.6 ± 0.8
$\text{N}_2\text{O}_5(\text{cr}) + \text{H}_2\text{O} \rightleftharpoons \text{NO}_3^- + 2\text{H}^+$	-94.25 ± 6.89	16.51 ± 1.21	109.80 ± 6.94	-81.07 ± 0.34	-46.80 ± 0.87
$\text{N}_2(\text{g}) \rightleftharpoons \text{N}_2(\text{aq})$	18.192	-3.19††	18.192		

* calculated from $\Delta_f G_m^\circ$ in [1982WAG/EVA]; † calculated from $\log_{10} K^\circ$ and $\Delta_f G_m^\circ$, or from $\Delta_f H_m^\circ$ in [2003GUI/FAN]; †† [2016SAN].

Table 3.4-2. Specific ion interaction coefficients for nitrogen ions

Specific ion interaction coefficient	Value	Reference
$\varepsilon(\text{H}^+, \text{NO}_3^-)$	0.07 ± 0.01	[1992GRE/FUG]
$\varepsilon(\text{Li}^+, \text{NO}_3^-)$	0.08 ± 0.01	
$\varepsilon(\text{Na}^+, \text{NO}_3^-)$	-0.04 ± 0.03	
$\varepsilon(\text{K}^+, \text{NO}_3^-)$	-0.11 ± 0.04	
$\varepsilon(\text{Li}^+, \text{NO}_2^-)$	0.06 ± 0.04	

Table 3.4-2. Continued

Specific ion interaction coefficient	Value	Reference
$\varepsilon(\text{Na}^+, \text{NO}_2^-)$	0.00 ± 0.02	
$\varepsilon(\text{K}^+, \text{NO}_2^-)$	-0.04 ± 0.02	
$\varepsilon(\text{Cs}^+, \text{NO}_2^-)$	-0.04 ± 0.02	[2002SPA]
$\varepsilon(\text{Na}^+, \text{N}_3^-)$	0.00 ± 0.10	[1992GRE/FUG]

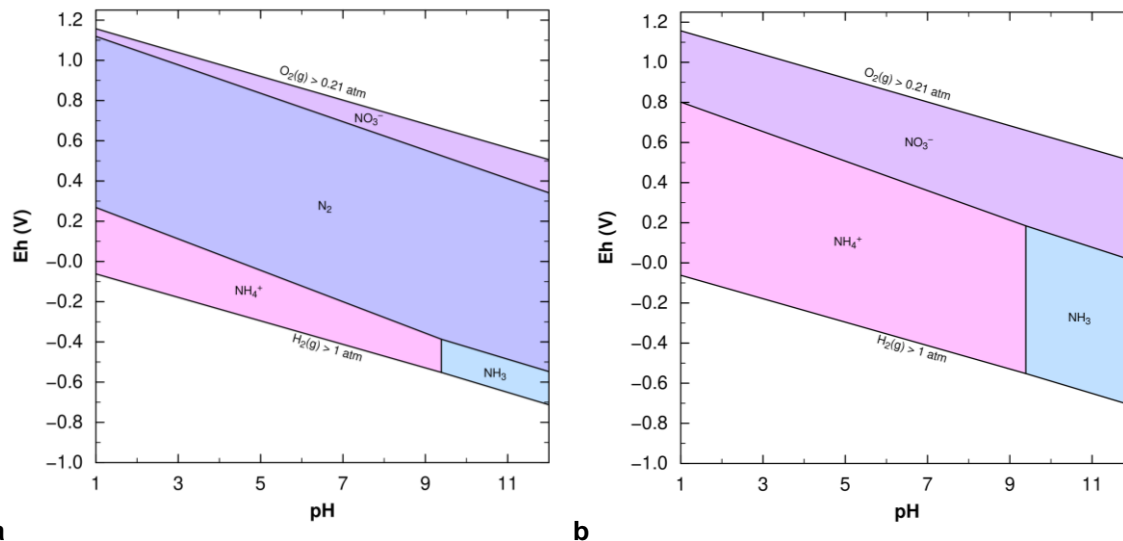


Figure 3.4-1. Pourbaix diagram of $10^{-4} \text{ mol kg}_w^{-1} \text{ N}$ in a $0.1 \text{ mol kg}_w^{-1} \text{ NaCl}$ solution (PHREEPLOT) including (a) and not including (b) $\text{N}(0)$, NO_2^- , and N_3^- .

3.4.2. Phosphor

The thermodynamic functions and constants for P(V) from NEA-OECD reviews [1992GRE/FUG; 2003GUI/FAN; 2020GRE/GAO], are accepted in PRODATA. The definition of the common master species can be either H_2PO_4^- , HPO_4^{2-} , or PO_4^{3-} . The specific ion interaction coefficients for are taken from the NEA-OECD reviews [1992GRE/FUG; 2003GUI/FAN; 2020GRE/GAO].

It can be noted that the uncertainty of the $\sigma(\Delta_f G_m^\circ)$ values of PO_4^{3-} , HPO_4^{2-} , H_2PO_4^- , are mostly the same. This is unlikely as the uncertainties of the $\log_{10} K^\circ$ values are not that different. The values of both $\Delta_f G_m^\circ$ and $\sigma(\Delta_f G_m^\circ)$ are recalculated in Table 3.4-3 from the selected $\log_{10} K^\circ$ and $\sigma(\log_{10} K^\circ)$ values, and referring to the selected value of $\Delta_f G_m^\circ(\text{PO}_4^{3-}) = -(1\ 025.491 \pm 1.576) \text{ kJ mol}^{-1}$.

The same occurs between $\Delta_f H_m^\circ(\text{HPO}_4^{2-})$ and $\Delta_f H_m^\circ(\text{H}_2\text{PO}_4^-)$, $S_{f,m}^\circ(\text{HPO}_4^{2-})$ and $S_{f,m}^\circ(\text{H}_2\text{PO}_4^-)$ that have the same uncertainty. The $\Delta_f H_m^\circ$ and $S_{f,m}^\circ$ values are recalculated in Table 3.4-3 from the $\Delta_r H_m^\circ$, $\sigma(\Delta_r H_m^\circ)$, $\Delta_r S_m^\circ$, and $\sigma(\Delta_r S_m^\circ)$ values, and referring to the selected value of $\Delta_f H_m^\circ(\text{PO}_4^{3-}) = -(1\ 284.400 \pm 4.085) \text{ kJ mol}^{-1}$, $S_{f,m}^\circ = -(220.970 \pm 12.846) \text{ J mol}^{-1} \text{ K}^{-1}$ in NEA-OECD reviews [2003GUI/FAN; 2020GRE/GAO].

Table 3.4-3. Thermodynamic constants and functions for the phosphate system with $\sigma(\Delta_f G^\circ_m)$ recalculated from the selected constants in NEA-OECD reviews [2003GUI/FAN; 2020GRE/GAO].

Reaction	$\log_{10} K^\circ$	$\Delta_r G_m^\circ$ (kJ mol ⁻¹)	$\Delta_f G_m^\circ$ (kJ mol ⁻¹)	$\Delta_r H_m^\circ$ (kJ mol ⁻¹)	$\Delta_f H_m^\circ$ (kJ mol ⁻¹)	$\Delta_r S_m^\circ$ (J K ⁻¹ mol ⁻¹)	$S_{f,m}^\circ$ (J K ⁻¹ mol ⁻¹)
$P(\text{cr}) + 1.25O_2(\text{g}) + 1.5H_2O \rightleftharpoons PO_4^{3-} + 3H^+$							
	117.34 ± 0.28	-669.781 ± 1.575	-1 025.491 ± 1.576	-855.655 ± 4.085	-1 284.400 ± 4.085	-623.425 ± 12.843	-220.970 ± 12.846
$P(\text{cr}) + 1.25O_2(\text{aq}) + 1.5H_2O \rightleftharpoons PO_4^{3-} + 3H^+$							
	120.93 ± 0.19	-690.254 ± 1.108		-841.030 ± 3.928		-505.710 ± 12.794	
$PO_4^{3-} + H^+ \rightleftharpoons HPO_4^{2-}$							
	12.35 ± 0.03	-70.494 ± 0.171	-1 095.985 ± 1.585	-14.600 ± 3.800	-1 299.000 ± 5.579	187.470 ± 12.758	-33.500 ± 18.105
$HPO_4^{2-} + H^+ \rightleftharpoons H_2PO_4^-$							
	7.212 ± 0.013	-41.166 ± 0.074	-1 137.151 ± 1.587	-3.600 ± 1.000	-1 302.600 ± 5.668	126.000 ± 3.363	92.500 ± 18.415
$H_2PO_4^- + H^+ \rightleftharpoons H_3PO_4(\text{aq})$							
	2.14 ± 0.03	-12.215 ± 0.171	-1 149.366 ± 1.596	8.480 ± 0.600	-1 294.120 ± 5.700	69.412 ± 2.093	161.912 ± 18.534
$PO_4^{3-} + 2H^+ \rightleftharpoons H_2PO_4^-$							
	19.562 ± 0.033	-111.660 ± 0.187		-18.200 ± 3.929			
$PO_4^{3-} + 3H^+ \rightleftharpoons H_3PO_4(\text{aq})$							
	21.702 ± 0.044	-123.875 ± 0.252		-9.720 ± 3.975			
$HPO_4^{2-} + 2H^+ \rightleftharpoons H_3PO_4(\text{aq})$							
	9.352 ± 0.033	-53.381 ± 0.187		4.880 ± 1.168			

a calculated from $\log_{10} K^\circ$ in [2003GUI/FAN]; b calculated from $\Delta_r G_m^\circ$ and $\Delta_f G_m^\circ(PO_4^{3-})$ in [2003GUI/FAN]

Even if not stable in water, the values for P(-III) from Wagman *et al.* [1982WAG/EVA] are included. The function of formation of P(V) being significantly different between Wagman *et al.* [1982WAG/EVA] and Guillaumont *et al.* [2003GUI/FAN], they are recalculated from the functions of reaction in Table 3.4-4.

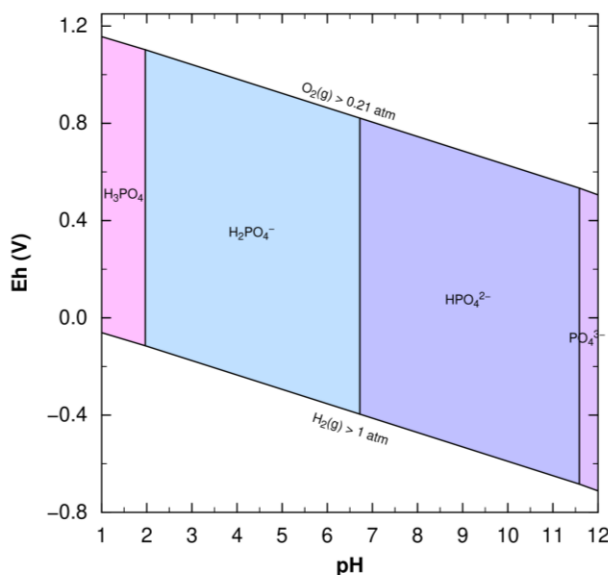


Figure 3.4-2. Pourbaix diagram of 10^{-4} mol kg_w⁻¹ P in a hypothetical indifferent 0.1 mol kg_w⁻¹ electrolyte solution (PHREEPLOT).

Table 3.4-4. Thermodynamic functions and constants of P(-III) calculated from Wagman *et al.* [1982WAG/EVA].

Reaction	$\Delta_r G_m^\circ$ ^a (kJ mol ⁻¹)	$\log_{10} K^\circ$	$\Delta_f G_m^\circ$ ^b (kJ mol ⁻¹)
$\text{PO}_4^{3-} + 8\text{e}^- + 12\text{H}^+ \rightleftharpoons \text{PH}_4^+ + 4\text{H}_2\text{O}$	162.240 ± 1.348	-28.42 ± 0.24	85.309 ± 0.800
$\text{PO}_4^{3-} + 4\text{H}^+ \rightleftharpoons \text{PH}_4^+ + 2\text{O}_2(\text{aq})$	1143.556 ± 1.167	-200.34 ± 0.20	
$\text{PO}_4^{3-} + 8\text{e}^- + 11\text{H}^+ \rightleftharpoons \text{PH}_3(\text{aq}) + 4\text{H}_2\text{O}$	95.500 ± 1.528	-16.73 ± 0.27	18.569 ± 0.351
$\text{PO}_4^{3-} + 3\text{H}^+ \rightleftharpoons \text{PH}_3(\text{aq}) + 2\text{O}_2(\text{aq})$	1076.816 ± 0.920	-188.65 ± 0.16	
$\text{PH}_3(\text{aq}) + \text{H}^+ \rightleftharpoons \text{PH}_4^+$	66.740 ± 0.719	-11.69 ± 0.13	85.309 ± 0.800
$\text{PH}_4^+ \rightleftharpoons \text{PH}_3(\text{g}) + \text{H}^+$	-78.7 ± 3.3	13.79 ± 0.58	6.609 ± 1.578

a calculated from $\Delta_f G_m^\circ$ of [1982WAG/EVA]; b calculated from $\log_{10} K^\circ$ and $\Delta_f G_m^\circ$ of [2003GUI/FAN].**Table 3.4-5. Specific ion interaction coefficients for phosphate ions.**

Specific ion interaction coefficient	Value	Reference
$\varepsilon(\text{Na}^+, \text{PO}_4^{3-})$	-0.25 ± 0.03	[2003GUI/FAN]
$\varepsilon(\text{K}^+, \text{PO}_4^{3-})$	-0.09 ± 0.02	
$\varepsilon(\text{Na}^+, \text{HPO}_4^{2-})$	-0.15 ± 0.06	
$\varepsilon(\text{K}^+, \text{HPO}_4^{2-})$	-0.10 ± 0.06	
$\varepsilon(\text{Na}^+, \text{H}_2\text{PO}_4^-)$	-0.08 ± 0.04	
$\varepsilon(\text{K}^+, \text{H}_2\text{PO}_4^-)$	-0.14 ± 0.04	

3.4.3. Arsenic

3.4.3.1. Inorganic Compounds

3.4.3.1.1 Oxo-compounds of As(III) and As(V)

The thermodynamic functions, constants, and specific interaction coefficients for As(III) — *i.e.*, the two allotropic forms of $\text{As}_4\text{O}_6(\text{cr})$, $\text{AsO}_2^-/\text{H}_2\text{AsO}_3^-$, $\text{HAsO}_2(\text{aq})/\text{H}_3\text{AsO}_3(\text{aq})$ — and As(V) — $\text{As}_2\text{O}_5(\text{cr})$, AsO_4^{3-} , HAsO_4^{2-} , H_2AsO_4^- , and $\text{H}_3\text{AsO}_4(\text{aq})$ — are taken from Olin *et al.* [2005OLI/NOL]. As the $\text{AsO}_2^-/\text{H}_2\text{AsO}_3^-$ and $\text{HAsO}_2(\text{aq})/\text{H}_3\text{AsO}_3(\text{aq})$ couples of molecules are equivalent, H_2AsO_3^- and $\text{H}_3\text{AsO}_3(\text{aq})$ are chosen for arsenite.

Table 3.4-6. Specific ion interaction coefficients for arsenic ions.

Specific ion interaction coefficient	Value	Reference
$\varepsilon(\text{Na}^+, \text{H}_2\text{AsO}_4^-)$	-0.01 ± 0.01	[2020LEM/PAL]
$\varepsilon(\text{K}^+, \text{H}_2\text{AsO}_4^-)$	-0.12 ± 0.02	[2002SPA]
$\varepsilon(\text{Na}^+, \text{HAsO}_4^{2-})$	-0.21 ± 0.06	
$\varepsilon(\text{K}^+, \text{HAsO}_4^{2-})$	-0.02 ± 0.01	

3.4.3.1.2 As(-III)

The thermodynamic functions and constants for As(-III) — *i.e.*, $\text{AsH}_3(\text{aq})$ and $\text{AsH}_3(\text{g})$ — are calculated from Ferguson and Gavis [1972FER/GAV].

Table 3.4-7. Thermodynamic functions and constants for As(-III).

Reaction	$\Delta_r G_m^\circ$ ^a	$\log_{10} K^\circ$	$\Delta_f G_m^\circ$ ^b
$\text{AsO}_3^{4-} + 3\text{H}^+ \rightleftharpoons \text{AsH}_3(\text{aq}) + 2\text{O}_2(\text{g})$	751.9	-131.7	103.389
$\text{AsH}_3(\text{g}) + 2\text{O}_2(\text{g}) \rightleftharpoons \text{AsO}_3^{4-} + 3\text{H}^+$	-721.4	126.4	

a calculated from $\Delta_f G_m^\circ$ in [1972FER/GAV]; b calculated from $\log_{10} K^\circ$ and $\Delta_f G_m^\circ$ in [2005OLI/NOL].

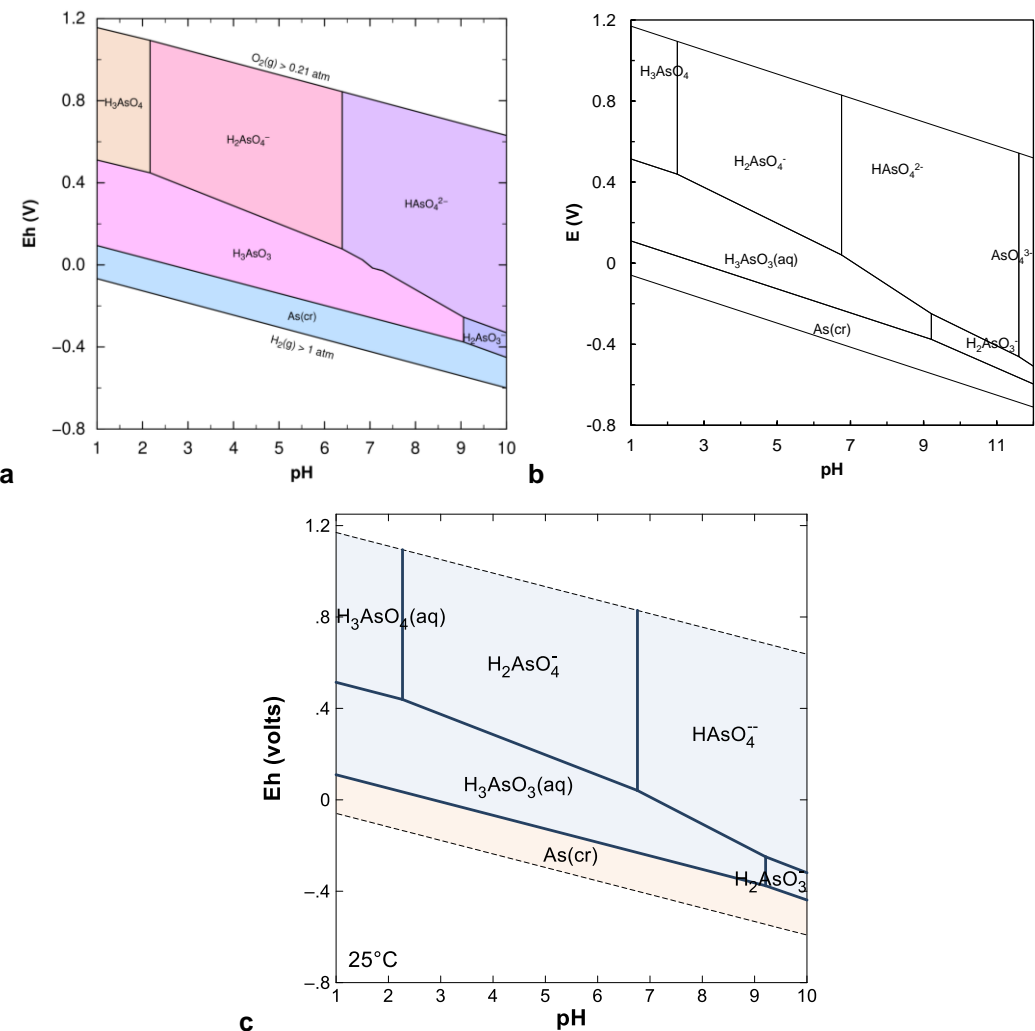


Figure 3.4-3. Pourbaix diagram of 10^{-4} mol kg_w⁻¹ As in a hypothetical indifferent 0.1 mol kg_w⁻¹ electrolyte solution using PHREEPLOT (a), CHESS (b), and GWB (c). All solid phases are allowed to precipitate.

3.4.3.1.3 Arsenosulphide

Arsenosulphide are particularly frequent compounds observed in mining context. The formation of arsenosulphide components are available in Naumov *et al.* [1974NAU/RYZ], Robie *et al.* [1979ROB/HEM], and Robie and Hemingway [1995ROB/HEM] for realgar (AsS), and in Naumov *et al.* [1974NAU/RYZ], Robie *et al.* [1979ROB/HEM], Wagman *et al.* [1982WAG/EVA] or Robie and Hemingway [1995ROB/HEM] for orpiment (As_2S_3). The functions of formation are different for each solid in function of the source. Values from Robie *et al.* [1979ROB/HEM] are taken from Wagman *et al.* [1968WAG/EVA] and are therefore coherent with Wagman *et al.* [1982WAG/EVA].

Values in Robie and Hemingway [1995ROB/HEM] are traced to more recent direct determination from Taras Bryndzia and Kleppa [1988TAR/KLE]. In Robie and Hemingway [1995ROB/HEM] the only arsenic form in reference state is native As(cr) — no soluble species are defined —, which $S_f^\circ = (35.69 \pm 0.84) \text{ J mol}^{-1} \text{ K}^{-1}$ value is in agreement with the one selected in NEA-OECD review of Se [2005OLI/NOL], $S_{f,m}^\circ = (35.100 \pm 0.600) \text{ J mol}^{-1} \text{ K}^{-1}$. The formation of realgar can be written relative to reference state of native elements,



$$\Delta_r S^\circ = -(4.24 \pm 0.59) \text{ J mol}^{-1} \text{ K}^{-1}$$

$$\Delta_r G^\circ = -(29.64 \pm 5.00) \text{ kJ mol}^{-1}$$

$$\log_{10} K = 5.19 \pm 0.88$$

$$\Delta_f G^\circ(\text{AsS}) = -(29.64 \pm 5.00) \text{ kJ mol}^{-1}$$

which is the value in Robie and Hemingway [1995ROB/HEM] for realgar. Contrary to HS^- , it does not seem to have any misprint.

The values of $\Delta_f G^\circ(\text{As}_2\text{S}_3)$ and $\Delta_f H^\circ(\text{As}_2\text{S}_3)$ in Robie and Hemingway [1995ROB/HEM] and Wagman *et al.* [1982WAG/EVA] are very different, when the $S_f^\circ(\text{As}_2\text{S}_3)$ are alike. Robie and Hemingway [1995ROB/HEM] do not give any functions of formation for the arsenic oxoanions. The formation from the native elements can then be compared.

	[1995ROB/HEM]	[1982WAG/EVA]
$2\text{As(cr)} + 3\text{S(cr)} \rightleftharpoons \text{As}_2\text{S}_3(\text{cr})$	$\Delta_r H^\circ = -(91.6 \pm 4.2) \text{ kJ mol}^{-1}$	$-(169.0 \pm 0.8) \text{ kJ mol}^{-1}$
	$\Delta_r S^\circ = -(3.93 \pm 0.53) \text{ J mol}^{-1} \text{ K}^{-1}$	$-(2.00 \pm 11.87) \text{ J mol}^{-1} \text{ K}^{-1}$
	$\Delta_r G^\circ = -(90.43 \pm 4.20) \text{ kJ mol}^{-1}$	$-168.4 \pm 3.45 \text{ kJ mol}^{-1}$
	$\log_{10} K_s = 15.84 \pm 0.74$	29.50 ± 0.60

The calculated $\Delta_r G^\circ$ and $\log_{10} K_s$ values are the same than the tabulated ones and no misprint seems to occur. Nevertheless, as the values in Wagman *et al.* [1982WAG/EVA] are difficult to trace, the value from Robie and Hemingway [1995ROB/HEM] — traced to direct determination in Taras Bryndzia and Kleppa [1988TAR/KLE] — will be selected in PRODATA.

The Pourbaix diagram of As-S system is seen in Figure 3.4-4.

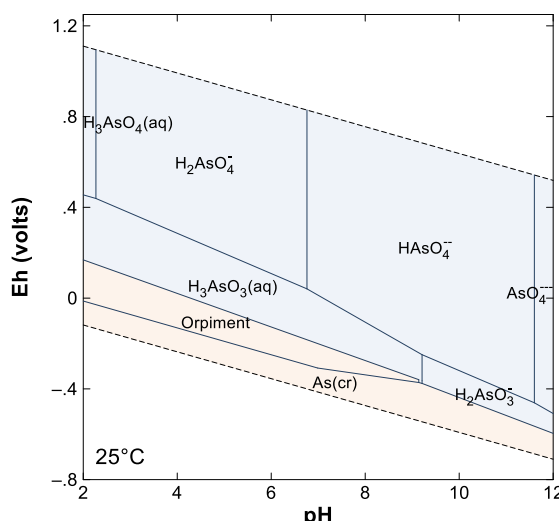


Figure 3.4-4. Pourbaix diagram of 10^{-4} mol kg_w⁻¹ As and S in a hypothetical indifferent 0.1 mol kg_w⁻¹ electrolyte solution using GWB. All solid phases are allowed to precipitate.

Table 3.4-8. Thermodynamic functions of arsenosulphide from native elements in Robie and Hemingway [1995ROB/HEM], and calculated dissolution to oxoanions from NEA-OECD review [2005OLI/NOL].

	$\Delta_r H^\circ$ (kJ mol ⁻¹)	$\Delta_r S^\circ$ (J mol ⁻¹ K ⁻¹)	$\Delta_r G^\circ$ ^b (kJ mol ⁻¹)	$\log_{10} K_s$	$\Delta_f G^\circ$ (kJ mol ⁻¹)
As(cr) + S(cr) ⇌ AsS(cr)	-30.9 ± 5.0 ^a	-4.24 ± 0.59 ^a	-29.64 ± 5.00	5.19 ± 0.88	-29.64 ± 5.00
AsS(cr) + 0.75O ₂ (g) + 2.5H ₂ O ⇌ AsO ₄ ³⁻ + HS ⁻ + 4H ⁺	-150.190 ± 2.685 ^b		-25.911 ± 2.219	4.54 ± 0.39	
AsS(cr) + 0.25O ₂ (g) + 2.5H ₂ O ⇌ H ₂ AsO ₃ ⁻ + HS ⁻ + 2H ⁺	17.310 ± 2.610 ^b		43.560 ± 2.127	-7.63 ± 0.37	
2As(cr) + 3S(cr) ⇌ As ₂ S ₃ (cr)	-91.6 ± 4.2 ^a	-3.93 ± 0.53 ^a	-90.43 ± 4.20	15.84 ± 0.74	-90.43 ± 4.20
As ₂ S ₃ + O ₂ (g) + 6H ₂ O ⇌ 2AsO ₄ ³⁻ + 3HS ⁻ + 9H ⁺	405.500 ± 9.141 ^b		453.358 ± 9.033	-79.42 ± 1.58	
As ₂ S ₃ + 6H ₂ O ⇌ 2H ₂ AsO ₃ ⁻ + 3HS ⁻ + 5H ⁺	328.100 ± 8.158 ^b		375.813 ± 9.317	-65.84 ± 1.63	

a [1995ROB/HEM]; b calculated using $\Delta_r H^\circ$ and $\Delta_r S^\circ$ from [1995ROB/HEM] and $\Delta_f G^\circ$ [2005OLI/NOL].

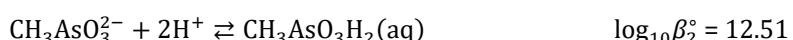
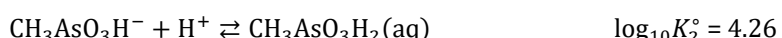
3.4.3.2. Organic Compounds

Due to microbial activity, the methylation of As(V) can occur leading to the formation of monomethylarsonic ($\text{CH}_3\text{AsO}_3\text{H}_2$ (aq)) and dimethylarsinic ($(\text{CH}_3)_2\text{AsO}_2\text{H}$ (aq)) acids [2002SME/KIN; 2019ALL/STA]. These acids are showing acid base properties that are to be taken into account in monitoring of mining activities. As(V) can also be included in arsenosugars and anarsenolipids [2019ALL/STA].

The methylation of As(III) can lead to the formation of monomethylarsonous acid ($\text{CH}_3\text{AsO}_2\text{H}_2$ (aq)), dimethylarsinous acid ($(\text{CH}_3)_2\text{AsOH}$ (aq)), and arsonobetaine AB zwitterion ($(\text{CH}_3)_3\text{As}^+\text{COO}^-$) [2019ALL/STA]. The protonation constants of these acids have not yet been traced in the literature.

As the thermodynamic functions of formation of monomethylarsenic acid and monomethylarsonate ions, and dimethylarsonic acid and dimethylarsinate ions are not known — and are metastable from the point of view of carbon chemistry —, the species will be defined as independent species as presented in Reiller and Descostes [2020REI/DES].

The protonation constants of monomethylarsonate ($\text{CH}_3\text{AsO}_3^{2-}$) — i.e. Monomethylarsonate-2 in PHREEQC, Monomethylarsonate[2-] in CHESS, and Monomethylarsonate-- in GWB — and dimethylarsinate ($(\text{CH}_3)_2\text{AsO}_2^-$) — i.e. Dimethylarsinate- in PHREEQC and GWB, and Dimethylarsinate[-] in CHESS — are taken from Aggett and Kadwani [1983AGG/KAD].



3.5. Carbon

Formation functions of native C as graphite are defined in NEA-OECD reviews [1992GRE/FUG; 2003GUI/FAN; 2020GRE/GAO] from CODATA [1989COX/WAG]. Formation functions of diamond is taken from Robie and Hemingway [1995ROB/HEM] — even of low relevance for monitoring of uranium mining operations. The most stable oxidation states of carbon are C(-IV), as CH_4 , and C(IV) as CO_2 . All the other oxidation states are to some extend metastable or have limited domain of stability. As an example, a Pourbaix diagram using the

thermodynamic functions of C species up to C₁₂ from Shock and Helgeson [1990SHO/HEL] can be drawn in Figure 3.5-1.

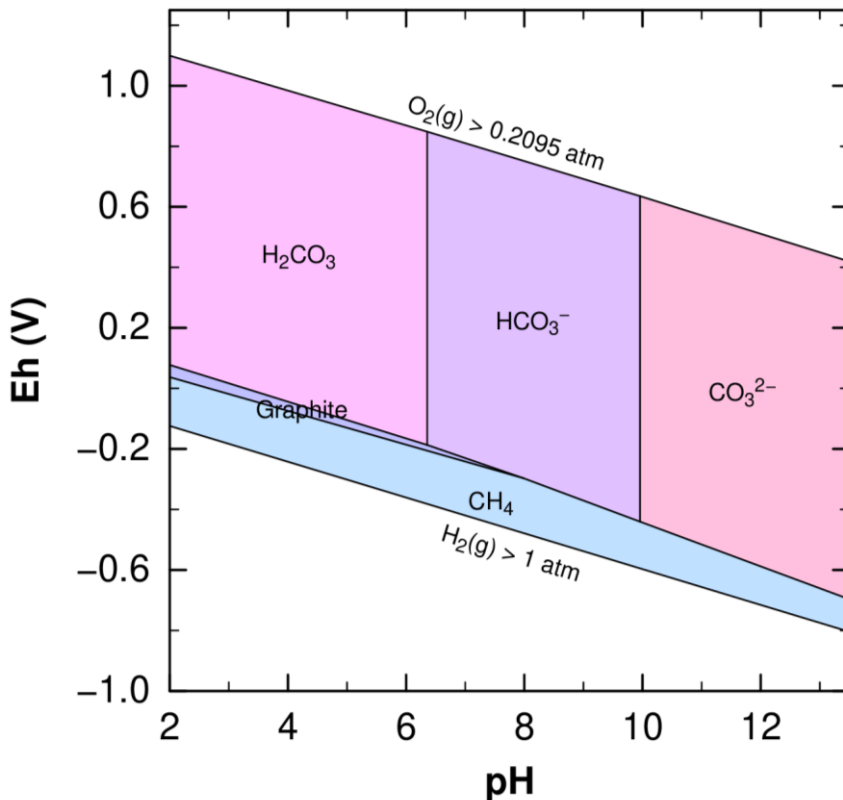


Figure 3.5-1. Pourbaix diagram of carbon $10^{-2} \text{ mol kg}^{-1}$ using PHREEPLOT and the thermodynamic constants calculated from thermodynamic functions for carbon species up to C₁₂ in Shock and Helgeson [1990SHO/HEL].

NEA-OECD reviews [1992GRE/FUG; 2003GUI/FAN; 2020GRE/GAO] provide the thermodynamic functions for CH₄(g), and the dissolution of CO₂(g) in water to the carbonate system, *i.e.* CO₂(aq), HCO₃⁻, and CO₃²⁻ taken from CODATA [1989COX/WAG]. The definition of the common master species can be made using either CO₃²⁻ or HCO₃⁻. The specific ion interaction coefficients for the carbonate ions are taken from NEA-OECD reviews [2003GUI/FAN; 2020GRE/GAO]. The specific ion interaction coefficient values are also given in NEA-OECD reviews [1992GRE/FUG; 2003GUI/FAN; 2020GRE/GAO] (Table 3.5-2). It can be noted that no $\varepsilon(\text{CO}_2(\text{aq}), \text{X}^-)$ are recommended in NEA-OECD reviews, even if Königsberger *et al.* [1999KÖN/KÖN] provided a value for $\lambda_{\text{ClO}_4^-, \text{CO}_2(\text{aq})}$ in the framework of the Pitzer [1991PIT] model.

As in the case of the O₂-H₂-H₂O system, the dissolution of CH₄(g) to CH₄(aq) is not selected in the NEA commissioned selections. The thermodynamic functions are then selected from the functions of reaction calculated from Wagman *et al.* [1982WAG/EVA].

Thermodynamic functions for organic ligands and complexes with metal ions have been selected in Hummel *et al.* [2005HUM/AND] or can be found elsewhere — *e.g.*, [1990SHO/HEL; 1995SHO; 1995SHO/KOR; 1999PRA/SHO] —, but are of no concern for the moment being.

Table 3.5-1. Thermodynamic functions and constants for C(-IV) and C(IV) [1982WAG/EVA; 1992GRE/FUG; 2003GUI/FAN; 2020GRE/GAO].

Reaction	$\Delta_r G_m^\circ$ (kJ mol ⁻¹)	$\log_{10} K^\circ$	$\Delta_f G_m^\circ$ (kJ mol ⁻¹)	$\Delta_r H_m^\circ$ (kJ mol ⁻¹)	$\Delta_f H_m^\circ$ (kJ mol ⁻¹)
$C + 2H_2(g) \rightleftharpoons CH_4(g)$	-50.777 ± 0.16	8.90 ± 0.22	-50.777 ± 0.16	-66.818 ± 0.064	-66.818 ± 0.064
$CH_4(g) \rightleftharpoons CH_4(aq)$	16.390 ± 0.179^a	-2.87 ± 0.03	-34.387 ± 0.240^b	-20.312 ± 0.326^a	-87.13 ± 0.32^b
$C + O_2(g) \rightleftharpoons CO_2(g)$	-394.373 ± 0.133	69.09 ± 0.02	-394.373 ± 0.133	-393.510 ± 0.130	-393.510 ± 0.130
$CO_2(g) \rightleftharpoons CO_2(aq)$	8.403 ± 0.235	-1.47 ± 0.04	-385.970 ± 0.270	-17.750 ± 0.152	-413.260 ± 0.200
$CO_2(g) + H_2O \rightleftharpoons HCO_3^- + H^+$	44.668 ± 0.209	-7.83 ± 0.04	-586.845 ± 0.251	-10.590 ± 0.242	-689.930 ± 0.200
$CO_2(g) + H_2O \rightleftharpoons CO_3^{2-} + 2H^+$	103.613 ± 0.364	-18.15 ± 0.06	-527.900 ± 0.390	4.110 ± 0.285	-675.230 ± 0.250
$HCO_3^- + H^+ \rightleftharpoons CO_2(aq) + H_2O$	-36.265 ± 0.108	6.35 ± 0.02			-9.160 ± 0.040
$CO_3^{2-} + 2H^+ \rightleftharpoons CO_2(aq) + H_2O$	-95.210 ± 0.278	16.68 ± 0.05			-23.860 ± 0.145
$CO_3^{2-} + H^+ \rightleftharpoons HCO_3^-$	-58.945 ± 0.298	10.33 ± 0.05			-14.700 ± 0.150

a calculated from the $\Delta_f G_m^\circ$ or $\Delta_f H_m^\circ$ in [1982WAG/EVA]; b calculated from $\log_{10} K^\circ$ and $\Delta_f G_m^\circ$ or $\Delta_f H_m^\circ$ in [2003GUI/FAN].

Table 3.5-2. Specific ion interaction coefficients for carbonate ions

Specific ion interaction coefficient	Value	Reference
$\varepsilon(Na^+, CO_3^{2-})$	-0.08 ± 0.03	[1992GRE/FUG]
$\varepsilon(K^+, CO_3^{2-})$	0.02 ± 0.01	
$\varepsilon(Na^+, HCO_3^-)$	0.00 ± 0.02	
$\varepsilon(K^+, HCO_3^-)$	-0.06 ± 0.05	

3.6. Metalloids

3.6.1. Silicon

3.6.1.1. Native Silicon and Silicic Acid

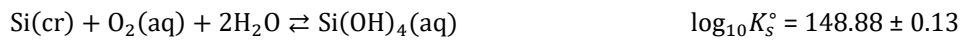
The thermodynamic functions of native silicon and quartz, and solubility constant are taken from Guillaumont *et al.* [2003GUI/FAN]. It can be noted that the functions of formation from forthcoming review of ancillary data are used in Grenthe *et al.* [2020GRE/GAO]. This does not change the constants, but the functions of formation of the complexes are modified. The functions of formation for the silicate ions will be changed when this review will be published.

The common master species is $Si(OH)_4(aq)$. Accounting for the dissolution of $O_2(g)$, the dissolution of $Si(cr)$ is written as follows.



$$\Delta_r G_m^\circ = -(359.175 \pm 1.144) \text{ kJ mol}^{-1}$$

$$\Delta_r H_m^\circ = -(313.640 \pm 3.159) \text{ kJ mol}^{-1}$$



$$\Delta_r H_m^\circ = -(873.600 \pm 3.033) \text{ kJ mol}^{-1}$$

Wagman *et al.* [1982WAG/EVA] are proposing a different value of $\Delta_f G^\circ(Si(OH)_4(aq)) = -1316.6 \text{ kJ mol}^{-1}$ than NEA-OECD [1992GRE/FUG; 2003GUI/FAN] — $\Delta_f G_m^\circ = -(1307.735 \pm 1.156) \text{ kJ mol}^{-1}$ —, or Robie and Hemingway

[1995ROB/HEM] — $\Delta_f G_m^\circ = -(1307.5 \pm 2.1) \text{ kJ mol}^{-1}$. This is changing the value of $\Delta_r G_m^\circ = -368.084 \text{ kJ mol}^{-1}$, $\log_{10} K_s^\circ = 64.49$, and $E^\circ = -0.954 \text{ V}$ for the $\text{Si(cr)} / \text{Si(OH)}_4(\text{cr})$ couple.

As it will be seen in the following, formation functions for silicate phases proposed in Wagman *et al.* [1982WAG/EVA] and Robie and Hemingway [1995ROB/HEM], will end up in large differences in *e.g.* silicate solubility constant calculated using either sources. For the sake of consistency, the phases in Robie and Hemingway [1995ROB/HEM] will be preferred.

3.6.1.2. Allotropic Forms of Solid SiO_2

The formation functions of quartz from Guillaumont *et al.* [2003GUI/FAN] is accepted in PRODATA. There are some other allotropic forms of SiO_2 . The low temperature solubility of quartz is taken from Rimstidt [1997RIM] as follows.

$$\log_{10} m = -\frac{(1107.12 \pm 10.77)}{T} - (0.0254 \pm 0.0247)$$

This is equivalent to the following expression.

$$\log_{10} K^\circ = -\frac{\Delta_r H_m^\circ}{R \ln 10} \times \frac{1}{T} + \frac{\Delta_r S^\circ}{R \ln 10}$$

The following equilibrium is accounted for in PRODATA only as $\log_{10} K_s^\circ$ and $\Delta_r H_m^\circ$. No formation function will be defined as it would change the $\Delta_f G_m^\circ$, $\Delta_f H_m^\circ$, and $S_{f,m}^\circ$ of $\text{Si(OH)}_4(\text{aq})$ from Guillaumont *et al.* [2003GUI/FAN].



$$\Delta_r H_m^\circ = -21.20 \pm 0.21 \text{ kJ mol}^{-1}$$

The same equilibrium for α - SiO_2 with the data from Wagman *et al.* [1982WAG/EVA] ends up with

$$\Delta_r G^\circ = 14.298 \text{ kJ mol}^{-1}$$

$$\log_{10} K_s^\circ = -2.50$$

and will not be included in PRODATA.

Other allotropic forms of SiO_2 are included in PRODATA. The thermodynamic functions of SiO_2 -alpha(cr), SiO_2 -beta(cr), coesite, cristobalite, stishovite, and tridymite are taken from Fabrichnaya *et al.* [2004FAB/SAX], which was developed within the framework of CODATA [1989COX/WAG]. The formation of SiO_2 (am) and chalcedony are taken from Nordstrom *et al.* [1990NOR/PLU]. Finally, the formation of silicatite is taken from Robie and Hemingway [1995ROB/HEM].

Several allotropic forms will be recommended in the forthcoming NEA-OECD review on ancillary data. These data will be included if necessary after publication.

Table 3.6-1. Thermodynamic functions and solubility constants of silica allotropic forms.

Reaction	$\Delta_f G_m^\circ$ (kJ mol ⁻¹)	$\Delta_r G_m^\circ$ (kJ mol ⁻¹)	$\log_{10} K_s^\circ$	$\Delta_f H_m^\circ$ (kJ mol ⁻¹)	$\Delta_r H_m^\circ$ (kJ mol ⁻¹)	Reference
$\text{SiO}_2 + 2\text{H}_2\text{O} \rightleftharpoons \text{Si(OH)}_4(\text{aq})$						
Quartz	-856.287 ± 1.002	22.832 ± 0.571	-4.00 ± 0.10	-910.70 ± 1.00	25.40 ± 3.00	[2003GUI/FAN]
Quartz-lowtemp			-3.74 ± 0.04		21.21 ± 0.21	[1997RIM]
Quartz- α (cr)	-856.283	22.828	-4.00	-910.700	25.400	[2004FAB/SAX]
Quartz- β (cr)	-856.151	22.696	-3.98	-910.495	25.195	[2004FAB/SAX]
Coesite	-851.726	18.271	-3.20	-906.400	21.100	[2004FAB/SAX]
Cristobalite	-852.987	19.532	-3.42	-906.034	20.734	[2004FAB/SAX]
Stishovite	-814.567	-18.888	3.31	-874.000	-11.300	[2004FAB/SAX]
Tridymite	-853.585	20.130	-3.53	-906.913	21.613	[2004FAB/SAX]

Table 3.6-1. Continued

Reaction	$\Delta_f G_m^\circ$ (kJ mol ⁻¹)	$\Delta_r G_m^\circ$ (kJ mol ⁻¹)	$\log_{10} K_s^\circ$	$\Delta_f H_m^\circ$ (kJ mol ⁻¹)	$\Delta_r H_m^\circ$ (kJ mol ⁻¹)	Reference
SiO ₂ (am)			-2.71		13.97	[1990NOR/PLU]
Chalcedony	-853.719	20.264	-3.55	-905.048	19.748	[1990NOR/PLU]
Silicatite	-852.355 ± 0.800	18.90 ± 0.83	-3.31 ± 0.15	-902.1 ± 0.8	16.800 ± 3.059	[1995ROB/HEM]

3.6.1.3. Silicate Ions

The thermodynamic functions and specific ion interaction coefficients of silicate ions are taken from Guillaumont *et al.* [2003GUI/FAN]. The $\varepsilon(\text{Si(OH)}_4\text{(aq)}, \text{X}^+\text{Y}^-)$ values are supposed to be nil.

Figure 3.6-1. Thermodynamic functions and constants for silicate ions [1982WAG/EVA; 1992GRE/FUG; 2003GUI/FAN; 2020GRE/GAO].

Reaction	$\Delta_r G_m^\circ$ (kJ mol ⁻¹)	$\log_{10} K^\circ$	$\Delta_f G_m^\circ$ (kJ mol ⁻¹)	$\Delta_r H_m^\circ$ (kJ mol ⁻¹)	$\Delta_f H_m^\circ$ (kJ mol ⁻¹)
$\text{Si(OH)}_4\text{(aq)} \rightleftharpoons \text{SiO(OH)}_3^- + \text{H}^+$	55.995 ± 0.118	-9.81 ± 0.02	-1 251.740 ± 1.162	25.600 ± 2.001	-1 431.360 ± 3.743
$\text{Si(OH)}_4\text{(aq)} \rightleftharpoons \text{SiO}_2\text{(OH)}_2^{2-} + 2\text{H}^+$	132.084 ± 0.514	-23.14 ± 0.09	-1 175.651 ± 1.265	75.000 ± 15.000	-1 381.960 ± 15.330
$2\text{Si(OH)}_4\text{(aq)} \rightleftharpoons \text{Si}_2\text{O}_3\text{(OH)}_4^{2-} + 2\text{H}^+ + \text{H}_2\text{O}$	108.452 ± 1.714	-19.00 ± 0.30	-2 269.878 ± 2.878		
$2\text{Si(OH)}_4\text{(aq)} \rightleftharpoons \text{Si}_2\text{O}_2\text{(OH)}_5^- + \text{H}^+ + \text{H}_2\text{O}$	46.234 ± 1.714	-8.10 ± 0.30	-2 332.096 ± 2.878		
$3\text{Si(OH)}_4\text{(aq)} \rightleftharpoons \text{Si}_3\text{O}_6\text{(OH)}_3^{3-} + 3\text{H}^+ + 3\text{H}_2\text{O}$	163.249 ± 1.722	-28.60 ± 0.30	-3 048.536 ± 3.870		
$3\text{Si(OH)}_4\text{(aq)} \rightleftharpoons \text{Si}_3\text{O}_5\text{(OH)}_5^{3-} + 3\text{H}^+ + 2\text{H}_2\text{O}$	156.970 ± 1.717	-27.50 ± 0.30	-3 291.955 ± 3.869		
$4\text{Si(OH)}_4\text{(aq)} \rightleftharpoons \text{Si}_4\text{O}_8\text{(OH)}_4^{4-} + 4\text{H}^+ + 4\text{H}_2\text{O}$	207.201 ± 2.865	-36.30 ± 0.50	-4 075.179 ± 5.437		
$4\text{Si(OH)}_4\text{(aq)} \rightleftharpoons \text{Si}_4\text{O}_7\text{(OH)}_5^{3-} + 3\text{H}^+ + 4\text{H}_2\text{O}$	145.554 ± 1.729	-25.50 ± 0.30	-4 136.826 ± 4.934		

Figure 3.6-2. Specific ion interaction coefficients for silicate ions.

Specific ion interaction coefficient	Value	Reference
$\varepsilon(\text{Na}^+, \text{SiO(OH)}_3^-)$	-0.08 ± 0.03	[2003GUI/FAN]
$\varepsilon(\text{Na}^+, \text{SiO}_2\text{(OH)}_2^{2-})$	-0.10 ± 0.07	
$\varepsilon(\text{Na}^+, \text{Si}_2\text{O}_2\text{(OH)}_5^-)$	-0.08 ± 0.04	
$\varepsilon(\text{Na}^+, \text{Si}_2\text{O}_3\text{(OH)}_4^{2-})$	-0.15 ± 0.06	
$\varepsilon(\text{Na}^+, \text{Si}_3\text{O}_5\text{(OH)}_5^{3-})$	-0.25 ± 0.03	
$\varepsilon(\text{Na}^+, \text{Si}_3\text{O}_6\text{(OH)}_3^{3-})$	-0.25 ± 0.03	
$\varepsilon(\text{Na}^+, \text{Si}_4\text{O}_7\text{(OH)}_5^{3-})$	-0.25 ± 0.03	

3.6.2. Lead

3.6.2.1. Native Metal and Free Ion

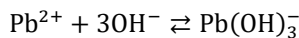
Lead is the end-result of the radioactive decomposition chain of uranium. The thermodynamic functions for Pb(cr) and Pb²⁺ from CODATA [1989COX/WAG], are selected in NEA-OECD reviews [2003GUI/FAN; 2020GRE/GAO] and are used within PRODATA (Table 3.6-2). The common master species is Pb²⁺.

The specific ion interaction coefficients from NEA-OECD reviews [1992GRE/FUG; 2003GUI/FAN; 2020GRE/GAO] will be used for $\varepsilon(\text{Pb}^{2+}, \text{ClO}_4^-)$ and $\varepsilon(\text{Pb}^{2+}, \text{NO}_3^-)$. Given the large uncertainty for the general estimation of $\varepsilon(\text{M}^{2+}, \text{Cl}^-)$ (Figure 2.6-2), the $\varepsilon(\text{Pb}^{2+}, \text{ClO}_4^-) = \varepsilon(\text{Pb}^{2+}, \text{Cl}^-)$ equivalence will be used (Table 3.6-7).

3.6.2.2. Oxo and Hydroxo Compounds

The lead(II) and lead(IV) oxides litharge (PbO(cr)) and plattnerite ($\text{PbO}_2(\text{cr})$) are available from Wagman *et al.* [1982WAG/EVA] or Robie and Hemingway [1995ROB/HEM].

The hydroxo complexes — $\text{Pb}_n(\text{OH})_m^{(2n-m)+}$, with $n = \{1; 2; 3; 4; 6\}$ and $m = \{2; 3; 4; 5; 8\}$ — from Brown and Ekberg [2016BRO/EKB] are accepted in the database. The formation constant and specific ion interaction coefficient of the trihydroxo complex ($\text{Pb}(\text{OH})_3^-$) is fitted using Equation 21, is re-evaluated using the classical SIT model of Equation 18 (Figure 3.6-3).



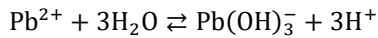
$$\log_{10} \beta_3^\circ = 13.97 \pm 0.14$$

$$\Delta\varepsilon = (0.26 \pm 0.05) \text{ kg}_w \text{ mol}^{-1}$$

$$\Delta_r G_m^\circ = -(79.742 \pm 0.799) \text{ kJ mol}^{-1}$$

$$\Delta_r G_m^\circ = -(575.639 \pm 0.919) \text{ kJ mol}^{-1}$$

$$\varepsilon(\text{Pb}(\text{OH})_3^-, \text{Na}^+) = (0.01 \pm 0.06) \text{ kg}_w \text{ mol}^{-1}$$



$$\log_{10} {}^*\beta_3^\circ = -28.03 \pm 0.14$$

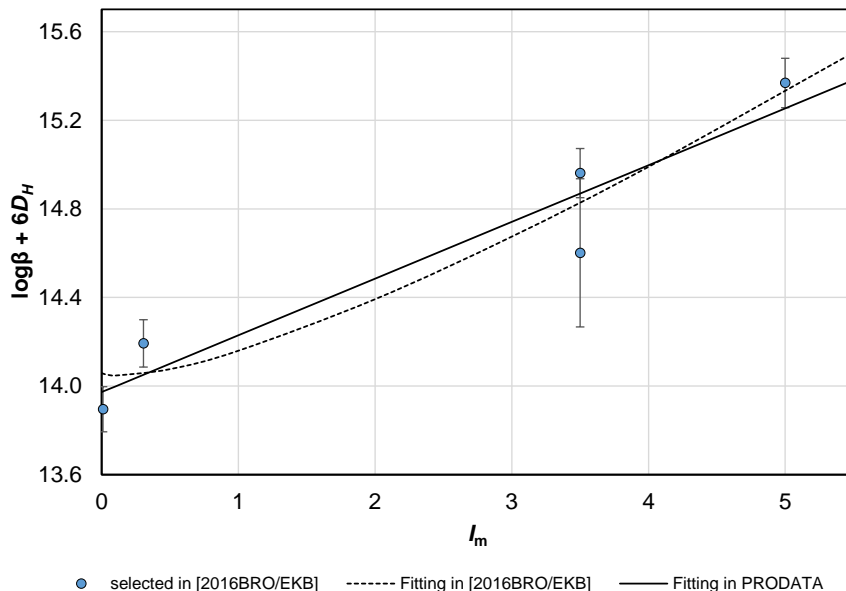
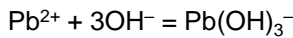


Figure 3.6-3. Re-estimation of $\log_{10}\beta_3^\circ$ and $\varepsilon(\text{Pb}(\text{OH})_3^-, \text{Na}^+)$ using selected data from Brown and Ekberg [2016BRO/EKB] (plain line), and estimation in Brown and Ekberg [2016BRO/EKB] (dashed line).

3.6.2.3. Halide Compounds

The functions of formation of cotunnite (PbCl_2) are defined in Robie and Hemingway [1995ROB/HEM]. The chloride complexes from Powell *et al.* [2009POW/BRO] are included in PRODATA. The specific ion interaction coefficients are calculated from the provided $\Delta\varepsilon$ values.

3.6.2.4. Sulphur and Selenium Compounds

3.6.2.4.1 Sulphur compounds

Wagman *et al.* [1982WAG/EVA] and Robie and Hemingway [1995ROB/HEM] proposed function of formation of galena (PbS), the values of which are relatively close to each other. The values from Robie and Hemingway [1995ROB/HEM] are included without modification even in view of the problem for the S(-II) function of formation (c.f. § 3.3), because S(cr) is considered reference in Robie and Hemingway [1995ROB/HEM].

Estimations of the functions of formation of $\text{Pb}(\text{HS})_n^{(2-n)+}$ complexes — with $n = \{2; 3\}$ — was proposed by Sverjensky *et al.* [1997SVE/SHO].

The solubility of anglesite (PbSO_4) can be retrieved from Wagman *et al.* [1982WAG/EVA], Robie and Hemingway [1995ROB/HEM], and Powell *et al.* [2009POW/BRO]. The values of the three source are in agreement with each other. The solubility constant from Robie and Hemingway [1995ROB/HEM] is not recalculated from the functions of formation of HS^- (c.f. § 3.3).

Oxo sulphate phases are reported in Wagman *et al.* [1982WAG/EVA], *i.e.*, PbSO_4 : $\text{PbO}(\text{cr})$, PbSO_4 : $2\text{PbO}(\text{cr})$, and PbSO_4 : $3\text{PbO}(\text{cr})$. The functions of reaction are used to calculate the $\log_{10} K_s$ and functions of formation relative to CODATA [1989COX/WAG].

Powell *et al.* [2009POW/BRO] recommended the formation constants of $\text{Pb}(\text{SO}_4)(\text{aq})$, with $\Delta\varepsilon = (0.02 \pm 0.03)$ $\text{kg}_w \text{ mol}^{-1}$ in ClO_4^- medium, which allows calculating the value of $\varepsilon(\text{Pb}(\text{SO}_4)(\text{aq}), \text{Na}^+\text{ClO}_4^-) = (0.05 \pm 0.07)$ $\text{kg}_w \text{ mol}^{-1}$. The formation constant for $\text{Pb}(\text{SO}_4)_2^{2-}$ is taken from Smith *et al.* [2004SMI/MAR], and the value of $\varepsilon(\text{Pb}(\text{SO}_4)_2^{2-}, \text{Na}^+)$ can be estimated using either Eq. 26 from $\varepsilon(\text{Pb}(\text{SO}_4)(\text{aq}), \text{Na}^+\text{ClO}_4^-)$ estimated above, or Eq. 27 from $\varepsilon(\text{Pb}^{2+}, \text{ClO}_4^-)$ [1992GRE/FUG; 2003GUI/FAN; 2020GRE/GAO], and $\varepsilon(\text{SO}_4^{2-}, \text{Na}^+)$ [1992GRE/FUG; 2003GUI/FAN; 2020GRE/GAO].

3.6.2.4.2 Selenium compounds

The functions of formation of clausthalite (PbSe) and $\text{PbSeO}_4(\text{cr})$ are taken from Olin *et al.* [2005OLI/NOL].

3.6.2.5. Phosphor and Arsenic Compounds

Nriagu [1984NRI] proposed Gibbs energies of formation and solubility product for numerous phosphate minerals. The general discussion on the account of these data will be done in this chapter, but will be valid for any other phase in Table 1 of Nriagu [1984NRI].

The considered equilibrium for the solubility and Gibbs energy of formation calculation is considered “to the stoichiometric ionization of the minerals” in Nriagu [1984NRI]. In page 320, the authors inform that the phases relations are calculated assuming “ HPO_4^{2-} as the dominant phosphate species”. In Table 1, the solubility of carbonate phases cerussite (PbCO_3) and smithsonite (ZnCO_3) are clearly given relative to CO_3^{2-} , and in page 322 the phase relation between a carbonate and a phosphate is written relative to HCO_3^- .

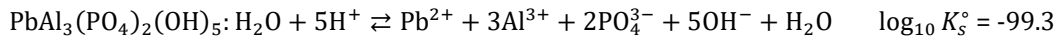
But it is apparent that the solubility of pyromorphite ($\text{Pb}_5(\text{PO}_4)_3\text{Cl}$) is written as follows.



The reported Gibbs energy of formation is calculated relative to National Bureau of Standard values [1968WAG/EVA; 1969WAG/EVA] — $\Delta_f G^\circ = -906.2 \text{ kcal mol}^{-1} = -3794.1 \text{ kJ mol}^{-1}$.

If the $\log_{10} K_s^\circ$ value is used as is, then the Gibbs energy of formation relative to Guillaumont *et al.* [2003GUI/FAN] should be $\Delta_f G^\circ = -3\ 810.639 \text{ kJ mol}^{-1}$, which is in agreement with the value given by Nriagu [1984NRI] knowing the differences in $\Delta_f G^\circ$ of the different species between Guillaumont *et al.* [2003GUI/FAN], Wagman *et al.* [1968WAG/EVA; 1969WAG/EVA] and even Wagman *et al.* [1982WAG/EVA].

The solubility of plumbogummite ($\text{PbAl}_3(\text{PO}_4)_2(\text{OH})_5 \cdot \text{H}_2\text{O}$) should be expressed as follows.



$$\Delta_r G^\circ = 566.8 \text{ kJ mol}^{-1}$$

The reported Gibbs energy of formation is calculated relative to National Bureau of Standard values [1968WAG/EVA; 1969WAG/EVA] — $\Delta_f G^\circ = -1\ 221 \text{ kcal mol}^{-1} = -5\ 112 \text{ kJ mol}^{-1}$.

The Gibbs energy of formation relative to Guillaumont *et al.* [2003GUI/FAN] is then $\Delta_f G^\circ(\text{PbAl}_3(\text{PO}_4)_2(\text{OH})_5 \cdot \text{H}_2\text{O}) = -5\ 139.790 \text{ kJ mol}^{-1}$, which is in agreement with the value given by Nriagu [1984NRI] given the differences in selected values for the functions of formation.

The $\Delta_r G^\circ$ and $\log_{10} K_s$ values of $\text{Pb}_3(\text{AsO}_4)_2(\text{s})$ can be calculated using the $\Delta_f G^\circ$ values from Naumov *et al.* [1974NAU/RYZ] for $\text{Pb}_3(\text{AsO}_4)_2(\text{s})$, Pb^{2+} , and AsO_4^{3-} .

3.6.2.6. Carbon compounds

The formation functions for cerussite (PbCO_3) is given in Wagman *et al.* [1982WAG/EVA], Robie and Hemingway [1995ROB/HEM]. Powell *et al.* [2009POW/BRO] proposed a solubility constant. The three values agree within their uncertainty limits. Functions of reactions of hydrocerussite ($\text{Pb}_3(\text{OH})_2(\text{CO}_3)_2$) and plumbonacrite ($\text{Pb}_{10}(\text{CO}_3)_6\text{O}(\text{OH})_6$) can be calculated from Taylor and Lopata [1984TAY/LOP] — it can be noted that functions of formation and uncertainties are from Robie *et al.* [1979ROB/HEM].

The solubility of $\text{Pb}_2(\text{CO}_3)\text{Cl}_2(\text{s})$ is available in Wagman *et al.* [1982WAG/EVA] (PbCl_2 : $\text{PbCO}_3(\text{cr})$), and Powell *et al.* [2009POW/BRO]. The two obtained values are very different $\log_{10} K_s$ — *i.e.*, -19.86 ± 0.23 [1982WAG/EVA], and -9.93 ± 0.08 [2009POW/BRO]. As the origin of the data onto which the analysis is done is available in literature, the value from Powell *et al.* [2009POW/BRO] will be used.

Powell *et al.* [2009POW/BRO] also gave an indicative value for $\text{Pb}(\text{CO}_3)(\text{aq})$, and two provisional values for $\text{Pb}(\text{CO}_3)_2^{2-}$ — with a $\Delta\varepsilon$ value — and PbHCO_3^+ — which ε value can be estimated from Eq. 26.

3.6.2.7. Silicate Compounds

$\text{Pb}_2\text{SiO}_4(\text{cr})$ and $\text{PbSiO}_3(\text{cr})$ functions of formation are not included from the functions of reaction calculated from Wagman *et al.* [1982WAG/EVA].

3.6.2.8. Tables of Thermodynamic Constants, Functions, and Specific Ion Interaction Coefficients for Pb

Table 3.6-2. Thermodynamic functions and constants for free ion, oxo, and hydroxo compounds of Pb.

Reaction	$\log_{10}\beta^\circ$	$\Delta_r G_m^\circ$ (kJ mol $^{-1}$)	$\Delta_f G_m^\circ$ (kJ mol $^{-1}$)	$\Delta_r H_m^\circ$ (kJ mol $^{-1}$)	$\Delta_f H_m^\circ$ (kJ mol $^{-1}$)
$\text{Pb}(\text{cr}) \rightleftharpoons \text{Pb}^{2+} + 2\text{e}^-$	4.25 ± 0.07	-24.238 ± 0.399	-24.238 ± 0.399^a	0.920 ± 0.250	0.920 ± 0.250^a
$\text{Pb}(\text{cr}) + 0.5\text{O}_2(\text{aq}) + 2\text{H}^+ \rightleftharpoons \text{Pb}^{2+} + \text{H}_2\text{O}$	47.23 ± 0.03	-269.567 ± 0.199		-279.060 ± 0.369	
Massicot					
$\text{PbO} + 2\text{H}^+ \rightleftharpoons \text{Pb}^{2+} + \text{H}_2\text{O}$	12.91 ± 0.12	-73.669 ± 0.675^b	-187.709 ± 0.785	-70.210 ± 5.603^b	-214.700 ± 5.609

Table 3.6-2. Continued

Reaction	$\log_{10}\beta^\circ$	$\Delta_r G_m^\circ$ (kJ mol ⁻¹)	$\Delta_f G_m^\circ$ * (kJ mol ⁻¹)	$\Delta_r H_m^\circ$ (kJ mol ⁻¹)	$\Delta_f H_m^\circ$ * (kJ mol ⁻¹)
Litharge					
$PbO + 2H^+ \rightleftharpoons Pb^{2+} + H_2O$	12.72 ± 0.01	-72.629 ± 0.072^b	-188.749 ± 0.408	-68.540 ± 5.559^b	-216.370 ± 5.564
$PbO: 0.333H_2O(cr) + 2H^+ \rightleftharpoons Pb^{2+} + 1.333H_2O$	12.97 ± 0.70	-74.023 ± 3.992^b	266.323 ± 4.012		
Plattnerite					
$PbO_2 + 2H^+ \rightleftharpoons Pb^{2+} + 0.5O_2(aq) + H_2O$	6.31 ± 0.28	-36.029 ± 1.602	-217.160 ± 1.711	-15.980 ± 5.387	-274.780 ± 5.411
Minium					
$Pb_3O_4 + 6H^+ \rightleftharpoons 3Pb^{2+} + 0.5O_2(aq) + 3H_2O$	30.71 ± 0.17	-175.288 ± 0.955	-600.657 ± 1.856	-150.040 ± 16.502	-710.540 ± 16.526
$Pb(OH)_2(cr) + 2H^+ \rightleftharpoons Pb^{2+} + 2H_2O$	8.14 ± 0.28	-46.488 ± 1.575	-452.030 ± 1.627		
$Pb^{2+} + H_2O \rightleftharpoons Pb(OH)^+ + H^+$	-7.49 ± 0.13^c	42.753 ± 0.742	-218.625 ± 0.843	56.000 ± 1.500^c	-228.910 ± 1.521
$Pb^{2+} + 2H_2O \rightleftharpoons Pb(OH)_2(aq) + 2H^+$	-16.99 ± 0.06^c	96.980 ± 0.342	-401.538 ± 0.532	90.000 ± 1.000^c	-480.740 ± 1.034
$Pb^{2+} + 3H_2O \rightleftharpoons Pb(OH)_3^- + 3H^+$	-28.03 ± 0.14^c	160.019 ± 0.819	-575.639 ± 0.919	135.800 ± 3.000^c	-720.770 ± 3.013
$2Pb^{2+} + H_2O \rightleftharpoons Pb_2(OH)^{3+} + H^+$	-6.73 ± 0.31^c	38.415 ± 1.769	-247.201 ± 1.941		
$3Pb^{2+} + 4H_2O \rightleftharpoons Pb_3(OH)_4^{2+} + 4H^+$	-23.46 ± 0.10^c	133.911 ± 0.571	-887.363 ± 1.336	111.400 ± 5.600^c	$-1\ 029.160 \pm 5.652$
$3Pb^{2+} + 5H_2O \rightleftharpoons Pb_3(OH)_5^+ + 4H^+$	-31.11 ± 0.10^c	177.577 ± 0.571	$-1\ 080.837 \pm 1.342$	146.000 ± 3.000	$-1\ 280.390 \pm 3.099$
$4Pb^{2+} + 4H_2O \rightleftharpoons Pb_4(OH)_4^{4+} + 4H^+$	-20.71 ± 0.18^c	118.214 ± 1.027	-927.298 ± 1.905	85.00 ± 2.000^c	$-1\ 054.640 \pm 2.242$
$6Pb^{2+} + 8H_2O \rightleftharpoons Pb_6(OH)_8^{4+} + 8H^+$	-43.27 ± 0.47^c	246.987 ± 2.683	$-1\ 795.561 \pm 3.611$	210.900 ± 7.100^c	$-2\ 070.220 \pm 7.264$

a [2003GUI/FAN]; b [1982WAG/EVA]; c [2016BRO/EKB].

* calculated from $\Delta_f G_m^\circ$ and $\Delta_f H_m^\circ$ from [2003GUI/FAN].

The Pourbaix diagram of the Pb-H₂O system is plotted in Figure 3.6-4. The slight difference in solubility limits are caused by the activity representation of GWB.

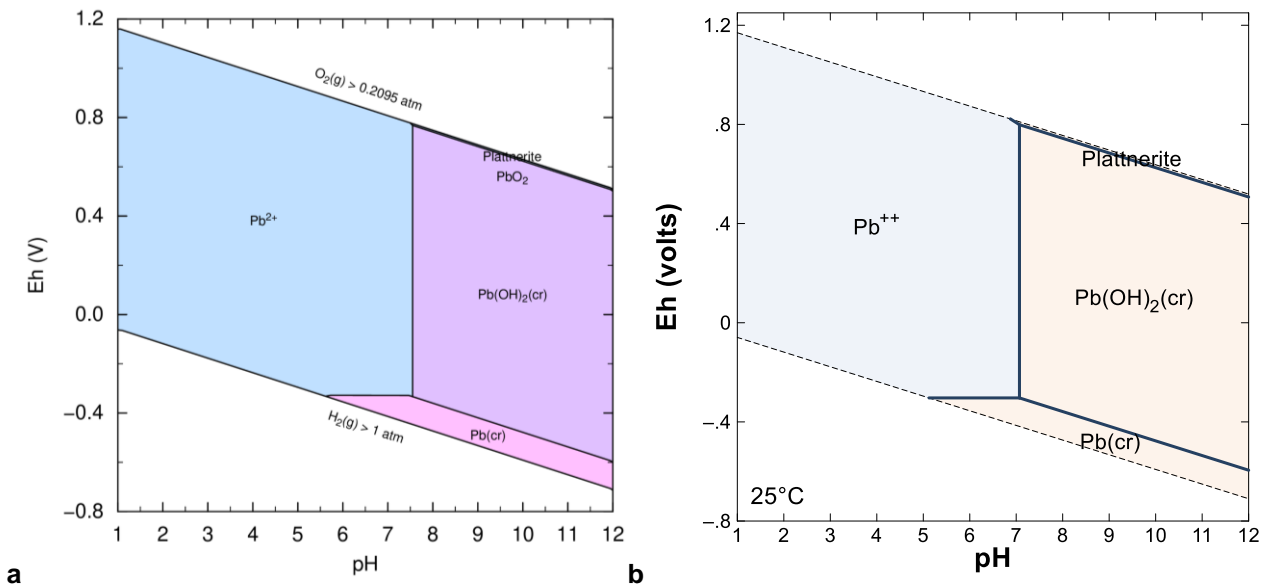


Figure 3.6-4. Pourbaix diagram of 10^{-6} mol kg_w⁻¹ Pb in a hypothetical indifferent 0.1 mol kg_w⁻¹ electrolyte solution using PHREEPLOT (a) and GWB (b). All solid phases are allowed to precipitate.

Table 3.6-3. Thermodynamic functions and constants for halogen compounds of Pb.

Reaction	$\log_{10}\beta^\circ$	$\Delta_r G_m^\circ$ (kJ mol ⁻¹)	$\Delta_f G_m^\circ$ * (kJ mol ⁻¹)	$\Delta_r H_m^\circ$ (kJ mol ⁻¹)	$\Delta_f H_m^\circ$ * (kJ mol ⁻¹)
PbF ₂ (cr) ⇄ Pb ²⁺ + 2F ⁻	-6.15 ± 0.21	35.090 ± 1.221 ^a	-622.374 ± 1.888	-2.960 ± 5.563 ^a	-666.820 ± 5.719
Cotunnite					
PbCl ₂ (cr) ⇄ Pb ²⁺ + 2Cl ⁻	-4.82 ± 0.11	27.500 ± 0.640 ^a	-314.172 ± 0.790	26.100 ± 0.200 ^a	-359.340 ± 0.377
Pb ²⁺ + F ⁻ ⇄ PbF ⁺	2.06	-11.757 ^b	-317.518	-0.925 ^b	-335.355
Pb ²⁺ + 2F ⁻ ⇄ PbF ₂ (aq)	3.42	-19.523 ^b	-606.807	-9.468 ^b	-679.248
Pb ²⁺ + Cl ⁻ ⇄ PbCl ⁺	1.50 ± 0.03 ^c	-8.562 ± 0.171	-164.017 ± 0.450	10.3 ± 1.5 ^c	-155.860 ± 1.524
Pb ²⁺ + 2Cl ⁻ ⇄ PbCl ₂ (aq)	2.10 ± 0.05 ^c	-11.987 ± 0.285	-298.659 ± 0.543	17.0 ± 0.6 ^c	-316.240 ± 0.680
Pb ²⁺ + 3Cl ⁻ ⇄ PbCl ₃ ⁻	2.00 ± 0.10 ^c	-11.416 ± 0.571	-429.305 ± 0.780	14.7 ± 1.0 ^c	-485.620 ± 1.074
Pb ²⁺ + Br ⁻ ⇄ PbBr ⁺	1.11 ± 0.98	-6.310 ± 5.570 ^a	-134.398 ± 5.587		
Pb ²⁺ + 2Br ⁻ ⇄ PbBr ₂ (aq)	1.45 ± 0.83	-8.250 ± 4.764 ^a	-240.188 ± 4.792		
Pb ²⁺ + 3Br ⁻ ⇄ PbBr ₃ ⁻	1.19 ± 0.08	-6.790 ± 0.478 ^a	-342.578 ± 0.799		
Pb ²⁺ + BrO ₃ ⁻ ⇄ PbBrO ₃ ⁺	1.84 ± 0.13	-10.500 ± 0.721 ^a	-15.668 ± 0.202		

a [1982WAG/EVA]; b [1997SVE/SHO]; c [2009POW/BRO].

* calculated from $\Delta_f G_m^\circ$ and $\Delta_f H_m^\circ$ from [2003GUI/FAN].**Table 3.6-4. Thermodynamic function and constants for S and Se compounds of Pb.**

Reaction	$\log_{10}\beta^\circ$	$\Delta_r G_m^\circ$ (kJ mol ⁻¹)	$\Delta_f G_m^\circ$ * (kJ mol ⁻¹)	$\Delta_r H_m^\circ$ (kJ mol ⁻¹)	$\Delta_f H_m^\circ$ * (kJ mol ⁻¹)
PbS(cr) + H ⁺ ⇄ Pb ²⁺ + HS ⁻	-14.78 ± 0.97	84.350 ± 5.558 ^a	-96.345 ± 5.960	81.100 ± 6.645 ^a	-96.480 ± 6.817
Galena					
PbS + H ⁺ ⇄ Pb ²⁺ + HS ⁻	-14.86 ± 0.14	84.805 ± 0.795 ^b	-96.800 ± 2.000	81.100 ± 1.833 ^b	-98.300 ± 2.000
Pb ²⁺ + 2HS ⁻ ⇄ Pb(HS) ₂ (aq)	14.71	-83.965 ^c	-83.717	-64.312 ^c	-95.992
Pb ²⁺ + 3HS ⁻ ⇄ Pb(HS) ₃ ⁻	16.01	-91.383 ^c	-78.892	-72.693 ^c	-120.673
Pb(SO ₄)(cr) ⇄ Pb ²⁺ + SO ₄ ²⁻	-7.74 ± 0.09	44.180 ± 0.521 ^a	-812.422 ± 0.250	8.970 ± 1.533 ^a	-917.390 ± 1.604
Pb(SO ₄)(s) ⇄ Pb ²⁺ + SO ₄ ²⁻	-7.80 ± 0.05 ^d	44.523 ± 0.285	-812.765 ± 0.644		
PbSO ₄ : PbO(cr) + 2H ⁺ ⇄ 2Pb ²⁺ + SO ₄ ²⁻ + H ₂ O					
	-0.28 ± 0.15	1.581 ± 0.840	-1 031.201 ± 0.953	-27.000 ± 1.763	-1 166.330 ± 2.765
PbSO ₄ : 2PbO(cr) + 4H ⁺ ⇄ 3Pb ²⁺ + SO ₄ ²⁻ + 2H ₂ O	10.88 ± 0.15	-62.078 ± 0.840 ^a	-1 228.920 ± 0.953	-86.930 ± 2.630 ^a	-1 391.310 ± 2.765
PbSO ₄ : 3PbO(cr) + 6H ⁺ ⇄ 4Pb ²⁺ + SO ₄ ²⁻ + 3H ₂ O	22.10 ± 0.22	-126.137 ± 1.227	-1 426.239 ± 1.109	-146.860 ± 2.713	-1 616.290 ± 2.922
Pb ²⁺ + SO ₄ ²⁻ ⇄ Pb(SO ₄)(aq)	2.72 ± 0.05 ^d	-15.526 ± 0.285	-783.768 ± 0.644		
Pb ²⁺ + 2SO ₄ ²⁻ ⇄ Pb(SO ₄) ₂ ²⁻	3.47 ^e				
PbSe(cr) + 2H ⁺ ⇄ Pb ²⁺ + H ₂ Se(aq)					
	-16.68 ± 1.30	95.193 ± 7.418	-97.936 ± 7.694 ^f	113.720 ± 7.322	-98.500 ± 7.600 ^f
PbSeO ₄ (cr) ⇄ Pb ²⁺ + SeO ₄ ²⁻	-6.90 ± 0.25	39.385 ± 1.427	-503.108 ± 2.060 ^f	4.720 ± 2.530	-607.300 ± 4.326 ^f

a [1982WAG/EVA]; b [1995ROB/HEM] with modified $\Delta_f G_m^\circ$ and $\Delta_f H_m^\circ$ for HS⁻; c [1997SVE/SHO]; d [2009POW/BRO]; e [2004SMI/MAR];

f [2005OLI/NOL].

* calculated from $\Delta_f G_m^\circ$ and $\Delta_f H_m^\circ$ from [2003GUI/FAN], unless otherwise noted.

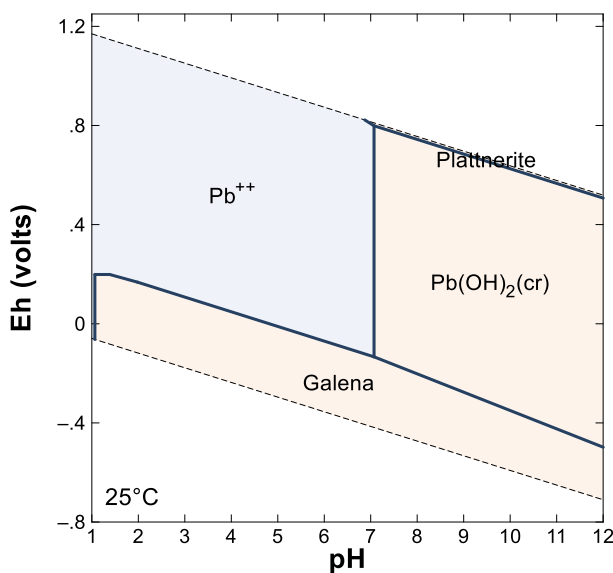


Figure 3.6-5. Pourbaix diagram of 10^{-6} mol $\text{kg}_{\text{w}}^{-1}$ Pb in a hypothetical $0.1 \text{ mol kg}_{\text{w}}^{-1}$ indifferent electrolyte solution containing 10^{-4} mol $\text{kg}_{\text{w}}^{-1}$ of S using GWB. All solid phases are allowed to precipitate.

Table 3.6-5. Thermodynamic function and constants for N, P, and As compounds of Pb.

Reaction	$\log_{10}\beta^\circ$	$\Delta_r G_m^\circ$ (kJ mol ⁻¹)	$\Delta_f G_m^\circ$ (* kJ mol ⁻¹)	$\Delta_r H_m^\circ$ (kJ mol ⁻¹)	$\Delta_f H_m^\circ$ (* kJ mol ⁻¹)
$\text{Pb}^{2+} + \text{NO}_3^- \rightleftharpoons \text{Pb}(\text{NO}_3)_+$	1.51 ± 1.12	-8.630 ± 6.374^a	-143.662 ± 6.400		
$\text{Pb}^{2+} + 2\text{NO}_3^- \rightleftharpoons \text{Pb}(\text{NO}_3)_2(\text{aq})$	0.88 ± 0.16	-4.600 ± 5.372^a	-250.846 ± 0.240		
$\text{PbHPO}_4(\text{s}) \rightleftharpoons \text{Pb}^{2+} + \text{HPO}_4^{2-}$	-11.4 ± 0.3^b	65.072 ± 1.712	-1185.295 ± 2.367		
$\text{PbHPO}_4(\text{s}) \rightleftharpoons \text{Pb}^{2+} + \text{PO}_4^{3-} + \text{H}^+$		-23.75 ± 0.30	135.566 ± 1.721		
$\text{Pb}(\text{H}_2\text{PO}_4)_2(\text{s}) \rightleftharpoons \text{Pb}^{2+} + 2\text{H}_2\text{PO}_4^-$		-9.84^c	56.191	-2354.731	
$\text{Pb}(\text{H}_2\text{PO}_4)_2(\text{s}) \rightleftharpoons \text{Pb}^{2+} + 2\text{PO}_4^{3-} + 4\text{H}^+$		-48.97	279.511		
$\text{Pb}_3(\text{PO}_4)_2(\text{cr}) \rightleftharpoons 3\text{Pb}^{2+} + 2\text{PO}_4^{3-}$		-44.4 ± 1.0^b	253.437 ± 5.718	-2377.133 ± 6.638	
Hydroxypyromorphite $\text{Pb}_5(\text{PO}_4)_3(\text{OH}) + 4\text{H}^+ \rightleftharpoons 5\text{Pb}^{2+} + 3\text{HPO}_4^{2-} + \text{H}_2\text{O}$		-25.76^c	147.026	-3793.311	
$\text{Pb}_5(\text{PO}_4)_3(\text{OH}) + \text{H}^+ \rightleftharpoons 5\text{Pb}^{2+} + 3\text{PO}_4^{3-} + \text{H}_2\text{O}$		-62.81	358.508		
Pyromorphite $\text{Pb}_5(\text{PO}_4)_3\text{Cl} \rightleftharpoons 5\text{Pb}^{2+} + 3\text{PO}_4^{3-} + \text{Cl}^-$		-84.4^d	481.759	-3810.639	
Plumbogummite $\text{PbAl}_3(\text{PO}_4)_2(\text{OH})_5:\text{H}_2\text{O} \rightleftharpoons \text{Pb}^{2+} + 3\text{Al}^{3+} + 2\text{PO}_4^{3-} + 5\text{OH}^- + \text{H}_2\text{O}$		-99.3^d	566.809	-5139.790	
$\text{PbAl}_3(\text{PO}_4)_2(\text{OH})_5:\text{H}_2\text{O} + 5\text{H}^+ \rightleftharpoons \text{Pb}^{2+} + 3\text{Al}^{3+} + 2\text{PO}_4^{3-} + 6\text{H}_2\text{O}$		-29.29	167.209		
Hinsdalite $\text{PbAl}_3(\text{PO}_4)(\text{OH})_6:\text{SO}_4 \rightleftharpoons \text{Pb}^{2+} + 3\text{Al}^{3+} + \text{PO}_4^{3-} + \text{SO}_4^{2-} + 6\text{OH}^-$		-99.1^d			
$\text{PbAl}_3(\text{PO}_4)(\text{OH})_6:\text{SO}_4 + 6\text{H}^+ \rightleftharpoons \text{Pb}^{2+} + 3\text{Al}^{3+} + \text{PO}_4^{3-} + \text{SO}_4^{2-} + 6\text{H}_2\text{O}$		-15.1			
$\text{Pb}^{2+} + \text{HPO}_4^{2-} \rightleftharpoons \text{PbHPO}_4(\text{aq})$		-3.20 ± 0.20^b	-18.837 ± 1.142	-1139.060 ± 1.994	
$\text{Pb}^{2+} + \text{PO}_4^{3-} + \text{H}^+ \rightleftharpoons \text{PbHPO}_4(\text{aq})$		15.65 ± 0.20	-89.331 ± 1.154		
$\text{Pb}^{2+} + 2\text{PO}_4^{3-} + 2\text{H}^+ \rightleftharpoons \text{Pb}(\text{P}_2\text{O}_7)^{2-} + \text{H}_2\text{O}$		31.99 ± 0.36	-182.599 ± 2.063^a	-2020.679 ± 2.416	
$\text{Pb}_3(\text{AsO}_4)_2(\text{s}) \rightleftharpoons 3\text{Pb}^{2+} + 2\text{AsO}_4^{3-}$		-33.94	193.719^e	-1563.153	

a [1982WAG/EVA]; b [2009POW/BRO]; c [1974NRI]; d [1984NRI]; e [1974NAU/RYZ].

* calculated from $\Delta_f G_m^\circ$ and $\Delta_f H_m^\circ$ from [2003GUI/FAN], unless otherwise noted.

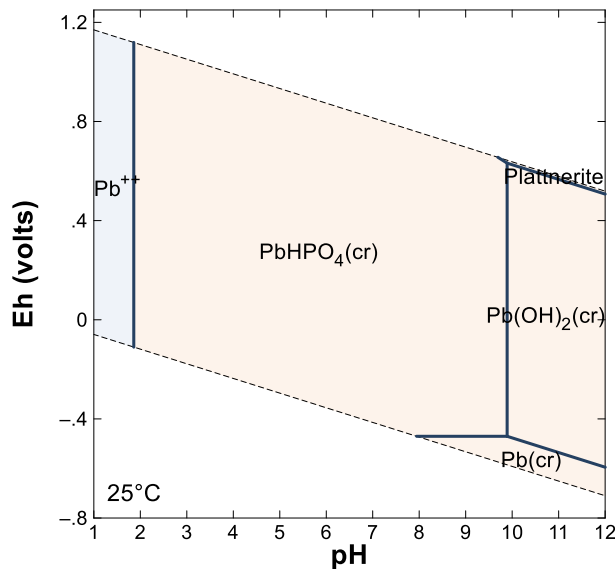


Figure 3.6-6. Pourbaix diagram of 10^{-6} mol kg_w⁻¹ Pb in a hypothetical indifferent 0.1 mol kg_w⁻¹ electrolyte solution containing 10^{-4} mol kg_w⁻¹ of P using GWB. All solid phases are allowed to precipitate.

Table 3.6-6. Thermodynamic function and constants for C compounds of Pb.

Reaction	$\log_{10}\beta^\circ$	$\Delta_r G_m^\circ$ (kJ mol ⁻¹)	$\Delta_f G_m^\circ$ (kJ mol ⁻¹)	$\Delta_r H_m^\circ$ (kJ mol ⁻¹)	$\Delta_f H_m^\circ$ (kJ mol ⁻¹)
Cerrusite					
$\text{Pb}(\text{CO}_3)(\text{s}) \rightleftharpoons \text{Pb}^{2+} + \text{CO}_3^{2-}$	-13.02 ± 0.26	74.300 ± 1.559^a	-626.438 ± 1.656	24.900 ± 1.158^a	-699.210 ± 1.210
$\text{PbO}: \text{PbCO}_3(\text{cr}) + 2\text{H}^+ \rightleftharpoons 2\text{Pb}^{2+} + \text{CO}_3^{2-} + \text{H}_2\text{O}$	-0.51 ± 0.35	2.901 ± 1.999	-816.417 ± 2.188	-47.970 ± 3.180	-911.250 ± 3.229
Hydrocerrusite					
$\text{Pb}_3(\text{OH})_2(\text{CO}_3)_2 + 2\text{H}^+ \rightleftharpoons 3\text{Pb}^{2+} + 2\text{CO}_3^{2-} + 2\text{H}_2\text{O}$	-17.82 ± 0.46	101.718 ± 2.626^b	-1704.512 ± 2.990		
Plumbonacrite					
$\text{Pb}_{10}(\text{CO}_3)_6\text{O}(\text{OH})_6 + 8\text{H}^+ \rightleftharpoons 10\text{Pb}^{2+} + 6\text{CO}_3^{2-} + 7\text{H}_2\text{O}$	-41.80 ± 0.61	238.613 ± 3.463^b	-5308.373 ± 3.080		
$\text{Pb}^{2+} + \text{CO}_3^{2-} \rightleftharpoons \text{Pb}(\text{CO}_3)(\text{aq})$	6.45 ± 0.72^c				
$\text{Pb}^{2+} + 2\text{CO}_3^{2-} \rightleftharpoons \text{Pb}(\text{CO}_3)_2^{2-}$	10.13 ± 0.24^c	-57.822 ± 1.370	-1137.860 ± 1.626		
$\text{Pb}^{2+} + \text{HCO}_3^- \rightleftharpoons \text{Pb}(\text{HCO}_3)^+$	1.86 ± 0.10^c	-10.617 ± 0.571	-621.700 ± 0.740		
$\text{Pb}^{2+} + \text{CO}_3^{2-} + \text{H}^+ \rightleftharpoons \text{Pb}(\text{HCO}_3)^+$	12.19 ± 0.09	-69.562 ± 0.487			
$\text{Pb}_2(\text{CO}_3)\text{Cl}_2(\text{s}) \rightleftharpoons 2\text{Pb}^{2+} + \text{CO}_3^{2-} + 2\text{Cl}^-$	-9.93 ± 0.08^c	56.681 ± 0.457	-895.491 ± 1.026		

a [1995ROB/HEM]; b [1984TAY/LOP]; c [2009POW/BRO]

* calculated from $\Delta_r G_m^\circ$ and $\Delta_f H_m^\circ$ from [2003GUI/FAN], unless otherwise noted.

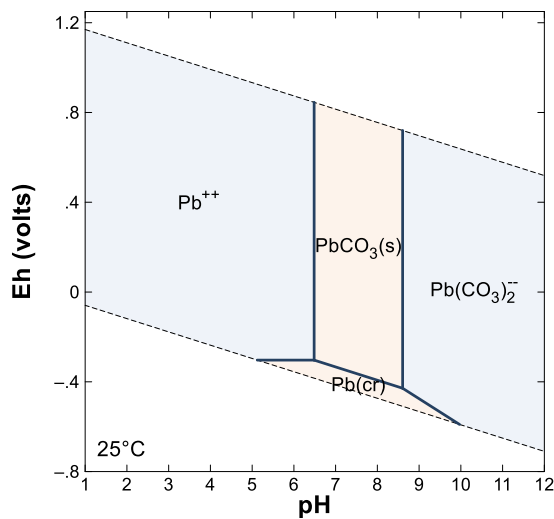


Figure 3.6-7. Pourbaix diagram of 10^{-6} mol kg^{-1} Pb in a hypothetical indifferent 0.1 mol kg^{-1} electrolyte solution in equilibrium with $P(\text{CO}_2) = 10^{-2}$ atm, using GWB; all solid phases are allowed to precipitate.

Table 3.6-7. Specific ion interaction coefficients for Pb complexes in PRODATA.

Specific ion interaction coefficient	Value $\pm \sigma$	Reference
$\varepsilon(\text{Pb}^{2+}, \text{ClO}_4^-/\text{Cl}^-)$	0.15 ± 0.02	[1992GRE/FUG]
$\varepsilon(\text{Pb}^{2+}, \text{NO}_3^-)$	-0.20 ± 0.12	[1992GRE/FUG]
$\varepsilon(\text{Pb}(\text{OH})^+, \text{NO}_3^-)$	0.19 ± 0.15	from $\Delta\varepsilon$ in [2016BRO/EKB]
$\varepsilon(\text{Pb}(\text{OH})^+, \text{ClO}_4^-/\text{Cl}^-)$	-0.44 ± 0.03	from $\Delta\varepsilon$ in [2016BRO/EKB]
$\varepsilon(\text{Pb}(\text{OH})_2(\text{aq}), \text{NO}_3^-)$	-0.49 ± 0.12	from $\Delta\varepsilon$ in [2016BRO/EKB]
$\varepsilon(\text{Pb}(\text{OH})_3^-, \text{Na}^+)$	0.01 ± 0.04	Extrapolation from [2016BRO/EKB]
$\varepsilon(\text{Pb}_2(\text{OH})^{3+}, \text{ClO}_4^-/\text{Cl}^-)$	0.27 ± 0.10	from $\Delta\varepsilon$ in [2016BRO/EKB]
$\varepsilon(\text{Pb}_3(\text{OH})^{3+}, \text{ClO}_4^-/\text{Cl}^-)$	-0.50 ± 0.10	from $\Delta\varepsilon$ in [2016BRO/EKB]
$\varepsilon(\text{Pb}_4(\text{OH})^{4+}, \text{ClO}_4^-/\text{Cl}^-)$	-0.50 ± 0.10	from $\Delta\varepsilon$ in [2016BRO/EKB]
$\varepsilon(\text{Pb}_6(\text{OH})^{8+}, \text{ClO}_4^-/\text{Cl}^-)$	-0.50 ± 0.10	from $\Delta\varepsilon$ in [2016BRO/EKB]
$\varepsilon(\text{PbF}^+, \text{Cl}^-)$	0.09	Estimation from [1990CIA] and $\varepsilon(\text{Pb}^{2+}, \text{Cl}^-) = \varepsilon(\text{Pb}^{2+}, \text{ClO}_4^-)$
$\varepsilon(\text{PbCl}^+, \text{Cl}^-)$	0.04 ± 0.01	from $\Delta\varepsilon$ in [2009POW/BRO] and $\varepsilon(\text{Pb}^{2+}, \text{Cl}^-) = \varepsilon(\text{Pb}^{2+}, \text{ClO}_4^-)$
$\varepsilon(\text{PbCl}_2(\text{aq}), \text{Na}^+\text{Cl}^-)$	-0.05 ± 0.02	Idem
$\varepsilon(\text{PbCl}_2^-, \text{Na}^+)$	-0.08 ± 0.03	Idem
$\varepsilon(\text{Pb}(\text{SO}_4)(\text{aq}), \text{Na}^+\text{ClO}_4^-/\text{Cl}^-)$	0.05 ± 0.07	from $\Delta\varepsilon$ in [2009POW/BRO]
$\varepsilon(\text{Pb}(\text{SO}_4)_2^{2-}, \text{Na}^+)$	-0.02 ± 0.04	Estimation from Eq. 26 [1990CIA]
	-0.03 ± 0.12	Estimation from Eq. 27 [1990CIA]
$\varepsilon(\text{Pb}(\text{CO}_3)(\text{aq}), \text{Na}^+\text{ClO}_4^-/\text{Cl}^-)$	0.04 ± 0.02	Estimation from Eq. 26 [1990CIA]
$\varepsilon(\text{Pb}(\text{CO}_3)_2^{2-}, \text{Na}^+)$	-0.20 ± 0.12	from $\Delta\varepsilon$ in [2009POW/BRO]
$\varepsilon(\text{PbHCO}_3^{\ddagger}, \text{ClO}_4^-/\text{Cl}^-)$	0.08 ± 0.03	Estimation from Eq. 26 [1990CIA]

3.6.3. Aluminium

3.6.3.1. Native Metal and Free ion

The thermodynamic functions of $\text{Al}(\text{cr})$ and Al^{3+} are taken from Guillaumont *et al.* [2003GUI/FAN]. The common master species is Al^{3+} . The only specific ion interaction coefficient selected is $\varepsilon(\text{Al}^{3+}, \text{Cl}^-)$ [1980CIA].

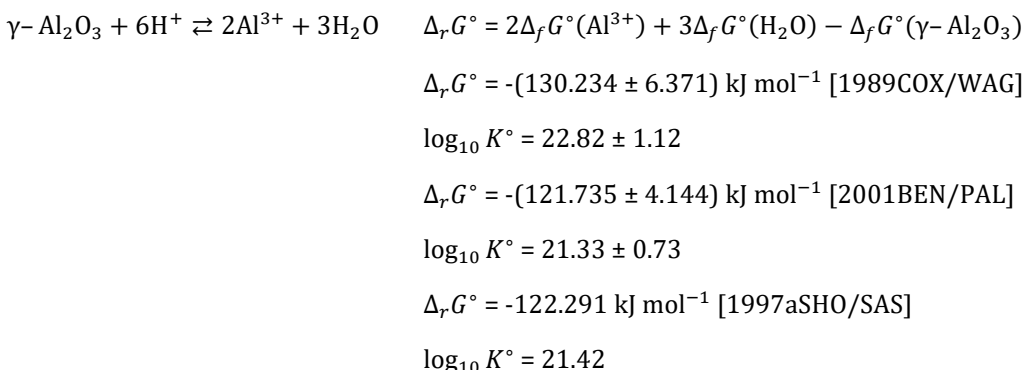
It can be noted that slight differences of functions of formation for Al^{3+} are existing in the literature, *i.e.*, $\Delta_f G^\circ = -(485 \pm 20) \text{ kJ mol}^{-1}$ [1982WAG/EVA], $\Delta_f G^\circ = -(491.507 \pm 3.308) \text{ kJ mol}^{-1}$ [2003GUI/FAN], and $\Delta_f G^\circ = -(487.2 \pm 2.3) \text{ kJ mol}^{-1}$ [2001BEN/PAL]. These are leading to slight differences in the potential of the $\text{Al}^{3+}/\text{Al}(\text{cr})$ couple.

$\text{Al}^{3+} + \text{e}^- \rightleftharpoons \text{Al(cr)}$	$\Delta_r G^\circ = 485 \pm 20$	$\log_{10} \beta^\circ = -84.97 \pm 3.50$	$E^\circ = -(1.68 \pm 0.07) \text{ V}$	[1982WAG/EVA]
	$\Delta_r G^\circ = 491.507 \pm 3.338$	$\log_{10} \beta^\circ = -86.11 \pm 0.58$	$E^\circ = -(1.70 \pm 0.01) \text{ V}$	[2003GUI/FAN]
	$\Delta_r G^\circ = 487.2 \pm 2.3$	$\log_{10} \beta^\circ = -85.35 \pm 0.40$	$E^\circ = -(1.68 \pm 0.01) \text{ V}$	[2001BEN/PAL]

For the sake of coherency the choice of NEA-OECD based on CODATA is done. The values of $\Delta_f G^\circ$ and associated uncertainties will be systematically recalculated to ease further modification.

3.6.3.2. Oxo and Hydroxo Compounds

The functions of reaction of corundum ($\alpha\text{-Al}_2\text{O}_3$), boehmite and diasporite (AlOOH), gibbsite (Al(OH)_3) are obtained from Robie and Hemingway [1995ROB/HEM]. Chen *et al.* [1995CHEN/ZEN] proposed functions of formation for $\gamma\text{-Al}_2\text{O}_3$ by measuring the heat capacities. The standard function of formation are calculated relative to Chase [1998CHA], which does not include the solution species. The calculated solubility value is then highly dependent on the chosen $\Delta_f G^\circ(\text{Al}^{3+})$. For instance slight differences can be obtained either considering the CODATA value [1989COX/WAG], estimation from Shock *et al.* [1997aSHO/SAS], or the value from Bénézeth *et al.* [2001BEN/PAL].

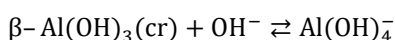


For the sake of consistency, the solubility relative to CODATA value [1989COX/WAG] is chosen.

The amorphous aluminium hydroxide solubility is taken from Nordstrom *et al.* [1990NOR/PLU].

Thermodynamic functions for the hydroxo complexes are taken from Tagirov and Schott [2001TAG/SCH] and adapted to the thermodynamic functions of formation of Al^{3+} and H_2O in Guillaumont *et al.* [2003GUI/FAN]. The calculated thermodynamic functions of reactions, $\log_{10}\beta_n^\circ$, and thermodynamic functions of formation are shown in Table 3.6-8.

Verdes *et al.* [1992VER/GOU] proposed a solubility study of bayerite ($\beta\text{-Al(OH)}_3(\text{cr})$) from the following reaction.



$$\text{with } \Delta_f G_m^\circ(\beta\text{-Al(OH)}_3(\text{cr})) = -(149.80 \pm 1.87) \text{ kJ mol}^{-1}$$

This value is linked to the value of $\Delta_f G^\circ(\text{Al(OH)}_4^-) = -1305.42 \text{ kJ mol}^{-1}$ evaluated in Verdes *et al.* [1992VER/GOU], which is $4.228 \text{ kJ mol}^{-1}$ higher than the value reestimated from Tagirov and Schott [2001TAG/SCH]. The value of $\Delta_f G^\circ(\text{OH}^-)$ is not given explicitly.

For the sake of consistency, the value of $\Delta_f G_m^\circ(\beta\text{-Al(OH)}_3(\text{cr}))$ is recalculated from the variation of pK_{s4} vs. T is given as follows,

$$pK_{s4} = -\log_{10} K_{s4} = \frac{1110.52}{T(K)} - 3.42$$

which is equivalent to the following expression.

$$\log_{10} K^\circ = -\frac{\Delta_r H^\circ}{R \ln 10} \times \frac{1}{T} + \frac{\Delta_r S^\circ}{R \ln 10} = -\frac{1110.52}{T(K)} + 3.42$$

The $\log_{10} K_{s4}$, $\Delta_r H^\circ$, and $\Delta_r S^\circ$ values at 25°C are calculated as follows,

$$\log_{10} K_{s4} = -0.30, \Delta_r H^\circ = 21.261 \text{ kJ mol}^{-1}, \Delta_r S^\circ = 65.48 \text{ J mol}^{-1} \text{ K}^{-1}$$

and Gibbs energy of formation can be calculated as follows.

$$\Delta_r G^\circ = 1.712 \text{ kJ mol}^{-1} = \Delta_f G^\circ(\text{Al(OH)}_4^-) - \Delta_f G^\circ(\text{OH}^-) - \Delta_f G^\circ(\text{Bayerite})$$

$$\Delta_f G^\circ(\text{Bayerite}) = -(1154.168 \pm 1.877) \text{ kJ mol}^{-1}$$

The uncertainty is estimated from the one proposed in Verdes *et al.* [1992VER/GOU].

This allows to propose the cumulative solubility equilibrium.



$$\log_{10} K_s = 8.50 \pm 0.48$$

The solubilities of the different oxides and hydroxides phases of Al(III) are calculated using Phreeplot and are plotted in Figure 3.6-8. The order of stability is:

Diaspore (AlOOH) > Gibbsite (Al(OH)_3), Boehmite ($\gamma\text{-AlOOH}$) > Bayerite ($\beta\text{-Al(OH)}_3$) > $\alpha\text{-Al}_2\text{O}_3$ < $\gamma\text{-Al}_2\text{O}_3$

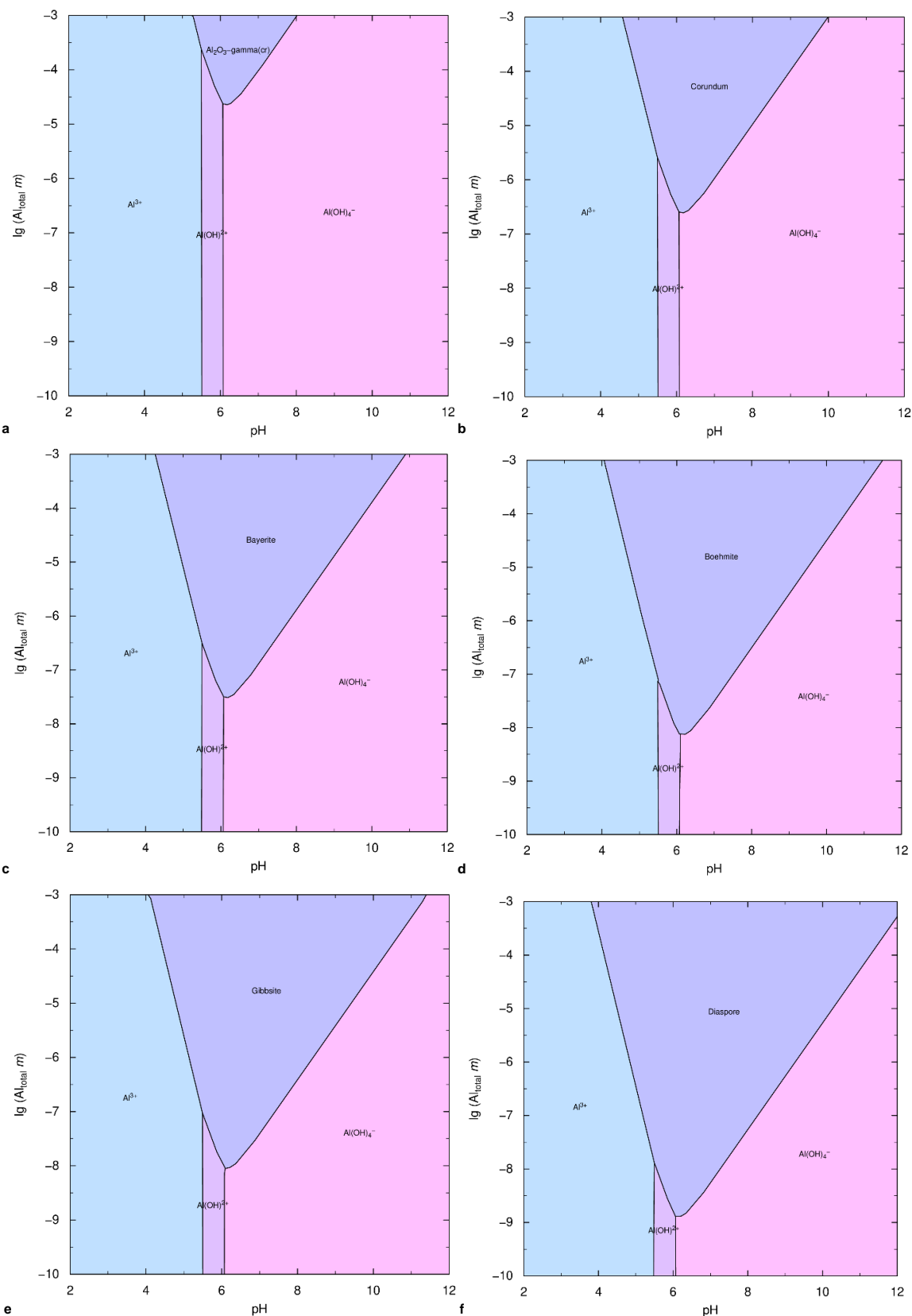


Figure 3.6-8. Solubility of aluminium oxides and hydroxide, using PHREEPLOT: $\gamma\text{-Al}_2\text{O}_3$ (a), corundum ($\alpha\text{-Al}_2\text{O}_3$) (b), bayerite ($\beta\text{-Al(OH)}_3$) (c), boehmite (AlOOH) (d), gibbsite (Al(OH)_3) (e), and diaspore (AlOOH) (f).

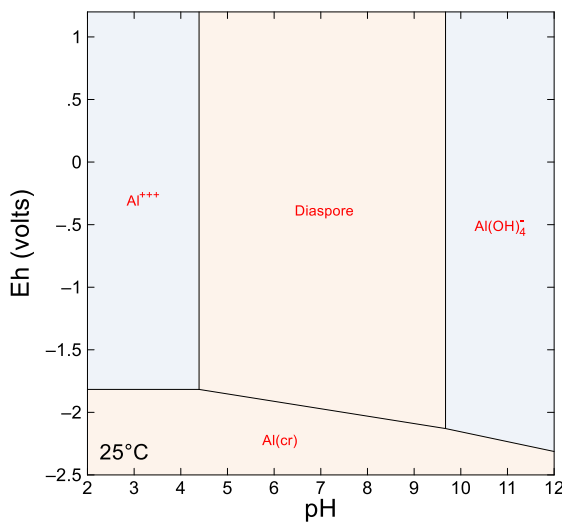


Figure 3.6-9. Pourbaix diagram of 10^{-6} mol kg_w⁻¹ Al in a hypothetical 0.1 mol kg_w⁻¹ indifferent electrolyte using GWB; all phases are allowed to precipitate.

3.6.3.3. Halogen Compounds

The functions of reaction of $\text{AlCl}_3(\text{cr})$ are calculated from the functions of formation in Wagman *et al.* [1982WAG/EVA].

Tagirov and Schott [2001TAG/SCH] recommended the thermodynamic functions of formation for $\text{AlF}_n^{(3-n)+}$ with $1 \leq n \leq 6$, and $\text{Al}(\text{OH})_2\text{F}_n^{(n-1)-}$ with $n = \{1; 2\}$ — values in coherence with Helgeson and Kirkham [1974aHEL/KIR] for H_2O . The calculated thermodynamic functions of reactions, $\log_{10}\beta_n^\circ$, and thermodynamic functions of formation adapted to the thermodynamic functions of formation of Al^{3+} and F^- in Guillaumont *et al.* [2003GUI/FAN] are shown in Table 3.6-8.

3.6.3.4. Sulphur Compounds

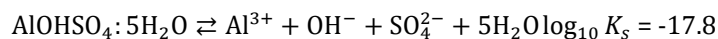
3.6.3.4.1 Sulphide compounds

The function of reaction for $\text{Al}_2\text{S}_3(\text{cr})$ are calculated from the functions of reaction given by Pankratz *et al.* [1987PAN/MAH].

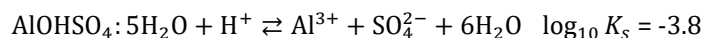
3.6.3.4.2 Sulphate compounds

Functions of formation for $\text{Al}_2(\text{SO}_4)_3$ and $\text{Al}_2(\text{SO}_4)_3 \cdot 6\text{H}_2\text{O}$ are taken from Wagman *et al.* [1982WAG/EVA]; Functions of formation for $\text{Al}_2(\text{SO}_4)_3$ are also available in Robie and Hemingway [1995ROB/HEM]. Adams and Rawajfih [1977ADA/RAW] measured the solubility of basaluminite ($\text{Al}_4(\text{OH})_{10}\text{SO}_4$).

The solubility constant of jurbanite ($\text{AlOHSO}_4 \cdot 5\text{H}_2\text{O}$),



is taken is taken as is from Nordstrom [1982NOR] and defined as follows.



Tagirov and Schott [2001TAG/SCH] recommended thermodynamic functions of formation for AlSO_4^+ . The calculated thermodynamic function of reactions, $\log_{10}\beta^\circ$, and thermodynamic function of formation adapted to the

thermodynamic functions of formation of Al^{3+} and SO_4^{2-} in Guillaumont *et al.* [2003GUI/FAN] are shown in Table 3.6-8.

a. Basaluminite

The solubility constant for basaluminite was recalculated from the original data from Adams and Rawajfih [1977ADA/RAW]. The solubility of this phase is reevaluated since both the choice of thermodynamic constants for the Al-OH-SO₄ system and the ionic strength descriptions are different in PRODATA and in the initial data determination. Using the original equilibrium concentration and pH, density of the solution imposed by NaClO₄ [1988NOV/SOH], complexation constants for Al-OH-SO₄, and assuming $\varepsilon(\text{Al}^{3+}, \text{ClO}_4^-) = \varepsilon(\text{Al}^{3+}, \text{Cl}^-)$, the SIT extrapolations in Figure 3.6-10 can be obtained for amorphous and crystalline phases.

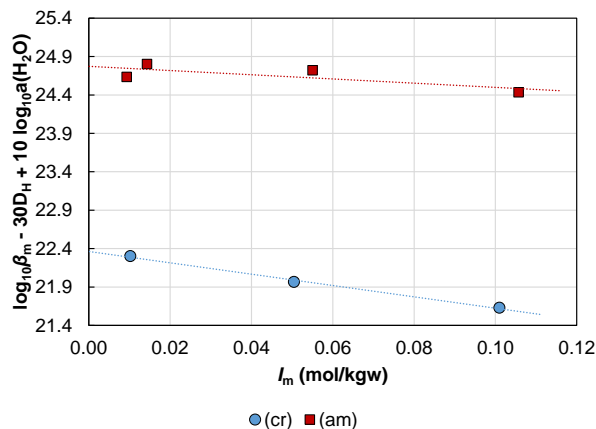
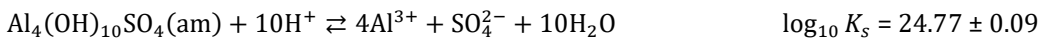
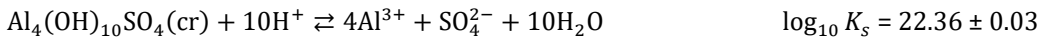
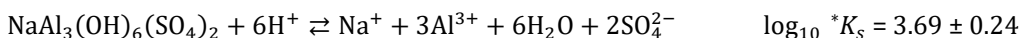
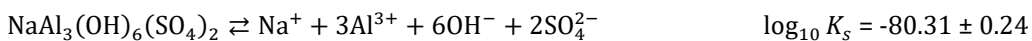


Figure 3.6-10. Extrapolation of solubility constant for $\text{Al}_4(\text{OH})_{10}\text{SO}_4$ from original data in Adams and Rawajfih [1977ADA/RAW].

b. Na-alunite

The solubility constant for Na-alunite ($\text{NaAl}_3(\text{OH})_6(\text{SO}_4)_2$) was recalculated from the original data from Adams and Rawajfih [1977ADA/RAW] (Figure 3.6-11).



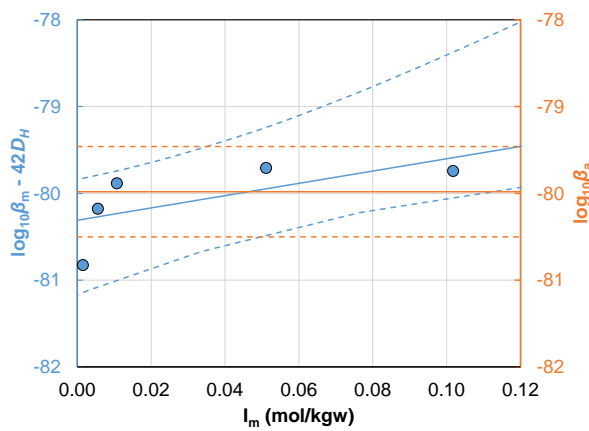
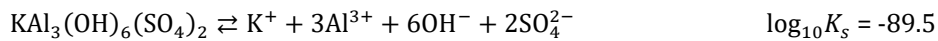


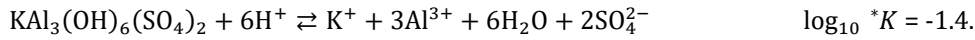
Figure 3.6-11. Extrapolation of solubility constant for $\text{NaAl}_3(\text{OH})_6(\text{SO}_4)_2$ from original data [1977ADA/RAW].

c. Alunite

The solubility constant for $\text{KAl}_3(\text{OH})_6(\text{SO}_4)_2$ was recalculated from the original data from Adams and Rawajfih [1977ADA/RAW]. The authors measured equilibrium concentrations of K, Al, SO_4 and pH, and different ionic strengths — from 1 to 300 mM NaClO_4 —, calculated the activity products using Debye-Hückel relationship [1937KIE], and thermodynamic constants from Adams [1971ADA] for Al-OH- SO_4 . The dissolution reaction,



which was reported in Nordstrom *et al.* [1990NOR/PLU] as,



The solubility of this phase is reevaluated since both the choice of thermodynamic constants for the Al-OH- SO_4 system and the ionic strength descriptions are different in PRODATA and in the initial data determination. Using the original equilibrium concentration and pH, density of the solution imposed by NaClO_4 [1988NOV/SOH], complexation constants for Al-OH- SO_4 , and assuming $\varepsilon(\text{Al}^{3+}, \text{ClO}_4^-) = \varepsilon(\text{Al}^{3+}, \text{Cl}^-)$, the SIT extrapolations and average activity products on Figure 3.6-12 can be obtained.

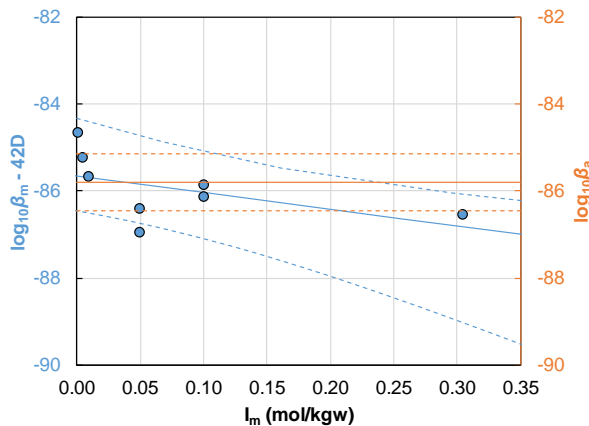
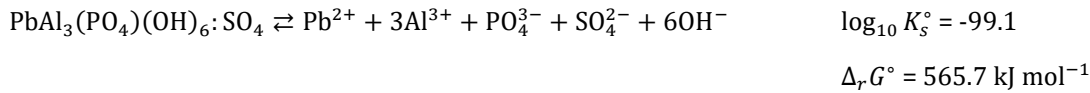


Figure 3.6-12. Extrapolation of solubility constant for $\text{KAl}_3(\text{OH})_6(\text{SO}_4)_2$ and average activity product from original data [1977ADA/RAW].

3.6.3.5. Group 15 Compounds

Berlinite (AlPO_4) [1995ROB/HEM] and mansfieldite ($\text{AlAsO}_4 \cdot 2\text{H}_2\text{O}$) [1974NAU/RYZ] are adapted to the functions of formation from NEA-OECD reviews [1992GRE/FUG; 2003GUI/FAN; 2020GRE/GAO]. The Gibbs energy of formation of PO_4^{3-} in Robie and Hemingway [1995ROB/HEM] are noticeably different from the one in the NEA-OECD review, *i.e.*, $\Delta_f G^\circ(\text{PO}_4^{3-}) = -(1\ 001.6 \pm 0.9) \text{ kJ mol}^{-1}$ [1995ROB/HEM], and $-(1\ 025.491 \pm 1.576) \text{ kJ mol}^{-1}$ [1992GRE/FUG; 2003GUI/FAN; 2020GRE/GAO].

The solubility of hinsdalite ($\text{PbAl}_3(\text{PO}_4)(\text{OH})_6 \cdot \text{SO}_4$) in Nriagu [1984NRI] should be written as the total ionization as follows.



The reported Gibbs energy of formation — $\Delta_f G^\circ = -1\ 368 \text{ kcal mol}^{-1} = -5\ 728 \text{ kJ mol}^{-1}$ — is not compatible with the one calculated using Guillaumont *et al.* [2003GUI/FAN], *i.e.* $-4\ 777.241 \text{ kJ mol}^{-1}$. A verification done with the Gibbs energy of formation from Wagman *et al.* [1968WAG/EVA; 1969WAG/EVA] ($-4\ 756.681 \text{ kJ mol}^{-1}$) or even Wagman *et al.* [1965WAG/EVA; 1966WAG/EVA] ($-4759.191 \text{ kJ mol}^{-1}$) is not satisfying either. The Gibbs energy of formation of this phase will then not be included, and the $\log_{10} K_s^\circ$ value will be included for scoping calculation only.

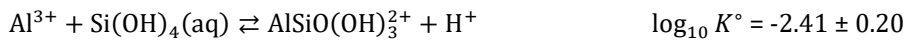
3.6.3.6. Silicate Compounds

The functions of reaction for Al_2SiO_5 phases — *i.e.*, andalusite, kyanite, and sillimanite — are calculated from Robie and Hemingway [1995ROB/HEM], and function of formation are recalculated relative to Guillaumont *et al.* [2003GUI/FAN].

The formation constant of $\text{AlSiO}(\text{OH})_3^{2+}$ is taken from Hummel *et al.* [2002HUM/BER],



which is expressed in PRODATA referring to $\text{Si}(\text{OH})_4(\text{aq})$ as follows.



3.6.3.7. Thermodynamic Constants, Functions, and Specific Ion Interaction Coefficients for Al

Table 3.6-8. Thermodynamic functions and constants for native metal, free ion, and oxo and hydroxo compounds of Al.

Reaction	$\Delta_r G_m^\circ$ (kJ mol ⁻¹)	$\log_{10} \beta^\circ$	$\Delta_f G_m^\circ$ (kJ mol ⁻¹)	$\Delta_r H_m^\circ$ (kJ mol ⁻¹)	$\Delta_f H_m^\circ$ (kJ mol ⁻¹)
$\text{Al}(\text{cr}) \rightleftharpoons \text{Al}^{3+} + 3\text{e}^-$	-491.507 ± 3.338	86.11 ± 0.58	-491.507 ± 3.338	-538.400 ± 1.500	-538.400 ± 1.500
$\text{Al}(\text{cr}) + 0.75\text{O}_2(\text{aq}) + 3\text{H}^+ \rightleftharpoons \text{Al}^{3+} + 1.5\text{H}_2\text{O}$	-859.501 ± 3.270	150.56 ± 0.57		-958.370 ± 1.343	
$\alpha-\text{Al}_2\text{O}_3 + 6\text{H}^+ \rightleftharpoons 2\text{Al}^{3+} + 3\text{H}_2\text{O}$	-107.800 ± 6.549^a	18.89 ± 1.15	$-1\ 586.634 \pm 1.304$	-259.290 ± 2.706^a	$-1\ 675.000 \pm 1.300$
$\gamma-\text{Al}_2\text{O}_3 + 6\text{H}^+ \rightleftharpoons 2\text{Al}^{3+} + 3\text{H}_2\text{O}$	-130.234 ± 6.371	22.82 ± 1.12	$-1\ 564.200 \pm 2.000^b$	-277.090 ± 2.601	$-1\ 657.200 \pm 1.500^b$
Boehmite $\text{AlO}(\text{OH}) + 3\text{H}^+ \rightleftharpoons \text{Al}^{3+} + 2\text{H}_2\text{O}$	-45.200 ± 2.507^a	7.92 ± 0.44	-920.587 ± 2.205	-113.660 ± 1.607^a	-996.400 ± 2.200
Diaspore $\text{AlO}(\text{OH}) + 3\text{H}^+ \rightleftharpoons \text{Al}^{3+} + 2\text{H}_2\text{O}$	-40.900 ± 2.592^a	7.165 ± 0.454	-924.887 ± 2.105	-108.760 ± 1.607^a	$-1\ 001.300 \pm 2.200$

Table 3.6-8. Continued.

Reaction	$\Delta_r G_m^\circ$ (kJ mol ⁻¹)	$\log_{10}\beta^\circ$	$\Delta_f G_m^\circ$ * (kJ mol ⁻¹)	$\Delta_r H_m^\circ$ (kJ mol ⁻¹)	$\Delta_f H_m^\circ$ * (kJ mol ⁻¹)
Gibbsite $\text{Al}(\text{OH})_3 + 3\text{H}^+ \rightleftharpoons \text{Al}^{3+} + 3\text{H}_2\text{O}$	-45.800 ± 3.116^a	8.02 ± 0.55	$-1\ 157.127 \pm 1.202$	-102.790 ± 0.908^a	$-1\ 293.100 \pm 1.200$
Bayerite $\beta\text{-Al}(\text{OH})_3 + \text{OH}^- \rightleftharpoons \text{Al}(\text{OH})_4^-$	1.712	-0.30 ^c	$-1\ 154.167 \pm 1.877$	21.261 ^c	
$\beta\text{-Al}(\text{OH})_3 + 3\text{H}^+ \rightleftharpoons \text{Al}^{3+} + 3\text{H}_2\text{O}$	-48.760 ± 2.763	8.54 ± 0.48			
$\text{Al}(\text{OH})_3(\text{am}) + 3\text{H}^+ \rightleftharpoons \text{Al}^{3+} + 3\text{H}_2\text{O}$		10.8 ^e			
$\text{Al}^{3+} + \text{H}_2\text{O} \rightleftharpoons \text{Al}(\text{OH})^{2+} + \text{H}^+$	28.334 ^d	-4.96	-700.313		
$\text{Al}^{3+} + 2\text{H}_2\text{O} \rightleftharpoons \text{Al}(\text{OH})_2^+ + 2\text{H}^+$	62.329 ^d	-10.92	-903.458		
$\text{Al}^{3+} + 3\text{H}_2\text{O} \rightleftharpoons \text{Al}(\text{OH})_3(\text{aq}) + 3\text{H}^+$	97.655 ^d	-17.11	-1 105.272		
$\text{Al}^{3+} + 4\text{H}_2\text{O} \rightleftharpoons \text{Al}(\text{OH})_4^- + 4\text{H}^+$	130.419 ^d	-22.85	-1 309.648		

a [1995ROB/HEM]; b [1995CHEN/ZEN]; c [1992VER/GOU]; d calculated from $\Delta_f G_m^\circ$ in [1974aHEL/KIR; 2001TAG/SCH];

e [1990NOR/PLU].

* calculated from $\log_{10}\beta^\circ$ and $\Delta_f G_m^\circ$ in [2003GUI/FAN].**Table 3.6-9. Thermodynamic functions and constants for halogen compounds of Al.**

Reaction	$\Delta_r G_m^\circ$ (kJ mol ⁻¹)	$\log_{10}\beta^\circ$	$\Delta_f G_m^\circ$ * (kJ mol ⁻¹)	$\Delta_r H_m^\circ$ (kJ mol ⁻¹)	$\Delta_f H_m^\circ$ * (kJ mol ⁻¹)
$\text{AlCl}_3(\text{cr}) \rightleftharpoons \text{Al}^{3+} + 3\text{Cl}^-$	-249.884 ± 19.163^a	43.78 ± 3.36	-635.274 ± 19.455	-328.277 ± 1.006^a	-711.363 ± 1.152
$\text{Al}^{3+} + \text{F}^- \rightleftharpoons \text{AlF}^{2+}$	-39.848 ^b	6.98	-812.878		
$\text{Al}^{3+} + 2\text{F}^- \rightleftharpoons \text{AlF}_2^+$	-71.931 ^b	12.60	-1 126.484		
$\text{Al}^{3+} + 3\text{F}^- \rightleftharpoons \text{AlF}_3(\text{aq})$	-95.052 ^b	16.652	-1 431.128		
$\text{Al}^{3+} + 4\text{F}^- \rightleftharpoons \text{AlF}_4^-$	-108.638 ^b	19.032	-1 726.237		
$\text{Al}^{3+} + 5\text{F}^- \rightleftharpoons \text{AlF}_5^{2-}$	-117.586 ^c	20.600	-2 016.708	7.704 ^c	-2 207.446
$\text{Al}^{3+} + 6\text{F}^- \rightleftharpoons \text{AlF}_6^{3-}$	-117.586 ^c	20.600	-2 298.231	-6.992 ^c	-2 557.492
$\text{Al}^{3+} + 2\text{H}_2\text{O} + \text{F}^- \rightleftharpoons \text{Al}(\text{OH})_2\text{F}(\text{aq}) + 2\text{H}^+$	24.196 ^b	-4.24	-1 223.114		
$\text{Al}^{3+} + 2\text{F}^- + \text{H}_2\text{O} \rightleftharpoons \text{Al}(\text{OH})\text{F}_2(\text{aq}) + \text{H}^+$	-0.870 ^b	0.15	-1 292.563		
$\text{Al}^{3+} + 2\text{H}_2\text{O} + 2\text{F}^- \rightleftharpoons \text{Al}(\text{OH})_2\text{F}_2^- + 2\text{H}^+$	11.711 ^b	-2.05	-1 517.122		

a [1982WAG/EVA]; b calculated from $\Delta_f G_m^\circ$ in [2001TAG/SCH] and [1974aHEL/KIR; 1997aSHO/SAS] for auxiliary data; c [1990NOR/PLU].* calculated from $\log_{10}\beta^\circ$ and $\Delta_f G_m^\circ$ in [2003GUI/FAN].**Table 3.6-10. Thermodynamic functions and constants for S compounds of Al.**

Reaction	$\Delta_r G_m^\circ$ (kJ mol ⁻¹)	$\log_{10}\beta^\circ$	$\Delta_f G_m^\circ$ * (kJ mol ⁻¹)	$\Delta_r H_m^\circ$ (kJ mol ⁻¹)	$\Delta_f H_m^\circ$ * (kJ mol ⁻¹)
$\text{Al}_2\text{S}_3 + 3\text{H}^+ \rightleftharpoons 2\text{Al}^{3+} + 3\text{HS}^-$	-305.991	53.61	-640.294 ^a	-474.670	-651.030 ^a
$\text{Al}_2(\text{SO}_4)_3 \rightleftharpoons 2\text{Al}^{3+} + 3\text{SO}_4^{2-}$	-103.650 ± 6.785 ^b	18.16 ± 1.19	-3 111.376 ± 0.321	-348.970 ± 3.215 ^b	-3 455.850 ± 0.321
$\text{Al}_2(\text{SO}_4)_3 \cdot 6\text{H}_2\text{O} \rightleftharpoons 2\text{Al}^{3+} + 3\text{SO}_4^{2-} + 6\text{H}_2\text{O}$	-4.284 ± 6.767 ^b	0.75 ± 1.18	-4 633.582 ± 0.642	-193.080 ± 3.239 ^b	-5 326.720 ± 0.080
Jurbanite $\text{AlOHSO}_4 \cdot 5\text{H}_2\text{O} \rightleftharpoons \text{Al}^{3+} + \text{OH}^- + \text{SO}_4^{2-} + 5\text{H}_2\text{O}$	97.493	-17.08 ^c	-2 675.924		
$\text{AlOHSO}_4 \cdot 5\text{H}_2\text{O} + \text{H}^+ \rightleftharpoons \text{Al}^{3+} + \text{SO}_4^{2-} + 6\text{H}_2\text{O}$	17.573	-3.08 ^c			
Basaluminite $\text{Al}_4(\text{OH})_{10}\text{SO}_4 + 10\text{H}^+ \rightleftharpoons 4\text{Al}^{3+} + \text{SO}_4^{2-} + 10\text{H}_2\text{O}$	-127.632 ± 0.171	22.36 ± 0.03 ^d	-4 953.800 ± 13.366		

Table 3.6-10. Continued.

Reaction	$\Delta_r G_m^\circ$ (kJ mol ⁻¹)	$\log_{10}\beta^\circ$	$\Delta_f G_m^\circ$ (kJ mol ⁻¹)	$\Delta_r H_m^\circ$ (kJ mol ⁻¹)	$\Delta_f H_m^\circ$ (kJ mol ⁻¹)
Basaluminite(am)					
$\text{Al}_4(\text{OH})_{10}\text{SO}_4 + 10\text{H}^+ \rightleftharpoons 4\text{Al}^{3+} + \text{SO}_4^{2-} + 10\text{H}_2\text{O}$	-141.445 ± 0.514	$24.78 \pm 0.09^{\text{d}}$			
$\text{Al}^{3+} + \text{SO}_4^{2-} \rightleftharpoons \text{AlSO}_4^+$	-18.071 ^e	3.17	-1 253.582		

a [1987PAN/MAH]; b [1982WAG/EVA]; c [1982NOR]; d recalculated from [1977ADA/RRAW]; e [1974aHEL/KIR; 2001TAG/SCH].

* calculated from $\log_{10}\beta^\circ$ and $\Delta_f G_m^\circ$ in [2003GUI/FAN] unless otherwise noted.**Table 3.6-11. Thermodynamic functions and constants for P, As, and Si compounds of Al.**

Reaction	$\Delta_r G_m^\circ$ (kJ mol ⁻¹)	$\log_{10}\beta^\circ$	$\Delta_f G_m^\circ$ (kJ mol ⁻¹)	$\Delta_r H_m^\circ$ (kJ mol ⁻¹)	$\Delta_f H_m^\circ$ (kJ mol ⁻¹)
Berlinite					
$\text{AlPO}_4 \rightleftharpoons \text{Al}^{3+} + \text{PO}_4^{3-}$	$126.900 \pm 3.373^{\text{a}}$	-22.23 ± 0.59	-1 643.898 ± 5.000	-64.200 $\pm 2.462^{\text{a}}$	-1 758.600 ± 5.000
Plumbogummite					
$\text{PbAl}_3(\text{PO}_4)_2(\text{OH})_5 \cdot \text{H}_2\text{O} \rightleftharpoons \text{Pb}^{2+} + 3\text{Al}^{3+} + 2\text{PO}_4^{3-} + 5\text{OH}^- + \text{H}_2\text{O}$	566.809	-99.3 ^b	5 139.790		
$\text{PbAl}_3(\text{PO}_4)_2(\text{OH})_5 \cdot \text{H}_2\text{O} + 5\text{H}^+ \rightleftharpoons \text{Pb}^{2+} + 3\text{Al}^{3+} + 2\text{PO}_4^{3-} + 6\text{H}_2\text{O}$	167.209	-29.29			
Hinsdalite					
$\text{PbAl}_3(\text{PO}_4)_2(\text{OH})_5 \cdot \text{SO}_4 \rightleftharpoons \text{Pb}^{2+} + 3\text{Al}^{3+} + \text{PO}_4^{3-} + \text{SO}_4^{2-} + 6\text{OH}^-$		-99.1 ^b			
$\text{PbAl}_3(\text{PO}_4)_2(\text{OH})_5 \cdot \text{SO}_4 + 6\text{H}^+ \rightleftharpoons \text{Pb}^{2+} + 3\text{Al}^{3+} + \text{PO}_4^{3-} + \text{SO}_4^{2-} + 6\text{H}_2\text{O}$		-15.1			
Mansfieldite					
$\text{AlAsO}_4 \cdot 2\text{H}_2\text{O} \rightleftharpoons \text{Al}^{3+} + \text{AsO}_4^{3-} + 2\text{H}_2\text{O}$	90.460 ^c	-15.85	-1 704.607		
Andalusite					
$\text{Al}_2\text{SiO}_5 + 6\text{H}^+ \rightleftharpoons 2\text{Al}^{3+} + \text{Si(OH)}_4(\text{aq}) + \text{H}_2\text{O}$	$-81.600 \pm 1.695^{\text{a}}$	14.30 ± 0.30	-2 446.289 ± 6.560	-232.700 $\pm 1.611^{\text{a}}$	-2 586.890 ± 4.051
Kyanite					
$\text{Al}_2\text{SiO}_5 + 6\text{H}^+ \rightleftharpoons 2\text{Al}^{3+} + \text{Si(OH)}_4(\text{aq}) + \text{H}_2\text{O}$	$-80.300 \pm 1.695^{\text{a}}$	14.07 ± 0.30	-2 447.589 ± 6.560	-228.800 $\pm 1.611^{\text{a}}$	-2 590.790 ± 4.051
Sillimanite					
$\text{Al}_2\text{SiO}_5 + 6\text{H}^+ \rightleftharpoons 2\text{Al}^{3+} + \text{Si(OH)}_4(\text{aq}) + \text{H}_2\text{O}$	$-84.300 \pm 1.695^{\text{a}}$	14.77 ± 0.30	-2 443.589 ± 6.560	-236.500 $\pm 1.611^{\text{a}}$	-2 583.090 ± 4.051
$\text{Al}^{3+} + \text{SiO}(\text{OH})_3^- \rightleftharpoons \text{AlSiO}(\text{OH})_3^{2+}$					
	-42.240 ± 1.142	7.4 $\pm 0.2^{\text{d}}$	-1 785.487 ± 3.714		
$\text{Al}^{3+} + \text{Si(OH)}_4(\text{aq}) \rightleftharpoons \text{AlSiO}(\text{OH})_3^{2+} + \text{H}^+$					
	13.755 ± 1.148	-2.41 ± 0.20			

a [1995ROB/HEM]; b [1984NRI]; c [1974NAU/RYZ]; d [2002HUM/BER].

* calculated from $\Delta_f G_m^\circ$ and $\Delta_f H_m^\circ$ from [2003GUI/FAN].**Table 3.6-12. Specific ion interaction coefficients for Al species.**

Specific ion interaction coefficient	Value $\pm \sigma$	Reference
$\varepsilon(\text{Al}^{3+}, \text{Cl}^-)$	0.33 ± 0.03	[1992GRE/FUG]
$\varepsilon(\text{Al}(\text{OH})^{2+}, \text{Cl}^-)$	0.09	[1992GRE/FUG]
$\varepsilon(\text{Al}(\text{OH})^{2+}, \text{ClO}_4^-)$	0.31	[1992GRE/FUG]
$\varepsilon(\text{Al}(\text{OH})_2^+, \text{Cl}^-)$	0.09	[1980CIA]

3.7. d-Transition Metals Series

3.7.1. Zinc

Zinc is a common metal in environmental mining context.

3.7.1.1. Native Metal and Free Ion

Based on CODATA selection [1989COX/WAG], the functions of formation for Zn(cr) and Zn²⁺ are available in the NEA-OECD reviews [1992GRE/FUG; 2003GUI/FAN; 2020GRE/GAO]. The common master species is Zn²⁺.

The specific ion interaction coefficients for Zn^{2+} are taken from Ciavatta [1980CIA] for ClO_4^- and NO_3^- , and Zhang and Muhammed [2001ZHA/MUH] for Cl^- .

3.7.1.2. Oxo and Hydroxo Compounds

Functions of formation values for zincite ($ZnO(cr)$) are recommended in the NEA-OECD reviews [1992GRE/FUG; 2003GUI/FAN; 2020GRE/GAO]. Brown and Ekberg [2016BRO/EKB] proposed a $\log_{10} K_s$ and a $\Delta_r H^\circ$ value for ϵ - $Zn(OH)_2(s)$, in agreement with the propositions from Powell *et al.* [2013POW/BRO], which was provisional. Powell *et al.* [2013POW/BRO] also recommended $\log_{10} K_s$ for β_1 - $Zn(OH)_2(s)$, β_2 - $Zn(OH)_2(s)$, γ - $Zn(OH)_2(s)$, and δ - $Zn(OH)_2(s)$.

The hydrolysis of Zn^{2+} ($Zn_n(OH)_m^{2n-m}$) is taken from Brown and Ekberg [2016BRO/EKB]. Zhang and Muhammed [2001ZHA/MUH] suggested the formation of $Zn_2(OH)_6^{2-}$ and $Zn_4(OH)_4^{4+}$ that Brown and Ekberg [2016BRO/EKB] have not selected. These latter species are added for scoping calculations. It is to be noted that the $\Delta_f G_m^\circ$ value for $Zn_2(OH)_6^{2-}$ is here recalculated from the $\log_{10} \beta_{2,6}^\circ$ value as it seems that an error occurred in this calculation in Zhang and Muhammed [2001ZHA/MUH]. Zhang and Muhammed [2001ZHA/MUH] also proposed ε values.

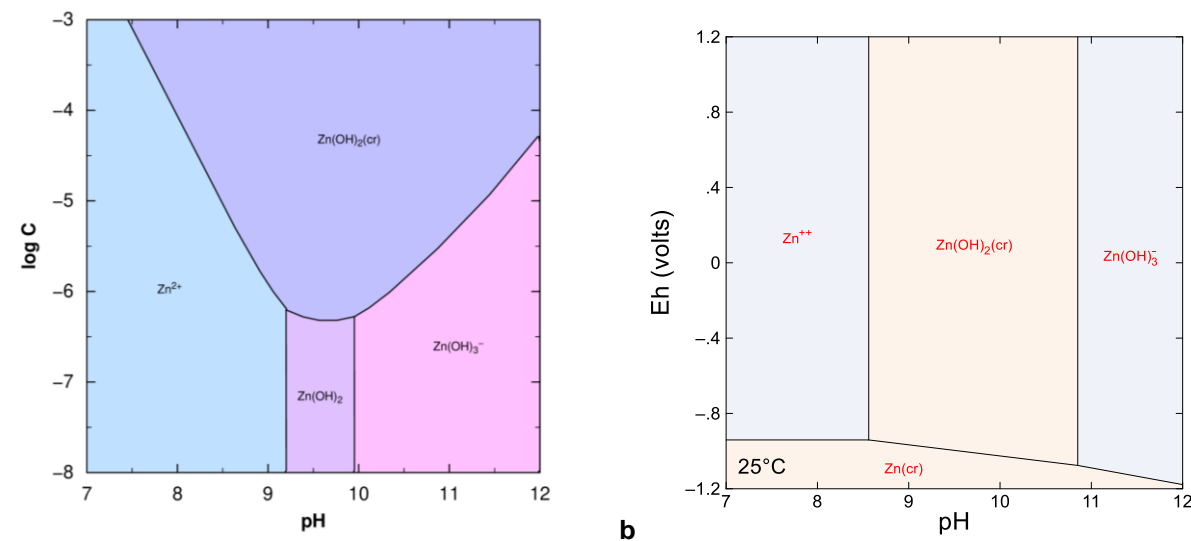


Figure 3.7-1. (a) Solubility of Zn (PHREEPLOT) in a hypothetical indifferent electrolyte at 0.1 mol kg^{-1} ; all phases are allowed to precipitate; (b) Pourbaix diagram (GWB) of Zn under the same conditions.

3.7.1.3. Chloro Compounds

The $ZnCl_n^{2-n}$ are taken from Powell *et al.* [2013POW/BRO], and the $\Delta\varepsilon$ values are used to calculate the $\varepsilon(ZnCl_n^{2-n}, Na^+ClO_4^-)$ values. No values were proposed for NaCl medium.

3.7.1.4. Sulphur and Selenium Compounds

Pankratz *et al.* [1987PAN/MAH] and Robie and Hemingway [1995ROB/HEM] proposed function of formation for sphalerite and wurstite (ZnS), which are in perfect agreement. The values of the former authors are included in PRODATA.

Zinkosite ($ZnSO_4$), bianchite ($ZnSO_4 \cdot 6H_2O$), and goslarite ($ZnSO_4 \cdot 7H_2O$) are taken from Robie and Hemingway [1995ROB/HEM]. A value of $ZnSO_4 \cdot H_2O$ is available in the wateq4f database [1991BAL/NOR]. $Zn(SO_4)(aq)$ is taken from Powell *et al.* [2013POW/BRO], who also suggested an indicative value for $Zn(SO_4)_2^{2-}$.

The $\Delta\epsilon$ values are proposed in LiClO_4 medium used to calculate the $\epsilon(\text{Zn}(\text{SO}_4)_n^{2-2n}, \text{Li}^+ \text{ClO}_4^-)$. The Eq. (26) and Eq. (27) from Ciavatta [1990CIA] are used to estimate the $\epsilon(\text{Zn}(\text{SO}_4)_n^{2-2n}, \text{Na}^+ \text{Cl}^-)$ values.

The solids $\alpha\text{-ZnSe(cr)}$ and $\text{ZnSeO}_4 \cdot 6\text{H}_2\text{O(cr)}$, and complexes $\text{Zn}(\text{SeCN})_n^{2-n}$ and $\text{ZnSeO}_4(\text{aq})$ are taken from Olin *et al.* [2005OLI/NOL].

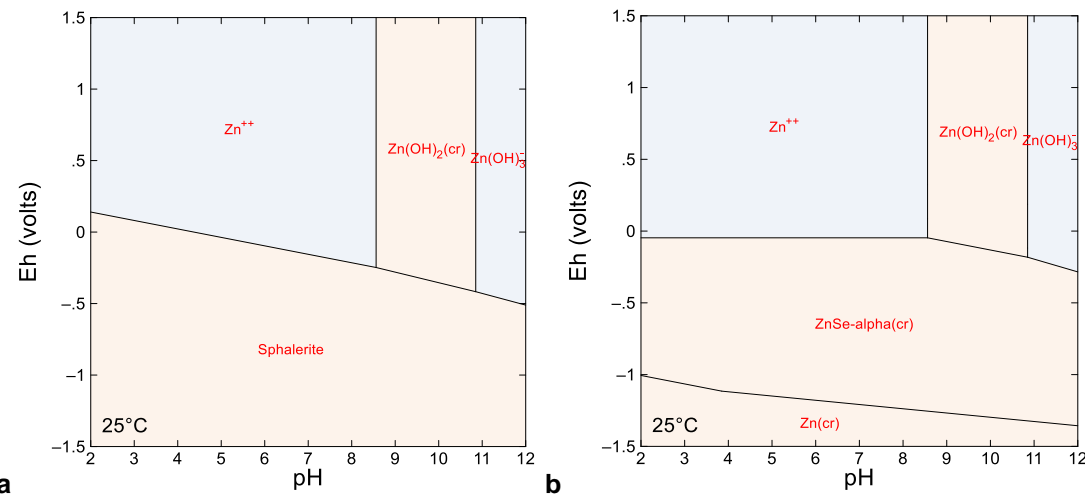


Figure 3.7-2. Pourbaix diagram of 10^{-6} mol kg⁻¹ Zn (GWB) in a hypothetical indifferent electrolyte 0.1 mol kg⁻¹, in presence of 10^{-4} mol kg⁻¹ of S (a) and Se (b).

3.7.1.5. Phosphor and Arsenic Compounds

The phosphate solids from Nriagu [1984NRI] are taken for hopeite ($\text{Zn}_3(\text{PO}_4)_2 \cdot 4\text{H}_2\text{O}$), spencerite ($\text{Zn}_4(\text{PO}_4)_2(\text{OH})_2 \cdot 3\text{H}_2\text{O}$), zinc pyromorphite ($\text{Zn}_5(\text{PO}_4)_3\text{OH}$), faustite ($\text{ZnAl}_6(\text{PO}_4)_4(\text{OH})_8 \cdot 4\text{H}_2\text{O}$), tarbuttite ($\text{Zn}_2(\text{PO}_4)\text{OH}$). Given the problem encountered for hinsdalite (c.f. § 3.6.2.3), the $\Delta_f G^\circ$ values were recalculated from the $\log_{10} K_S^\circ$ values, relative to Guillaumont *et al.* [2003GUI/FAN]. The obtained values are in agreement with the proposed values in Nriagu [1984NRI].

Powell *et al.* [2013POW/BRO] have suggested an indicative formation constant for $\text{ZnHPO}_4(\text{aq})$.

The Gibbs energy of reaction and solubility for $(\text{Zn}_3(\text{AsO}_4)_2 \cdot 2.5\text{H}_2\text{O(s)})$ can be calculated from Naumov *et al.* [1974NAU/RYZ].

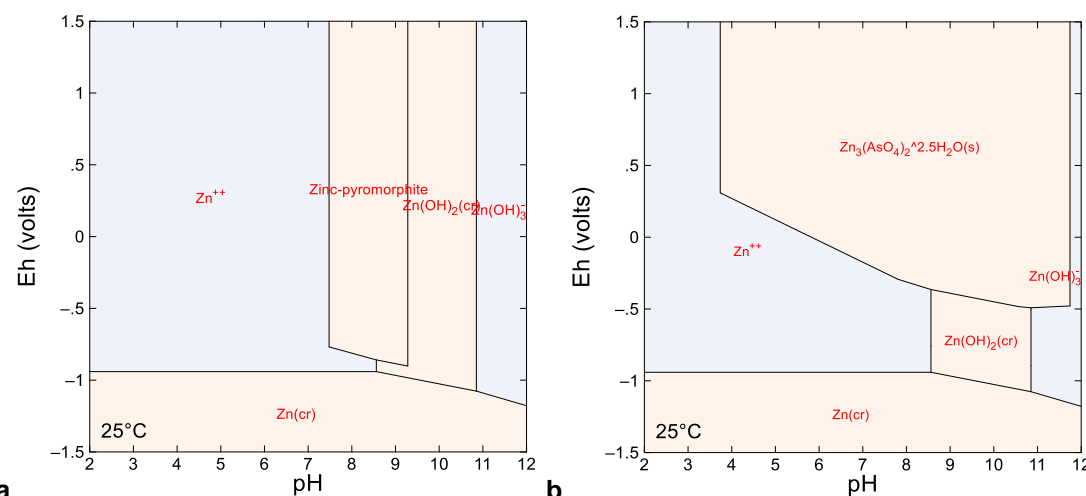


Figure 3.7-3. Pourbaix diagram of 10^{-6} mol kg⁻¹ Zn (GWB) in a hypothetical indifferent electrolyte 0.1 mol kg⁻¹, in presence of 10^{-4} mol kg⁻¹ of P (a) and As (b).

3.7.1.6. Carbon and Silicium Compounds

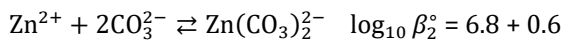
Robie and Hemingway [1995ROB/HEM] and Powell *et al.* [2013POW/BRO] proposed functions of formation and solubility constants, respectively, for smithsonite ($\text{ZnCO}_3(\text{s})$).

Powell *et al.* [2013POW/BRO] proposed a provisional constants for $\text{Zn}(\text{CO}_3)(\text{aq})$ and ZnHCO_3^+ , and an indicative constants for $\text{Zn}(\text{CO}_3)_2^{2-}$ — $\log_{10} \beta_2 = 5.4 \pm 0.6$ in synthetic sea water $0.68 \text{ kg}_w \text{ mol}^{-1}$. The authors also proposed $\Delta\epsilon$ values for the formation of ZnHCO_3^+ but did not noted in any medium.

The estimation *a priori* of $\epsilon(\text{Zn}(\text{CO}_3)_2^{2-}, \text{Na}^+)$ could tentatively be done referring to other analogous complexes of the transition metals series. As only two discordant values can be proposed — *i.e.*, $\text{Cu}(\text{CO}_3)_2^{2-}$ [2007POW/BRO] and $\text{Fe}(\text{CO}_3)_2^{2-}$ [2013LEM/BER] —, we will rather use Eq. 27 from Ciavatta [1990CIA].

$$\epsilon(\text{Zn}(\text{CO}_3)_2^{2+}, \text{Na}^+) = \frac{\epsilon(\text{Zn}^{2+}, \text{Cl}^-) + 2\epsilon(\text{CO}_3^{2-}, \text{Na}^+)}{3} = (0.04 \pm 0.06) \text{ kg}_w \text{ mol}^{-1}$$

Using this value, then the $\log_{10} \beta_2^\circ$ value can be estimated as follows.



Ferri *et al.* [1985FER/GRE] proposed the formation of $\text{Zn}_2\text{CO}_3^{2+}$ in 3 M NaClO_4 .

Even if this kind of justification can be biased [2020aSHA/REI], we will used this estimation as a first approximation, instead of the estimation from the frequency distribution in § 2.6.3.3.2 — it can be observed that the value of $0.4 \text{ kg}_w \text{ mol}^{-1}$ is commonly used in analogy for +2 ions in NaClO_4 .

Wagman *et al.* [1982WAG/EVA] and Robie and Hemingway [1995ROB/HEM] proposed functions of formation for willemite (Zn_2SiO_4). The tabulated values of $\Delta_f G^\circ$ are mostly the same, but as seen in § 3.6.1.1 the $\Delta_f G^\circ(\text{Si(OH)}_4(\text{aq}))$ are 9.1 kJ mol^{-1} different. The calculated $\log_{10} K_s^\circ$ are then two orders of magnitude different. As the Gibbs energy value of $\text{Si(OH)}_4(\text{aq})$ in NEA-OECD reviews [1992GRE/FUG; 2003GUI/FAN] is coherent with Robie and Hemingway [1995ROB/HEM], this latter value will be used in PRODATA — the value reported in Grenthe *et al.* [2020GRE/GAO] for the forthcoming ancillary data review is *ca.* 1.5 kJ mol^{-1} lower than the former one and 7.4 kJ mol^{-1} higher than the value in Wagman *et al.* [1982WAG/EVA].

3.7.1.7. Thermodynamic Constants and Functions, and Specific Ion Interaction Coefficients for Zn

Table 3.7-1. Thermodynamic constants and functions for native metal, free ion, oxo, hydroxo-, and chloro-compounds of Zn.

Reaction	$\log_{10} \beta_n^\circ$	$\Delta_r G_m^\circ$ (kJ mol ⁻¹)	$\Delta_f G_m^\circ$ (kJ mol ⁻¹)	$\Delta_r H_m^\circ$ (kJ mol ⁻¹)	$\Delta_f H_m^\circ$ (kJ mol ⁻¹)
$\text{Zn(cr)} \rightleftharpoons \text{Zn}^{2+} + 2\text{e}^-$	25.79 ± 0.04	-147.203 ± 0.254	-147.203 ± 0.254^a	-153.390 ± 0.200	-153.390 ± 0.200^a
$\text{Zn(cr)} + 0.5\text{O}_2(\text{aq}) + 2\text{H}^+ \rightleftharpoons \text{Zn}^{2+} + \text{H}_2\text{O}$	68.77 ± 0.06	-392.532 ± 0.366		-433.370 ± 0.398	
Zincite					
$\text{ZnO(cr)} + 2\text{H}^+ \rightleftharpoons \text{Zn}^{2+} + \text{H}_2\text{O}$	11.19 ± 0.03	-63.864 ± 0.152	-320.479 ± 0.299^a	-88.760 ± 0.177	-350.460 ± 0.270^a
$\epsilon\text{-Zn(OH)}_2(\text{s}) + 2\text{H}^+ \rightleftharpoons \text{Zn}^{2+} + 2\text{H}_2\text{O}$	11.38 ± 0.20^b	-64.958 ± 1.142	-556.525 ± 1.172	-99.000 ± 3.700^b	-626.050 ± 3.706
$\beta_1\text{-Zn(OH)}_2(\text{s}) + 2\text{H}^+ \rightleftharpoons \text{Zn}^{2+} + 2\text{H}_2\text{O}$	11.72 ± 0.04^d	-66.898 ± 0.228	-554.585 ± 0.351		
$\beta_2\text{-Zn(OH)}_2(\text{s}) + 2\text{H}^+ \rightleftharpoons \text{Zn}^{2+} + 2\text{H}_2\text{O}$	11.76 ± 0.04^d	-67.127 ± 0.228	-554.356 ± 0.351		
$\gamma\text{-Zn(OH)}_2(\text{s}) + 2\text{H}^+ \rightleftharpoons \text{Zn}^{2+} + 2\text{H}_2\text{O}$	11.70 ± 0.04^d	-66.784 ± 0.228	-554.699 ± 0.351		
$\delta\text{-Zn(OH)}_2(\text{s}) + 2\text{H}^+ \rightleftharpoons \text{Zn}^{2+} + 2\text{H}_2\text{O}$	11.81 ± 0.04^d	-67.412 ± 0.228	-554.071 ± 0.351		

Table 3.7-1. Continued.

Reaction	$\log_{10} \beta_n^{\circ}$	$\Delta_r G_m^{\circ}$ (kJ mol ⁻¹)	$\Delta_f G_m^{\circ}$ * (kJ mol ⁻¹)	$\Delta_r H_m^{\circ}$ (kJ mol ⁻¹)	$\Delta_f H_m^{\circ}$ * (kJ mol ⁻¹)
Zn ²⁺ + H ₂ O ⇌ Zn(OH) ⁺ + H ⁺	-8.94 ± 0.06 ^b	51.030 ± 0.342	-333.313 ± 0.428	56.700 ± 0.700 ^b	-382.520 ± 0.729
Zn ²⁺ + 2H ₂ O ⇌ Zn(OH) ₂ (aq) + 2H ⁺	-17.89 ± 0.15 ^b	102.117 ± 0.856	-519.366 ± 0.897	107.100 ± 3.100 ^b	-617.950 ± 3.107
Zn ²⁺ + 3H ₂ O ⇌ Zn(OH) ₃ ⁻ + 3H ⁺	-27.98 ± 0.10 ^b	159.711 ± 0.571	-698.912 ± 0.637	143.480 ± 2.489 ^b	-867.400 ± 2.500
Zn ²⁺ + 4H ₂ O ⇌ Zn(OH) ₄ ²⁻ + 4H ⁺	-40.35 ± 0.22 ^b	230.319 ± 1.256	-865.444 ± 1.292	178.210 ± 5.894 ^b	-1 118.500 ± 5.900
2Zn ²⁺ + H ₂ O ⇌ Zn ₂ (OH) ³⁺ + H ⁺	-7.89 ± 0.31 ^b	45.036 ± 1.769	-486.510 ± 1.841	59.610 ± 4.984 ^b	-533.000 ± 5.000
2Zn ²⁺ + 6H ₂ O ⇌ Zn ₂ (OH) ₆ ²⁻ + 6H ⁺	-54.3 ± 0.4 ^c	309.947 ± 2.283	-1407.299 ± 2.352		
4Zn ²⁺ + 4H ₂ O ⇌ Zn ₄ (OH) ₄ ⁴⁺ + 4H ⁺	-27 ± 1 ^c	154.117 ± 5.708	-1383.255 ± 5.800	106.920 ± 9.967 ^c	-1 649.960 ± 10
Zn ²⁺ + Cl ⁻ ⇌ ZnCl ⁺	0.40 ± 0.09 ^d	-2.283 ± 0.514	-280.703 ± 0.585		
Zn ²⁺ + 2Cl ⁻ ⇌ ZnCl ₂ (aq)	0.69 ± 0.15 ^d	-3.939 ± 0.856	-413.576 ± 0.923		
Zn ²⁺ + 3Cl ⁻ ⇌ ZnCl ₃	0.48 ± 0.54 ^d	-2.740 ± 3.083	-543.594 ± 3.113		

a [2003GUI/FAN]; b [2016BRO/EKB]; c [2001ZHA/MUH]; d [2013POW/BRO].

* calculated from $\Delta_r G_m^{\circ}$ or $\Delta_r H_m^{\circ}$, and $\Delta_f G_m^{\circ}$ or $\Delta_f H_m^{\circ}$ in [2003GUI/FAN].**Table 3.7-2. Thermodynamic constants and functions of S and Se compounds of Zn.**

Reaction	$\log_{10} \beta_n^{\circ}$	$\Delta_r G_m^{\circ}$ (kJ mol ⁻¹)	$\Delta_f G_m^{\circ}$ * (kJ mol ⁻¹)	$\Delta_r H_m^{\circ}$ (kJ mol ⁻¹)	$\Delta_f H_m^{\circ}$ * (kJ mol ⁻¹)
Zinkosite $\text{ZnSO}_4 \rightleftharpoons \text{Zn}^{2+} + \text{SO}_4^{2-}$	3.96 ± 0.13	-22.6 ± 0.8 ^a	-868.607 ± 0.9	-82.6 ± 0.7 ^a	-980.13 ± 0.8
$\text{ZnSO}_4 \cdot \text{H}_2\text{O}(\text{s}) \rightleftharpoons \text{Zn}^{2+} + \text{SO}_4^{2-} + \text{H}_2\text{O}$	-0.57 ^b			-44.52 ^b	
Bianchite $\text{ZnSO}_4 \cdot 6\text{H}_2\text{O} \rightleftharpoons \text{Zn}^{2+} + \text{SO}_4^{2-} + 6\text{H}_2\text{O}$	-1.87 ± 0.15	10.7 ± 0.7 ^a	-2324.747 ± 1.000	0.30 ± 0.86 ^a	2 778.010 ± 1.000
Goslarite $\text{ZnSO}_4 \cdot 7\text{H}_2\text{O} \rightleftharpoons \text{Zn}^{2+} + \text{SO}_4^{2-} + 7\text{H}_2\text{O}$	-1.98 ± 0.15	11.3 ± 0.8 ^a	-2562.487 ± 0.100	14.20 ± 0.52 ^a	3 077.740 ± 0.083
$\text{Zn}^{2+} + \text{SO}_4^{2-} \rightleftharpoons \text{Zn}(\text{SO}_4)(\text{aq})$	2.30 ± 0.04 ^d	-13.151 ± 0.240	-904.358 ± 0.545	6.0 ± 0.5 ^d	-1 056.730 ± 0.671
$\text{Zn}^{2+} + 2\text{SO}_4^{2-} \rightleftharpoons \text{Zn}(\text{SO}_4)_2^{2-}$	3.2 ± 0.2 ^d				
$\text{ZnSe}-\alpha + 2\text{H}^+ \rightleftharpoons \text{Zn}^{2+} + \text{H}_2\text{Se}(\text{aq})$	-8.20 ± 0.61	46.780 ± 3.468	-172.488 ± 4.013 ^c	36.910 ± 3.446	-176.000 ± 4.000 ^c
$\text{ZnSeO}_4 \cdot 6\text{H}_2\text{O}(\text{cr}) \rightleftharpoons \text{Zn}^{2+} + \text{SeO}_4^{2-} + 6\text{H}_2\text{O}$	-1.54 ± 0.07	8.781 ± 0.387	-2 018.309 ± 1.524 ^c	-13.330 ± 4.373	-2 458.540 ± 5.610 ^c
$\text{Zn}^{2+} + \text{SeCN}^- \rightleftharpoons \text{Zn}(\text{SeCN})^+$	1.21 ± 0.06	-6.906 ± 0.344	-18.058 ± 3.824 ^c		
$\text{Zn}^{2+} + 2\text{SeCN}^- \rightleftharpoons \text{Zn}(\text{SeCN})_2(\text{aq})$	1.68 ± 0.11	-9.588 ± 0.626	115.311 ± 7.630 ^c		
$\text{Zn}^{2+} + \text{SeO}_4^{2-} \rightleftharpoons \text{Zn}(\text{SeO}_4)(\text{aq})$	2.16 ± 0.06	-12.329 ± 0.342	-599.017 ± 1.493 ^c	4.6 ± 4.0	-752.290 ± 5.319 ^c

a [1995ROB/HEM]; b [1991BAL/NOR]; c [2005OLI/NOL]; d [2013POW/BRO].

* calculated from $\Delta_r G_m^{\circ}$ or $\Delta_r H_m^{\circ}$, and $\Delta_f G_m^{\circ}$ or $\Delta_f H_m^{\circ}$ in [2003GUI/FAN].**Table 3.7-3. Thermodynamic constants and functions of P and As compounds of zinc.**

Reaction	$\log_{10} \beta_n^{\circ}$	$\Delta_r G_m^{\circ}$ (kJ mol ⁻¹)	$\Delta_f G_m^{\circ}$ * (kJ mol ⁻¹)	$\Delta_r H_m^{\circ}$ (kJ mol ⁻¹)	$\Delta_f H_m^{\circ}$ * (kJ mol ⁻¹)
$\text{Zn}_3(\text{PO}_4)_2 \cdot 4\text{H}_2\text{O} \rightleftharpoons 3\text{Zn}^{2+} + 2\text{PO}_4^{3-} + 4\text{H}_2\text{O}$	-35.3 ^a	201.494	-3 642.645		
$\text{Zn}_4(\text{PO}_4)_2(\text{OH})_2 \cdot 3\text{H}_2\text{O} \rightleftharpoons 4\text{Zn}^{2+} + 2\text{PO}_4^{3-} + 2\text{OH}^- + 3\text{H}_2\text{O}$	-52.8 ^a	301.385	-3 967.039		
$\text{Zn}_4(\text{PO}_4)_2(\text{OH})_2 \cdot 3\text{H}_2\text{O} + 2\text{H}^+ \rightleftharpoons 4\text{Zn}^{2+} + 2\text{PO}_4^{3-} + 5\text{H}_2\text{O}$	-24.8	127.506			

Table 3.7-3. Continued.

Reaction	$\log_{10} \beta_n^\circ$	$\Delta_r G_m^\circ$ (kJ mol ⁻¹)	$\Delta_f G_m^\circ$ * (kJ mol ⁻¹)	$\Delta_r H_m^\circ$ (kJ mol ⁻¹)	$\Delta_f H_m^\circ$ * (kJ mol ⁻¹)
$Zn_2(PO_4)OH \rightleftharpoons 2Zn^{2+} + PO_4^{3-} + OH^-$	-26.6 ^a	151.834	-1 628.951		
$Zn_2(PO_4)OH + H^+ \rightleftharpoons 2Zn^{2+} + PO_4^{3-} + H_2O$	-12.6	71.914			
$Zn_5(PO_4)_3OH \rightleftharpoons 5Zn^{2+} + 3PO_4^{3-} + OH^-$	-63.1 ^a	360.177	-4 329.885		
$Zn_5(PO_4)_3OH + H^+ \rightleftharpoons 5Zn^{2+} + 3PO_4^{3-} + H_2O$	-49.1	280.257			
$ZnAl_6(PO_4)_4(OH)_8 \cdot 4H_2O \rightleftharpoons Zn^{2+} + 6Al^{3+} + 4PO_4^{3-} + 8OH^- + 4H_2O$	-177.7 ^a	1014.319	-10 418.848		
$ZnAl_6(PO_4)_4(OH)_8 \cdot 4H_2O + 8H^+ \rightleftharpoons Zn^{2+} + 6Al^{3+} + 4PO_4^{3-} + 12H_2O$	-65.7	374.959			
$Zn_3(AsO_4)_2 \cdot 2.5H_2O(s) \rightleftharpoons 3Zn^{2+} + 2AsO_4^{3-} + 2.5H_2O$	-47.78	272.724	-2 603.903		
$Zn^{2+} + PO_4^{3-} + H^+ \rightleftharpoons Zn(HPO_4)(aq)$	15.64 ± 0.20^b				

a [1984NRI]; b [2013POW/BRO].

* calculated from $\Delta_r G_m^\circ$ or $\Delta_r H_m^\circ$, and $\Delta_f G_m^\circ$ or $\Delta_f H_m^\circ$ in [2003GUI/FAN].**Table 3.7-4. Thermodynamic constants and functions of C and Si compounds of zinc.**

Reaction	$\log_{10} \beta_n^\circ$	$\Delta_r G_m^\circ$ (kJ mol ⁻¹)	$\Delta_f G_m^\circ$ * (kJ mol ⁻¹)	$\Delta_r H_m^\circ$ (kJ mol ⁻¹)	$\Delta_f H_m^\circ$ * (kJ mol ⁻¹)
Smithsonite					
$ZnCO_3 \rightleftharpoons Zn^{2+} + CO_3^{2-}$	-10.55 ± 0.54	60.197 ± 3.065^a	-735.300 ± 3.100	-11.620 ± 3.083^a	-817.000 ± 3.100
$ZnCO_3(s) \rightleftharpoons Zn^{2+} + CO_3^{2-}$	-10.93 ± 0.04^b	62.389 ± 0.228	-737.492 ± 0.518		
$Zn^{2+} + CO_3^{2-} \rightleftharpoons Zn(CO_3)(aq)$	4.75 ± 0.05^b	-27.113 ± 0.285	-702.216 ± 0.546		
$Zn^{2+} + CO_3^{2-} \rightleftharpoons Zn(CO_3)_2^{2-}$	$6.8 + 0.6^b$				
$Zn^{2+} + HCO_3^- \rightleftharpoons Zn(HCO_3)^+$	1.62 ± 0.10^b	-9.247 ± 0.570	-743.295 ± 0.673		
$Zn^{2+} + CO_3^{2-} + H^+ \rightleftharpoons Zn(HCO_3)^+$	11.95 ± 0.08	-68.192 ± 0.486			
$2Zn^{2+} + H_2O + CO_2(g) \rightleftharpoons Zn_2(CO_3)^{2+} + 2H^+$					
	-13.47 ± 0.05^c				
	3 M NaClO_4				
	-14.29 ± 0.05	81.568 ± 0.285	-844.351 ± 0.967		
	0 M				
$2Zn^{2+} + CO_3^{2-} \rightleftharpoons Zn_2(CO_3)^{2+}$	3.86 ± 0.13	-22.045 ± 0.725			
Willemite					
$Zn_2SiO_4 + 4H^+ \rightleftharpoons 2Zn^{2+} + Si(OH)_4(aq)$	13.83 ± 0.20	-78.940 ± 1.168^a	$-1 523.201 \pm 0.480$	-130.060 ± 3.172^a	-1633.680 ± 0.320

a [1995ROB/HEM]; b [2013POW/BRO]; c [1985FER/GRE].

* calculated from $\Delta_r G_m^\circ$ or $\Delta_r H_m^\circ$, and $\Delta_f G_m^\circ$ or $\Delta_f H_m^\circ$ in [2003GUI/FAN].**Table 3.7-5. Specific ion interaction coefficient for Zn(II) complexes.**

Specific ion interaction coefficient	Value	Comment or reference
$\epsilon(Zn^{2+}, ClO_4^-)$	0.33 ± 0.03	[1980CIA]
$\epsilon(Zn^{2+}, Cl^-)$	0.29 ± 0.11	[2001ZHA/MUH]
$\epsilon(Zn^{2+}, NO_3^-)$	0.16 ± 0.02	[1980CIA]
$\epsilon(Zn(OH)^+, ClO_4^-)$	0.17 ± 0.03	from $\Delta\epsilon$ in [2016BRO/EKB]
$\epsilon(Zn(OH)^+, Cl^-)$	0.17 ± 0.03	Estimation from Eq. 26 [1990CIA]
$\epsilon(Zn(OH)^+, NO_3^-)$	0.10 ± 0.03	Estimation from Eq. 26 [1990CIA]
$\epsilon(Zn(OH)_2(aq), Na^+ClO_4^-)$	-0.02 ± 0.05	[2001ZHA/MUH]
$\epsilon(Zn(OH)_3^-, Na^+)$	-0.06 ± 0.05	[2001ZHA/MUH]
$\epsilon(Zn(OH)_3^-, K^+)$	-0.05 ± 0.04	[2001ZHA/MUH]
$\epsilon(Zn_2(OH)^{3+}, ClO_4^-)$	0.6 ± 0.2	Analogy to Co(II), Ni(II) and Cu(II) [2001ZHA/MUH]
$\epsilon(Zn_4(OH)_4^{4+}, ClO_4^-)$	0.9 ± 0.3	Analogy to Co(II), Ni(II) and Cu(II) [2001ZHA/MUH]
$\epsilon(Zn_2(OH)_6^{2-}, Na^+)$	0.10 ± 0.08	[2001ZHA/MUH]
$\epsilon(Zn_2(OH)_6^{2-}, K^+)$	0.32 ± 0.09	[2001ZHA/MUH]
$\epsilon(Zn(OH)_4^{2-}, Na^+)$	0.05 ± 0.04	[2001ZHA/MUH]
$\epsilon(Zn(OH)_4^{2-}, K^+)$	0.20 ± 0.04	[2001ZHA/MUH]

Table 3.7-5. Continued.

Specific ion interaction coefficient	Value	Comment or reference
$\varepsilon(\text{ZnCl}^+, \text{ClO}_4^-)$	0.22 ± 0.04	from $\Delta\varepsilon$ in [2013POW/BRO]
$\varepsilon(\text{ZnCl}_2(\text{aq}), \text{Na}^+\text{ClO}_4^-)$	0.19 ± 0.05	from $\Delta\varepsilon$ in [2013POW/BRO]
$\varepsilon(\text{ZnCl}_3^-, \text{Na}^+)$	0.15 ± 0.14	from $\Delta\varepsilon$ in [2013POW/BRO]
$\varepsilon(\text{Zn}(\text{SO}_4)(\text{aq}), \text{Li}^+\text{ClO}_4^-)$	0.25 ± 0.06	from $\Delta\varepsilon$ in [2013POW/BRO]
$\varepsilon(\text{Zn}(\text{SO}_4)_2^{2-}, \text{Li}^+)$	0.36 ± 0.12	from $\Delta\varepsilon$ in [2013POW/BRO]
$\varepsilon(\text{ZnHCO}_3^+, \text{ClO}_4^-)$	0.43 ± 0.05	from $\Delta\varepsilon$ in [2013POW/BRO]
$\varepsilon(\text{Zn}(\text{CO}_3)_2^{2-}, \text{Na}^+)$	0.04 ± 0.06	Estimation from Eq. 27 [1990CIA]

3.7.2. Cadmium

3.7.2.1. Native Metal and Free Ion

Based on CODATA selection [1989COX/WAG], the functions of formation for $\gamma\text{-Cd(cr)}$, and Cd^{2+} are available in Guillaumont *et al.* [2003GUI/FAN]. The common master species is Cd^{2+} .

The value of $\varepsilon(\text{Cd}^{2+}, \text{ClO}_4^-)$ and $\varepsilon(\text{Cd}^{2+}, \text{Cl}^-)$ are not present in any NEA-OECD selection [1992GRE/FUG; 2003GUI/FAN; 2020GRE/GAO]. Ciavatta [1980CIA] reported a range of 0.27-0.34 for Ca^{2+} , Mg^{2+} , Co^{2+} , Cu^{2+} , Zn^{2+} , and Hg^{2+} in ClO_4^- . A selection from the different values in Figure 2.6-1 for the transition metals series is shown in Figure 3.7-4 as a function of $1/r$ [1976SHA]. Grand average values of $\varepsilon(\text{Cd}^{2+}, \text{ClO}_4^-) = (0.35 \pm 0.02) \text{ kg}_w \text{ mol}^{-1}$ and $\varepsilon(\text{Cd}^{2+}, \text{Cl}^-) = (0.17 \pm 0.08) \text{ kg}_w \text{ mol}^{-1}$ can be estimated.

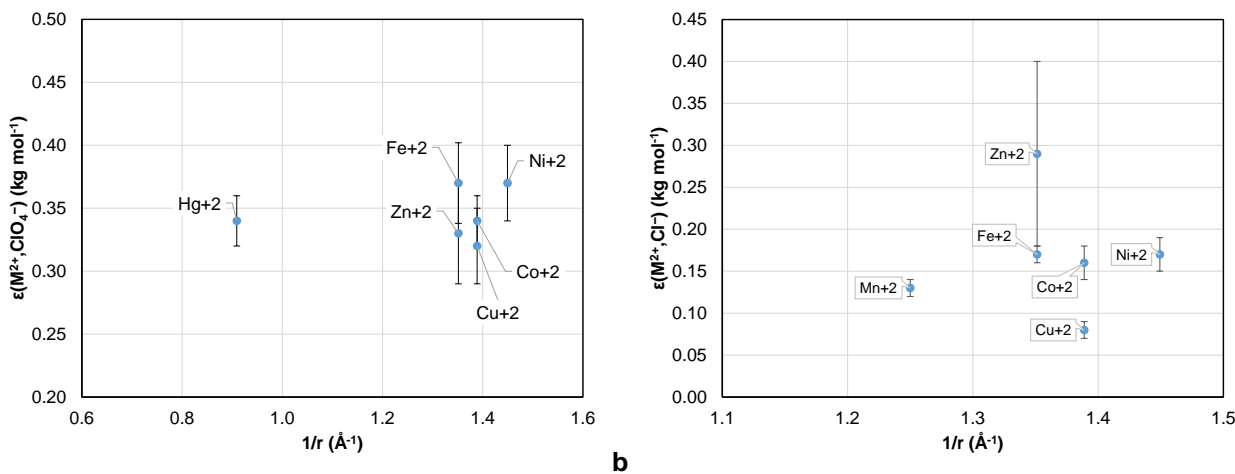


Figure 3.7-4. Values of $\varepsilon(\text{M}^{2+}, \text{ClO}_4^-)$ (a) and $\varepsilon(\text{M}^{2+}, \text{Cl}^-)$ for transition metals vs. $1/r$ [1976SHA].

3.7.2.2. Oxo and Hydroxo Compounds

The function of formation for $\gamma\text{-Cd(cr)}$, CdO(cr) , and Cd^{2+} are taken from Guillaumont *et al.* [2003GUI/FAN].

The solubility of $\text{Cd}(\text{OH})_2(\text{s})$ and the hydrolysis of $\text{Cd}^{2+} \rightarrow \text{Cd}(\text{OH})_{n-}^{2-n}$ are taken from Powell *et al.* [2011POW/BRO]. More recently, Brown and Ekberg [2016BRO/EKB] also proposed the estimation of solubility and hydrolysis, which does not change significantly from the estimations of Powell *et al.* [2011POW/BRO], with the exception of non-propagation of $\text{Cd}(\text{OH})$. For the sake of coherency, the constants and functions from Powell *et al.* [2011POW/BRO] are used in PRODATA.

The $\Delta\varepsilon$ values for $\text{Cd}(\text{OH})^+$, $\text{Cd}(\text{OH})_2(\text{aq})$, and $\text{Cd}_2(\text{OH})^{3+}$ in Powell *et al.* [2011POW/BRO], and the estimated value for $\varepsilon(\text{Cd}^{2+}, \text{ClO}_4^-/\text{Cl}^-)$ in § 3.7.2.1 allow calculating the ε values in Table 3.7-9.

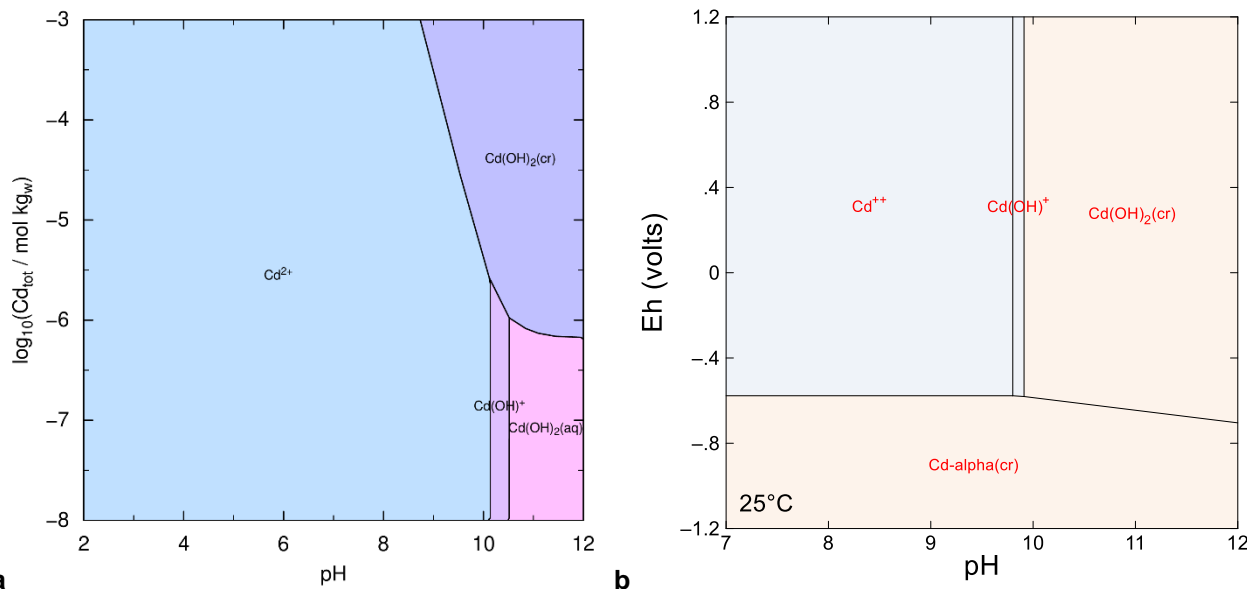


Figure 3.7-5. (a) Solubility of Cd in a hypothetical indifferent electrolyte at 0.1 mol kg_w⁻¹ using PHREEPLOT; all phases are allowed to precipitate; (b) Pourbaix diagram of Cd in the same conditions using GWB.

3.7.2.3. Chloro Complexes

The functions of reaction for CdCl₂(cr) and CdCl₂: H₂O(cr) are calculated from [1982WAG/EVA].

The constants and $\Delta_r H^\circ$ for CdCl_n²⁻ⁿ with n = {1; 2; 3} complexes are taken from Powell *et al.* [2011POW/BRO]. The authors also proposed $\Delta\varepsilon$ values for the complexes that are used to calculate the ε values in Table 3.7-9.

The $\varepsilon(\text{CdCl}^+, \text{ClO}_4^-) = 0.23 \text{ kg}_w \text{ mol}^{-1}$ corresponds to the value in Spahiu [1983SPA].

3.7.2.4. Sulphur and Selenium Compounds

Wagman *et al.* [1982WAG/EVA] reported functions of formation for CdS(cr), and Robie and Hemingway [1995ROB/HEM] reported those of greenockite. As in the case of S(-II), there is a great discrepancy in the $\Delta_f G^\circ$ values — *i.e.*, $-(156.5 \pm 4.0) \text{ kJ mol}^{-1}$ [1982WAG/EVA], and $-(146.1 \pm 1.3) \text{ kJ mol}^{-1}$ [1995ROB/HEM] — that would yield in different $\log_{10} K_s$ values.

Concerning the problem of the sign of $\Delta_f H^\circ(\text{HS}^-)$ it also yields to different $\Delta_r H^\circ$ values. If the functions of formation for HS⁻ in § 3.3 are used instead, the $\log_{10} K_s$ values are more in agreement

Table 3.7-6. Thermodynamic functions and constants for the CdS solids.

Reaction	$\Delta_r G^\circ (\text{kJ mol}^{-1})$	$\log_{10} K_s$	$\Delta_r H^\circ (\text{kJ mol}^{-1})$	References
CdS(cr) + H ⁺ \rightleftharpoons Cd ²⁺ + HS ⁻	90.968 ± 3.948	-15.94 ± 0.69	68.4 ± 7.673	[1982WAG/EVA]
Greenockite + H ⁺ \rightleftharpoons Cd ²⁺ + HS ⁻	113.3 ± 1.1^a	-19.85 ± 0.19^a	90.0 ± 1.1^a	[1995ROB/HEM]
	80.7 ± 1.1^b	-14.14 ± 0.19^b	57.4 ± 1.1^b	

a using function of formation in [1995ROB/HEM]; b using re-estimated functions in § 3.3

The solubility of CdSO₄(cr) can be retrieved from the functions in Wagman *et al.* [1982WAG/EVA].

Powell *et al.* [2011POW/BRO] recommended a value for the formation of Cd(SO₄)(aq), and proposed an indicative value for the formation of Cd(SO₄)₂²⁻. The given $\Delta\varepsilon$ values are used to calculate the ε values in Table 3.7-9.

Olin *et al.* [2005OLI/NOL] selected a value for the formation of α-CdSe(cr), CdSeO₃(cr), and CdSeO₄(aq).

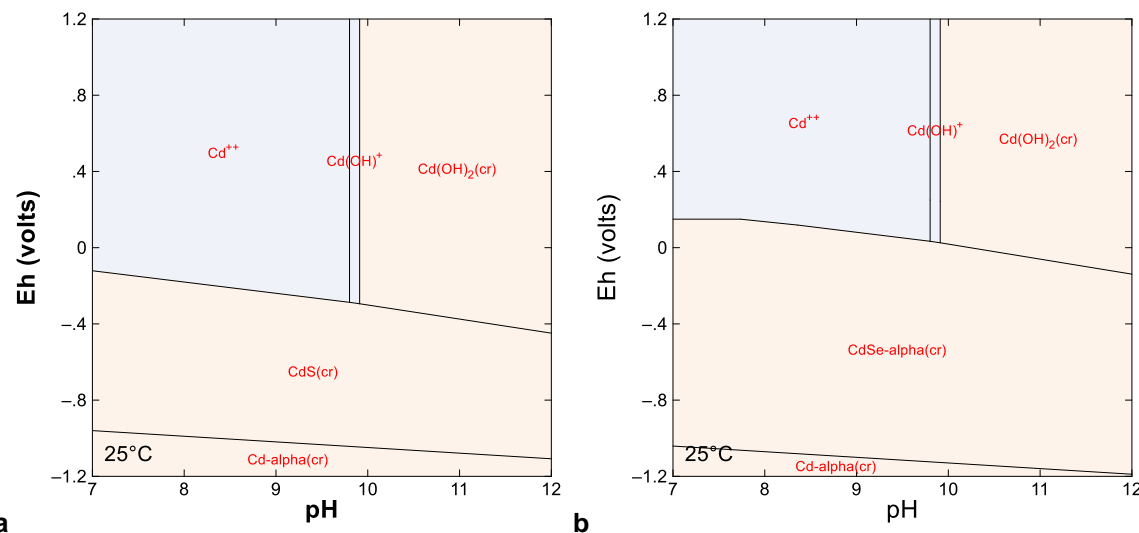
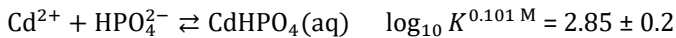


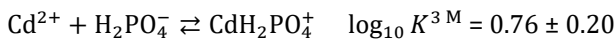
Figure 3.7-6. Pourbaix diagram (GWB) of 10^{-6} mol kg_w⁻¹ Cd in a hypothetical indifferent 0.1 mol kg_w⁻¹ electrolyte solution containing 10^{-4} mol kg_w⁻¹ of S (a) and Se (b). All solid phases are allowed to precipitate.

3.7.2.5. Phosphor Compounds

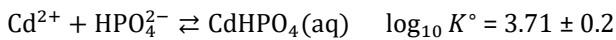
The formation of phosphate complexes was noted provisional by Powell *et al.* [2011POW/BRO]. The formation of CdHPO₄(aq) at 0.101 kg_w mol⁻¹ NaClO₄,



and of CdH₂PO₄⁺ at 3 mol dm⁻³ NaClO₄ was reported.



The value of $\varepsilon(\text{CdHPO}_4(\text{aq}), \text{NaClO}_4)$ could be considered nil, and the following extrapolation to infinite dilution could eventually be proposed.



Ciavatta [1980CIA] proposed a way to estimate the missing specific ion interaction theory parameters. This would give the following expression in the case of the formation of CdH₂PO₄⁺.

$$\varepsilon(\text{CdH}_2\text{PO}_4^+, \text{ClO}_4^-) = \frac{\varepsilon(\text{Cd}^{2+}, \text{ClO}_4^-) + \varepsilon(\text{H}_2\text{PO}_4^-, \text{Na}^+)}{2} = 0.13 \text{ kg}_w \text{ mol}^{-1}$$

The extrapolation to infinite dilution is then



The values of $\log_{10} K^\circ$ referring to HPO₄²⁻ and PO₄³⁻ are calculated using the acidity constants of phosphate system [2003GUI/FAN].

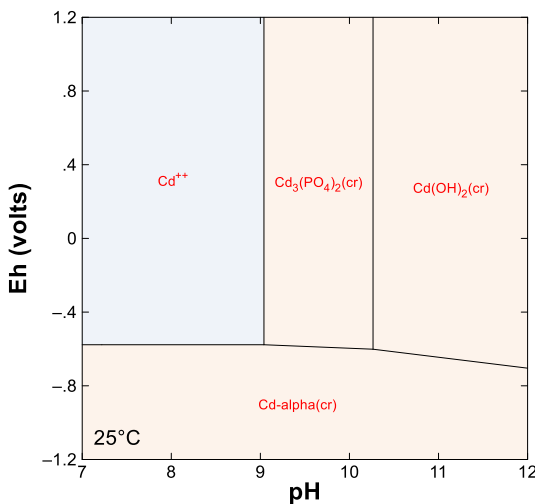


Figure 3.7-7. Pourbaix diagram (GWB) of 10^{-6} mol kg_w⁻¹ Cd in a hypothetical indifferent 0.1 mol kg_w⁻¹ electrolyte solution containing 10^{-4} mol kg_w⁻¹ P. All solid phases are allowed to precipitate.

3.7.2.6. Carbon Compounds

Powell *et al.* [2011POW/BRO] proposed a provisional value for the formation of Cd(CO₃)(aq), and the solubility of CdCO₃(cr). The function of formation for CdSeCN_n⁽²⁻ⁿ⁾⁺ are taken from Olin *et al.* [2005OLI/NOL].

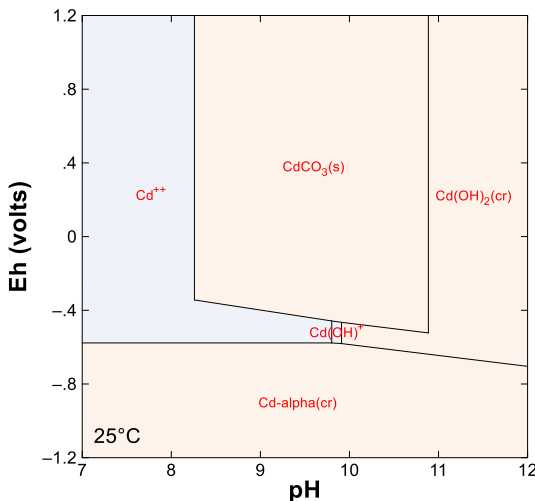


Figure 3.7-8. Pourbaix diagram (GWB) of 10^{-6} mol kg_w⁻¹ Cd in a hypothetical indifferent 0.1 mol kg_w⁻¹ electrolyte solution containing 10^{-4} mol kg_w⁻¹ C. All solid phases are allowed to precipitate.

3.7.2.7. Tables of Thermodynamic Constants and Functions, and Specific Ion Interaction Coefficients for Cd

Table 3.7-7. Thermodynamic constants and functions for the native element, free ion, and oxo and hydroxo compounds of Cd.

Reaction	$\log_{10} K^\circ$	$\Delta_r G^\circ$ kJ mol ⁻¹	$\Delta_f G^\circ$ * kJ mol ⁻¹	$\Delta_r H^\circ$ kJ mol ⁻¹	$\Delta_f H^\circ$ * kJ mol ⁻¹
Cd-γ(cr) ⇌ Cd ²⁺ + 2e ⁻	13.62 ± 0.13	-77.733 ± 0.750	-77.733 ± 0.750^a	-75.920 ± 0.600	-75.920 ± 0.600^a
Cd ²⁺ + 2e ⁻ ⇌ Cd-α(cr)	-13.49 ± 0.13	77.022 ± 0.720^b	-0.711 ± 0.868	75.310 ± 7.164^b	-0.610 ± 0.744
Cd-γ(cr) + 0.5O ₂ (aq) + 2H ⁺ ⇌ Cd ²⁺ + H ₂ O		56.60 ± 0.11	-323.062 ± 0.603		-355.900 ± 0.401
Cd-α(cr) + 0.5O ₂ (aq) + 2H ⁺ ⇌ Cd ²⁺ + H ₂ O		56.47 ± 0.11	-322.351 ± 0.624		-355.290 ± 0.627

Table 3.7-7. Continued.

Reaction	$\log_{10} K^\circ$	$\Delta_r G^\circ$ kJ mol ⁻¹	$\Delta_f G^\circ$ * kJ mol ⁻¹	$\Delta_r H^\circ$ kJ mol ⁻¹	$\Delta_f H^\circ$ * kJ mol ⁻¹
$\text{CdO(cr)} + 2\text{H}^+ \rightleftharpoons \text{Cd}^{2+} + \text{H}_2\text{O}$	15.10 ± 0.08	-86.212 ± 0.449	-228.661 ± 0.602^a	-103.400 ± 0.449	-258.350 ± 0.400^a
$\text{Cd(OH)}_2(\text{cr}) + 2\text{H}^+ \rightleftharpoons \text{Cd}^{2+} + 2\text{H}_2\text{O}$	13.71 ± 0.10	-78.270 ± 0.582^b	-473.743 ± 0.480	-86.860 ± 5.567^b	-560.720 ± 5.600
$\text{Cd(OH)}_2(\text{s}) + 2\text{H}^+ \rightleftharpoons \text{Cd}^{2+} + 2\text{H}_2\text{O}$	13.72 ± 0.12^c	-78.329 ± 0.695	-473.684 ± 1.026		
$\text{Cd}^{2+} + \text{H}_2\text{O} \rightleftharpoons \text{Cd(OH)}^+ + \text{H}^+$	-9.80 ± 0.10^c	55.939 ± 0.571	-258.934 ± 0.943	54.800 ± 2.000^c	-306.950 ± 2.088
$\text{Cd}^{2+} + 2\text{H}_2\text{O} \rightleftharpoons \text{Cd(OH)}_2(\text{aq}) + 2\text{H}^+$	-20.19 ± 0.13^c	115.245 ± 0.742	-436.768 ± 1.058	111.690 ± 0.581^c	-535.890 ± 0.170
$\text{Cd}^{2+} + 3\text{H}_2\text{O} \rightleftharpoons \text{Cd(OH)}_3^- + 3\text{H}^+$	-33.5 ± 0.5^c	191.219 ± 2.854	-597.934 ± 2.953		
$\text{Cd}^{2+} + 4\text{H}_2\text{O} \rightleftharpoons \text{Cd(OH)}_4^{2-} + 4\text{H}^+$	-47.28 ± 0.15^c	269.876 ± 0.856	-756.417 ± 1.150		
$2\text{Cd}^{2+} + \text{H}_2\text{O} \rightleftharpoons \text{Cd}_2(\text{OH})^{3+} + \text{H}^+$	-8.73 ± 0.01^c	49.831 ± 0.856	-342.775 ± 1.728	-94.6 ± 2.0^c	-532.270 ± 2.333

a [2003GUI/FAN]; b [1982WAG/EVA]; c [2011POW/BRO].

* calculated from $\Delta_r G_m^\circ$ or $\Delta_r H_m^\circ$, and $\Delta_f G_m^\circ$ or $\Delta_f H_m^\circ$ in [2003GUI/FAN], unless noted otherwise.**Table 3.7-8. Thermodynamic constants and functions for the Cl, S, Se, P, and C compounds of Cd.**

Reaction	$\log_{10} K^\circ$	$\Delta_r G^\circ$ kJ mol ⁻¹	$\Delta_f G^\circ$ * kJ mol ⁻¹	$\Delta_r H^\circ$ kJ mol ⁻¹	$\Delta_f H^\circ$ * kJ mol ⁻¹
$\text{CdCl}_2(\text{cr}) \rightleftharpoons \text{Cd}^{2+} + 2\text{Cl}^-$	-0.68 ± 0.13	3.862 ± 0.748^a	-344.029 ± 0.240	-18.718 ± 3.948^a	-391.362 ± 4.000
$\text{CdCl}_2 \cdot \text{H}_2\text{O}(\text{cr}) \rightleftharpoons \text{Cd}^{2+} + 2\text{Cl}^- + \text{H}_2\text{O}$	-1.71 ± 0.14	9.778 ± 0.786^a	-587.085 ± 0.040	-7.470 ± 0.547^a	-688.302 ± 0.320
$\text{Cd}^{2+} + \text{Cl}^- \rightleftharpoons \text{CdCl}^+$	1.98 ± 0.06^b	-11.302 ± 0.342	-220.252 ± 0.833	3.3 ± 0.6^b	-239.700 ± 0.854
$\text{Cd}^{2+} + 2\text{Cl}^- \rightleftharpoons \text{CdCl}_2(\text{aq})$	2.64 ± 0.09^b	-15.069 ± 0.514	-355.236 ± 0.939	7.8 ± 1.4^b	-402.280 ± 1.536
$\text{Cd}^{2+} + 3\text{Cl}^- \rightleftharpoons \text{CdCl}_3^-$	2.30 ± 0.21^b	-13.128 ± 1.199	-484.512 ± 1.457		
$\text{CdS(cr)} + \text{H}^+ \rightleftharpoons \text{Cd}^{2+} + \text{HS}^-$	-15.94 ± 0.69	90.968 ± 3.948^a	-156.458 ± 0.800	68.4 ± 7.673^a	-160.620 ± 1.300
Greenockite					
$\text{CdS} + \text{H}^+ \rightleftharpoons \text{Cd}^{2+} + \text{HS}^-$	-14.14 ± 0.19	80.7 ± 1.1^c	-146.190 ± 1.301	57.4 ± 1.1^c	-149.620 ± 1.300
$\text{CdSO}_4(\text{cr}) \rightleftharpoons \text{Cd}^{2+} + \text{SO}_4^{2-}$	-0.10 ± 0.15	0.578 ± 0.844^a	-822.315 ± 0.160	-51.890 ± 0.332^a	-933.370 ± 0.640
$\text{Cd}^{2+} + \text{SO}_4^{2-} \rightleftharpoons \text{Cd}(\text{SO}_4)(\text{aq})$	2.36 ± 0.04^b	-13.471 ± 0.228	-835.208 ± 0.888	8.3 ± 0.5^b	-976.960 ± 0.877
$\text{Cd}^{2+} + 2\text{SO}_4^{2-} \rightleftharpoons \text{Cd}(\text{SO}_4)_2^-$	3.32 ± 0.16^b				
$\text{CdSe(cr)} + \text{H}^+ \rightleftharpoons \text{Cd}^{2+} + \text{H}_2\text{Se}(\text{aq})$	-14.83 ± 0.17	84.659 ± 0.946	-140.897 ± 1.918^d	81.480 ± 0.916	-143.100 ± 1.900^d
$\text{CdSeO}_3(\text{cr}) \rightleftharpoons \text{Cd}^{2+} + \text{SeO}_3^{2-}$	-9.34 ± 1.08	53.307 ± 6.179	-493.432 ± 6.467^d	-6.280 ± 2.148	-576.800 ± 2.500^d
$\text{Cd}^{2+} + \text{SeO}_3^{2-} \rightleftharpoons \text{Cd}(\text{SeO}_4)(\text{aq})$	2.27 ± 0.06	-12.957 ± 0.345	-530.175 ± 1.652^d	8.3 ± 4.0	-671.120 ± 5.349^d
$\text{Cd}_3(\text{PO}_4)_2(\text{cr}) \rightleftharpoons 3\text{Cd}^{2+} + 2\text{PO}_4^{3-}$	-32.60 ± 0.53	186.064 ± 3.029^a	-2470.245 ± 2.414		
$\text{Cd}^{2+} + \text{HPO}_4^{2-} \rightleftharpoons \text{CdHPO}_4(\text{aq})$	3.71 ± 0.2^b				
$\text{Cd}^{2+} + \text{PO}_4^{3-} + \text{H}^+ \rightleftharpoons \text{CdHPO}_4(\text{aq})$		16.06 ± 0.2			
$\text{Cd}^{2+} + \text{H}_2\text{PO}_4^- \rightleftharpoons \text{CdH}_2\text{PO}_4^+$	1.38 ± 0.2^b				
$\text{Cd}^{2+} + \text{PO}_4^{3-} + 2\text{H}^+ \rightleftharpoons \text{CdH}_2\text{PO}_4^+$		20.94 ± 0.2			
$\text{Cd}_3(\text{AsO}_4)_2(\text{cr}) \rightleftharpoons 3\text{Cd}^{2+} + 2\text{AsO}_4^{3-}$	-32.66 ± 1.35	186.444 ± 3.029^a	-1716.363 ± 3.142		
$\text{CdCO}_3(\text{cr}) \rightleftharpoons \text{Cd}^{2+} + \text{CO}_3^{2-}$	-11.21 ± 0.23	63.978 ± 1.330^a	-669.611 ± 1.576	-2.440 ± 2.129^a	-748.710 ± 2.226
$\text{Cd}^{2+} + \text{CO}_3^{2-} \rightleftharpoons \text{Cd}(\text{CO}_3)(\text{aq})$	4.4 ± 0.2^b				
$\text{Cd}(\text{SeCN})_2(\text{cr}) \rightleftharpoons \text{Cd}^{2+} + 2\text{SeCN}^-$	-5.70 ± 0.50	32.535 ± 2.855	-161.834 ± 8.153^d		

a [1982WAG/EVA]; b [2011POW/BRO]; c [1995ROB/HEM] using reestimate function of formation for HS^- in § 3.3; d [2005OLI/NOL].* calculated from $\Delta_r G_m^\circ$ or $\Delta_r H_m^\circ$, and $\Delta_f G_m^\circ$ or $\Delta_f H_m^\circ$ in [2003GUI/FAN], unless noted otherwise.**Table 3.7-9. Specific ion interaction coefficients for the Cd complexes.**

Specific ion interaction coefficient	Value	Comments and references
$\varepsilon(\text{Cd}^{2+}, \text{ClO}_4^{2-})$	0.35 ± 0.02	Estimation from other transition metals
$\varepsilon(\text{Cd}^{2+}, \text{Cl}^-)$	0.17 ± 0.08	Estimation from other transition metals
$\varepsilon(\text{Cd}^{2+}, \text{NO}_3^-)$	0.09 ± 0.02	[2003GUI/FAN]
$\varepsilon(\text{Cd}(\text{OH})^+, \text{ClO}_4^-)$	0.15 ± 0.11	from $\Delta\varepsilon$ in [2011POW/BRO]

Table 3.7-9. Continued

Specific ion interaction coefficient	Value	Comments and references
$\epsilon(\text{Cd}(\text{OH})_2(\text{aq}), \text{Na}^+\text{ClO}_4^-)$	0.10 ± 0.10	from $\Delta\epsilon$ in [2011POW/BRO]
$\epsilon(\text{Cd}(\text{OH})_3^-, \text{Na}^+)$	0.07 ± 0.10	estimation using Eq. 26 [1990CIA]
$\epsilon(\text{Cd}(\text{OH})_4^{2-}, \text{Na}^+)$	0.06 ± 0.10	estimation using Eq. 26 [1990CIA]
$\epsilon(\text{Cd}_2(\text{OH})^{3+}, \text{ClO}_4^-)$	0.78 ± 0.10	from $\Delta\epsilon$ in [2011POW/BRO]
$\epsilon(\text{CdCl}^+, \text{ClO}_4^-)$	0.23 ± 0.10	from $\Delta\epsilon$ in [2011POW/BRO]
$\epsilon(\text{CdCl}_2(\text{aq}), \text{Na}^+\text{ClO}_4^-)$	0.13 ± 0.11	from $\Delta\epsilon$ in [2011POW/BRO]
$\epsilon(\text{CdCl}_3^-, \text{Na}^+)$	0.03 ± 0.13	from $\Delta\epsilon$ in [2011POW/BRO]
$\epsilon(\text{Cd}(\text{SO}_4)(\text{aq}), \text{Na}^+\text{ClO}_4^-)$	0.13 ± 0.12	from $\Delta\epsilon$ in [2011POW/BRO]
$\epsilon(\text{Cd}(\text{SO}_4)_2^{2-}, \text{Na}^+)$	0.21 ± 0.16	from $\Delta\epsilon$ in [2011POW/BRO]
$\epsilon(\text{CdSeO}_4(\text{aq}), \text{Na}^+\text{X}^-)$	0	
$\epsilon(\text{CdHPO}_4(\text{aq}), \text{Na}^+\text{X}^-)$	0	
$\epsilon(\text{CdH}_2\text{PO}_4^+, \text{ClO}_4^-)$	0.13 ± 0.05	estimation using Eq. 26 [1990CIA]
$\epsilon(\text{CdCO}_3(\text{aq}), \text{Na}^+\text{X}^-)$	0	

3.7.3. Mercury

3.7.3.1. Native Metal and Free Ions

Functions of formation for native liquid metal Hg(l) , Hg^{2+} , and Hg_2^{2+} ions are taken from Guillaumont *et al.* [2003GUI/FAN]. The specific ion interaction coefficients for Hg^{2+} and Hg_2^{2+} in ClO_4^- and NO_3^- are taken from Grenthe *et al.* [1992GRE/FUG]. No values are given for Cl^- media. In view of the relatively low influence of $1/r$ for +2 free ions in general, and for transition elements in particular, the grand average value for transition elements in § 3.7.2.1 is also applied to Hg^{2+} , i.e. $\epsilon(\text{Hg}^{2+}, \text{Cl}^-) = (0.17 \pm 0.08) \text{ kg}_w \text{ mol}^{-1}$. This analogy is not done on Hg_2^{2+} as it is not an M(II) free ion and the values are let as nil.

3.7.3.2. Oxo and Hydroxo Compounds

Grenthe *et al.* [1992GRE/FUG] selected functions of formation for montroydite (HgO(cr)).

Powell *et al.* [2005POW/BRO] proposed a $\log_{10} K_s$ and a $\Delta_r H^\circ$ value for the dissolution of HgO(s) , which can represent the three form of HgO — *i.e.*, red (montroydite), yellow, and hexagonal —, and $\log_{10} K_s$ for the three forms.

Powell *et al.* [2005POW/BRO] proposed formation constants for Hg(OH)_n^{2-n} with $n = \{1; 2\}$, and a provisional value for the formation of Hg(OH)_3^- ; an enthalpy of reaction for $n = 2$ is also recommended.

Only $\Delta\epsilon$ values in ClO_4^- are available in Powell *et al.* [2005POW/BRO], which values are used to calculate ϵ for $\text{Hg(OH)}_n^{(2-n)+}$. Using the estimation of $\epsilon(\text{Hg}^{2+}, \text{Cl}^-)$ (*vide supra*) and Eq. 26 and 27, ϵ values could be cautiously proposed for the first two hydroxo complex.

$$\begin{aligned} \text{Hg}^{2+} + \text{OH}^- &\rightleftharpoons \text{Hg(OH)}^+ & \epsilon(\text{Hg(OH)}^+, \text{Cl}^-) &= \frac{\epsilon(\text{Hg}^{2+}, \text{Cl}^-) + \epsilon(\text{OH}^-, \text{Na}^+)}{2} = \frac{0.17 + 0.04}{2} \\ && \epsilon(\text{Hg(OH)}^+, \text{Cl}^-) &= (0.11 \pm 0.08) \text{ kg}_w \text{ mol}^{-1} \\ \text{Hg}^{2+} + 2\text{OH}^- &\rightleftharpoons \text{Hg(OH)}_2(\text{aq}) & \epsilon(\text{Hg(OH)}_2(\text{aq}), \text{Na}^+\text{Cl}^-) &= \frac{\epsilon(\text{Hg}^{2+}, \text{Cl}^-) + 2\epsilon(\text{OH}^-, \text{Na}^+)}{3} \\ && \epsilon(\text{Hg(OH)}_2(\text{aq}), \text{Na}^+\text{Cl}^-) &= \frac{(0.17 + 2 \times 0.04)}{3} = (0.08 \pm 0.08) \text{ kg}_w \text{ mol}^{-1} \end{aligned}$$

The third hydroxo complex could be proposed from the $\Delta\epsilon$ values for $\text{Hg(OH)}_2(\text{aq})$ in NaClO_4 .

$$\begin{aligned} \text{Hg(OH)}_2(\text{aq}) + \text{OH}^- &\rightleftharpoons \text{Hg(OH)}_3^- & \epsilon(\text{Hg(OH)}_3^-, \text{Na}^+) &= \frac{\epsilon(\text{Hg(OH)}_2(\text{aq}), \text{Na}^+\text{ClO}_4^-) + \epsilon(\text{OH}^-, \text{Na}^+)}{2} \\ && \epsilon(\text{Hg(OH)}_3^-, \text{Na}^+) &= \frac{-0.08 + 0.04}{2} = -(0.02 \pm 0.05) \text{ kg}_w \text{ mol}^{-1} \end{aligned}$$

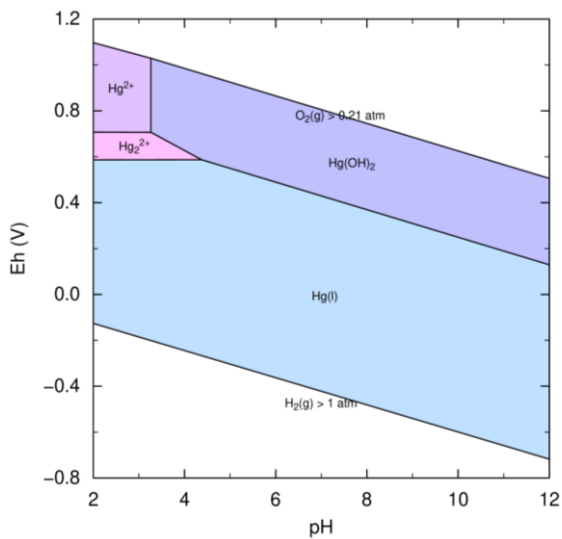


Figure 3.7-9. Pourbaix diagram (PHREEPLOT) of $10^{-6} \text{ mol kg}_{\text{w}}^{-1}$ Hg in a hypothetical indifferent $0.1 \text{ mol kg}_{\text{w}}^{-1}$ electrolyte solution; all solid phases are allowed to precipitate.

3.7.3.3. Halogeno Compounds

The Gibbs energy of reaction of Hg^{2+} complex can be calculated from Wagman *et al.* [1982WAG/EVA].

Powell *et al.* [2005POW/BRO] recommended formation constants and enthalpies of reactions for the formation of HgCl_n^{2-n} complexes, with $n = \{1; 2; 3; 4\}$, and a formation constant for $\text{HgOHCl}(\text{aq})$.

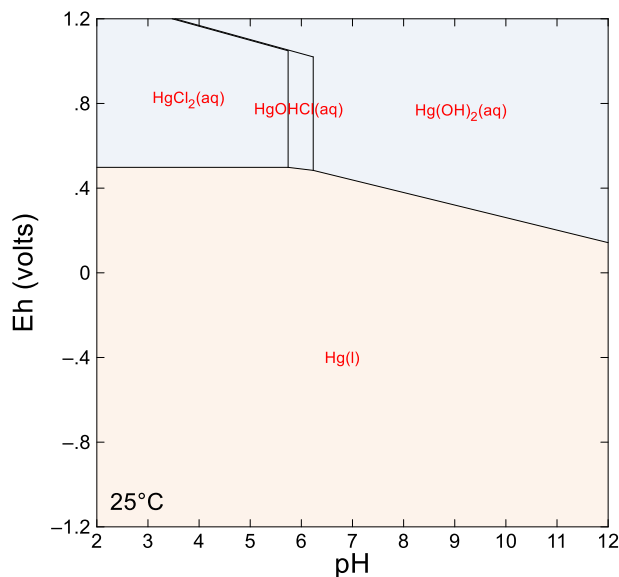


Figure 3.7-10. Pourbaix diagram (GWB) of $10^{-6} \text{ mol kg}_{\text{w}}^{-1}$ Hg in a hypothetical indifferent $0.1 \text{ mol kg}_{\text{w}}^{-1}$ electrolyte solution containing $10^{-4} \text{ mol kg}_{\text{w}}^{-1}$ Cl. All solid phases are allowed to precipitate.

3.7.3.4. Group 16 Compounds

3.7.3.4.1 Sulphur Compounds

Sulphide solids $\text{HgS}(\text{cr})$ cinnabar and metacinnabar can be retrieved in Wagman *et al.* [1982WAG/EVA], and Robie and Hemingway [1995ROB/HEM]. The $\Delta_f G^\circ$ values are notably different between the two sources, *i.e.*, *ca.* 10 and 4 kJ mol^{-1} for cinnabar and metacinnabar, respectively. In addition, as noted in § 3.3, there is a large difference between functions of formation for the S(-II) species. The $\Delta_r G^\circ$ for the solubility or phase

transformations of the allotropic forms of HgS(cr) can be written in Table 3.7-10. It can be seen that it is then difficult to ascertain a value. Nevertheless, the very low solubility of these phases is evident, and the use of the functions evaluated in § 3.3 for HS⁻ are giving closer values between the two sources. The two values will be included noted HgS-red(cr) and HgS-black(cr) [1982WAG/EVA], and cinnabar and meta-cinnabar [1995ROB/HEM].

Table 3.7-10. Gibbs energies of reaction for the solubility of mercury sulphide phases from different sources.

Reaction	$\Delta_r G^\circ \text{ (kJ mol}^{-1}\text{)}$	$\log_{10} K_s$	Reference
HgS-red(cr) + H ⁺ ⇌ Hg ²⁺ + HS ⁻	227.08 ± 5.80	-39.78 ± 1.02	[1982WAG/EVA]
Cinnabar + H ⁺ ⇌ Hg ²⁺ + HS ⁻	249.0 ± 2.7 ^a	-43.62 ± 0.47 ^a	[1995ROB/HEM]
	216.4 ± 2.7 ^b	-37.91 ± 0.47 ^b	
HgS-black(cr) + H ⁺ ⇌ Hg ²⁺ + HS ⁻	224.18 ± 6.48	-39.27 ± 0.96	[1982WAG/EVA]
Metacinnabar + H ⁺ ⇌ Hg ²⁺ + HS ⁻	251.6 ± 0.9 ^a	-44.08 ± 0.16 ^a	[1995ROB/HEM]
	219.0 ± 0.8 ^b	-38.37 ± 0.14 ^b	

a using functions for HS⁻ in [1995ROB/HEM]; b using re-evaluated function in § 3.3

The sulphide complexes Hg(HS)₃⁻, HgS(H₂S)₂(aq), and HgS₂²⁻ are taken from Spycher and Reed [1989SPY/REE].

The solubility of Hg₂SO₄(cr) is taken from Guillaumont *et al.* [2003GUI/FAN].

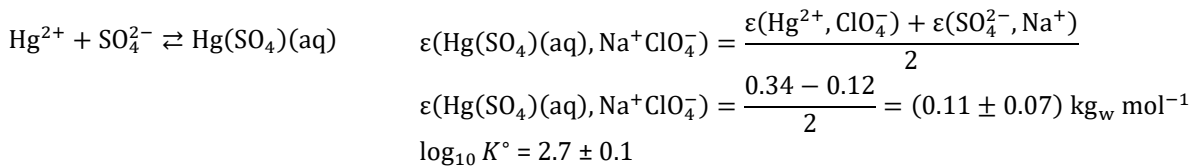
Powell *et al.* [2005POW/BRO] proposed a provisional value for the formation of HgSO₄(aq) at 0.5 M NaClO₄, but judged the formation value of Hg(SO₄)₂²⁻ as doubtful. This formation constant for HgSO₄(aq) is extrapolated using the SIT assuming that $\varepsilon(\text{HgSO}_4\text{(aq)}, \text{Na}^+\text{ClO}_4^-) = 0$, and then,

$$\Delta\varepsilon = \varepsilon(\text{HgSO}_4\text{(aq)}) - \varepsilon(\text{Hg}^{2+}, \text{ClO}_4^-) - \varepsilon(\text{SO}_4^{2-}, \text{Na}^+)$$



$$\log_{10} K^\circ = 2.6 \pm 0.1$$

This value could be compared to the one obtained using the other possible hypothesis, *i.e.*, Eq. 26 from Ciavatta [1980CIA].



In view of the weak difference between the two hypotheses, the nil hypothesis will be favoured.

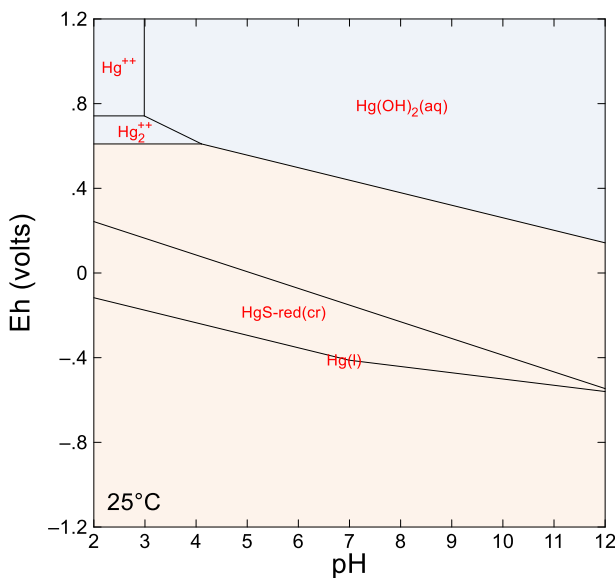


Figure 3.7-11. Pourbaix diagram (GWB) of 10^{-6} mol $\text{kg}_{\text{w}}^{-1}$ Hg in a hypothetical indifferent 0.1 mol $\text{kg}_{\text{w}}^{-1}$ electrolyte solution containing 10^{-4} mol $\text{kg}_{\text{w}}^{-1}$ S. All solid phases are allowed to precipitate.

3.7.3.4.2 Selenium Compounds

The diselenide HgSe_2^{2-} and selenocyanate complexes HgSeCN_n^{2-n} with $n = \{2; 3; 4\}$, are taken from Olin *et al.* [2005OLI/NOL].

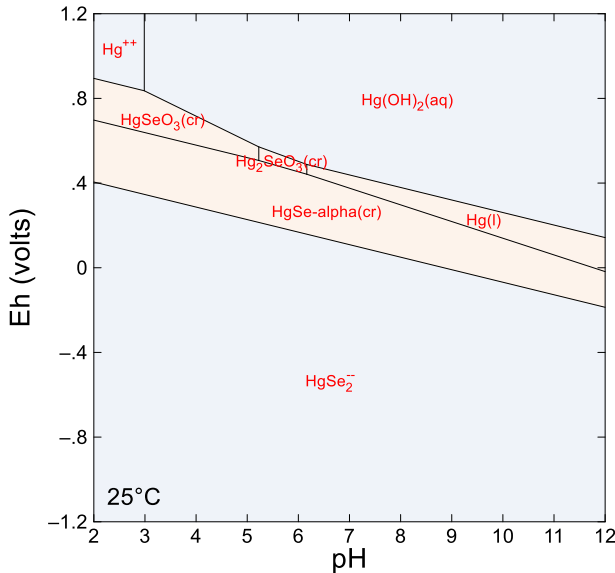
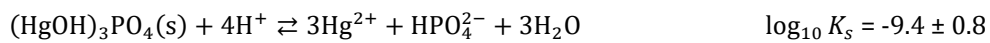


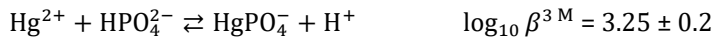
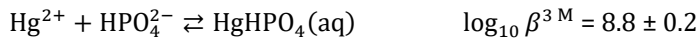
Figure 3.7-12. Pourbaix diagram (GWB) of 10^{-6} mol $\text{kg}_{\text{w}}^{-1}$ Hg in a hypothetical indifferent 0.1 mol $\text{kg}_{\text{w}}^{-1}$ electrolyte solution containing 10^{-4} mol $\text{kg}_{\text{w}}^{-1}$ Se. All solid phases are allowed to precipitate.

3.7.3.5. Phosphor Compounds

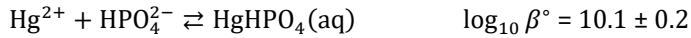
Powell *et al.* [2005POW/BRO] selected values for phosphate solids.



Powell *et al.* [2005POW/BRO] selected values for phosphate complexes at 3 mol L⁻¹ NaClO₄ — *i.e.*, 3.502 kg_w mol⁻¹ [1988NOV/SOH].



The formation of HgHPO₄(aq) can be extrapolated to infinite dilution assuming that $\varepsilon(\text{HgHPO}_4(\text{aq}), \text{Na}^+ \text{ClO}_4^-) = 0$.

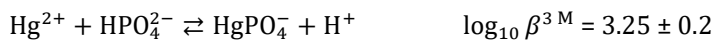


The formation of HgPO₄⁻ cannot be properly extrapolated using either assumption from Equations 26 or 27 [1990CIA], because of the implication of H⁺. The acidity constants for H₃PO₄(aq) selected in Powell *et al.* [2005POW/BRO] are slightly different from Guillaumont *et al.* [2003GUI/FAN].

Table 3.7-11. Acidity constants and variation of specific ion interaction coefficients for the phosphate system selected in Powell *et al.* [2005POW/BRO] and Guillaumont *et al.* [2003GUI/FAN].

Reaction	[2005POW/BRO]		[2003GUI/FAN]	
	$\log_{10} K_n^\circ$	$\Delta\varepsilon$	$\log_{10} K_n^\circ$	$\Delta\varepsilon$
PO ₄ ³⁻ + H ⁺ ⇌ HPO ₄ ²⁻	12.338 ± 0.028	-0.078 ± 0.019	12.350 ± 0.030	-0.04 ± 0.05
HPO ₄ ²⁻ + H ⁺ ⇌ H ₂ PO ₄ ⁻	7.200 ± 0.008	-0.061 ± 0.016	7.212 ± 0.014	-0.07 ± 0.05
H ₂ PO ₄ ⁻ + H ⁺ ⇌ H ₃ PO ₄ (aq)	2.141 ± 0.010	-0.043 ± 0.017	2.140 ± 0.030	-0.06 ± 0.04

The formation of HgPO₄⁻ can then be expressed relative to PO₄³⁻ at 3 M using the $\Delta\varepsilon$ values from Powell *et al.* [2005POW/BRO].



From this expression, then the $\varepsilon(\text{HgPO}_4^-, \text{Na}^+)$ value can be evaluated using the Equation 26 [1990CIA] and the ε values from Guillaumont *et al.* [2003GUI/FAN],

$$\varepsilon(\text{HgPO}_4^-, \text{Na}^+) = \frac{\varepsilon(\text{Hg}^{2+}, \text{ClO}_4^-) + \varepsilon(\text{PO}_4^{3-}, \text{Na}^+)}{2} = (0.05 \pm 0.02) \text{ kg}_w \text{ mol}^{-1}$$

which allows extrapolating the $\log_{10} K^\circ$ value.



The values of $\log_{10} \beta^\circ(\text{HgPO}_4^-)$ for the swapped values relative to HPO₄²⁻ or H₂PO₄⁻ will recalculated accounting for the $\log_{10} K_n^\circ$ — or more precisely $\log_{10} \beta_n^\circ$ — of H₃PO₄(aq) from Guillaumont *et al.* [2003GUI/FAN] with uncertainties in Table 3.4-3 (cf. § 3.4.2).

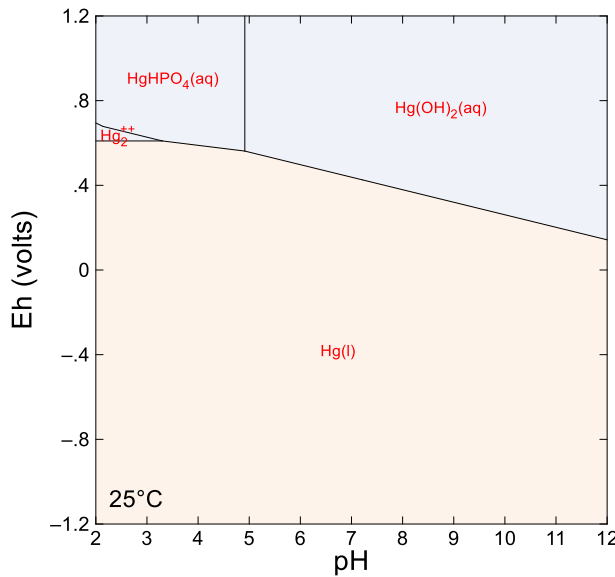
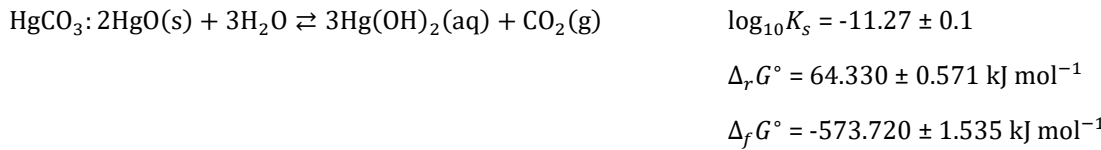


Figure 3.7-13. Pourbaix diagram (GWB) of 10^{-6} mol $\text{kg}_{\text{w}}^{-1}$ Hg in a hypothetical indifferent 0.1 mol $\text{kg}_{\text{w}}^{-1}$ electrolyte solution containing 10^{-4} mol $\text{kg}_{\text{w}}^{-1}$ P. All solid phases are allowed to precipitate.

3.7.3.6. Carbon Compounds

Powell *et al.* [2005POW/BRO] recommended solubility of HgCO_3 : 2HgO(s) .



The transposition to the solubility in carbonate system is written as follows,



and formation constants for $\text{HgCO}_3\text{(aq)}$, HgHCO_3^+ and $\text{Hg(OH)}\text{CO}_3^-$.

3.7.3.7. Tables of Thermodynamic Constants and Functions, and Specific Ion Interaction Coefficients for Hg

Table 3.7-12. Thermodynamic constants and functions for native element, free ions, and oxo and hydroxo compounds of Hg.

Reaction	$\log_{10} K^\circ$	$\Delta_r G^\circ$ (kJ mol ⁻¹)	$\Delta_f G^\circ$ (kJ mol ⁻¹)	$\Delta_r H^\circ$ (kJ mol ⁻¹)	$\Delta_f H^\circ$ (kJ mol ⁻¹)
$\text{Hg(l)} \rightleftharpoons \text{Hg}^{2+} + 2\text{e}^-$	-28.85 ± 0.05	164.667 ± 0.313	$164.667 \pm 0.313^{\text{a}}$	170.210 ± 0.200	$170.21 \pm 0.20^{\text{a}}$
$2\text{Hg}^{2+} + \text{H}_2\text{O} \rightleftharpoons \text{Hg}_2^{2+} + 0.5\text{O}_2\text{(aq)} + 2\text{H}^+$	-12.19 ± 0.06	69.562 ± 0.345	$153.567 \pm 0.559^{\text{a}}$	106.430 ± 0.782	$166.87 \pm 0.50^{\text{a}}$
$\text{HgO(cr)} + 2\text{H}^+ \rightleftharpoons \text{Hg}^{2+} + \text{H}_2\text{O}$	2.44 ± 0.05	-13.950 ± 0.276	$-58.523 \pm 0.154^{\text{a}}$	-24.830 ± 0.165	$-90.790 \pm 0.120^{\text{a}}$
$\text{HgO(s)} + 2\text{H}^+ \rightleftharpoons \text{Hg}^{2+} + \text{H}_2\text{O}$	$2.37 \pm 0.08^{\text{b}}$	-13.528 ± 0.457	-58.945 ± 0.555	$-25.300 \pm 0.200^{\text{b}}$	-90.320 ± 0.286
$\text{Hg}^{2+} + \text{H}_2\text{O} \rightleftharpoons \text{Hg(OH)}^+ + \text{H}^+$	$-3.40 \pm 0.08^{\text{b}}$	19.407 ± 0.457	-53.066 ± 0.555		
$\text{Hg}^{2+} + 2\text{H}_2\text{O} \rightleftharpoons \text{Hg(OH)}_2\text{(aq)} + 2\text{H}^+$	$-5.98 \pm 0.06^{\text{b}}$	34.134 ± 0.342	-275.479 ± 0.471	$51.5 \pm 1.8^{\text{b}}$	-349.950 ± 1.813
$\text{Hg}^{2+} + 3\text{H}_2\text{O} \rightleftharpoons \text{Hg(OH)}_3^- + 3\text{H}^+$	$-21.1 \pm 0.3^{\text{b}}$				
$\text{Hg}^{2+} + \text{Cl}^- \rightleftharpoons \text{HgCl}^+$	$7.31 \pm 0.04^{\text{b}}$	-41.726 ± 0.228	-8.276 ± 0.405	$-21.3 \pm 0.7^{\text{b}}$	-18.170 ± 0.735
$\text{Hg}^{2+} + 2\text{Cl}^- \rightleftharpoons \text{HgCl}_2\text{(aq)}$	$14.00 \pm 0.07^{\text{b}}$	-79.913 ± 0.400	-177.680 ± 0.559	$-49.1 \pm 1.0^{\text{b}}$	-213.050 ± 1.039
$\text{HgCl}_2\text{(aq)} + \text{Cl}^- \rightleftharpoons \text{HgCl}_3^-$	$0.925 \pm 0.09^{\text{b}}$	-5.280 ± 0.566	-314.177 ± 0.707	$0.5 \pm 2.5^{\text{b}}$	-379.630 ± 2.709
$\text{Hg}^{2+} + 3\text{Cl}^- \rightleftharpoons \text{HgCl}_4^{2-}$	$14.93 \pm 0.09^{\text{b}}$	-85.193 ± 0.528		$-48.600 \pm 2.685^{\text{b}}$	
$\text{HgCl}_3^- + \text{Cl}^- \rightleftharpoons \text{HgCl}_4^{2-}$	$0.61 \pm 0.12^{\text{b}}$	-3.482 ± 0.685	-448.876 ± 0.991		-557.210 ± 3.688

Table 3.7-12. Continued.

Reaction	$\log_{10} K^\circ$	$\Delta_r G^\circ$ (kJ mol ⁻¹)	$\Delta_f G^\circ$ (kJ mol ⁻¹)	$\Delta_r H^\circ$ (kJ mol ⁻¹)	$\Delta_f H^\circ$ (kJ mol ⁻¹)
$Hg^{2+} + 4Cl^- \rightleftharpoons HgCl_4^{2-}$	15.54 ± 0.14^b	-88.675 ± 0.816		-59.100 ± 3.661^b	
$Hg^{2+} + Cl^- + H_2O \rightleftharpoons HgClOH(aq)$	4.27 ± 0.35^b				

a [1992GRE/FUG]; b [2005POW/BRO].

* calculated from $\Delta_r G_m^\circ$ or $\Delta_r H_m^\circ$, and $\Delta_f G_m^\circ$ or $\Delta_f H_m^\circ$ in [2003GUI/FAN], unless noted otherwise.**Table 3.7-13. Thermodynamic constants and functions for S and Se compounds of Hg.**

Reaction	$\log_{10} K^\circ$	$\Delta_r G^\circ$ (kJ mol ⁻¹)	$\Delta_f G^\circ$ (kJ mol ⁻¹)	$\Delta_r H^\circ$ (kJ mol ⁻¹)	$\Delta_f H^\circ$ (kJ mol ⁻¹)
Cinnabar + $H^+ \rightleftharpoons Hg^{2+} + HS^-$	-37.91 ± 0.47	216.4 ± 2.7^a	-39.490 ± 3.425	208.2 ± 2.1^a	-54.290 ± 2.573
$HgS\text{-red(cr)} + H^+ \rightleftharpoons Hg^{2+} + HS^-$	-39.78 ± 0.83	227.08 ± 4.75^b	-50.170 ± 5.215	211.700 ± 4.596^b	-57.790 ± 4.838
meta-Cinnabar + $H^+ \rightleftharpoons Hg^{2+} + HS^-$	-38.37 ± 0.14	219.0 ± 0.7^a	-42.090 ± 2.254	200.6 ± 1.5^a	-46.690 ± 2.112
$HgS\text{-black(cr)} + H^+ \rightleftharpoons Hg^{2+} + HS^-$	-39.27 ± 0.96	224.18 ± 5.56^b	-47.270 ± 5.959	207.100 ± 0.800^b	-53.190 ± 1.712
$Hg^{2+} + 3HS^- \rightleftharpoons Hg(HS)3$		42.28^c			
$Hg^{2+} + 2HS^- \rightleftharpoons HgS_2^{2-} + 2H^+$		24.29^c			
$Hg^{2+} + 3HS^- + H^+ \rightleftharpoons HgS(H_2S)2(aq)$		48.53^c			
$Hg_2SO_4\text{(cr)} \rightleftharpoons Hg_2^{2+} + SO_4^{2-}$	-6.19 ± 0.10	35.343 ± 0.564	-625.780 ± 0.411^d	0.62 ± 0.50	-743.09 ± 0.40^d
$Hg^{2+} + SO_4^{2-} \rightleftharpoons HgSO_4\text{(aq)}$		2.57 ± 0.1^e			
$Hg^{2+} + 2H_2Se\text{(aq)} \rightleftharpoons HgSe_2^{2-} + 4H^+$	24.93 ± 0.69	-142.323 ± 3.916	65.334 ± 5.641^f		

a [1995ROB/HEM]; b [1982WAG/EVA]; c [1989SPY/REE]; d [2003GUI/FAN]; e [2005POW/BRO]; f [2005OLI/NOL].

* calculated from $\Delta_r G_m^\circ$ or $\Delta_r H_m^\circ$, and $\Delta_f G_m^\circ$ or $\Delta_f H_m^\circ$ in [2003GUI/FAN], unless noted otherwise.**Table 3.7-14. Thermodynamic constants and functions for P and C compounds of Hg.**

Reaction	$\log_{10} K^\circ$	$\Delta_r G^\circ$ (kJ mol ⁻¹)	$\Delta_f G^\circ$ (kJ mol ⁻¹)	$\Delta_r H^\circ$ (kJ mol ⁻¹)	$\Delta_f H^\circ$ (kJ mol ⁻¹)
$Hg_3(PO_4)_2(s) + 2H^+ \rightleftharpoons 3Hg^{2+} + 2HPO_4^{2-}$	-24.6 ± 0.6^a	140.418 ± 3.425			
$Hg_3(PO_4)_2(s) \rightleftharpoons 3Hg^{2+} + 2PO_4^{3-}$	-49.30 ± 0.60	281.406 ± 3.441			
$Hg_3(PO_4)_2(s) + 4H^+ \rightleftharpoons 3Hg^{2+} + 2H_2PO_4^-$	-10.18 ± 0.60	58.086 ± 3.421			
$(HgOH)_3PO_4(s) + 4H^+ \rightleftharpoons 3Hg^{2+} + HPO_4^{2-} + 3H_2O$	-9.4 ± 0.8^a	53.656 ± 4.566	-1367.060 ± 4.926		
$(HgOH)_3PO_4(s) \rightleftharpoons 3Hg^{2+} + PO_4^{2-} + 3H_2O$	-21.75 ± 0.80	124.150 ± 4.570			
$(HgOH)_3PO_4(s) + 8H^+ \rightleftharpoons 3Hg^{2+} + H_2PO_4^- + 3H_2O$	-2.19 ± 0.80	12.490 ± 4.566			
$HgHPO_4(s) \rightleftharpoons Hg^{2+} + HPO_4^{2-}$	-13.1 ± 0.1^a	74.775 ± 0.571	-1006.093 ± 1.713		
$HgHPO_4(s) \rightleftharpoons Hg^{2+} + PO_4^{3-} + H^+$	-25.45 ± 0.10	145.269 ± 0.595			
$HgHPO_4(s) \rightleftharpoons Hg^{2+} + H_2PO_4^-$	-5.89 ± 0.10	33.609 ± 0.565			
$Hg^{2+} + HPO_4^{2-} \rightleftharpoons HgHPO_4\text{(aq)}$	11.1 ± 0.2^a				
$Hg^{2+} + PO_4^{3-} + H^+ \rightleftharpoons HgHPO_4\text{(aq)}$		22.5 ± 0.2			
$Hg^{2+} + H_2PO_4^- \rightleftharpoons HgHPO_4\text{(aq)} + H^+$		2.9 ± 0.2			
$Hg^{2+} + PO_4^{3-} \rightleftharpoons HgPO_4^-$	17.2 ± 0.2^a				
$Hg^{2+} + HPO_4^{2-} \rightleftharpoons HgPO_4^- + H^+$	4.85 ± 0.2				
$Hg^{2+} + H_2PO_4^- \rightleftharpoons HgPO_4^- + 2H^+$	-2.36 ± 0.2				
$HgCO_3: 2HgO(s) + 3H_2O \rightleftharpoons 3Hg(OH)_2(aq) + CO_2(g)$	-11.27 ± 0.10^a	64.330 ± 0.571	-573.720 ± 2.454		
$HgCO_3 \cdot 2HgO(s) + 4H^+ \rightleftharpoons 3Hg^{2+} + CO_3^{2-} + 2H_2O$	-11.48 ± 0.39	65.541 ± 2.232			
$HgCO_3 \cdot 2HgO(s) + 5H^+ \rightleftharpoons 3Hg^{2+} + HCO_3^- + 2H_2O$	-1.16 ± 0.39	6.596 ± 2.252			
$Hg(OH)_2(aq) + CO_2(g) \rightleftharpoons HgCO_3(aq) + H_2O$	-0.70 ± 0.20	3.996 ± 1.142	-428.716 ± 1.243		
$Hg^{2+} + CO_3^{2-} \rightleftharpoons HgCO_3(aq)$	11.47 ± 0.20^a	-65.483 ± 1.138			

Table 3.7-14. Continued.

Reaction	$\log_{10} K^\circ$	$\Delta_r G^\circ$ (kJ mol ⁻¹)	$\Delta_f G^\circ$ (kJ mol ⁻¹)	$\Delta_r H^\circ$ (kJ mol ⁻¹)	$\Delta_f H^\circ$ (kJ mol ⁻¹)
$Hg^{2+} + HCO_3^- \rightleftharpoons HgCO_3(aq) + H^+$	1.15 ± 0.21	-6.538 ± 1.177			
$Hg(OH)_2(aq) + CO_2(g) + H^+ \rightleftharpoons HgHCO_3^+ + H_2O$	3.63 ± 0.1^a	20.720 ± 0.571	-453.432 ± 0.753		
$Hg^{2+} + CO_3^{2-} + H^+ \rightleftharpoons HgHCO_3^+$	15.80 ± 0.10	-90.199 ± 0.563			
$Hg^{2+} + HCO_3^- \rightleftharpoons HgHCO_3^+$	5.48 ± 0.11	-31.254 ± 0.638			
$Hg(OH)_2(aq) + HCO_3^- \rightleftharpoons Hg(OH)CO_3^- + H_2O$	0.98 ± 0.1^a	5.594 ± 0.571	-630.778 ± 0.783		
$Hg^{2+} + H_2O + CO_3^{2-} \rightleftharpoons Hg(OH)CO_3^- + H^+$	5.33 ± 0.10	-30.405 ± 0.601			

^a [2005POW/BRO]* calculated from $\Delta_r G_m^\circ$ or $\Delta_r H_m^\circ$, and $\Delta_f G_m^\circ$ or $\Delta_f H_m^\circ$ in [2003GUI/FAN], unless noted otherwise.**Table 3.7-15. Specific ion interaction coefficients for Hg soluble species**

Specific ion interaction coefficient	Value $\pm \sigma$	Reference
$\epsilon(Hg^{2+}, Cl^-)$	0.17 ± 0.08	From transition M ²⁺
$\epsilon(Hg^{2+}, ClO_4^-)$	0.34 ± 0.03	[2003GUI/FAN]
$\epsilon(Hg^{2+}, NO_3^-)$	-0.1 ± 0.1	[2003GUI/FAN]
$\epsilon(Hg_2^{2+}, ClO_4^-)$	0.09 ± 0.02	[2003GUI/FAN]
$\epsilon(Hg_2^{2+}, NO_3^-)$	-0.2 ± 0.1	[2003GUI/FAN]
$\epsilon(Hg(OH)^+, Cl^-)$	0.11 ± 0.08	From Eq. 26 considering OH ⁻
$\epsilon(Hg(OH)^+, ClO_4^-)$	0.06 ± 0.05	From $\Delta\epsilon$ in [2005POW/BRO]
$\epsilon(Hg(OH)_2(aq), Na^+ClO_4^-)$	-0.08 ± 0.05	From $\Delta\epsilon$ in [2005POW/BRO]
$\epsilon(Hg(OH)_3^-, Na^+)$	-0.02 ± 0.05	From Eq. 26 [1990CIA]
$\epsilon(HgCl^+, ClO_4^-)$	0.15 ± 0.05	From $\Delta\epsilon$ in [2005POW/BRO]
$\epsilon(HgCl_2(aq), Na^+ClO_4^-)$	0.01 ± 0.05	From $\Delta\epsilon$ in [2005POW/BRO]
$\epsilon(HgCl_3^-, Na^+)$	0.05 ± 0.07	From $\Delta\epsilon$ in [2005POW/BRO]
$\epsilon(HgCl_4^{2-}, Na^+)$	0.08 ± 0.09	From $\Delta\epsilon$ in [2005POW/BRO]
$\epsilon(HgSO_4(aq), Na^+ClO_4^-)$	0	Nil charge approximation
	0.11 ± 0.07	From Eq. 26 [1990CIA]
$\epsilon(HgHPO_4(aq), Na^+ClO_4^-)$	0	Nil charge approximation
	0.10 ± 0.05	From Eq. 26 considering HPO ₄ ²⁻ [1990CIA]
$\epsilon(HgPO_4^-, Na^+)$	0.05 ± 0.04	From Eq. 26 considering PO ₄ ³⁻ [1990CIA]

3.7.4. Copper

Copper is forming insoluble compounds with uranium [2013CRE/SZE]

3.7.4.1. Native Metal and free Ions

Copper is present in aqueous solution as Cu(I) and Cu(II). The thermodynamic functions of formation for native Cu(cr) and Cu²⁺ are taken from Guillaumont *et al.* [2003GUI/FAN], and the ones for Cu⁺ are calculated for the functions of reaction from Wang *et al.* [1997WAN/ZHA]. The common master species is Cu²⁺.

The specific ion interaction coefficients are taken from the NEA-OECD reviews [1992GRE/FUG; 2003GUI/FAN; 2020GRE/GAO].

3.7.4.2. Hydroxo Compounds

The $\log_{10} K_s$ of Cu(OH)₂(cr) is estimated by Brown and Ekberg [2016BRO/EKB]. The thermodynamic constants for the hydrolysis of both cations are taken from Brown and Ekberg [2016BRO/EKB], and thermodynamic functions of formation are recalculated referring to NEA-OECD [1992GRE/FUG; 2003GUI/FAN; 2020GRE/GAO]. The specific ion interaction coefficients are calculated from the $\Delta\epsilon$ values selected in Brown and Ekberg [2016BRO/EKB] and the ϵ values in NEA-OECD [1992GRE/FUG; 2003GUI/FAN; 2020GRE/GAO].

3.7.4.3. Halogen Compounds

The Gibbs energy of reaction for $\text{CuF}_2 \cdot 2\text{H}_2\text{O}(\text{cr})$ can be retrieved from Wagman *et al.* [1982WAG/EVA], and Gibbs energy of formation can be calculated relative to NEA-OECD [1992GRE/FUG; 2003GUI/FAN; 2020GRE/GAO].

Wang *et al.* [1997WAN/ZHA] proposed the solubility constant, enthalpy and entropy of reaction for nantokite ($\text{CuCl}(\text{cr})$). The Gibbs energy of reaction for $\text{CuCl}_2 \cdot 3\text{Cu}(\text{OH})_2(\text{cr})$ is available in Wagman *et al.* [1982WAG/EVA].

Wang *et al.* [1997WAN/ZHA] proposed estimation of the formation of Cu^+ and Cu^{2+} chloro compounds. The estimations of the chloro complexes were updated in Powell *et al.* [2007POW/BRO], but without the enthalpy and entropy values. As the differences between the two evaluations are very slight, the former will be used in PRODATA together with the ε values.

3.7.4.4. Sulphur Compounds

Copper sulphide can be retrieved from Wagman *et al.* [1982WAG/EVA] — $\text{Cu}_2\text{S}-\alpha(\text{cr})$, $\text{CuS}(\text{cr})$ —, Robie and Hemingway [1995ROB/HEM] — chalcocite (Cu_2S), digenite ($\text{Cu}_{1.80}\text{S}$), djurleite ($\text{Cu}_{1.95}\text{S}$), ailite ($\text{Cu}_{1.75}\text{S}$), covellite (CuS) —, or from the Minteq database [1998EPA] — Blaublei_II ($\text{Cu}_{0.6}\text{Cu}_{0.8}\text{S}$), Blaublei_I ($\text{Cu}_{0.9}\text{Cu}_{0.2}\text{S}$).

Copper sulphate and hydroxosulphate are available in Wagman *et al.* [1982WAG/EVA] — $\text{CuSO}_4 \cdot \text{H}_2\text{O}(\text{s})$, $\text{CuSO}_4 \cdot 3\text{H}_2\text{O}(\text{s})$, $\text{CuSO}_4 \cdot 5\text{H}_2\text{O}(\text{s})$, Antlerite ($\text{Cu}_3(\text{SO}_4)(\text{OH})_4$), Langite ($\text{Cu}_4(\text{SO}_4)(\text{OH})_6 \cdot \text{H}_2\text{O}$) —, and Robie and Hemingway [1995ROB/HEM] — brochantite ($\text{Cu}_4(\text{SO}_4)(\text{OH})_6$), chalcantite ($\text{CuSO}_4 \cdot 5\text{H}_2\text{O}$), chalcocyanite (CuSO_4).

The NEA-OECD review only selected chalcocyanite ($\text{CuSO}_4(\text{cr})$) [2003GUI/FAN].

Powell *et al.* [2007POW/BRO] recommended the formation of $\text{CuSO}_4(\text{aq})$ — $\log_{10} \beta^\circ$, $\Delta_r H^\circ$, and $\Delta_r S^\circ$ —, and a provisional value for $\Delta\varepsilon$.

3.7.4.5. Selenium Compounds

Functions of reaction for $\text{Cu}_2\text{Se}-\alpha(\text{cr})$ and $\text{Cu}_3\text{Se}_2(\text{cr})$ can be calculated from Naumov *et al.* [1974NAU/RYZ]. The function of formation of $\text{CuSeO}_3(\text{cr})$ are taken form the NE-OECD review [2005OLI/NOL].

3.7.4.6. Phosphor Compounds

The copper phosphate phases are taken from Nriagu [1984NRI] for libethenite ($\text{Cu}_2(\text{PO}_4)\text{OH}$), tagilite ($\text{Cu}_2(\text{PO}_4)\text{OH} \cdot \text{H}_2\text{O}$), cornetite ($\text{Cu}_3(\text{PO}_4)(\text{OH})_3$), pseudomalachite ($\text{Cu}_5(\text{PO}_4)_2(\text{OH})_4$), pyromorphite-Cu ($\text{Cu}_5(\text{PO}_4)_3\text{OH}$), tsumebite ($\text{Pb}_2\text{Cu}(\text{PO}_4)(\text{OH})_3 \cdot 3\text{H}_2\text{O}$), turquoise ($\text{CuAl}_6(\text{PO}_4)_4(\text{OH})_8 \cdot 4\text{H}_2\text{O}$), and veszelyite ($\text{CuZn}_2\text{PO}_4(\text{OH})_3 \cdot 2\text{H}_2\text{O}$). The Gibbs energies of formation are recalculated referring to Wagman *et al.* [1968WAG/EVA; 1969WAG/EVA] as for the case of lead phosphate (c.f. § 3.6.2.3). Only veszelyite is showing a significant difference — *i.e.*, $\Delta_f G^\circ = -2\ 456.469$ and $-2\ 462.219\ \text{kJ mol}^{-1}$ for Wagman *et al.* [1968WAG/EVA; 1969WAG/EVA] and Guillaumont *et al.* [2003GUI/FAN], respectively. The recalculated value referring to Guillaumont *et al.* [2003GUI/FAN] is chosen.

Powell *et al.* [2007POW/BRO] proposed a provisional constant for $\text{CuHPO}_4(\text{aq})$ extrapolated to infinite dilution using the Davies [1962DAV] equation. It will be adapted to the other ions of the phosphate system using the constants and uncertainties in Table 3.4-3.

3.7.4.7. Arsenic Compounds

The $\Delta_f G^\circ$ of $\text{Cu}_3(\text{AsO}_4)_2 \cdot 6\text{H}_2\text{O}(\text{s})$ is available in Naumov *et al.* [1974NAU/RYZ]. Using the $\Delta_f G^\circ$ values of Cu^{2+} , AsO_4^{3-} , and H_2O in Naumov *et al.* [1974NAU/RYZ], the Gibbs energy of reaction $\Delta_r G^\circ$ and $\log_{10} K_s$ values are obtained.

The evolution of $\log_{10} K_s$ vs. T of arsenosulphide phase enargite (Cu_3AsS_4) is proposed in SOLTHERM-XPT database [2015PAL; 2016REE/SPY] from Spycher and Reed [1989SPY/REE]. The analysis using the Van't Hoff relationship in Figure 3.7-14 allows calculating the functions of formation from the following reaction.

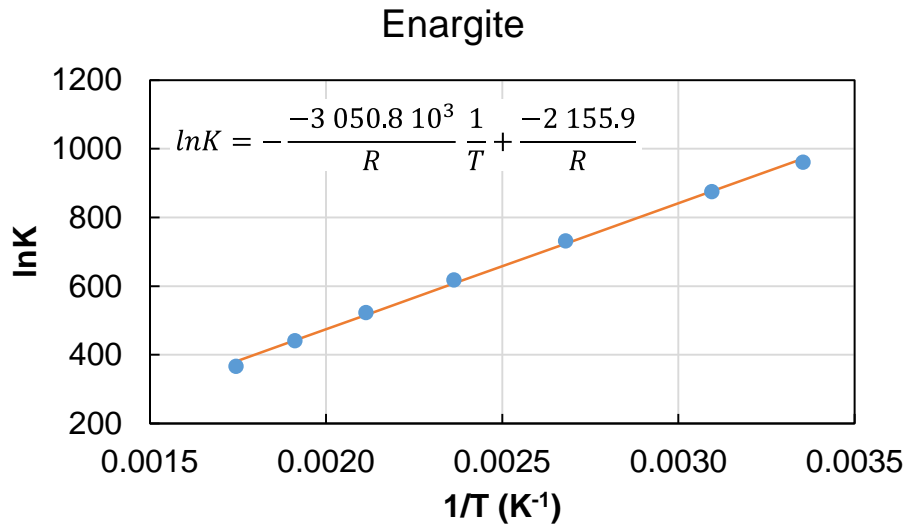
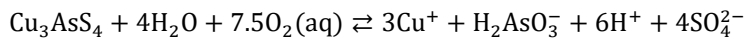
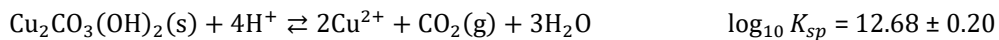
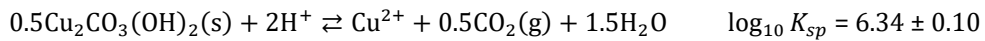


Figure 3.7-14. Evolution of the $\ln K$ values vs. $1/T$ (blue circles) for the dissolution of enargite (Cu_3AsS_4) in the SOLTHERM-XPT database [2015PAL; 2016REE/SPY], and estimation of the formation functions by the Van't Hoff relationship (orange plain line).

3.7.4.8. Carbon Compounds

The solubility of malachite ($\text{Cu}_2\text{CO}_3(\text{OH})_2$) and azurite ($\text{Cu}_3(\text{CO}_3)_2(\text{OH})_2$) can be traced in Wagman *et al.* [1982WAG/EVA], Robie and Hemingway [1995ROB/HEM] and Powell *et al.* [2007POW/BRO]. For malachite, the calculation of $\log_{10} K_s$ using Robie and Hemingway [1995ROB/HEM] leads to 2 orders of magnitude difference with the value in Powell *et al.* [2007POW/BRO]. Original data that are used in Powell *et al.* [2007POW/BRO] are pointing particularly to Preis and Gamsjäger [2002PRE/GAM], where functions of formation are given in reference to CODATA values [1989COX/WAG]. The reaction in Preis and Gamsjäger [2002PRE/GAM] is

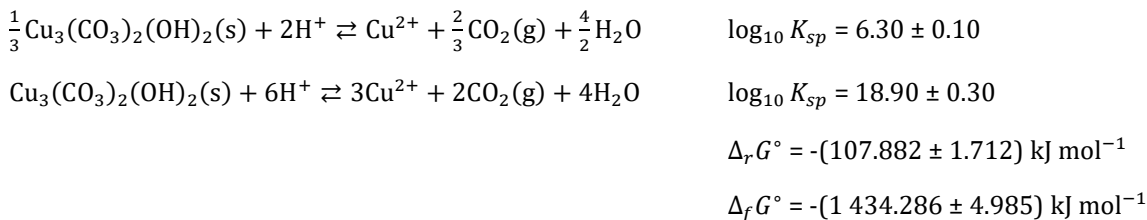


$$\Delta_r G^\circ = -(72.378 \pm 1.142) \text{ kJ mol}^{-1}$$

$$\Delta_f G^\circ = -(903.323 \pm 3.322) \text{ kJ mol}^{-1}$$

Preis and Gamsjäger [2002PRE/GAM] seem to disqualify the data from the compilation from Robie and Hemingway [1995ROB/HEM] based on the too high partial pressure of $\text{CO}_2(\text{g})$ that would be needed to obtain the malachite precipitation. Only the data from Preis and Gamsjäger [2002PRE/GAM] will be included.

In the case of azurite, there is a *ca.* 76 kJ mol⁻¹ difference in Gibbs energies of formation between Wagman *et al.* [1982WAG/EVA] (-1315.5 kJ mol⁻¹) and Robie and Hemingway [1995ROB/HEM] (-1391.4 kJ mol⁻¹). Powell *et al.* [2007POW/BRO] proposed a solubility constant — $\log_{10} K_s = -44.9 \pm 0.2$ for the full ionization — that is not coherent with both of the previous value as it has a *ca.* 7 and *ca.* 20 orders of magnitude difference in K_s . The value from Powell *et al.* [2007POW/BRO] come from Preis and Gamsjäger [2002PRE/GAM] who wrote the following solubility equilibrium.



Only the data from Preis and Gamsjäger [2002PRE/GAM] will be included in PRODATA. As in the case of malachite, Preis and Gamsjäger [2002PRE/GAM] provided functions of formation for azurite in reference to CODATA values [1989COX/WAG].

Powell *et al.* [2007POW/BRO] recommended $\log_{10} \beta^\circ$ values for the formation of $\text{Cu}(\text{CO}_3)(\text{aq})$, $\text{Cu}(\text{CO}_3)_2^{2-}$, and $\text{Cu}(\text{HCO}_3)^+$ that are used in PRODATA (Table 3.7-16). The $\Delta\varepsilon$ values are used to calculate the corresponding ε values (Table 3.7-21).

3.7.4.9. Thermodynamic Constants and Functions, and Specific Ion Interaction Coefficients for Cu

Table 3.7-16. Thermodynamic constants and functions for free ions, oxo, and hydroxo Cu compounds.

Reaction	$\log_{10} \beta_n^\circ$	$\Delta_r G_m^\circ$ (kJ mol ⁻¹)	$\Delta_f G_m^\circ$ (kJ mol ⁻¹)	$\Delta_r H_m^\circ$ (kJ mol ⁻¹)	$\Delta_f H_m^\circ$ (kJ mol ⁻¹)
$\text{Cu}(\text{cr}) \rightleftharpoons \text{Cu}^{2+} + 2\text{e}^-$	-11.40 ± 0.27	65.046 ± 1.557	65.046 ± 1.557	64.9 ± 1.0	64.9 ± 1.0
$\text{Cu}(\text{cr}) \rightleftharpoons \text{Cu}^+ + \text{e}^-$	-8.58 ± 0.04	48.990 ± 0.24	48.990 ± 0.24 ^a	76.35 ± 3.60	76.35 ± 3.60 ^a
$\text{Cu}^{2+} + 0.5\text{H}_2\text{O} \rightleftharpoons \text{Cu}^+ + 0.25\text{O}_2(\text{aq}) + \text{H}^+$	-18.68 ± 0.27	106.609 ± 1.522		151.440 ± 4.129	
$\text{Cu}^+ + \text{H}_2\text{O} \rightleftharpoons \text{Cu}(\text{OH})(\text{aq}) + \text{H}^+$	-7.85 ± 0.41 ^b	44.808 ± 2.340	-143.342 ± 2.353	41.3 ± 4.4 ^b	-168.180 ± 5.947
$\text{Cu}^+ + 2\text{H}_2\text{O} \rightleftharpoons \text{Cu}(\text{OH})_2^- + 2\text{H}^+$	-18.64 ± 0.60 ^b	106.398 ± 3.425	-318.892 ± 3.434	61 ± 12 ^b	-434.310 ± 12.649
Tenorite					
$\text{CuO} + 2\text{H}^+ \rightleftharpoons \text{Cu}^{2+} + \text{H}_2\text{O}$	7.63 ± 0.05 ^b	-43.609 ± 0.342	128.485 ± 1.595	-64.9 ± 2.3 ^b	156.030 ± 2.508
$\text{Cu}^{2+} + \text{H}_2\text{O} \rightleftharpoons \text{Cu}(\text{OH})^+ + \text{H}^+$	-7.64 ± 0.17 ^b	43.609 ± 0.970	-128.485 ± 1.835	66 ± 2.8 ^b	-154.930 ± 2.973
$\text{Cu}^{2+} + 2\text{H}_2\text{O} \rightleftharpoons \text{Cu}(\text{OH})_2(\text{aq}) + 2\text{H}^+$	-16.24 ± 0.03 ^b	92.699 ± 0.175	-316.535 ± 1.569	89.9 ± 0.7 ^b	-416.860 ± 1.223
$\text{Cu}^{2+} + 3\text{H}_2\text{O} \rightleftharpoons \text{Cu}(\text{OH})_3^- + 3\text{H}^+$	-26.65 ± 0.13 ^b	152.119 ± 0.742	-494.255 ± 1.729		
$\text{Cu}^{2+} + 4\text{H}_2\text{O} \rightleftharpoons \text{Cu}(\text{OH})_4^{2-} + 4\text{H}^+$	-39.70 ± 0.19 ^b	226.609 ± 1.085	-656.905 ± 1.905	167.0 ± 5.7 ^b	-911.420 ± 5.789
$2\text{Cu}^{2+} + \text{H}_2\text{O} \rightleftharpoons \text{Cu}_2(\text{OH})_3^{2+} + \text{H}^+$	-6.71 ± 0.30 ^b	38.301 ± 1.712	-68.747 ± 3.554	27 ± 8 ^b	-129.03 ± 8.246
$2\text{Cu}^{2+} + 2\text{H}_2\text{O} \rightleftharpoons \text{Cu}_2(\text{OH})_2^{2+} + 2\text{H}^+$	-10.55 ± 0.19 ^b	60.220 ± 0.109	-283.968 ± 3.117	71.4 ± 5 ^b	-370.46 ± 5.386
$3\text{Cu}^{2+} + 4\text{H}_2\text{O} \rightleftharpoons \text{Cu}_3(\text{OH})_4^{2+} + 4\text{H}^+$	-21.2 ± 0.4 ^b	121.010 ± 2.284	-632.412 ± 5.202	119.6 ± 1.7 ^b	-829.02 ± 3.452

a [1997WAN/ZHA]; b [2016BRO/EKB]

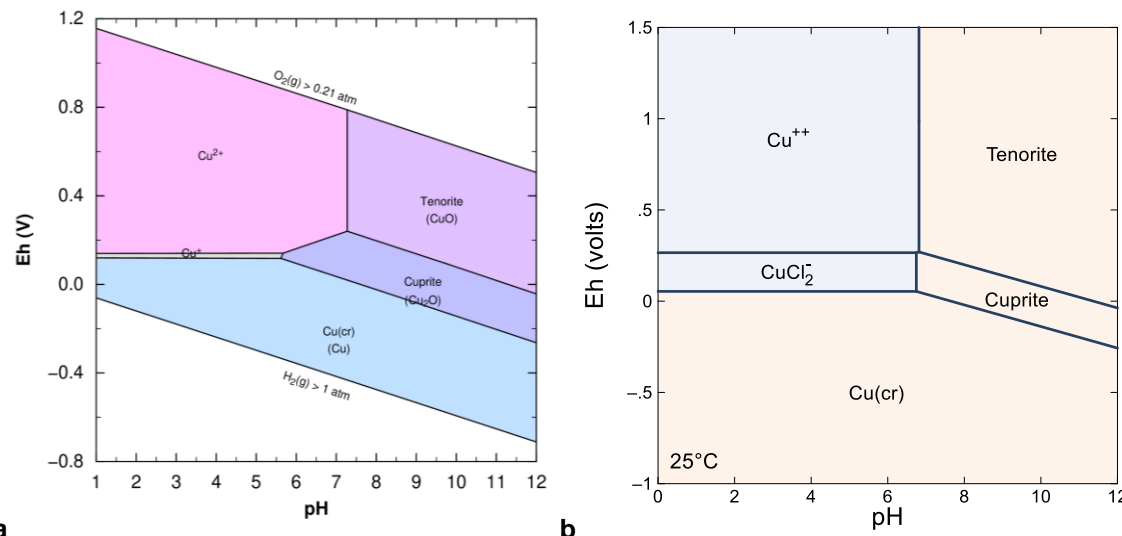
* calculated from $\Delta_r G_m^\circ$ or $\Delta_r H_m^\circ$, and $\Delta_f G_m^\circ$ or $\Delta_f H_m^\circ$ in [2003GUI/FAN], unless noted otherwise.

The Pourbaix diagram of 10^{-6} mol kg_w⁻¹ Cu is plotted in Figure 3.7-15.

Table 3.7-17. Thermodynamic constants and functions for halogen compounds of Cu.

Reaction	$\log_{10} \beta_n^{\circ}$	$\Delta_r G_m^{\circ}$ (kJ mol ⁻¹)	$\Delta_f G_m^{\circ *}$ (kJ mol ⁻¹)	$\Delta_r H_m^{\circ}$ (kJ mol ⁻¹)	$\Delta_f H_m^{\circ *}$ (kJ mol ⁻¹)
$\text{CuF}_2 + 2\text{H}_2\text{O}(\text{cr}) \rightleftharpoons \text{Cu}^{2+} + 2\text{F}^- + 2\text{H}_2\text{O}$	-2.64 ± 0.43	15.052 ± 2.453^a	-987.332 ± 3.219		
$\text{Cu}^{2+} + \text{F}^- \rightleftharpoons \text{CuF}^+$	1.26 ± 0.65	-7.200 ± 3.683^a	-223.677 ± 4.058		
Nantokite					
$\text{CuCl}(\text{cr}) \rightleftharpoons \text{Cu}^+ + \text{Cl}^-$	-6.82 ± 0.12^b	38.929 ± 0.685	-111.156 ± 0.735	47.3 ± 4.0^b	-138.030 ± 5.382
$\text{CuCl}_2(\text{cr}) \rightleftharpoons \text{Cu}^{2+} + 2\text{Cl}^-$	3.73 ± 0.94	-21.266 ± 5.388^a	-176.122 ± 5.613	-49.448 ± 0.634^a	-219.812 ± 0.799
$\text{CuCl}_2 + 3\text{Cu}(\text{OH})_3(\text{cr}) + 6\text{H}^+ \rightleftharpoons 4\text{Cu}^{2+} + \text{Cl}^- + 6\text{H}_2\text{O}$	14.68 ± 0.84	-83.770 ± 4.781^a	-1341.320 ± 4.005		
$\text{Cu}^+ + 2\text{Cl}^- \rightleftharpoons \text{CuCl}_2^-$	5.68 ± 0.14^b	-32.422 ± 0.799	-245.866 ± 0.866	-20.0 ± 4.0^b	-277.810 ± 5.660
$\text{Cu}^+ + 3\text{Cl}^- \rightleftharpoons \text{CuCl}_3^{2-}$	5.02 ± 0.12^b	-28.654 ± 0.685	-373.315 ± 0.806	-33.0 ± 4.0^b	-457.890 ± 5.665
$\text{Cu}^{2+} + \text{Cl}^- \rightleftharpoons \text{CuCl}^+$	0.64 ± 0.06^b	-3.653 ± 0.342	-69.824 ± 1.598	8.4 ± 1.3^b	-93.780 ± 1.643
$\text{Cu}^{2+} + 2\text{Cl}^- \rightleftharpoons \text{CuCl}_2(\text{aq})$	0.60 ± 0.37^b	-3.425 ± 2.112	-200.813 ± 2.634	23 ± 6^b	-246.260 ± 6.086

a [1982WAG/EVA]; b [1997WAN/ZHA]

* calculated from $\Delta_r G_m^{\circ}$ or $\Delta_r H_m^{\circ}$, and $\Delta_f G_m^{\circ}$ or $\Delta_f H_m^{\circ}$ in [2003GUI/FAN], unless noted otherwise.**Figure 3.7-15. Pourbaix diagram of 10^{-6} mol kg_w⁻¹ Cu (PHREEPLOT) (a) and with 10^{-2} mol kg_w⁻¹ of Cl (GWB) (b) in a hypothetical indifferent 0.1 mol kg_w⁻¹ electrolyte solution; all solid phases are allowed to precipitate.****Table 3.7-18. Thermodynamic constants and functions for S and Se compounds of Cu.**

Reaction	$\log_{10} \beta_n^{\circ}$	$\Delta_r G_m^{\circ}$ (kJ mol ⁻¹)	$\Delta_f G_m^{\circ *}$ (kJ mol ⁻¹)	$\Delta_r H_m^{\circ}$ (kJ mol ⁻¹)	$\Delta_f H_m^{\circ *}$ (kJ mol ⁻¹)
$\text{CuS}(\text{cr}) + \text{H}^+ \rightleftharpoons \text{Cu}^{2+} + \text{HS}^-$	-22.98 ± 0.70	131.170 ± 4.018^a	-53.881 ± 4.800	100.270 ± 1.616^a	-51.670 ± 0.800
Covellite					
$\text{CuS} + \text{H}^+ \rightleftharpoons \text{Cu}^{2+} + \text{HS}^-$	-23.23 ± 0.06	132.600 ± 0.316^b	-55.311 ± 2.607	102.800 ± 1.883^b	-54.200 ± 2.607
Blaublei_I					
$\text{Cu}_{0.9}\text{Cu}_{0.2}\text{S} + \text{H}^+ \rightleftharpoons 0.2\text{Cu}^+ + 0.9\text{Cu}^{2+} + \text{HS}^-$					
		-24.16^c			
Blaublei_II					
$\text{Cu}_{0.6}\text{Cu}_{0.8}\text{S} + \text{H}^+ \rightleftharpoons 0.6\text{Cu}^+ + 0.8\text{Cu}^{2+} + \text{HS}^-$					
		-27.28^c			
Anilite					
$\text{Cu}_{1.75}\text{S} + \text{H}^+ \rightleftharpoons 1.5\text{Cu}^+ + 0.25\text{Cu}^{2+} + \text{HS}^-$					
	-31.88 ± 0.07	181.975 ± 0.390^b	-79.986 ± 2.145	180.675 ± 5.184^b	-66.225 ± 2.145
Digenite					
$\text{Cu}_{1.80}\text{S} + \text{H}^+ \rightleftharpoons 1.6\text{Cu}^+ + 0.2\text{Cu}^{2+} + \text{HS}^-$					
	-32.15 ± 0.11	183.520 ± 0.605^b	-79.884 ± 2.086	184.320 ± 0.616^b	-65.480 ± 5.923
Djurleite					
$\text{Cu}_{1.95}\text{S} + \text{H}^+ \rightleftharpoons 1.9\text{Cu}^+ + 0.05\text{Cu}^{2+} + \text{HS}^-$					
	-34.10 ± 0.08	194.655 ± 0.429^b	-86.079 ± 2.122	201.955 ± 0.534^b	-69.945 ± 6.982

Table 3.7-18. Continued.

Reaction	$\log_{10} \beta_n^\circ$	$\Delta_r G_m^\circ$ (kJ mol ⁻¹)	$\Delta_f G_m^\circ$ * (kJ mol ⁻¹)	$\Delta_r H_m^\circ$ (kJ mol ⁻¹)	$\Delta_f H_m^\circ$ * (kJ mol ⁻¹)
$\text{Cu}_2\text{S}-\alpha(\text{cr}) + \text{H}^+ \rightleftharpoons 2\text{Cu}^+ + \text{HS}^-$	-34.73 ± 0.15	198.240 ± 0.846^a	-88.017 ± 1.997	205.240 ± 1.697^a	-68.840 ± 7.156
Chalcocite					
$\text{Cu}_2\text{S} + \text{H}^+ \rightleftharpoons 2\text{Cu}^+ + \text{HS}^-$	-35.28 ± 0.18	201.400 ± 1.019^b	-91.177 ± 1.914	211.000 ± 1.031^b	-74.600 ± 7.282
$\text{CuSO}_4(\text{cr}) \rightleftharpoons \text{Cu}^{2+} + \text{SO}_4^{2-}$	2.94 ± 0.19	-16.773 ± 1.070	-662.185 ± 1.206	-73.040 ± 0.529	-771.400 ± 1.200
$\text{CuSO}_4 \cdot \text{H}_2\text{O}(\text{cr}) \rightleftharpoons \text{Cu}^{2+} + \text{SO}_4^{2-} + \text{H}_2\text{O}$	-0.34 ± 0.15	1.941 ± 0.871^a	-918.039 ± 1.357	-44.500 ± 0.890^a	-1085.770 ± 0.608
$\text{CuSO}_4 \cdot 3\text{H}_2\text{O}(\text{cr}) \rightleftharpoons \text{Cu}^{2+} + \text{SO}_4^{2-} + 3\text{H}_2\text{O}$	-1.67 ± 0.14	9.533 ± 0.782^a	-1399.911 ± 1.415	-17.680 ± 0.949^a	-1684.250 ± 0.523
$\text{CuSO}_4 \cdot 5\text{H}_2\text{O}(\text{cr}) \rightleftharpoons \text{Cu}^{2+} + \text{SO}_4^{2-} + 5\text{H}_2\text{O}$	-2.64 ± 0.16	15.060 ± 0.899^a	-1879.718 ± 1.354	6.000 ± 0.949^a	-2279.590 ± 0.547
Antlerite					
$\text{Cu}_3(\text{SO}_4)(\text{OH})_4 + 4\text{H}^+ \rightleftharpoons 3\text{Cu}^{2+} + \text{SO}_4^{2-} + 4\text{H}_2\text{O}$	8.78 ± 0.77	-50.116 ± 4.380^a	-1447.310 ± 1.685		
Brochantite					
$\text{Cu}_4(\text{SO}_4)(\text{OH})_6 + 6\text{H}^+ \rightleftharpoons 4\text{Cu}^{2+} + \text{SO}_4^{2-} + 6\text{H}_2\text{O}$	15.37 ± 1.03	-87.754 ± 5.876^b	-1818.906 ± 2.121		
Langite					
$\text{Cu}_4(\text{SO}_4)(\text{OH})_6 \cdot \text{H}_2\text{O} + 6\text{H}^+ \rightleftharpoons 4\text{Cu}^{2+} + \text{SO}_4^{2-} + 7\text{H}_2\text{O}$	17.29 ± 1.07	-98.683 ± 6.083^a	-2045.117 ± 1.428	-165.874 ± 4.424	-2484.676 ± 5.984
$\text{Cu}^{2+} + \text{SO}_4^{2-} \rightleftharpoons \text{Cu}(\text{SO}_4)(\text{aq})$	2.35 ± 0.05^d	-13.414 ± 0.284	-692.372 ± 1.637	7.3 ± 1.5^d	-837.140 ± 1.847
$\text{Cu}_2\text{Se}(\text{cr}) + 2\text{H}^+ \rightleftharpoons 2\text{Cu}^+ + \text{H}_2\text{Se}(\text{aq})$	-32.21	183.884^e	64.409	218.090 ± 7.472^e	51.090 ± 0.319
$\text{Cu}_3\text{Se}_2(\text{cr}) + 4\text{H}^+ \rightleftharpoons 2\text{Cu}^+ + \text{Cu}^{2+} + 2\text{H}_2\text{Se}(\text{aq})$	-55.76	318.267^e	-112.251	337.586^e	-91.386
$\text{CuSe}-\alpha(\text{cr}) + 2\text{H}^+ \rightleftharpoons 2\text{Cu}^{2+} + \text{H}_2\text{Se}(\text{aq})$	-21.61 ± 0.43	123.376 ± 2.474	-36.835 ± 0.563^f	118.700 ± 2.200	-39.500 ± 0.500^f
$\text{CuSe}-\beta(\text{cr}) + 2\text{H}^+ \rightleftharpoons 2\text{Cu}^{2+} + \text{H}_2\text{Se}(\text{aq})$	-21.28 ± 0.43	121.451 ± 2.474	-34.910 ± 0.563^f	116.000 ± 2.200	-36.800 ± 0.500^f
$\text{CuSeO}_3(\text{cr}) \rightleftharpoons \text{Cu}^{2+} + \text{SeO}_3^{2-}$	-7.67 ± 0.39	43.790 ± 2.206^a	-341.136 ± 0.800		
$\text{CuSeO}_4 \cdot 5\text{H}_2\text{O} \rightleftharpoons \text{Cu}^{2+} + \text{SeO}_4^{2-} + 5\text{H}_2\text{O}$	-2.17 ± 0.20	12.361 ± 1.159	-1572.500 ± 2.420^f	5.580 ± 2.298	-1973.330 ± 2.830^f

a [1982WAG/EVA]; b [1995ROB/HEM]; c [1998EPA]; d [2007POW/BRO]; e [1974NAU/RYZ]; f [2005OLI/NOL].

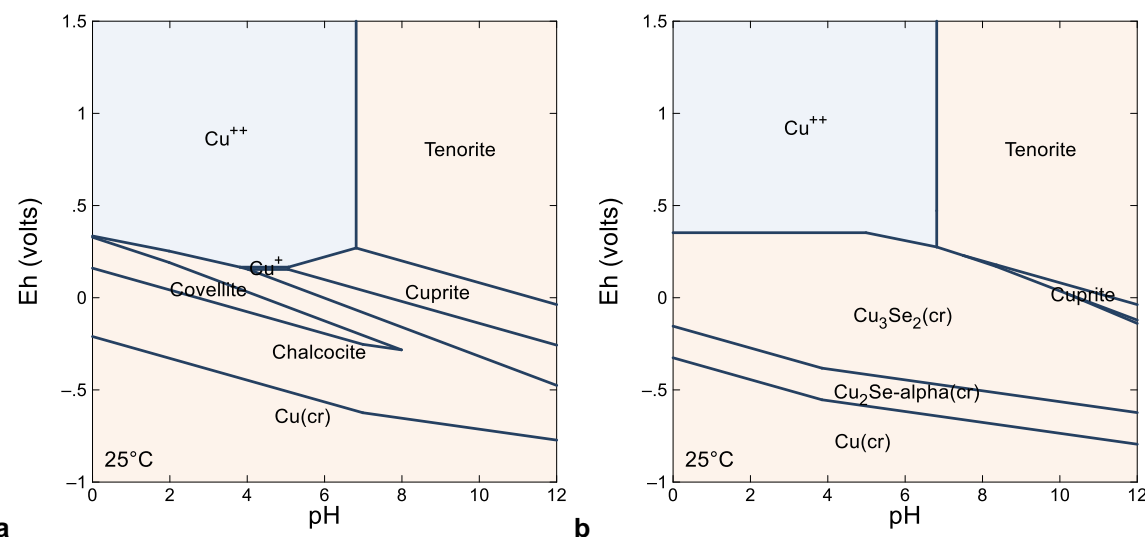
* calculated from $\Delta_r G_m^\circ$ or $\Delta_r H_m^\circ$, and $\Delta_f G_m^\circ$ or $\Delta_f H_m^\circ$ in [2003GUI/FAN], unless noted otherwise.**Figure 3.7-16. Pourbaix diagram (GWB) of 10^{-6} mol kg⁻¹ Cu in a hypothetical indifferent 0.1 mol kg⁻¹ electrolyte solution containing 10^{-4} mol kg⁻¹ of S (a) and Se (b); all solid phases are allowed to precipitate.**

Table 3.7-19. Thermodynamic constants and functions for N, P, and As compounds of Cu.

Reaction	$\log_{10} \beta_n^{\circ}$	$\Delta_r G_m^{\circ a}$ (kJ mol ⁻¹)	$\Delta_f G_m^{\circ b}$ (kJ mol ⁻¹)	$\Delta_r H_m^{\circ}$ (kJ mol ⁻¹)	$\Delta_f H_m^{\circ}$ (kJ mol ⁻¹)
$\text{Cu}_4(\text{NO}_3)_2(\text{OH})_6(\text{cr}) + 6\text{H}^+ \rightleftharpoons 4\text{Cu}^{2+} + 2\text{NO}_3^- + 6\text{H}_2\text{O}$	17.62 ± 1.06	-100.604 ± 6.042^a	-1283.640 ± 1.743	-126.074 ± 3.957^a	-1743.006 ± 1.019
$\text{Cu}_3(\text{PO}_4)_2(\text{cr}) \rightleftharpoons 3\text{Cu}^{2+} + 2\text{PO}_4^{3-}$	-36.86 ± 0.91	210.370 ± 5.212^a	2066.214 ± 2.143		
$\text{Cu}_2\text{P}_2\text{O}_7(\text{cr}) \rightleftharpoons 2\text{Cu}^{2+} + \text{P}_2\text{O}_7^{4-}$	-15.12 ± 0.20	86.280 ± 1.121	-1891.691 ± 5.637		
$\text{Cu}_2\text{P}_2\text{O}_7(\text{cr}) + \text{H}_2\text{O} \rightleftharpoons 2\text{Cu}^{2+} + 2\text{PO}_4^{3-} + 2\text{H}^+$	-36.43 ± 0.61	207.941 ± 3.485			
Libenthenite					
$\text{Cu}_2(\text{PO}_4)\text{OH} \rightleftharpoons 2\text{Cu}^{2+} + \text{PO}_4^{3-} + \text{OH}^-$	-28.0^b	159.825		-1212.444	
$\text{Cu}_2(\text{PO}_4)\text{OH} + \text{H}^+ \rightleftharpoons 2\text{Cu}^{2+} + \text{PO}_4^{3-} + \text{H}_2\text{O}$	-14.0	79.905			
Tagilite					
$\text{Cu}_2(\text{PO}_4)\text{OH}: \text{H}_2\text{O} \rightleftharpoons 2\text{Cu}^{2+} + \text{PO}_4^{3-} + \text{OH}^- + \text{H}_2\text{O}$	-27.9^b	159.3		-1449.013	
$\text{Cu}_2(\text{PO}_4)\text{OH}: \text{H}_2\text{O} + \text{H}^+ \rightleftharpoons 2\text{Cu}^{2+} + \text{PO}_4^{3-} + 2\text{H}_2\text{O}$	-13.9	79.334			
Cornetite					
$\text{Cu}_3(\text{PO}_4)(\text{OH})_3 \rightleftharpoons 3\text{Cu}^{2+} + \text{PO}_4^{3-} + 3\text{OH}^-$	-48.0^b	273.986		-1575.999	
$\text{Cu}_3(\text{PO}_4)(\text{OH})_3 + 3\text{H}^+ \rightleftharpoons 3\text{Cu}^{2+} + \text{PO}_4^{3-} + 3\text{H}_2\text{O}$	-6.0	34.226			
Pseudomalachite					
$\text{Cu}_5(\text{PO}_4)_2(\text{OH})_4 \rightleftharpoons 5\text{Cu}^{2+} + 2\text{PO}_4^{3-} + 4\text{OH}^-$	-75.8^b	432.7		-2787.302	
$\text{Cu}_5(\text{PO}_4)_2(\text{OH})_4 + 4\text{H}^+ \rightleftharpoons 5\text{Cu}^{2+} + 2\text{PO}_4^{3-} + 4\text{H}_2\text{O}$	-19.8	112.990			
Cu-pyromorphite					
$\text{Cu}_5(\text{PO}_4)_3\text{OH} \rightleftharpoons 5\text{Cu}^{2+} + 3\text{PO}_4^{3-} + \text{OH}^-$	-65.6^b	374.448		-3282.911	
$\text{Cu}_5(\text{PO}_4)_3\text{OH} + \text{H}^+ \rightleftharpoons 5\text{Cu}^{2+} + 3\text{PO}_4^{3-} + \text{H}_2\text{O}$	-51.6	294.528			
Tsumebite					
$\text{Pb}_2\text{Cu}(\text{PO}_4)(\text{OH})_3 \cdot 3\text{H}_2\text{O} \rightleftharpoons 2\text{Pb}^{2+} + \text{Cu}^{2+} + \text{PO}_4^{3-} + 3\text{OH}^- + 3\text{H}_2\text{O}$	-51.3^b	292.8		-2484.824	
$\text{Pb}_2\text{Cu}(\text{PO}_4)(\text{OH})_3 \cdot 3\text{H}_2\text{O} + 3\text{H}^+ \rightleftharpoons 2\text{Pb}^{2+} + \text{Cu}^{2+} + \text{PO}_4^{3-} + 6\text{H}_2\text{O}$	-9.3	53.063			
Turquoise					
$\text{CuAl}_6(\text{PO}_4)_4(\text{OH})_8 \cdot 4\text{H}_2\text{O} \rightleftharpoons \text{Cu}^{2+} + 6\text{Al}^{3+} + 4\text{PO}_4^{3-} + 8\text{OH}^- + 4\text{H}_2\text{O}$	-179.0^b	1021.740		-10214.020	
$\text{CuAl}_6(\text{PO}_4)_4(\text{OH})_8 \cdot 4\text{H}_2\text{O} + 8\text{H}^+ \rightleftharpoons \text{Cu}^{2+} + 6\text{Al}^{3+} + 4\text{PO}_4^{3-} + 12\text{H}_2\text{O}$	-66.99	382.380			
Veszelyite					
$\text{CuZn}_2\text{PO}_4(\text{OH})_3 \cdot 2\text{H}_2\text{O} \rightleftharpoons \text{Cu}^{2+} + 2\text{Zn}^{2+} + \text{PO}_4^{3-} + 3\text{OH}^- + 2\text{H}_2\text{O}$	-45.8^b	261.428		-2462.219	
$\text{CuZn}_2\text{PO}_4(\text{OH})_3 \cdot 2\text{H}_2\text{O} + 3\text{H}^+ \rightleftharpoons \text{Cu}^{2+} + 2\text{Zn}^{2+} + \text{PO}_4^{3-} + 5\text{H}_2\text{O}$	-3.8	21.668			
$\text{Cu}^{2+} + \text{HPO}_4^{2-} \rightleftharpoons \text{CuHPO}_4(\text{aq})$		4.15 ± 0.30^c			
$\text{Cu}^{2+} + \text{PO}_4^{3-} + \text{H}^+ \rightleftharpoons \text{CuHPO}_4(\text{aq})$		16.49 ± 0.3			
$\text{Cu}^{2+} + \text{P}_2\text{O}_7^{4-} \rightleftharpoons \text{Cu}(\text{P}_2\text{O}_7)^{2-}$	6.64 ± 1.49	-37.890 ± 8.481^a	-1908.347 ± 9.756		
$\text{Cu}^{2+} + 2\text{PO}_4^{3-} + 2\text{H}^+ \rightleftharpoons \text{Cu}(\text{P}_2\text{O}_7)^{2-} + \text{H}_2\text{O}$	27.95 ± 1.59	-159.551 ± 9.101	-1908.347 ± 9.756		
$\text{Cu}^{2+} + 2\text{P}_2\text{O}_7^{4-} \rightleftharpoons \text{Cu}(\text{P}_2\text{O}_7)_2^{6-}$	8.92 ± 1.36	-50.890 ± 7.755^a	-3856.850 ± 12.076		
$\text{Cu}^{2+} + 4\text{PO}_4^{3-} + 4\text{H}^+ \rightleftharpoons \text{Cu}(\text{P}_2\text{O}_7)_2^{6-} + 2\text{H}_2\text{O}$	51.54 ± 1.78	-294.212 ± 10.183	-3856.850 ± 12.076		
Enargite					
$\text{Cu}_3\text{AsS}_4 + 4\text{H}_2\text{O} + 7.5\text{O}_2(\text{aq}) \rightleftharpoons 3\text{Cu}^+ + \text{H}_2\text{AsO}_3^- + 6\text{H}^+ + 4\text{SO}_4^{2-}$	421.9 ± 12.8	-2408.00 ± 73.22	-182.40 ± 73.04	-2408.00 ± 73.22	-484.03 ± 73.83

Table 3.7-19. Continued.

Reaction	$\log_{10} \beta_n^\circ$	$\Delta_r G_m^\circ$ (kJ mol ⁻¹)	$\Delta_f G_m^\circ$ (kJ mol ⁻¹)	$\Delta_r H_m^\circ$ (kJ mol ⁻¹)	$\Delta_f H_m^\circ$ (kJ mol ⁻¹)
$\text{Cu}_3\text{AsS}_4 + 4\text{H}_2\text{O} \rightleftharpoons 3\text{Cu}^{+} + \text{H}_2\text{AsO}_3^- + 4\text{HS}^- + 0.5\text{O}_2(\text{aq}) + 2\text{H}^+$	-131.0 ± 12.7	748.01 ± 72.44		1 070.56 ± 72.68	
$\text{Cu}_3(\text{AsO}_4)_2 \cdot 6\text{H}_2\text{O} \rightleftharpoons 3\text{Cu}^{2+} + 2\text{AsO}_4^{3-} + 6\text{H}_2\text{O}$	-33.22 ^d	189.611	-2 714.033		

a [1982WAG/EVA]; b [1984NRI]; c [2007POW/BRO]; d [1974NAU/RYZ].

* calculated from $\Delta_r G_m^\circ$ or $\Delta_r H_m^\circ$, and $\Delta_f G_m^\circ$ or $\Delta_f H_m^\circ$ in [2003GUI/FAN], unless noted otherwise.**Table 3.7-20. Thermodynamic constants and functions for C compounds of Cu.**

Reaction	$\log_{10} \beta_n^\circ$	$\Delta_r G_m^\circ$ (kJ mol ⁻¹)	$\Delta_f G_m^\circ$ (kJ mol ⁻¹)	$\Delta_r H_m^\circ$ (kJ mol ⁻¹)	$\Delta_f H_m^\circ$ (kJ mol ⁻¹)
$\text{CuCO}_3(\text{cr}) \rightleftharpoons \text{Cu}^{2+} + \text{CO}_3^{2-}$	-11.50 ^a	65.642	-528.496		
$\text{Cu}_2\text{CO}_3(\text{OH})_2(\text{s}) + 4\text{H}^+ \rightleftharpoons 2\text{Cu}^{2+} + \text{CO}_2(\text{g}) + 3\text{H}_2\text{O}$	12.68 ± 0.10 ^b	-72.378 ± 1.142	-903.323 ± 3.322		-1 067.1 ± 3.4 ^b
$\text{Cu}_2\text{CO}_3(\text{OH})_2(\text{s}) + 2\text{H}^+ \rightleftharpoons 2\text{Cu}^{2+} + \text{CO}_3^{2-} + 2\text{H}_2\text{O}$	-5.47 ± 0.19	31.235 ± 1.085			
$\text{Cu}_3(\text{CO}_3)_2(\text{OH})_2(\text{s}) + 6\text{H}^+ \rightleftharpoons 3\text{Cu}^{2+} + 2\text{CO}_2(\text{g}) + 4\text{H}_2\text{O}$	18.90 ± 0.30 ^b	-71.921 ± 1.142	-1 470.247 ± 4.819		-1 675.1 ± 5.1 ^b
$\text{Cu}_3(\text{CO}_3)_2(\text{OH})_2(\text{s}) + 2\text{H}^+ \rightleftharpoons 3\text{Cu}^{2+} + 2\text{CO}_3^{2-} + 2\text{H}_2\text{O}$	-17.40 ± 0.27	99.344 ± 1.554		-52.320 ± 4.093	
$\text{Cu}^{2+} + \text{CO}_3^{2-} \rightleftharpoons \text{Cu}(\text{CO}_3)(\text{aq})$	6.75 ± 0.03 ^c	-38.529 ± 0.169	-501.383 ± 1.614		
$\text{Cu}^{2+} + \text{HCO}_3^- \rightleftharpoons \text{Cu}(\text{HCO}_3)^+$	1.84 ± 0.10 ^c	-10.503 ± 0.570	-532.302 ± 1.677		
$\text{Cu}^{2+} + \text{CO}_3^{2-} + \text{H}^+ \rightleftharpoons \text{Cu}(\text{HCO}_3)^+$	12.17 ± 0.09	-69.448 ± 0.486			
$\text{Cu}^{2+} + 2\text{CO}_3^{2-} \rightleftharpoons \text{Cu}(\text{CO}_3)_2^{2-}$	10.3 ± 0.1 ^c	-58.793 ± 0.572	-1 049.547 ± 1.833		

a [2004SMI/MAR]; b [2002PRE/GAM]; c [2007POW/BRO]

* calculated from $\Delta_f G_m^\circ$ and $\Delta_f H_m^\circ$ in [2003GUI/FAN]**Table 3.7-21. Specific ion interaction coefficients for Cu species**

Specific ion interaction coefficient	Values ± 1σ	Reference and comments
$\varepsilon(\text{Cu}^+, \text{ClO}_4^-)$	0.11 ± 0.01	[1980CIA]
$\varepsilon(\text{Cu}^{2+}, \text{Cl}^-)$	0.08 ± 0.01	[2003GUI/FAN]
$\varepsilon(\text{Cu}^{2+}, \text{ClO}_4^-)$	0.32 ± 0.02	[2003GUI/FAN]
$\varepsilon(\text{Cu}^{2+}, \text{NO}_3^-)$	0.11 ± 0.01	[2003GUI/FAN]
$\varepsilon(\text{Cu}(\text{OH})^+, \text{ClO}_4^-)$	-0.07 ± 0.04	from Δε in [2016BRO/EKB]
$\varepsilon(\text{Cu}(\text{OH})_2(\text{aq}), \text{Na}^+\text{ClO}_4^-)$	0.30 ± 0.11	from Δε in [2016BRO/EKB]
$\varepsilon(\text{Cu}(\text{OH})_3^-, \text{Na}^+)$	0.40 ± 0.09	from Δε in [2016BRO/EKB]
$\varepsilon(\text{Cu}(\text{OH})_4^{2-}, \text{Na}^+)$	0.19 ± 0.05	[1997PLY/WAN]
$\varepsilon(\text{Cu}(\text{OH})_4^{2-}, \text{K}^+)$	0.29 ± 0.05	[1997PLY/WAN]
$\varepsilon(\text{Cu}_2(\text{OH})^{3+}, \text{ClO}_4^-)$	1.00 ± 0.23	from Δε in [2016BRO/EKB]
$\varepsilon(\text{Cu}_2(\text{OH})_2^{2+}, \text{ClO}_4^-)$	0.63 ± 0.11	from Δε in [2016BRO/EKB]
$\varepsilon(\text{Cu}_2(\text{OH})_2^{2+}, \text{NO}_3^-)$	0.35 ± 0.18	from Δε in [2016BRO/EKB]
$\varepsilon(\text{CuCl}^+, \text{Na}^+)$	0.06 ± 0.03	from Δε in [2007POW/BRO]
$\varepsilon(\text{CuCl}_2(\text{aq}), \text{Na}^+\text{ClO}_4^{\pm})$	0.24 ± 0.07	from Δε in [2007POW/BRO]
$\varepsilon(\text{Cu}(\text{SO}_4)(\text{aq}), \text{Na}^+\text{ClO}_4^{\pm})$	-0.06 ± 0.04	from Δε in [2007POW/BRO]
$\varepsilon(\text{Cu}(\text{CO}_3)(\text{aq}), \text{Na}^+\text{ClO}_4^{\pm})$	0.06 ± 0.05	from Δε in [2007POW/BRO]
$\varepsilon(\text{Cu}(\text{HCO}_3)^+, \text{Na}^+)$	0.46 ± 0.15	from Δε in [2007POW/BRO]
$\varepsilon(\text{Cu}(\text{CO}_3)_2^{2-}, \text{Na}^+\text{ClO}_4^-)$	0.46 ± 0.21	from Δε in [2007POW/BRO]

3.7.5. Silver

3.7.5.1. Native Metal and Free Ions

The thermodynamic functions for $\text{Ag}(\text{cr})$, $\text{Ag}(\text{g})$, and the common master species Ag^+ are taken from the NEA-OECD reviews [1992GRE/FUG; 2003GUI/FAN]. No other data in solution are selected in any NEA-OECD commissioned review, yet. The specific ion interaction coefficients for Ag^+ are taken from Grenthe *et al.* [1992GRE/FUG].

Function of formation for Ag^{2+} is taken from Bard *et al.* [1985BAR/PAR] — even if it is unstable in water.

3.7.5.2. Oxo and Hydroxo Compounds

The function of formation of $\text{Ag}_2\text{O}(\text{cr})$ from Wagman *et al.* [1982WAG/EVA] are used to calculate the functions of reaction and solubility constants.

Thermodynamic functions of formation from Wagman *et al.* [1982WAG/EVA] for $\text{Ag(OH)}(\text{aq})$, and Bard *et al.* [1985BAR/PAR] for Ag(OH)_2^- — the values of the Gibbs energy seem to be based on Wagman *et al.* [1982WAG/EVA].

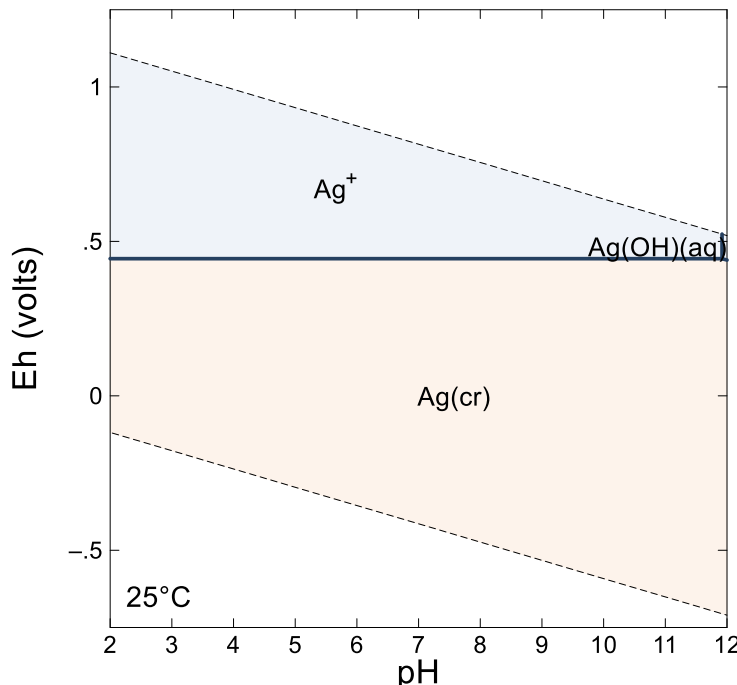


Figure 3.7-17. Pourbaix diagram (GWB) of $10^{-6} \text{ mol kg}_w^{-1} \text{ Ag}$.

3.7.5.3. Halogen Compounds

The functions of formation for $\text{AgCl}(\text{cr})$ is given in the NEA-OECD reviews [1992GRE/FUG; 2003GUI/FAN]. The functions of formation of $\text{AgF}(\text{cr})$, $\text{AgBr}(\text{cr})$, and $\text{AgI}(\text{cr})$ are available in Bard *et al.* [1985BAR/PAR]. The functions of formation of $\text{AgF}: 2\text{H}_2\text{O}(\text{cr})$ and $\text{AgF}: 4\text{H}_2\text{O}(\text{cr})$ are used to calculate the functions of reaction.

Functions of formation for $\text{AgF}(\text{aq})$ $\text{AgCl}(\text{aq})$, AgCl_2^- , $\text{AgBr}_n^{(1-n)+}$ — with $n = \{1; 2; 3\}$ —, and $\text{AgI}_n^{(1-n)+}$ — with $n = \{1; 2; 3; 4\}$ — from Wagman *et al.* [1982WAG/EVA] are used to calculate the function of reaction, and formation constants. The functions of formation are then recalculated in relation to NEA-OECD reviews Guillaumont *et al.* [2003GUI/FAN].

Finally the Gibbs energies for AgCl_3^{2-} and AgCl_4^{3-} are taken from Bard *et al.* [1985BAR/PAR].

3.7.5.4. Group 16 Compounds

The functions of formation of the allotropic forms of $\text{Ag}_2\text{S}(\text{cr})$ are available in Wagman *et al.* [1982WAG/EVA]. Robie and Hemingway [1995ROB/HEM] gives only the value for acanthite ($\beta - \text{Ag}_2\text{S}$). Knowing the already noticed problem on the Gibbs energy and enthalpy of HS^- in Robie and Hemingway [1995ROB/HEM], the functions of reaction and constant are calculated relative to the corrected $\Delta_f G^\circ(\text{HS}^-)$ in § 3.3.

Spycher and Reed [1989SPY/REE] proposed variations of $\log_{10} K^\circ$ for sulphide complexes — $\text{Ag}(\text{HS})_n^{(1-n)+}$ with $n = \{1; 2\}$ — that are used to calculate the thermodynamic function of reaction and $\log_{10} \beta^\circ$ value, which were used also to recalculate $\Delta_f G_m^\circ$ and $\Delta_f H_m^\circ$ used in the database.

The functions of formation of $\text{Ag}_2\text{Se}(\text{cr})$, $\text{Ag}_2\text{SeO}_3(\text{cr})$ and $\text{Ag}_2\text{SeO}_4(\text{cr})$ are taken from the NEA-OECD review on selenium [2005OLI/NOL].

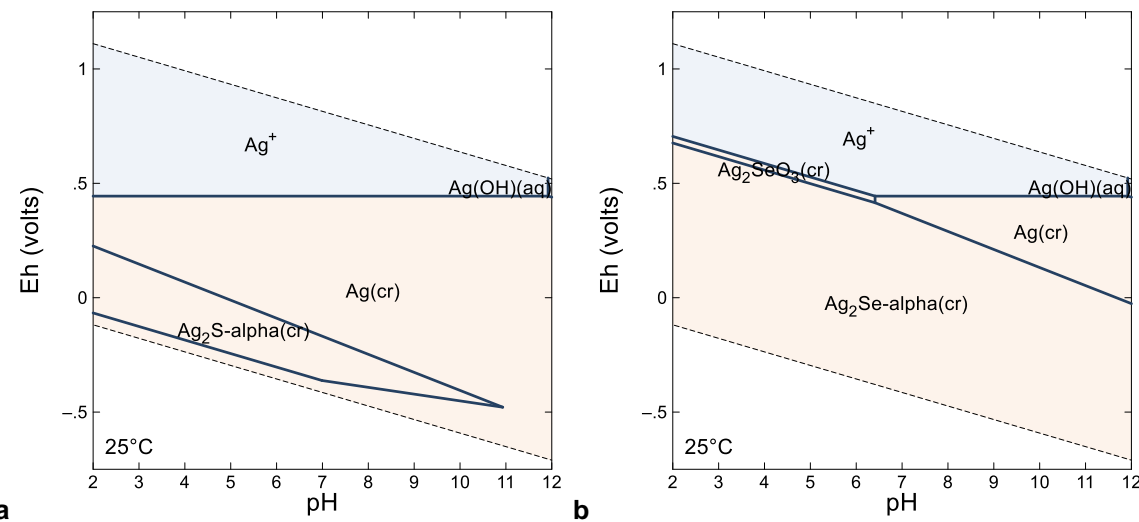


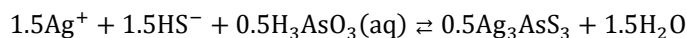
Figure 3.7-18. Pourbaix diagram (GWB) of 10^{-6} mol kg_w⁻¹ Ag and 10^{-4} mol kg_w⁻¹ S (a) and Se (b).

3.7.5.5. Group 15 Compounds

The functions of formation of $\text{AgNO}_3(\text{cr})$ from Wagman *et al.* [1982WAG/EVA] are used to calculate the functions of reaction.

Silver is forming several arsenosulphide components: smithite and trechmannite (AgAsS_2), and xanthoconite and proustite (Ag_3AsS_3) [1989TAR/KLE; 1997MEY/SCH]. Only the value of entropy is available for arsenosulphide solid proustite, in Robie and Hemingway [1995ROB/HEM]. Taras Bryndzia and Kleppa [1989TAR/KLE] proposed $\Delta_f H_m^\circ$ for smithite, trechmanite and proustite, and enthalpies of transformation as well as entropies of transformation at 593 K of trechmanite to proustite.

Spycher and Reed [1989SPY/REE] proposed variations of $\log_{10} K^\circ$ for proustite between 25 and 300°C (Figure 3.7-19) for the following reaction.



The data at temperature lower than 150°C can be used to estimate the functions of formation of proustite with the help of the Van't Hoff equation (Table 3.7-22).

Meyer and Scholz [1997MEY/SCH] proposed values of $\Delta_r G^\circ = 19.7 \pm 3.5 \text{ kJ mol}^{-1}$ ($\log_{10} K^\circ = -3.45 \pm 0.61$) and $\Delta_r H^\circ = 54.8 \pm 9.6 \text{ kJ mol}^{-1}$ for the transformation of xanthoconite to proustite, which can lead to the following estimation for xanthoconite.

$$\Delta_f G^\circ(\text{xanthoconite}) = \Delta_f G^\circ(\text{Proustite}) - \Delta_r G^\circ = -128.75 \pm 9.34 \text{ kJ mol}^{-1}$$

$$\Delta_f H^\circ(\text{xanthoconite}) = \Delta_f H^\circ(\text{Proustite}) - \Delta_r H^\circ = -119.74 \pm 5.60 \text{ kJ mol}^{-1}$$

Table 3.7-22. Thermodynamic functions and constants for proustite and xanthoconite (Ag_3AsS_3)

Reaction	$\Delta_r H_m^\circ$ kJ mol ⁻¹	$\Delta_r S_m^\circ$ J mol ⁻¹ K ⁻¹	$\Delta_r G_m^\circ$ kJ mol ⁻¹	$\Delta_f H_m^\circ$ kJ mol ⁻¹	$\Delta_f S_m^\circ$ kJ mol ⁻¹	$\Delta_f G_m^\circ$ kJ mol ⁻¹	$\log_{10} K_s^\circ$
Proustite							
$0.5\text{Ag}_3\text{AsS}_3 + 1.5\text{H}_2\text{O} \rightleftharpoons 1.5\text{Ag}^+ + 1.5\text{HS}^- + 0.5\text{H}_3\text{AsO}_3(\text{aq})$	224.348 ± 2.475	-0.18 ± 7.172	224.40 ± 3.271	-32.468 ± 3.899	203.434 ± 10.407	-54.525 ± 4.985	-39.3 ± 0.6
$\text{Ag}_3\text{AsS}_3 + 3\text{H}_2\text{O} \rightleftharpoons 3\text{Ag}^+ + 3\text{HS}^- + \text{H}_2\text{AsO}_3^- + \text{H}^+$	476.106 ± 4.953	-84.87 ± 8.87	501.409 ± 6.548	-64.936 ± 7.799	406.868 ± 20.813	-109.050 ± 9.970	-87.84 ± 1.15
$\text{Ag}_3\text{AsS}_3(\text{Xanthoconite}) \rightleftharpoons \text{Ag}_3\text{AsS}_3(\text{Proustite})$	54.8 ± 9.6	19.7 ± 3.5		-119.74 ± 5.60		-128.75 ± 9.34	-3.45 ± 0.61
$\text{Ag}_3\text{AsS}_3 + 3\text{H}_2\text{O} \rightleftharpoons 3\text{Ag}^+ + 3\text{HS}^- + \text{H}_2\text{AsO}_3^- + \text{H}^+$	530.906 ± 2.226		521.109 ± 5.533				-91.29 ± 0.97

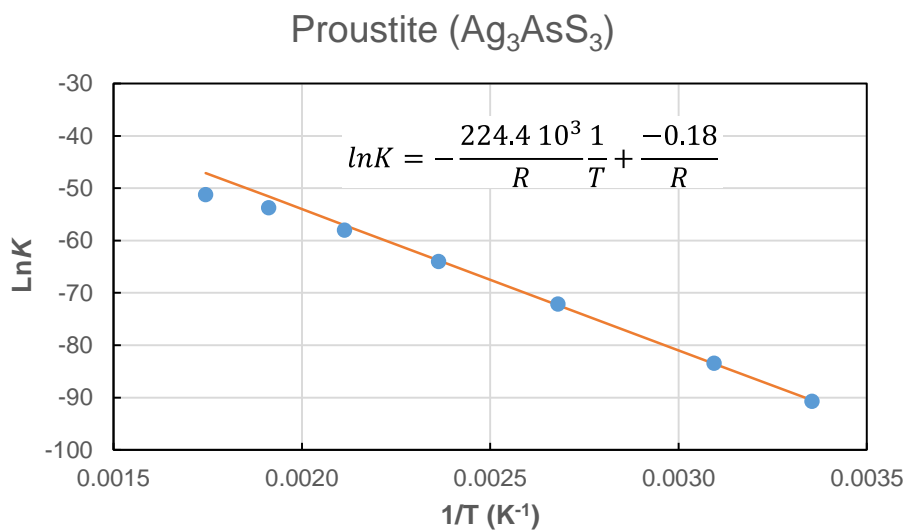


Figure 3.7-19. Evolution of the $\ln K$ values vs. $1/T$ (blue circles) for the dissolution of proustite (Ag_3AsS_3) in Spycher and Reed [1989SPY/REE], and estimation of the formation functions by the Van't Hoff relationship (orange plain line).

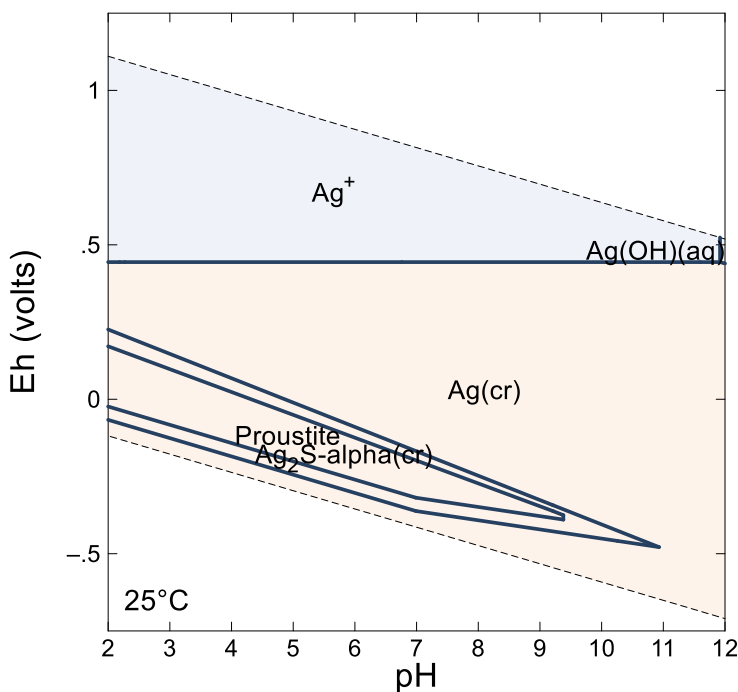


Figure 3.7-20. Pourbaix diagram (GWB) of 10^{-6} mol kg^{-1} Ag and 10^{-4} mol kg^{-1} S and As.

3.7.5.6. Carbon Compounds

The functions of formation for $\text{Ag}(\text{CO}_3)$ (aq) and $\text{Ag}(\text{CO}_3)_2^{2-}$ are estimated in Sverjensky *et al.* [1997SVE/SHO].

The $\text{Ag}(\text{SeCN})_3^{2-}$ complex from [2005OLI/NOL] is included.

3.7.5.7. Thermodynamic Constants and Functions for Ag

Table 3.7-23. Thermodynamic constants and functions for native element, free ions, and oxo and hydroxo compounds of Ag.

Reaction	$\log_{10} \beta^\circ$	$\Delta_r G^\circ$ kJ mol ⁻¹	$\Delta_f G^\circ$ kJ mol ⁻¹	$\Delta_r H^\circ$ kJ mol ⁻¹	$\Delta_f H^\circ$ kJ mol ⁻¹
$\text{Ag}(\text{cr}) + \text{H}^+ \rightleftharpoons \text{Ag}^+ + 0.5\text{H}_2(\text{g})$	-13.51 ± 0.03	77.096 ± 0.156	77.096 ± 0.156^a	105.790 ± 0.080	105.790 ± 0.080^a
$\text{Ag}(\text{cr}) + 0.25\text{O}_2(\text{aq}) + \text{H}^+ \rightleftharpoons \text{Ag}^+ + 0.5\text{H}_2\text{O}$	7.98 ± 0.03	-45.569 ± 0.159		-34.200 ± 0.208	
$\text{Ag}^+ + 0.25\text{O}_2(\text{g}) + \text{H}^+ \rightleftharpoons \text{Ag}^{2+} + 0.5\text{H}_2\text{O}$	-12.86	73.411^b	269.077	20.195^b	268.900
$\text{Ag}^+ + 0.25\text{O}_2(\text{aq}) + \text{H}^+ \rightleftharpoons \text{Ag}^{2+} + 0.5\text{H}_2\text{O}$	-12.14	69.317		23.120	
$\text{Ag}_2\text{O}(\text{cr}) + 2\text{H}^+ \rightleftharpoons 2\text{Ag}^+ + \text{H}_2\text{O}$	12.56 ± 0.275	-71.715 ± 1.569	-11.233 ± 1.600^a	-43.622 ± 0.101	-30.628 ± 0.130^a
$\text{Ag}^+ + \text{H}_2\text{O} \rightleftharpoons \text{Ag}(\text{OH})(\text{aq}) + \text{H}^+$	-11.92 ± 0.14	68.057 ± 0.784^c	-91.987 ± 0.800		
$\text{Ag}^+ + 2\text{H}_2\text{O} \rightleftharpoons \text{Ag}(\text{OH})_2^- + 2\text{H}^+$	-24.00 ± 0.28	137.021 ± 1.604^c	-260.163 ± 1.613		

a [2003GUI/FAN]; b [1985BAR/PAR]; c [1982WAG/EVA].

* calculated from $\Delta_f G_m^\circ$ and $\Delta_f H_m^\circ$ from [2003GUI/FAN].

Table 3.7-24. Thermodynamic constants and functions for halogen compounds of Ag.

Reaction	$\log_{10} \beta^\circ$	$\Delta_r G^\circ$ kJ mol ⁻¹	$\Delta_f G^\circ$ kJ mol ⁻¹	$\Delta_r H^\circ$ kJ mol ⁻¹	$\Delta_f H^\circ$ kJ mol ⁻¹
$\text{AgF}(\text{cr}) \rightleftharpoons \text{Ag}^+ + \text{F}^-$	2.40	-13.680^c	-190.747	-23.000^c	-206.560
$\text{AgF}: 2\text{H}_2\text{O}(\text{cr}) \rightleftharpoons \text{Ag}^+ + \text{F}^- + 2\text{H}_2\text{O}$	0.87 ± 1.40	-4.941 ± 8.001^b	-673.766 ± 8.033	2.089 ± 0.658^b	-803.309 ± 0.041
$\text{AgF}: 4\text{H}_2\text{O}(\text{cr}) \rightleftharpoons \text{Ag}^+ + \text{F}^- + 4\text{H}_2\text{O}$	0.56 ± 9.81	-3.199 ± 0.800^b	-1149.788 ± 56.000	17.929 ± 2.303^b	-1390.809 ± 2.400
$\text{Ag}^+ + \text{F}^- \rightleftharpoons \text{AgF}(\text{aq})$	0.35 ± 0.99	-2.017 ± 5.631^b	-206.444 ± 5.675	-11.849 ± 7.246^b	-241.409 ± 7.276
$\text{AgCl}(\text{cr}) \rightleftharpoons \text{Ag}^+ + \text{Cl}^-$	-9.75 ± 0.03	55.644 ± 0.169	-109.765 ± 0.098^a	65.720 ± 0.118	-127.010 ± 0.050^a
$\text{Ag}^+ + \text{Cl}^- \rightleftharpoons \text{AgCl}(\text{aq})$	3.27 ± 1.12	-18.679 ± 6.399^b	-72.800 ± 6.402	-11.510 ± 6.399^b	-72.510 ± 6.400
$\text{Ag}^+ + 2\text{Cl}^- \rightleftharpoons \text{AgCl}_2^-$	5.26 ± 0.56	-30.051 ± 3.187^b	-215.389 ± 3.200	-16.461 ± 1.585^b	-244.831 ± 1.600
$\text{Ag}^+ + 3\text{Cl}^- \rightleftharpoons \text{AgCl}_3^{2-}$	5.25	-29.961^c	-346.516		
$\text{Ag}^+ + 4\text{Cl}^- \rightleftharpoons \text{AgCl}_4^{3-}$	5.50	-31.395^c	-479.167		
$\text{AgBr}(\text{cr}) \rightleftharpoons \text{Ag}^+ + \text{Br}^-$	-12.29	70.140^c	-96.894	84.500^c	-100.120
$\text{Ag}^+ + \text{Br}^- \rightleftharpoons \text{AgBr}(\text{aq})$	4.23 ± 0.08	-24.147 ± 0.477^b	-50.901 ± 0.529		
$\text{Ag}^+ + 2\text{Br}^- \rightleftharpoons \text{AgBr}_2^-$	7.29 ± 0.55	-41.587 ± 3.127^b	-172.191 ± 3.148		
$\text{Ag}^+ + 3\text{Br}^- \rightleftharpoons \text{AgBr}_3^{2-}$	8.71 ± 0.69	-49.727 ± 3.912^b	-77.096 ± 0.156		
$\text{AgI}(\text{cr}) \rightleftharpoons \text{Ag}^+ + \text{I}^-$	-16.07	91.710^c	-66.338	111.560^c	-62.550
$\text{Ag}^+ + \text{I}^- \rightleftharpoons \text{AgI}(\text{aq})$	6.59 ± 0.14	-37.637 ± 0.788^b	-12.265 ± 0.811		
$\text{Ag}^+ + 2\text{I}^- \rightleftharpoons \text{AgI}_2^-$	10.68 ± 0.13	-60.969 ± 0.755^b	-87.321 ± 0.803		
$\text{Ag}^+ + 3\text{I}^- \rightleftharpoons \text{AgI}_3^{2-}$	13.37 ± 1.26	-76.299 ± 7.213^b	-154.375 ± 7.222	-122.009 ± 0.782^b	-186.559 ± 0.800
$\text{Ag}^+ + 4\text{I}^- \rightleftharpoons \text{AgI}_4^{3-}$	14.09 ± 0.84	-80.429 ± 4.777^b	-210.229 ± 4.800		

a [2003GUI/FAN]; b [1982WAG/EVA]; c [1985BAR/PAR].

Table 3.7-25. Thermodynamic constants and functions for S, Se, N, and C compounds of Ag.

Reaction	$\log_{10} \beta^\circ$	$\Delta_r G^\circ$ kJ mol ⁻¹	$\Delta_f G^\circ$ kJ mol ⁻¹	$\Delta_r H^\circ$ kJ mol ⁻¹	$\Delta_f H^\circ$ kJ mol ⁻¹
$\text{Ag}_2\text{S}-\alpha + \text{H}^+ \rightleftharpoons 2\text{Ag}^+ + \text{HS}^-$	-36.26 ± 0.36	206.964 ± 2.063^a	-40.529 ± 0.560	226.148 ± 1.499^a	-30.868 ± 0.170
$\text{Ag}_2\text{S}-\beta + \text{H}^+ \rightleftharpoons 2\text{Ag}^+ + \text{HS}^-$	-36.05 ± 0.35	205.754 ± 2.083^a	-39.319 ± 0.480	222.968 ± 1.506^a	-27.688 ± 0.090
$\text{Ag}_2\text{S} + \text{H}^+ \rightleftharpoons 2\text{Ag}^+ + \text{HS}^-$	-36.11 ± 0.33	206.100 ± 1.890^b	-39.665 ± 1.000	227.300 ± 1.129^b	-32.020 ± 1.000

Table 3.7-25. Continued.

Reaction	$\log_{10} \beta^\circ$	$\Delta_r G^\circ$ kJ mol ⁻¹	$\Delta_f G^\circ$ kJ mol ⁻¹	$\Delta_r H^\circ$ kJ mol ⁻¹	$\Delta_f H^\circ$ kJ mol ⁻¹
$\text{Ag}^+ + \text{HS}^- \rightleftharpoons \text{Ag}(\text{HS})(\text{aq})$	13.92 ± 0.63	$-79.473 \pm 3.611^{\text{c}}$	9.866 ± 4.188	$-71.524 \pm 2.733^{\text{c}}$	17.966 ± 3.119
$\text{Ag}^+ + 2\text{HS}^- \rightleftharpoons \text{Ag}(\text{HS})_2^-$	17.68 ± 0.52	$-100.908 \pm 2.947^{\text{c}}$	0.674 ± 5.158	$-94.082 \pm 2.230^{\text{c}}$	-20.892 ± 3.739
$\text{Ag}_2\text{Se}-\alpha + 2\text{H}^+ \rightleftharpoons 2\text{Ag}^+ + \text{H}_2\text{Se}(\text{aq})$	-39.00 ± 0.27	222.587 ± 1.555	$-46.900 \pm 1.300^{\text{d}}$	266.009 ± 1.542	$-40.129 \pm 1.318^{\text{d}}$
$\text{Ag}_2\text{SeO}_3(\text{cr}) \rightleftharpoons 2\text{Ag}^+ + \text{SeO}_3^{2-}$	-15.80 ± 0.29	90.200 ± 1.665	$-298.400 \pm 2.440^{\text{d}}$	67.860 ± 0.512	$-363.440 \pm 1.020^{\text{d}}$
$\text{Ag}_2\text{SeO}_4(\text{cr}) \rightleftharpoons 2\text{Ag}^+ + \text{SeO}_4^{2-}$	-7.86 ± 0.50	44.857 ± 2.845	$-330.150 \pm 3.200^{\text{d}}$	30.590 ± 2.789	$-422.510 \pm 2.120^{\text{d}}$
$\text{AgNO}_3(\text{cr}) \rightleftharpoons \text{Ag}^+ + \text{NO}_3^-$	-0.31 ± 0.08	$1.777 \pm 0.437^{\text{a}}$	-35.475 ± 0.085	$24.969 \pm 0.605^{\text{a}}$	-126.029 ± 0.729
$\text{Ag}^+ + \text{CO}_3^{2-} \rightleftharpoons \text{Ag}(\text{CO}_3)^-$	2.69	-15.339^{f}	-466.143	-26.738^{f}	-596.178
$\text{Ag}^+ + 2\text{CO}_3^{2-} \rightleftharpoons \text{Ag}(\text{CO}_3)_2^{3-}$	2.15	-12.280^{f}	-990.984	-28.103^{f}	-1272.773
$\text{AgSeCN}(\text{cr}) \rightleftharpoons \text{Ag}^+ + \text{SeCN}^-$	-14.00 ± 0.51	79.900 ± 2.900	133.247 ± 4.783		
$\text{Ag}^+ + 3\text{SeCN}^- \rightleftharpoons \text{Ag}(\text{SeCN})_3^{2-}$	13.85 ± 0.30	-79.056 ± 1.713	$406.193 \pm 11.529^{\text{d}}$		

a [1982WAG/EVA]; b [1995ROB/HEM]; c [1989SPY/REE]; d [2005OLI/NOL]; f [1997SVE/SHO]

Table 3.7-26. Specific ion interaction coefficients for Ag aqueous species.

Specific ion interaction coefficient	Value $\pm \sigma$	Reference
$\varepsilon(\text{Ag}^+, \text{Cl}^-)$	0	Equivalence $\text{ClO}_4^-/\text{Cl}^-$
$\varepsilon(\text{Ag}^+, \text{ClO}_4^-)$	0.00 ± 0.01	[2003GUI/FAN]
$\varepsilon(\text{Ag}^+, \text{NO}_3^-)$	-0.12 ± 0.05	[2003GUI/FAN]

3.7.6. Nickel

Nickel is often associated to uranium ores.

3.7.6.1. General Data

The values selected in Gamsjäger *et al.* [2005GAM/BUG] are accepted in the database. The common master species is Ni^{2+} . The $\text{NiSe}_2(\text{cr})$, $\text{NiSeO}_3 \cdot 2\text{H}_2\text{O}(\text{cr})$, $\text{NiSeO}_4 \cdot 6\text{H}_2\text{O}(\text{cr})$ solids, and $\text{NiSeCN}_n^{(2-n)+}$ and $\text{NiSeO}_4(\text{aq})$ species from Olin *et al.* [2005OLI/NOL] are directly included since they were proposed in the same framework.

The specific ion interaction coefficients from the NEA-OECD reviews are accepted [2003GUI/FAN; 2005GAM/BUG 1476; 2020GRE/GAO].

3.7.6.2. Complementary Data

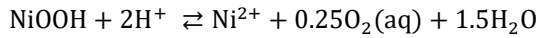
3.7.6.2.1 Oxides and Hydroxides

Brown and Ekberg [2016BRO/EKB] proposed the Gibbs energy of formation of $\beta\text{-NiOOH}(\text{cr})$, which solubility can be written, as follows.



$$\Delta_r G^\circ = -(194.653 \pm 5.957) \text{ kJ mol}^{-1}$$

$$\log_{10} K_s = 34.10 \pm 1.04$$



$$\Delta_r G^\circ = -(71.989 \pm 5.946) \text{ kJ mol}^{-1}$$

$$\log_{10} K_s = 12.61 \pm 1.04$$

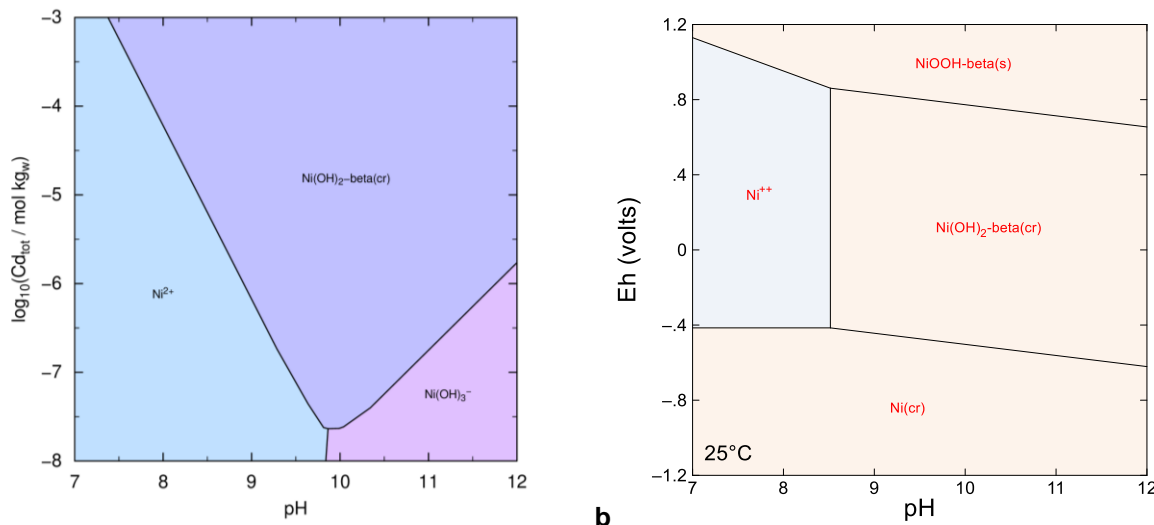


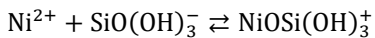
Figure 3.7-21. (a) Solubility of Ni in a hypothetical indifferent electrolyte at 0.1 mol kg_w⁻¹ (PHREEPLOT); all phases are allowed to precipitate; (b) Pourbaix diagram of Ni in the same conditions (GWB).

3.7.6.2.2 Group 14

For scoping calculation the value for NiHCO₃⁺ and Ni(CO₃)₂²⁻ proposed in Baeyens *et al.* [2003BAE/BRA] are added to the database.

Robie and Hemingway [1995ROB/HEM] proposed the functions of formation of liebenbergite (Ni₂SiO₄) — which functions of formation are close to Ni₂SiO₄ olivine in Gamsjäger *et al.* [2005GAM/BUG] — and the slightly more soluble Ni₂SiO₄- spinel.

Finally, the constant value from Pathak and Choppin [2006PAT/CHO] for NiOSi(OH)₃⁺ is used,



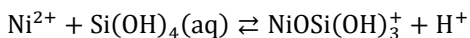
$$\log_{10} \beta^\circ = 6.34 \pm 0.03$$

$$\Delta_r G_m^\circ = -(36.189 \pm 0.144) \text{ kJ mol}^{-1}$$

which give the following Gibbs energy of formation.

$$\Delta_f G_m^\circ = -(1\ 333.702 \pm 1.405) \text{ kJ mol}^{-1}$$

The formation reaction relative to Si(OH)₄(aq) is then written as follows.

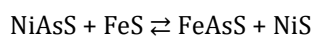


$$\log_{10} \beta^\circ = -3.47 \pm 0.04$$

$$\Delta_r G_m^\circ = (19.806 \pm 0.208) \text{ kJ mol}^{-1}$$

3.7.6.2.3 Arsenosulphide

The arsenosulphide phases of nickel are important in environmental monitoring of mining activities. Goodgame [1997GOO] estimated the data for gersdorffite (NiAsS) postulating that $\Delta_r G = 0$ for the following reaction.



Goodgame [1997GOO] proposed $\Delta_f G_m^\circ = -88.73 \text{ kJ mol}^{-1}$, but no $\Delta_f H_m^\circ$ or $S_{f,m}^\circ$ were proposed. In the SOLTHERM-XPT database [2015PAL; 2016REE/SPY], a variation of $\log_{10} \beta^\circ(T)$ between 25 and 300°C is given for the following reaction.



The variation are represented in Figure 3.7-22. The variation at $T < 100^\circ\text{C}$ — *i.e.*, $1/T > 0.0027\text{ K}^{-1}$ — could be approximated to a straight line and treated using the Van't Hoff equation. The formation function for the phases Gersdorffite could be estimated, using the same hypothesis as in Goodgame [1997GOO] in Table 3.7-27 using the formation functions for Ni^{2+} [2005GAM/BUG], and from Guillaumont *et al.* [2003GUI/FAN] for H_2O , H_3AsO_3 , HS^- , and SO_4^{2-} . It can be noted that the obtained value for gersdorffite is lower than the data estimated by Goodgame [1997GOO].

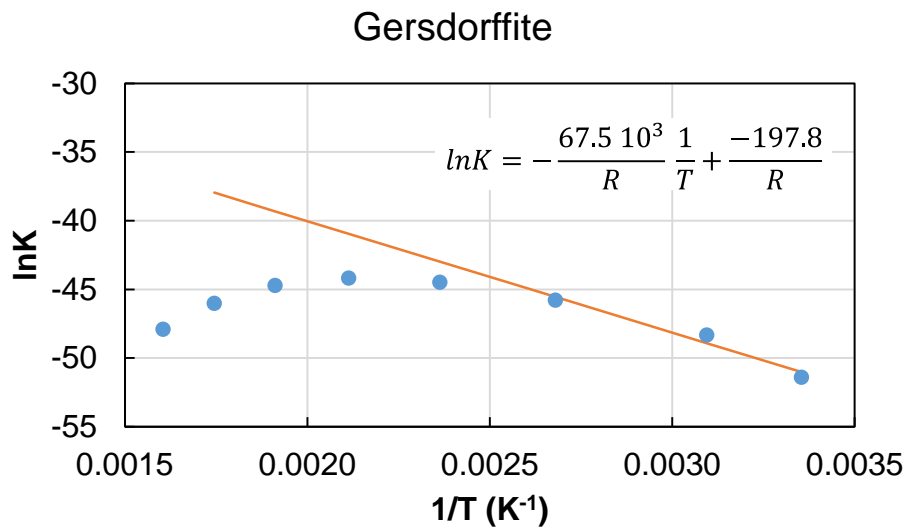


Figure 3.7-22. Evolution of the $\ln K$ values vs. $1/T$ (blue circles) for the dissolution of gersdorffite (NiAsS) in the SOLTHERM-XPT database [2015PAL; 2016REE/SPY], and estimation of the formation functions by the Van't Hoff relationship (orange line).

Table 3.7-27. Thermodynamic functions and constants estimated for gersdorffite (NiAsS) in the SOLTHERM-XPT database [2015PAL; 2016REE/SPY].

Reaction	$\Delta_r H_m^\circ$ kJ mol^{-1}	$\Delta_r S_m^\circ$ $\text{J mol}^{-1} \text{K}^{-1}$	$\Delta_r G_m^\circ$ kJ mol^{-1}	$\Delta_f H_m^\circ$ kJ mol^{-1}	$\Delta_f S_m^\circ$ kJ mol^{-1}	$\Delta_f G_m^\circ$ kJ mol^{-1}	$\log_{10} K_s^\circ$
Gersdorffite	67.5 ± 12.9	-197.81 ± 39.44	126.5 ± 17.5	-89.967 ± 13.692	156.763 ± 40.025	-107.805 ± 18.204	-22.2 ± 3.1

The hypothesis used to estimate the formation functions and dissolution reaction could be verified comparing to an analytical expression, which allows adjusting the $\log_{10} K_s$ variations,

$$\log_{10} K_s = A_1 + A_2 T + \frac{A_3}{T}$$

with the calculated values using the Van't Hoff relationship (Figure 3.7-23).

$$\log_{10} K_s(\text{Gersdorffite}) = 14.15 - 0.0365T - \frac{7603}{T}$$

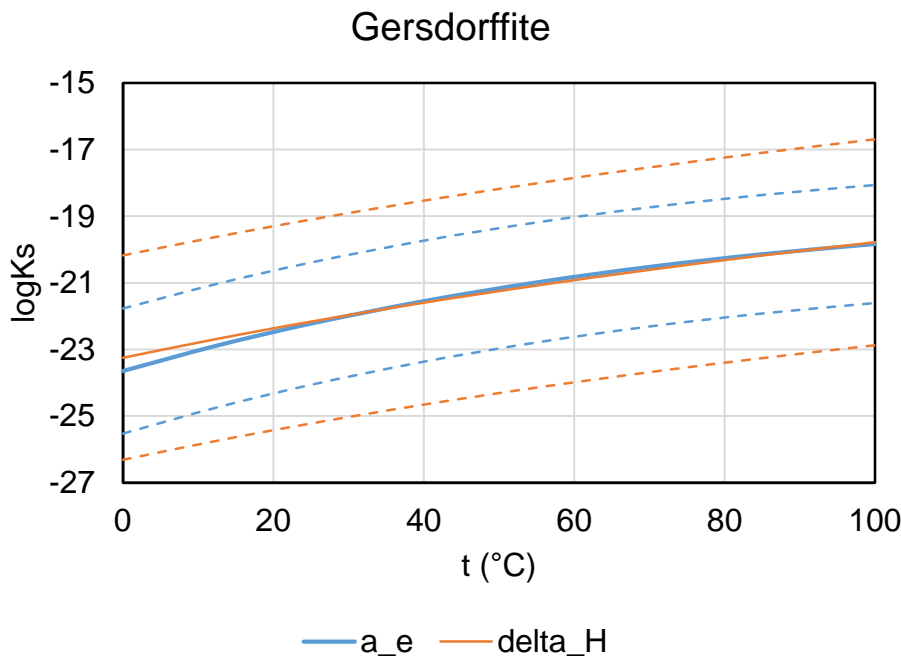


Figure 3.7-23. Evolutions of the $\log_{10} K_s$ of NiAsS(cr) with functions of formation from Table 3.7-27.

3.7.6.3. Additional Thermodynamic Constants and Functions for Ni

Table 3.7-28. Thermodynamic functions and constants for hydroxide, Si, and AsS compounds of Ni

Reaction	$\Delta_r G^\circ$ kJ mol ⁻¹	$\log_{10} \beta^\circ$	$\Delta_f G^\circ$ kJ mol ⁻¹	$\Delta_r H^\circ$ kJ mol ⁻¹	$\Delta_f H^\circ$ kJ mol ⁻¹
$\text{NiOOH} + e^- + 3\text{H}^+ \rightleftharpoons \text{Ni}^{2+} + 2\text{H}_2\text{O}$	-194.653 ± 5.957	34.10 ± 1.04	-305.4 ± 6.000^a		
$\text{NiOOH} + 2\text{H}^+ \rightleftharpoons \text{Ni}^{2+} + 0.250_2(\text{aq}) + 1.5\text{H}_2\text{O}$	12.61 ± 1.04	-71.989 ± 5.946			
$\text{Ni}^{2+} + \text{SiO}(\text{OH})_3^- \rightleftharpoons \text{NiOSi}(\text{OH})_3^+$	-36.189 ± 0.144	6.34 ± 0.03^b	$-1\ 333.702 \pm 1.405$		
$\text{Ni}^{2+} + \text{Si}(\text{OH})_4(\text{aq}) \rightleftharpoons \text{NiOSi}(\text{OH})_3^+ + \text{H}^+$	19.806 ± 0.208	-3.47 ± 0.04			
<hr/>					
Gersdorffite					
$\text{NiAsS} + 1.5\text{H}_2\text{O} + 1.375\text{H}^+ + 0.375\text{SO}_4^{2-} \rightleftharpoons \text{Ni}^{2+} + \text{H}_3\text{AsO}_3(\text{aq}) + 1.375\text{HS}^-$	126.5 ± 17.5^c	-22.16 ± 3.07	-107.805 ± 18.204	67.5 ± 12.9^c	-89.967 ± 13.692
<hr/>					
Gersdorffite					
$\text{NiAsS} + 0.750_2(\text{aq}) + 1.5\text{H}_2\text{O} \rightleftharpoons \text{Ni}^{2+} + \text{H}_2\text{AsO}_3^- + \text{HS}^-$	-169.377 ± 17.627	29.67 ± 3.08		-258.615 ± 12.996	
<hr/>					
Ni₂SiO₄–spinel					
$\text{Ni}_2\text{SiO}_4 + 4\text{H}^+ \rightleftharpoons 2\text{Ni}^{2+} + \text{Si}(\text{OH})_4(\text{aq})$	-117.800 ± 3.706^d	20.64 ± 0.65	$-1\ 281.481 \pm 4.177$	-178.300 ± 3.358^d	$-1\ 388.684 \pm 4.936$

a [2016BRO/EKB]; b [2006PAT/CHO]; c calculated from $\log_{10} K_s = f(T)$ in [2016REE/SPY], d [1995ROB/HEM]

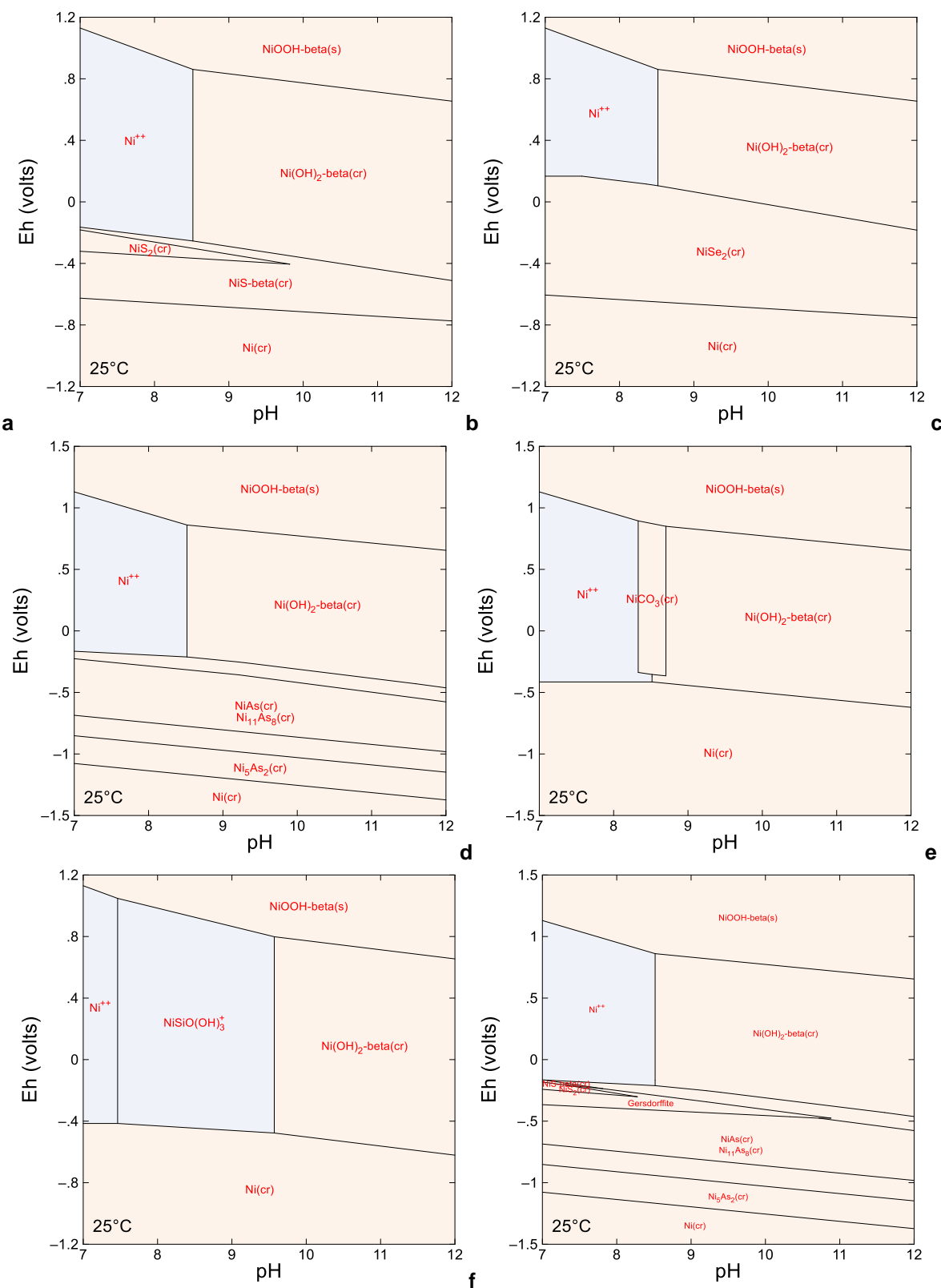


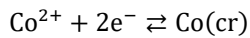
Figure 3.7-24. Pourbaix diagram using GWB of 10^{-6} mol kg_w⁻¹ Cd in a hypothetical indifferent 0.1 mol kg_w⁻¹ electrolyte solution containing 10^{-4} mol kg_w⁻¹ S (a) and Se (b), 10^{-4} mol kg_w⁻¹ As (c), 10^{-3} mol kg_w⁻¹ C (d), at equilibrium with quartz (SiO₂) (e), and 10^{-4} mol kg_w⁻¹ S and As (f); all solid phases are allowed to precipitate.

3.7.7. Cobalt

Cobalt can be found in some instance in mining and post mining activities. It occurs in solution as Co(II) and Co(III), the latter being highly insoluble and forms spinel type Co_3O_4 solid. The common master species is Co^{2+} .

3.7.7.1. Native Metal and Free Ions

The data for redox potential for the couple Co(0)/Co(II) is difficult to obtain [1998PLY/ZHA]. No function of formation value was selected in any NEA-OECD review. In the later review, Grenthe *et al.* [2020GRE/GAO] used values from another compilation without any discussion, which is unusual. This lead to slightly different selected thermodynamic functions of formation [1982WAG/EVA; 1998PLY/ZHA] that are reflecting the contrasting results of electromotive force measurements — *i.e.*, $-0.298 < E_h (\text{V}) < -0.246$ [1998PLY/ZHA, and references therein].



$$\Delta_r G_m^\circ = (54.4 \pm 3.2) \text{ kJ mol}^{-1} \text{ [1982WAG/EVA]}$$

$$\log_{10} K^\circ = -9.53 \pm 0.56$$

$$E^\circ = -0.282 \pm 0.017 \text{ V}$$

$$\Delta_r G_m^\circ = (55.6 \pm 2.2) \text{ kJ mol}^{-1} \text{ [1998PLY/ZHA]}$$

$$\log_{10} K^\circ = -9.74 \pm 0.39$$

$$E^\circ = -0.288 \pm 0.012 \text{ V}$$

$$\Delta_r G_m^\circ = 53.64 \pm 0.38 \text{ kJ mol}^{-1} \text{ [2020GRE/GAO]}$$

$$\log_{10} K^\circ = -9.40 \pm 0.07$$

$$E^\circ = -0.278 \pm 0.002 \text{ V}$$

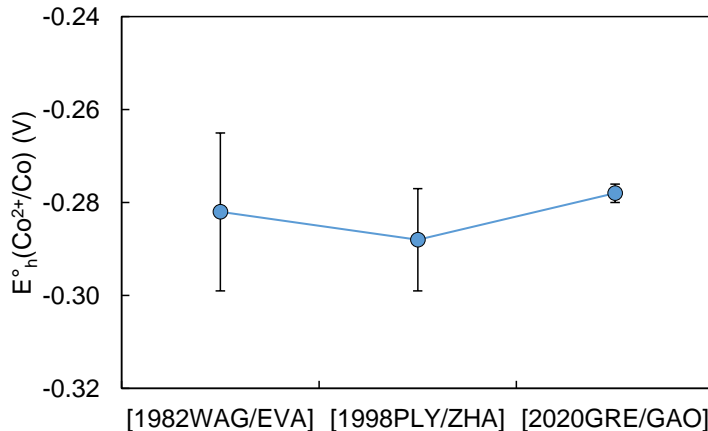
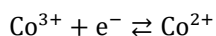


Figure 3.7-25. Comparison of the $E_h^o(\text{Co}^{2+}/\text{Co})$ calculated from different origin of $\Delta_f G_m^\circ$.

Plyasunova *et al.* [1998PLY/ZHA] proposed the $\Delta_f G_m^\circ$ value from the enthalpy and entropy analyses. Unfortunately, the authors did not provide an analysis for the Co(III)/Co(II) couple. This redox couple can be estimated using the thermodynamic functions in Wagman *et al.* [1982WAG/EVA].



$$\Delta_r G_m^\circ = -(188.4 \pm 7.7) \text{ kJ mol}^{-1}$$

$$\log_{10} K^\circ = 33.01 \pm 1.35$$

$$E_h = 1.953 \pm 0.080 \text{ V}$$

From here, three options are opened:

1. Adopting the analysis from Plyasunova *et al.* [1998PLY/ZHA] and then accepting all their analysis on hydrolysis constants, including the polynuclear species $\text{Co}_2(\text{OH})^{3+}$, and $\text{Co}_4(\text{OH})^{4+}$, but not Co(III);
2. Adopting the hydrolysis constants from Brown and Ekberg [2016BRO/EKB], which are sat on the data in Wagman *et al.* [1982WAG/EVA], and also provides analysis on Co(III), but do not include either $\text{Co}(\text{OH})_4^{2-}$ or the polynuclear species;
3. Adopting the choice of the later NEA-OECD review [2020GRE/GAO] for Co^{2+} , and recalculate the functions of formation for Co(II) hydrolysis and Co(III).

Comparing the analyses from Plyasunova *et al.* [1998PLY/ZHA], Brown and Ekberg [2016BRO/EKB], and Grenthe *et al.* [2020GRE/GAO] is showing only small differences. As Co(III) is included in the latter review, the thermodynamic functions of formation from Wagman *et al.* [1982WAG/EVA] will be accepted in PRODATA for the sake of consistency. Data for $\text{Co}(\text{OH})_4^{2-}$, $\text{Co}_2(\text{OH})^{3+}$, and $\text{Co}_4(\text{OH})^{4+}$ will be adapted to the thermodynamic functions in Wagman *et al.* [1982WAG/EVA].

The values for $\varepsilon(\text{Co}^{2+}, \text{Cl}^-)$, $\varepsilon(\text{Co}^{2+}, \text{ClO}_4^-)$, and $\varepsilon(\text{Co}^{2+}, \text{NO}_3^-)$ are available in Ciavatta [1980CIA]. The values for $\varepsilon(\text{Co}^{3+}, \text{X}^-)$ are estimated from the ones for $\varepsilon(\text{Fe}^{3+}, \text{X}^-)$ in Lemire *et al.* [2013LEM/BER; 2020LEM/PAL].

3.7.7.2. Oxo and Hydroxo Compounds

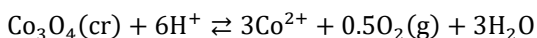
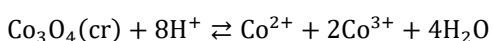
The oxides and hydroxides of Co(II) are $\text{CoO}(\text{cr})$ and $\text{Co}(\text{OH})_2$. Different values are existing in reviews [1982WAG/EVA; 1995ROB/HEM; 1998PLY/ZHA; 2016BRO/EKB]. The differences for $\text{CoO}(\text{cr})$ between Wagman *et al.* [1982WAG/EVA] and Robie and Hemingway [1995ROB/HEM] are marginal, and the former will be included for the sake of consistency with the choice for Co^{2+} (*vide supra*) — the $\Delta_f G^\circ$ values will nevertheless be corrected for the slight difference in $\Delta_f G^\circ(\text{H}_2\text{O})$.

The case of hydroxides is more confusing. Wagman *et al.* [1982WAG/EVA] gave different thermodynamic functions for the “pink” and “blue” phase with *ca.* 4 kJ mol^{-1} difference. Plyasunova *et al.* [1998PLY/ZHA] reported two different recommendations from Baes and Mesmer [1976BAE/MES] and Smith and Martell [1989SMI/MAR]. Brown and Ekberg [2016BRO/EKB] reinterpreted data from literature and proposed the thermodynamic functions for β - $\text{Co}(\text{OH})_2$.

The phases in Wagman *et al.* [1982WAG/EVA] and the estimation from Brown and Ekberg [2016BRO/EKB] are included in PRODATA.

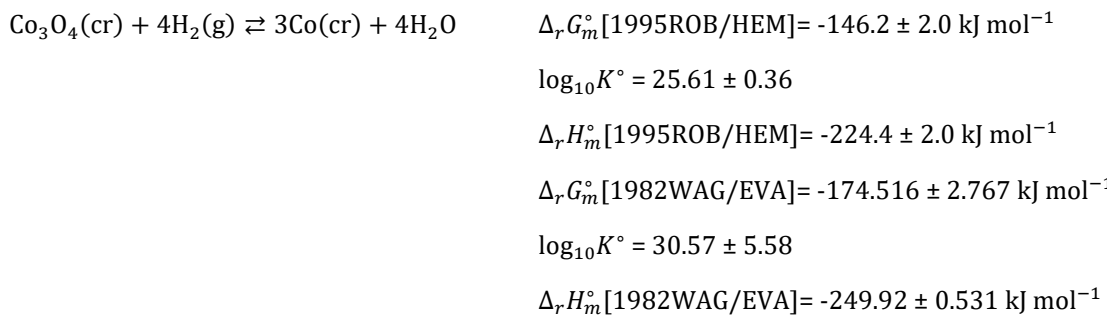
The hydrolysis constants and $\Delta_r H_m^\circ$ estimated in Brown and Ekberg [2016BRO/EKB] are shown in Table 3.7-30. The $\Delta_f G_m^\circ$ and $\Delta_f H_m^\circ$ are recalculated in order to avoid rounding problems.

Brown and Ekberg [2016BRO/EKB] accepted the data for the spinel $\text{Co}_3\text{O}_4(\text{cr})$ ($\text{CoO}, \text{Co}_2\text{O}_3$) from Robie and Hemingway [1995ROB/HEM]. The solubility equilibria,



cannot be calculated as no thermodynamic functions for either Co^{2+} or Co^{3+} are given in Robie and Hemingway [1995ROB/HEM] — the reference state being $\text{Co}(\text{cr})$, even if the functions of formation of both Co^{2+} and Co^{3+} were present in Robie *et al.* [1979ROB/HEM]. There is a 28.2 kJ mol^{-1} difference between the $\Delta_r G^\circ$ values, and a 25.52

kJ mol^{-1} difference between the Δ_rH° in Robie and Hemingway [1995ROB/HEM] and Wagman *et al.* [1982WAG/EVA], which ends up for the phase transformation to *ca.* 5 order of magnitude difference.



This would end up in the same gap between the expression relative to Co^{2+} and/or Co^{3+} . Both values will be included in PRODATA with a different phase name, *i.e.*, $\text{Co}_3\text{O}_4(\text{cr})$ [1982WAG/EVA] and Tricobalt_tetraoxide [1995ROB/HEM]. The solubility equilibria will be expressed referring to Co^{2+} .

3.7.7.3. Halogeno Compounds

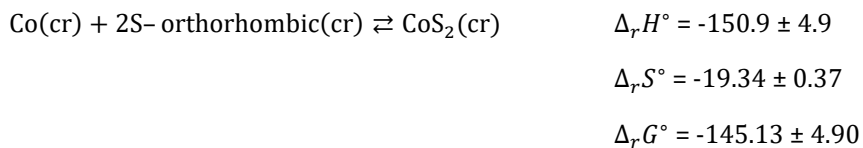
$\text{CoF}_2(\text{cr})$ was proposed in Wagman *et al.* [1982WAG/EVA]. No fluoride complexes have been retrieved up to now.

Three chloride solids have been proposed in Wagman *et al.* [1982WAG/EVA] — $\text{CoCl}_2 \cdot n\text{H}_2\text{O}$ with $n = \{0, 2, 6\}$. Pan and Susak [1989PAN/SUS] proposed the formation of higher complexes for CoCl_n^{2-n} up to $n = 4$. Sverjensky *et al.* [1997SVE/SHO] estimated formation properties for CoCl^+ .

3.7.7.4. Group 16 Compounds

The formation of sulphur compounds of cobalt is particularly important in the ore chemistry of cobalt through the formation of sulphides Co_xS_y . The formation functions for jaipurite (CoS) are taken from Naumov *et al.* [1974NAU/RYZ], and adapted to the choice for the formation functions for Co^{2+} . Allotropic forms α - and β - CoS are reported in Dyrssen and Kremling [1990DYR/KRE] but the origin of the data is not clear. Pankratz *et al.* [1987PAN/MAH] proposed formation functions for cattierite (CoS_2), pentlandite (Co_9S_8 or $\text{CoS}_{0.89}$) and linnaeite (spinel Co_3S_4 or $\text{CoS}, \text{Co}_2\text{S}_3$). Robie and Hemingway [1995ROB/HEM] proposed functions of formation for cattierite and linnaeite, even if one must stay cautious in view of the preceding comments on S(-II) chemistry (c.f. § 3.3) and various sulphide species (*vide ante*), there is no difference in calculated and tabulated Δ_fG° .

As no formation functions are proposed for Co^{2+} in Robie and Hemingway [1995ROB/HEM], the functions of reaction can only be calculated referring to $\text{Co}(\text{cr})$.



The formation constants for the $\text{Co}(\text{HS})_n^{2-n}$ complexes are scarcely found. Values in Khodakovsky [1966KHO] could be used to calculate $\Delta_rG_m^\circ$ and $\Delta_fG_m^\circ$.

The precipitation of $\text{CoSO}_4 \cdot n\text{H}_2\text{O}$ phases, with $n = \{0; 6; 7\}$, and of $\text{CoSO}_4 \cdot 3\text{Co}(\text{OH})_2$ is taken from Wagman *et al.* [1982WAG/EVA]. The function of formation are adapted to the ones in Guillaumont *et al.* [2003GUI/FAN] for SO_4^{2-} .

Olin *et al.* [2005OLI/NOL] selected the selenide solid $\text{Co}_{0.84}\text{Se}(\text{cr})$ ($\text{Co}_5\text{Se}_6(\text{cr})$), and selenite complex $\text{CoSeO}_4(\text{aq})$, which are included in PRODATA. Olin *et al.* [2005OLI/NOL] also proposed the $\Delta_f H_m^\circ$ and $S_{f,m}^\circ$ of $\text{CoSe}_2(\text{cr})$, but not the $\Delta_f G_m^\circ$, as no functions of formation are selected. It can nevertheless be tentatively calculated using the following reaction,



where the $\Delta_r H_m^\circ$ and $\Delta_r S_m^\circ$ can be calculated to evaluate $\Delta_r G_m^\circ$ and finally $\Delta_f G_m^\circ(\text{CoSe}_2(\text{cr}))$ using $\Delta_f G_m^\circ$ in NEA-OECD reviews [2005OLI/NOL] and Brown and Ekberg [2016BRO/EKB].

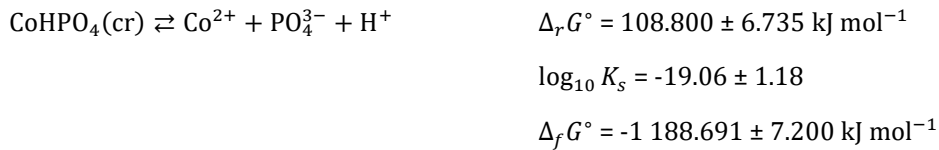
3.7.7.5. Group 15 Compounds

3.7.7.5.1 Nitrogen Compounds

Amino complexes $\text{Co}(\text{NH}_3)_n^{2+}$ (with $1 \leq n \leq 4$) and $\text{Co}(\text{NH}_3)_6^{3+}$ are taken from Wagman *et al.* [1982WAG/EVA].

3.7.7.5.2 Phosphor Compounds

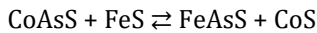
The Gibbs energy of formation of $\text{CoHPO}_4(\text{cr})$ is available in Wagman *et al.* [1982WAG/EVA]. Using the value of $\Delta_f G^\circ(\text{Co}^{2+})$ allows calculating the Gibbs energy of reaction, solubility reaction, and Gibb energy of formation relative to Wagman *et al.* [1982WAG/EVA] for Co^{2+} as follows.



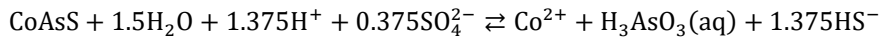
3.7.7.5.3 Arsenic Compounds

Arsenide compounds — modderite (CoAs) and safflorite (CoAs_2) —, and arsenate compounds — $\text{Co}_3(\text{AsO}_4)_2(\text{cr})$, and $\text{Co}_3(\text{AsO}_4)_2 \cdot 8\text{H}_2\text{O}(\text{s})$ — are taken from Naumov *et al.* [1974NAU/RYZ]. The functions of formation are recalculated relative to Wagman *et al.* [1982WAG/EVA] for Co^{2+} and Olin *et al.* [2005OLI/NOL] for arsenic.

The formation of arsenosulphide solids is also particularly important in geochemistry of cobalt, *e.g.*, cobaltite CoAsS . As in the case of gersdorffite (c.f. § 3.7.6.2.3), Goodgame [1997GOO] estimated these data postulating that $\Delta_r G = 0$ for the following reaction.



Goodgame [1997GOO] proposed $\Delta_f G_m^\circ = -98.84 \text{ kJ mol}^{-1}$, but no $\Delta_f H_m^\circ$ or $S_{f,m}^\circ$ were proposed. In the SOLTHERM-XPT database [2015PAL; 2016REE/SPY], two variations of $\log_{10}\beta(T)$ between 25 and 300 °C are given for the following reaction.



The variation are represented in Figure 3.7-26. In both case the variation at $T < 100 \text{ }^\circ\text{C}$ — *i.e.*, $1/T > 0.0027 \text{ K}^{-1}$ — could be approximated to a straight line and treated using the Van't Hoff equation. The formation function for the phases Cobaltite and Cobaltite-1 could be estimated, using the same hypothesis as in Goodgame [1997GOO] in Table 3.7-29 using the formation functions for Co^{2+} [1982WAG/EVA], and from Guillaumont *et al.*

[2003GUI/FAN] for H₂O, H₃AsO₃(aq), HS⁻, and SO₄²⁻. It can be noted that the obtained value for Cobaltite-1 is in agreement with the data estimated by Goodgame [1997GOO].

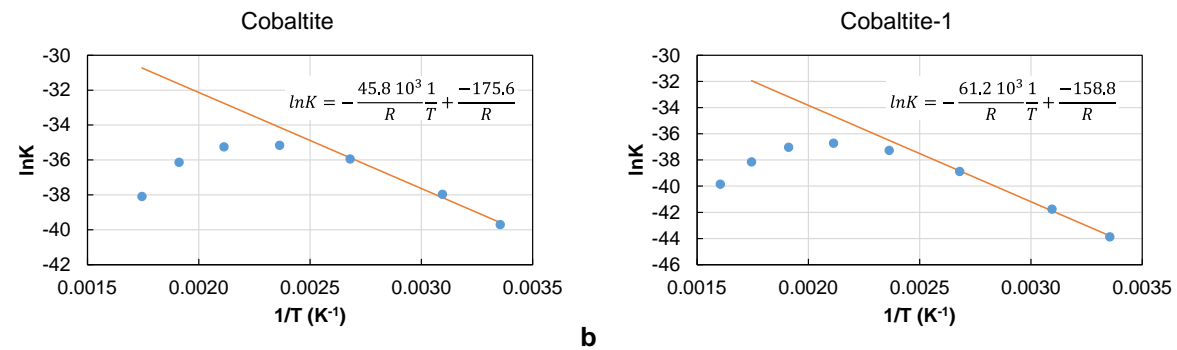


Figure 3.7-26. Evolution of the $\ln K$ vs. $1/T$ values (blue circles) for the dissolution of CoAsS phases in the SOLTHERM-XPT database [2015PAL; 2016REE/SPY], and estimation of the formation functions by the Van't Hoff relationship (orange line).

Table 3.7-29. Thermodynamic functions and constants estimated for the CoAsS phases in the SOLTHERM-XPT database [2015PAL; 2016REE/SPY].

Reaction	$\Delta_r H_m^\circ$ (kJ mol ⁻¹)	$\Delta_r S_m^\circ$ (J mol ⁻¹ K ⁻¹)	$\Delta_r G_m^\circ$ (kJ mol ⁻¹)	$\Delta_f H_m^\circ$ (kJ mol ⁻¹)	$\Delta_f S_m^\circ$ (J mol ⁻¹ K ⁻¹)	$\Delta_f G_m^\circ$ (kJ mol ⁻¹)	$\log_{10} K^\circ$
Cobaltite	45.8 ± 4.0	-175.6 ± 12.1	98.1 ± 5.3	-71.355 ± 6.316	153.463 ± 14.048	-88.032 ± 7.526	-17.2 ± 0.9
Cobaltite-1	61.2 ± 2.9	-158.80 ± 8.776	108.6 ± 3.9	-86.755 ± 5.718	136.663 ± 11.362	-98.532 ± 6.606	-19.0 ± 0.7

The hypothesis used to estimate the formation functions and dissolution reaction could be verified comparing to an analytical expression, which allows adjusting the $\log_{10} K$ variations,

$$\log_{10} K_s = A_1 + A_2 T + \frac{A_3}{T}$$

with the calculated values using the Van't Hoff relationship (Figure 3.7-27).

$$\log_{10} K_s(\text{Cobaltite}) = 14.5 - 0.035T - \frac{6415}{T}$$

$$\log_{10} K_s(\text{Cobaltite-1}) = 14.0 - 0.032T - \frac{7034}{T}$$

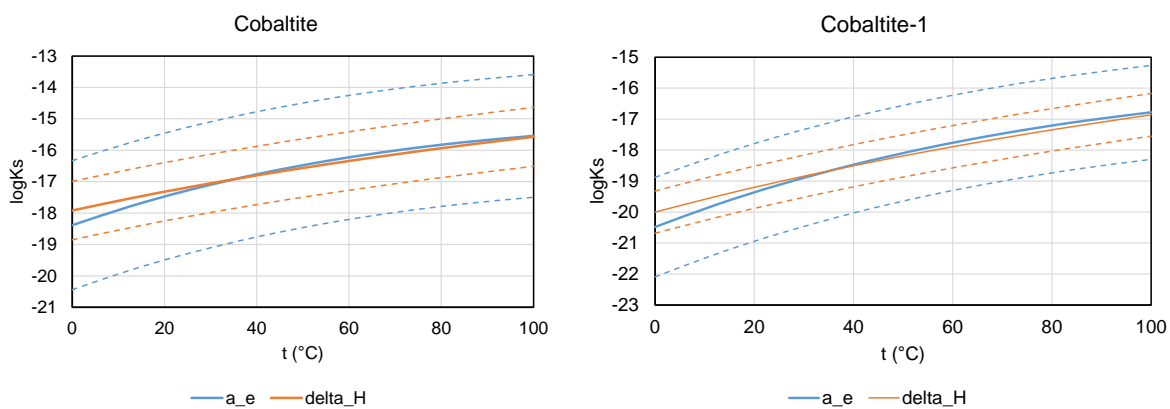


Figure 3.7-27. Evolutions of the $\log_{10} K_s$ vs. t (°C) of CoAsS(cr) with formation functions from Table 3.7-29.

3.7.7.6. Carbon Compounds

The formation of $\text{Co}(\text{CO}_3)_n^{(2-2n)+}$ complexes is still in controversy. During their analysis of the literature data, Glaus *et al.* [2000GLA/HUM] remarked that the values in thermodynamic compilations of data were not satisfactory. They estimated the values from the ones of $\text{Zn}(\text{CO}_3)_n^{(2-n)+}$ instead. The values proposed by Glaus *et al.* [2000GLA/HUM] will be used in PRODATA.

3.7.7.7. Silicate Compounds

The functions of formation of $\text{Co}_2\text{SiO}_4(\text{cr})$ are available in Robie and Hemingway [1995ROB/HEM]. As for oxides, the functions of reaction relative to Co^{2+} are impossible to calculate. As for other silicate minerals, the function of formation of $\text{Si}(\text{OH})_4(\text{aq})$ is different from the values selected in NEA-OECD reviews. Hence, the functions of formation will be used as is in PRODATA.

Pathak and Choppin [2005PAT/CHO] proposed the formation of the complex,



which is modified to the following reaction.



3.7.7.8. Thermodynamic Constants and Functions, and Estimation of Specific Ion Interaction Coefficients for Co

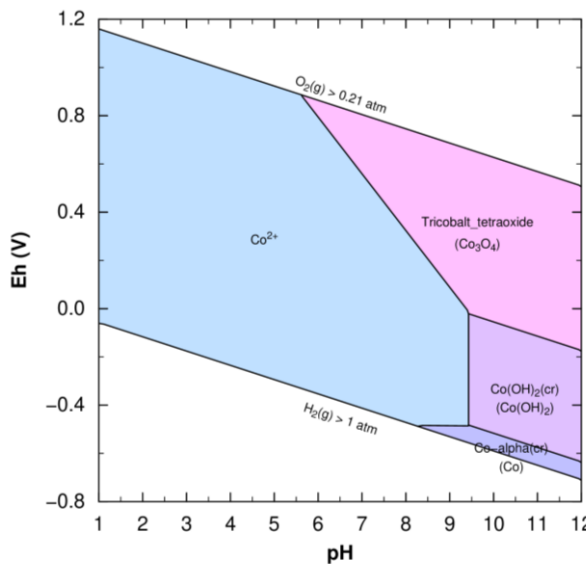
Table 3.7-30. Thermodynamic constants and functions for native metals, free metals, oxo and hydroxo compounds of Co.

Reaction	$\log_{10} \beta^\circ$	$\Delta_r G_m^\circ$ (kJ mol ⁻¹)	$\Delta_f G_m^\circ$ (kJ mol ⁻¹)	$\Delta_r H_m^\circ$ (kJ mol ⁻¹)	$\Delta_f H_m^\circ$ (kJ mol ⁻¹)
$\text{Co}-\alpha(\text{cr}) \rightleftharpoons \text{Co}-\beta(\text{cr})$	-0.04 ± 0.07	0.25 ± 0.40 ^a	0.25 ± 0.40	0.46 ± 0.48 ^a	0.46 ± 0.48
$\text{Co}-\alpha(\text{cr}) + 0.5\text{O}_2(\text{aq}) \rightleftharpoons \text{Co}^{2+} + \text{H}_2\text{O}$	52.51 ± 0.34	-299.729 ± 1.950 ^b	-54.400 ± 2.000	-338.080 ± 1.950 ^b	-58.1 ± 2.0
$\text{Co}-\beta(\text{cr}) + 0.5\text{O}_2(\text{aq}) \rightleftharpoons \text{Co}^{2+} + \text{H}_2\text{O}$	52.55 ± 0.33	-299.979 ± 1.908		-338.540 ± 1.890	
$\text{Co}^{2+} + \text{H}^+ \rightleftharpoons \text{Co}^{3+} + 0.5\text{H}_2(\text{g})$	-33.01 ± 1.36	188.400 ± 7.746 ^a	134.000 ± 8.000	150.10 ± 16.12 ^a	92.0 ± 16.0
$\text{Co}^{2+} + 0.25\text{O}_2(\text{aq}) + \text{H}^+ \rightleftharpoons \text{Co}^{3+} + 0.5\text{H}_2\text{O}$	-11.52 ± 1.36	65.736 ± 7.743		10.110 ± 16.126	
$\text{CoO}(\text{cr}) + 2\text{H}^+ \rightleftharpoons \text{Co}^{2+} + \text{H}_2\text{O}$	13.55 ± 0.05	-77.318 ± 0.259 ^a	-214.222 ± 1.984	-106.090 ± 0.876 ^a	237.840 ± 1.799
$\beta\text{-Co(OH)}_2(\text{cr}) + 2\text{H}^+ \rightleftharpoons \text{Co}^{2+} + 2\text{H}_2\text{O}$	13.26 ± 0.12 ^b	-75.574 ± 0.685	-453.106 ± 2.116	-92.7 ± 1.2 ^b	-537.060 ± 2.334
$\text{Co}^{2+} + \text{H}_2\text{O} \rightleftharpoons \text{Co}(\text{OH})^+ + \text{H}^+$	-9.61 ± 0.17 ^b	54.854 ± 0.970	-236.686 ± 2.223	41.3 ± 4.4 ^b	-168.180 ± 5.947
$\text{Co}^{2+} + 2\text{H}_2\text{O} \rightleftharpoons \text{Co}(\text{OH})_2(\text{aq}) + 2\text{H}^+$	-19.77 ± 0.11 ^b	112.848 ± 0.628	-415.832 ± 2.098	93.0 ± 2.6 ^b	-536.760 ± 3.281
$\text{Co}^{2+} + 3\text{H}_2\text{O} \rightleftharpoons \text{Co}(\text{OH})_3^- + 3\text{H}^+$	-32.01 ± 0.33 ^b	182.714 ± 1.884	-583.106 ± 2.750		
$\text{Co}^{2+} + 4\text{H}_2\text{O} \rightleftharpoons \text{Co}(\text{OH})_4^{2-} + 3\text{H}^+$	-46.42 ± 0.43 ^b	264.967 ± 2.454	-737.993 ± 3.170		
$2\text{Co}^{2+} + \text{H}_2\text{O} \rightleftharpoons \text{Co}_2(\text{OH})^{3+} + \text{H}^+$	-9.83 ± 0.39 ^b	56.110 ± 2.226	-289.830 ± 4.578	30.03 ± 6.49 ^b	-372.00 ± 7.62
$4\text{Co}^{2+} + 4\text{H}_2\text{O} \rightleftharpoons \text{Co}_4(\text{OH})_4^{4+} + 4\text{H}^+$	-29.88 ± 0.35 ^b	170.556 ± 1.998	-995.604 ± 8.247	149.72 ± 12.72 ^b	-1226 ± 15
$\text{Co}_3\text{O}_4(\text{cr}) + 6\text{H}^+ \rightleftharpoons 3\text{Co}^{2+} + 0.5\text{O}_2(\text{g}) + 3\text{H}_2\text{O}$	17.62 ± 0.99	-100.587 ± 5.625 ^a	-774.033 ± 2.092	-141.090 ± 2.761 ^a	-890.700 ± 5.328
$\text{Co}_3\text{O}_4(\text{cr}) + 6\text{H}^+ \rightleftharpoons 3\text{Co}^{2+} + 0.5\text{O}_2(\text{aq}) + 3\text{H}_2\text{O}$	16.19 ± 0.99	-92.398 ± 5.643		-146.940 ± 2.797	

Table 3.7-30. Continued.

Reaction	$\log_{10} \beta_n^\circ$	$\Delta_r G_m^\circ$ (kJ mol ⁻¹)	$\Delta_f G_m^\circ$ (kJ mol ⁻¹)	$\Delta_r H_m^\circ$ (kJ mol ⁻¹)	$\Delta_f H_m^\circ$ (kJ mol ⁻¹)
$\text{Co}_3\text{O}_4(\text{cr}) + 6\text{H}^+ \rightleftharpoons 3\text{Co}^{2+} + 0.5\text{O}_2(\text{g}) + 3\text{H}_2\text{O}$	12.69 ± 0.99	-72.420 ± 5.658^c	-802.2 ± 2.0	-118.840 ± 5.676^c	-918.8 ± 2.0
$\text{Co}_3\text{O}_4(\text{cr}) + 6\text{H}^+ \rightleftharpoons 3\text{Co}^{2+} + 0.5\text{O}_2(\text{aq}) + 3\text{H}_2\text{O}$	11.25 ± 0.99^c	-64.231 ± 5.676			

a [1982WAG/EVA]; b [2016BRO/EKB]; c [1995ROB/HEM]

* calculated from the $\Delta_f G_m^\circ$ and $\Delta_f H_m^\circ$ from [2016BRO/EKB] for Co^{2+} , and [2003GUI/FAN]**Figure 3.7-28. Pourbaix diagram (PHREEPLOT) of 10^{-6} mol kg⁻¹ Co in a hypothetical indifferent 0.1 mol kg⁻¹ electrolyte solution; all solid phases are allowed to precipitate.****Table 3.7-31. Thermodynamic constants and functions for halogen compounds of Co.**

Reaction	$\log_{10} \beta_n^\circ$	$\Delta_r G_m^\circ$ (kJ mol ⁻¹)	$\Delta_f G_m^\circ$ (kJ mol ⁻¹)	$\Delta_r H_m^\circ$ (kJ mol ⁻¹)	$\Delta_f H_m^\circ$ (kJ mol ⁻¹)
$\text{CoF}_2(\text{cr}) \rightleftharpoons \text{Co}^{2+} + 2\text{F}^-$	-6.17 ± 0.15	35.220 ± 0.849^a	-652.666 ± 2.279	-31.460 ± 2.144^a	-697.340 ± 3.208
$\text{CoCl}_2(\text{cr}) \rightleftharpoons \text{Co}^{2+} + 2\text{Cl}^-$	8.24 ± 0.24	-47.056 ± 1.383^a	-269.778 ± 1.463	-80.018 ± 1.980^a	-312.242 ± 0.349
$\text{CoCl}_2 \cdot 2\text{H}_2\text{O}(\text{cr}) \rightleftharpoons \text{Co}^{2+} + 2\text{Cl}^- + 2\text{H}_2\text{O}$	4.63 ± 0.24	-26.414 ± 1.388^a	-764.700 ± 1.461	-41.178 ± 3.987^a	-922.742 ± 4.465
$\text{CoCl}_2 \cdot 6\text{H}_2\text{O}(\text{cr}) \rightleftharpoons \text{Co}^{2+} + 2\text{Cl}^- + 6\text{H}_2\text{O}$	2.53 ± 0.08	-14.430 ± 0.437^a	-1725.244 ± 1.981	7.902 ± 1.758^a	-2115.142 ± 1.003
$\text{Co}^{2+} + \text{Cl}^- \rightleftharpoons \text{CoCl}^+$	0.57	-3.255 ^b	-188.872	-0.552 ^b	-225.732
$\text{Co}^{2+} + 2\text{Cl}^- \rightleftharpoons \text{CoCl}_2(\text{aq})$	0.02	-0.114 ^c	-316.948		
$\text{Co}^{2+} + 3\text{Cl}^- \rightleftharpoons \text{CoCl}_3^-$	-1.71	9.761 ^c	-438.290		
$\text{Co}^{2+} + 4\text{Cl}^- \rightleftharpoons \text{CoCl}_4^{2-}$	-4.51	25.743 ^c	-553.525		

a [1982WAG/EVA]; b [1997SVE/SHO]; c [1989PAN/SUS].

* calculated from the $\Delta_f G_m^\circ$ and $\Delta_f H_m^\circ$ from [2016BRO/EKB] for Co^{2+} , and [2003GUI/FAN].**Table 3.7-32. Thermodynamic constants and functions for the S and Se compounds of Co.**

Reaction	$\log_{10} \beta_n^\circ$	$\Delta_r G_m^\circ$ (kJ mol ⁻¹)	$\Delta_f G_m^\circ$ (kJ mol ⁻¹)	$\Delta_r H_m^\circ$ (kJ mol ⁻¹)	$\Delta_f H_m^\circ$ (kJ mol ⁻¹)
$\text{CoS-}\beta + \text{H}^+ \rightleftharpoons \text{Co}^{2+} + \text{HS}^-$	-11.07 ± 0.30^a	63.188 ± 1.720	-105.345 ± 3.381		
$\text{CoS(jaipurite)} + \text{H}^+ \rightleftharpoons \text{Co}^{2+} + \text{HS}^-$	-7.09	40.460 ^b	-82.617	6.690 ^b	-81.090
$\text{CoS}_2(\text{cattierite}) + \text{H}_2\text{O} \rightleftharpoons \text{Co}^{2+} + 0.5\text{O}_2(\text{aq}) + 2\text{HS}^-$	-63.16 ± 0.24	360.515 ± 1.385^c	-145.100 ± 4.900	340.180 ± 3.288^c	150.900 ± 4.900
$\text{CoS}_2(\text{cr}) + \text{H}_2\text{O} \rightleftharpoons \text{Co}^{2+} + 0.5\text{O}_2(\text{aq}) + 2\text{HS}^-$	-63.56	362.780	-147.365 ^d	342.414	-153.134 ^d

Table 3.7-32. Continued.

Reaction	$\log_{10} \beta_n^o$	$\Delta_r G_m^o$ (kJ mol ⁻¹)	$\Delta_f G_m^o$ (kJ mol ⁻¹)	$\Delta_r H_m^o$ (kJ mol ⁻¹)	$\Delta_f H_m^o$ (kJ mol ⁻¹)
Linnaeite					
$\text{Co}_3\text{S}_4 + 2\text{H}^+ + \text{H}_2\text{O} \rightleftharpoons 3\text{Co}^{2+} + 0.5\text{O}_2(\text{aq}) + 4\text{HS}^-$	-81.64 ± 1.29	466.001 ± 7.381 ^c	-334.900 ± 7.300	387.980 ± 4.348 ^c	-347.500 ± 7.300
$\text{Co}_3\text{S}_4(\text{cr}) + 2\text{H}^+ + \text{H}_2\text{O} \rightleftharpoons 3\text{Co}^{2+} + 0.5\text{O}_2(\text{aq}) + 4\text{HS}^-$	-83.64	477.448	-346.347 ^d	399.467	-358.987 ^d
Pentlandite					
$\text{Co}_9\text{S}_8 + 0.5\text{O}_2(\text{aq}) + 10\text{H}^+ \rightleftharpoons 9\text{Co}^{2+} + 8\text{HS}^- + \text{H}_2\text{O}$	-216.34	1 234.857	-1 871.842 ^d	973.243	-1 906.523 ^d
$\text{Co}^{2+} + \text{HS}^- \rightleftharpoons \text{Co}(\text{HS})^+$	5.67 ^a	-32.365	-74.522		
$\text{Co}^{2+} + 2\text{HS}^- \rightleftharpoons \text{Co}(\text{HS})_2(\text{aq})$	8.77 ^a	-50.060	-79.974		
$\text{CoSO}_4(\text{cr}) \rightleftharpoons \text{Co}^{2+} + \text{SO}_4^{2-}$	2.91 ± 0.22	-16.630 ± 1.259 ^f	-781.774 ± 2.400	-79.140 ± 1.265 ^f	-888.3 ± 2.4
$\text{CoSO}_4 \cdot 6\text{H}_2\text{O}(\text{cr}) \rightleftharpoons \text{Co}^{2+} + \text{SO}_4^{2-} + 6\text{H}_2\text{O}$	-2.39 ± 0.35	13.656 ± 2.001 ^f	-2 234.900 ± 0.480	1.580 ± 31.934 ^f	-2 684 ± 32
Bieberite					
$\text{CoSO}_4 \cdot 7\text{H}_2\text{O}(\text{cr}) \rightleftharpoons \text{Co}^{2+} + \text{SO}_4^{2-} + 7\text{H}_2\text{O}$	-2.56 ± 0.36	14.587 ± 2.057 ^f	-2 472.971 ± 0.160	11.680 ± 2.045 ^f	-2 979.93 ± 0.24
$\text{CoSO}_4 \cdot 3\text{Co}(\text{OH})_2(\text{cr}) + 6\text{H}^+ \rightleftharpoons 4\text{Co}^{2+} + \text{SO}_4^{2-} + 6\text{H}_2\text{O}$	33.18 ± 1.22	-189.404 ± 6.945 ^f	-2 195.040 ± 4.000	-379.250 ± 4.823 ^f	-2 477.47 ± 6.40
$\text{CoSe}_2(\text{cr}) + 2\text{H}^+ + \text{H}_2\text{O} \rightleftharpoons \text{Co}^{2+} + 2\text{H}_2\text{Se}(\text{aq}) + 0.5\text{O}_2(\text{g})$	-57.13 ± 2.24	326.112 ± 12.814 ^g	-100.382 ± 13.574	361.830 ± 14.306 ^g	-105.5 ± 15.0
$\text{CoSe}_2(\text{cr}) + 2\text{H}^+ + \text{H}_2\text{O} \rightleftharpoons \text{Co}^{2+} + 2\text{H}_2\text{Se}(\text{aq}) + 0.5\text{O}_2(\text{aq})$	-58.57 ± 2.24	334.301 ± 12.807		355.980 ± 14.299	
$\text{Co}_{0.84}\text{Se}(\text{cr})$					
$\text{Co}_5\text{Se}_6 + 12\text{H}^+ \rightleftharpoons 3\text{Co}^{2+} + 2\text{Co}^{3+} + 6\text{H}_2\text{Se}(\text{aq})$	-100.13 ± 5.77	571.570 ± 32.887	-337.800 ± 39.000 ^g	-427.900 ± 9.424	-332.4 ± 36.0 ^g
$\text{Co}^{2+} + \text{SeO}_4^{2-} \rightleftharpoons \text{CoSeO}_4(\text{aq})$	2.70 ± 0.05 ^g	-15.412 ± 0.285	-509.297 ± 2.476		

a [1990DYR/KRE]; b [1974NAU/RYZ]; c [1995ROB/HEM]; d [1987PAN/MAH]; e [1966KHO]; f [1982WAG/EVA]; g [2005OLI/NOL].

* calculated from the $\Delta_f G_m^o$ and $\Delta_f H_m^o$ from [2016BRO/EKB] for Co^{2+} , and [2003GUI/FAN], unless otherwise noted.

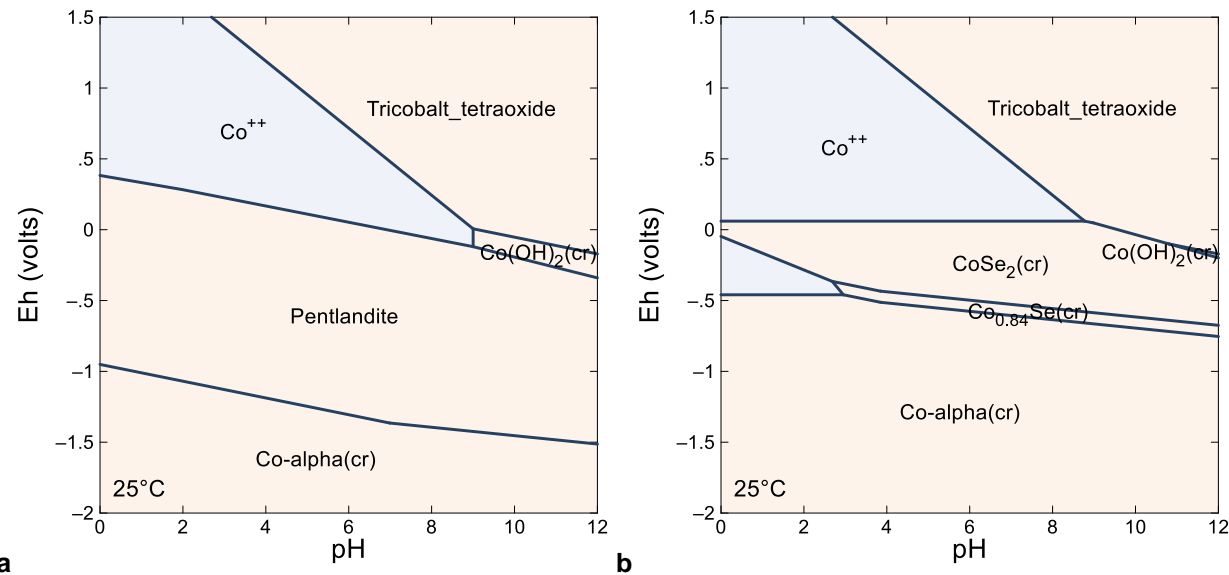


Figure 3.7-29. Pourbaix diagram (GWB) of 10^{-6} mol kg⁻¹ Co and 10^{-4} mol kg⁻¹ S (a) and Se(b) in a hypothetical indifferent 0.1 mol kg⁻¹ electrolyte solution; all solid phases are allowed to precipitate.

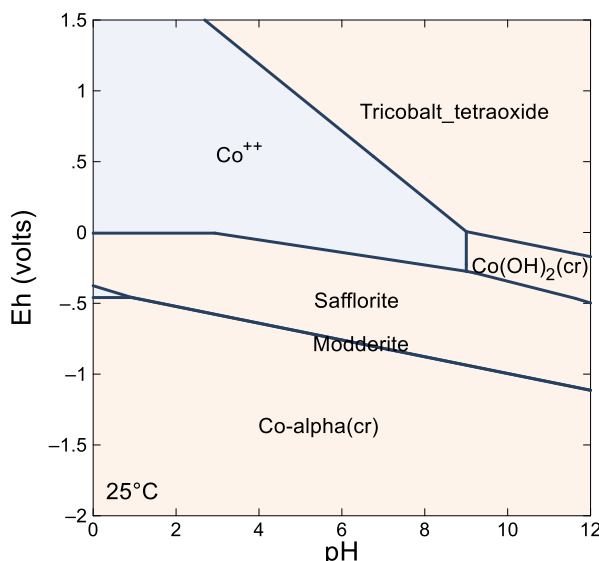
Table 3.7-33. Thermodynamic constants and functions for the P and As compounds of Co.

Reaction	$\log_{10} \beta_n^o$	$\Delta_r G_m^o$ (kJ mol ⁻¹)	$\Delta_f G_m^o$ (kJ mol ⁻¹)	$\Delta_r H_m^o$ (kJ mol ⁻¹)	$\Delta_f H_m^o$ (kJ mol ⁻¹)
$\text{CoHPO}_4(\text{cr}) \rightleftharpoons \text{Co}^{2+} + \text{PO}_4^{3-} + \text{H}^+$	-19.06 ± 1.18	108.800 ± 6.735 ^a	-1 188.691 ± 7.200		
Modderite					
$\text{CoAs} + 1.75\text{O}_2(\text{g}) + 0.5\text{H}_2\text{O} \rightleftharpoons \text{Co}^{2+} + \text{AsO}_4^{3-} + \text{H}^+$	94.69 ± 0.44	-540.501 ± 2.521 ^b	-43.689 ± 3.702	-752.246 ± 11.737 ^b	-51.079 ± 12.560

Table 3.7-33. Continued.

Reaction	$\log_{10} \beta_n^{\circ}$	$\Delta_r G_m^{\circ}$ (kJ mol ⁻¹)	$\Delta_f G_m^{\circ*}$ (kJ mol ⁻¹)	$\Delta_r H_m^{\circ}$ (kJ mol ⁻¹)	$\Delta_f H_m^{\circ*}$ (kJ mol ⁻¹)
$\text{CoAs} + 1.75\text{O}_2(\text{aq}) + 0.5\text{H}_2\text{O} \rightleftharpoons \text{Co}^{2+} + \text{AsO}_4^{3-} + \text{H}^+$	99.71 ± 0.35	-569.163 ± 1.975		-731.771 ± 11.841	
Safflorite					
$\text{CoAs}_2 + 3\text{O}_2(\text{g}) + 2\text{H}_2\text{O} \rightleftharpoons \text{Co}^{2+} + 2\text{AsO}_4^{3-} + 4\text{H}^+$	138.33 ± 1.29	-789.614 ± 7.348^b	-87.226 ± 3.776	-1179.403 ± 9.475^b	-83.317 ± 12.560
$\text{CoAs}_2 + 3\text{O}_2(\text{aq}) + 2\text{H}_2\text{O} \rightleftharpoons \text{Co}^{2+} + 2\text{AsO}_4^{3-} + 4\text{H}^+$	146.94 ± 1.20	-838.748 ± 6.839		-1144.303 ± 9.848	
$\text{Co}_3(\text{AsO}_4)_2(\text{cr}) \rightleftharpoons 3\text{Co}^{2+} + 2\text{AsO}_4^{3-}$	-28.17 ± 0.36	160.780 ± 2.057^a	-1620.700 ± 9.799		
$\text{Co}_3(\text{AsO}_4)_2(\text{cr}):8\text{H}_2\text{O} \rightleftharpoons 3\text{Co}^{2+} + 2\text{AsO}_4^{3-} + 8\text{H}_2\text{O}$	-28.18	160.832^b	-3517.872		
Cobaltite					
$\text{CoAsS} + 1.5\text{H}_2\text{O} + 0.375\text{H}^+ + 0.375\text{SO}_4^{2-} \rightleftharpoons \text{Co}^{2+} + \text{H}_2\text{AsO}_3^- + 1.375\text{HS}^-$	-17.19 ± 0.93	98.100 ± 5.305^c	-88.032 ± 7.526	45.800 ± 3.957^c	-71.355 ± 6.316
Cobaltite-1					
$\text{CoAsS} + 1.5\text{H}_2\text{O} + 0.375\text{H}^+ + 0.375\text{SO}_4^{2-} \rightleftharpoons \text{Co}^{2+} + \text{H}_2\text{AsO}_3^- + 1.375\text{HS}^-$	-19.03 ± 0.68	108.600 ± 3.892^c	-98.532 ± 6.606	61.200 ± 2.910^c	-86.755 ± 5.718

a [1982WAG/EVA]; b [1974NAU/RYZ]; c [1997GOO].

* calculated from the $\Delta_f G_m^{\circ}$ and $\Delta_f H_m^{\circ}$ from [2016BRO/EKB] for Co^{2+} , and [2003GUI/FAN], unless otherwise noted.**Figure 3.7-30. Pourbaix diagram (GWB) of 10^{-6} mol kg_w⁻¹ Co and 10^{-4} mol kg_w⁻¹ of As in a hypothetical indifferent 0.1 mol kg_w⁻¹ electrolyte solution; all solid phases are allowed to precipitate.****Table 3.7-34. Thermodynamic constants and functions for the C and Si compounds of Co.**

Reaction	$\log_{10} \beta_n^{\circ}$	$\Delta_r G_m^{\circ}$ (kJ mol ⁻¹)	$\Delta_f G_m^{\circ*}$ (kJ mol ⁻¹)	$\Delta_r H_m^{\circ}$ (kJ mol ⁻¹)	$\Delta_f H_m^{\circ*}$ (kJ mol ⁻¹)
$\text{Co}^{2+} + \text{CO}_3^{2-} \rightleftharpoons \text{Co}(\text{CO}_3)(\text{aq})$	4.7^a				
$\text{Co}^{2+} + 2\text{CO}_3^{2-} \rightleftharpoons \text{Co}(\text{CO}_3)_2^{2-}$	7.1^a				
$\text{Co}_2\text{SiO}_4(\text{cr}) + 4\text{H}^+ \rightleftharpoons 2\text{Co}^{2+} + \text{Si}(\text{OH})_4(\text{aq})$	18.89 ± 0.64	-107.835 ± 3.652^b	-1308.700 ± 2.000	-161.160 ± 4.691^b	-1412.000 ± 2.000
$\text{Co}^{2+} + \text{Si}(\text{OH})_4(\text{aq}) \rightleftharpoons \text{CoSiO}(\text{OH})_3^+ + \text{H}^+$	-4.19 ± 0.11^c	23.916 ± 0.639	-1338.219 ± 2.397		

a [2000GLA/HUM]; b [1995ROB/HEM]; c [2005PAT/CHO].

* calculated from the $\Delta_f G_m^{\circ}$ and $\Delta_f H_m^{\circ}$ from [2003GUI/FAN].

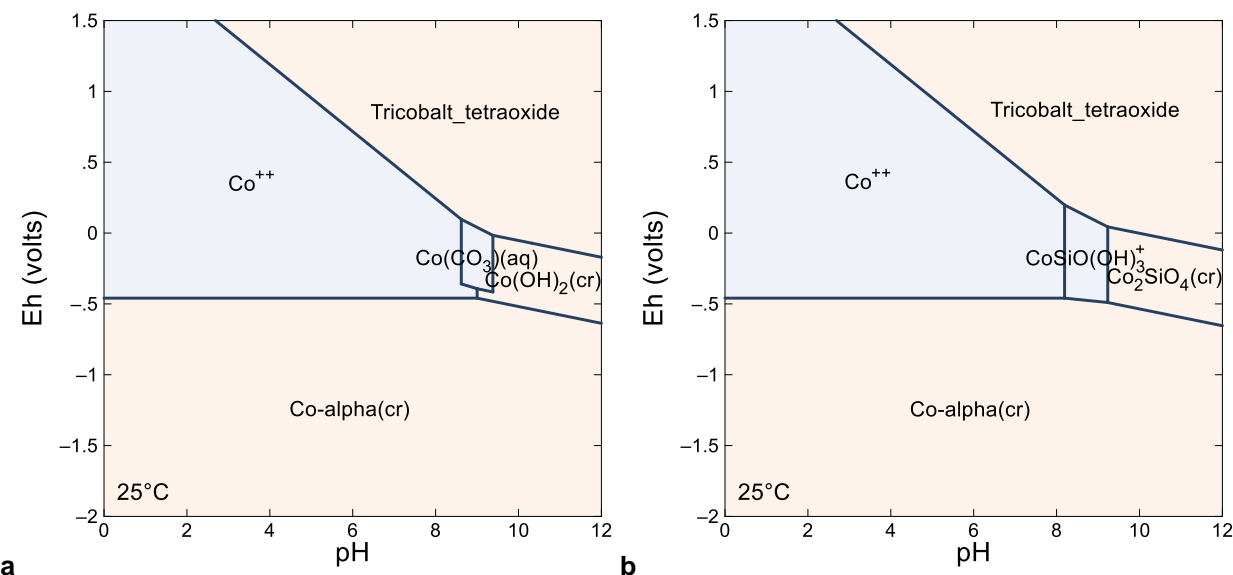


Figure 3.7-31. Pourbaix diagram (GWB) of 10^{-6} mol kg_w⁻¹ Co and 10^{-3} mol kg_w⁻¹ C (a), and in equilibrium with quartz (SiO_2) (b); all phases are allowed to precipitate.

Table 3.7-35. Specific ion interaction coefficients for Co aqueous species and complexes.

Specific ion interaction coefficient	Value $\pm 1\sigma$	Reference and comments
$\varepsilon(\text{Co}^{2+}, \text{Cl}^-)$	0.16 ± 0.02	[1980CIA]
$\varepsilon(\text{Co}^{2+}, \text{NO}_3^-)$	0.14 ± 0.01	[1980CIA]
$\varepsilon(\text{Co}^{2+}, \text{ClO}_4^-)$	0.34 ± 0.03	[1980CIA]
$\varepsilon(\text{Co}^{3+}, \text{ClO}_4^-)$	0.73 ± 0.04	analogy Fe^{3+}
$\varepsilon(\text{Co}^{3+}, \text{Cl}^-)$	0.76 ± 0.03	analogy Fe^{3+}
$\varepsilon(\text{Co}^{3+}, \text{NO}_3^-)$	0.42 ± 0.08	analogy Fe^{3+}
$\varepsilon(\text{Co}(\text{OH})^+, \text{ClO}_4^-)$	0.30 ± 0.19	[1998PLY/ZHA]
$\varepsilon(\text{Co}(\text{OH})^{2+}, \text{ClO}_4^-)$	0.50 ± 0.07	from $\Delta\varepsilon$ in [2016BRO/EKB]
$\varepsilon(\text{Co}(\text{OH})_2(\text{aq}), \text{Na}^+\text{ClO}_4^-)$	-0.15 ± 0.10	[1998PLY/ZHA]
$\varepsilon(\text{Co}(\text{OH})_3^-, \text{Na}^+)$	-0.14 ± 0.05	[1998PLY/ZHA]
$\varepsilon(\text{Co}(\text{OH})_3^-, \text{K}^+)$	-0.01 ± 0.03	[1998PLY/ZHA]
$\varepsilon(\text{Co}(\text{OH})_4^{2-}, \text{Na}^+)$	-0.06 ± 0.02	[1998PLY/ZHA]
$\varepsilon(\text{Co}(\text{OH})_4^{2-}, \text{K}^+)$	0.14 ± 0.01	[1998PLY/ZHA]
$\varepsilon(\text{Co}_2(\text{OH})^{3+}, \text{ClO}_4^-)$	0.71 ± 0.2	[1998PLY/ZHA]
$\varepsilon(\text{Co}_4(\text{OH})_4^{4+}, \text{ClO}_4^-)$	0.92 ± 0.17	[1998PLY/ZHA]
$\varepsilon(\text{Co}(\text{CO}_3)(\text{aq}), \text{Na}^+\text{ClO}_4^-)$	0.13 ± 0.03	Estimation from Eq. 26 [1990CIA]
$\varepsilon(\text{Co}(\text{CO}_3)_2^{2-}, \text{Na}^+)$	0.06 ± 0.04	Estimation from Eq. 27 [1990CIA]
$\varepsilon(\text{CoSiO}(\text{OH})_3^+, \text{ClO}_4^-)$	0.66 ± 0.15	[2014THO/HUM]

3.7.8. Iron

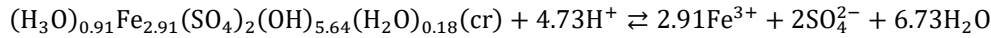
Iron is a ubiquitous element on Earth. The values selected in the NEA-OECD reviews [2013LEM/BER; 2020LEM/PAL] are accepted in the PRODATA database.

3.7.8.1. Free Ion and Hydroxo Compound

The common master species could be swapped between either Fe^{2+} or Fe^{3+} . The NEA-OECD reviews [2013LEM/BER; 2020LEM/PAL] only accepted the $\text{Fe}(\text{OH})^+$, $\text{Fe}(\text{OH})^{2+}$, $\text{Fe}(\text{OH})_2^+$, and $\text{Fe}_2(\text{OH})_2^{4+}$ hydroxo complexes. The data are completed by $\text{Fe}(\text{OH})_2(\text{aq})$, $\text{Fe}(\text{OH})_3^-$, $\text{Fe}(\text{OH})_4^{2-}$, $\text{Fe}(\text{OH})_3(\text{aq})$ and $\text{Fe}(\text{OH})_4^-$ from Chivot [2004CHI]. The Pourbaix diagram is plotted in Figure 3.7-32.

3.7.8.2. Sulphate Compounds

The phases from the jarosite family are important in the Fe-SO₄²⁻ system. The first NEA-OECD review on iron [2013LEM/BER] discuss of several values, but only select the formation functions of stoichiometric hydronium jarosite ((H₃O)_{0.91}Fe_{2.91}(SO₄)₂(OH)_{5.64}(H₂O)_{0.18}(cr)). The solubility constant is not selected but can be calculated from the following solubility equilibrium.



$$\Delta_r G_m^\circ = 32.675 \pm 6.603 \text{ kJ mol}^{-1}$$

$$\Delta_r H_m^\circ = -194.079 \pm 5.790 \text{ kJ mol}^{-1}$$

$$\log_{10} K_s = -5.72 \pm 1.16$$

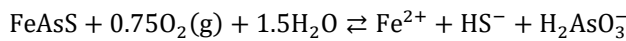
3.7.8.3. Phosphor Compounds

Only the entropy of formation of strengite (FePO₄: 2H₂O) is selected in Lemire *et al.* [2020LEM/PAL]. The complete functions of formation are available in Robie and Hemingway [1995ROB/HEM], out of which the functions reaction are calculated.

The solubility product for corkite (PbFe₃PO₄(OH)₆SO₄), phosphophyllite (Zn₂Fe(PO₄)₂ : 4H₂O(cr)), zinc-rockbridgeite (ZnFe₄(PO₄)₃(OH)₅(cr)) and chalcosiderite (CuFe₆(PO₄)₄(OH)₈: 4H₂O) are taken from Nriagu [1984NRI] — *vide ante* for the origin of the Gibbs energies of formation § 3.6.2.3. The value of Δ_fG° for Fe³⁺ and Fe²⁺ are different in Wagman *et al.* [1969WAG/EVA] — used in Nriagu [1984NRI] — and in Lemire *et al.* [2013LEM/BER; 2020LEM/PAL]. However, contrary to hinsdalite (c.f. § 3.6.2.3) there is almost no difference between the Δ_fG° values given in Nriagu [1984NRI], and the one that can be calculated with Wagman *et al.* [1968WAG/EVA; 1969WAG/EVA]. Hence the Δ_fG° values are recalculated from the log₁₀ K_s relative to Lemire *et al.* [2013LEM/BER; 2020LEM/PAL] and Guillaumont *et al.* [2003GUI/FAN] (Table 3.7-38).

3.7.8.4. Arsenosulphide

The function of reaction of arsenopyrite (FeAsS) can be calculated from Wagman *et al.* [1982WAG/EVA] from the following reaction.



Spycher and Reed [1989SPY/REE] proposed the solubility for the following reaction.



3.7.8.5. Thermodynamic Functions and Constants for Compounds of Fe

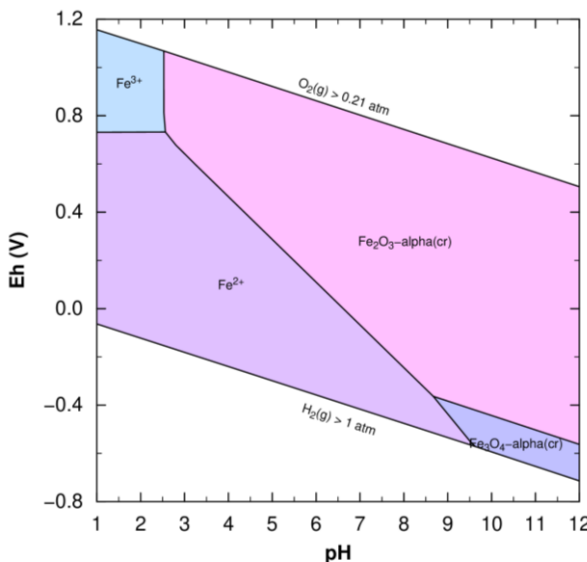
Table 3.7-36. Thermodynamic constants and functions for hydroxo compounds of Fe.

Reaction	log ₁₀ K°	Δ _r G° (kJ mol ⁻¹)	Δ _f G°* (kJ mol ⁻¹)	Δ _r H° (kJ mol ⁻¹)	Δ _f H°* (kJ mol ⁻¹)
Fe-alpha(cr) ⇌ Fe ²⁺ + 2e ⁻	15.89 ± 0.11	-90.719 ± 0.641	-90.719 ± 0.641 ^a	-90.295 ± 0.522	-90.295 ± 0.522 ^a
Fe-alpha(cr) + 0.5O ₂ (aq) + 2H ⁺ ⇌ Fe ²⁺ + H ₂ O	58.87 ± 0.08	-336.048 ± 0.461		-370.275 ± 0.271	
Fe-alpha(cr) ⇌ Fe ³⁺ + 3e ⁻	2.84 ± 0.11	-16.226 ± 0.650	-16.226 ± 0.650 ^a	-50.056 ± 0.973	-50.056 ± 0.973 ^a
Fe-alpha(cr) + 0.75O ₂ (aq) + 3H ⁺ ⇌ Fe ³⁺ + 1.5H ₂ O	67.31 ± 0.03	-384.220 ± 0.157		-470.026 ± 0.707	
Fe ²⁺ + H ₂ O ⇌ Fe(OH) ⁺ + H ⁺	-9.10 ± 0.40	51.943 ± 2.283	-275.916 ± 2.372 ^a	55.229 ^b	-320.896
Fe ²⁺ + 2H ₂ O ⇌ Fe(OH) ₂ (aq) + 2H ⁺	-20.6 ^b	117.586	-447.413	119.662 ^b	-542.293
Fe ²⁺ + 3H ₂ O ⇌ Fe(OH) ₃ ⁻ + 3H ⁺	-31.8 ^b	181.516	-620.623	138.070 ^b	-809.715
Fe ²⁺ + 4H ₂ O ⇌ Fe(OH) ₄ ²⁻ + 4H ⁺	-46.3 ^b	264.282	-774.997	160.460 ^b	-1 073.155
Fe ²⁺ ⇌ Fe ³⁺ + e ⁻	-13.051 ± 0.019	74.493 ± 0.108		40.24 ± 1.10	

Table 3.7-36. Continued.

Reaction	$\log_{10} K^\circ$	$\Delta_r G^\circ$ (kJ mol ⁻¹)	$\Delta_f G^\circ$ (kJ mol ⁻¹)	$\Delta_r H^\circ$ (kJ mol ⁻¹)	$\Delta_f H^\circ$ (kJ mol ⁻¹)
$\text{Fe}^{2+} + 0.25\text{O}_2(\text{aq}) + \text{H}^+ \rightleftharpoons \text{Fe}^{3+} + 0.5\text{H}_2\text{O}$	-8.439 ± 0.034	48.172 ± 0.195		99.751 ± 1.127	
$\text{Fe}^{3+} + \text{H}_2\text{O} \rightleftharpoons \text{Fe}(\text{OH})^{2+} + \text{H}^+$	-2.15 ± 0.07	12.272 ± 0.399	-241.094 ± 0.764 ^a	36.0 ± 3.0	-299.886 ± 3.154 ^a
$\text{Fe}^{3+} + 2\text{H}_2\text{O} \rightleftharpoons \text{Fe}(\text{OH})_2^+ + 2\text{H}^+$	-4.80 ± 0.40	27.399 ± 2.283	-463.107 ± 2.375 ^a	71.546 ^b	-550.170
$\text{Fe}^{3+} + 3\text{H}_2\text{O} \rightleftharpoons \text{Fe}(\text{OH})_3(\text{aq}) + 3\text{H}^+$	-12.56 ^b	71.693	-655.953	103.764 ^b	-803.782
$\text{Fe}^{3+} + 4\text{H}_2\text{O} \rightleftharpoons \text{Fe}(\text{OH})_4^- + 4\text{H}^+$	-21.26 ^b	121.353	-843.433	133.471 ^b	-1 059.905
$2\text{Fe}^{3+} + 2\text{H}_2\text{O} \rightleftharpoons \text{Fe}_2(\text{OH})_2^{4+} + 2\text{H}^+$	-2.82 ± 0.11	16.097 ± 0.628	-490.635 ± 1.446	43.999 ± 2.999	-627.773 ± 3.576
$\text{Fe}_2\text{O}_3\text{-alpha}(\text{cr}) + 6\text{H}^+ \rightleftharpoons 2\text{Fe}^{3+} + 3\text{H}_2\text{O}$	-0.10 ± 0.40	0.576 ± 2.285	-744.448 ± 2.632 ^a	-131.312 ± 1.765	-826.290 ± 2.630 ^a
$\text{Fe}_2\text{O}_3\text{-gamma}(\text{cr}) + 6\text{H}^+ \rightleftharpoons 2\text{Fe}^{3+} + 3\text{H}_2\text{O}$	2.81 ± 0.48	-16.042 ± 2.731	-727.830 ± 3.027 ^a	-149.612 ± 2.310	-807.990 ± 3.023 ^a
Wustite					
$\text{Fe}_{0.947}\text{O} + 2\text{H}^+ \rightleftharpoons 0.106\text{Fe}^{3+} + 0.841\text{Fe}^{2+} + \text{H}_2\text{O}$	12.20 ± 0.10	-69.660 ± 0.586 ^c	-245.494 ± 0.800	-101.405 ± 0.660 ^c	-265.670 ± 0.800
$\text{Fe}_{0.932}\text{O}(\text{cr}) + 2\text{H}^+ \rightleftharpoons 0.136\text{Fe}^{3+} + 0.796\text{Fe}^{2+} + \text{H}_2\text{O}$	11.73 ± 0.32	-66.966 ± 1.834	-244.593 ± 1.906 ^a	-98.712 ± 1.849	-265.800 ± 1.900 ^a
$\text{FeOOH}\text{-alpha}(\text{cr}) + 3\text{H}^+ \rightleftharpoons \text{Fe}^{3+} + 2\text{H}_2\text{O}$	0.17 ± 0.33	-0.969 ± 1.885	-489.537 ± 1.996 ^a	-61.256 ± 1.734	-560.460 ± 1.990 ^a
$\text{FeOOH}\text{-gamma}(\text{cr}) + 3\text{H}^+ \rightleftharpoons \text{Fe}^{3+} + 2\text{H}_2\text{O}$	1.86 ± 0.33	-10.625 ± 1.895	-479.881 ± 2.005 ^a	-72.516 ± 1.746	-549.200 ± 2.000 ^a
$\text{Fe}_3\text{O}_4\text{-alpha}(\text{cr}) + 8\text{H}^+ \rightleftharpoons 2\text{Fe}^{3+} + \text{Fe}^{2+} + 4\text{H}_2\text{O}$	10.34 ± 0.12	-59.012 ± 0.679	-1 012.719 ± 1.609 ^a	-217.947 ± 1.235	-1 115.780 ± 1.600 ^a

a [2013LEM/BER]; b [2004CHI]; c [1995ROB/HEM].

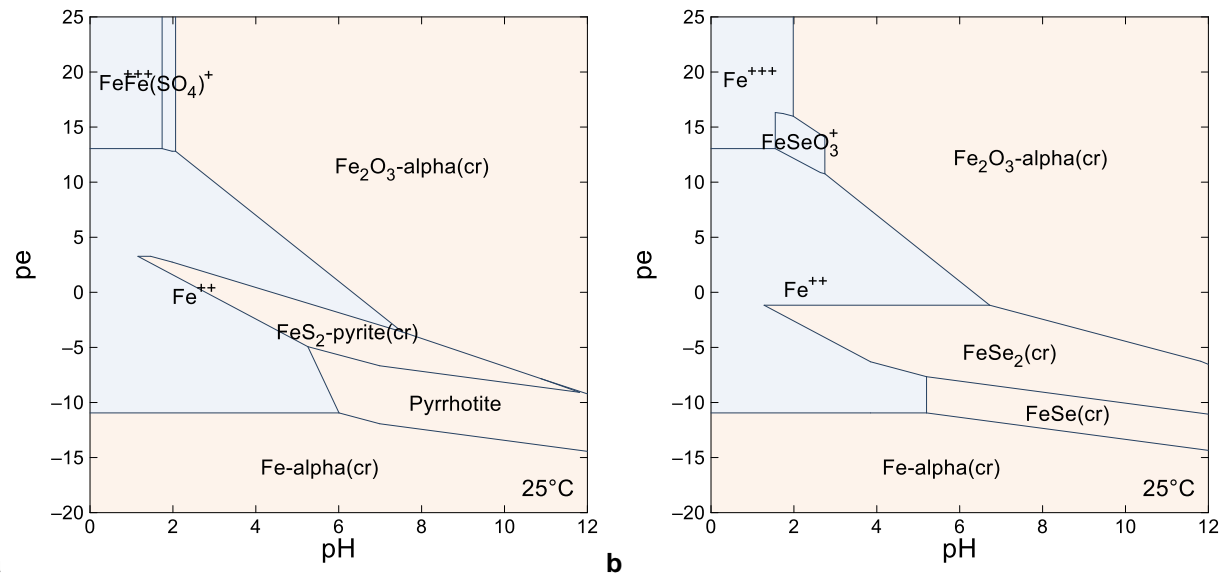
* calculated from $\Delta_f G^\circ$ and $\Delta_f H^\circ$ from [2003GUI/FAN; 2013LEM/BER; 2020LEM/PAL], unless otherwise noted.**Figure 3.7-32. Pourbaix diagram (PHREEPLOT) of 10^{-6} mol kg_w⁻¹ Fe in a 0.1 mol kg_w⁻¹ solution; all solid phases are allowed to precipitate.****Table 3.7-37. Thermodynamic constants and functions for halogen compounds of Fe.**

Reaction	$\log_{10} K^\circ$	$\Delta_r G^\circ$ (kJ mol ⁻¹)	$\Delta_f G^\circ$ (kJ mol ⁻¹)	$\Delta_r H^\circ$ (kJ mol ⁻¹)	$\Delta_f H^\circ$ (kJ mol ⁻¹)
$\text{Fe}^{2+} + \text{F}^- \rightleftharpoons \text{FeF}^+$	1.70 ± 0.20	-9.704 ± 1.142	-381.946 ± 1.481 ^a		
$\text{Fe}^{3+} + \text{F}^- \rightleftharpoons \text{FeF}^{2+}$	6.09 ± 0.11	-34.762 ± 0.650	-332.511 ± 0.692 ^a	12.800 ± 7.400	-372.606 ± 7.492
$\text{Fe}^{3+} + \text{Cl}^- \rightleftharpoons \text{FeCl}^{2+}$	1.52 ± 0.10	-8.676 ± 0.571	-156.119 ± 0.873 ^a	22.480 ± 4.600	-194.656 ± 4.703
$\text{Fe}^{3+} + 2\text{Cl}^- \rightleftharpoons \text{FeCl}_2^+$	2.22 ± 0.22	-12.672 ± 1.266	-291.332 ± 1.442 ^a		
$\text{Fe}^{3+} + 3\text{Cl}^- \rightleftharpoons \text{FeCl}_3(\text{aq})$	1.02 ± 0.30	-5.823 ± 1.688	-415.700 ± 1.843 ^a		
$\text{Fe}^{3+} + 4\text{Cl}^- \rightleftharpoons \text{FeCl}_4^-$	-0.98 ± 0.76	5.593 ± 4.329	-535.501 ± 4.402 ^a		
$\text{Fe}^{2+} + \text{SO}_4^{2-} \rightleftharpoons \text{Fe}(\text{SO}_4)(\text{aq})$	2.44 ± 0.03	-13.928 ± 0.170	-848.651 ± 0.784 ^a	8.400 ± 6.200	-991.235 ± 6.235
$\text{Fe}^{3+} + \text{SO}_4^{2-} \rightleftharpoons \text{Fe}(\text{SO}_4)^+$	4.25 ± 0.10	-24.258 ± 0.570	-784.488 ± 0.960 ^a		
$\text{Fe}^{3+} + 2\text{SO}_4^{2-} \rightleftharpoons \text{Fe}(\text{SO}_4)_2^-$	6.22 ± 0.13	-35.504 ± 0.726	-1 539.738 ± 1.284 ^a		
$\text{FeSe}(\text{cr}) + 2\text{H}^+ \rightleftharpoons \text{Fe}^{2+} + 2\text{H}_2\text{Se}(\text{aq})$	-0.95	5.429 ^b	74.653		
$\text{FeSe}_2(\text{cr}) + \text{H}_2\text{O} + 2\text{H}^+ \rightleftharpoons \text{Fe}^{2+} + 0.5\text{O}_2(\text{aq}) + 2\text{H}_2\text{Se}(\text{aq})$	-54.19 ± 1.41	309.322 ± 8.046	-111.722 ± 9.022	338.285 ± 8.011	-120.000 ± 9.000

Table 3.7-37. Continued.

Reaction	$\log_{10} K^\circ$	$\Delta_r G^\circ$ (kJ mol ⁻¹)	$\Delta_f G^{\circ\ddagger}$ (kJ mol ⁻¹)	$\Delta_r H^\circ$ (kJ mol ⁻¹)	$\Delta_f H^{\circ\ddagger}$ (kJ mol ⁻¹)
$\text{Fe}_3\text{Se}_4(\text{cr}) + \text{H}_2\text{O} + 6\text{H}^+ \rightleftharpoons 3\text{Fe}^{2+} + 0.5\text{O}_2(\text{aq}) + 4\text{H}_2\text{Se}(\text{aq})$	-55.39 ± 3.24	316.152 ± 18.482	-257.000 ± 20.240	314.295 ± 18.219	-248.000 ± 20.000
$\text{Fe}_7\text{Se}_8(\text{cr}) + 0.5\text{O}_2(\text{aq}) + 18\text{H}^+ \rightleftharpoons 3\text{Fe}^{2+} + 4\text{Fe}^{3+} + 8\text{H}_2\text{Se}(\text{aq}) + \text{H}_2\text{O}$	-23.94 ± 6.21	136.654 ± 35.453	-547.084 ± 39.038	-115.689 ± 35.241	-521.000 ± 39.000
$\text{Fe}_2(\text{SeO}_3)_3 \cdot 3\text{H}_2\text{O}(\text{cr}) \rightleftharpoons 2\text{Fe}^{3+} + 3\text{SeO}_3^{2-} + 3\text{H}_2\text{O}$	-44.30 ± 0.54	252.868 ± 3.088			
$\text{Fe}^{3+} + \text{SeO}_3^{2-} \rightleftharpoons \text{Fe}(\text{SeO}_3)^+$	11.90 ± 0.42	-67.926 ± 2.405	-446.544 ± 3.048		
$(\text{H}_3\text{O})_{0.91}\text{Fe}_{2.91}(\text{SO}_4)_2(\text{OH})_{5.64}(\text{H}_2\text{O})_{0.18}(\text{cr}) + 4.73\text{H}^+ \rightleftharpoons 2.91\text{Fe}^{3+} + 2\text{SO}_4^{2-} + 6.73\text{H}_2\text{O}$	-5.72 ± 1.16	32.675 ± 6.603	-3163.853 ± 6.925	-194.079 ± 5.790	-3693.900 ± 6.500

a [2013LEM/BER]; b [1974NAU/RYZ]; c [2020LEM/PAL].

**Figure 3.7-33. Pourbaix diagram (GWB) of 10^{-6} mol $\text{kg}_{\text{w}}^{-1}$ Fe with 10^{-4} mol $\text{kg}_{\text{w}}^{-1}$ S (a) and Se (b); all phases are allowed to precipitate.****Table 3.7-38. Thermodynamic constants and functions for complementary P and As compounds of Fe.**

Reaction	$\log_{10} K^\circ$	$\Delta_r G^\circ$ (kJ mol ⁻¹)	$\Delta_f G^{\circ\ddagger}$ (kJ mol ⁻¹)	$\Delta_r H^\circ$ (kJ mol ⁻¹)	$\Delta_f H^{\circ\ddagger}$ (kJ mol ⁻¹)
Strengite $\text{FePO}_4 \cdot 2\text{H}_2\text{O} \rightleftharpoons \text{Fe}^{3+} + \text{PO}_4^{3-} + 2\text{H}_2\text{O}$	-29.38 ± 0.24	167.700 ± 1.383^a	-1683.697 ± 1.000	7.900 ± 4.102^a	-1914.016 ± 0.900
Vivianite $\text{Fe}_3(\text{PO}_4)_2 \cdot 8\text{H}_2\text{O} \rightleftharpoons 3\text{Fe}^{2+} + 2\text{PO}_4^{3-} + 8\text{H}_2\text{O}$	-36.00 ± 0.40	205.489 ± 2.259	-4425.748 ± 4.341^b		
Corkite $\text{PbFe}_3\text{PO}_4(\text{OH})_6\text{SO}_4 \rightleftharpoons \text{Pb}^{2+} + 3\text{Fe}^{3+} + \text{PO}_4^{3-} + 6\text{OH}^- + \text{SO}_4^{2-}$	-112.6^c	642.726	-3428.457		
$\text{PbFe}_3\text{PO}_4(\text{OH})_6\text{SO}_4 + 6\text{H}^+ \rightleftharpoons \text{Pb}^{2+} + 3\text{Fe}^{3+} + \text{PO}_4^{3-} + 6\text{H}_2\text{O} + \text{SO}_4^{2-}$	-28.59	163.206			
Phosphophyllite $\text{Zn}_2\text{Fe}(\text{PO}_4)_2 \cdot 4\text{H}_2\text{O} \rightleftharpoons 2\text{Zn}^{2+} + \text{Fe}^{2+} + 2\text{PO}_4^{3-} + 4\text{H}_2\text{O}$	-35.8^c	204.348	-3589.015		
Zinc rockbridgeite $\text{ZnFe}_4(\text{PO}_4)_3(\text{OH})_5 \rightleftharpoons \text{Zn}^{2+} + 4\text{Fe}^{3+} + 3\text{PO}_4^{3-} + 5\text{OH}^-$	-138.6^c	791.1	-4865.815		
$\text{ZnFe}_4(\text{PO}_4)_3(\text{OH})_5 + 5\text{H}^+ \rightleftharpoons \text{Zn}^{2+} + 4\text{Fe}^{3+} + 3\text{PO}_4^{3-} + 5\text{H}_2\text{O}$	-68.59	391.535			
Chalcosiderite $\text{CuFe}_6(\text{PO}_4)_4(\text{OH})_8 \cdot 4\text{H}_2\text{O} \rightleftharpoons \text{Cu}^{2+} + 6\text{Fe}^{3+} + 4\text{PO}_4^{3-} + 8\text{OH}^- + 4\text{H}_2\text{O}$	-205.7^c	1174.144	-7514.738		
$\text{CuFe}_6(\text{PO}_4)_4(\text{OH})_8 \cdot 4\text{H}_2\text{O} + 8\text{H}^+ \rightleftharpoons \text{Cu}^{2+} + 6\text{Fe}^{3+} + 4\text{PO}_4^{3-} + 12\text{H}_2\text{O}$	-93.69	534.784			
Loellingite $\text{FeAs}_2 + 2\text{O}_2(\text{g}) + 2\text{H}_2\text{O} \rightleftharpoons \text{Fe}^{2+} + 2\text{H}_2\text{AsO}_3^-$	129.23 ± 1.36	-737.656 ± 7.777^a	-52.939 ± 2.045	-891.280 ± 7.751^a	-56.935 ± 2.045
$\text{FeAs}_2 + 2\text{O}_2(\text{aq}) + 2\text{H}_2\text{O} \rightleftharpoons \text{Fe}^{2+} + 2\text{H}_2\text{AsO}_3^-$	134.97 ± 1.33	-770.412 ± 7.568		-867.880 ± 7.542	

Table 3.7-38. Continued.

Reaction	$\log_{10} K^\circ$	$\Delta_f G^\circ$ (kJ mol ⁻¹)	$\Delta_f G^{\circ\ddagger}$ (kJ mol ⁻¹)	$\Delta_f H^\circ$ (kJ mol ⁻¹)	$\Delta_f H^{\circ\ddagger}$ (kJ mol ⁻¹)
Scorodite $\text{FeAsO}_4 \cdot 2\text{H}_2\text{O} \rightleftharpoons \text{Fe}^{3+} + \text{AsO}_4^{3-} + 2\text{H}_2\text{O}$	-25.30 ± 0.42	144.403 ± 2.415	-1283.269 ± 4.725^b	-2.676 ± 2.225	-1507.180 ± 4.680^b
Kankite $\text{FeAsO}_4 \cdot 3.5\text{H}_2\text{O} \rightleftharpoons \text{Fe}^{3+} + \text{AsO}_4^{3-} + 3.5\text{H}_2\text{O}$	-23.43 ± 0.43	133.764 ± 2.438	-1628.340 ± 4.738^b	-0.011 ± 2.179	-1938.590 ± 4.660^b
$\text{Fe}_4(\text{AsO}_4)_4 \cdot 3\text{H}_2\text{O} \rightleftharpoons 4\text{Fe}^{3+} + 4\text{AsO}_4^{3-} + 3\text{H}_2\text{O}$	-105.41 ± 1.49	601.693 ± 8.501	-3971.457 ± 18.332	-50.590 ± 8.113	-4559.684 ± 18.357
Arsenopyrite $\text{FeAsS} + 0.75\text{O}_2(g) + 1.5\text{H}_2\text{O} \rightleftharpoons \text{Fe}^{2+} + \text{HS}^- + \text{H}_2\text{AsO}_3^-$	43.49 ± 0.09	-248.257 ± 0.525^d	-61.587 ± 4.456	-350.745 ± 1.466^d	-41.895 ± 4.456
$\text{FeAsS} + 0.75\text{O}_2(aq) + 1.5\text{H}_2\text{O} \rightleftharpoons \text{Fe}^{2+} + \text{HS}^- + \text{H}_2\text{AsO}_3^-$	45.64 ± 0.07	-260.540 ± 0.419		-341.970 ± 1.613	

a [1995ROB/HEM]; b [2020LEM/PAL]; c [1984NRI]; d [1982WAG/EVA].

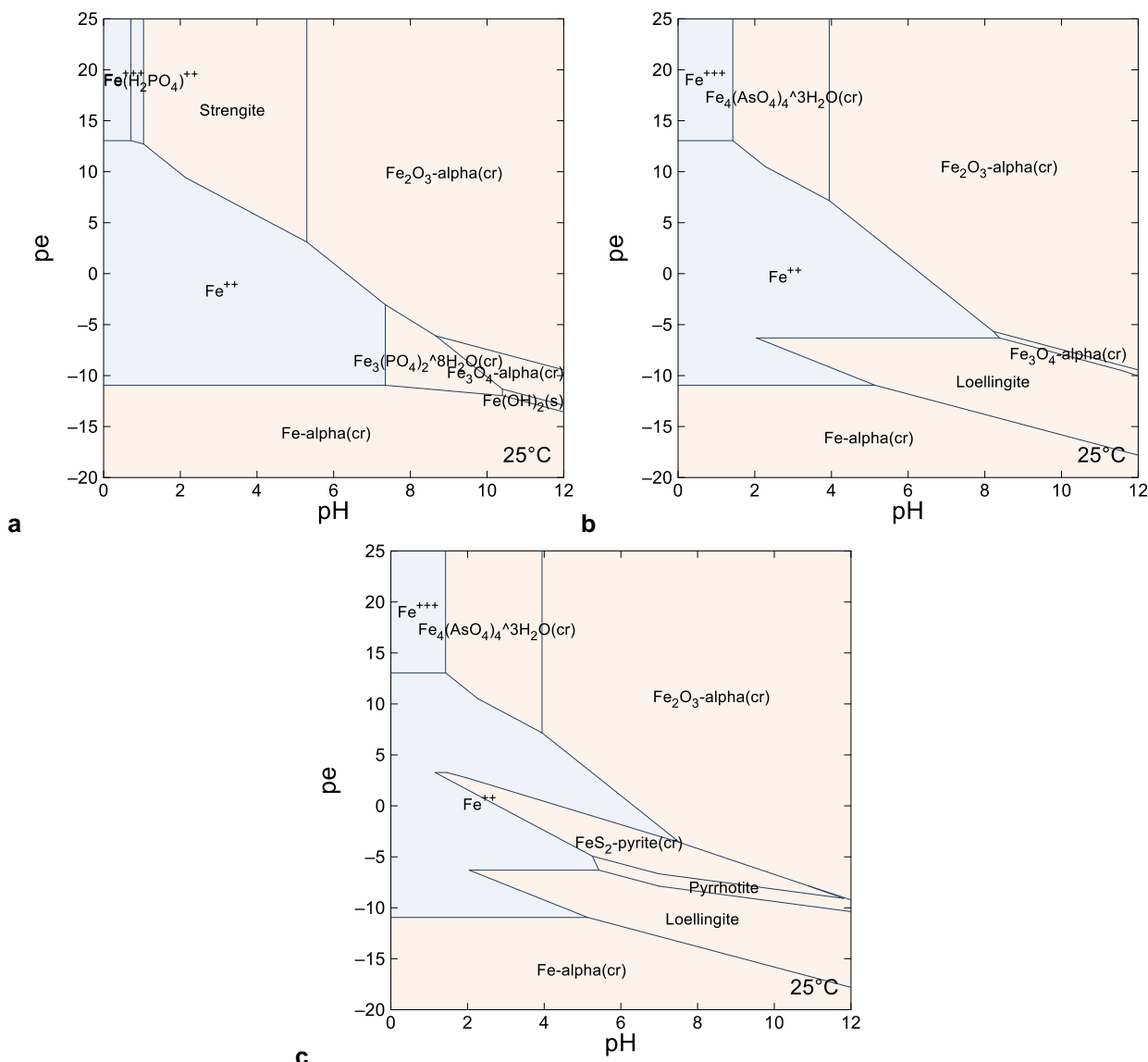
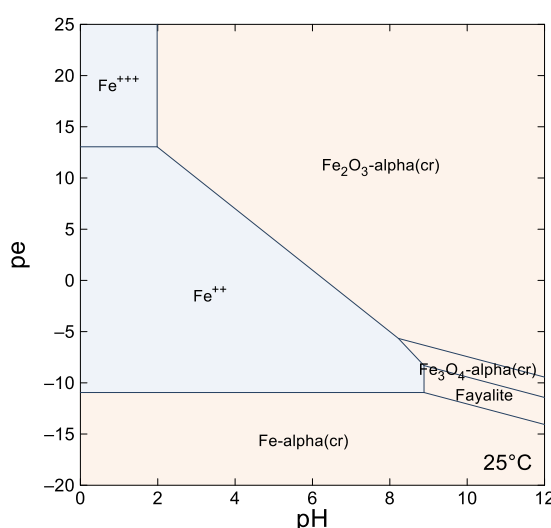
* calculated from $\Delta_f G^\circ$ and $\Delta_f H^\circ$ from [2003GUI/FAN; 2013LEM/BER; 2020LEM/PAL].

Figure 3.7-34. Pourbaix diagram (GWB) of 10^{-6} mol kg_w⁻¹ Fe and 10^{-4} mol kg_w⁻¹ P (a), As (b), and As and S (c); all phases are allowed to precipitate.

Table 3.7-39. Thermodynamic constants and functions for C and Si compounds of Fe.

Reaction	$\log_{10} K^\circ$	$\Delta_f G^\circ$ (kJ mol ⁻¹)	$\Delta_f G^{**}$ (kJ mol ⁻¹)	$\Delta_f H^\circ$ (kJ mol ⁻¹)	$\Delta_f H^{**}$ (kJ mol ⁻¹)
Siderite $\text{FeCO}_3 \rightleftharpoons \text{Fe}^{2+} + \text{CO}_3^{2-}$	-10.68 ± 0.09	60.938 ± 0.527	-679.557 ± 0.917 ^a	-12.916 ± 0.683	-752.609 ± 0.895 ^a
$\text{Fe}_3\text{C(cr)} + 3.25\text{O}_2(\text{g}) + 7\text{H}^+ \rightleftharpoons 3\text{Fe}^{3+} + \text{CO}_3^{2-} + 3.5\text{H}_2\text{O}$	243.86 ± 0.11	-1 391.962 ± 0.642 ^b	-14.607 ± 2.095	-1 848.145 ± 2.442 ^b	22.342 ± 1.625
$\text{Fe}_3\text{C(cr)} + 3.25\text{O}_2(\text{aq}) + 7\text{H}^+ \rightleftharpoons 3\text{Fe}^{3+} + \text{CO}_3^{2-} + 3.5\text{H}_2\text{O}$	253.18 ± 0.52	-1 445.190 ± 2.980		-1 810.120 ± 1.582	
$\text{Fe}^{2+} + \text{CO}_3^{2-} \rightleftharpoons \text{FeCO}_3(\text{aq})$	5.27 ± 0.18	-30.058 ± 1.043	-648.677 ± 1.285 ^a		
$\text{Fe}^{2+} + 2\text{CO}_3^{2-} \rightleftharpoons \text{Fe}(\text{CO}_3)_2^{2-}$	7.03 ± 0.14	-40.151 ± 0.808	-1 186.670 ± 1.293 ^a		
$\text{Fe}^{2+} + \text{CO}_3^{2-} + \text{H}_2\text{O} \rightleftharpoons \text{Fe(OH)}\text{CO}_3^- + \text{H}^+$	-4.03 ^c	23.011	-832.748		
$\text{Fe}^{3+} + 3\text{CO}_3^{2-} \rightleftharpoons \text{Fe}(\text{CO}_3)_3^{3-}$	24.00 ± 2.00	-136.992 ± 11.416	-1 736.918 ± 11.494 ^a		
$\text{Fe}^{2+} + \text{CO}_3^{2-} + \text{H}_2\text{O} \rightleftharpoons \text{Fe(OH)}\text{CO}_3(\text{aq}) + \text{H}^+$	10.70 ± 2.00	-61.076 ± 11.416	-842.342 ± 11.441 ^a		
Fayalite $\text{Fe}_2\text{SiO}_4 + 4\text{H}^+ \rightleftharpoons 2\text{Fe}^{2+} + \text{Si(OH)}_4(\text{aq})$	19.53 ± 10.24	-111.453 ± 11.350	-1 377.720 ± 11.076	-160.760 ± 13.154	-1 476.790 ± 11.070

a [2013LEM/BER]; b [1982WAG/EVA]; c [2004CHI].

* calculated from $\Delta_f G^\circ$ and $\Delta_f H^\circ$ from [2003GUI/FAN; 2013LEM/BER; 2020LEM/PAL], unless otherwise noted.**Figure 3.7-35. Pourbaix diagram (GWB) of 10^{-6} mol kg_w⁻¹ Fe at equilibrium with quartz (SiO₂); all phases are allowed to precipitate.**

3.7.9. Manganese

Manganese is often controlling the redox properties of geochemical sites [2000DUR/ARC] and is thus important to add to PRODATA.

3.7.9.1. Native Metal and Free Ions

The S_f° and C_p° of α -Mn(cr) are available in Wagman *et al.* [1982WAG/EVA] and Robie and Hemingway [1995ROB/HEM] and is chosen in Brown and Ekberg [2016BRO/EKB]. The thermodynamic functions for Mn(II), and Mn(III) are chosen in Brown and Ekberg [2016BRO/EKB]. The uncertainty for $\Delta_f G^\circ(\text{Mn}^{3+})$ is increased in view of the value of the corresponding uncertainty of $\Delta_f H^\circ(\text{Mn}^{3+})$. The redox reactions from Mn(II) to Mn(VI) and Mn(VII) are chosen from the ones estimated in Shock *et al.* [1997aSHO/SAS] and adapted to the formation functions in Brown and Ekberg [2016BRO/EKB] in Table 3.7-40. The common master species is Mn²⁺.

An estimation of $\varepsilon(\text{Mn}^{2+}, \text{NO}_3^-)$ is possible using the data compiled in Figure 2.6-1c. An extraction concerning only the d-transition series elements is shown in Figure 3.7-36. A value of $\varepsilon(\text{Mn}^{2+}, \text{NO}_3^-) = (0.10 \pm 0.07) \text{ kg}_w \text{ mol}^{-1}$ can be proposed.

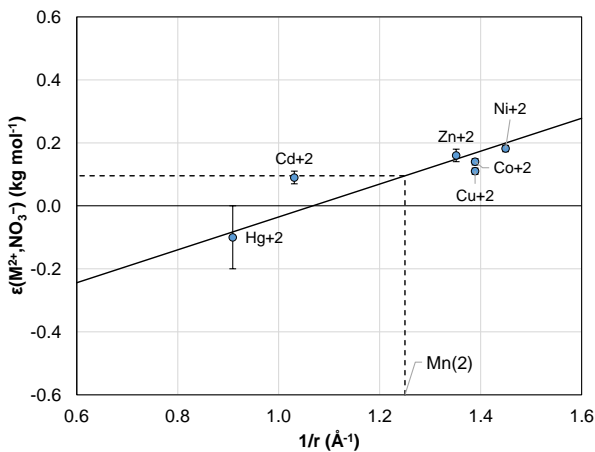


Figure 3.7-36. Values of $\epsilon(M^{2+}, \text{NO}_3^-)$ for d-transition element series, and estimation of $\epsilon(\text{Mn}^{2+}, \text{NO}_3^-)$.

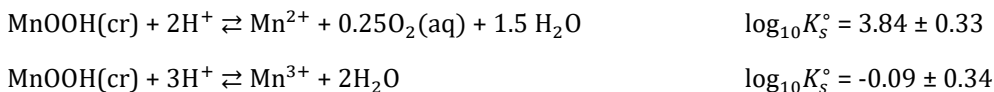
3.7.9.2. Hydroxo Compounds

The Mn(II) oxide from Robie and Hemingway [1995ROB/HEM] — *i.e.*, manganosite (MnO(cr)) — is accepted in Brown and Ekberg [2016BRO/EKB]. As the thermodynamic functions of Mn^{2+} in Brown and Ekberg [2016BRO/EKB] are taken from Robie and Hemingway [1995ROB/HEM], no change in the thermodynamic functions of the phases are done before inclusion in PRODATA.

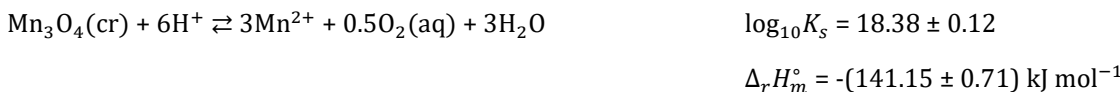
The dissolution of Mn(III) oxide — bixbyite, $\text{Mn}_2\text{O}_3(\text{cr})$ — is chosen from the thermodynamic functions in Robie and Hemingway [1995ROB/HEM].



For the Mn(III) oxo-hydroxide, manganite, the estimation of $\Delta_f G_m^\circ(\text{MnOOH(cr)}) = -(555.8 \pm 2.0) \text{ kJ mol}^{-1}$ in Brown and Ekberg [2016BRO/EKB] is accepted.



The manganese spinel hausmannite, $\text{Mn}_3\text{O}_4(\text{cr})$, is chosen in Robie and Hemingway [1995ROB/HEM] in agreement with Brown and Ekberg [2016BRO/EKB].



The Mn(IV) oxide pyrolusite ($\text{MnO}_2(\text{cr})$) is also accepted in PRODATA and corrected to the functions of Brown and Ekberg [2016BRO/EKB].



The hydroxo complexes of Mn(II), $\text{Mn(OH)}_n^{(2-n)+}$, and Mn(OH)^{2+} in Brown and Ekberg [2016BRO/EKB] are accepted in the database.

$\Delta\epsilon(\text{Mn(OH)}^+, \text{NO}_3^-)$ from Brown and Ekberg [2016BRO/EKB] is not included in PRODATA as the estimation of $\log_{10} * \beta_1^\circ$ is slightly different than the one selected from the temperature dependency. Brown and Ekberg

[2016BRO/EKB] has fitted the evolution of using the Ciavatta [1980CIA] hypothesis (Eq. 21), which could be refitted using the more classical linear relationship (Eq. 18), even if the distribution of residuals is more satisfying in the former case than in the latter.

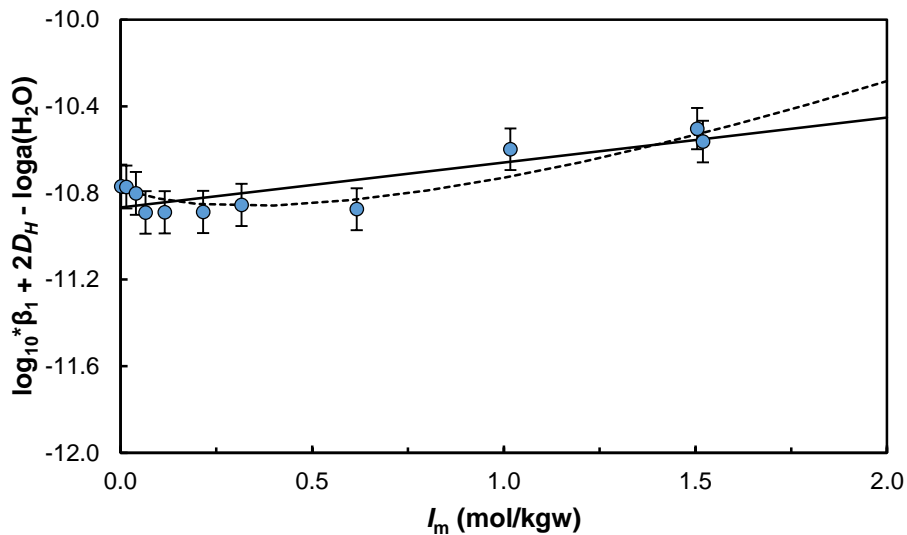


Figure 3.7-37. Dependence of $\log_{10} * \beta_1$ of Mn(OH)^+ on ionic strength in potassium nitrate media: the dashed line is obtained using the interaction coefficients and stability constant at zero ionic strength from Brown and Ekberg [2016BRO/EKB], and solid line represents the linear fitting.

3.7.9.3. Halogen Compounds

The formation of MnF^+ can be found in Nordstrom *et al.* [1990NOR/PLU]. Higher complexes can be found in Chandratillake *et al.* [1988CHA/NEW]. In view of the very high difference between MnF^+ and $\text{MnF}_2(\text{aq})$, the constants from Chandratillake *et al.* [1988CHA/NEW] are not included in PRODATA.

The solubility of scacchite ($\text{MnCl}_2(\text{cr})$) is taken from Robie and Hemingway [1995ROB/HEM]. The chloride complexes are taken from Nordstrom *et al.* [1990NOR/PLU].

3.7.9.4. Group 16 Compounds

The sulphide and disulphide phases of Mn(II) can be found in [1982WAG/EVA] (MnS(cr)), Pankratz *et al.* [1987PAN/MAH] ($\text{MnS}_2(\text{cr})$), Dyrssen and Kremling [1990DYR/KRE] (MnS-green(cr) , MnS-pink(cr)), and Robie and Hemingway [1995ROB/HEM] for alabandite (MnS) — which must be corrected by the values of HS^- in § 3.3 — and hauerite (MnS_2) — which must be expressed relative to HS^- as S_2^{2-} is not available in Robie and Hemingway [1995ROB/HEM].

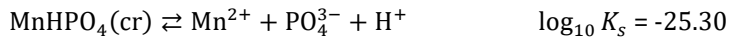
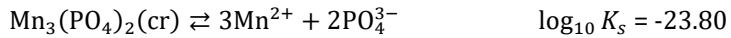
The functions of reaction of $\text{MnSO}_4(\text{cr})$ is calculated from Robie and Hemingway [1995ROB/HEM], and the ones of $\text{MnSO}_4(\text{aq})$ are from Wagman *et al.* [1982WAG/EVA].

The functions of formation of MnSe(cr) are available in Wagman *et al.* [1982WAG/EVA]. Olin *et al.* [2005OLI/NOL] selected the $\log_{10} \beta^\circ$ value for the formation of $\text{MnSeO}_4(\text{aq})$.

3.7.9.5. Group 15 Compounds

Naumov *et al.* [1974NAU/RYZ] only report the $\Delta_f H^\circ$ of $\text{Mn}_3(\text{PO}_4)_2(\text{cr})$. Solubility values of $\text{MnHPO}_4(\text{cr})$, and $\text{Mn}_3(\text{PO}_4)_2(\text{cr})$ are available in different database compilations [1988CHA/NEW; 1991WAT/DUF]; Falck *et al.*

[1996FAL/REA], which are difficult to trace to the original data. For scoping calculation, the solubility from Falck *et al.* [1996FAL/REA].



are included in PRODATA.

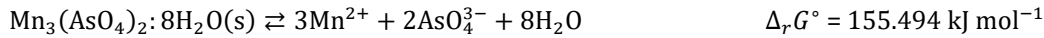
The $\text{Mn}(\text{HPO}_4)^{(2-2n)+}$ complexes can be found in various databases [1988CHA/NEW; 1991WAT/DUF]; Falck *et al.* [1996FAL/REA].

The functions of formation of kaneite ($\text{MnAs}(\text{cr})$) and $\text{Mn}_3(\text{AsO}_4)_2 \cdot 8\text{H}_2\text{O}(\text{s})$ are available in Naumov *et al.* [1974NAU/RYZ]. Using the function of formation of Mn^{2+} , AsO_4^{3-} , and H_2O in Naumov *et al.* [1974NAU/RYZ], the functions of reaction and $\log_{10} K_s$ for the following reactions are calculated.



$$\log_{10} K_s = 124.13$$

$$\Delta_r H^\circ = -908.666 \text{ kJ mol}^{-1}$$



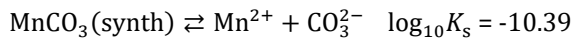
$$\log_{10} K_s = -27.24$$

The functions of formation relative to the NEA-OECD reviews [1992GRE/FUG; 2003GUI/FAN; 2020GRE/GAO] are then calculated in PRODATA.

3.7.9.6. Carbonate Compounds

The thermodynamic functions of rhodocrosite, $\text{MnCO}_3(\text{cr})$, in Robie and Hemingway [1995ROB/HEM] is accepted.

Nordstrom *et al.* [1990NOR/PLU] proposed the dissolution of the synthetic rhodocrosite from $\Delta_f G_m^\circ$ in Garrels *et al.* [1960GAR/THO]. The $\Delta_f G_m^\circ(\text{Mn}^{2+})$ value that allowed calculating the $\Delta_f G_m^\circ(\text{Rhodocrosite(synth)})$ seems to be linked to an NBS values at that particular time [1952ROS/WAG] — *i.e.* $\Delta_f G_m^\circ(\text{Mn}^{2+}) = -53.4 \text{ kcal mol}^{-1}$ (-223.4 kJ mol^{-1}), and $\Delta_f G_m^\circ(\text{CO}_3^{2-}) = -126.22 \text{ kcal mol}^{-1}$ (-528.10 kJ mol^{-1}) —, which are different from the more recent values [1989COX/WAG; 1995ROB/HEM; 2003GUI/FAN; 2016BRO/EKB].



3.7.9.7. Silicate Compounds

The thermodynamic functions of reaction for $\text{MnSiO}_3(\text{cr})$ and $\text{Mn}_2\text{SiO}_4(\text{cr})$ are from Wagman *et al.* [1982WAG/EVA] are not added for the reason of coherency of function of formation of $\text{Si(OH)}_4(\text{aq})$. The ones for rhodonite and pyroxmangite (MnSiO_3), tephroite (Mn_2SiO_4) and braunite ($\text{Mn}_7\text{SiO}_{12}$) are from Robie and Hemingway [1995ROB/HEM].

3.7.9.8. Zinc Phase

The multiple oxide hetaerolite (ZnMn_2O_4) can be retrieved from Robie and Hemingway [1995ROB/HEM].

3.7.9.9. Thermodynamic Functions and Constants, and Specific Ion Interaction Coefficients for Mn

Table 3.7-40. Thermodynamic functions and constants for native metal, free ions, and oxo and hydroxo compounds of Mn.

Reaction	$\Delta_r G_m^\circ$ kJ mol ⁻¹	$\log_{10} K^\circ$	$\Delta_f G_m^\circ$ kJ mol ⁻¹	$\Delta_r H_m^\circ$ kJ mol ⁻¹	$\Delta_f H_m^\circ$ kJ mol ⁻¹
$Mn \rightleftharpoons Mn^{2+} + 2e^-$	-228.100 ± 0.500	39.96 ± 0.09	-228.100 ± 0.500 ^a	-220.800 ± 0.500	-220.800 ± 0.500 ^a
$Mn\text{-alpha(cr)} + 0.5O_2(aq) + 2H^+ \rightleftharpoons Mn^{2+} + H_2O$	-473.429 ± 0.226	82.94 ± 0.04		-500.780 ± 0.226	
$Mn^{2+} \rightleftharpoons Mn^{3+} + e^-$	145.100 ± 1.936	-25.42 ± 0.34	-83 ± 2 ^a	107.800 ± 2.062	-113 ± 2 ^a
$Mn^{2+} + 0.25O_2(aq) + H^+ \rightleftharpoons Mn^{3+} + 0.5H_2O$	22.436 1.924	-3.931 0.337		-32.190 2.074	
$Mn^{2+} + 4H_2O \rightleftharpoons MnO_4^{2-} + 4e^- + 8H^+$	675.498 ^b	-118.34	-501.162	709.439 ^b	-654.681
$Mn^{2+} + O_2(aq) + 2H_2O \rightleftharpoons MnO_4^{2-} + 4H^+$	184.840	-32.38		149.479	
$Mn^{2+} + 4H_2O \rightleftharpoons MnO_4^- + 5e^- + 8H^+$	729.054 ^b	-127.72	-447.606	821.152 ^b	-542.968
$Mn^{2+} + 1.25O_2(aq) + 1.5H_2O \rightleftharpoons MnO_4^- + 3H^+$	115.732	-20.28		121.202	
Manganosite					
$MnO + 2H^+ \rightleftharpoons Mn^{2+} + H_2O$	-102.300 ± 0.329 ^c	17.92 ± 0.06	-362.940 ± 0.600	-121.400 ± 0.040 ^c	-385.230 ± 0.500
Manganite					
$MnOOH + 2H^+ \rightleftharpoons Mn^{2+} + 0.25O_2(g) + 1.5H_2O$	-26.010 ± 1.923 ^c	4.56 ± 0.34	-557.800 ± 2.000		
$MnOOH + 2H^+ \rightleftharpoons Mn^{2+} + 0.25O_2(aq) + 1.5H_2O$	-21.916 ± 1.923	3.84 ± 0.34			
Bixbyite					
$Mn_2O_3 + 4H^+ \rightleftharpoons 2Mn^{2+} + 0.5O_2(g) + 2H_2O$	-48.260 ± 0.080 ^c	8.45 ± 0.01	-882.220 ± 1.000	-54.170 ± 0.079 ^c	-959.090 ± 1.000
$Mn_2O_3 + 4H^+ \rightleftharpoons 2Mn^{2+} + 0.5O_2(aq) + 2H_2O$	-40.071 ± 0.455	7.02 ± 0.08		-60.020 ± 0.455	
$Mn_2O_3 + 6H^+ \rightleftharpoons 2Mn^{3+} + 3H_2O$	4.800 ± 0.122	-0.84 ± 0.02		-124.400 ± 3.875	
Hausmannite					
$Mn_3O_4 + 6H^+ \rightleftharpoons 3Mn^{2+} + 0.5O_2(g) + 3H_2O$	-113.100 ± 0.711 ^c	19.81 ± 0.10	-1 282.620 ± 1.400	-135.300 ± 0.552 ^c	-1 384.590 ± 1.400
$Mn_3O_4 + 6H^+ \rightleftharpoons 3Mn^{2+} + 0.5O_2(aq) + 3H_2O$	-104.911 ± 0.711	18.38 ± 0.13		-141.150 ± 0.710	
Pyrolusite					
$MnO_2 + 2H^+ \rightleftharpoons Mn^{2+} + 0.5O_2(g) + H_2O$	-0.200 ± 0.532 ^c	0.04 ± 0.09	-465.040 ± 0.732	13.370 ± 0.488 ^c	-520.000 ± 0.700
$MnO_2 + 2H^+ \rightleftharpoons Mn^{2+} + 0.5O_2(aq) + H_2O$	7.989 ± 0.288	-1.40 ± 0.05		7.520 ± 0.195	
Pyrochroite					
$Mn(OH)_2 + 2H^+ \rightleftharpoons Mn^{2+} + 2H_2O$	-86.705 ± 0.507	15.19 ± 0.09 ^a	-615.675 ± 0.011	-97.060	-695.400 ^a
$Mn^{2+} + H_2O \rightleftharpoons Mn(OH)^+ + H^+$	60.391 ± 0.228	-10.58 ± 0.04 ^a	-404.849 ± 0.551	57.300 ± 1.100 ^a	-449.330 ± 1.209
$Mn^{2+} + 2H_2O \rightleftharpoons Mn(OH)_2(aq) + 2H^+$	126.604 ± 1.142	-22.18 ± 0.20 ^a	-575.776 ± 1.249	117.400 ± 2.600 ^a	-675.060 ± 2.649
$Mn^{2+} + 3H_2O \rightleftharpoons Mn(OH)_3^- + 3H^+$	196.014 ± 2.569	-34.34 ± 0.45 ^a	-743.506 ± 2.620	171.900 ± 3.100 ^a	-906.390 ± 3.142
$Mn^{2+} + 4H_2O \rightleftharpoons Mn(OH)_4^{2-} + 4H^+$	275.584 ± 2.283	-48.28 ± 0.40 ^a	-901.076 ± 2.343	256.400 ± 5.200 ^a	-1 107.720 ± 5.226
Hetaerolite					
$ZnMn_2O_4 + 6H^+ \rightleftharpoons Zn^{2+} + 2Mn^{2+} + 0.5O_2(g) + 3H_2O$	-87.000 ± 3.837 ^c	15.24 ± 0.68	-1 227.823 ± 4.000	-115.400 ± 3.840 ^c	-1 337.080 ± 4.000
$ZnMn_2O_4 + 6H^+ \rightleftharpoons Zn^{2+} + 2Mn^{2+} + 0.5O_2(aq) + 3H_2O$	-78.811 ± 3.837	13.81 ± 0.67		-121.250 ± 3.840	

a [2016BRO/EKB]; b [1997aSHO/SAS]; c [1995ROB/HEM]

* calculated from $\Delta_f G_m^\circ$ or $\Delta_f H_m^\circ$ in [2016BRO/EKB], unless noted otherwise.

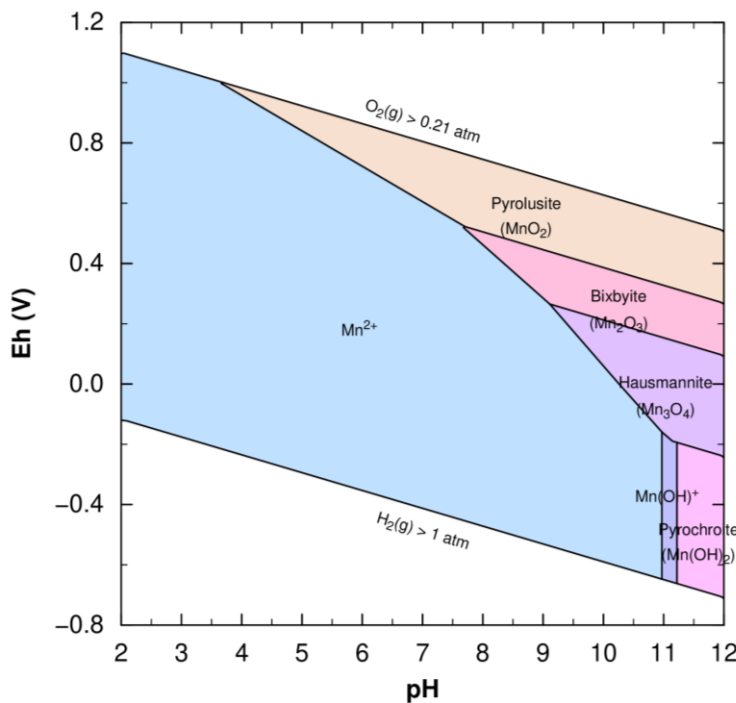


Figure 3.7-38. Pourbaix diagram (PHREEPLOT) of 10^{-6} mol $\text{kg}_{\text{w}}^{-1}$ Mn in a $0.1 \text{ mol kg}_{\text{w}}^{-1}$ solution; all solid phases are allowed to precipitate.

Table 3.7-41. Thermodynamic functions and constants for halogen, S, and Se compounds of Mn.

Reaction	$\Delta_r G_m^\circ$ kJ mol ⁻¹	$\log_{10} K^\circ$	$\Delta_f G_m^\circ$ kJ mol ⁻¹	$\Delta_r H_m^\circ$ kJ mol ⁻¹	$\Delta_f H_m^\circ$ kJ mol ⁻¹
$\text{Mn}^{2+} + \text{F}^- \rightleftharpoons \text{MnF}^+$	-4.795	0.84 ^a			
Scacchite $\text{MnCl}_2 \rightleftharpoons \text{Mn}^{2+} + 2\text{Cl}^-$	-50.000 ± 0.128^b	8.76 ± 0.02	-440.534 ± 0.537	-73.660 ± 0.347^b	-481.300 ± 0.411
$\text{Mn}^{2+} + \text{Cl}^- \rightleftharpoons \text{MnCl}^+$	-3.482	0.610 ^a	-362.799		
$\text{Mn}^{2+} + 2\text{Cl}^- \rightleftharpoons \text{MnCl}_2(\text{aq})$	-1.427	0.250 ^a	-491.961		
$\text{Mn}^{2+} + 3\text{Cl}^- \rightleftharpoons \text{MnCl}_3^-$	1.769	-0.310 ^a	-619.982		
$\text{MnS(cr)} + \text{H}^+ \rightleftharpoons \text{Mn}^{2+} + \text{HS}^-$	2.380 ± 0.506^c	-0.42 ± 0.09	-218.237 ± 2.114	-24.150 ± 3.955^c	-212.950 ± 4.259
Alabantite $\text{MnS(cr)} + \text{H}^+ \rightleftharpoons \text{Mn}^{2+} + \text{HS}^-$	2.800 ± 0.686^b	-0.49 ± 0.12	-218.657 ± 2.062	-23.200 ± 0.592^b	-213.900 ± 1.466
Hauerite $\text{MnS}_2(\text{cr}) + \text{H}_2\text{O} \rightleftharpoons \text{Mn}^{2+} + 2\text{HS}^- + 0.5\text{O}_2(\text{g})$	258.040 ± 7.944^b	-45.21 ± 1.39	-224.514 ± 9.014	256.230 ± 9.005^b	-223.800 ± 9.505
$\text{MnS}_2(\text{cr}) \rightleftharpoons \text{Mn}^{2+} + \text{S}_2^{2-}$	81.120	-14.21		38.041	
$\text{MnSO}_4(\text{cr}) \rightleftharpoons \text{Mn}^{2+} + \text{SO}_4^{2-}$	-10.000 ± 1.351^b	1.752 ± 0.237	-962.104 ± 1.500	-64.400 ± 0.894^b	$-1\ 065.740 \pm 1.100$
$\text{Mn}^{2+} + \text{SO}_4^{2-} \rightleftharpoons \text{MnSO}_4(\text{aq})$	-13.596 ± 5.562^c	2.382 ± 0.974	-985.700 ± 5.600	14.240 ± 7.171^c	$-1\ 115.900 \pm 7.200$
$\text{MnSe(cr)} + 2\text{H}^+ \rightleftharpoons \text{Mn}^{2+} + \text{H}_2\text{Se(aq)}$	-94.200 ± 4.431^c	16.50 ± 0.78	-112.405 ± 4.889	-94.850 ± 4.468^c	-111.650 ± 4.930
$\text{Mn}^{2+} + \text{SeO}_4^{2-} \rightleftharpoons \text{MnSeO}_4(\text{aq})$	-13.871	2.43 ± 0.05^d			

a [1990NOR/PLU]; b [1995ROB/HEM]; c [1982WAG/EVA]; d [2005OLI/NOL]

* calculated from $\Delta_f G_m^\circ$ or $\Delta_f H_m^\circ$ in [2016BRO/EKB], unless noted otherwise.

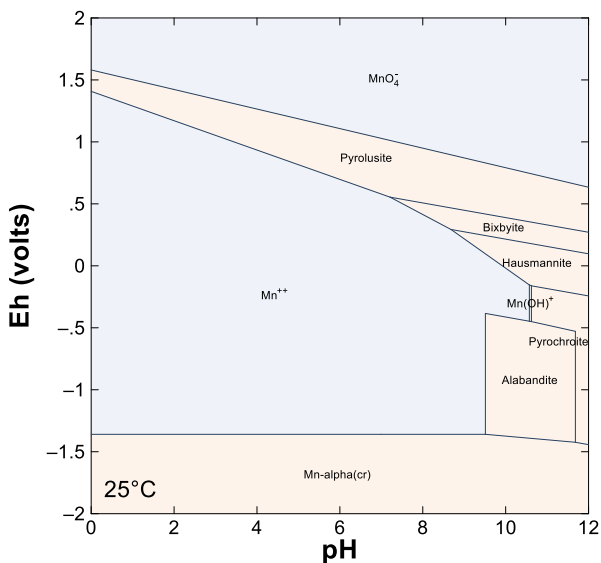


Figure 3.7-39. Pourbaix diagram (GWB) of 10^{-6} mol kg_w⁻¹ Mn and 10^{-4} mol kg_w⁻¹ S; all phases are allowed to precipitate.

Table 3.7-42. Thermodynamic functions and constants for As, P, C and Si compounds of Mn.

Reaction	$\Delta_r G_m^\circ$ (kJ mol ⁻¹)	$\log_{10} K^\circ$	$\Delta_f G_m^\circ$ (kJ mol ⁻¹)	$\Delta_r H_m^\circ$ (kJ mol ⁻¹)	$\Delta_f H_m^\circ$ (kJ mol ⁻¹)
$MnAs + 1.75O_2(g) + 0.5H_2O \rightleftharpoons Mn^{2+} + AsO_4^{3-} + H^+$	-708.515 ^a	124.126	-49.375	-908.666 ^a	-57.359
$MnAs + 1.75O_2(aq) + 0.5H_2O \rightleftharpoons Mn^{2+} + AsO_4^{3-} + H^+$	-737.176	129.147		-888.191	
$Mn_3(AsO_4)_2 \cdot 8H_2O(s) \rightleftharpoons 3Mn^{2+} + 2AsO_4^{3-} + 8H_2O$	155.494 ^a	-27.241	-4 033.634		
Rhodocrosite					
$MnCO_3 \rightleftharpoons Mn^{2+} + CO_3^{2-}$	64.000 ± 0.205^b	-11.212 ± 0.036	-820.000 ± 0.600	-3.100 ± 0.250^b	892.930 ± 0.500
$Mn^{2+} + HCO_3^- \rightleftharpoons MnHCO_3^+$	-11.131	1.95 ^c	-826.076		
$Mn^{2+} + H^+ + CO_3^{2-} \rightleftharpoons MnHCO_3^+$	-70.08	12.277			
$Mn^{2+} + CO_3^{2-} \rightleftharpoons MnCO_3(aq)$	-27.969	4.90 ^c	-783.969		
Rhodonite					
$MnSiO_3 + H_2O + 2H^+ \rightleftharpoons Mn^{2+} + Si(OH)_4(aq)$	-53.800 ± 0.660^b	9.43 ± 0.12	$-1 244.895 \pm 1.072^b$	-73.400 ± 0.966	$-1 318.530 \pm 3.053$
Pyroxmangite					
$MnSiO_3 + H_2O + 2H^+ \rightleftharpoons Mn^{2+} + Si(OH)_4(aq)$	-53.500 ± 0.245^b	9.37 ± 0.04	$-1 245.195 \pm 1.283^b$	-72.700 ± 0.966	$-1 319.230 \pm 3.053$
Tephroite					
$Mn_2SiO_4(cr) + 4H^+ \rightleftharpoons 2Mn^{2+} + Si(OH)_4(aq)$	-132.700 ± 1.895^b	23.25 ± 0.33	$-1 631.235 \pm 2.434$	-170.600 ± 2.261^b	$-1 727.960 \pm 4.014$
Braunite					
$Mn_7SiO_{12} + 14H^+ \rightleftharpoons 7Mn^{2+} + 1.5O_2(aq) + Si(OH)_4(aq) + 5H_2O$	-120.433 ± 0.754^b	21.099 ± 0.132	$-3 945.135 \pm 4.000$	-192.150 ± 2.846^b	$-4 257.110 \pm 4.000$

a [1974NAU/RYZ]; b [1995ROB/HEM]; c [1990NOR/PLU]

* calculated from $\Delta_f G_m^\circ$ or $\Delta_f H_m^\circ$ in [2016BRO/EKB], unless noted otherwise.

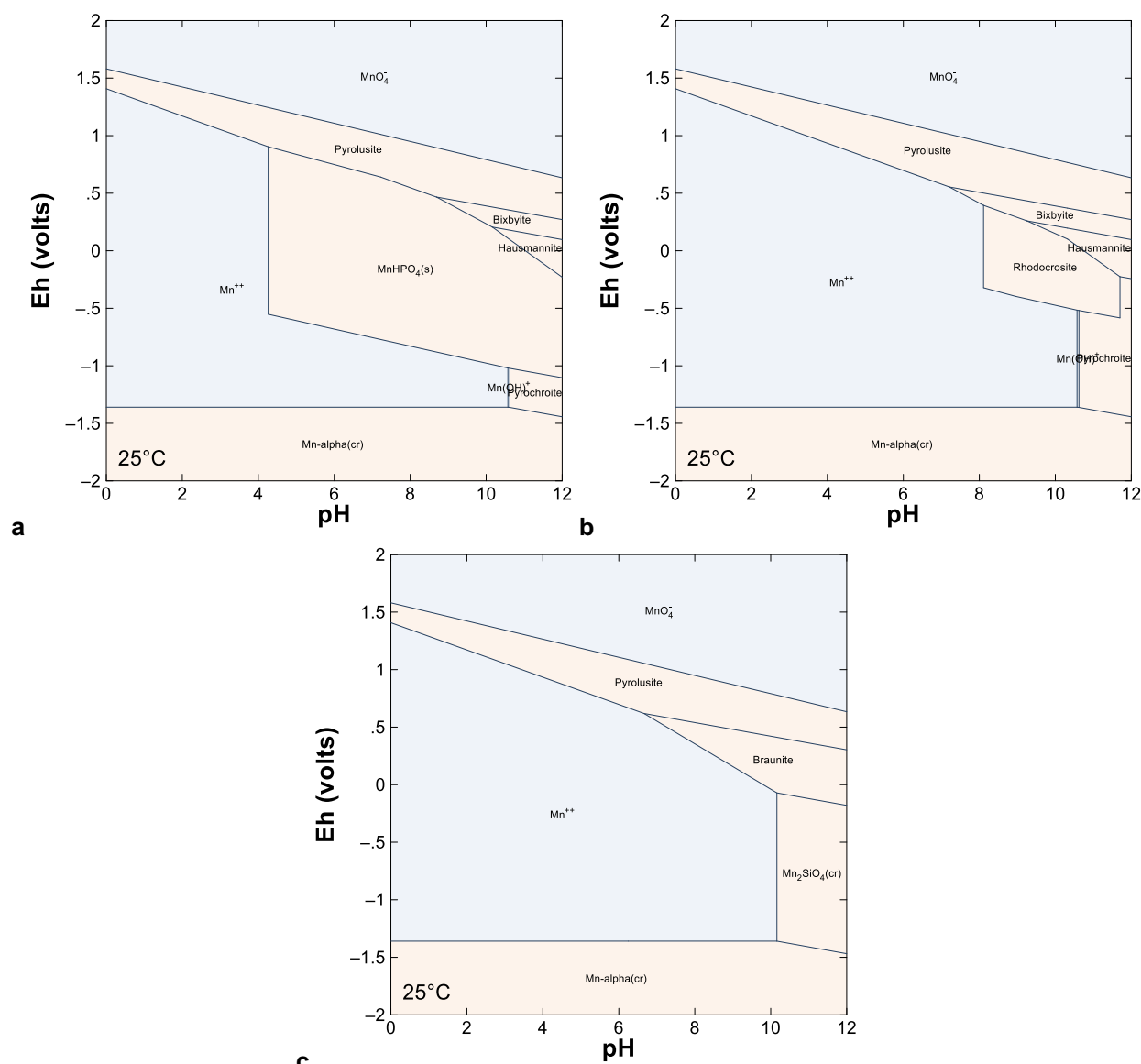


Figure 3.7-40. Pourbaix diagram (GWB) of $10^{-6} \text{ mol kg}^{-1} \text{ Mn}$ and $10^{-4} \text{ mol kg}^{-1} \text{ P}$ (a), $10^{-3} \text{ mol kg}^{-1} \text{ C}$ (b), and at equilibrium with quartz (SiO_2) (c).

3.7.10. Molybdenum

Molybdenum is often associated with uranium ores and can be a secondary contaminant.

3.7.10.1. Native Element and Free Ions

Native metallic $\text{Mo}(\text{cr})$, molybdenum free ion Mo^{3+} , $\text{MoO}_4(\text{aq})$ [1985BAR/PAR], and MoO_4^{2-} [1974OHA]. The common master species is MoO_4^{2-} .

3.7.10.2. Oxides and Molybdates

Molybdenum(IV) oxide ($\text{MoO}_2(\text{cr})$) [1985BAR/PAR], and molybdenum(VI) oxide (molybdite, $\text{MoO}_3(\text{cr})$) [1985BAR/PAR; 1995ROB/HEM]. It can be noted that no solution species is defined in Robie and Hemingway [1995ROB/HEM], which precludes any correction.

The solubility of molybdic acid ($\text{H}_2\text{MoO}_4(\text{cr})$) is taken from Bard *et al.* [1985BAR/PAR].

The acidity of molybdate ion to $\text{H}_2\text{MoO}_4(\text{aq})$, HMnO_4^- [1975CRU/ROH; 1997aSHO/SAS], and H_3MoO_4^+ [1976CRU/HEY] is included.

The solubility of $\text{Ag}_2\text{MoO}_4(\text{cr})$, $\text{PbMoO}_4(\text{cr})$, $\text{FeMoO}_4(\text{cr})$ are taken from Wagman *et al.* [1982WAG/EVA].

3.7.10.3. Sulphur Compounds

Molybdenum sulphide $\text{MoS}_2(\text{cr})$, $\text{MoS}_3(\text{cr})$, $\text{Mo}_2\text{S}_3(\text{cr})$ are taken from Bard *et al.* [1985BAR/PAR] and Robie and Hemingway [1995ROB/HEM].

3.7.10.4. Thermodynamic Functions and Constants for Mo

Table 3.7-43. Thermodynamic functions and constants of Mo compounds.

Reaction	$\Delta_r G_m^\circ$ kJ mol ⁻¹	$\log_{10} K^\circ$	$\Delta_f G_m^\circ$ kJ mol ⁻¹	$\Delta_r H_m^\circ$ kJ mol ⁻¹	$\Delta_f H_m^\circ$ kJ mol ⁻¹
$\text{Mo}(\text{cr}) + 1.5\text{O}_2(\text{g}) + \text{H}_2\text{O} \rightleftharpoons \text{MoO}_4^{2-} + 2\text{H}^+$	-599.470 ± 2.930	105.02 ± 0.51	$-836.610 \pm 2.930^{\text{a}}$	-711.170 ± 0.799	$-997.000 \pm 0.800^{\text{a}}$
$\text{Mo}(\text{cr}) + 1.5\text{O}_2(\text{aq}) + \text{H}_2\text{O} \rightleftharpoons \text{MoO}_4^{2-} + 2\text{H}^+$	-624.037 ± 2.604	109.33 ± 0.46		-693.620 ± 1.079	
$\text{MoO}_4^{2-} + 3\text{e}^- + 8\text{H}^+ \rightleftharpoons \text{Mo}^{3+} + 4\text{H}_2\text{O}$	-167.855	29.41^{b}	-55.905		
$\text{MoO}_4^{2-} + 5\text{H}^+ \rightleftharpoons \text{Mo}^{3+} + 0.75\text{O}_2(\text{aq}) + 2.5\text{H}_2\text{O}$	200.139	-35.06			
$\text{MoO}_4^{2-} \rightleftharpoons \text{MoO}_4(\text{aq}) + 2\text{e}^-$	258.200	-45.23^{b}	-578.410		
$\text{MoO}_4^{2-} + 0.5\text{O}_2(\text{aq}) + 2\text{H}^+ \rightleftharpoons \text{MoO}_4(\text{aq}) + \text{H}_2\text{O}$	12.871	-2.25			
$\text{MoO}_2(\text{cr}) + 0.5\text{O}_2(\text{aq}) + \text{H}_2\text{O} \rightleftharpoons \text{MoO}_4^{2-} + 2\text{H}^+$	-74.649	13.08	-533.010^{b}	-116.380	-588.940^{b}
Molybdate					
$\text{MoO}_3 + \text{H}_2\text{O} \rightleftharpoons \text{MoO}_4^{2-} + 2\text{H}^+$	68.630 ± 2.902	-12.02 ± 0.51	$-668.100 \pm 0.400^{\text{c}}$	34.030 ± 0.692	$745.200 \pm 0.400^{\text{c}}$
$\text{H}_2\text{MoO}_4(\text{cr}) \rightleftharpoons \text{MoO}_4^{2-} + 2\text{H}^+$	75.390	-13.21	-912.000^{a}	49.000	$-1\,046.000^{\text{a}}$
$\text{MoO}_4^{2-} + \text{H}^+ \rightleftharpoons \text{HMnO}_4^-$	-23.803 ± 0.399	$4.17 \pm 0.07^{\text{d}}$	-860.413 ± 2.957	-0.837^{e}	-997.837
$\text{MoO}_4^{2-} + 2\text{H}^+ \rightleftharpoons \text{H}_2\text{MoO}_4(\text{aq})$	-47.605 ± 0.565	$8.34 \pm 0.10^{\text{d}}$	-884.215 ± 2.984	-10.500^{e}	$-1\,007.500$
$\text{MoO}_4^{2-} + 3\text{H}^+ \rightleftharpoons \text{H}_3\text{MoO}_4^+$	-55.825 ± 0.576	$9.78 \pm 0.10^{\text{f}}$	-892.435 ± 2.986		
$\text{PbMoO}_4(\text{cr}) \rightleftharpoons \text{Pb}^{2+} + \text{MoO}_4^{2-}$	$90.670 \pm 1.223^{\text{g}}$	-15.88 ± 0.21	-951.518 ± 3.200	$55.820 \pm 7.151^{\text{g}}$	$1\,051.900 \pm 7.200$
$\text{Ag}_2\text{MoO}_4(\text{cr}) \rightleftharpoons 2\text{Ag}^+ + \text{MoO}_4^{2-}$	$-0.186 \pm 6.569^{\text{g}}$	0.03 ± 1.15	-682.232 ± 7.200	$1.180 \pm 4.730^{\text{g}}$	-786.600 ± 4.800
$\text{FeMoO}_4(\text{cr}) \rightleftharpoons \text{Fe}^{2+} + \text{MoO}_4^{2-}$	$59.800 \pm 39.887^{\text{g}}$	-10.48 ± 6.99	$-1\,075.295 \pm 40.000$	$-12.000 \pm 39.989^{\text{g}}$	987.129 ± 40.000
Molybdenite					
$\text{MoS}_2 + 0.5\text{O}_2(\text{aq}) + 3\text{H}_2\text{O} \rightleftharpoons \text{MoO}_4^{2-} + 2\text{HS}^- + 4\text{H}^+$	153.907 ± 1.501	-26.96 ± 0.26	$-262.800 \pm 4.900^{\text{c}}$	105.540 ± 3.819	$-271.800 \pm 4.900^{\text{c}}$
$\text{MoS}_3(\text{cr}) + 4\text{H}_2\text{O} \rightleftharpoons \text{MoO}_4^{2-} + 3\text{HS}^- + 5\text{H}^+$	386.402	-67.69	-237.723^{b}	354.650	-257.230^{b}
$\text{Mo}_2\text{S}_3 + 3\text{H}^+ \rightleftharpoons 2\text{Mo}^{3+} + 3\text{HS}^-$	318.650^{b}	-55.825	-397.321		

a [1974OHA]; b [1985BAR/PAR]; c [1995ROB/HEM]; d [1975CRU/ROH], e [1997aSHO/SAS]; f [1976CRU/HEY]; g [1982WAG/EVA].

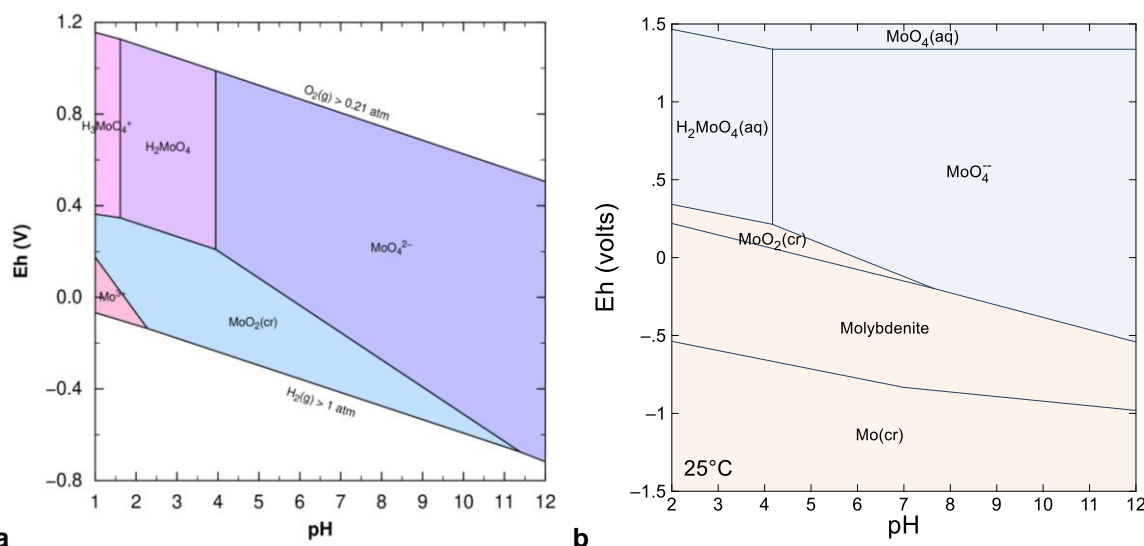


Figure 3.7-41. Pourbaix diagram of 10^{-6} mol $\text{kg}_{\text{w}}^{-1}$ Mo in a hypothetical indifferent $0.1 \text{ mol kg}_{\text{w}}^{-1}$ electrolyte solution using PHREEPLOT (a), and with 10^{-4} mol $\text{kg}_{\text{w}}^{-1}$ S using GWB (b); all solid phases are allowed to precipitate.

3.7.11. Vanadium

Vanadium forms insoluble vanadate compounds with uranium.

3.7.11.1. Native Element and Free Ions

The functions of formation for vanadium(V) have been recently selected in NEA-OECD review [2020GRE/GAO], with some data being nevertheless selected from another compilation,* which is unusual for the NEA-OECD reviews. The hydrolysis of V(V) is not accounted and only V(cr), $\text{V}_2\text{O}_5(\text{cr})$, VO_2^+ , and VO_4^{3-} are reported. The Gibbs energies of formation of V^{2+} , V^{3+} , and VO^{2+} are available in Brown and Ekberg [2016BRO/EKB] — from the data in Bard *et al.* [1985BAR/PAR] —, with estimation of the uncertainties.

Due to the importance of V(V) chemistry on uranium, the common master species could be either VO_2^+ or H_2VO_4^- .

There is discrepancy between values of $\Delta_f G^\circ(\text{V}^{3+})$ within vanadium analysis in Bard *et al.* [1985BAR/PAR]. In Table 1 p. 509 $\Delta_r G^\circ(\text{V}^{3+}) = -251.3 \text{ kJ mol}^{-1}$ [1985BAR/PAR], and later in the text another value is recalled from Hill *et al.* [1971HIL/WOR] $\Delta_f G^\circ(\text{V}^{3+}) = -242.3 \text{ kJ mol}^{-1}$ [1985BAR/PAR, p. 522],

Shock *et al.* [1997aSHO/SAS] estimated the function of formation of different vanadium species, which is leading to slightly different redox potentials compared to the selection of Brown and Ekberg [2016BRO/EKB] — and thus of Bard *et al.* [1985BAR/PAR] —, mainly because of a very different value between $\Delta_f G^\circ(\text{V}^{3+}) = -57.9 \text{ kcal mol}^{-1}$ or $-242.3 \text{ kJ mol}^{-1}$ [1997aSHO/SAS], and $-251.3 \text{ kJ mol}^{-1}$ [1985BAR/PAR] Table 1 p. 509. It can be noticed that the value from Shock *et al.* [1997aSHO/SAS] is in agreement with the standard potential determined or selected elsewhere [1944JON/COL; 1971HIL/WOR]. It is then highly probable that the value in Table 1 from Bard *et al.* [1985BAR/PAR] is a misprint. Hence, in PRODATA the value of $\Delta_f G^\circ(\text{V}^{3+}) = -242.3 \text{ kJ mol}^{-1}$ [1944JON/COL; 1971HIL/WOR; 1997aSHO/SAS], will be used.

* <http://www.chem.msu.su/rus/tsiv/V/table.V.T7.html>

The enthalpy and entropy of formation for V^{3+} can be estimated from the experiments in Jones and Colvin [1944]JON/COL]. The authors reported the extrapolation of the $E^\circ(V^{3+}/V^{2+})$ at infinite dilution at 0 and 25°C: $E_{25^\circ C}^\circ(V^{3+}/V^{2+}) = 255.3 \pm 0.8$ mV and $E_0^\circ(V^{3+}/V^{2+}) = 265.4 \pm 1.0$ mV, which is giving $\Delta_r H^\circ = -(36.254 \pm 1.427)$ kJ mol⁻¹, and $\Delta_r S^\circ = -(38.980 \pm 4.792)$ J mol⁻¹ K⁻¹, and finally $\Delta_r G^\circ = -(24.633 \pm 2.019)$ kJ mol⁻¹. This allow attribution of the uncertainties

One can also note a slight difference in the functions of formation for VO_2^+ in Shock *et al.* [1997aSHO/SAS] ($\Delta_f G^\circ = -140.3$ kcal mol⁻¹ or -587.0 kJ mol⁻¹) and Brown and Ekberg [2016BRO/EKB] ($\Delta_f G^\circ = -587.0 \pm 1.0$ kJ mol⁻¹) — taken from Bard *et al.* [1985BAR/PAR] —, and in the NEA-OECD selection [2020GRE/GAO] ($\Delta_f G_m^\circ(VO_2^+) = -590.28$ kJ mol⁻¹). The latter authors re-analysed original V_2O_5 (cr) solubility data and extrapolated the obtained $\log_{10} K_s$ to zero ionic strength. The function of formation of the different hydrolysed species in Grenthe *et al.* [2020GRE/GAO] are recalculated within PRODATA using Brown and Ekberg [2016BRO/EKB], but all the vanadium data will have to be recalculated in coherence with the extrapolation to infinite dilution of VO_2^+ using the standard potential values.

Table 3.7-44. Comparison of the Gibbs energies of reaction, $\log_{10}\beta^\circ$ and E_h° calculated from Shock *et al.* [1997aSHO/SAS] — H₂O from Helgeson and Kirkham [1974aHEL/KIR] — and Brown and Ekberg [2016BRO/EKB] for vanadium free ions.

Reaction	[1997aSHO/SAS]				[2016BRO/EKB]		
	$\Delta_r G^\circ$ kcal mol ⁻¹	$\Delta_r G^\circ$ kJ mol ⁻¹	$\log_{10}\beta^\circ$	E_h° V	$\Delta_r G^\circ$ kJ mol ⁻¹	$\log_{10}\beta^\circ$	E_h° V
$V^{2+} \rightleftharpoons V^{3+} + e^-$	-5.9	-24.7	4.32	0.256	-33.300	5.83	0.345
$V^{2+} + H_2O \rightleftharpoons VO^{2+} + 2e^- + 2H^+$	1.987	8.314	-1.46	-0.086	8.740	-1.53	-0.091
$V^{2+} + 2H_2O \rightleftharpoons VO_2^+ + 3e^- + 4H^+$	25.074	104.910	-18.38	1.087	105.280	-18.44	1.091
$V^{3+} + H_2O \rightleftharpoons VO^{2+} + e^- + 2H^+$	7.887	32.999	-5.78	0.342	42.040	-7.37	0.436
$V^{3+} + 2H_2O \rightleftharpoons VO_2^+ + 2e^- + 4H^+$	30.974	129.595	-22.70	0.672	279.180	-48.91	1.447
$VO^{2+} + H_2O \rightleftharpoons VO_2^+ + e^- + 2H^+$	23.087	96.596	16.92	1.001	96.540	-16.91	1.001
$V(\text{cr}) + 2H_2O \rightleftharpoons VO_2^+ + 5e^- + 4H^+$	-26.926	-112.658	-19.74	-0.234	-116.000	20.32	-0.240

The calculation of the Gibbs energies of reaction from the standard redox potentials from the Latimer's diagram page 522 in Bard *et al.* [1985BAR/PAR] can be seen afterwards, considering $\Delta_f G_m^\circ(V(\text{cr})) = 0$ and $\Delta_f G_m^\circ(H_2O) = -(237.140 \pm 0.041)$ kJ mol⁻¹ [1992GRE/FUG; 2003GUI/FAN; 2020GRE/GAO].

$V^{2+} + 2e^- \rightleftharpoons V(\text{cr})$	$E_h^\circ = -1.13$ V	$\Delta_r G^\circ = 218.056$ kJ mol ⁻¹	$\log_{10}\beta^\circ = -38.20$	$\Delta_f G^\circ(V^{2+}) = -218.056$ kJ mol ⁻¹
$V^{3+} + e^- \rightleftharpoons V^{2+}$	$E_h^\circ = -0.255$ V	$\Delta_r G^\circ = 24.604$ kJ mol ⁻¹	$\log_{10}\beta^\circ = -4.31$	$\Delta_f G^\circ(V^{3+}) = -242.660$ kJ mol ⁻¹
$VO^{2+} + e^- + 2H^+ \rightleftharpoons V^{3+} + H_2O$	$E_h^\circ = 0.337$ V	$\Delta_r G^\circ = -32.515$ kJ mol ⁻¹	$\log_{10}\beta^\circ = -5.70$	$\Delta_f G^\circ(VO^{2+}) = -447.285$ kJ mol ⁻¹
$VO_2^+ + e^- + 2H^+ \rightleftharpoons VO^{2+} + H_2O$	$E_h^\circ = 1.000$ V	$\Delta_r G^\circ = -96.485$ kJ mol ⁻¹	$\log_{10}\beta^\circ = -16.90$	$\Delta_f G^\circ(VO_2^+) = -587.940$ kJ mol ⁻¹
$VO_2^+ + 5e^- + 4H^+ \rightleftharpoons V(\text{cr}) + 2H_2O$	$\Delta_r G^\circ = 113.660$ kJ mol ⁻¹	$\log_{10}\beta^\circ = -19.91$		$E_h^\circ = -0.236$ V
$VO_2^+ + 3e^- + 4H^+ \rightleftharpoons V^{2+} + 2H_2O$	$\Delta_r G^\circ = -104.396$ kJ mol ⁻¹	$\log_{10}\beta^\circ = -18.29$		$E_h^\circ = 0.361$ V
$VO_2^+ + 2e^- + 4H^+ \rightleftharpoons V^{3+} + 2H_2O$	$\Delta_r G^\circ = -129.000$ kJ mol ⁻¹	$\log_{10}\beta^\circ = -22.60$		$E_h^\circ = 0.668$ V

Hence, the value of $\Delta_f G^\circ(V^{3+})$ in Table 1 from Bard *et al.* [1985BAR/PAR], selected by Brown and Ekberg [2016BRO/EKB], will not be used as the calculated standard redox potential implying V^{3+} are over estimated, at least regarding Latimer's diagram page 522 in Bard *et al.* [1985BAR/PAR], reproduced in Figure 3.7-42.

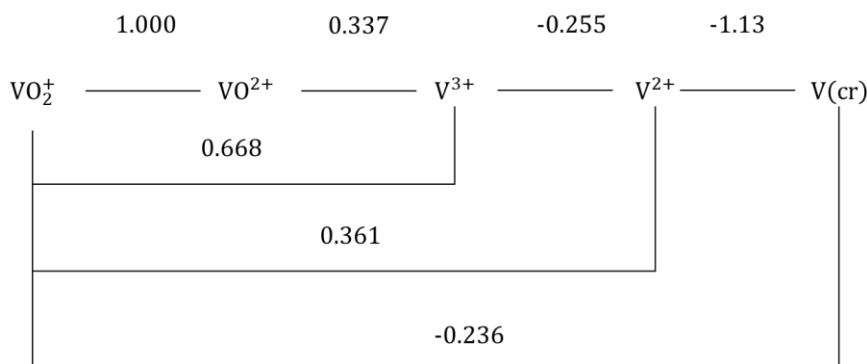


Figure 3.7-42. Latimer diagram for vanadium native metal and free ions [1985BAR/PAR].

3.7.11.2. Oxo, Hydroxo, Chloride and Sulphate Compounds

The functions of reaction of $\text{VO}(\text{cr})$, $\text{V}_2\text{O}_3(\text{cr})$, and $\text{V}_2\text{O}_4(\text{cr})$ can be calculated from Wagman *et al.* [1982WAG/EVA]. The Gibbs energy of formation of $\text{V}_2\text{O}_3 \cdot \text{H}_2\text{O}(\text{s})$ is taken from Brown and Ekberg [2016BRO/EKB].

Brown and Ekberg [2016BRO/EKB] provided a thorough proposition of hydrolysis reactions from which hydrolysis constants of the mononuclear and polynuclear species have been proposed. The $\log_{10} * \beta_n^\circ$ values in Brown and Ekberg [2016BRO/EKB] are accompanied by $\Delta \varepsilon_1$ and $\Delta \varepsilon_2$ (Eq. 21) values. In only two instances the $\Delta \varepsilon_2$ value is nil: $\text{VO}_2(\text{OH})(\text{aq})$ and $\text{VO}_2(\text{OH})_2^- — \text{H}_3\text{VO}_4(\text{aq})$ and H_2VO_4^- .

As the authors did not provide estimations of $\varepsilon(\text{V}^{2+}, \text{X}^-)$, $\varepsilon(\text{V}^{3+}, \text{X}^-)$, $\varepsilon(\text{VO}^{2+}, \text{X}^-)$, or $\varepsilon(\text{VO}_2^+, \text{X}^-)$. The proposition of Thoenen *et al.* [2014THO/HUM] gives $\varepsilon(\text{V}^{2+}, \text{Cl}^-) = (0.15 \pm 0.10) \text{ kg}_w \text{ mol}^{-1}$, $\varepsilon(\text{V}^{3+}, \text{Cl}^-) = (0.25 \pm 0.10) \text{ kg}_w \text{ mol}^{-1}$, $\varepsilon(\text{VO}^{2+}, \text{Cl}^-) = (0.15 \pm 0.10) \text{ kg}_w \text{ mol}^{-1}$, and $\varepsilon(\text{VO}_2^+, \text{Cl}^-) = (0.05 \pm 0.10) \text{ kg}_w \text{ mol}^{-1}$. This allows calculating $\varepsilon(\text{VO}_2(\text{OH})(\text{aq}), \text{Na}^+\text{ClO}_4^-) = \varepsilon(\text{H}_3\text{VO}_4(\text{aq}), \text{Na}^+\text{ClO}_4^-) = (0.25 \pm 0.24) \text{ kg}_w \text{ mol}^{-1}$ from $\Delta \varepsilon_1 = (0.30 \pm 0.20) \text{ kg}_w \text{ mol}^{-1}$, and $\varepsilon(\text{VO}_2(\text{OH})_2^-, \text{Na}^+) = \varepsilon(\text{H}_2\text{VO}_4^-, \text{Na}^+) = (0.36 \pm 0.25) \text{ kg}_w \text{ mol}^{-1}$ from $\Delta \varepsilon_1 = (0.55 \pm 0.23) \text{ kg}_w \text{ mol}^{-1}$.

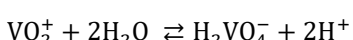
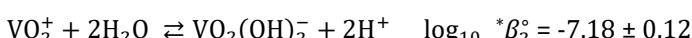
As PHREEQC does not support Eq. 21, some of the variations have been reinterpreted. The variation of the following stepwise reactions are plotted in Figure 3.7-43,



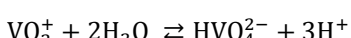
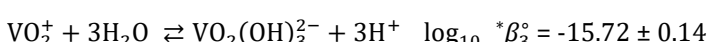
which were interpreted using Eq. 21 (dashed line).

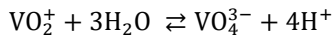
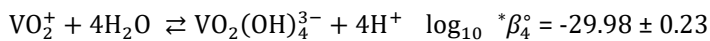
The reinterpretation using Eq. 18 (solid line) gives $\log_{10} K_3^\circ = 5.46 \pm 0.08$ or $\log_{10} * K_3^\circ = -8.54 \pm 0.08$, and $\Delta \varepsilon = -(0.07 \pm 0.06) \text{ kg}_w \text{ mol}^{-1}$; the second hydrolysis gives $\log_{10} K_4^\circ = -0.27 \pm 0.18$ or $\log_{10} * K_4^\circ = -14.27 \pm 0.18$, and $\Delta \varepsilon = -(0.05 \pm 0.10) \text{ kg}_w \text{ mol}^{-1}$

Using the value of,



the cumulative reactions can be written as follows.





The $\varepsilon(\text{VO}_2(\text{OH})_3^{2-}, \text{Na}^+) = \varepsilon(\text{HVO}_4^{2-}, \text{Na}^+) = (0.33 \pm 0.27) \text{ kg}_w \text{ mol}^{-1}$, and $\varepsilon(\text{VO}_2(\text{OH})_4^{3-}, \text{Na}^+) = \varepsilon(\text{VO}_4^{3-}, \text{Na}^+) = (0.32 \pm 0.29) \text{ kg}_w \text{ mol}^{-1}$ can be proposed.

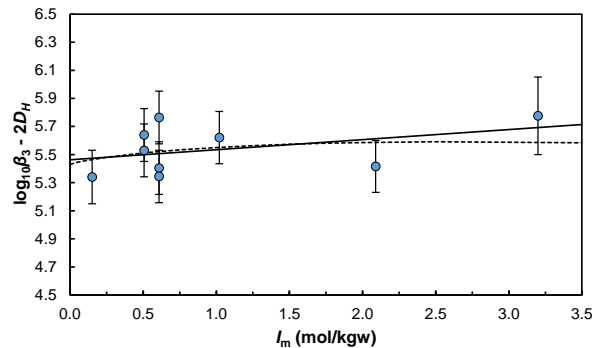
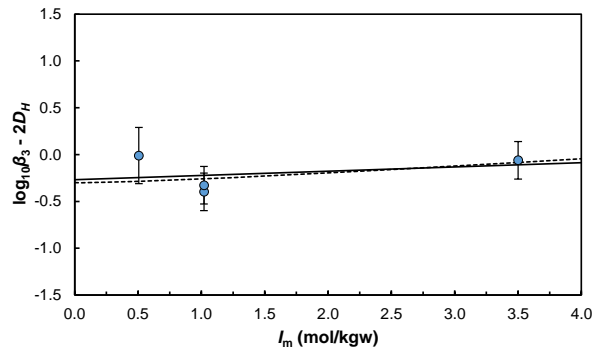
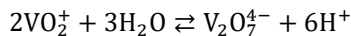
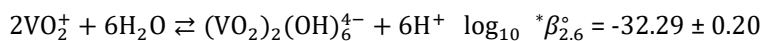
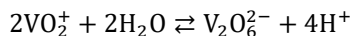
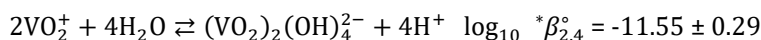
**a****b**

Figure 3.7-43. Dependence of (a) $\log_{10}K_3^\circ$ of $\text{VO}_2(\text{OH})_3^{2-}$ (HVO_4^{2-}) and (b) $\log_{10}K_4^\circ$ of $\text{VO}_2(\text{OH})_4^{3-}$ (VO_4^{3-}) vs. ionic strength in $\text{NaCl}/\text{NaClO}_4$: the dashed line is obtained using the interaction coefficients and stability constants at zero ionic strength from Brown and Ekberg [2016BRO/EKB], and solid line represents the linear fittings.

For the sake of inner coherency some of the polynuclear species can be reanalysed using Eq. 18. The dimerization of $\text{VO}_2(\text{OH})_3^{2-}$ (HVO_4^{2-}) to $(\text{VO}_2)_2(\text{OH})_6^{4-}$ ($\text{V}_2\text{O}_7^{4-}$), and of $\text{VO}_2(\text{OH})_2^-$ (H_2VO_4^-) to $(\text{VO}_2)_2(\text{OH})_4^{2-}$ ($\text{V}_2\text{O}_6^{2-}$) are represented in Figure 3.7-44. The dimerization constant $\log_{10} K_D^\circ (\text{V}_2\text{O}_7^{4-}) = -0.86 \pm 0.05$ and $\log_{10} * \beta_2^\circ$ are giving the following reaction,



the dimerization constant $\log_{10} K_D^\circ (\text{V}_2\text{O}_6^{2-}) = 2.81 \pm 0.16$ and $\log_{10} * \beta_2^\circ$ are giving the following reaction,



The $\varepsilon((\text{VO}_2)_2(\text{OH})_6^{4-}, \text{Na}^+) = \varepsilon(\text{V}_2\text{O}_7^{4-}, \text{Na}^+) = (0.58 \pm 0.12) \text{ kg}_w \text{ mol}^{-1}$, and $\varepsilon((\text{VO}_2)_2(\text{OH})_4^{2-}, \text{Na}^+) = \varepsilon(\text{V}_2\text{O}_6^{2-}, \text{Na}^+) = (0.87 \pm 0.51) \text{ kg}_w \text{ mol}^{-1}$ are obtained.

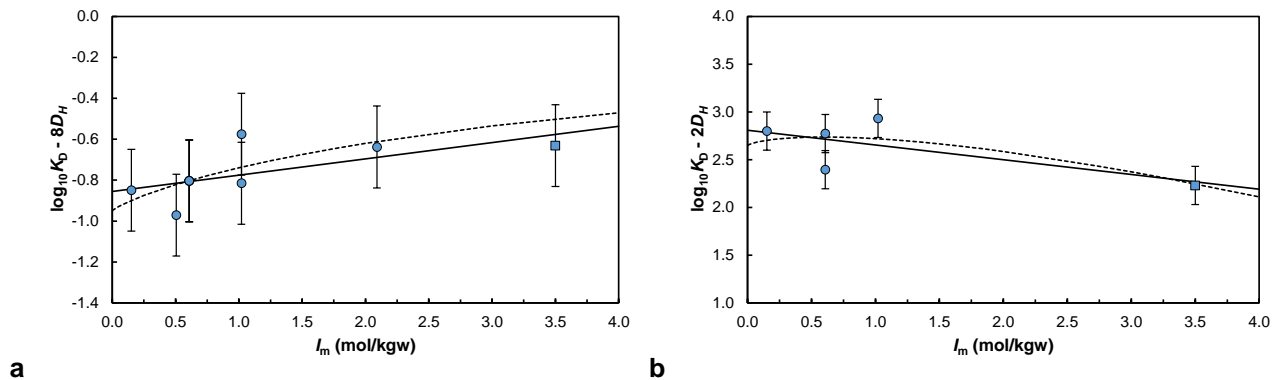
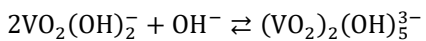


Figure 3.7-44. Dependence of $\log_{10} K^\circ d$ of (a) $(\text{VO}_2)_2(\text{OH})_6^{4-}$ ($\text{V}_2\text{O}_7^{4-}$) and (b) $(\text{VO}_2)_2(\text{OH})_4^{2-}$ ($\text{V}_2\text{O}_6^{2-}$) on ionic strength in NaCl (circles) and NaClO₄ (squares): the dashed line is obtained using the interaction coefficients and stability constants at zero ionic strength from Brown and Ekberg [2016BRO/EKB], and solid line represents the linear fittings.

The hydroxylation reaction,



can be re-estimated from Figure 3.7-45 to $\log_{10} K^\circ = 7.36 \pm 0.09$ and $\Delta\varepsilon = (0.00 \pm 0.05) \text{ kg}_w \text{ mol}^{-1}$.

This yields to the following cumulative formation.

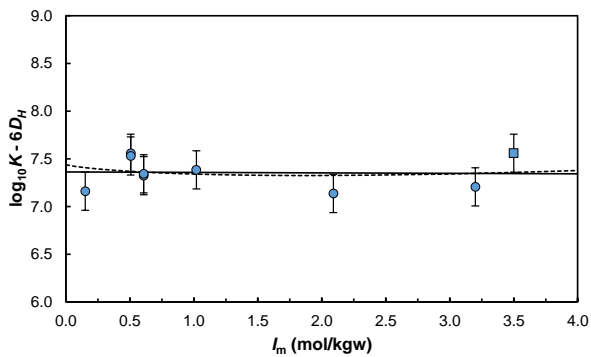
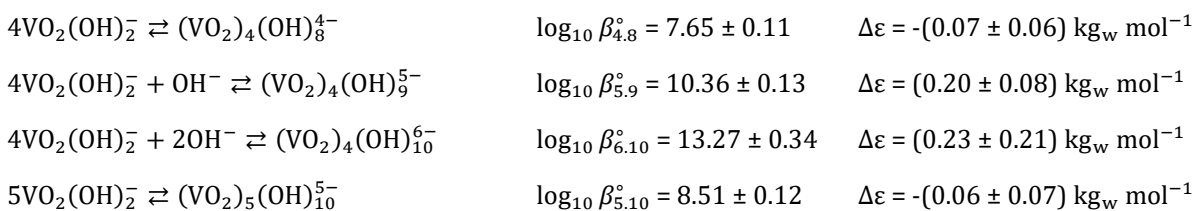


Figure 3.7-45. Dependence of $\log_{10} K^\circ$ of $(\text{VO}_2)_2(\text{OH})_5^{3-}$ ($\text{HV}_2\text{O}_7^{3-}$) on ionic strength in NaCl (circles) and NaClO₄ (squares): the dashed line is obtained using the interaction coefficients and stability constants at zero ionic strength from Brown and Ekberg [2016BRO/EKB] (Eq. 21), and solid line represents the linear fittings (Eq. 18).

The tetra- and pentamerization reactions can be reanalyzed in Figure 3.7-46 using both NaCl and NaClO₄ data — as done by Brown and Ekberg [2016BRO/EKB] — as follows.



In the light of recent work on multi-centered complexes [2020aSHA/REI; 2020bSHA/REI] evidencing differences in comportment between NaCl and NaClO₄, the fitting could be done considering only the NaCl data, which is only slightly increasing the quality of the adjustment in view of the very slight slope.

$4\text{VO}_2(\text{OH})_2^- \rightleftharpoons (\text{VO}_2)_4(\text{OH})_8^{4-}$	$\log_{10} K_{4.8}^\circ = 7.75 \pm 0.11$	$\Delta\varepsilon = -(0.08 \pm 0.11) \text{ kg}_w \text{ mol}^{-1}$
$4\text{VO}_2(\text{OH})_2^- + \text{OH}^- \rightleftharpoons (\text{VO}_2)_4(\text{OH})_9^{5-}$	$\log_{10} K_{5.9}^\circ = 10.49 \pm 0.13$	$\Delta\varepsilon = (0.38 \pm 0.11) \text{ kg}_w \text{ mol}^{-1}$
$4\text{VO}_2(\text{OH})_2^- + 2\text{OH}^- \rightleftharpoons (\text{VO}_2)_4(\text{OH})_{10}^{6-}$	$\log_{10} K_{6.10}^\circ = 13.73 \pm 0.20$	$\Delta\varepsilon = (0.90 \pm 0.20) \text{ kg}_w \text{ mol}^{-1}$
$5\text{VO}_2(\text{OH})_2^- \rightleftharpoons (\text{VO}_2)_5(\text{OH})_{10}^{5-}$	$\log_{10} K_{5.10}^\circ = 8.65 \pm 0.12$	$\Delta\varepsilon = (0.14 \pm 0.08) \text{ kg}_w \text{ mol}^{-1}$

The cumulative reactions can then be proposed.

$4\text{VO}_2^+ + 8\text{H}_2\text{O} \rightleftharpoons (\text{VO}_2)_4(\text{OH})_8^{4-} + 8\text{H}^+$	$\log_{10} {}^*\beta_{4.8}^\circ = -20.97 \pm 0.49$
$4\text{VO}_2^+ + 4\text{H}_2\text{O} \rightleftharpoons \text{V}_4\text{O}_{12}^{4-} + 10\text{H}^+$	$\varepsilon((\text{VO}_2)_4(\text{OH})_8^{4-}, \text{Na}^+) = \varepsilon(\text{V}_4\text{O}_{12}^{4-}, \text{Na}^+) = (1.52 \pm 1.01) \text{ kg}_w \text{ mol}^{-1}$
$4\text{VO}_2^+ + 9\text{H}_2\text{O} \rightleftharpoons (\text{VO}_2)_4(\text{OH})_9^{5-} + 9\text{H}^+$	$\log_{10} {}^*\beta_{4.9}^\circ = -32.23 \pm 0.50$
$4\text{VO}_2^+ + 10\text{H}_2\text{O} \rightleftharpoons \text{HV}_4\text{O}_{13}^{5-} + 9\text{H}^+$	$\varepsilon((\text{VO}_2)_4(\text{OH})_9^{5-}, \text{Na}^+) = \varepsilon(\text{HV}_4\text{O}_{13}^{5-}, \text{Na}^+) = (1.86 \pm 1.01) \text{ kg}_w \text{ mol}^{-1}$
$4\text{VO}_2^+ + 10\text{H}_2\text{O} \rightleftharpoons (\text{VO}_2)_4(\text{OH})_{10}^{6-} + 10\text{H}^+$	$\log_{10} {}^*\beta_{4.10}^\circ = -42.99 \pm 0.52$
$4\text{VO}_2^+ + 5\text{H}_2\text{O} \rightleftharpoons \text{V}_4\text{O}_{13}^{6-} + 10\text{H}^+$	$\varepsilon((\text{VO}_2)_4(\text{OH})_{10}^{6-}, \text{Na}^+) = \varepsilon(\text{V}_4\text{O}_{13}^{6-}, \text{Na}^+) = (2.38 \pm 1.02) \text{ kg}_w \text{ mol}^{-1}$
$5\text{VO}_2^+ + 10\text{H}_2\text{O} \rightleftharpoons (\text{VO}_2)_5(\text{OH})_{10}^{5-} + 10\text{H}^+$	$\log_{10} {}^*\beta_{5.10}^\circ = -27.25 \pm 0.61$
$5\text{VO}_2^+ + 5\text{H}_2\text{O} \rightleftharpoons \text{V}_5\text{O}_{15}^{5-} + 10\text{H}^+$	$\varepsilon((\text{VO}_2)_5(\text{OH})_{10}^{5-}, \text{Na}^+) = \varepsilon(\text{V}_5\text{O}_{15}^{5-}, \text{Na}^+) = (1.94 \pm 1.25) \text{ kg}_w \text{ mol}^{-1}$

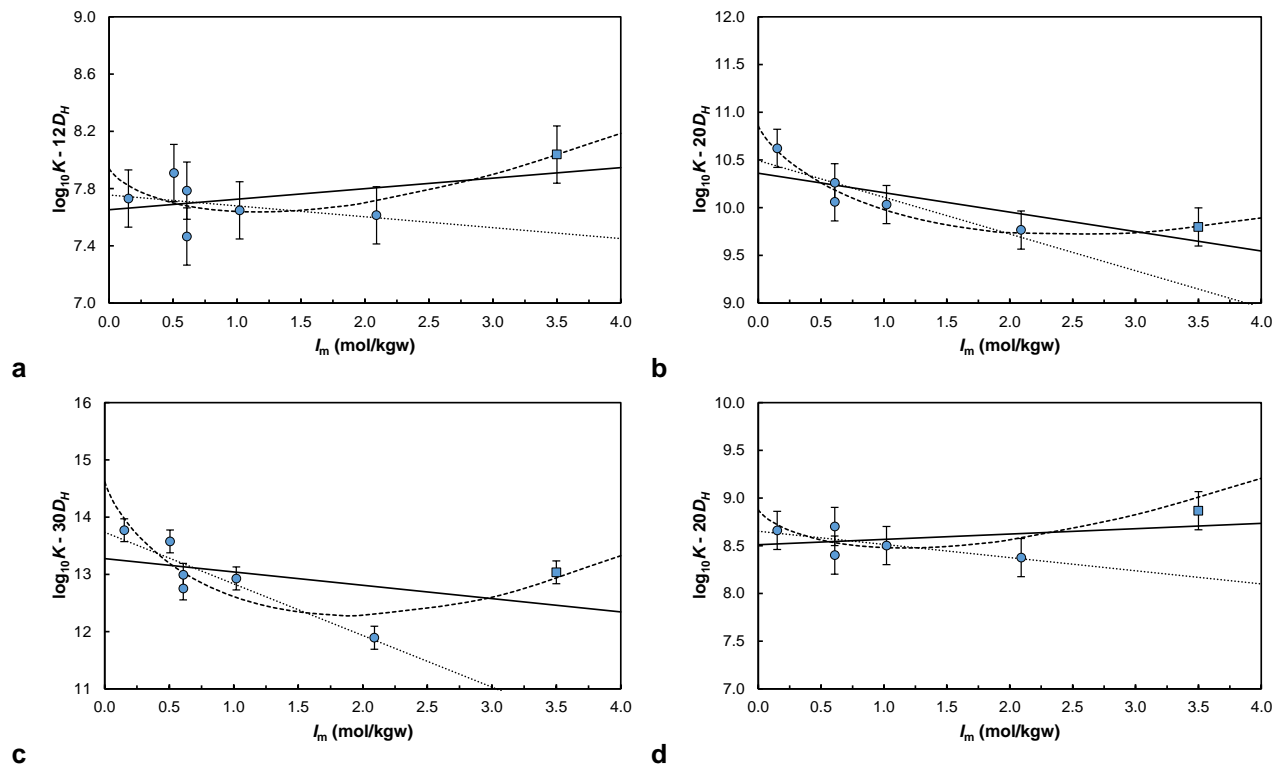
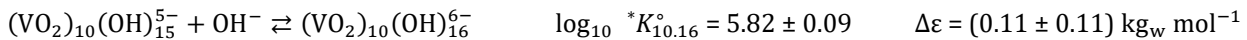
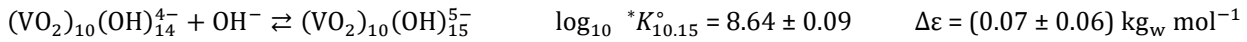
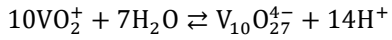


Figure 3.7-46. Dependence of $\log_{10} K^\circ$ of (a) $(\text{VO}_2)_4(\text{OH})_8^{4-}$ ($\text{V}_4\text{O}_{12}^{4-}$), (b) $(\text{VO}_2)_4(\text{OH})_9^{5-}$ ($\text{HV}_4\text{O}_{13}^{5-}$), (c) $(\text{VO}_2)_4(\text{OH})_{10}^{6-}$ ($\text{V}_4\text{O}_{13}^{6-}$), and (d) $(\text{VO}_2)_5(\text{OH})_{10}^{5-}$ ($\text{V}_5\text{O}_{15}^{5-}$) on ionic strength in NaCl (circles) and NaClO₄ (squares): the dashed line is obtained using the interaction coefficients and stability constants at zero ionic strength from Brown and Ekberg [2016BRO/EKB] (Eq. 21), and solid lines represent the linear fittings (Eq. 18) — the linear fitting on NaCl only are plotted in dotted line.

Finally, the decamerization reactions can be reanalyzed. Even if $(VO_2)_{10}(OH)_{16}^{6-}$ is not showing a $\Delta\epsilon_2$ value, it is also reanalyzed to provide the final cumulative constant. For $(VO_2)_{10}(OH)_{14}^{4-}$ only the data at 25°C are used in the extrapolation — but are plotted with an empty symbol —, and the data at zero ionic strength from Baes and Mesmer [1976BAE/MES] is not included. All the data at 20 and 25°C are used for $(VO_2)_{10}(OH)_{15}^{5-}$ and $(VO_2)_{10}(OH)_{16}^{6-}$.



For the formation of $(VO_2)_{10}(OH)_{14}^{4-}$, only data in $NaClO_4$ are available, which implies the use of $\epsilon(VO_2^+, ClO_4^-) = (0.2 \pm 0.1) \text{ kg}_w \text{ mol}^{-1}$ from Thoenen *et al.* [2014THO/HUM] to estimate $\epsilon(V_{10}O_{27}^{4-}, Na^+) = -(0.25 \pm 1.05) \text{ kg}_w \text{ mol}^{-1}$. The final $\log_{10} * \beta_{10.15}^\circ$ and $\log_{10} * \beta_{10.16}^\circ$ can be calculated.

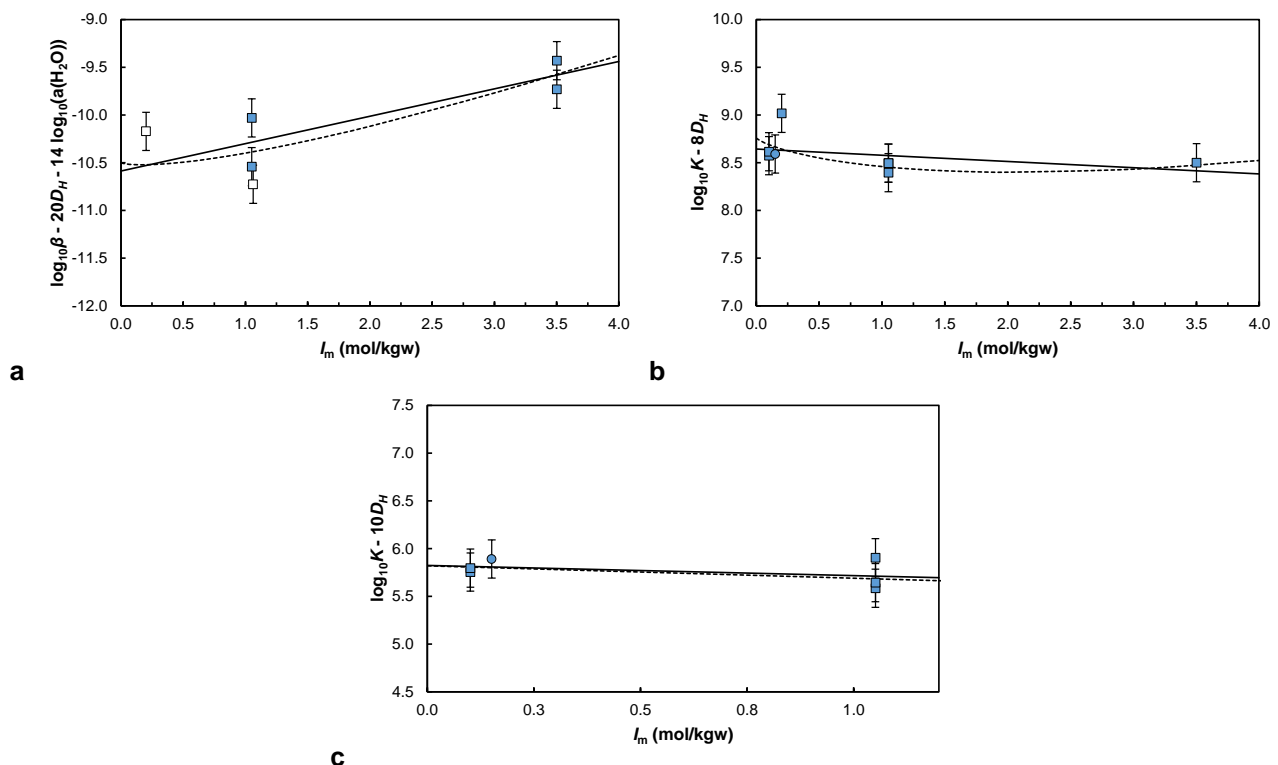
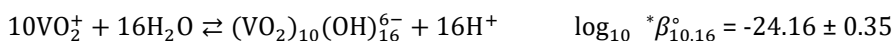
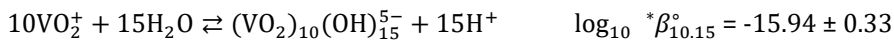


Figure 3.7-47. Dependence of $\log_{10}K^\circ$ of (a) $(VO_2)_{10}(OH)_{14}^{4-}$ ($V_{10}O_{27}^{4-}$), (b) $(VO_2)_{10}(OH)_{15}^{5-}$ ($HV_{10}O_{28}^{5-}$), and (c) $(VO_2)_{10}(OH)_{16}^{6-}$ ($V_{10}O_{28}^{6-}$) on ionic strength in $NaCl$ (circles) and $NaClO_4$ (squares): the dashed line is obtained using the interaction coefficients and stability constants at zero ionic strength from Brown and Ekberg [2016BRO/EKB] (Eq. 21), and solid line represents the linear fittings (Eq. 18).

The enthalpy and entropy values for V(V) hydrolysed mononuclear species are not selected in Brown and Ekberg [2016BRO/EKB]. As for redox species, they were estimated in Shock *et al.* [1997aSHO/SAS]. The obtained functions of reaction are relatively close. The $\Delta_r H^\circ$ values will be used rounded to the nearest integer values to calculate the $\Delta_f H^\circ$ values.

The functions of formation of $\text{VCl}_2(\text{cr})$, $\text{VCl}_3(\text{cr})$, $\text{VOCl}(\text{cr})$, $\text{VOCl}_2(\text{cr})$, and $\text{VO}_2\text{Cl}(\text{cr})$ are available in Wagman *et al.* [1982WAG/EVA].

Hill *et al.* [1971HIL/WOR] and Wagman *et al.* [1982WAG/EVA] reported the formation of VOSO_4 . The differences between the Vanadyl hydrolyses are generally minimal except for the formation of VO_4^{3-} . The values from Brown and Ekberg [2016BRO/EKB] will be preferred.

Reaction	[1982WAG/EVA]	[1971HIL/WOR]
$\text{VO}^{2+} + \text{SO}_4^{2-} \rightleftharpoons \text{VOSO}_4(\text{aq})$	$\Delta_r G^\circ = -(13.97 \pm 6.45) \text{ kJ mol}^{-1}$ $\log_{10} \beta^\circ = 2.45$	$\Delta_r G^\circ = -RT \ln(3.0 \cdot 10^2) = -14.14 \text{ kJ mol}^{-1}$ $\log_{10} \beta^\circ = 2.48$

Reaction	$\Delta_r G^\circ$ kJ mol ⁻¹	$\Delta_r H^\circ$ kJ mol ⁻¹	$\log_{10} \beta^\circ$	$\Delta_r G^\circ$ kJ mol ⁻¹	$\log_{10} \beta^\circ$
[1982WAG/EVA]					[1971HIL/WOR]
$\text{VO}_2^+ + 2\text{H}_2\text{O} \rightleftharpoons \text{H}_3\text{VO}_4(\text{aq}) + \text{H}^+$	18.719	30.669	-3.28	18.551	-3.25
$\text{VO}_2^+ + 2\text{H}_2\text{O} \rightleftharpoons \text{H}_2\text{VO}_4^- + 2\text{H}^+$	40.518	47.321	-7.10	40.984	-7.18
$\text{VO}_2^+ + 2\text{H}_2\text{O} \rightleftharpoons \text{HVO}_4^{2-} + 3\text{H}^+$	86.500	62.467	-15.15	89.845	-15.74
$\text{VO}_2^+ + 2\text{H}_2\text{O} \rightleftharpoons \text{VO}_4^{3-} + 4\text{H}^+$	162.230	89.245	-28.42	171.413	-30.03

Table 3.7-45. Thermodynamic constants and functions for native, free ions of vanadium, and dihydrogenovanadate ion.

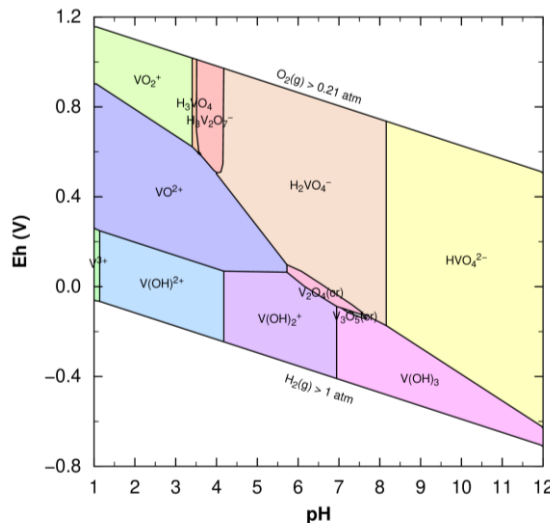
Reaction	$\Delta_r G_m^\circ$ kJ mol ⁻¹	$\log_{10} K^\circ$	$\Delta_f G_m^\circ$ kJ mol ⁻¹	$\Delta_r H_m^\circ$ kJ mol ⁻¹	$\Delta_f H_m^\circ$ kJ mol ⁻¹
$\text{V}(\text{cr}) \rightleftharpoons \text{V}^{2+} + 2\text{e}^-$	-218.000 ± 5.000	38.19 ± 0.88	$-218.000 \pm 5.000^{\text{a}}$	-225.936	-225.936 ^b
$\text{V}(\text{cr}) + 0.5\text{O}_2(\text{aq}) + 2\text{H}^+ \rightleftharpoons \text{V}^{2+} + \text{H}_2\text{O}$	-463.329 ± 4.980	81.17 ± 0.87		-505.916	
$\text{VO}_2^+ + 3\text{e}^- + 4\text{H}^+ \rightleftharpoons \text{V}^{2+} + 2\text{H}_2\text{O}$	-105.280 ± 4.900	18.44 ± 0.86	$-587.000 \pm 1.000^{\text{a}}$	-147.80	$-649.800 \pm 1.000^{\text{a}}$
$\text{VO}_2^+ + \text{H}^+ \rightleftharpoons \text{V}^{2+} + 0.75\text{O}_2(\text{aq}) + 0.5\text{H}_2\text{O}$	262.714 ± 4.945	-46.03 ± 0.86		272.174	
$\text{VO}_2^+ + 2\text{e}^- + 4\text{H}^+ \rightleftharpoons \text{V}^{3+} + 2\text{H}_2\text{O}$	$-129.534 \pm 0.082^{\text{b}}$	22.69 ± 0.01	-242.254 ± 1.000	-181.27 ^b	-259.408
$\text{VO}_2^+ + 2\text{H}^+ \rightleftharpoons \text{V}^{3+} + 0.5\text{O}_2(\text{aq}) + \text{H}_2\text{O}$	115.795 ± 0.450	-20.29 ± 0.08		98.712	
$\text{VO}_2^+ + \text{e}^- + 2\text{H}^+ \rightleftharpoons \text{VO}^{2+} + \text{H}_2\text{O}$	-96.540 ± 0.041	16.91 ± 0.01	$-446.4 \pm 1.000^{\text{a}}$	-122.63 ± 1.41	$-486.6 \pm 1.000^{\text{a}}$
$\text{VO}_2^+ + \text{H}^+ \rightleftharpoons \text{VO}^{2+} + 0.25\text{O}_2(\text{aq}) + 0.5\text{H}_2\text{O}$	26.125 ± 0.225	-4.58 ± 0.04		17.360 ± 1.432	
$\text{H}_2\text{VO}_4^- + 3\text{e}^- + 6\text{H}^+ \rightleftharpoons \text{V}^{2+} + 4\text{H}_2\text{O}$	-146.264 ± 4.891	25.62 ± 0.86	-1020.296 ± 1.050	-195.14	-1174.114
$\text{H}_2\text{VO}_4^- + 3\text{H}^+ \rightleftharpoons \text{V}^{2+} + 0.75\text{O}_2(\text{aq}) + 2.5\text{H}_2\text{O}$	221.730 ± 4.935	-38.85 ± 0.86		224.828	
$\text{H}_2\text{VO}_4^- + 2\text{e}^- + 6\text{H}^+ \rightleftharpoons \text{V}^{3+} + 4\text{H}_2\text{O}$	-170.518 ± 0.670	29.87 ± 0.12			
$\text{H}_2\text{VO}_4^- + 4\text{H}^+ \rightleftharpoons \text{V}^{3+} + 0.5\text{O}_2(\text{aq}) + 3\text{H}_2\text{O}$	74.811 ± 0.510	-13.11 ± 0.09			
$\text{H}_2\text{VO}_4^- + \text{e}^- + 4\text{H}^+ \rightleftharpoons \text{VO}^{2+} + 3\text{H}_2\text{O}$	-137.524 ± 0.296	24.09 ± 0.05		-169.98	
$\text{H}_2\text{VO}_4^- + 3\text{H}^+ \rightleftharpoons \text{VO}^{2+} + 0.25\text{O}_2(\text{aq}) + 2.5\text{H}_2\text{O}$	-14.859 ± 0.644	2.60 ± 0.11		-29.640	

a [2016BRO/EKB], b [1997aSHO/SAS].

Table 3.7-46. Thermodynamic functions and constants for oxides of V.

Reaction	$\Delta_r G_m^\circ$ kJ mol ⁻¹	$\log_{10} K^\circ$	$\Delta_f G_m^\circ$ kJ mol ⁻¹	$\Delta_r H_m^\circ$ kJ mol ⁻¹	$\Delta_f H_m^\circ$ kJ mol ⁻¹
$\text{VO}(\text{cr}) + 2\text{H}^+ \rightleftharpoons \text{V}^{2+} + \text{H}_2\text{O}$	$-50.935 \pm 4.962^{\text{a}}$	8.92 ± 0.87	-404.206 ± 0.620	-79.966^{a}	-431.800 ± 0.938
Karelianite $\text{V}_2\text{O}_3(\text{cr}) + 6\text{H}^+ \rightleftharpoons 2\text{V}^{3+} + 3\text{H}_2\text{O}$	$-74.720 \pm 1.321^{\text{a}}$	13.09 ± 0.23	$-1\ 139.3 \pm 2.4$		$-1\ 218.8 \pm 6.4^{\text{a}}$
Montroseite $\text{V}_2\text{O}_3 \cdot \text{H}_2\text{O}(\text{s}) + 6\text{H}^+ \rightleftharpoons 2\text{V}^{3+} + 4\text{H}_2\text{O}$	$-86.460 \pm 3.803^{\text{b}}$	15.15 ± 0.67	$-1\ 364.7 \pm 4.3$		
$\text{V}_2\text{O}_4(\text{cr}) + 4\text{H}^+ \rightleftharpoons 2\text{VO}^{2+} + 2\text{H}_2\text{O}$	$-48.780 \pm 1.324^{\text{a}}$	8.55 ± 0.23	$-1\ 318.3 \pm 2.4$	$-117.660 \pm 2.497^{\text{a}}$	$-1\ 427.2 \pm 3.2$
$\text{V}_2\text{O}_5(\text{cr}) + 2\text{H}^+ \rightleftharpoons 2\text{VO}_2^+ + \text{H}_2\text{O}$	$7.360 \pm 1.201^{\text{a}}$	-1.29 ± 0.21	$-1\ 418.5 \pm 1.6$	$-24.230 \pm 1.323^{\text{a}}$	$-1\ 561.2 \pm 1.5$
$\text{V}_2\text{O}_5(\text{s}) + 3\text{H}_2\text{O} \rightleftharpoons 2\text{H}_2\text{VO}_4^- + 2\text{H}^+$	89.328 ± 1.355	-15.65 ± 0.24		70.462	
$\text{V}_3\text{O}_5(\text{cr}) + 1.25\text{O}_2(\text{g}) + 3\text{H}^+ \rightleftharpoons 3\text{VO}_2^+ + 1.5\text{H}_2\text{O}$	$-334.183 \pm 7.500^{\text{a}}$	58.55 ± 1.31	$-1\ 803.000 \pm 8.000$	$-430.520 \pm 7.500^{\text{a}}$	$-1\ 933.000 \pm 8.000$
$\text{V}_3\text{O}_5(\text{cr}) + 1.25\text{O}_2(\text{aq}) + 4.5\text{H}_2\text{O} \rightleftharpoons 3\text{H}_2\text{VO}_4^- + 3\text{H}^+$	-211.231 ± 7.440	37.01 ± 1.30	$-1\ 803.0 \pm 8.0$	-288.482	$-1\ 933. \pm 8.$
$\text{V}_4\text{O}_7(\text{cr}) + 1.5\text{O}_2 + 4\text{H}^+ \rightleftharpoons 4\text{VO}_2^+ + 2\text{H}_2\text{O}$	$-390.847 \pm 47.852^{\text{a}}$	68.47 ± 8.38	$-2\ 456.000 \pm 48.000$	$-513.310 \pm 7.057^{\text{a}}$	$-2\ 640.000 \pm 8.000$
$\text{V}_4\text{O}_7(\text{cr}) + 1.5\text{O}_2(\text{aq}) + 6\text{H}_2\text{O} \rightleftharpoons 4\text{H}_2\text{VO}_4^- + 4\text{H}^+$	-226.911 ± 47.773	39.75 ± 8.37		-325.310	

a [1982WAG/EVA]; b [2016BRO/EKB].

**Figure 3.7-48. Pourbaix diagram of 10^{-6} mol kg_w⁻¹ vanadium in a 0.1 mol kg_w⁻¹ solution using PHREEPLOT; all solid phases are allowed to precipitate.****Table 3.7-47. Thermodynamic functions and constants for hydroxide complexes of V [2016BRO/EKB].**

Reaction	$\Delta_r G_m^\circ$ kJ mol ⁻¹	$\log_{10} K^\circ$	$\Delta_f G_m^\circ$ kJ mol ⁻¹	$\Delta_r H_m^\circ$ kJ mol ⁻¹	$\Delta_f H_m^\circ$ kJ mol ⁻¹
$\text{V}^{2+} + \text{H}_2\text{O} \rightleftharpoons \text{V}(\text{OH})^+ + \text{H}^+$	38.240 ± 1.757	-6.70 ± 0.31	-416.9 ± 5.3	34.372	-477.394
$\text{V}^{3+} + \text{H}_2\text{O} \rightleftharpoons \text{V}(\text{OH})^{2+} + \text{H}^+$	11.740 ± 0.456	-2.06 ± 0.08	-476.7 ± 1.1		-499.570
$\text{V}^{3+} + 2\text{H}_2\text{O} \rightleftharpoons \text{V}(\text{OH})_2^+ + \text{H}^+$	33.380 ± 0.676	-5.85 ± 0.12	-692.20 ± 1.21		-457.730
$\text{V}^{3+} + 3\text{H}_2\text{O} \rightleftharpoons \text{V}(\text{OH})_3(\text{aq}) + 3\text{H}^+$	71.946	-12.60	-890.774		
$2\text{V}^{3+} + 2\text{H}_2\text{O} \rightleftharpoons \text{V}_2(\text{OH})_2^{4+} + 2\text{H}^+$	18.680 ± 1.522	-3.27 ± 0.27	-958.2 ± 1.3		
$\text{VO}^{2+} + \text{H}_2\text{O} \rightleftharpoons \text{VO}(\text{OH})^+ + \text{H}^+$	30.240 ± 0.662	-5.30 ± 0.12	-653.3 ± 1.2	54.630 ± 5.001	-717.8 ± 5.1

Table 3.7-47. Continued.

Reaction	$\Delta_r G_m^\circ$ kJ mol ⁻¹	$\log_{10} K^\circ$	$\Delta_f G_m^\circ$ kJ mol ⁻¹	$\Delta_r H_m^\circ$ kJ mol ⁻¹	$\Delta_f H_m^\circ$ kJ mol ⁻¹
$2\text{VO}^{2+} + 2\text{H}_2\text{O} \rightleftharpoons (\text{VO})_2(\text{OH})_2^{2+} + 2\text{H}^+$	38.280 ± 1.325	-6.71 ± 0.23	$-1\ 328.8 \pm 1.5$	53.060 ± 4.799	$-1\ 491.8 \pm 5.2$
$\text{VO}_2^+ + 2\text{H}_2\text{O} \rightleftharpoons \text{H}_3\text{VO}_4(\text{aq}) + \text{H}^+$	18.551 ± 0.625	-3.25 ± 0.11	$-1\ 042.729 \pm 1.182$	31.000	$-1\ 190.460$
$\text{VO}_2^+ + 2\text{H}_2\text{O} \rightleftharpoons \text{H}_2\text{VO}_4^- + 2\text{H}^+$	40.984 ± 0.685	-7.18 ± 0.12	$-1\ 020.296 \pm 1.215$	47.000	$-1\ 174.460$
$\text{VO}_2^+ + 2\text{H}_2\text{O} \rightleftharpoons \text{HVO}_4^{2-} + \text{H}^+$	89.730 ± 0.806	-15.72 ± 0.14	-971.550 ± 1.287	62.000	$-1\ 159.460$
$\text{VO}_2^+ + 2\text{H}_2\text{O} \rightleftharpoons \text{VO}_4^{3-} + 4\text{H}^+$	171.127 ± 1.321	-29.98 ± 0.23	-890.153 ± 1.659	89.000	$-1\ 132.460$
$2\text{VO}_2^+ + 2\text{H}_2\text{O} \rightleftharpoons \text{V}_2\text{O}_6^{2-} + 4\text{H}^+$	65.928 ± 1.663	-11.55 ± 0.29	$-1\ 582.352 \pm 2.603$		
$2\text{VO}_2^+ + 3\text{H}_2\text{O} \rightleftharpoons \text{V}_2\text{O}_7^{4-} + 6\text{H}^+$	184.313 ± 1.168	-32.29 ± 0.20	$-1\ 701.107 \pm 2.319$		
$2\text{VO}_2^+ + 3\text{H}_2\text{O} \rightleftharpoons \text{HV}_2\text{O}_7^{4-} + 5\text{H}^+$	119.869 ± 1.495	-21.00 ± 0.26	$-1\ 765.551 \pm 2.500$		
$2\text{VO}_2^+ + 3\text{H}_2\text{O} \rightleftharpoons \text{H}_3\text{V}_2\text{O}_7^{4-} + 3\text{H}^+$	22.639 ± 6.075	-3.97 ± 1.06	$-1\ 862.781 \pm 6.397$		
$4\text{VO}_2^+ + 4\text{H}_2\text{O} \rightleftharpoons \text{V}_4\text{O}_{12}^{4-} + 8\text{H}^+$	119.698 ± 2.017	-20.97 ± 0.35	$-3\ 176.862 \pm 3.458$		
$4\text{VO}_2^+ + 5\text{H}_2\text{O} \rightleftharpoons \text{HV}_4\text{O}_{13}^{5-} + 9\text{H}^+$	183.970 ± 2.875	-32.23 ± 0.50	$-3\ 349.730 \pm 4.930$		
$4\text{VO}_2^+ + 5\text{H}_2\text{O} \rightleftharpoons \text{V}_4\text{O}_{13}^{5-} + 10\text{H}^+$	245.389 ± 2.996	-42.99 ± 0.52	$-3\ 288.311 \pm 5.002$		
$5\text{VO}_2^+ + 5\text{H}_2\text{O} \rightleftharpoons \text{V}_5\text{O}_{15}^{5-} + 10\text{H}^+$	155.544 ± 3.506	-27.25 ± 0.61	$-3\ 965.156 \pm 6.110$		
$10\text{VO}_2^+ + 7\text{H}_2\text{O} \rightleftharpoons \text{V}_{10}\text{O}_{27}^{4-} + 14\text{H}^+$	60.448 ± 1.860	-10.59 ± 0.33	$-7\ 469.532 \pm 10.176$		
$10\text{VO}_2^+ + 8\text{H}_2\text{O} \rightleftharpoons \text{HV}_{10}\text{O}_{28}^{5-} + 15\text{H}^+$	90.986 ± 1.975	-15.94 ± 0.35	$-7\ 676.134 \pm 10.198$		
$10\text{VO}_2^+ + 8\text{H}_2\text{O} \rightleftharpoons \text{V}_{10}\text{O}_{28}^{6-} + 16\text{H}^+$	137.906 ± 2.051	-24.16 ± 0.36	$-7\ 629.214 \pm 10.213$		
$\text{H}_2\text{VO}_4^- + \text{H}^+ \rightleftharpoons \text{H}_3\text{VO}_4(\text{aq})$	-22.433 ± 0.281	3.93 ± 0.05		-16.000	
$\text{H}_2\text{VO}_4^- \rightleftharpoons \text{HVO}_4^{2-} + \text{H}^+$	48.746 ± 0.425	-8.54 ± 0.07		15.000	
$\text{H}_2\text{VO}_4^{2-} \rightleftharpoons \text{VO}_4^{3-} + 2\text{H}^+$	130.143 ± 1.130	-22.80 ± 0.20		42.000	
$2\text{H}_2\text{VO}_4^- \rightleftharpoons \text{V}_2\text{O}_6^{2-} + 2\text{H}_2\text{O}$	-16.040 ± 0.936	2.81 ± 0.16			
$2\text{H}_2\text{VO}_4^- \rightleftharpoons \text{V}_2\text{O}_7^{4-} + \text{H}_2\text{O} + 2\text{H}^+$	102.345 ± 0.723	-17.93 ± 0.13			
$2\text{H}_2\text{VO}_4^- \rightleftharpoons \text{HV}_2\text{O}_7^{4-} + \text{H}_2\text{O} + \text{H}^+$	37.901 ± 0.591	-6.64 ± 0.10			
$2\text{H}_2\text{VO}_4^- + \text{H}^+ \rightleftharpoons \text{H}_3\text{V}_2\text{O}_7^- + \text{H}_2\text{O}$	-59.329 ± 5.917	10.39 ± 1.04			
$4\text{H}_2\text{VO}_4^- \rightleftharpoons \text{V}_4\text{O}_{12}^{4-} + 4\text{H}_2\text{O}$	-44.238 ± 3.410	7.75 ± 0.60			
$4\text{H}_2\text{VO}_4^- \rightleftharpoons \text{HV}_4\text{O}_{13}^{5-} + 3\text{H}_2\text{O} + \text{H}^+$	20.034 ± 0.842	-3.51 ± 0.15			
$4\text{H}_2\text{VO}_4^- \rightleftharpoons \text{V}_4\text{O}_{13}^{5-} + 3\text{H}_2\text{O} + 2\text{H}^+$	81.453 ± 1.192	-14.27 ± 0.21			
$5\text{H}_2\text{VO}_4^- \rightleftharpoons \text{V}_5\text{O}_{15}^{5-} + 5\text{H}_2\text{O}$	-49.376 ± 0.692	8.65 ± 0.12			
$10\text{H}_2\text{VO}_4^- + 6\text{H}^+ \rightleftharpoons \text{V}_{10}\text{O}_{27}^{4-} + 13\text{H}_2\text{O}$	-349.392 ± 6.615	61.21 ± 1.16			
$10\text{H}_2\text{VO}_4^- + 5\text{H}^+ \rightleftharpoons \text{HV}_{10}\text{O}_{28}^{5-} + 12\text{H}_2\text{O}$	-318.854 ± 6.583	55.86 ± 1.15			
$10\text{H}_2\text{VO}_4^- + 4\text{H}^+ \rightleftharpoons \text{V}_{10}\text{O}_{28}^{6-} + 12\text{H}_2\text{O}$	-271.934 ± 6.560	47.64 ± 1.15			

Table 3.7-48. Thermodynamic functions and constants for Cl and S compounds of V.

Reaction	$\Delta_r G_m^\circ$ kJ mol ⁻¹	$\log_{10} K^\circ$	$\Delta_f G_m^\circ$ kJ mol ⁻¹	$\Delta_r H_m^\circ$ kJ mol ⁻¹	$\Delta_f H_m^\circ$ kJ mol ⁻¹
$VCl_2(\text{cr}) \rightleftharpoons V^{2+} + 2Cl^-$	-74.434 ± 47.74^a	13.04 ± 8.36	$-406. \pm 48.$	-108.096	452 ± 16^a
$VCl_3(\text{cr}) \rightleftharpoons V^{2+} + 3Cl^-$	-124.751 ± 1.199^a	21.86 ± 0.21	-511.2 ± 1.6		-580.7 ± 5.6
$VOCl(\text{cr}) + 2H^+ \rightleftharpoons V^{3+} + H_2O + Cl^-$	-54.657 ± 47.989^a	9.58 ± 8.41	$-556. \pm 48.$		$-607. \pm 56.$
$VOCl_2(\text{cr}) \rightleftharpoons VO^{2+} + 2Cl^-$	-72.834 ± 47.989^a	12.76 ± 8.41	$-636. \pm 48.$	-117.760 ± 23.978^a	$703. \pm 24.$
$VO_2Cl(\text{cr}) \rightleftharpoons VO_2^+ + Cl^-$	1.783 ± 1.004^a	-0.31 ± 0.18	-720.0 ± 0.8	-40.280 ± 4.694^a	776.6 ± 4.8
$VO^{2+} + SO_4^{2-} \rightleftharpoons VOSO_4(\text{aq})$	-14.156	2.48^b	-1204.560		

a [1982WAG/EVA]; b [1971HIL/WOR].

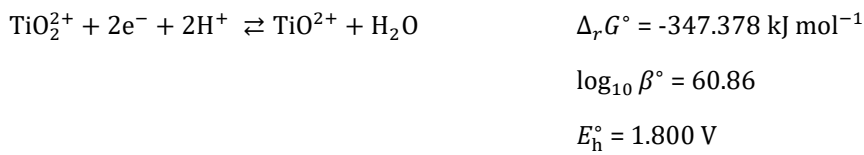
3.7.12. Titanium

Titanium in the form of oxide are common in environmental mining context. A titanate phase is an important uranium ore.

3.7.12.1. Native Element and Free Ions

The native element, and free ions Ti^{2+} , Ti^{3+} , TiO_2^{2+} are taken from Bard *et al.* [1985BAR/PAR], and TiO^{2+} from Brown and Ekberg [2016BRO/EKB]. The common master species is TiO^{2+} .

It can be noted that the $\Delta_f G_m^\circ(TiO^{2+}) = -577.4 \text{ kJ mol}^{-1}$ in Bard *et al.* [1985BAR/PAR] differs strongly from the one in Brown and Ekberg [2016BRO/EKB], $\Delta_f G_m^\circ(TiO^{2+}) = -(631.3 \pm 1.2) \text{ kJ mol}^{-1}$. Hence, it is necessary to recalculate the $\Delta_f G_m^\circ(TiO_2^{2+})$ given in Bard *et al.* [1985BAR/PAR] from the potential calculated as follows,



which leads to the corrected $\Delta_f G_m^\circ(TiO_2^{2+}) = -521.062 \text{ kJ mol}^{-1}$ accounting for Brown and Ekberg [2016BRO/EKB].

3.7.12.2. Oxo and Hydroxo Compounds

The functions of formation of $TiO(\text{cr})$ and $Ti(OH)_3(\text{cr})$ are taken from Bard *et al.* [1985BAR/PAR]. The functions of formation of $Ti_2O_3(\text{cr})$, anatase and rutile ($TiO_2(\text{cr})$), and $Ti_2O_3(\text{cr})$ are taken from Robie and Hemingway [1995ROB/HEM]. The function of formation of $Ti_3O_5(\text{cr})$ is available in Wagman *et al.* [1982WAG/EVA].

Brown and Ekberg [2016BRO/EKB] selected the solubility of $TiO(OH)_2(\text{am})$.

The hydrolysis of TiO^{2+} is taken from Brown and Ekberg [2016BRO/EKB].

3.7.12.3. Multiple Oxides

The functions of formation of $MgTi_2O_5(\text{cr})$, $Mg_2TiO_4(\text{cr})$, and $(CaO)_3:2TiO_2(\text{cr})$ are given in Wagman *et al.* [1982WAG/EVA].

The functions of formation of $Zn_2TiO_4(\text{cr})$, ilmenite ($FeTiO_3$), ulvöspinel (Fe_2TiO_4), pyrophanite ($MnTiO_3$), geikielite ($MgTiO_3$), perovskite ($CaTiO_3$), $BaTiO_3(\text{cr})$, and $Ba_2TiO_4(\text{cr})$ are available in Robie and Hemingway [1995ROB/HEM].

3.7.12.4. Halogen Compounds

$\text{TiF}_2(\text{cr})$, $\text{TiF}_3(\text{cr})$, and $\text{TiF}_4(\text{cr})$, and $\text{TiCl}_2(\text{cr})$ are taken from Bard *et al.* [1985BAR/PAR]. The formation of TiF_6^{2-} in Bard *et al.* [1985BAR/PAR] is also included in PRODATA.

3.7.12.5. Sulphur Compounds

The Gibbs energy of $\text{TiS}(\text{cr})$ is taken from Pankratz *et al.* [1987PAN/MAH].

3.7.12.6. Thermodynamic Functions and Constants for Ti

Table 3.7-49. Thermodynamic functions and constants of Ti.

Reaction	$\Delta_r G^\circ$ kJ mol ⁻¹	$\log_{10} \beta^\circ$	$\Delta_f G^\circ$ kJ mol ⁻¹	$\Delta_r H^\circ$ kJ mol ⁻¹	$\Delta_f H^\circ$ kJ mol ⁻¹
$\text{Ti}(\text{cr}) + \text{O}_2(\text{aq}) + 2\text{H}^+ \rightleftharpoons \text{TiO}^{2+} + \text{H}_2\text{O}$	-884.818 ± 0.800	155.01 ± 0.14	$-631.300 \pm 1.200^{\text{a}}$		
$\text{Ti}(\text{cr}) \rightleftharpoons \text{Ti}^{2+} + 2\text{e}^-$	-314.542	55.11^{b}	-314.542		
$\text{TiO}^{2+} \rightleftharpoons \text{Ti}^{2+} + 0.5\text{O}_2(\text{aq})$	324.948	-56.928			
$\text{TiO}^{2+} + \text{H}^+ \rightleftharpoons \text{Ti}^{3+} + 0.25\text{O}_2(\text{aq}) + 0.5\text{H}_2\text{O}$	166.874 ± 4.859	-29.24 ± 0.85	$-349.951 \pm 5.000^{\text{b}}$		
$\text{TiO}^{2+} + \text{H}_2\text{O} \rightleftharpoons \text{TiO}_2^{2+} + 2\text{e}^- + 2\text{H}^+$	347.378	-60.96^{b}	-521.062		
$\text{TiO}^{2+} + \text{O}_2(\text{aq}) \rightleftharpoons \text{TiO}_2^{2+}$	155.911	-27.31			
$\text{TiO}(\text{cr}) + 2\text{H}^+ \rightleftharpoons \text{Ti}^{2+} + \text{H}_2\text{O}$	-62.481	10.95	-489.200^{b}		
$\text{TiO}(\text{OH})_2(\text{am}) + 2\text{H}^+ \rightleftharpoons \text{TiO}^{2+} + 2\text{H}_2\text{O}$		-0.50^{a}			
$\text{TiO}_2(\text{cr}) + 2\text{H}^+ \rightleftharpoons \text{TiO}^{2+} + \text{H}_2\text{O}$					
Rutile	20.360 ± 0.665	-3.57 ± 0.12	$-888.8 \pm 1.0^{\text{c}}$		$-944.0 \pm 0.8^{\text{c}}$
Anatase	14.760 ± 1.723	-2.59 ± 0.30	$-883.2 \pm 2.1^{\text{c}}$		$-938.1 \pm 2.1^{\text{c}}$
$\text{Ti}_2\text{O}_3(\text{cr}) + 6\text{H}^+ \rightleftharpoons 2\text{Ti}^{3+} + 3\text{H}_2\text{O}$	22.578 ± 5.427	-3.96 ± 0.95	$-1\ 433.9 \pm 8.4^{\text{c}}$		$-1\ 520.9 \pm 8.4^{\text{c}}$
$\text{Ti}(\text{OH})_3(\text{cr}) + 3\text{H}^+ \rightleftharpoons \text{Ti}^{3+} + 3\text{H}_2\text{O}$	-11.571	2.03	$-1\ 049.800^{\text{b}}$		
$\text{Ti}_3\text{O}_5(\text{cr}) + 4\text{H}^+ \rightleftharpoons 3\text{TiO}^{2+} + 2\text{e}^- + 2\text{H}_2\text{O}$	-50.780 ± 1.651	8.90 ± 0.29	$-2\ 317.4 \pm 3.2^{\text{d}}$		$-2\ 459.4 \pm 3.2^{\text{d}}$
$\text{Ti}_3\text{O}_5(\text{cr}) + 0.5\text{O}_2(\text{aq}) + 6\text{H}^+ \rightleftharpoons 3\text{TiO}^{2+} + 3\text{H}_2\text{O}$	-296.109 ± 1.592	51.88 ± 0.28			
$\text{TiO}^{2+} + \text{H}_2\text{O} \rightleftharpoons \text{TiO}(\text{OH})^+ + \text{H}^+$					
	14.156 ± 0.572	$-2.48 \pm 0.10^{\text{a}}$	-854.284 ± 1.330		
$\text{TiO}^{2+} + 2\text{H}_2\text{O} \rightleftharpoons \text{TiO}(\text{OH})_2(\text{aq}) + 2\text{H}^+$					
	31.337 ± 0.799	$-5.49 \pm 0.14^{\text{a}}$	$-1\ 074.243 \pm 1.444$		
$\text{TiO}^{2+} + 3\text{H}_2\text{O} \rightleftharpoons \text{TiO}(\text{OH})_3^- + 3\text{H}^+$					
	99.320 ± 2.854	$-17.40 \pm 0.50^{\text{a}}$	$-1\ 243.400 \pm 3.098$		
$\text{Ti}^{3+} + \text{H}_2\text{O} \rightleftharpoons \text{TiOH}^{2+} + \text{H}^+$					
	9.391 ± 0.041	$-1.65 \pm 0.01^{\text{a}}$	-577.700 ± 5.000		
$2\text{Ti}^{3+} + 2\text{H}_2\text{O} \rightleftharpoons \text{Ti}_2(\text{OH})_2^{4+} + 2\text{H}^+$					
	14.882 ± 8.661	$-2.61 \pm 1.52^{\text{a}}$	$-1\ 159.300 \pm 5.000$		
$\text{Zn}_2\text{TiO}_4(\text{cr}) + 6\text{H}^+ \rightleftharpoons 2\text{Zn}^{2+} + \text{TiO}^{2+} + 3\text{H}_2\text{O}$	$-98.726 \pm 1.512^{\text{c}}$	17.30 ± 0.26	$-1\ 538.4 \pm 2.0$		$-1\ 652.1 \pm 2.0^{\text{c}}$
Ilmenite					
$\text{FeTiO}_3 + 4\text{H}^+ \rightleftharpoons \text{Mn}^{2+} + \text{TiO}^{2+} + 2\text{H}_2\text{O}$	$-40.799 \pm 2.096^{\text{c}}$	7.15 ± 0.37	$-1\ 155.5 \pm 2.5$		$-1\ 232.0 \pm 2.5^{\text{c}}$
Ulvospinel					
$\text{Fe}_2\text{TiO}_4 + 6\text{H}^+ \rightleftharpoons 2\text{Fe}^{2+} + \text{TiO}^{2+} + 3\text{H}_2\text{O}$	$-124.258 \pm 1.145^{\text{c}}$	21.77 ± 0.20	$-1\ 399.9 \pm 2.1$		$-1\ 493.8 \pm 2.0^{\text{c}}$
Pyrophanite					
$\text{MnTiO}_3 + 4\text{H}^+ \rightleftharpoons \text{Mn}^{2+} + \text{TiO}^{2+} + 2\text{H}_2\text{O}$	$-52.780 \pm 3.782^{\text{c}}$	9.25 ± 0.66	$-1\ 280.900 \pm 4.000$		$-1\ 360.10 \pm 4.00^{\text{c}}$
Geikielite					
$\text{MgTiO}_3 + 4\text{H}^+ \rightleftharpoons \text{Mg}^{2+} + \text{TiO}^{2+} + 2\text{H}_2\text{O}$	$-76.555 \pm 1.338^{\text{c}}$	13.41 ± 0.23	$-1\ 484.4 \pm 1.2$		$-1\ 572.8 \pm 1.2^{\text{c}}$
$\text{MgTi}_2\text{O}_5(\text{cr}) \rightleftharpoons \text{Mg}^{2+} + 2\text{TiO}^{2+} + 3\text{H}_2\text{O}$	$-62.595 \pm 5.780^{\text{d}}$	10.97 ± 1.013	$-2\ 366.8 \pm 6.4$		$-2\ 509.6 \pm 4.8^{\text{c}}$

Table 3.7-49. Continued.

Reaction	$\Delta_r G^\circ$ kJ mol ⁻¹	$\log_{10} \beta^\circ$	$\Delta_f G^\circ$ kJ mol ⁻¹	$\Delta_r H^\circ$ kJ mol ⁻¹	$\Delta_f H^\circ$ kJ mol ⁻¹
Perovskite					
$\text{CaTiO}_3 + 4\text{H}^+ \rightleftharpoons \text{Ca}^{2+} + \text{TiO}^{2+} + 2\text{H}_2\text{O}$	$-83.586 \pm 0.831^{\text{c}}$	14.64 ± 0.15	$-1\ 574.8 \pm 1.8$		$-1\ 660.6 \pm 1.7^{\text{c}}$
$(\text{CaO})_2: 2\text{TiO}_2(\text{cr}) + 10\text{H}^+ \rightleftharpoons 3\text{Ca}^{2+} + 2\text{TiO}^{2+} + 5\text{H}_2\text{O}$	$-355.418 \pm 3.157^{\text{d}}$	62.27 ± 0.553	$-3\ 751.3 \pm 2.4$		$-3\ 950.5 \pm 4.0^{\text{d}}$
$\text{BaTiO}_3 + 4\text{H}^+ \rightleftharpoons \text{Ba}^{2+} + \text{TiO}^{2+} + 2\text{H}_2\text{O}$	$-90.936 \pm 1.534^{\text{d}}$	15.93 ± 0.27	$-1\ 572.300 \pm 2.400$		$-1\ 659.8 \pm 6.4^{\text{d}}$
$\text{Ba}_2\text{TiO}_4 + 6\text{H}^+ \rightleftharpoons 2\text{Ba}^{2+} + \text{TiO}^{2+} + 3\text{H}_2\text{O}$	$-325.132 \pm 4.870^{\text{d}}$	56.96 ± 0.85	$-2\ 132.900 \pm 7.200$		$-2\ 243.0 \pm 0.08^{\text{d}}$
$\text{TiF}_2(\text{cr}) \rightleftharpoons \text{Ti}^{2+} + 2\text{F}^-$	-94.787^{b}	16.61	-782.800		
$\text{TiF}_3(\text{cr}) \rightleftharpoons \text{Ti}^{3+} + 3\text{F}^-$	22.580^{b}	-3.96	$-1\ 217.100$		$-1\ 318.000^{\text{b}}$
$\text{TiF}_4(\text{cr}) + \text{H}_2\text{O} \rightleftharpoons \text{TiO}^{2+} + 4\text{F}^- + 2\text{H}^+$	-71.352^{b}	12.50	$-1\ 448.900$		$-1\ 548.000^{\text{b}}$
$\text{TiO}^{2+} + 6\text{F}^- + 2\text{H}^+ \rightleftharpoons \text{TiF}_6^{2-} + \text{H}_2\text{O}$	-105.258^{b}	18.44	$-2\ 188.556$		$-2\ 322.500^{\text{b}}$
$\text{TiS}(\text{cr}) + \text{H}^+ \rightleftharpoons \text{Ti}^{2+} + \text{HS}^-$	-25.075	4.39	-277.223^{e}		

a [2016BRO/EKB]; b [1985BAR/PAR]; c [1995ROB/HEM]; d [1982WAG/EVA]; e [1987PAN/MAH].

3.7.13. Zirconium

Zirconium oxides are often found in environmental contexts. The thermodynamic constants and function values in Brown *et al.* [2005BRO/CUR], as well as the specific ion interaction coefficients, are accepted in the database. The common master species is Zr^{4+} .

It can be noted that Brown and Ekberg [2016BRO/EKB] proposed a slightly different interpretations of the hydrolysis and solubility values of Zr(IV). Until a further analysis, PRODATA will keep the NEA-OECD analysis in Brown *et al.* [2005BRO/CUR]. Altmaier *et al.* [2008ALT/NEC] evidenced the formation of ion pair species $\text{Ca}_n[\text{Zr}(\text{OH})_6]^{(2n-2)+}$, which are of no importance for the mining activities of ORANO.

The functions of formation of $\text{CaZrO}_3(\text{cr})$ are available in Wagman *et al.* [1982WAG/EVA], but as no function of formation are given for Zr^{4+} in solution, the function of reactions are calculated relative to Brown *et al.* [2005BRO/CUR].

Table 3.7-50. Thermodynamic functions and constants of native, free metal and oxo and hydroxo compounds of Zr from Brown *et al.* [2005BRO/CUR].

Reaction	$\log_{10} \beta^\circ$	$\Delta_r G^\circ$ kJ mol ⁻¹	$\Delta_f G^\circ$ kJ mol ⁻¹	$\Delta_r H^\circ$ kJ mol ⁻¹	$\Delta_f H^\circ$ kJ mol ⁻¹
$\text{Zr}(\text{cr}) \rightleftharpoons \text{Zr}^{4+} + 4\text{e}^-$	92.59 ± 1.62	-528.509 ± 9.227	-528.509 ± 9.227	-608.5 ± 5.0	-608.5 ± 5.0
$\text{Zr}^{4+} + \text{H}_2\text{O} \rightleftharpoons \text{Zr}(\text{OH})^{3+} + \text{H}^+$	0.32 ± 0.22	-1.827 ± 1.255	-767.476 ± 9.312		
$\text{ZrO}_2 + 4\text{H}^+ \rightleftharpoons \text{Zr}^{4+} + 2\text{H}_2\text{O}$	-7.00 ± 1.60	39.957 ± 9.133	$-1\ 042.746 \pm 1.313$	-79.560 ± 4.829	$-1\ 100.600 \pm 1.300$
$\text{Zr}(\text{OH})_4\text{-fresh(am)} + 4\text{H}^+ \rightleftharpoons \text{Zr}^{4+} + 4\text{H}_2\text{O}$	-3.24 ± 0.1				
$\text{Zr}^{4+} + \text{H}_2\text{O} \rightleftharpoons \text{Zr}(\text{OH})^{3+} + \text{H}^+$	0.32 ± 0.22	-1.827 ± 1.255	-767.476 ± 9.312		
$\text{Zr}^{4+} + 2\text{H}_2\text{O} \rightleftharpoons \text{Zr}(\text{OH})_2^{2+} + 2\text{H}^+$	0.98 ± 1.06	-5.595 ± 6.050	$-1\ 008.384 \pm 11.034$		
$\text{Zr}^{4+} + 4\text{H}_2\text{O} \rightleftharpoons \text{Zr}(\text{OH})_4\text{(aq)} + 4\text{H}^+$	-2.19 ± 1.70	12.499 ± 9.703	$-1\ 464.570 \pm 13.391$		
$\text{Zr}^{4+} + 6\text{H}_2\text{O} \rightleftharpoons \text{Zr}(\text{OH})_6^{2-} + 6\text{H}^+$	-29.00 ± 0.70	165.531 ± 3.996	$-1\ 785.818 \pm 10.058$		
$3\text{Zr}^{4+} + 4\text{H}_2\text{O} \rightleftharpoons \text{Zr}_3(\text{OH})_4^{8+} + 4\text{H}^+$	0.40 ± 0.30	-2.286 ± 1.722	$-2\ 536.373 \pm 27.735$	-1.980 ± 11.181	$-2\ 970.800 \pm 10.000$

Table 3.7-50. Continued.

Reaction	$\log_{10} \beta^\circ$	$\Delta_r G^\circ$ kJ mol ⁻¹	$\Delta_f G^\circ$ kJ mol ⁻¹	$\Delta_r H^\circ$ kJ mol ⁻¹	$\Delta_f H^\circ$ kJ mol ⁻¹
$3\text{Zr}^{4+} + 9\text{H}_2\text{O} \rightleftharpoons \text{Zr}_3(\text{OH})_9^{3+} + 9\text{H}^+$	12.19 ± 0.09	-69.585 ± 0.501	$-3\ 789.372 \pm 27.688$		
$4\text{Zr}^{4+} + 8\text{H}_2\text{O} \rightleftharpoons \text{Zr}_4(\text{OH})_8^{8+} + 8\text{H}^+$	6.52 ± 0.65	-37.221 ± 3.716	$-4\ 048.377 \pm 37.096$		
$4\text{Zr}^{4+} + 15\text{H}_2\text{O} \rightleftharpoons \text{Zr}_4(\text{OH})_{15}^{+} + 15\text{H}^+$	12.58 ± 0.24	-71.814 ± 1.382	$-5\ 742.950 \pm 36.939$		
$4\text{Zr}^{4+} + 16\text{H}_2\text{O} \rightleftharpoons \text{Zr}_4(\text{OH})_{16}^{-(aq)} + 16\text{H}^+$	8.39 ± 0.80	-47.897 ± 4.573	301.120 ± 18.670	$-5\ 956.173 \pm 37.196$	$-6\ 706.160 \pm 7.200$

Table 3.7-51. Thermodynamic functions and constants of halogeno compounds of Zr from Brown *et al.* [2005BRO/CUR].

Reaction	$\log_{10} \beta^\circ$	$\Delta_r G^\circ$ kJ mol ⁻¹	$\Delta_f G^\circ$ kJ mol ⁻¹	$\Delta_r H^\circ$ kJ mol ⁻¹	$\Delta_f H^\circ$ kJ mol ⁻¹
$\text{Zr}^{4+} + \text{F}^- \rightleftharpoons \text{ZrF}^{3+}$	10.12 ± 0.07	-57.766 ± 0.410	-867.798 ± 9.262	-17.500 ± 0.697	-961.350 ± 5.090
$\text{Zr}^{4+} + 2\text{F}^- \rightleftharpoons \text{ZrF}_2^{2+}$	18.55 ± 0.31	-105.885 ± 1.772	$-1\ 197.440 \pm 9.497$	-16.800 ± 0.999	$-1\ 296.000 \pm 5.262$
$\text{Zr}^{4+} + 3\text{F}^- \rightleftharpoons \text{ZrF}_3^+$	24.44 ± 0.38	-139.504 ± 2.173	$-1\ 512.582 \pm 9.704$	-11.200 ± 1.701	$-1\ 625.750 \pm 5.630$
$\text{Zr}^{4+} + 4\text{F}^- \rightleftharpoons \text{ZrF}_4^{-(aq)}$	30.11 ± 0.40	-171.870 ± 2.287	$-1\ 826.471 \pm 9.901$	-22.000 ± 2.700	$-1\ 971.900 \pm 6.249$
$\text{Zr}^{4+} + 5\text{F}^- \rightleftharpoons \text{ZrF}_5^-$	34.58 ± 0.37	-197.380 ± 2.130	$-2\ 133.504 \pm 10.082$		
$\text{Zr}^{4+} + 6\text{F}^- \rightleftharpoons \text{ZrF}_6^{2-}$	38.09 ± 0.38	-217.415 ± 2.197	$-2\ 435.062 \pm 10.354$		
$\text{ZrCl}_3(\text{cr}) \rightleftharpoons \text{Zr}^{4+} + \text{e}^- + 3\text{Cl}^-$	40.72 ± 1.53	-232.418 ± 8.728	-689.742 ± 3.013	-349.640 ± 4.011	-760.100 ± 3.000
$\text{ZrCl}_3(\text{cr}) + 0.25\text{O}_2(\text{aq}) + \text{H}^+ \rightleftharpoons \text{Zr}^{4+} + 3\text{Cl}^- + 0.5\text{H}_2\text{O}$	62.21 ± 1.53	-355.083 ± 8.725		-489.630 ± 4.005	
$\text{ZrCl}_4(\text{cr}) \rightleftharpoons \text{Zr}^{4+} + 4\text{Cl}^-$	28.60 ± 1.61	-163.227 ± 9.162	-890.150 ± 1.188	-296.020 ± 4.935	-980.800 ± 0.900
$\text{ZrI}_3(\text{cr}) \rightleftharpoons \text{Zr}^{4+} + \text{e}^- + 3\text{I}^-$	52.22 ± 2.07	-298.101 ± 11.823	-385.580 ± 15.001	-387.240 ± 14.141	-391.600 ± 15.000
$\text{ZrI}_3(\text{cr}) + 0.25\text{O}_2(\text{aq}) + \text{H}^+ \rightleftharpoons \text{Zr}^{4+} + 3\text{I}^- + 0.5\text{H}_2\text{O}$	73.71 ± 2.07	-420.766 ± 11.825		-527.230 ± 14.143	
$\text{ZrI}_4(\text{cr}) \rightleftharpoons \text{Zr}^{4+} + 4\text{I}^-$	44.59 ± 1.48	-254.543 ± 8.458	-480.862 ± 3.714	-346.720 ± 3.369	-488.900 ± 3.700

Table 3.7-52. Thermodynamic functions and constants of S compounds of Zr from Brown *et al.* [2005BRO/CUR].

Reaction	$\log_{10} \beta^\circ$	$\Delta_r G^\circ$ kJ mol ⁻¹	$\Delta_f G^\circ$ kJ mol ⁻¹	$\Delta_r H^\circ$ kJ mol ⁻¹	$\Delta_f H^\circ$ kJ mol ⁻¹
$\text{ZrS}_2(\text{cr}) \rightleftharpoons \text{Zr}^{4+} + 2\text{HS}^-$	-10.81 ± 1.13	61.727 ± 6.429	-565.750 ± 12.015	-67.900 ± 10.488	-573.200 ± 12.000
$\text{Zr}(\text{SO}_3)_2(\text{cr}) \rightleftharpoons \text{Zr}^{4+} 2\text{SO}_3^{2-}$	-58.06 ± 1.23	331.417 ± 7.010	$-1\ 834.870 \pm 10.032$	140.380 ± 8.623	$-2\ 011.000 \pm 10.000$
$\text{Zr}(\text{SO}_4)_2(\text{cr}) \rightleftharpoons \text{Zr}^{4+} 2\text{SO}_4^{2-}$	1.24 ± 1.58	-7.063 ± 9.004	$-2\ 009.454 \pm 2.183$	-181.980 ± 4.608	$-2\ 245.200 \pm 2.100$
$\text{Zr}(\text{SO}_4)_2 \cdot 4\text{H}_2\text{O}(\text{cr}) \rightleftharpoons \text{Zr}^{4+} 2\text{SO}_4^{2-} + 4\text{H}_2\text{O}$	-7.65 ± 1.56	43.685 ± 8.892	$-3\ 008.762 \pm 2.607$	-99.600 ± 4.348	$-3\ 470.900 \pm 2.600$

3.8. Actinides

3.8.1. Uranium

There is a large body of thermodynamic data on uranium. A large part of which has been the subject of critical analyses by groups of experts commissioned by the NEA-OECD [1992GRE/FUG; 1995SIL/BID; 2003GUI/FAN; 2020GRE/GAO]. The selected thermodynamic constants and functions are mostly included in this database. The choice of the common master species can be made using either U^{4+} or UO_2^{2+} . Only the data that are not included or modified in PRODATA will be discussed.

3.8.1.1. Free Ions

The enthalpies and entropies of reaction of U^{4+} and UO_2^+ were not selected in NEA-OECD reviews [1992GRE/FUG; 2003GUI/FAN; 2020GRE/GAO], but can be calculated from functions of formation estimated using the Gibbs-Helmholtz equation in NEA-OECD reviews [2003GUI/FAN; 2020GRE/GAO].

3.8.1.2. Oxo and Hydroxo Compounds

The thorough selection of thermodynamic functions and constants, and SIT parameters from NEA-OECD reviews [2003GUI/FAN; 2020GRE/GAO] is accepted in this database.

3.8.1.2.1 Uranium(IV)

The thermodynamic constant and functions of reaction of $\text{UO}_2(\text{cr})$ were not selected Guillaumont *et al.* [2003GUI/FAN], but can be calculated from functions of formation estimated using the Gibbs-Helmholtz equation in Guillaumont *et al.* [2003GUI/FAN]. The solubility of $\text{UO}_2\text{-hyd(am)}$ relative to OH^-



is written relative to H^+ in PRODATA.



Only U(OH)^{3+} and $\text{U(OH)}_4(\text{aq})$ are selected in Guillaumont *et al.* [2003GUI/FAN]. The selected value of the latter complexes markedly differs from the first selection in Grenthe *et al.* [1992GRE/FUG]. The $\Delta_r H_m^\circ$ and $\Delta_r S_m^\circ$ values of $\text{U(OH)}_4(\text{aq})$ were not selected, but can be calculated from the $\Delta_f H_m^\circ$ and $S_{f,m}^\circ$ estimated using the Gibbs-Helmholtz equation in Guillaumont *et al.* [2003GUI/FAN]. The $\log_{10}\beta^\circ$ and $\Delta_f G_m^\circ$ of U(OH)_2^{2+} and U(OH)_3^+ were recently selected in Grenthe *et al.* [2020GRE/GAO].

Neck and Kim [2001NEC/KIM] also proposed a tentative value for U(OH)_5^- , the existence of which was already not selected in Grenthe *et al.* [1992GRE/FUG]. This value is included in PRODATA, but is not apparent in the extraction files.

3.8.1.2.2 Uranium(VI)

The solubility constants and functions of reactions of U(VI) oxides and hydroxydes are not selected in the NEA-OECD reviews [2003GUI/FAN; 2020GRE/GAO], but are calculated from the functions of formation.

Some thermodynamic functions have not been selected for U(VI) hydrolysis — *e.g.*, $\Delta_r H_m^\circ$ and $\Delta_r S_m^\circ$ for $\text{UO}_2(\text{OH})_n^{(2-n)+}$ with $n > 1$. Shock *et al.* [1997bSHO/SAS] proposed estimations of these values based on the first NEA-OECD review [1992GRE/FUG]. Using the proposed thermodynamic functions and properties of water from Helgeson and Kirkham [1974aHEL/KIR], one can calculate the values in Table 3.8-1. It can be seen that the reaction data do not correspond to the latter selections in date [2003GUI/FAN; 2020GRE/GAO]. However, the $\Delta_r H_m^\circ$ for $\text{UO}_2(\text{OH})_n^{(2-n)+}$ with $n = \{2; 3; 4\}$ rounded to the first digit are included in PRODATA — even if there is an inevitable lack of consistency using the $S_{f,m}^\circ$ values.

The $\varepsilon(\text{Cation}^+, \text{Anion}^-)$ values selected in Grenthe *et al.* [2020GRE/GAO] are accepted in this database.

Table 3.8-1. Thermodynamic function of reaction for the hydroxouranyl(VI) complexes calculated from the thermodynamic function of formation estimated in Shock *et al.* [1997bSHO/SAS].

Equilibrium	$\Delta_r G_m^\circ$ kJ mol ⁻¹	$\Delta_r H_m^\circ$ kJ mol ⁻¹	$\Delta_r S_m^\circ$ J mol ⁻¹ K ⁻¹	$\log_{10} \beta_n^\circ$
$\text{UO}_2^{2+} + 2\text{H}_2\text{O} \rightleftharpoons \text{UO}_2(\text{OH})_2(\text{aq}) + 2\text{H}^+$	58.856	51.3	-25.6	-10.31
$\text{UO}_2^{2+} + 3\text{H}_2\text{O} \rightleftharpoons \text{UO}_2(\text{OH})_3^- + 3\text{H}^+$	109.847	72.3	-125.6	-19.24
$\text{UO}_2^{2+} + 4\text{H}_2\text{O} \rightleftharpoons \text{UO}_2(\text{OH})_4^{2-} + 4\text{H}^+$	188.506	142.2	-227.3	-33.02

The Pourbaix diagram of uranium at 10^{-4} mol kg_w⁻¹ in a hypothetical indifferent 0.1 mol kg_w⁻¹ electrolyte solution is plotted in Figure 3.8-1.

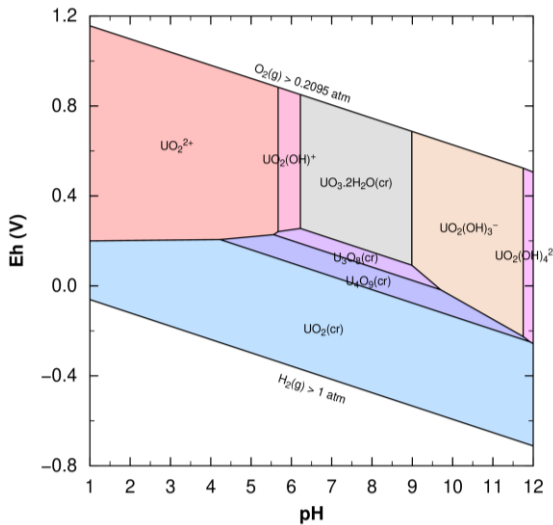


Figure 3.8-1. Pourbaix diagram of 10^{-6} mol kg_w⁻¹ U in a hypothetical indifferent 0.1 mol kg_w⁻¹ electrolyte solution using PHREEPLOT; all solid phases are allowed to precipitate.

3.8.1.3. Group 17 Compounds

Karbowiak *et al.* [2004KAR/HUB] proposed the formation of $\text{UO}_2\text{IO}_4^\ddagger$,



the formation constant of which is added for scoping calculation.

3.8.1.4. Group 16 Compounds

In addition to already selected uranyl sulphate solids — *i.e.*, $\text{UO}_2\text{SO}_4(\text{cr})$, $\text{UO}_2\text{SO}_4 \cdot 2.5\text{H}_2\text{O}(\text{cr})$, $\text{UO}_2\text{SO}_4 \cdot 3\text{H}_2\text{O}(\text{cr})$, and $\text{UO}_2\text{SO}_4 \cdot 3.5\text{H}_2\text{O}(\text{cr})$ —, it was stated page 249 in Grenthe *et al.* [1992GRE/FUG] that there was no “thermodynamic data for mono hydrate α -, β -, or γ - $\text{UO}_2\text{SO}_4 \cdot \text{H}_2\text{O}(\text{cr})$ ”. Nonetheless, functions of formation are proposed in Wagman *et al.* [1982WAG/EVA], and $\log_{10} K_s$ vs. T are available in the CHESS 3.0 and SOLTHERM-XPT [2015PAL; 2016REE/SPY] databases. The latter value is flagged to EQ3/6 database [1990WOL/JAC]. The solubility constants obtained using functions of formation in Wagman *et al.* [1982WAG/EVA] and in SOLTHERM-XPT database [2015PAL; 2016REE/SPY] are not in agreement.

	[1982WAG/EVA]	[2015PAL; 2016REE/SPY]
$\text{UO}_2\text{SO}_4 \cdot \text{H}_2\text{O}(\text{cr}) \rightleftharpoons \text{UO}_2^{2+} + \text{SO}_4^{2-} + \text{H}_2\text{O}$	$\Delta_r G^\circ = -(5.959 \pm 0.950) \text{ kJ mol}^{-1}$	
	$\log_{10} K_s^\circ = 1.04 \pm 0.17$	-5.96
	$\Delta_r H^\circ = -(68.300 \pm 1.447) \text{ kJ mol}^{-1}$	

These solubility values are not traceable to the original data. It can be noted that the value from Wagman *et al.* [1982WAG/EVA] is between the values for $\text{UO}_2\text{SO}_4(\text{cr})$ and $\text{UO}_2\text{SO}_4 \cdot 2.5\text{H}_2\text{O}(\text{cr})$ selected in NEA-OECD reviews Grenthe *et al.* [1992GRE/FUG]. The value of SOLTHERM-XPT [2015PAL; 2016REE/SPY] — and also from CHESS 3.0 and apparently from EQ3/6 —, will give a much lower solubility. Neither of these values will be exported by default.

3.8.1.5. Group 15 Compounds

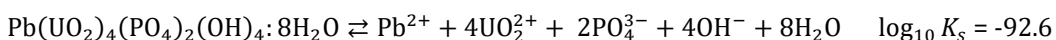
3.8.1.5.1 Phosphate Solids

The phosphate solids are extremely important for uranium mining exploration and exploitation. Due to its standard of review, the selection from the review commissioned by NEA-OECD are necessarily incomplete [1992GRE/FUG; 2003GUI/FAN; 2020GRE/GAO].

Muto [1965MUT] proposed Gibbs energy and enthalpy of formation for ningyoite $(\text{CaU}(\text{PO}_4)_2 \cdot 2\text{H}_2\text{O})$. The Gibbs energy and enthalpy of reaction and solubility constant can be calculated from the available data.

The functions of formation for $(\text{UO}_2)_3(\text{PO}_4)_2 \cdot 4\text{H}_2\text{O}(\text{cr})$ has been proposed by Rai *et al.* [2005RAI/XIA].

Parsonsite $(\text{Pb}_2\text{UO}_2(\text{PO}_4)_2 \cdot 2\text{H}_2\text{O})$, dumontite* $(\text{Pb}_2(\text{UO}_2)_3(\text{PO}_4)_2(\text{OH})_4 \cdot 3\text{H}_2\text{O})$, dewindtite $(\text{Pb}(\text{UO}_2)_4(\text{PO}_4)_2(\text{OH})_4 \cdot 8\text{H}_2\text{O})$, renardite $(\text{Pb}(\text{UO}_2)_4(\text{PO}_4)_2(\text{OH})_4 \cdot 7\text{H}_2\text{O})$, przhevalskite $(\text{Pb}(\text{UO}_2)_2(\text{PO}_4)_2 \cdot 4\text{H}_2\text{O})$, and torbernite $(\text{Cu}(\text{UO}_2)_2(\text{PO}_4)_2 \cdot 10\text{H}_2\text{O})$ are taken from Nriagu [1984NRI] — Nriagu [1984NRI] also proposed metatorbernite $(\text{Cu}(\text{UO}_2)_2(\text{PO}_4)_2 \cdot 8\text{H}_2\text{O})$, which Gibbs energy of formation has recently been selected in Grenthe *et al.* [2020GRE/GAO]. The Gibbs energies of formation of the uranyl constituting species are not available in Wagman *et al.* [1968WAG/EVA; 1969WAG/EVA] as stated in the paper. The data in Wagman *et al.* [1981WAG/EVA] are tested instead. There are a large differences between the $\Delta_f G^\circ$ values in Nriagu 1984NRI and the ones that can be calculated using Wagman *et al.* [1968WAG/EVA; 1969WAG/EVA] and Wagman *et al.* [1981WAG/EVA]. As an example, for dewindtite the solubility equilibrium,



ends up with a value of $\Delta_f G^\circ = -8937 \text{ kJ mol}^{-1}$, when a value of $-2169 \text{ kcal mol}^{-1}$ ($-9081 \text{ kJ mol}^{-1}$) is reported in Nriagu [1984NRI] — *i.e.*, a difference of -144 kJ mol^{-1} . The $\log_{10} K_s$ values will be used to recalculated the $\Delta_f G_m^\circ$ in coherence with NEA-OECD values [2003GUI/FAN; 2020GRE/GAO].

As already noted, copper is forming insoluble solids with uranium(VI) such as meta-Torbernite $(\text{H}_{0.4}\text{Cu}_{0.8}(\text{UO}_2)_2(\text{PO}_4)_2 \cdot 8\text{H}_2\text{O}(\text{cr}))$. Cretaz *et al.* [2013CRE/SZE] proposed functions of reaction and $\log_{10} K_s$, the values of which were used to calculate functions of formation used in PRODATA in addition to the value for $\text{Cu}(\text{UO}_2)_2(\text{PO}_4)_2 \cdot 8\text{H}_2\text{O}(\text{cr})$ in Grenthe *et al.* [2020GRE/GAO].

* Dumontite is incorrectly written $\text{Pb}_2(\text{UO}_2)_2(\text{PO}_4)_2(\text{OH})_4 \cdot 3\text{H}_2\text{O}$ in Table 1 of Nriagu [1984NRI], which does not assure a charge and matter balance of the solubility reaction.

Langmuir [1978LAN] reported the function of formation for saleeite ($\text{Mg}(\text{UO}_2)_2(\text{PO}_4)_2 \cdot 10\text{H}_2\text{O}$). They are included in addition to the values for $\text{Mg}(\text{UO}_2)_2(\text{PO}_4)_2 \cdot 8\text{H}_2\text{O}(\text{cr})$ from Grenthe *et al.* [2020GRE/GAO].

Muto [1965MUT] proposed the Gibbs energy for $\text{Ca}(\text{UO}_2)_2(\text{PO}_4)_2 \cdot 10\text{H}_2\text{O}(\text{s})$. The Gibbs energy and enthalpy of reaction and solubility constant can be calculated from the available data. Gorman-Lewis *et al.* [2009GOR/SHV] proposed the solubility of $(\text{Ca}(\text{UO}_2)_2(\text{PO}_4)_2 \cdot 3\text{H}_2\text{O})$. These two phases are included in addition to $\text{Ca}(\text{UO}_2)_2(\text{PO}_4)_2 \cdot 6\text{H}_2\text{O}(\text{cr})$ from Grenthe *et al.* [2020GRE/GAO].

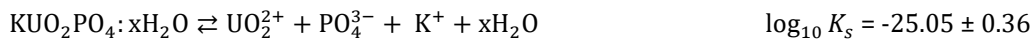
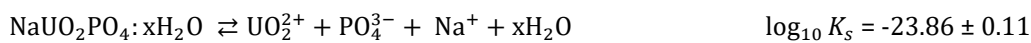
Vesely *et al.* [1965VES/PEK] measured the solubility of $\text{KUO}_2\text{PO}_4 \cdot x\text{H}_2\text{O}(\text{am})$, which constant can be recalculated from the available data.

Van Haverbeke *et al.* [1996HAV/VOC] reported the solubility products on a molar basis of chernikovite ($\text{H}(\text{UO}_2)(\text{PO}_4) \cdot 3\text{H}_2\text{O}$) and meta-Ankoleite ($\text{KUO}_2\text{PO}_4 \cdot 4\text{H}_2\text{O}$) using different uranium(VI) and phosphate chemistry than NEA-OECD selections. Even if the ionic strength of the experiments were not controlled, the solubility data can be used to calculate the solubility products on an basis activity using PHREEQC and the aqueous data from NEA-OECD reviews [2003GUI/FAN; 2020GRE/GAO].

Table 3.8-2. Reinterpretation of the solubility data of chernikovite and meta-ankoleite from Van Haverbeke *et al.* [1996HAV/VOC] using U(VI) and P(V) chemistry from NEA-OECD reviews .

pH	Solubility	$\log_{10} K_s$ [1996HAV/VOC]	$\log_{10} K_s$
Chernikovite ($\text{H}(\text{UO}_2)\text{PO}_4 \cdot 3\text{H}_2\text{O}$)			
0.93	$1.22 \cdot 10^{-2}$	-22.46	-24.44
1.12	$6.30 \cdot 10^{-3}$	-22.81	-24.63
1.38	$3.21 \cdot 10^{-3}$	-22.91	-24.64
		-22.73 ± 0.24	-24.57 ± 0.11
Meta-Ankoleite ($\text{KUO}_2\text{PO}_4 \cdot 4\text{H}_2\text{O}$)			
2.60	$2.26 \cdot 10^{-4}$	-23.20	-25.77
4.13	$4.70 \cdot 10^{-6}$	-25.07	-27.40
4.90	$2.26 \cdot 10^{-6}$	-24.71	-26.98
5.24	$2.15 \cdot 10^{-6}$	-24.21	-26.57
		-24.30 ± 0.81	-26.68 ± 0.69

The solubility constant of $\text{NaUO}_2\text{PO}_4 \cdot x\text{H}_2\text{O}(\text{am})$ and $\text{KUO}_2\text{PO}_4 \cdot x\text{H}_2\text{O}(\text{am})$ are recalculated using the elemental concentration from the data in Table 3 in Vesely *et al.* [1965VES/PEK] as input for a PHREEQC calculation using PRODATA. The activity products are giving the following data.



$\text{UO}_2(\text{PO}_3)_2(\text{s})$ is added from llnl.dat database at the request from ORANO and is noted as non-identified.

$\text{UO}_2\text{HPO}_4 \cdot 3\text{H}_2\text{O}(\text{cr})$ is taken from Gorman-Lewis *et al.* [2009GOR/SHV].

Table 3.8-3. Thermodynamic constants and functions of reaction for the uranyl(VI)phosphate phases, and functions of formation calculated relative to Guillaumont *et al.* [2003GUI/FAN].

Reaction	$\log_{10} K_s$	Reference	$\Delta_r G_m^\circ$ kJ mol ⁻¹	$\Delta_f G_m^\circ$ kJ mol ⁻¹	$\Delta_r H_m^\circ$ kJ mol ⁻¹	$\Delta_f H_m^\circ$ kJ mol ⁻¹
<hr/>						
Parsonsite $Pb_2(UO_2)_2 \cdot 2H_2O \rightleftharpoons 2Pb^{2+} + UO_2^{2+} + 2PO_4^{3-} + 2H_2O$	-45.8	[1984NRI]	261.428	-3 787.717		
<hr/>						
Dumontite $Pb_2(UO_2)_2(PO_4)_2 \cdot 3H_2O \rightleftharpoons 2Pb^{2+} + 2UO_2^{2+} + 2PO_4^{3-} + 4OH^- + 3H_2O$	-91.4	[1984NRI]	521.715	-5 866.575		
$Pb_2(UO_2)_2(PO_4)_2 \cdot (OH)_4 \cdot 3H_2O + 4H^+ \rightleftharpoons 2Pb^{2+} + 2UO_2^{2+} + 2PO_4^{3-} + 7H_2O$	-35.4		202.035			
<hr/>						
Dewindtite $Pb(UO_2)_4(PO_4)_2 \cdot (OH)_4 \cdot 8H_2O \rightleftharpoons Pb^{2+} + 4UO_2^{2+} + 2PO_4^{3-} + 4OH^- + 8H_2O$	-92.6	[1984NRI]	528.565	-8 939.989		
$Pb(UO_2)_4(PO_4)_2 \cdot (OH)_4 \cdot 8H_2O + 4H^+ \rightleftharpoons Pb^{2+} + 4UO_2^{2+} + 2PO_4^{3-} + 12H_2O$	-36.6		208.885			
<hr/>						
Renardite $Pb(UO_2)_4(PO_4)_2 \cdot (OH)_4 \cdot 7H_2O \rightleftharpoons Pb^{2+} + 4UO_2^{2+} + 2PO_4^{3-} + 4OH^- + 7H_2O$	-93.7	[1984NRI]	534.844	-8 709.128		
$Pb(UO_2)_4(PO_4)_2 \cdot (OH)_4 \cdot 7H_2O + 4H^+ \rightleftharpoons Pb^{2+} + 4UO_2^{2+} + 2PO_4^{3-} + 11H_2O$	-37.7		215.164			
<hr/>						
Przhevalskite $Pb(UO_2)_2 \cdot 4H_2O \rightleftharpoons Pb^{2+} + 2UO_2^{2+} + 2PO_4^{3-} + 4H_2O$	-47.4	[1984NRI]	270.561	-5 199.443		
<hr/>						
Torbernite $Cu(UO_2)_2 \cdot 10H_2O \rightleftharpoons Cu^{2+} + 2UO_2^{2+} + 2PO_4^{3-} + 10H_2O$	-41.0	[1984NRI]	234.030	-6 496.468		
<hr/>						
Meta-torbernite $Cu(UO_2)_2 \cdot 8H_2O \rightleftharpoons Cu^{2+} + 2UO_2^{2+} + 2PO_4^{3-} + 8H_2O$	-41.3	[1984NRI]	235.742	-6023.900		
<hr/>						
Meta-torbernite $H_{0.4}Cu_{0.8}(UO_2)_2(PO_4)_2 \cdot 8H_2O \rightleftharpoons 0.8Cu^{2+} + 2UO_2^{2+} + 2PO_4^{3-} + 8H_2O + 0.4H^+$	-52.90 ± 0.10	[2013CRE/SZE]	301.96 ± 0.57	$-6 103.123 \pm 4.912$	301.96 ± 0.57	$-6 882.133 \pm 8.958$
$NaUO_2PO_4 \cdot xH_2O \rightleftharpoons UO_2^{2+} + PO_4^{3-} + Na^+ + xH_2O$	-23.86	[1965VES/PEK]				
$KUO_2PO_4 \cdot xH_2O \rightleftharpoons UO_2^{2+} + PO_4^{3-} + K^+ + xH_2O$	-25.05 ± 0.36					
$UO_2HPO_4 \cdot 3H_2O \rightleftharpoons UO_2^{2+} + PO_4^{3-} + 3H_2O + H^+$	-25.52 ± 0.11	[2009GOR/SHV]	145.68 ± 0.65	$-2 835.140 \pm 2.445$	62.33 ± 3.87	$-3 223.220 \pm 1.995$

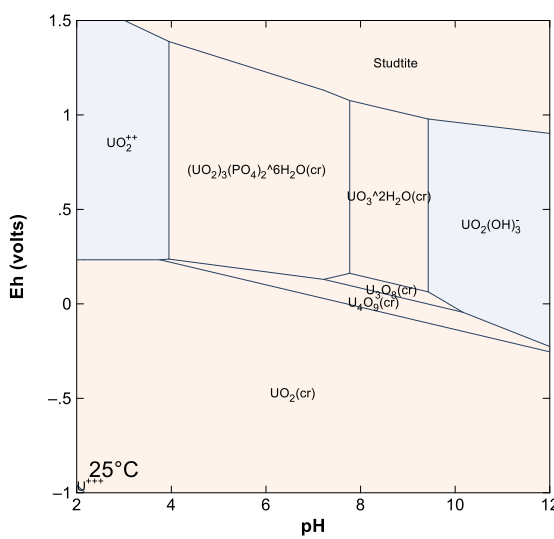


Figure 3.8-2. Pourbaix diagram of 10^{-6} mol kgw⁻¹ U with 10^{-4} mol kgw⁻¹ P using GWB.

3.8.1.5.2 Arsenate Compounds

Several uranium arsenate solids have been selected in Grenthe *et al.* [2020GRE/GAO]. The Gibbs energy of reaction for $\text{KUO}_2\text{AsO}_4(\text{s})$ can be obtained from Naumov *et al.* [1974NAU/RYZ].

Table 3.8-4. Thermodynamic constants and functions of reaction for the As(V) phases of U(VI).

Reaction	$\log_{10} K_s$	$\Delta_f G_m^\circ$ kJ mol ⁻¹	$\Delta_f G_m^\circ$ kJ mol ⁻¹	$\Delta_r H_m^\circ$ kJ mol ⁻¹	$\Delta_f H_m^\circ$ kJ mol ⁻¹
$\text{UO}_2(\text{AsO}_3)_2 + 2\text{H}_2\text{O} \rightleftharpoons \text{UO}_2^{2+} + 2\text{AsO}_4^{3-} + 4\text{H}^+$	-29.77 ± 1.54	169.920 ± 8.766	-1 944.911 ± 12.006 ^a	-67.020 ± 1.498	-2 156.600 ± 8.000 ^a
$(\text{UO}_2)_3(\text{AsO}_4)_2 \rightleftharpoons 3\text{UO}_2^{2+} + 2\text{AsO}_4^{3-}$	-27.40 ± 1.27	156.416 ± 7.242	-4 310.789 ± 12.007 ^a	-143.880 ± 4.500	-4 689.400 ± 8.000 ^a
$(\text{UO}_2)_3(\text{AsO}_4)_2: 12\text{H}_2\text{O}(\text{cr}) \rightleftharpoons 3\text{UO}_2^{2+} + 2\text{AsO}_4^{3-} + 12\text{H}_2\text{O}$	-45.33 ± 1.00	258.744 ± 5.708	-7 258.797 ± 11.160 ^b		
$(\text{UO}_2)_2\text{As}_2\text{O}_7 + \text{H}_2\text{O} \rightleftharpoons 2\text{UO}_2^{2+} + 2\text{AsO}_4^{3-} + 2\text{H}^+$	-29.01 ± 1.44	165.572 ± 8.227	-3 130.254 ± 12.006 ^a	-102.450 ± 3.000	3 426.000 ± 8.000 ^a
$\text{UO}_2\text{HAsO}_4: 4\text{H}_2\text{O} \rightleftharpoons \text{UO}_2^{2+} + \text{AsO}_4^{3-} + \text{H}^+ + 4\text{H}_2\text{O}$	-23.00 ± 0.30	131.284 ± 1.711	-2 680.755 ± 4.698 ^b	32.833 ± 3.566	-3 083.293 ± 5.567 ^b
$\text{NH}_4(\text{UO}_2\text{AsO}_4): 3\text{H}_2\text{O} \rightleftharpoons \text{NH}_4^+ + \text{UO}_2^{2+} + \text{AsO}_4^{3-} + 3\text{H}_2\text{O}$	-24.70 ± 1.00	140.988 ± 5.709	-2 532.717 ± 7.197 ^b		
$\text{Pb}(\text{UO}_2)_2(\text{AsO}_4)_2: 10\text{H}_2\text{O} \rightleftharpoons \text{Pb}^{2+} + 2\text{UO}_2^{2+} + 2\text{AsO}_4^{3-} + 10\text{H}_2\text{O}$	-46.30 ± 1.00	264.281 ± 5.708	-5 861.741 ± 10.458 ^b		
$\text{Zn}(\text{UO}_2)_2(\text{AsO}_4)_2: 8\text{H}_2\text{O} \rightleftharpoons \text{Zn}^{2+} + 2\text{UO}_2^{2+} + 2\text{AsO}_4^{3-} + 8\text{H}_2\text{O}$	-45.10 ± 1.00	257.431 ± 5.709	-5 503.576 ± 10.451 ^b		
$\text{Cd}(\text{UO}_2)_2(\text{AsO}_4)_2: 8\text{H}_2\text{O} \rightleftharpoons \text{Cd}^{2+} + 2\text{UO}_2^{2+} + 2\text{AsO}_4^{3-} + 8\text{H}_2\text{O}$	-45.40 ± 1.00	259.144 ± 5.708	-5 435.819 ± 10.475 ^b		
$\text{Cu}(\text{UO}_2)_2(\text{AsO}_4)_2: 8\text{H}_2\text{O} \rightleftharpoons \text{Cu}^{2+} + 2\text{UO}_2^{2+} + 2\text{AsO}_4^{3-} + 8\text{H}_2\text{O}$	-45.70 ± 1.00	260.862 ± 5.708	-5 294.758 ± 10.563 ^b		
$\text{Ni}(\text{UO}_2)_2(\text{AsO}_4)_2: 10\text{H}_2\text{O} \rightleftharpoons \text{Ni}^{2+} + 2\text{UO}_2^{2+} + 2\text{AsO}_4^{3-} + 10\text{H}_2\text{O}$	-45.90 ± 1.00	261.998 ± 5.708	-5 880.993 ± 10.479 ^b		
$\text{Co}(\text{UO}_2)_2(\text{AsO}_4)_2: 8\text{H}_2\text{O} \rightleftharpoons \text{Co}^{2+} + 2\text{UO}_2^{2+} + 2\text{AsO}_4^{3-} + 8\text{H}_2\text{O}$	-46.50 ± 1.00	265.422 ± 5.708	-5 418.764 ± 10.637 ^b		
$\text{Fe}(\text{UO}_2)_2(\text{AsO}_4)_2: 8\text{H}_2\text{O} \rightleftharpoons \text{Fe}^{2+} + 2\text{UO}_2^{2+} + 2\text{AsO}_4^{3-} + 8\text{H}_2\text{O}$	-46.10 ± 2.20	263.139 ± 12.557	-5 452.800 ± 15.319 ^b		
$\text{Mn}(\text{UO}_2)_2(\text{AsO}_4)_2: 8\text{H}_2\text{O} \rightleftharpoons \text{Mn}^{2+} + 2\text{UO}_2^{2+} + 2\text{AsO}_4^{3-} + 8\text{H}_2\text{O}$	-44.40 ± 1.00	253.437 ± 5.708	-5 580.479 ± 10.460 ^b		
$\text{Mg}(\text{UO}_2)_2(\text{AsO}_4)_2: 10\text{H}_2\text{O} \rightleftharpoons \text{Mg}^{2+} + 2\text{UO}_2^{2+} + 2\text{AsO}_4^{3-} + 10\text{H}_2\text{O}$	-44.60 ± 0.50	254.577 ± 2.855	-6 283.174 ± 9.304 ^b		
$\text{Ca}(\text{UO}_2)_2(\text{AsO}_4)_2: 6\text{H}_2\text{O} \rightleftharpoons \text{Ca}^{2+} + 2\text{UO}_2^{2+} + 2\text{AsO}_4^{3-} + 6\text{H}_2\text{O}$	-45.10 ± 1.00	257.431 ± 5.708	-5 434.899 ± 10.498 ^b		
$\text{Ca}(\text{UO}_2)_2(\text{AsO}_4)_2: 10\text{H}_2\text{O} \rightleftharpoons \text{Ca}^{2+} + 2\text{UO}_2^{2+} + 2\text{AsO}_4^{3-} + 10\text{H}_2\text{O}$	-45.10 ± 1.00	257.431 ± 5.708	-6 383.459 ± 10.503 ^b		
$\text{Ba}(\text{UO}_2)_2(\text{AsO}_4)_2: 7\text{H}_2\text{O} \rightleftharpoons \text{Ba}^{2+} + 2\text{UO}_2^{2+} + 2\text{AsO}_4^{3-} + 7\text{H}_2\text{O}$	-44.70 ± 1.00	255.148 ± 5.708	-5 674.606 ± 10.761 ^b		
$\text{LiUO}_2\text{AsO}_4: 4\text{H}_2\text{O} \rightleftharpoons \text{Li}^+ + \text{UO}_2^{2+} + \text{AsO}_4^{3-} + 4\text{H}_2\text{O}$	-20.40 ± 1.00	116.443 ± 5.708	-2 958.832 ± 7.193 ^b		
$\text{NaUO}_2\text{AsO}_4: 3\text{H}_2\text{O} \rightleftharpoons \text{Na}^+ + \text{UO}_2^{2+} + \text{AsO}_4^{3-} + 3\text{H}_2\text{O}$	-22.80 ± 1.00	130.143 ± 5.708	-2 704.427 ± 7.192 ^b		
$\text{KUO}_2\text{AsO}_4(\text{s}) \rightleftharpoons \text{K}^+ + \text{UO}_2^{2+} + \text{AsO}_4^{3-}$	-21.90	125.030 ^c	2 008.451		
$\text{KUO}_2\text{AsO}_4: 3\text{H}_2\text{O} \rightleftharpoons \text{K}^+ + \text{UO}_2^{2+} + \text{AsO}_4^{3-} + 3\text{H}_2\text{O}$	-23.30 ± 1.00	132.997 ± 5.708	-2 727.838 ± 7.192 ^b		
$\text{RbUO}_2\text{AsO}_4: 3\text{H}_2\text{O} \rightleftharpoons \text{Rb}^+ + \text{UO}_2^{2+} + \text{AsO}_4^{3-} + 3\text{H}_2\text{O}$	-24.60 ± 1.00	140.417 ± 5.708	-2 736.757 ± 7.193 ^b		
$\text{CsUO}_2\text{AsO}_4: 2.5\text{H}_2\text{O} \rightleftharpoons \text{Cs}^+ + \text{UO}_2^{2+} + \text{AsO}_4^{3-} + 2.5\text{H}_2\text{O}$	-25.20 ± 1.00	143.842 ± 5.708	-2 629.059 ± 7.211 ^b		

a [2003GUI/FAN]; b [2020GRE/GAO]; c [1974NAU/RYZ]

3.8.1.6. Carbonate Compounds

The main gap in the NEA-OECD selected data up to Guillaumont *et al.* [2003GUI/FAN] were for the $\text{M}_n\text{UO}_2(\text{CO}_3)^{(4-2n)-}_3$ complexes that were first evidenced by Bernhard *et al.* [1996BER/GEI]. These determinations — see also Kalmykov and Choppin [2000KAL/CHO] — were not selected in Guillaumont *et al.* [2003GUI/FAN].

Since then, further determinations have been reported [2006DON/BRO; 2008DON/BRO; 2008GEI/AMA; 2013LEE/YUN; 2014END/RAO; 2017LEE/VES; 2019JO/KIR; 2020aSHA/REI; 2020bSHA/REI], out of which the evolution as a function of ionic strength [2000KAL/CHO; 2008DON/BRO; 2020aSHA/REI; 2020bSHA/REI], and the influence of temperature [2014END/RAO; 2019JO/KIR] were scarcely studied.

Part of these gaps have been addressed in Grenthe *et al.* [2020GRE/GAO], with the selection of some $M_nUO_2(CO_3)_3^{(4-2n)-}$ complexes. Nonetheless, no specific ion interaction coefficients have been selected. Slightly different selections will be made in PRODATA, mainly due to the works from Jo *et al.* [2019JO/KIR; 2019JO/KIM], and Shang *et al.* [2020aSHA/REI; 2020bSHA/REI; 2021aSHA/REI], which were published after the 2018 cut-off date of Grenthe *et al.* [2020GRE/GAO].

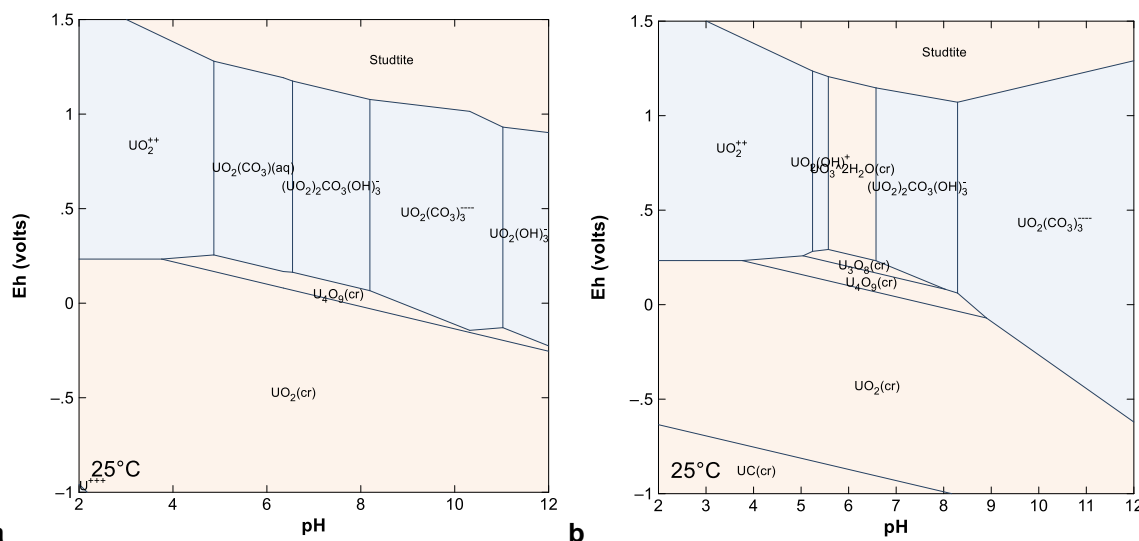


Figure 3.8-3. Pourbaix diagram using GWB of $10^{-6} \text{ mol kg}_w^{-1} \text{ U}$ and $10^{-3} \text{ mol kg}_w^{-1} \text{ C}$ (a), and in equilibrium with $P(CO_2) = 10^{-3.5} \text{ atm}$ (b).

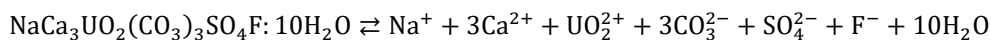
3.8.1.6.1 Carbonate Solids

The formation of triscarbonatouranyl phases of alkaline earths has been evidenced since the mid-19th century [1848SMI; 1851SMI]. Thermodynamic functions have been evaluated by solubility study [1980ALW; 1980ALW/WIL], of bayleyite ($Mg_2UO_2(CO_3)_3 \cdot 18H_2O$), liebigite ($Ca_2UO_2(CO_3)_3 \cdot 11H_2O$), swartzite ($MgCaUO_2(CO_3)_3 \cdot 12H_2O$), and andersonite ($Na_2CaUO_2(CO_3)_3 \cdot 6H_2O$). These values were not selected in the first NEA commissioned selection [1992GRE/FUG], because of evident problems in calculations for andersonite in Alwan and Williams [1980ALW/WIL]. It should nevertheless be noted that O'Brien and Williams [19830BR/WIL] proposed a correction of the $\Delta_f G_m^\circ$ of andersonite, which was not noted in any review [1992GRE/FUG; 1995SIL/BID; 2003GUI/FAN; 2020GRE/GAO]. O'Brien and Williams [19830BR/WIL] also proposed solubility values for schröckingerite ($NaCa_3UO_2(CO_3)_3SO_4F \cdot 10H_2O$) and grimselite ($K_3NaUO_2(CO_3)_3 \cdot H_2O$).

Chen *et al.* [1999CHE/EWI] recalculated the $\Delta_f G_m^\circ$ for the phases from the $\log_{10} K_{SP}$ — which estimation is not described — and $\Delta_f G_m^\circ$ selected in Grenthe *et al.* [1992GRE/FUG]. Kubatko *et al.* [2005KUB/HEL] reported $\Delta_f H_m^\circ$ for andersonite and recalled the previous wrong value from Alwan and Williams [1980ALW/WIL]. Later, Gorman-Lewis *et al.* [2008GOR/BUR] seem to propose inconsistent values of $\log_{10} K_{SP}$ from a mix of the $\Delta_f G_m^\circ$ from Alwan and Williams [1980ALW/WIL] — initially calculated using $\Delta_f G_m^\circ$ (ions, water) from Barner and Scheuerman [1978BAR/SCH] and $\Delta_f G_m^\circ$ (ions, water) from Grenthe *et al.* [1992GRE/FUG]. As stressed by Endrizzi *et al.*

[2016END/LEG], the differences between $\Delta_f G_m^\circ(\text{UO}_2^{2+})$ in Barner and Scheuerman [1978BAR/SCH] and the one selected in Grenthe *et al.* [1992GRE/FUG] is leading to a difference of *ca.* -37 kJ mol⁻¹ in the final value of $\Delta_r G_m^\circ$, and 6.5 order of magnitude in the final $\log_{10} K_{\text{SP}}$ — which corresponds approximately to the difference in $\log_{10} K_{\text{SP}}$ given in Table 1 from Gorman-Lewis *et al.* [2008GOR/BUR] and the one which can be extrapolated from Figure 2 in Alwan and Williams [1980ALW/WIL].

The functions of reaction and solubilities of schröckingerite and grimselite in O'Brien and Williams [1983OBR/WIL] can also be eventually calculated from the function of formation in Barner and Scheuerman [1978BAR/SCH], even if it is not explicitly written as it is in Alwan and Williams [1980ALW/WIL]. As for the phases in Alwan and Williams [1980ALW/WIL], this leads to a particular difference as in addition to the aforementioned -37 kJ mol⁻¹ difference for $\Delta_f G^\circ(\text{UO}_2^{2+})$, a -40 kJ mol⁻¹ difference for $\Delta_f G^\circ(\text{SO}_4^{2-})$ is showing between Barner and Scheuerman [1978BAR/SCH] and Grenthe *et al.* [1992GRE/FUG].

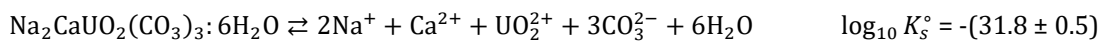
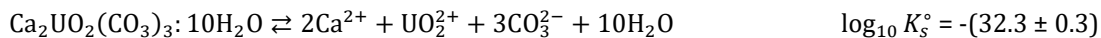


$$\Delta_r G^\circ = 146.11 \text{ kJ mol}^{-1}$$

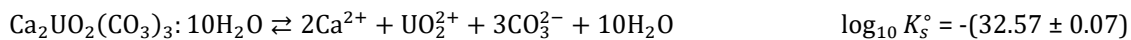
$$\log_{10} K^\circ = -25.60$$

As the presence of the $\text{Ca}_n\text{UO}_2(\text{CO}_3)_3^{(4-2n)-}$ complexes were not accounted for, the solubility should be recalculated accordingly.

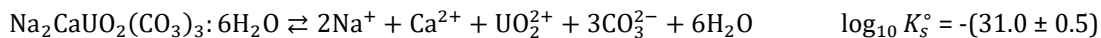
Lee *et al.* [2019LEE/AMA] studied the solubility of liebigite at varying temperature and proposed the formation of $\text{Ca}_2\text{UO}_2(\text{CO}_3)_3: 10\text{H}_2\text{O}$ instead of $\text{Ca}_2\text{UO}_2(\text{CO}_3)_3: 11\text{H}_2\text{O}$. The authors reported that at 5.61 mol kg_w⁻¹ NaCl liebigite transforms to andersonite. A reinterpretation of the data from Alwan and Williams [1980ALW/WIL] was done, and new experiments were reported. The authors proposed the following solubility constants taking into account the $\text{Ca}_n\text{UO}_2(\text{CO}_3)_3^{(4-2n)-}$ complexation constants from Lee and Yun [2013LEE/YUN].



Using the elemental data in Lee *et al.* [2019LEE/AMA] and the thermodynamic data in Shang and Reiller [2020aSHA/REI] detailed further (*vide infra*) the solubility constants can be recalculated as follows.

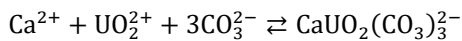


For the sole experiment in which andersonite was evidenced the value of activity product is the following



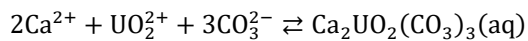
3.8.1.6.2 Calcium(II)triscarbonatouranyl(VI) Complexes

The most complete study on $\text{Ca}_n\text{UO}_2(\text{CO}_3)_3^{(4-2n)-}$ complexes to date is from the Chengming Shang's PhD Shang and Reiller [2020aSHA/REI] and Shang *et al.* [2020bSHA/REI], the $\log_{10} \beta^\circ$ and ε values are included in PRODATA (Table 3.8-6).



$$\log_{10} \beta^\circ = 27.20 \pm 0.04$$

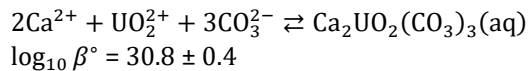
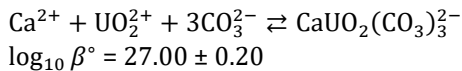
$$\varepsilon(\text{CaUO}_2(\text{CO}_3)_3^{2-}, \text{Na}^+) = 0.29 \text{ kg}_w \text{ mol}^{-1}$$



$$\log_{10} \beta^\circ = 30.49 \pm 0.05$$

$$\varepsilon(\text{Ca}_2\text{UO}_2(\text{CO}_3)_3(\text{aq}), \text{NaCl}) = 0.66 \text{ kg}_w \text{ mol}^{-1}$$

One can compare these latter data to the one selected from analysis of earlier studies in NEA-OECD review [2020GRE/GAO].



but with no ε values.

An illustration of the differences in speciation results between the constants and ε values from Shang and Reiller [2020aSHA/REI], and the constants and $\varepsilon = 0$ as selected in NEA-OECD [2020GRE/GAO] can be seen in Figure 3.8-4. In both cases, $\text{CaUO}_2(\text{CO}_3)_3^{2-}$ is the dominant complex at pH > 7.25 but slight differences between both cases can be noted. A clear predominance of $\text{CaUO}_2(\text{CO}_3)_3^{2-}$ is obtained, with $\text{Ca}_2\text{UO}_2(\text{CO}_3)_3(\text{aq})$ and $\text{UO}_2(\text{CO}_3)_3^{4-}$ sharing subdominance using data from Shang and Reiller [2020aSHA/REI] at pH > 7.25 (Figure 3.8-4a). For the data selected in NEA-OECD [2020GRE/GAO] (Figure 3.8-4b) the $\text{Ca}_n\text{UO}_2(\text{CO}_3)_3^{(4-2n)-}$ complexes are sharing predominance with $\text{UO}_2(\text{CO}_3)_3^{4-}$ being subdominant. This comes from the higher stepwise constant in the latter case.

	[2020aSHA/REI]	[2020GRE/GAO]
$\text{CaUO}_2(\text{CO}_3)_3^{2-} + \text{Ca}^{2+} \rightleftharpoons \text{Ca}_2\text{UO}_2(\text{CO}_3)_3(\text{aq})$	$\log_{10} K^\circ = 3.29 \pm 0.26$	$\log_{10} K^\circ = 3.8$

Greater differences can occur when considering higher ionic strengths — *vide post* § 4.6.2 —. An illustration is shown in Figure 3.8-4c,d at $I_m = 0.5 \text{ mol kg}_w^{-1}$ NaCl and $[\text{Ca}]_{\text{total}} = 10 \text{ mmol kg}_w^{-1}$ and pH fixed by NaOH, where $\text{CaUO}_2(\text{CO}_3)_3^{2-}$ is dominant at pH > 7 using data from Shang and Reiller [2020aSHA/REI], and $\text{Ca}_2\text{UO}_2(\text{CO}_3)_3(\text{aq})$ is dominant using NEA-OECD [2020GRE/GAO]. The free energy of formation for the two complexes are calculated using the thermodynamic functions for UO_2^{2+} , CO_3^{2-} , and Ca^{2+} selected in NEA-OECD Guillaumont *et al.* [2003GUI/FAN].

Endrizzi and Rao [2014END/RAO] — which were selected in Grenthe *et al.* [2020GRE/GAO] — and Jo *et al.* [2019JO/KIR] — which were published after the cut-off date of Grenthe *et al.* [2020GRE/GAO] — proposed estimations of $\Delta_r H_m^\circ$ for $\text{Ca}_n\text{UO}_2(\text{CO}_3)_3^{(4-2n)-}$. Since then, Maia *et al.* [2021MAI/RIB] and Shang and Reiller [2021bSHA/REI] also determined the $\Delta_r H_m^\circ$ and $\Delta_r S_m^\circ$ values for the $\text{Ca}_n\text{UO}_2(\text{CO}_3)_3^{(4-2n)-}$ complexes.

The comparison between the stepwise $\Delta_r H_m^\circ$ and $-T\Delta_r S_m^\circ$ values from the different authors is presented in Figure 3.8-5. It can be seen that the stepwise $\Delta_r H_m^\circ$ values are typically weak and not statistically different from nil — except for $\text{CaUO}_2(\text{CO}_3)_3^{2-}$ in Maia *et al.* [2021MAI/RIB]. The stepwise complexation phenomena are mainly driven by entropy.

In order to be conservative, the average values all the studies [2014END/RAO; 2019JO/KIR; 2021MAI/RIB; 2021bSHA/REI] will be used in PRODATA (Table 3.8-6 and Figure 3.8-5).

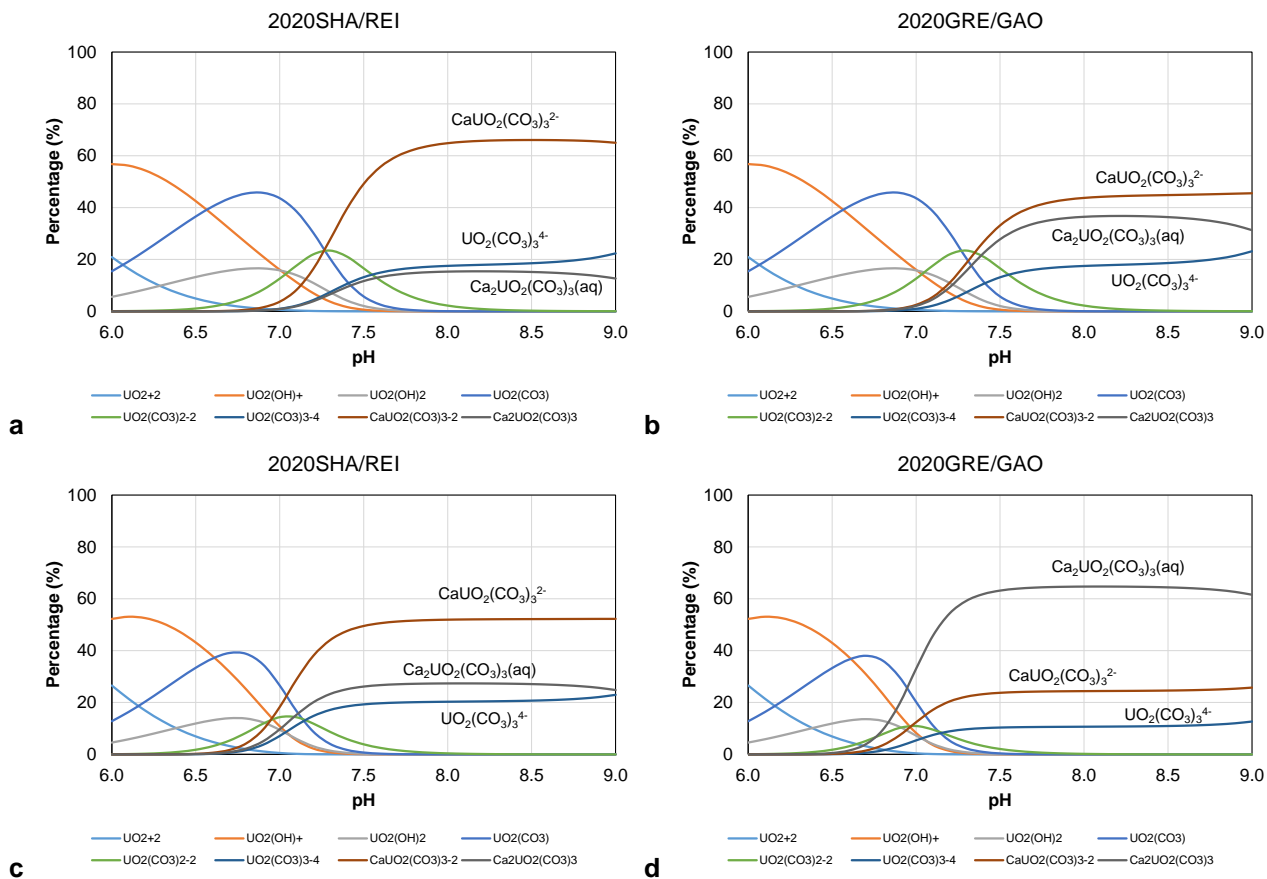


Figure 3.8-4. Speciation of uranium(VI) at equilibrium with $P(\text{CO}_2\text{(g)}) = 10^{-3.5}$ atm at ionic strength $I_m = 0.1 \text{ mol kg}^{-1} \text{ NaCl}$ with $[\text{Ca}]_{\text{total}} = 1 \text{ mmol kg}^{-1}$ (a,b), and $I_m = 0.5 \text{ mol kg}^{-1}$ with $[\text{Ca}]_{\text{total}} = 10 \text{ mmol kg}^{-1}$ (c,d) using thermodynamic constants and specific ion interaction coefficients from Shang and Reiller [2020aSHA/REI] (a,c), and constants and $\varepsilon = 0$ from NEA-OECD [2020GRE/GAO] (b,d); pH fixed by NaOH, PHREEQC extraction for SIT calculation.

Table 3.8-5. Comparision of thermodynamic functions $\Delta_r H^\circ_m$ and $T\Delta_r S^\circ_m$ for the stepwise and cumulative formation of $\text{CaUO}_2(\text{CO}_3)_3^{2-}$ and $\text{Ca}_2\text{UO}_2(\text{CO}_3)_3(\text{aq})$.

	[2014END/RAO]	[2019J0/KIR]	[2021MAI/RIB]	[2021bSHA/REI]
	$\Delta_r H_m^\circ$ kJ mol ⁻¹	$T\Delta_r S_m^\circ$ kJ mol ⁻¹	$\Delta_r H_m^\circ$ kJ mol ⁻¹	$T\Delta_r S_m^\circ$ kJ mol ⁻¹
$\text{Ca}^{2+} + \text{UO}_2(\text{CO}_3)_3^{4-} \rightleftharpoons \text{CaUO}_2(\text{CO}_3)_3^{2-}$	-8 ± 6	12 ± 6	-1.2 ± 0.3	28.4 ± 0.9
				14.8 ± 3.5
				45.5 ± 3.9
				4.8 ± 5.9
				36.5 ± 6.0
$\text{Ca}^{2+} + \text{UO}_2^{2+} + 3\text{CO}_3^{2-} \rightleftharpoons \text{CaUO}_2(\text{CO}_3)_3^{2-}$	-47 ± 7*	107 ± 6	-40.4 ± 4.1	45.1 ± 5.8
				-24.4 ± 2.2
				131 ± 5
				-34.4 ± 7.2
				51.1 ± 8.29
$\text{Ca}^{2+} + \text{CaUO}_2(\text{CO}_3)_3^{2-} \rightleftharpoons \text{Ca}_2\text{UO}_2(\text{CO}_3)_3(\text{aq})$	0 ± 7	22 ± 7	-1.9 ± 3.0	46.6 ± 3.1
				21 ± 48
				0 ± 1
				-1.3 ± 11.9
				50.2 ± 11.9
$2\text{Ca}^{2+} + \text{UO}_2^{2+} + 3\text{CO}_3^{2-} \rightleftharpoons \text{Ca}_2\text{UO}_2(\text{CO}_3)_3(\text{aq})$	-47 ± 8*	129 ± 7	-42.3 ± 5.1	43.2 ± 5.14
				-3 ± 10
				167 ± 10
				-40.5 ± 11.9
				45.0 ± 12.6

* the uncertainty is recalculated

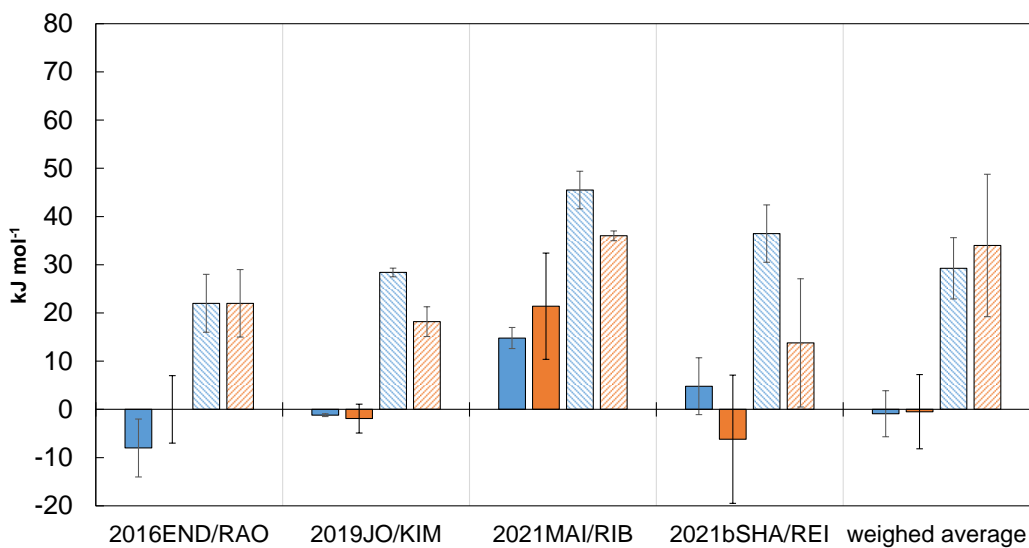
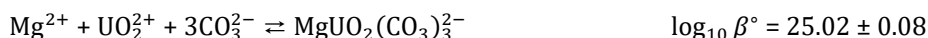


Figure 3.8-5. Comparision of thermodynamic functions $\Delta_rH_m^\circ$ and $-T\Delta_rS_m^\circ$ for the stepwise formation of $\text{CaUO}_2(\text{CO}_3)_3^{2-}$ and $\text{Ca}_2\text{UO}_2(\text{CO}_3)_3(\text{aq})$.

3.8.1.6.3 Magnesium(II)triscarbonatouranyl(VI) Complexes

The $\text{Mg}_n\text{UO}_2(\text{CO}_3)_3^{(4-2n)-}$ complexes as up to now received limited attention [2006DON/BRO; 2008DON/BRO; 2017LEE/VES] from the point of view of ionic strength dependence. Dong and Brooks [2006DON/BRO; 2008DON/BRO] did not succeed in evidencing $\text{Mg}_2\text{UO}_2(\text{CO}_3)_3(\text{aq})$, and only Dong and Brooks [2008DON/BRO] proposed the ionic strength evolution of $\text{MgUO}_2(\text{CO}_3)_3^{2-}$ in NaNO_3 , for which they obtained a rather high and unexpected dependence. The constant and ϵ parameter for the formation of $\text{MgUO}_2(\text{CO}_3)_3^{2-}$ according to Dong and Brooks [2008DON/BRO] would end up as follows.



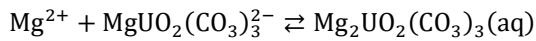
$$\epsilon(\text{Na}^+, \text{MgUO}_2(\text{CO}_3)_3^{2-}) = -3.2 \text{ kg}_w \text{ mol}^{-1}$$

This was slightly lower than the value extrapolated from 0.1 M NaNO_3 to infinite dilution using the Davies [1962DAV] equation in Dong and Brooks [2006DON/BRO], i.e., $\log_{10} \beta^\circ = 26.11 \pm 0.04$.

The use of this $\epsilon(\text{Na}^+, \text{MgUO}_2(\text{CO}_3)_3^{2-})$ value in Reiller and Descostes [2020REI/DES] led to a predominance of $\text{MgUO}_2(\text{CO}_3)_3^{2-}$ in media where high ionic strengths can be anticipated. This trend must be questioned with other observations.

Lee *et al.* [2017LEE/VES] proposed in TRLFS the formation of both $\text{Mg}_n\text{UO}_2(\text{CO}_3)_3^{(4-2n)-}$ complexes, and only extrapolated the $\log_{10} \beta^\circ$ values from 0.1 M NaClO_4 using a charged-like hypothesis where $\epsilon(\text{Na}^+, \text{MgUO}_2(\text{CO}_3)_3^{2-}) = \epsilon(\text{Na}^+, \text{UO}_2(\text{CO}_3)_2^{2-}) = -0.02 \text{ kg}_w \text{ mol}^{-1}$, and assuming $\epsilon(\text{Mg}_2\text{UO}_2(\text{CO}_3)_3(\text{aq}), \text{NaClO}_4) = 0$, which have been shown not to be applicable by Shang and Reiller [2020aSHA/REI] in the case of $\text{Ca}_n\text{UO}_2(\text{CO}_3)_3^{(4-2n)-}$ complexes. It is also worthy to notice that Oher *et al.* [2020OHE/VER] seem to show from DFT calculation of the excited states that $\text{MgUO}_2(\text{CO}_3)_3^{2-}$ and $\text{Mg}_2\text{UO}_2(\text{CO}_3)_3(\text{aq})$ are not likely to be distinguished from their luminescence spectra.

In the latter NEA-OECD review [2020GRE/GAO], the $\log_{10} \beta^\circ (\text{MgUO}_2(\text{CO}_3)_3^{2-}) = 26.2 \pm 0.2$ and $\log_{10} \beta^\circ (\text{Mg}_2\text{UO}_2(\text{CO}_3)_3(\text{aq})) = 27.1 \pm 0.6$ were selected. This means that the second stepwise reaction, is very weak.



$$\log_{10} K^\circ = 0.9$$

Shang and Reiller [2021aSHA/REI] proposed the formation constant of $\text{MgUO}_2(\text{CO}_3)_3^{2-}$ using TRLFS, but as Dong and Brooks [2006DON/BRO; 2008DON/BRO] did not observe the formation of $\text{Mg}_2\text{UO}_2(\text{CO}_3)_3(\text{aq})$. The authors also determined the $\varepsilon(\text{Na}^+, \text{MgUO}_2(\text{CO}_3)_3^{2-}) = (0.09 \pm 0.16) \text{ kg}_w \text{ mol}^{-1}$ in agreement with their determined value of $\varepsilon(\text{Na}^+, \text{CaUO}_2(\text{CO}_3)_3^{2-})$. This latter value will be included in PRODATA.

Jo *et al.* [2019JO/KIM] and Shang and Reiller [2021bSHA/REI] proposed variation of $\log_{10} K(T)$.

The slight differences between values in NEA-OECD review [2020GRE/GAO] and Shang and Reiller [2021aSHA/REI] under different conditions are illustrated in Figure 3.8-6.

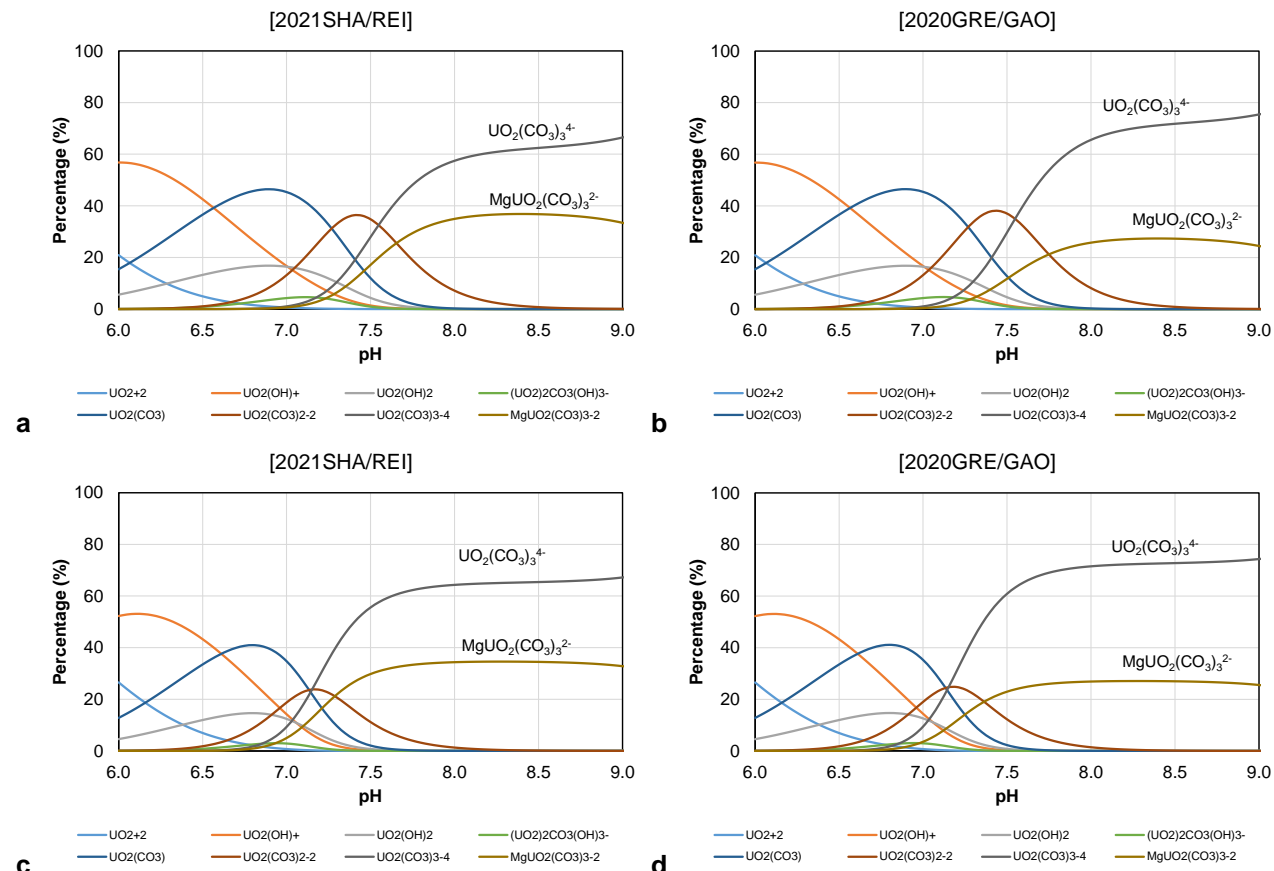


Figure 3.8-6. Speciation of uranium(VI) at equilibrium with $P(\text{CO}_2(\text{g})) = 10^{-3.5} \text{ atm}$ at ionic strength $I_m = 0.1 \text{ mol kg}_w^{-1} \text{ NaCl}$ with $[\text{Mg}]_{\text{total}} = 1 \text{ mmol kg}_w^{-1}$ (a,b), and $I_m = 0.5 \text{ mol kg}^{-1}$ with $[\text{Mg}]_{\text{total}} = 10 \text{ mmol kg}_w^{-1}$ (c,d) using thermodynamic constants and specific ion interaction coefficients from Shang and Reiller [2021aSHA/REI] (a,c), and constants and $\varepsilon = 0$ from NEA-OECD [2020GRE/GAO] (b,d); pH fixed by NaOH, PHREEQC extraction for SIT calculation.

3.8.1.6.4 Other Alkaline Earth(II)triscarbonatouranyl(VI) Complexes

Dong and Brooks [2006DON/BRO] proposed complexation constants for $\text{SrUO}_2(\text{CO}_3)_3^{2-}$ and $\text{Ba}_n\text{UO}_2(\text{CO}_3)_3^{(4-2n)-}$ ($n = \{1; 2\}$) after extrapolation from 0.1 M NaNO_3 to infinite dilution using the Davies [1962DAV] equation (Table 3.8-6). The luminescence spectrum of $\text{SrUO}_2(\text{CO}_3)_3^{2-}$ was evidenced in Beccia *et al.* [2017BEC/MAT]. These extrapolations are included in PRODATA, but neither $\varepsilon(\text{Na}^+, \text{MUO}_2(\text{CO}_3)_3^{2-})$ nor $\varepsilon(\text{M}_2\text{UO}_2(\text{CO}_3)_3(\text{aq}), \text{Na}^+\text{Cl}^-)$ values are given.

Table 3.8-6. Thermodynamic constants and functions for the alkaline earth(II)triscarbonatouranyl(VI) complexes.

Reaction	$\log_{10}\beta^\circ$	$\Delta_r G_m^\circ$ kJ mol ⁻¹	$\Delta_f G_m^\circ$ [*] kJ mol ⁻¹	$\Delta_r H_m^\circ$ kJ mol ⁻¹	$\Delta_f H_m^\circ$ [*] kJ mol ⁻¹
$\text{Ca}^{2+} + \text{UO}_2^{2+} + 3\text{CO}_3^{2-} \rightleftharpoons \text{CaUO}_2(\text{CO}_3)_3^{2-}$	$27.20 \pm 0.04^{\text{a}}$	-155.259 ± 0.228	$-3\ 244.316 \pm 2.361$	$4.9 \pm 5.9^{\text{f}}$	$-3\ 622.0 \pm 7.5$
$2\text{Ca}^{2+} + \text{UO}_2^{2+} + 3\text{CO}_3^{2-} \rightleftharpoons \text{Ca}_2\text{UO}_2(\text{CO}_3)_3(\text{aq})$	$30.49 \pm 0.05^{\text{a}}$	-174.038 ± 0.285	$-3\ 815.901 \pm 2.985$	$-6.2 \pm 13.3^{\text{f}}$	$-4\ 171.2 \pm 15.3$
$\text{Mg}^{2+} + \text{UO}_2^{2+} + 3\text{CO}_3^{2-} \rightleftharpoons \text{MgUO}_2(\text{CO}_3)_3^{2-}$	$25.02 \pm 0.08^{\text{b}}$	-142.815 ± 0.457	—	—	—
$\text{Mg}^{2+} + \text{UO}_2^{2+} + 3\text{CO}_3^{2-} \rightleftharpoons \text{MgUO}_2(\text{CO}_3)_3^{2-}$	$26.11 \pm 0.04^{\text{c}}$	-149.037 ± 0.228	—	—	—
$\text{Mg}^{2+} + \text{UO}_2^{2+} + 3\text{CO}_3^{2-} \rightleftharpoons \text{MgUO}_2(\text{CO}_3)_3^{2-}$	$25.8 \pm 0.3^{\text{d}}$	-147.267 ± 1.733	—		
$2\text{Mg}^{2+} + \text{UO}_2^{2+} + 3\text{CO}_3^{2-} \rightleftharpoons \text{Mg}_2\text{UO}_2(\text{CO}_3)_3(\text{aq})$	$27.1 \pm 0.6^{\text{d}}$	-154.688 ± 3.425	—		
$\text{Mg}^{2+} + \text{UO}_2^{2+} + 3\text{CO}_3^{2-} \rightleftharpoons \text{MgUO}_2(\text{CO}_3)_3^{2-}$	$26.40 \pm 0.07^{\text{e}}$	-150.692 ± 0.400	$-3\ 142.308 \pm 2.523$	$-11.7 \pm 10.3^{\text{f}}$	$-3\ 562.5 \pm 11.2$
$\text{Sr}^{2+} + \text{UO}_2^{2+} + 3\text{CO}_3^{2-} \rightleftharpoons \text{SrUO}_2(\text{CO}_3)_3^{2-}$	$26.86 \pm 0.04^{\text{c}}$	-153.312 ± 0.228	—	—	—
$\text{Ba}^{2+} + \text{UO}_2^{2+} + 3\text{CO}_3^{2-} \rightleftharpoons \text{BaUO}_2(\text{CO}_3)_3^{2-}$	$26.68 \pm 0.04^{\text{c}}$	-152.285 ± 0.228	—	—	—
$2\text{Ba}^{2+} + \text{UO}_2^{2+} + 3\text{CO}_3^{2-} \rightleftharpoons \text{Ba}_2\text{UO}_2(\text{CO}_3)_3(\text{aq})$	$29.74 \pm 0.07^{\text{c}}$	-169.751 ± 0.400	—	—	—

a [2020aSHA/REI]; b [2008DON/BRO]; c [2006DON/BRO]; d [2017LEE/VES]; e [2021aSHA/REI]; f [2021bSHA/REI].

* calculated from $\Delta_f G_m^\circ$ or $\Delta_f H_m^\circ$ in [2003GUI/FAN; 2020GRE/GAO]. -4 171.237 ± 15.257

values in italic are not included in PRODATA.

3.8.1.7. Silicate Compounds

Silicate phases of uranium have been selected in Grenthe *et al.* [2020GRE/GAO]. Nevertheless, the thermodynamic functions used for $\text{Si(OH)}_4(\text{cr})$ are announced from the forthcoming ancillary data review, which is still under peer-review. Hence, the selected data will be corrected to the functions of formation of $\text{Si(OH)}_4(\text{cr})$ in Guillaumont *et al.* [2003GUI/FAN].

Coffinite ($\text{USiO}_4(\text{cr})$) is present in the NEA-OECD selected data since Grenthe *et al.* [1992GRE/FUG]. The solubility of U(IV) phases is often largely influenced by amorphous phase like $\text{USiO}_4(\text{am})$, for which Thoenen *et al.* [2014THO/HUM] provided an estimation of the $\log_{10} K_s$ value.

The selected solubility constant for soddyite ($(\text{UO}_2)_2\text{SiO}_4 \cdot 2\text{H}_2\text{O}$) from Gorman-Lewis *et al.* [2007GOR/MAZ] is used to recalculate $\Delta_f G_m^\circ((\text{UO}_2)_2\text{SiO}_4 \cdot 2\text{H}_2\text{O})$ using $\Delta_f G_m^\circ(\text{Si(OH)}_4(\text{aq}))$ from Guillaumont *et al.* [2003GUI/FAN] — the value in Grenthe *et al.* [2020GRE/GAO] is calculated from the forthcoming ancillary data selection given in advance but still currently under peer-review.

The functions of formation of boltwoodite ($\text{KUO}_2(\text{SiO}_3\text{OH}) \cdot \text{H}_2\text{O}$) and Na-boltwoodite $\text{NaUO}_2(\text{SiO}_3\text{OH}) \cdot \text{H}_2\text{O}$ selected in Grenthe *et al.* [2020GRE/GAO] are used to calculate the $\Delta_f G_m^\circ$ using $\Delta_f G_m^\circ(\text{Si(OH)}_4(\text{aq}))$ from Guillaumont *et al.* [2003GUI/FAN].

The calcium silicate phase uranophane ($\text{Ca}(\text{UO}_2)_2(\text{SiO}_3\text{OH})_2 \cdot 5\text{H}_2\text{O}(\text{cr})$) has been suspected to control the solubility of uranium in silicate rich medium, such altered cement pore water [2004POI/LAN]. The Gibbs energy of formation selected in Grenthe *et al.* [2020GRE/GAO] is used to calculate the $\Delta_f G_m^\circ$ using $\Delta_f G_m^\circ(\text{Si(OH)}_4(\text{aq}))$ from Guillaumont *et al.* [2003GUI/FAN].

Table 3.8-7. Thermodynamic constants and thermodynamic functions of Si phases of U.

Reaction	$\log_{10} K_s^\circ$	$\Delta_r G_m^\circ \text{ kJ mol}^{-1}$	$\Delta_f G_m^\circ \text{ kJ mol}^{-1}$	$\Delta_r H_m^\circ \text{ kJ mol}^{-1}$	$\Delta_f H_m^\circ \text{ kJ mol}^{-1}$
$\text{USiO}_4(\text{am}) + 4\text{H}^+ \rightleftharpoons \text{U}^{4+} + \text{Si(OH)}_4(\text{aq})$	$-1.5 \pm 1.0^{\text{a}}$	8.562 ± 5.708			
$(\text{UO}_2)_2\text{SiO}_4 \cdot 2\text{H}_2\text{O} + 4\text{H}^+ \rightleftharpoons 2\text{UO}_2^{2+} + \text{Si(OH)}_4(\text{aq}) + 2\text{H}_2\text{O}$	$5.75 \pm 0.26^{\text{b}}$	-31.794 ± 1.438	$-3654.296 \pm 3.969^{\text{c}}$		
$\text{KUO}_2(\text{HSiO}_4) \cdot \text{H}_2\text{O} \rightleftharpoons \text{K}^+ + \text{UO}_2^{2+} + \text{Si(OH)}_4(\text{aq}) + \text{H}^+ + \text{H}_2\text{O}$	$4.48 \pm 1.17^{\text{b}}$	-25.572 ± 6.678	$-2754.364 \pm 6.975^{\text{c}}$	$-27.047 \pm 7.018^{\text{b}}$	$-2986.883 \pm 7.843^{\text{c}}$
$\text{NaUO}_2(\text{HSiO}_4) \cdot \text{H}_2\text{O} \rightleftharpoons \text{Na}^+ + \text{UO}_2^{2+} + \text{Si(OH)}_4(\text{aq}) + \text{H}^+ + \text{H}_2\text{O}$	$5.81 \pm 0.44^{\text{b}}$	-33.164 ± 2.512	$-2726.215 \pm 3.226^{\text{c}}$		
$\text{Ca}(\text{UO}_2)_2(\text{SiO}_3\text{OH})_2 \cdot 5\text{H}_2\text{O}(\text{cr}) + 6\text{H}^+ \rightleftharpoons \text{Ca}^{2+} + 2\text{UO}_2^{2+} + 2\text{Si(OH)}_4(\text{aq}) + 5\text{H}_2\text{O}$	$11.52 \pm 0.16^{\text{b}}$	-65.757 ± 0.913	$-6193.321 \pm 4.281^{\text{c}}$		

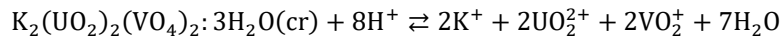
a Thoenen *et al.* [2014THO/HUM]; b selected in Grenthe *et al.* [2020GRE/GAO]; c recalculated using the functions of $\text{Si(OH)}_4(\text{aq})$ from Guillaumont *et al.* [2003GUI/FAN].

3.8.1.8. d-Transition Series Compounds

3.8.1.8.1 Vanadate Compounds

Vanadate phases of uranium have been selected in the last NEA-OECD review [2020GRE/GAO]. As noted earlier (c.f. § 3.7.11), the selected functions of formation are only accounting for vanadium(V), including $\text{VO}_2^+ - \Delta_f G_m^\circ$, $\Delta_f H_m^\circ$ and $S_{f,m}^\circ - \Delta_f G_m^\circ$ only. For VO_2^+ , the functions of formation are slightly different than the choice of Brown and Ekberg [2016BRO/EKB]. As the choice of the hydrolysis constants have been made, the function of reaction will be calculated relative to VO_2^+ , and the functions of formations will be recalculated accordingly.

In Grenthe *et al.* [2020GRE/GAO], $\text{K}_2(\text{UO}_2)_2(\text{VO}_4)_2 \cdot 3\text{H}_2\text{O}(\text{cr})$ selected the $\log_{10} K_s = -1.10 \pm 0.40$ for



and $\Delta_f G_m^\circ$ values, which can be recalculated using the VO_2^+ functions of formation values from the standard redox potentials.

The other vanadate and pyrovanadate phases functions of formation are selected from thermochemistry measurements and Gibbs-Helmholtz equation.

Table 3.8-8. Thermodynamic functions and constants for the solubility of U(VI) vanadate phases.

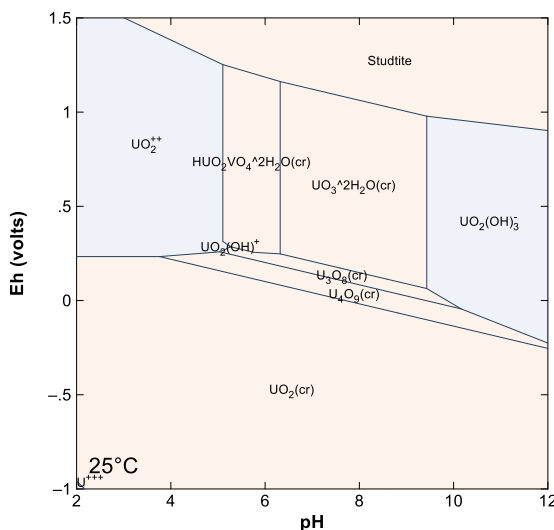
Reaction	$\Delta_r G^\circ * \text{ (kJ mol}^{-1}\text{)}$	$\log_{10} K^\circ$	$\Delta_f G_m^\circ \dagger \text{ (kJ mol}^{-1}\text{)}$	$\Delta_r H^\circ * \text{ (kJ mol}^{-1}\text{)}$	$\Delta_f H_m^\circ \dagger \text{ (kJ mol}^{-1}\text{)}$
$\text{HUO}_2\text{VO}_4 \cdot 2\text{H}_2\text{O}(\text{cr}) + 3\text{H}^+ \rightleftharpoons \text{UO}_2^{2+} + \text{VO}_2^+ + 4\text{H}_2\text{O}$	-11.312 ± 2.562	1.98 ± 0.45	-2476.799 ± 3.262	-56.560 ± 2.639	-2755.560 ± 3.200
$(\text{UO}_2)_2\text{V}_2\text{O}_7(\text{cr}) + 6\text{H}^+ \rightleftharpoons 2\text{UO}_2^{2+} + 2\text{VO}_2^+ + 3\text{H}_2\text{O}$	-135.184 ± 4.629	23.68 ± 0.81	-3655.338 ± 6.136	-259.970 ± 4.919	-3935.120 ± 6.100
$\text{Ca}(\text{UO}_2)_2(\text{VO}_4)_2 \cdot 5\text{H}_2\text{O}(\text{cr}) + 8\text{H}^+ \rightleftharpoons \text{Ca}^{2+} + 2\text{UO}_2^{2+} + 2\text{VO}_2^+ + 9\text{H}_2\text{O}$	-26.944 ± 5.869	4.72 ± 1.03	-5739.224 ± 7.204	-129.850 ± 6.023	-6323.220 ± 7.100
$\text{Ca}(\text{UO}_2)_2(\text{VO}_4)_2 \cdot 8\text{H}_2\text{O}(\text{cr}) + 8\text{H}^+ \rightleftharpoons \text{Ca}^{2+} + 2\text{UO}_2^{2+} + 2\text{VO}_2^+ + 12\text{H}_2\text{O}$	-26.712 ± 5.645	4.68 ± 0.99	-6450.876 ± 7.030	-110.940 ± 5.897	-7199.620 ± 7.000
$\text{Sr}(\text{UO}_2)_2(\text{VO}_4)_2 \cdot 5\text{H}_2\text{O}(\text{cr}) + 8\text{H}^+ \rightleftharpoons \text{Sr}^{2+} + 2\text{UO}_2^{2+} + 2\text{VO}_2^+ + 9\text{H}_2\text{O}$	14.127 ± 16.230	-2.47 ± 2.84	-5791.353 ± 16.744	-92.950 ± 16.294	-6368.020 ± 16.700
$\text{NaUO}_2\text{VO}_4(\text{cr}) + 4\text{H}^+ \rightleftharpoons \text{Na}^+ + \text{UO}_2^{2+} + \text{VO}_2^+ + 2\text{H}_2\text{O}$	-8.729 ± 3.793	1.53 ± 0.66	-2267.055 ± 4.296	-52.540 ± 3.792	-2428.260 ± 4.200
$\text{NaUO}_2\text{VO}_4 \cdot 2\text{H}_2\text{O}(\text{cr}) + 4\text{H}^+ \rightleftharpoons \text{Na}^+ + \text{UO}_2^{2+} + \text{VO}_2^+ + 4\text{H}_2\text{O}$	7.125 ± 4.761	-1.25 ± 0.83	-2757.189 ± 5.173	-21.600 ± 4.768	-3030.860 ± 5.100
$\text{KUO}_2\text{VO}_4(\text{cr}) + 4\text{H}^+ \rightleftharpoons \text{K}^+ + \text{UO}_2^{2+} + \text{VO}_2^+ + 2\text{H}_2\text{O}$	-14.699 ± 5.658	2.58 ± 0.99	-2281.642 ± 6.007	-47.940 ± 5.722	-2444.660 ± 6.000
$\text{K}_2(\text{UO}_2)_2(\text{VO}_4)_2 \cdot 3\text{H}_2\text{O}(\text{cr}) + 8\text{H}^+ \rightleftharpoons 2\text{K}^+ + 2\text{UO}_2^{2+} + 2\text{VO}_2^+ + 7\text{H}_2\text{O}$	6.259 ± 3.251	-1.10 ± 0.40	-5310.361 ± 4.643		

Table 3.8-8. Continued.

Reaction	$\Delta_r G^\circ$ * (kJ mol ⁻¹)	$\log_{10} K^\circ$	$\Delta_f G_m^\circ$ † (kJ mol ⁻¹)	$\Delta_r H^\circ$ * (kJ mol ⁻¹)	$\Delta_f H_m^\circ$ † (kJ mol ⁻¹)
$\text{RbUO}_2\text{VO}_4(\text{cr}) + 4\text{H}^+ \rightleftharpoons \text{Rb}^+ + \text{UO}_2^{2+} + \text{VO}_2^+ + 2\text{H}_2\text{O}$	-33.440 ± 0.617	5.86 ± 0.11	-2264.400 ± 1.924	-62.820 ± 0.586	-2428.760 ± 1.900
$\text{CsUO}_2\text{VO}_4(\text{cr}) + 4\text{H}^+ \rightleftharpoons \text{Cs}^+ + \text{UO}_2^{2+} + \text{VO}_2^+ + 2\text{H}_2\text{O}$	-37.001 ± 1.899	6.48 ± 0.33	-2268.286 ± 2.820	-64.100 ± 2.082	-2434.360 ± 2.800

* calculated from $\Delta_f G_m^\circ$ in [2020GRE/GAO]; † calculated from $\log_{10} K^\circ$ and $\Delta_f G_m^\circ$ in [2003GUI/FAN] and $\Delta_f G_m^\circ$ in § 3.7.11.

Uranyl vanadate of *d* transition series elements are also discussed but not selected. The $\Delta_r G_m^\circ$ and $\log_{10} K_s^\circ$ values are calculated from the functions of formation selected in the NEA-OECD reviews — and in other selection without discussion —, and from the values reported in Grenthe *et al.* [2020GRE/GAO] for Co^{2+} and Mn^{2+} — see § 3.3 and § 3.7.9. It is not clear how the final functions of formation values are obtained. Particularly, one can notice that the difference between $\Delta_f G_m^\circ(\text{Ni}(\text{UO}_2)_2(\text{VO}_4)_2(\text{cr}))$ and $\Delta_f G_m^\circ(\text{Co}(\text{UO}_2)_2(\text{VO}_4)_2(\text{cr}))$ is larger than between values in the original publication [2002CHE/KAR]. This ends up in a great difference between the obtained $\log_{10} K_s^\circ$ values: $\Delta_f G_m^\circ(\text{Ni}(\text{UO}_2)_2(\text{VO}_4)_2(\text{cr})) = -3971 \text{ kJ mol}^{-1}$ and $\Delta_f G_m^\circ(\text{Co}(\text{UO}_2)_2(\text{VO}_4)_2(\text{cr})) = -3992 \text{ kJ mol}^{-1}$ [2002CHE/KAR]; $\Delta_f G_m^\circ(\text{Ni}(\text{UO}_2)_2(\text{VO}_4)_2(\text{cr})) = -(4378.493 \pm 12.902) \text{ kJ mol}^{-1}$ and $\Delta_f G_m^\circ(\text{Co}(\text{UO}_2)_2(\text{VO}_4)_2(\text{cr})) = -(3981.161 \pm 12.996) \text{ kJ mol}^{-1}$ in Table 9-88 in Grenthe *et al.* [2020GRE/GAO]. These phases are included as possible phases in PRODATA, but $\text{Ni}(\text{UO}_2)_2(\text{VO}_4)_2(\text{cr})$ will not be included.

**Figure 3.8-7. Pourbaix diagram using GWB of $10^{-6} \text{ mol kg}^{-1}$ U in the presence of $10^{-3} \text{ mol kg}^{-1}$ V.****Table 3.8-9. Thermodynamic functions and constants for the solubility of U(VI) vanadate phases of the first transition elements series discussed but not selected in Grenthe *et al.* [2020GRE/GAO].**

Reaction	$\Delta_r G^\circ$ * (kJ mol ⁻¹)	$\log_{10} K^\circ$	$\Delta_f G_m^\circ$ † (kJ mol ⁻¹)	$\Delta_r H^\circ$ * (kJ mol ⁻¹)	$\Delta_f H_m^\circ$ † (kJ mol ⁻¹)
$\text{Zn}(\text{UO}_2)_2(\text{VO}_4)_2(\text{cr}) + 8\text{H}^+ \rightleftharpoons \text{Cd}^{2+} + 2\text{UO}_2^{2+} + 2\text{VO}_2^+ + 4\text{H}_2\text{O}$	-143.651 ± 12.232	25.17 ± 2.14	-4031.214 ± 12.881	-320.390 ± 11.536	-4313.920 ± 12.089
$\text{Zn}(\text{UO}_2)_2(\text{VO}_4)_2 \cdot 4\text{H}_2\text{O}(\text{cr}) + 8\text{H}^+ \rightleftharpoons \text{Cd}^{2+} + 2\text{UO}_2^{2+} + 2\text{VO}_2^+ + 8\text{H}_2\text{O}$	-65.686 ± 12.233	11.51 ± 2.14	-5057.739 ± 12.885	-216.010 ± 11.535	-5561.620 ± 12.091
$\text{Zn}(\text{UO}_2)_2(\text{VO}_4)_2 \cdot 5\text{H}_2\text{O}(\text{cr}) + 8\text{H}^+ \rightleftharpoons \text{Cd}^{2+} + 2\text{UO}_2^{2+} + 2\text{VO}_2^+ + 9\text{H}_2\text{O}$	-68.419 ± 12.233	11.99 ± 2.14	-5292.146 ± 12.886	-212.140 ± 11.534	-5851.320 ± 12.092
$\text{Cd}(\text{UO}_2)_2(\text{VO}_4)_2(\text{cr}) + 8\text{H}^+ \rightleftharpoons \text{Cd}^{2+} + 2\text{UO}_2^{2+} + 2\text{VO}_2^+ + 4\text{H}_2\text{O}$	-132.519 ± 13.398	23.22 ± 2.35	-3972.876 ± 14.011	-306.820 ± 12.774	-4250.020 ± 13.287
$\text{Cd}(\text{UO}_2)_2(\text{VO}_4)_2 \cdot 4\text{H}_2\text{O}(\text{cr}) + 8\text{H}^+ \rightleftharpoons \text{Cd}^{2+} + 2\text{UO}_2^{2+} + 2\text{VO}_2^+ + 8\text{H}_2\text{O}$	-82.954 ± 12.212	14.53 ± 2.14	-4971.001 ± 12.885	-224.840 ± 11.521	-5475.320 ± 12.091
$\text{Cd}(\text{UO}_2)_2(\text{VO}_4)_2 \cdot 8\text{H}_2\text{O}(\text{cr}) + 8\text{H}^+ \rightleftharpoons \text{Cd}^{2+} + 2\text{UO}_2^{2+} + 2\text{VO}_2^+ + 12\text{H}_2\text{O}$	-99.389 ± 12.210	17.41 ± 2.14	-5903.126 ± 12.888	-214.860 ± 11.517	-6628.620 ± 12.093

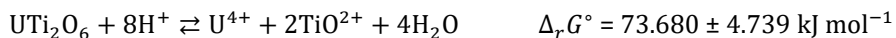
Table 3.8-9. Continued.

Reaction	$\Delta_r G^\circ *$ (kJ mol ⁻¹)	$\log_{10} K^\circ$	$\Delta_f G_m^\circ \dagger$ (kJ mol ⁻¹)	$\Delta_r H^\circ *$ (kJ mol ⁻¹)	$\Delta_f H_m^\circ \dagger$ (kJ mol ⁻¹)
$\text{Cu}(\text{UO}_2)_2(\text{VO}_4)_2(\text{cr}) + 8\text{H}^+ \rightleftharpoons \text{Cu}^{2+} + 2\text{UO}_2^{2+} + 2\text{VO}_2^+ + 4\text{H}_2\text{O}$					
-211.523 ± 12.133	37.06 ± 2.13	-3751.093 ± 12.879	-384.600 ± 11.493	-4031.420 ± 12.088	
$\text{Cu}(\text{UO}_2)_2(\text{VO}_4)_2 \cdot 4\text{H}_2\text{O}(\text{cr}) + 8\text{H}^+ \rightleftharpoons \text{Cd}^{2+} + 2\text{UO}_2^{2+} + 2\text{VO}_2^+ + 8\text{H}_2\text{O}$					
-132.857 ± 12.135	23.28 ± 2.13	-4778.319 ± 12.884	-279.520 ± 11.493	-5279.820 ± 12.091	
$\text{Cu}(\text{UO}_2)_2(\text{VO}_4)_2 \cdot 9\text{H}_2\text{O}(\text{cr}) + 8\text{H}^+ \rightleftharpoons \text{Cd}^{2+} + 2\text{UO}_2^{2+} + 2\text{VO}_2^+ + 13\text{H}_2\text{O}$					
-109.226 ± 12.132	19.14 ± 2.13	-5987.650 ± 12.888	-222.870 ± 11.488	-6765.620 ± 12.093	
$\text{Ni}(\text{UO}_2)_2(\text{VO}_4)_2(\text{cr}) + 8\text{H}^+ \rightleftharpoons \text{Ni}^{2+} + 2\text{UO}_2^{2+} + 2\text{VO}_2^+ + 4\text{H}_2\text{O}$					
298.498 ± 12.212	-52.29 ± 2.14	-4371.933 ± 12.883	115.588 ± 11.505	-4651.520 ± 12.089	
$\text{Ni}(\text{UO}_2)_2(\text{VO}_4)_2 \cdot 4\text{H}_2\text{O}(\text{cr}) + 8\text{H}^+ \rightleftharpoons \text{Ni}^{2+} + 2\text{UO}_2^{2+} + 2\text{VO}_2^+ + 8\text{H}_2\text{O}$					
-18.537 ± 12.211	3.25 ± 2.14	-5003.458 ± 12.885	-175.032 ± 11.503	-5504.220 ± 12.091	
$\text{Co}(\text{UO}_2)_2(\text{VO}_4)_2(\text{cr}) + 8\text{H}^+ \rightleftharpoons \text{Co}^{2+} + 2\text{UO}_2^{2+} + 2\text{VO}_2^+ + 4\text{H}_2\text{O}$					
-106.701 ± 12.172	18.69 ± 2.13	-3975.361 ± 12.977	-283.410 ± 11.473	-4255.610 ± 12.193	
$\text{Co}(\text{UO}_2)_2(\text{VO}_4)_2 \cdot 4\text{H}_2\text{O}(\text{cr}) + 8\text{H}^+ \rightleftharpoons \text{Co}^{2+} + 2\text{UO}_2^{2+} + 2\text{VO}_2^+ + 8\text{H}_2\text{O}$					
-27.735 ± 11.709	4.86 ± 2.05	-5002.887 ± 12.546	-178.030 ± 11.472	-5504.310 ± 12.194	
$\text{Fe}(\text{UO}_2)_2(\text{VO}_4)_2(\text{cr}) + 8\text{H}^+ \rightleftharpoons \text{Ni}^{2+} + 2\text{UO}_2^{2+} + 2\text{VO}_2^+ + 4\text{H}_2\text{O}$					
-142.637 ± 12.218	24.99 ± 2.14	-3975.744 ± 12.881	-316.595 ± 11.525	-4254.620 ± 12.088	
$\text{Fe}(\text{UO}_2)_2(\text{VO}_4)_2 \cdot 4\text{H}_2\text{O}(\text{cr}) + 8\text{H}^+ \rightleftharpoons \text{Fe}^{2+} + 2\text{UO}_2^{2+} + 2\text{VO}_2^+ + 8\text{H}_2\text{O}$					
-63.072 ± 12.417	11.05 ± 2.18	-5003.869 ± 13.073	-210.615 ± 11.734	-5503.920 ± 12.291	
$\text{Mn}(\text{UO}_2)_2(\text{VO}_4)_2(\text{cr}) + 8\text{H}^+ \rightleftharpoons \text{Mn}^{2+} + 2\text{UO}_2^{2+} + 2\text{VO}_2^+ + 4\text{H}_2\text{O}$					
-129.196 ± 12.413	22.63 ± 2.17	-4126.566 ± 13.060	-291.160 ± 11.738	-4410.560 ± 12.290	
$\text{Mn}(\text{UO}_2)_2(\text{VO}_4)_2 \cdot 4\text{H}_2\text{O}(\text{cr}) + 8\text{H}^+ \rightleftharpoons \text{Mn}^{2+} + 2\text{UO}_2^{2+} + 2\text{VO}_2^+ + 8\text{H}_2\text{O}$					
-37.530 ± 12.317	6.57 ± 2.16	-5166.792 ± 12.972	-173.080 ± 11.632	-5671.960 ± 12.193	

* calculated from $\Delta_f G_m^\circ$ from [2020GRE/GAO]; † calculated from $\log_{10} K^\circ$ and $\Delta_f G_m^\circ$ in [2003GUI/FAN] and $\Delta_f G_m^\circ$ in § 3.7.11.

3.8.1.8.2 Titanate Compounds

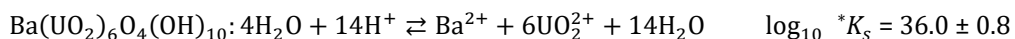
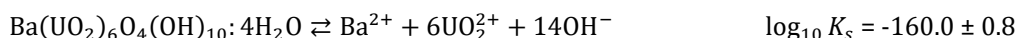
Donaldson *et al.* [2005DON/STE] proposed the functions of formation of brannerite (UTi_2O_6), from which the solubility constant is calculated.



$$\log_{10} K_s = -12.91 \pm 0.83$$

3.8.1.9. Alkaline Earth Compounds

Vochten and Van Haverbeke [1990VOC/HAV] measured the solubility of billietite ($\text{Ba}(\text{UO}_2)_6\text{O}_4(\text{OH})_{10} \cdot 4\text{H}_2\text{O}$) at $4 < \text{pH} < 5.6$ without controlling the ionic strength. Using the total uranium solubility, the following activity product can be calculated using PHREEQC and the database.



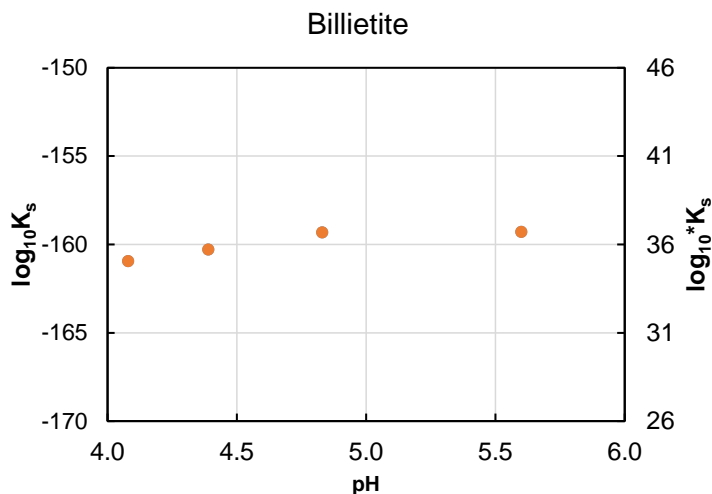


Figure 3.8-8. Activity products of billietite ($\text{Ba}(\text{UO}_2)_6\text{O}_4(\text{OH})_{10}\cdot 4\text{H}_2\text{O}$) from the solubility data in Vochten and Van Haverbeke [1990VOC/HAV] calculated using PHREEQC and PRODATA.

3.8.1.10. Alkaline Compounds

Gorman-Lewis *et al.* [2008GOR/FEI] measured the solubility of compreignacite ($\text{K}_2(\text{UO}_2)_6\text{O}_4(\text{OH})_6\cdot 7\text{H}_2\text{O}$), sodium compreignacite ($\text{Na}_2(\text{UO}_2)_6\text{O}_4(\text{OH})_6\cdot 7\text{H}_2\text{O}$) and clarkeite ($\text{Na}(\text{UO}_2)\text{O}(\text{OH})$). This study is cited in the recent NEA-OECD review [2020GRE/GAO], but is discussed anywhere. The $\log_{10} K^\circ$ values are used to calculate the $\Delta_f G_m^\circ$, and the $\Delta_f H_m^\circ$ and $S_{f,m}^\circ$ values from the authors are directly used as they were calculated in agreement with the preceding NEA-OECD review [2003GUI/FAN].

Table 3.8-10. Thermodynamic functions and constants for the solubility of uranyl(VI) oxides of alkaline metals phases from Gorman-Lewis *et al.* [2008GOR/FEI].

Reaction	$\Delta_r G^\circ *$ (kJ mol ⁻¹)	$\log_{10} K^\circ$	$\Delta_f G_m^\circ \dagger$ (kJ mol ⁻¹)	$\Delta_r H^\circ *$ (kJ mol ⁻¹)	$\Delta_f H_m^\circ \dagger$ (kJ mol ⁻¹)
<hr/>					
Clarkeite $\text{NaUO}_2\text{OOH}(\text{cr}) + 3\text{H}^+ \rightleftharpoons \text{UO}_2^{2+} + \text{Na}^+ + 2\text{H}_2\text{O}$	-53.656 ± 5.137	9.40 ± 0.9	$-1\,635.128 \pm 5.428$	-107.000 ± 2.060	$-1\,724.000 \pm 2.550$
<hr/>					
Na-compreignacite $\text{Na}_2(\text{UO}_2)_6\text{O}_4(\text{OH})_6\cdot 7\text{H}_2\text{O} + 14\text{H}^+ \rightleftharpoons 6\text{UO}_2^{2+} + 2\text{Na}^+ + 17\text{H}_2\text{O}$	-224.897 ± 6.279	39.4 ± 1.1	$-10\,045.695 \pm 12.240$	-517.390 ± 11.348	$10\,936.400 \pm 14.500$
<hr/>					
Compreignacite $\text{K}_2(\text{UO}_2)_6\text{O}_4(\text{OH})_6\cdot 7\text{H}_2\text{O} + 14\text{H}^+ \rightleftharpoons 6\text{UO}_2^{2+} + 2\text{K}^+ + 17\text{H}_2\text{O}$	-204.348 ± 2.854	35.8 ± 0.5	$-10\,107.358 \pm 10.888$		

3.8.2. Thorium

Thorium is part of the radioactive decay chain of uranium. The values from the NEA-OECD review [2009RAN/FUG] are accepted in PRODATA. The common master species is Th^{4+} .

3.8.2.1. Hydroxo Compounds

As for uranium(IV), the formation of $\text{Th}(\text{OH})_3^+$ is not selected in Rand *et al.* [2009RAN/FUG]. Neck and Kim [2001NEC/KIM] proposed the formation,



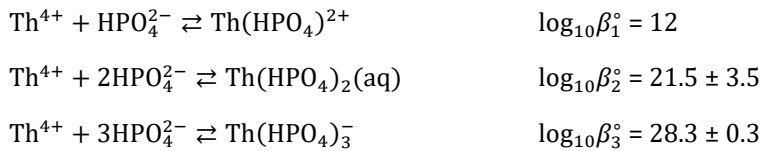
which can be rewritten as follows.



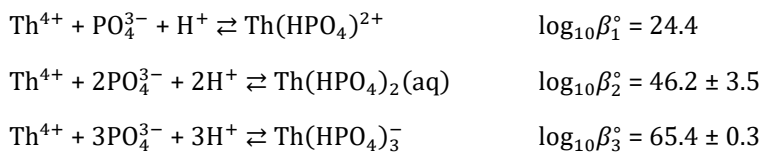
This latter complex is accepted in PRODATA.

3.8.2.2. Phosphate Complexes

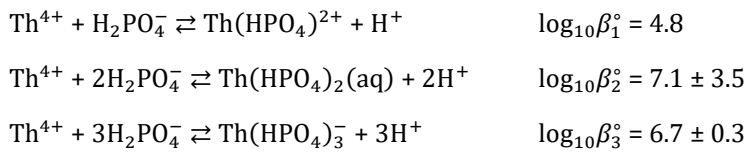
Ekberg *et al.* [2011EKB/KNU] proposed the formation of three hydrogenophosphate complexes, which was tentatively extrapolated to infinite dilution in Reiller *et al.* [2012REI/VER] as follows.



These reactions are accepted in PRODATA and can be rewritten relative to PO_4^{3-} using phosphate constants in Guillaumont *et al.* [2003GUI/FAN] as follows.



The swap to H_2PO_4^- are handled from the $\log_{10} K^\circ$ of PO_4^{3-} protonation.

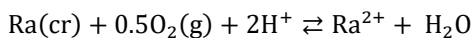


3.9. Alkaline Earth Metals

The alkaline earth metals are major ions in geochemical environments (Mg , Ca), important radionuclides in the nuclear fuel cycle — ${}^{90}\text{Sr}$ is one of the major daughter of the ${}^{235}\text{U}$ fission [1993ENG/RID] —, or are forming solid solution with radium (Sr , Ba). Beryllium will not be considered in PRODATA. Knowing their very strong chemical analogy from Mg to Ra in the column IIA, these elements will be treated altogether in this document.

3.9.1. Native Metals and Free Ions

The functions of formation for $\text{Mg}(\text{cr})$ and Mg^{2+} , $\text{Ca}(\text{cr})$ and Ca^{2+} , $\text{Sr}(\text{cr})$ and Sr^{2+} , and $\text{Ba}(\text{cr})$ and Ba^{2+} are available in Guillaumont *et al.* [2003GUI/FAN]. The functions of formation for $\text{Ra}(\text{cr})$ and Ra^{2+} are taken from Wagman *et al.* [1982WAG/EVA]. The values are corrected from the differences between the functions of formation of H_2O between Wagman *et al.* [1982WAG/EVA] and Guillaumont *et al.* [2003GUI/FAN] in the following reaction.



The common master species are Mg^{2+} , Ca^{2+} , Sr^{2+} , Ba^{2+} , and Ra^{2+} .

Table 3.9-1. Thermodynamic functions of reactions and constants for the native metal oxidation for alkaline earths.

Reaction	$\Delta_r G_m^\circ$ (kJ mol ⁻¹)	$\log_{10} \beta^\circ$	$\Delta_f G_m^\circ$ (kJ mol ⁻¹)	$\Delta_r H_m^\circ$ (kJ mol ⁻¹)	$\Delta_f H_m^\circ$ (kJ mol ⁻¹)
Mg(cr) \rightleftharpoons Mg ²⁺ + 2e ⁻	-455.375 ± 1.335	79.78 ± 0.23	-455.375 ± 1.335 ^a	-467.000 ± 0.600	-467.000 ± 0.600 ^a
Mg(cr) + 0.5O ₂ (aq) + 2H ⁺ \rightleftharpoons Mg ²⁺ + H ₂ O	-700.704 ± 1.258	122.76 ± 0.22		-746.980 ± 0.401	
Ca(cr) \rightleftharpoons Ca ²⁺ + 2e ⁻	-552.806 ± 1.050	96.85 ± 0.18	-552.806 ± 1.050 ^a	-543.000 ± 1.000	-543.000 ± 1.000 ^a
Ca(cr) + 0.5O ₂ (aq) + 2H ⁺ \rightleftharpoons Ca ²⁺ + H ₂ O	-798.135 ± 0.951	139.83 ± 0.17		-822.980 ± 0.895	
Sr(cr) \rightleftharpoons Sr ²⁺ + 2e ⁻	-563.864 ± 0.781	98.78 ± 0.14	-563.864 ± 0.781 ^a	-550.900 ± 0.500	-550.900 ± 0.500 ^a
Sr(cr) + 0.5O ₂ (aq) + 2H ⁺ \rightleftharpoons Sr ²⁺ + H ₂ O	-809.193 ± 0.641	141.76 ± 0.11		-830.880 ± 0.226	
Ba(cr) \rightleftharpoons Ba ²⁺ + 2e ⁻	-557.656 ± 2.582	97.70 ± 0.45	-557.656 ± 2.582 ^a	-534.800 ± 2.500	-534.800 ± 2.500 ^a
Ba(cr) + 0.5O ₂ (aq) + 2H ⁺ \rightleftharpoons Ba ²⁺ + H ₂ O	-802.985 ± 2.543	140.68 ± 0.45		-814.780 ± 2.460	
Ra(cr) \rightleftharpoons Ra ²⁺ + 2e ⁻	-561.489 ± 4.000	98.37 ± 0.70	-561.489 ± 4.000 ^b	-527.600 ± 4.800	-527.600 ± 4.800 ^b
Ra(cr) + 0.5O ₂ (aq) + 2H ⁺ \rightleftharpoons Ra ²⁺ + H ₂ O	-806.818 ± 3.975	141.35 ± 0.70		-807.580 ± 4.779	

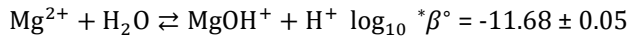
a [2003GUI/FAN]; b [1982WAG/EVA]

3.9.2. Oxo and Hydroxo Compounds

The functions of formation for oxides are taken from Guillaumont *et al.* [2003GUI/FAN] for MgO(cr), CaO(cr), SrO(cr) and BaO(cr). Only the $\Delta_f H^\circ$ value is given for RaO(cr) in Wagman *et al.* [1982WAG/EVA].

The formation of brucite ($\text{Mg}(\text{OH})_2(\text{cr})$) can be found in different references [1982WAG/EVA; 1995ROB/HEM; 2003ALT/MET]. There is no difference between the two former references. The latter reference is added being coherent with the two former ones, and a direct experimental determination.

The hydrolysis reaction for the alkaline earth metals are obtained from the estimation in Shock *et al.* [1997aSHO/SAS], except for the determination of the hydrolysis constant for magnesium,



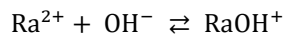
which is taken from Palmer and Wesolowski [1997PAL/WES].

The functions of formation of portlandite ($\text{Ca}(\text{OH})_2(\text{cr})$) are taken from [1995ROB/HEM]. The formation of ($\text{Sr}(\text{OH})_2(\text{cr})$) is taken from the JANAF database [1998CHA] and the solubility of $\text{Sr}(\text{OH})_2 \cdot 8\text{H}_2\text{O}$ is taken from Felmy *et al.* [1998FEL/DIX]. Only the $\Delta_f H^\circ(\text{Ba}(\text{OH})_2(\text{cr}))$ value is given in Wagman *et al.* [1982WAG/EVA]. The functions of formation of $\text{Ba}(\text{OH})_2 \cdot 8\text{H}_2\text{O}$ are taken from Wagman *et al.* [1982WAG/EVA].

The hydroxo complexes of Ca, Sr, and Ba are taken from Shock *et al.* [1997aSHO/SAS].

The $\Delta_r G_m^\circ$, $\log_{10} \beta^\circ$, and $\Delta_r H_m^\circ$ for the considered reactions are shown in Table 3.9-2, as well as the $\Delta_f G_m^\circ$ and $\Delta_f H_m^\circ$ recalculated in coherence with the data from Guillaumont *et al.* [2003GUI/FAN].

The hydroxo complex formation and $\Delta_r H_m^\circ$ for Ra²⁺ are taken from Langmuir and Riese [1985LAN/RIE] for the following reaction.



The $\Delta_f G_m^\circ$ and $\Delta_f H_m^\circ$ are calculated in Table 3.9-2 in coherence with the data from Guillaumont *et al.* [2003GUI/FAN].

Table 3.9-2. Thermodynamic functions and constants for the oxo and hydroxo-alkaline earth compounds.

	$\Delta_r G_m^\circ$ kcal mol ⁻¹	$\log_{10} \beta^\circ$	$\Delta_f G_m^\circ$ * kJ mol ⁻¹	$\Delta_r H_m^\circ$ kcal mol ⁻¹	$\Delta_f H_m^\circ$ * kJ mol ⁻¹		
MgO(cr) + 2H ⁺ ⇌ Mg ²⁺ + H ₂ O	-123.203 ± 1.300	21.58 ± 0.23	-569.312 ± 0.305 ^a	-151.230 ± 0.521	-601.600 ± 0.300 ^a		
Mg(OH) ₂ (cr) + 2H ⁺ ⇌ Mg ²⁺ + 2H ₂ O	-95.548 ± 1.335 ^b	16.74 ± 0.23	-834.107 ± 0.080	-113.970 ± 0.514 ^b	-924.690 ± 0.320		
Brucite							
Mg(OH) ₂ (cr) + 2H ⁺ ⇌ Mg ²⁺ + 2H ₂ O	-97.608 ± 0.200	17.10 ± 0.04 ^c	-832.047 ± 1.352				
CaO(cr) + 2H ⁺ ⇌ Ca ²⁺ + H ₂ O	-186.650 0.515	32.70 0.09	-603.296 0.916 ^a	-193.910 0.438	-634.920 0.900 ^a		
Portlandite							
Ca(OH) ₂ (cr) + 2H ⁺ ⇌ Ca ²⁺ + 2H ₂ O	-129.8 ± 0.7	22.74 ± 0.13	897.286 ± 1.300 ^d				
Sr(OH) ₂ (cr) + 2H ⁺ ⇌ Sr ²⁺ + 2H ₂ O	-157.046 ^e	27.51	-881.098	-153.671 ^e	-968.889		
Sr(OH) ₂ :8H ₂ O(cr) + 2H ⁺ ⇌ Sr ²⁺ + 10H ₂ O		24.32 ^f					
Ba(OH) ₂ :8H ₂ O(cr) + 2H ⁺ ⇌ Sr ²⁺ + 10H ₂ O	-139.260 ± 5.834 ^b	24.34 ± 1.02	-2 789.796 ± 6.393	-50.900 ± 1.962 ^b	-3 342.200 ± 1.600		
Mg ²⁺ + H ₂ O ⇌ MgOH ⁺ + H ⁺		-11.68 ^h	-625.845	-3.993 ^g	-16.707	-769.537	
Ca ²⁺ + OH ⁻ ⇌ CaOH ⁺	-1.585 ^g	-6.632	1.16	-716.658	5.177 ^g	21.661	-751.354
Ca ²⁺ + H ₂ O ⇌ CaOH ⁺ + H ⁺			-12.84				
Sr ²⁺ + OH ⁻ ⇌ SrOH ⁺	-0.945 ^g	-3.954	0.69	-725.038	6.647 ^g	27.811	-753.104
Sr ²⁺ + H ₂ O ⇌ SrOH ⁺ + H ⁺			-13.31				
Ba ²⁺ + OH ⁻ ⇌ BaOH ⁺	-0.675 ^g	-2.824	0.49	-717.700	7.577 ^g	31.702	-733.113
Ba ²⁺ + H ₂ O ⇌ BaOH ⁺ + H ⁺			-13.51				
Ra ²⁺ + OH ⁻ ⇌ RaOH ⁺	-2.854	0.5 ⁱ	-721.563	1.097 ⁱ	4.590	-753.025	
Ra ²⁺ + H ₂ O ⇌ RaOH ⁺ + H ⁺	77.066	-13.5			60.405		

a [2003GUI/FAN]; b [1982WAG/EVA]; c [2003ALT/MET]; d [1995ROB/HEM]; e [1998CHA]; f [1998FEL/DIX]; g calculated from $\Delta_f G_m^\circ$ or $\Delta_f H_m^\circ$ in [1997aSHO/SAS]; h [1997PAL/WES]; i [1985LAN/RIE].

* calculated from the $\Delta_r G_m^\circ$ or $\Delta_r H_m^\circ$ using $\Delta_f G_m^\circ$ or $\Delta_f H_m^\circ$ in [2003GUI/FAN].

3.9.3. Halogen Compounds

The functions of formation of MgF₂(cr) are taken from Guillaumont *et al.* [2003GUI/FAN]. The functions of reaction of CaF₂(cr), SrF₂(cr), and BaF₂(cr) are calculated from Wagman *et al.* [1982WAG/EVA].

The functions of formation of SrCl₂(cr) and BaCl₂(cr) are taken from Guillaumont *et al.* [2003GUI/FAN].

The functions of reaction of MgCl₂(cr), MgCl₂:H₂O(cr), MgCl₂:2H₂O(cr), and MgCl₂:4H₂O(cr), BaCl₂:H₂O(cr), BaCl₂:2H₂O(cr), and RaCl₂:2H₂O(cr) are taken from Wagman *et al.* [1982WAG/EVA].

The solubility of Bischofite (MgCl₂:6H₂O(cr)) is taken from Harvie *et al.* [1984HAR/MØL].

The functions of reaction of hydrophylite (CaCl₂(cr)) are taken from Robie and Hemingway [1995ROB/HEM].

The solubility of CaCl₂:H₂O(cr), CaCl₂:2H₂O(cr), CaCl₂:4H₂O(cr), and antarticite (CaCl₂:6H₂O(cr)) are taken from CODATA works [1987GAR/PAR].

The functions of reaction for MF^+ and MCl^+ complexes are obtained from the estimation in Sverjensky *et al.* [1997SVE/SHO] for the complexes, and Shock *et al.* [1997aSHO/SAS] for the free ions and ligands. The thermodynamic functions of formation as well as the obtained $\log_{10}\beta^\circ$ values are shown in Table 3.9-3.

Table 3.9-3. Thermodynamic functions and constants for the halogeno compounds of alkaline earth(II).

Reaction	$\Delta_r G_m^\circ$	$\log_{10}\beta^\circ$	$\Delta_f G_m^\circ$ ^b	$\Delta_r H_m^\circ$	$\Delta_f H_m^\circ$ ^b
$\text{MgF}_2(\text{cr}) \rightleftharpoons \text{Mg}^{2+} + 2\text{F}^-$	52.630 ± 1.495	-9.22 ± 0.26	$-1\ 071.051 \pm 1.210$	-13.500 ± 0.781	$-1\ 124.200 \pm 1.200$
$\text{CaF}_2(\text{cr}) \rightleftharpoons \text{Ca}^{2+} + 2\text{F}^-$	51.448 ± 1.656 ^c	-9.01 ± 0.29	$-1\ 167.300 \pm 2.400$	5.900 ± 4.511 ^c	$-1\ 219.600 \pm 4.800$
$\text{SrF}_2(\text{cr}) \rightleftharpoons \text{Sr}^{2+} + 2\text{F}^-$	47.740 ± 6.255 ^c	-8.36 ± 1.10	$-1\ 174.650 \pm 6.454$	5.240 ± 1.980 ^c	$-1\ 226.840 \pm 2.421$
$\text{BaF}_2(\text{cr}) \rightleftharpoons \text{Ba}^{2+} + 2\text{F}^-$	38.450 ± 5.705 ^c	-6.74 ± 1.00	$-1\ 159.152 \pm 6.413$	4.200 ± 2.701 ^c	$-1\ 209.700 \pm 0.802$
$\text{MgCl}_2(\text{cr}) \rightleftharpoons \text{Mg}^{2+} + 2\text{Cl}^-$	-125.466 ± 1.148 ^c	21.98 ± 0.20	-592.343 ± 0.721	-159.848 ± 0.612 ^c	-641.312 ± 0.160
$\text{MgCl}_2 \cdot \text{H}_2\text{O}(\text{cr}) \rightleftharpoons \text{Mg}^{2+} + 2\text{Cl}^- + \text{H}_2\text{O}$	-93.209 ± 1.318 ^c	16.33 ± 0.23	-861.740 ± 0.320	-120.360 ± 0.587 ^c	-966.630 ± 0.240
$\text{MgCl}_2 \cdot 2\text{H}_2\text{O}(\text{cr}) \rightleftharpoons \text{Mg}^{2+} + 2\text{Cl}^- + 2\text{H}_2\text{O}$	-73.514 ± 1.355 ^c	12.88 ± 0.24	$-1\ 118.575 \pm 0.080$	-93.108 ± 0.617 ^c	$-1\ 279.712 \pm 0.160$
$\text{MgCl}_2 \cdot 4\text{H}_2\text{O}(\text{cr}) \rightleftharpoons \text{Mg}^{2+} + 2\text{Cl}^- + 4\text{H}_2\text{O}$	-43.079 ± 1.160 ^c	7.55 ± 0.20	$-1\ 623.290 \pm 0.720$	-45.490 ± 0.305 ^c	$-1\ 898.990 \pm 0.720$
Bischofite					
$\text{MgCl}_2 \cdot 6\text{H}_2\text{O}(\text{cr}) \rightleftharpoons \text{Mg}^{2+} + 2\text{Cl}^- + 6\text{H}_2\text{O}$	-24.936 ± 5.789 ^d	4.37 ± 1.01	$-2\ 115.713 \pm 5.951$	-17.120 ± 0.657	$-2\ 499.020 \pm 0.160$
$\text{CaCl}_2(\text{cr}) \rightleftharpoons \text{Ca}^{2+} + 2\text{Cl}^-$	-67.936 ± 0.720	11.90 ± 0.13	-747.304 ± 0.799	-81.348 ± 4.690	-795.812 ± 4.800
Hydrophylite					
$\text{CaCl}_2(\text{cr}) \rightleftharpoons \text{Ca}^{2+} + 2\text{Cl}^-$	-68.300 ± 0.719 ^e	11.97 ± 0.13	-746.940 ± 0.800	-81.400 ± 0.742 ^e	-795.760 ± 0.700
$\text{CaCl}_2 \cdot \text{H}_2\text{O}(\text{cr}) \rightleftharpoons \text{Ca}^{2+} + 2\text{Cl}^- + \text{H}_2\text{O}$	-44.807 ± 1.443 ^f	7.85 ± 0.25	$-1\ 007.573 \pm 1.800$	-52.190 ± 1.720 ^f	$-1\ 110.800 \pm 2.000$
$\text{CaCl}_2 \cdot 2\text{H}_2\text{O}(\text{cr}) \rightleftharpoons \text{Ca}^{2+} + 2\text{Cl}^- + 2\text{H}_2\text{O}$	-45.412 ± 1.564 ^f	7.96 ± 0.27	$-1\ 244.108 \pm 1.900$	-44.820 ± 1.481 ^f	$-1\ 404.000 \pm 1.800$
$\alpha\text{-CaCl}_2 \cdot 4\text{H}_2\text{O}(\text{cr}) \rightleftharpoons \text{Ca}^{2+} + 2\text{Cl}^- + 4\text{H}_2\text{O}$	30.600 ± 0.711 ^f	5.36 ± 0.12	$-1\ 733.200 \pm 1.300$	-11.344 ± 0.946 ^f	$-2\ 009.136 \pm 1.400$
$\beta\text{-CaCl}_2 \cdot 4\text{H}_2\text{O}(\text{cr}) \rightleftharpoons \text{Ca}^{2+} + 2\text{Cl}^- + 4\text{H}_2\text{O}$	-31.300 ± 1.032 ^f	5.48 ± 0.18	$-1\ 732.500 \pm 1.500$		
$\gamma\text{-CaCl}_2 \cdot 4\text{H}_2\text{O}(\text{cr}) \rightleftharpoons \text{Ca}^{2+} + 2\text{Cl}^- + 4\text{H}_2\text{O}$	-31.500 ± 1.032 ^f	5.52 ± 0.18	$-1\ 732.300 \pm 1.500$		
$\text{CaCl}_2 \cdot 6\text{H}_2\text{O}(\text{cr}) \rightleftharpoons \text{Ca}^{2+} + 2\text{Cl}^- + 6\text{H}_2\text{O}$	22.490 ± 0.471 ^f	3.94 ± 0.08	$-2\ 215.590 \pm 1.200$	13.960 ± 0.770 ^f	$-2\ 606.100 \pm 1.300$
$\text{SrCl}_2(\text{cr}) \rightleftharpoons \text{Sr}^{2+} + 2\text{Cl}^-$	-41.324 ± 0.394	7.24 ± 0.07	-784.974 ± 0.714	-51.210 ± 0.447	-833.850 ± 0.700
$\text{BaCl}_2 \cdot \text{H}_2\text{O}(\text{cr}) \rightleftharpoons \text{Ba}^{2+} + 2\text{Cl}^- + \text{H}_2\text{O}$	-4.725 ± 2.582	0.83 ± 0.45	$-1\ 052.505 \pm 0.240$	5.810 ± 2.081	$-1\ 160.600 \pm 1.400$
$\text{BaCl}_2 \cdot 2\text{H}_2\text{O}(\text{cr}) \rightleftharpoons \text{Ba}^{2+} + 2\text{Cl}^- + 2\text{H}_2\text{O}$	-1.164 ± 2.589	0.20 ± 0.45	$-1\ 293.206 \pm 0.160$	19.510 ± 2.498	$-1\ 460.130 \pm 0.240$
$\text{RaCl}_2 \cdot 2\text{H}_2\text{O}(\text{cr}) \rightleftharpoons \text{Ra}^{2+} + 2\text{Cl}^- + 2\text{H}_2\text{O}$	4.586 ± 4.990 ^c	-0.80 ± 0.87	$-1\ 302.789 \pm 6.400$	30.422 ± 31.634 ^c	$-1\ 463.842 \pm 31.997$
$\text{Mg}^{2+} + \text{F}^- \rightleftharpoons \text{MgF}^+$	-7.719 ^a	1.35	-744.617	2.372 ^a	-799.976
$\text{Ca}^{2+} + \text{F}^- \rightleftharpoons \text{CaF}^+$	-3.891 ^a	0.68	-838.220	5.648 ^a	-872.702
$\text{Sr}^{2+} + \text{F}^- \rightleftharpoons \text{SrF}^+$	-0.795 ^a	0.14	-846.182	4.812 ^a	-881.438
$\text{Ba}^{2+} + \text{F}^- \rightleftharpoons \text{BaF}^+$	1.046 ^a	-0.18	-838.133	8.954 ^a	-861.196
$\text{Mg}^{2+} + \text{Cl}^- \rightleftharpoons \text{MgCl}^+$	0.799 ^a	-0.14	-585.793	1.536 ^a	-632.544
$\text{Ca}^{2+} + \text{Cl}^- \rightleftharpoons \text{CaCl}^+$	1.700 ^a	-0.30	-682.323	4.714 ^a	-705.366
$\text{Ca}^{2+} + 2\text{Cl}^- \rightleftharpoons \text{CaCl}_2(\text{aq})$	4.000 ^a	-0.70	-811.240	-5.837 ^a	-882.997

Table 3.9-3. Continued

Reaction	$\Delta_r G_m^\circ$	$\log_{10} \beta^\circ$	$\Delta_f G_m^\circ$ ^b	$\Delta_r H_m^\circ$	$\Delta_f H_m^\circ$ ^b
$\text{Sr}^{2+} + \text{Cl}^- \rightleftharpoons \text{SrCl}^+$	1.167 ^a	-0.20	-693.914	7.590 ^a	-710.390
$\text{Ba}^{2+} + \text{Cl}^- \rightleftharpoons \text{BaCl}^+$	2.841 ^a	-0.50	-686.032	13.021 ^a	-688.859

a calculated from $\Delta_f G_m^\circ$ in [1997SVE/SHO] for the complexes and [1997aSHO/SAS] for the free metals and ligands; b calculated from $\Delta_r G_m^\circ$ or $\Delta_r H_m^\circ$ using $\Delta_f G_m^\circ$ in [2003GUI/FAN]; c [1982WAG/EVA]; d [1984HAR/MØL]; e [1995ROB/HEM]; f [1987GAR/PAR].

3.9.4. Sulphur Compounds

The functions of formation from niningerite (MgS(cr)), oldhamite (CaS(cr)) are taken from Robie and Hemingway [1995ROB/HEM]. The functions of reaction are calculated using the correction of functions of formation for HS^- in § 3.3. SrS(cr) and BaS(cr) can be calculated from Pankratz *et al.* [1987PAN/MAH] or Wagman *et al.* [1982WAG/EVA].

The functions of reaction of anhydrite ($\text{Ca}(\text{SO}_4)(\text{cr})$), gypsum ($\text{Ca}(\text{SO}_4) \cdot 2\text{H}_2\text{O(cr)}$), and celestite ($\text{SrSO}_4(\text{aq})$) are taken from Robie and Hemingway [1995ROB/HEM]. The functions of reaction of barite ($\text{BaSO}_4(\text{cr})$) are available in Wagman *et al.* [1982WAG/EVA] and Robie and Hemingway [1995ROB/HEM], giving slightly different solubility values.

The solubility and enthalpy of reaction of $\text{RaSO}_4(\text{cr})$ is taken from Langmuir and Riese [1985LAN/RIE].

3.9.5. Selenium Compounds

The functions of reaction of CaSe(cr) are taken from Wagman *et al.* [1982WAG/EVA].

Functions of formation of $\text{MgSeO}_3 \cdot 6\text{H}_2\text{O(cr)}$, $\text{MgSeO}_4 \cdot 6\text{H}_2\text{O(cr)}$, $\text{CaSeO}_3 \cdot \text{H}_2\text{O(cr)}$, $\text{CaSeO}_4 \cdot 2\text{H}_2\text{O(cr)}$, SrSeO_3 , BaSeO_3 , and BaSeO_4 are taken from the NEA-OECD reviews [2003GUI/FAN; 2005OLI/NOL].

Table 3.9-4. Thermodynamic functions and constants for the S and Se compounds of alkaline earth(II).

Reaction	$\Delta_r G_m^\circ$	$\log_{10} \beta^\circ$	$\Delta_f G_m^\circ$ *	$\Delta_r H_m^\circ$	$\Delta_f H_m^\circ$ *
Niningerite $\text{MgS} + \text{H}^+ \rightleftharpoons \text{Mg}^{2+} + \text{HS}^-$	-101.800 ± 2.036^a	17.83 ± 0.36	-341.332 ± 1.452	-137.600 ± 1.033^a	-345.700 ± 1.242
Oldhamite $\text{CaS} + \text{H}^+ \rightleftharpoons \text{Ca}^{2+} + \text{HS}^-$	-71.900 ± 1.350^a	12.60 ± 0.24	-468.663 ± 1.937	-84.400 ± 0.710^a	-474.900 ± 1.937
Anhydrite $\text{SrS(cr)} + \text{H}^+ \rightleftharpoons \text{Sr}^{2+} + \text{HS}^-$	-79.600 ± 1.945^b	13.95 ± 0.34	-472.021 ± 1.141	-91.000 ± 1.549^b	-476.200 ± 0.316
BaS(cr) + $\text{H}^+ \rightleftharpoons \text{Ba}^{2+} + \text{HS}^-$	-92.690 ± 5.071^b	16.24 ± 0.89	-452.723 ± 6.071	-95.240 ± 2.762^b	-455.860 ± 0.933
$\text{MgSO}_4(\text{cr}) \rightleftharpoons \text{Mg}^{2+} + \text{SO}_4^{2+}$	-28.900 ± 0.589^a	5.06 ± 0.10	$-1\ 170.479 \pm 1.269$	-91.400 ± 0.632^a	$-1\ 284.940 \pm 0.346$
$\text{MgSO}_4 \cdot \text{H}_2\text{O(cr)} \rightleftharpoons \text{Mg}^{2+} + \text{SO}_4^{2+} + \text{H}_2\text{O}$	-7.759 ± 0.823^b	1.36 ± 0.14	$-1\ 428.760 \pm 1.623$	-59.850 ± 0.575^b	$-1\ 602.320 \pm 0.437$
$\text{MgSO}_4 \cdot 6\text{H}_2\text{O(cr)} \rightleftharpoons \text{Mg}^{2+} + \text{SO}_4^{2+} + 6\text{H}_2\text{O}$	9.696 ± 1.226^b	-1.70 ± 0.21	$-2\ 631.915 \pm 1.876$	-4.100 ± 7.405^b	$-3\ 087.220 \pm 7.444$
Epsomite $\text{MgSO}_4 \cdot 7\text{H}_2\text{O} \rightleftharpoons \text{Mg}^{2+} + \text{SO}_4^{2+} + 7\text{H}_2\text{O}$	12.100 ± 0.669^a	-2.12 ± 0.12	$-2\ 871.459 \pm 1.262$	11.800 ± 0.444^a	$-3\ 388.950 \pm 0.634$
Anhydrite $\text{CaSO}_4 \rightleftharpoons \text{Ca}^{2+} + \text{SO}_4^{2+}$	24.200 ± 3.844^a	-4.24 ± 0.67	$-1\ 321.010 \pm 4.007$	-17.900 ± 3.763^a	$-1\ 434.440 \pm 3.914$
Gypsum $\text{CaSO}_4 \cdot 2\text{H}_2\text{O} \rightleftharpoons \text{Ca}^{2+} + \text{SO}_4^{2+} + 2\text{H}_2\text{O}$	25.200 ± 1.301^a	-4.41 ± 0.23	$-1\ 796.290 \pm 1.726$	-0.900 ± 1.351^a	$-2\ 023.100 \pm 1.730$
Celestite $\text{SrSO}_4 \rightleftharpoons \text{Sr}^{2+} + \text{SO}_4^{2+}$	31.800 ± 1.655^a	-5.57 ± 0.29	$-1\ 339.668 \pm 1.877$	-7.000 ± 1.825^a	$-1\ 453.240 \pm 1.934$

Table 3.9-4. Continued.

Reaction	$\Delta_r G_m^\circ$	$\log_{10} \beta^\circ$	$\Delta_f G_m^\circ$ *	$\Delta_r H_m^\circ$	$\Delta_f H_m^\circ$ *
Barite $\text{BaSO}_4 \rightleftharpoons \text{Ba}^{2+} + \text{SO}_4^{2-}$	$63.100 \pm 0.853^{\text{b}}$	-11.05 ± 0.15	$-1\ 364.760 \pm 2.473$	$31.800 \pm 0.632^{\text{a}}$	$-1\ 475.940 \pm 2.452$
$\text{RaSO}_4(\text{s}) \rightleftharpoons \text{Ra}^{2+} + \text{SO}_4^{2-}$	58.576^{c}	-10.26	$-1\ 364.069$	39.246^{c}	$-1\ 476.186$
$\text{CaSe}(\text{cr}) + 2\text{H}^+ \rightleftharpoons \text{Ca}^{2+} + \text{H}_2\text{Se}(\text{aq})$	$-168.180 \pm 1.161^{\text{b}}$	29.46 ± 0.20	-363.131 ± 1.941	$-155.430 \pm 1.175^{\text{b}}$	-373.270 ± 1.926

a [1995ROB/HEM]; b [1982WAG/EVA]; c [1985LAN/RIE].

* calculated from $\Delta_r G_m^\circ$ or $\Delta_r H_m^\circ$ using $\Delta_f G_m^\circ$ or $\Delta_f H_m^\circ$ in [2003GUI/FAN].

3.9.6. Nitrate Compounds

The functions of reaction for $\text{Mg}(\text{NO}_3)_2(\text{cr})$, $\text{Mg}(\text{NO}_3)_2 \cdot 6\text{H}_2\text{O}(\text{cr})$, $\text{Ca}(\text{NO}_3)_2(\text{cr})$, $\text{Ca}(\text{NO}_3)_2 \cdot 2\text{H}_2\text{O}(\text{cr})$, $\text{Ca}(\text{NO}_3)_2 \cdot 3\text{H}_2\text{O}(\text{cr})$, $\text{Ca}(\text{NO}_3)_2 \cdot 4\text{H}_2\text{O}(\text{cr})$, $\text{Sr}(\text{NO}_3)_2 \cdot 4\text{H}_2\text{O}(\text{cr})$, $\text{Ba}(\text{NO}_3)_2(\text{cr})$ and $\text{Ra}(\text{NO}_3)_2(\text{cr})$ are available in Wagman *et al.* [1982WAG/EVA].

Table 3.9-5. Thermodynamic functions and constants for the N compounds of alkaline earth(II) calculated from Wagman *et al.* [1982WAG/EVA].

Reaction	$\Delta_r G_m^\circ$	$\log_{10} \beta^\circ$	$\Delta_f G_m^\circ$ *	$\Delta_r H_m^\circ$	$\Delta_f H_m^\circ$ *
$\text{Mg}(\text{NO}_3)_2(\text{cr}) \rightleftharpoons \text{Mg}^{2+} + \text{NO}_3^-$	-82.880 ± 0.566	14.52 ± 0.10	-594.083 ± 1.469	-86.200 ± 0.849	-794.500 ± 0.528
$\text{Mg}(\text{NO}_3)_2 \cdot 6\text{H}_2\text{O}(\text{cr}) \rightleftharpoons \text{Mg}^{2+} + \text{NO}_3^- + 6\text{H}_2\text{O}$	-14.754 ± 1.467	2.58 ± 0.26	$-2\ 085.049 \pm 0.622$	21.450 ± 0.942	$-2\ 617.130 \pm 0.412$
$\text{Ca}(\text{NO}_3)_2(\text{cr}) \rightleftharpoons \text{Ca}^{2+} + \text{NO}_3^-$	-27.990 ± 0.574	4.90 ± 0.10	-746.404 ± 1.212	-14.440 ± 0.607	-942.260 ± 1.127
$\text{Ca}(\text{NO}_3)_2 \cdot 2\text{H}_2\text{O}(\text{cr}) \rightleftharpoons \text{Ca}^{2+} + \text{NO}_3^- + 2\text{H}_2\text{O}$	-16.208 ± 0.672	2.84 ± 0.12	$-1\ 232.466 \pm 1.163$	16.270 ± 0.833	$-1\ 544.630 \pm 0.976$
$\text{Ca}(\text{NO}_3)_2 \cdot 3\text{H}_2\text{O}(\text{cr}) \rightleftharpoons \text{Ca}^{2+} + \text{NO}_3^- + 3\text{H}_2\text{O}$	-10.747 ± 1.398	1.88 ± 0.24	$-1\ 475.067 \pm 1.941$	23.810 ± 0.616	$-1\ 841.870 \pm 1.129$
$\text{Ca}(\text{NO}_3)_2 \cdot 4\text{H}_2\text{O}(\text{cr}) \rightleftharpoons \text{Ca}^{2+} + \text{NO}_3^- + 4\text{H}_2\text{O}$	-6.426 ± 0.506	1.13 ± 0.09	$-1\ 716.528 \pm 1.253$	36.180 ± 0.954	$-2\ 132.330 \pm 0.870$
$\text{Sr}(\text{NO}_3)_2(\text{cr}) \rightleftharpoons \text{Sr}^{2+} + \text{NO}_3^-$	3.060 ± 0.651	-0.54 ± 0.11	-788.512 ± 0.939	22.420 ± 1.231	-987.020 ± 1.551
$\text{Sr}(\text{NO}_3)_2 \cdot 4\text{H}_2\text{O}(\text{cr}) \rightleftharpoons \text{Sr}^{2+} + \text{NO}_3^- + 4\text{H}_2\text{O}$	4.914 ± 0.736	-0.86 ± 0.13	$-1\ 738.926 \pm 0.890$	55.680 ± 1.906	$-2\ 163.600 \pm 2.133$
$\text{Ba}(\text{NO}_3)_2(\text{cr}) \rightleftharpoons \text{Ba}^{2+} + \text{NO}_3^-$	18.340 ± 0.762	-3.21 ± 0.13	-797.584 ± 2.604	43.570 ± 0.770	-992.070 ± 2.509
$\text{Ra}(\text{NO}_3)_2(\text{cr}) \rightleftharpoons \text{Ra}^{2+} + \text{NO}_3^-$	17.120 ± 1.364	-3.00 ± 0.24	-800.197 ± 3.852	54.400 ± 3.975	-995.700 ± 2.807

* calculated from $\Delta_r G_m^\circ$ or $\Delta_r H_m^\circ$ using $\Delta_f G_m^\circ$ or $\Delta_f H_m^\circ$ in [2003GUI/FAN]

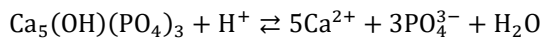
3.9.7. Phosphate Compounds

3.9.7.1. Magnesium solids

The Gibbs energy of formation of the solubility of nissonite ($\text{CuMg}(\text{PO}_4)_2 \cdot 2.5\text{H}_2\text{O}$) in Nriagu [1984NRI] is verified relative to Wagman *et al.* [1968WAG/EVA; 1969WAG/EVA] for H_2O , PO_4^{2-} and Cu^{2+} , and Parker *et al.* [1971PAR/WAG] for Mg^{2+} — the latter references is not explicitly cited in Nriagu [1984NRI]. Only a difference of $-2.4\ \text{kJ mol}^{-1}$ between the $\Delta_f G^\circ$ value in Nriagu [1984NRI] and the one calculated from the $\log_{10} K_s$ values is noted. Hence, the $\Delta_f G_m^\circ$ is recalculated relative to Guillaumont *et al.* [2003GUI/FAN].

3.9.7.2. Calcium solids

Several data are available for the formation of hydroxyapatite, $\text{Ca}_5(\text{OH})(\text{PO}_4)_3$. Robie and Hemingway [1995ROB/HEM] proposed thermodynamic functions — *e.g.*, $\Delta_f G_m^\circ(\text{Ca}_5(\text{OH})(\text{PO}_4)_3) = -(6\ 337.1 \pm 5.0)\ \text{kJ mol}^{-1}$ — that leads to the following solubility equilibrium,



$$\Delta_r G^\circ = (327.2 \pm 2.7) \text{ kJ mol}^{-1}$$

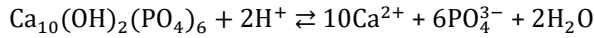
$$\log_{10} K_s^\circ = -57.32 \pm 0.65$$



$$\Delta_r G^\circ = (407.0 \pm 2.7) \text{ kJ mol}^{-1}$$

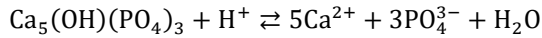
$$\log_{10} K_s^\circ = -71.30 \pm 0.65$$

Wagman *et al.* [1982WAG/EVA] proposed thermodynamic functions — *e.g.*, $\Delta_f G_m^\circ(\text{Ca}_{10}(\text{OH})_2(\text{PO}_4)_6) = -12\ 677 \text{ kJ mol}^{-1}$ or $\Delta_f G_m^\circ(\text{Ca}_5(\text{OH})(\text{PO}_4)_3) = -6\ 338.5 \text{ kJ mol}^{-1}$ — that leads to the following solubility equilibria,



$$\Delta_r G^\circ = 554.7 \text{ kJ mol}^{-1}$$

$$\log_{10} K_s^\circ = -97.18$$



$$\Delta_r G^\circ = 277.4 \text{ kJ mol}^{-1}$$

$$\log_{10} K_s^\circ = -48.60$$



$$\Delta_r G^\circ = 714.5 \text{ kJ mol}^{-1}$$

$$\log_{10} K_s^\circ = -125.17$$



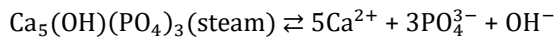
$$\Delta_r G^\circ = 357.3 \text{ kJ mol}^{-1}$$

$$\log_{10} K_s^\circ = -62.60$$

It is interesting to note that the formation functions in Robie and Hemingway [1995ROB/HEM] are referred to the values of Wagman *et al.* [1982WAG/EVA], when apparently they have nothing in common. This comes from the different value for $\Delta_f G^\circ(\text{PO}_4^{3-}) = -1\ 018.7 \text{ kJ mol}^{-1}$ [1982WAG/EVA] compared to the choice in Robie and Hemingway [1995ROB/HEM] — *c.f. § 3.3.*

As for MnS phases, some thermodynamic functions of the products and reactants from Robie and Hemingway [1995ROB/HEM] are not the same as those selected by Guillaumont *et al.* [2003GUI/FAN] — *e.g.*, $\Delta_f G_m^\circ(\text{PO}_4^{3-}) = -(1\ 001.6 \pm 0.9) \text{ kJ mol}^{-1}$ [1995ROB/HEM] and $-(1\ 025.491 \pm 1.576) \text{ kJ mol}^{-1}$ [2003GUI/FAN] —, which can lead to discrepancies when back calculating $\log_{10} K_s$ values. Tracing the original data leads to Moreno *et al.* [1968MOR/GRE], and McDowell *et al.* [1977McD/GRE] who also analysed data from other authors.

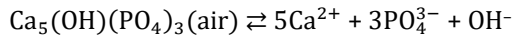
Moreno *et al.* [1968MOR/GRE] studied the solubility at 25°C of synthetic $\text{Ca}_5(\text{OH})(\text{PO}_4)_3$ either steam- or air-heated at 1000°C [1968MOR/GRE]. The solubility were found to be as follows relative to OH^- — $K_s^\circ(\text{steam}) = (3.7_3 \pm 0.5) \cdot 10^{-58}$, and $K_s^\circ(\text{air}) = (2.5_1 \pm 0.4) \cdot 10^{-55}$ — with obtained Gibbs energies of formation in agreement with Guillaumont *et al.* [2003GUI/FAN].



$$\log_{10} K_s = -57.43 \pm 0.06$$

$$\Delta_r G_m^\circ = (327.803 \pm 0.332) \text{ kJ mol}^{-1}$$

$$\Delta_f G_m^\circ = -(6\ 325.526 \pm 7.073) \text{ kJ mol}^{-1}$$

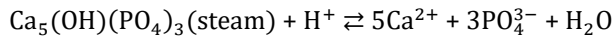


$$\log_{10} K_s = -54.60 \pm 0.07$$

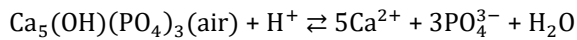
$$\Delta_r G_m^\circ = (311.661 \pm 0.395) \text{ kJ mol}^{-1}$$

$$\Delta_f G_m^\circ = -(6\ 309.384 \pm 7.077) \text{ kJ mol}^{-1}$$

The calculated Gibbs energies of formation allow calculating the solubilities relative to $\text{H}_2\text{O}/\text{H}^+$.



$$\log_{10} K_s = -43.43 \pm 0.06$$

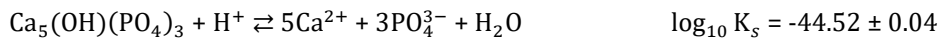


$$\log_{10} K_s = -40.60 \pm 0.07$$

McDowell *et al.* [1977McD/GRE] proposed the following solubility at 25 °C of $\text{Ca}_5(\text{OH})(\text{PO}_4)_3$, obtained from titration of a boiling suspension of $\text{Ca}(\text{OH})_2$ by H_3PO_4 , which solubility equilibrium relative to OH^- — $K_s = (3.04 \pm 0.25) 10^{-59}$ — was written as follows.



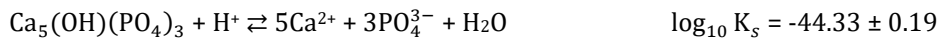
Using Gibbs energies from Guillaumont *et al.* [2003GUI/FAN] allow calculating the following solubility equilibrium relative to $\text{H}_2\text{O}/\text{H}^+$.



The authors compiled data from Moreno *et al.* [1968MOR/GRE] and other sources, and finally proposed that the best estimated value for hydroxyapatite should be $K_s^\circ = (4.7 \pm 2.0) 10^{-59}$, which is written as follows.



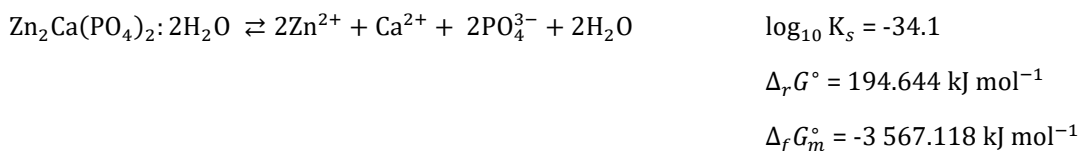
This finally leads to the equilibrium relative to $\text{H}_2\text{O}/\text{H}^+$ as follows.



In PRODATA, the final value from McDowell *et al.* [1977McD/GRE] is retained and the values of steam- and air-heated phases are added and duly addressed as Hydroxyapatite-steamheated and Hydroxyapatite-airheated.

The functions of reaction of fluorapatite ($\text{Ca}_5(\text{PO}_4)_3\text{F}$) are calculated from Robie and Hemingway [1995ROB/HEM].

As for hinsdalite (c.f. § 3.6.2.3), the Gibbs energy of formation of the solubility of scholzite ($(\text{Zn}_2\text{Ca}(\text{PO}_4)_2 \cdot 2\text{H}_2\text{O}(\text{cr}))$ in Nriagu [1984NRI] is verified relative to Wagman *et al.* [1968WAG/EVA; 1969WAG/EVA] for H_2O , PO_4^{2-} and Zn^{2+} , and Parker *et al.* [1971PAR/WAG] for Ca^{2+} — the latter references is not explicitly cited in Nriagu [1984NRI]. No significant difference is noted, hence, the $\Delta_f G^\circ$ is recalculated relative to Guillaumont *et al.* [2003GUI/FAN] as follows.



3.9.7.3. Strontium solid

Functions of reaction of $\text{SrHPO}_4(\text{cr})$ can be retrieved from Wagman *et al.* [1982WAG/EVA].

3.9.7.4. Phosphate complexes

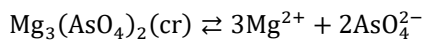
Turner *et al.* [1981TUR/WHI] proposed complexation constants for $\text{MgH}_2\text{PO}_4^+$, $\text{MgHPO}_4(\text{aq})$, MgPO_4^- , $\text{CaH}_2\text{PO}_4^+$, $\text{CaHPO}_4(\text{aq})$, and CaPO_4^- . The Gibbs energy of formation are calculated from the constants and function of formation of the phosphate species in Guillaumont *et al.* [2003GUI/FAN], which allows calculating constants for the other phosphate species.

Table 3.9-6. Thermodynamic constants and Gibbs energies of reaction of P(V) compounds of Mg(II) and Ca(II), and Gibbs energies of formation using Guillaumont *et al.* [2003GUI/FAN]

Reaction	$\log_{10} \beta^\circ$	$\Delta_r G_m^\circ$ kJ mol ⁻¹	$\Delta_f G_m^\circ$ kJ mol ⁻¹
$\text{CuMg}(\text{PO}_4)(\text{OH}): 2.5\text{H}_2\text{O} \rightleftharpoons \text{Cu}^{2+} + \text{Mg}^{2+} + \text{PO}_4^{3-} + \text{OH}^- + 2.5\text{H}_2\text{O}$	-23.6	134.710	-2 300.600
$\text{CuMg}(\text{PO}_4)(\text{OH}): 2.5\text{H}_2\text{O} + \text{H}^+ \rightleftharpoons \text{Cu}^{2+} + \text{Mg}^{2+} + \text{PO}_4^{3-} + 3.5\text{H}_2\text{O}$	-9.6	54.790	-6 325.526 ± 7.073
$\text{Ca}_5(\text{OH})(\text{PO}_4)_3(\text{air}) \rightleftharpoons 5\text{Ca}^{2+} + 3\text{PO}_4^{3-} + \text{OH}^-$	-54.60 ± 0.07	311.661 ± 0.395	-6 309.384 ± 7.077
$\text{Ca}_5(\text{OH})(\text{PO}_4)_3(\text{air}) + \text{H}^+ \rightleftharpoons 5\text{Ca}^{2+} + 3\text{PO}_4^{3-} + \text{H}_2\text{O}$	-40.60 ± 0.07		
$\text{Ca}_5(\text{OH})(\text{PO}_4)_3(\text{steam}) \rightleftharpoons 5\text{Ca}^{2+} + 3\text{PO}_4^{3-} + \text{OH}^-$	-57.43 ± 0.06	327.803 ± 0.332	
$\text{Ca}_5(\text{OH})(\text{PO}_4)_3(\text{steam}) + \text{H}^+ \rightleftharpoons 5\text{Ca}^{2+} + 3\text{PO}_4^{3-} + \text{H}_2\text{O}$	-43.43 ± 0.06		
$\text{Zn}_2\text{Ca}(\text{PO}_4)_2: 2\text{H}_2\text{O} \rightleftharpoons 2\text{Zn}^{2+} + \text{Ca}^{2+} + 2\text{PO}_4^{3-} + 2\text{H}_2\text{O}$	-34.1	194.644	-3 567.118
$\text{Mg}^{2+} + \text{PO}_4^{3-} \rightleftharpoons \text{MgPO}_4^-$	4.85	-27.684	-1 508.550
$\text{Mg}^{2+} + \text{HPO}_4^{2-} \rightleftharpoons \text{MgHPO}_4(\text{aq})$	2.88	-16.439	-1 567.799
$\text{Mg}^{2+} + \text{H}_2\text{PO}_4^- \rightleftharpoons \text{MgH}_2\text{PO}_4^+$	1.17	-6.678	-1 599.204
$\text{Ca}^{2+} + \text{PO}_4^{3-} \rightleftharpoons \text{CaPO}_4^-$	6.46	-36.874	-1 615.171
$\text{Ca}^{2+} + \text{HPO}_4^{2-} \rightleftharpoons \text{CaHPO}_4(\text{aq})$	2.55	-14.556	-1 663.347
$\text{Ca}^{2+} + \text{H}_2\text{PO}_4^- \rightleftharpoons \text{CaH}_2\text{PO}_4^+$	1.40	-7.991	-1 697.948

3.9.8. Arsenic Compounds

The solubility of $\text{Mg}_3(\text{AsO}_4)_2(\text{cr})$ is calculated from the functions of formation from Wagman *et al.* [1982WAG/EVA].



$$\Delta_r G^\circ = 136.900 \pm 2.321 \text{ kJ mol}^{-1}$$

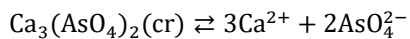
$$\log_{10} K_s = -23.98 \pm 0.41$$

$$\Delta_f G_m^\circ = -3 554.007 \pm 5.600 \text{ kJ mol}^{-1}$$

$$\Delta_r H^\circ = -174.650 \pm 6.215 \text{ kJ mol}^{-1}$$

$$\Delta_f H^\circ = -3 795.150 \pm 5.6 \text{ kJ mol}^{-1}$$

The solubility of $\text{Ca}_3(\text{AsO}_4)_2(\text{cr})$ is calculated from the functions of formation from Wagman *et al.* [1982WAG/EVA].



$$\Delta_r G^\circ = 105.440 \pm 1.753$$

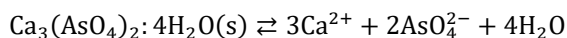
$$\log_{10} K_s = -18.47 \pm 0.08$$

$$\Delta_f G_m^\circ = -3 060.578 \pm 8.432 \text{ kJ mol}^{-1}$$

$$\Delta_r H^\circ = -106.070 \pm 5.517 \text{ kJ mol}^{-1}$$

$$\Delta_f H^\circ = -3 299.210 \pm 6.524 \text{ kJ mol}^{-1}$$

The solubility of $\text{Ca}_3(\text{AsO}_4)_2: 4\text{H}_2\text{O}(\text{s})$ is calculated from the functions of formation from Naumov *et al.* [1974NAU/RYZ].

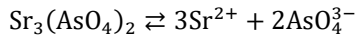


$$\Delta_r G^\circ = 107.986 \text{ kJ mol}^{-1}$$

$$\log_{10} K_s = -18.92$$

$$\Delta_f G_m^\circ = -4 011.684 \text{ kJ mol}^{-1}$$

The functions of reaction of $\text{Sr}_3(\text{AsO}_4)_2(\text{cr})$ can be retrieved from Wagman *et al.* [1982WAG/EVA].



$$\Delta_r G^\circ = 104.840 \pm 8.313 \text{ kJ mol}^{-1}$$

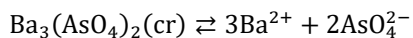
$$\log_{10} K_s = -18.37$$

$$\Delta_f G_m^\circ = -3093.152 \pm 0.800 \text{ kJ mol}^{-1}$$

$$\Delta_r H^\circ = -96.580 \pm 8.100 \text{ kJ mol}^{-1}$$

$$\Delta_f H^\circ = -3332.400 \pm 0.800 \text{ kJ mol}^{-1}$$

The solubility of $\text{Ba}_3(\text{AsO}_4)_2(\text{cr})$ is calculated from the solubility from Essington [1988ESS].



$$\log_{10} K_s = -21.62$$

$$\Delta_r G^\circ = 123.408 \text{ kJ mol}^{-1}$$

$$\Delta_f G_m^\circ = -3093.096 \text{ kJ mol}^{-1}$$

It can be noted that a -30 orders of magnitude difference $\log_{10} K_s$ value is reported in the wateq4f database, which origin is unknown. A similar value from a Russian study is cited in Robins [1985ROB]. The data from Essington [1988ESS] will be used in PRODATA

3.9.9. Carbonato Compounds

3.9.9.1. Solids

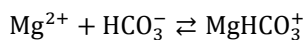
The functions of reaction of magnesite (MgCO_3) and nesquehonite ($\text{MgCO}_3 \cdot 3\text{H}_2\text{O}$) are taken from Robie and Hemingway [1995ROB/HEM]. The functions of reaction of lansfordite ($\text{MgCO}_3 \cdot 5\text{H}_2\text{O}$) are taken from Wagman *et al.* [1982WAG/EVA]. The hydroxocarbonate phases hydromagnesite ($(\text{MgCO}_3)_4(\text{Mg}(\text{OH})_2) \cdot 4\text{H}_2\text{O}$), and artinite ($(\text{Mg}_2(\text{OH})_2\text{CO}_3 \cdot 3\text{H}_2\text{O}$) are taken from Robie and Hemingway [1995ROB/HEM].

The functions of reaction for allotropic forms of CaCO_3 (aragonite, calcite, and vaterite), ikaite ($\text{CaCO}_3 \cdot 6\text{H}_2\text{O}$), and monohydrocalcite ($\text{CaCO}_3 \cdot \text{H}_2\text{O}$), as well as dolomite ($\text{CaMg}(\text{CO}_3)_2$) and huntite ($\text{CaMg}_3(\text{CO}_3)_4$) are taken from Robie and Hemingway [1995ROB/HEM].

The formation functions of strontianite (SrCO_3) are taken from Busenberg *et al.* [1984BUS/PLU]. The solubility of witherite (BaCO_3) is taken from Busenberg and Plummer [1986BUS/PLU]. The functions of reaction of barytocalcite, and alstonite ($\text{BaCa}(\text{CO}_3)_2$) are calculated from Wagman *et al.* [1982WAG/EVA].

3.9.9.2. Complexes

Nordstrom *et al.* [1990NOR/PLU] proposed the formation constant and enthalpy of reaction of MgHCO_3^- , which are used to calculate the Gibbs energy and enthalpy of formation.



$$\log_{10} K^\circ = 1.07$$

$$\Delta_r G^\circ = -6.108 \text{ kJ mol}^{-1}$$

$$\Delta_r H^\circ = 0.79 \text{ kcal mol}^{-1} = 3.31 \text{ kJ mol}^{-1}$$

$$\Delta_f G^\circ = -1048.328 \text{ kJ mol}^{-1}$$

$$\Delta_r H^\circ = -1153.625 \text{ kJ mol}^{-1}$$

Sverjensky *et al.* [1997SVE/SHO] estimated the thermodynamic function of formation for the carbonato complexes of alkaline earth metals. From these values the formation of $\text{MgCO}_3(\text{aq})$ can be estimated as follows,

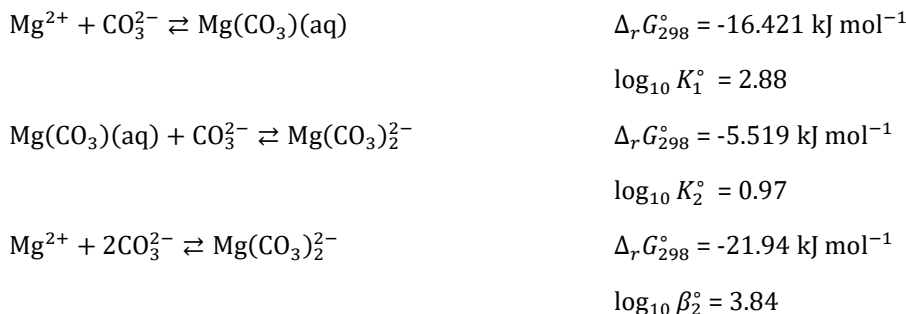
using the functions of formation from the free ion and ligand from Shock and Helgeson [1988SHO/HEL] (Table 3.9-7).



Königsberger *et al.* [1999KÖN/KÖN] proposed the enthalpy and entropy of formation of $\text{Mg}(\text{CO}_3)_2^{2-}$.

$$\Delta_f H_{298}^\circ = -1839.4 \text{ kJ mol}^{-1}, S_{298}^\circ = -237.0 \text{ J mol}^{-1} \text{ K}^{-1}$$

Using the functions of formation of Mg^{2+} and CO_3^{2-} in Königsberger *et al.* [1999KÖN/KÖN], the Gibbs energy of reaction and thermodynamic constants can be proposed.



The first carbonation constant is slightly lower than the one estimated in Sverjensky *et al.* [1997SVE/SHO], and as awaited the formation of $\text{Mg}(\text{CO}_3)_2^{2-}$ is more difficult than the formation of the monocarbonatomagnesium(II) complex.

Plotting the speciation of Mg-CO₃ in Figure 3.9-1 — not accounting for MgHCO_3^+ — shows that the impact of $\text{Mg}(\text{CO}_3)_2^{2-}$ is minor — the thermodynamic constant of CO₂(aq), HCO₃⁻, and CO₃²⁻ in Königsberger *et al.* [1999KÖN/KÖN] are the same as in Guillaumont *et al.* [2003GUI/FAN]. It would only be occurring at P(CO₂) higher than 10%. It is included in PRODATA for scoping calculation.

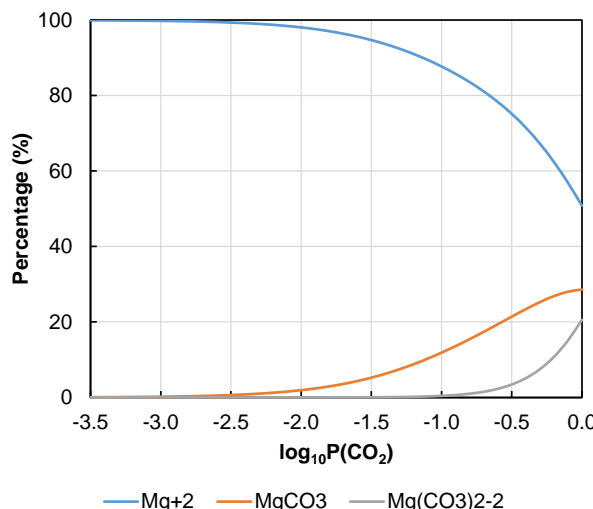


Figure 3.9-1. Speciation of Mg-CO₃ with increasing concentration of carbonate plotted as percentage of species vs. equivalent P(CO₂) in equilibrium using the data from Königsberger *et al.* [1999KÖN/KÖN]: C_{Mg} = 0.1 mmol kg_w⁻¹, pH = 8, [NaClO₄] = 0.1 mol kg_w⁻¹.

Plummer and Busenberg [1982PLU/BUS] estimated the solubility *vs.* temperature of calcite, aragonite, and vaterite (CaCO_3), as well as the formation of $\text{CaCO}_3(\text{aq})$ and CaHCO_3^+ . It can be noted that the estimation of the formation of $\text{CaCO}_3(\text{aq})$ in Sverjensky *et al.* [1997SVE/SHO] ($\log_{10} K^\circ = 3.33$) is slightly higher than the one from Plummer and Busenberg [1982PLU/BUS] — see Table 3.9-7.

Busenberg *et al.* [1984BUS/PLU] estimated the solubility *vs.* temperature of strontianite ($\text{SrCO}_3(\text{s})$) and the formation of $\text{SrCO}_3(\text{aq})$, and SrHCO_3^+ . The estimation of $\text{SrCO}_3(\text{aq})$ in Sverjensky *et al.* [1997SVE/SHO] ($\log_{10} K^\circ = 2.87$) is slightly lower than the one from Busenberg *et al.* [1984BUS/PLU] — see Table 3.9-7.

Busenberg and Plummer [1986BUS/PLU] estimated the solubility of witherite ($\text{BaCO}_3(\text{s})$) and the formation of $\text{BaCO}_3(\text{aq})$ and BaHCO_3^+ . The estimation of $\text{BaCO}_3(\text{aq})$ in Sverjensky *et al.* [1997SVE/SHO] ($\log_{10} K^\circ = 2.65$) is slightly higher than the one from Busenberg *et al.* [1984BUS/PLU] — see Table 3.9-7.

Table 3.9-7. Thermodynamic functions and constants for the C compounds of alkaline earth(II).

Reaction	$\Delta_r G_m^\circ$ (kJ mol ⁻¹)	$\log_{10} \beta^\circ$	$\Delta_f G_m^\circ$ * (kJ mol ⁻¹)	$\Delta_r H_m^\circ$ (kJ mol ⁻¹)	$\Delta_f H_m^\circ$ * (kJ mol ⁻¹)
Magnesite $\text{MgCO}_3(\text{cr}) \rightleftharpoons \text{Mg}^{2+} + \text{CO}_3^{2-}$	$47.100 \pm 1.229^{\text{a}}$	-8.25 ± 0.22	$-1\ 030.375 \pm 0.651$	$-28.900 \pm 0.608^{\text{a}}$	$-1\ 113.330 \pm 0.947$
Nesquehonite $\text{MgCO}_3 \cdot 3\text{H}_2\text{O} \rightleftharpoons \text{Mg}^{2+} + \text{CO}_3^{2-} + 3\text{H}_2\text{O}$	$30.100 \pm 0.539^{\text{a}}$	-5.27 ± 0.09	$-1\ 724.795 \pm 1.288$	$-22.300 \pm 0.608^{\text{a}}$	$-1\ 977.420 \pm 0.259$
Lansfordite $\text{MgCO}_3 \cdot 5\text{H}_2\text{O} \rightleftharpoons \text{Mg}^{2+} + \text{CO}_3^{2-} + 5\text{H}_2\text{O}$	$30.945 \pm 5.881^{\text{a}}$	-5.42 ± 1.03	$-2\ 199.920 \pm 6.046$		
Hydromagnesite $(\text{MgCO}_3)_4(\text{Mg(OH)}_2) \cdot 4\text{H}_2\text{O} + 2\text{H}^+ \rightleftharpoons 5\text{Mg}^{2+} + 4\text{CO}_3^{2-} + 6\text{H}_2\text{O}$	$56.600 \pm 6.771^{\text{a}}$	-9.92 ± 0.52	$-5\ 867.915 \pm 6.181$	$-235.700 \pm 2.883^{\text{a}}$	$-6\ 515.200 \pm 1.322$
Artinitie $\text{Mg}_2(\text{OH})_2\text{CO}_3 \cdot 3\text{H}_2\text{O} + 2\text{H}^+ \rightleftharpoons 2\text{Mg}^{2+} + \text{CO}_3^{2-} + 5\text{H}_2\text{O}$	$-54.900 \pm 1.068^{\text{a}}$	9.62 ± 0.19	$-2\ 569.450 \pm 2.487$	$-117.600 \pm 1.100^{\text{a}}$	$-2\ 920.780 \pm 0.577$
Calcite $\text{CaCO}_3 \rightleftharpoons \text{Ca}^{2+} + \text{CO}_3^{2-}$	$47.900 \pm 0.192^{\text{a}}$	-8.39 ± 0.03	$-1\ 128.606 \pm 1.104$	$-10.800 \pm 0.235^{\text{a}}$	$-1\ 207.430 \pm 1.057$
Aragonite $\text{CaCO}_3 \rightleftharpoons \text{Ca}^{2+} + \text{CO}_3^{2-}$	$46.800 \pm 0.503^{\text{a}}$	-8.20 ± 0.09	$-1\ 127.506 \pm 1.228$	$-10.800 \pm 0.570^{\text{a}}$	$-1\ 207.430 \pm 1.178$
Vaterite $\text{CaCO}_3 \rightleftharpoons \text{Ca}^{2+} + \text{CO}_3^{2-}$	$44.900 \pm 0.503^{\text{a}}$	-7.87 ± 0.09	$-1\ 125.606 \pm 1.228$		
Monohydrocalcite $\text{CaCO}_3 \cdot \text{H}_2\text{O} \rightleftharpoons \text{Ca}^{2+} + \text{CO}_3^{2-} + \text{H}_2\text{O}$	$43.900 \pm 0.894^{\text{a}}$	-7.69 ± 0.16	$-1\ 361.746 \pm 0.675$	$-5.700 \pm 1.262^{\text{a}}$	$-1\ 498.360 \pm 1.63$
Ikaite $\text{CaCO}_3 \cdot \text{H}_2\text{O} \rightleftharpoons \text{Ca}^{2+} + \text{CO}_3^{2-} + \text{H}_2\text{O}$	$37.700 \pm 4.574^{\text{a}}$	-6.60 ± 0.80	$-2\ 541.246 \pm 4.715$	$21.100 \pm 4.625^{\text{a}}$	$-2\ 954.310 \pm 4.744$
Dolomite $\text{MgCa}(\text{CO}_3)_2 \rightleftharpoons \text{Mg}^{2+} + \text{Ca}^{2+} + 2\text{CO}_3^{2-}$	$98.300 \pm 1.082^{\text{a}}$	-17.22 ± 0.19	$-2\ 162.281 \pm 1.524$	$-35.900 \pm 0.922^{\text{a}}$	$-2\ 324.560 \pm 0.872$
Dolomite-dissordered $\text{MgCa}(\text{CO}_3)_2 \rightleftharpoons \text{Mg}^{2+} + \text{Ca}^{2+} + 2\text{CO}_3^{2-}$	94.411^{b}	-16.54	$-2\ 158.392$	-46.401	$-2\ 314.059$
Huntite $\text{CaMg}_3(\text{CO}_3)_4 \rightleftharpoons 3\text{Mg}^{2+} + \text{Ca}^{2+} + 4\text{CO}_3^{2-}$	$175.300 \pm 1.766^{\text{a}}$	-30.71 ± 0.31	$-4\ 205.831 \pm 4.057$	$-115.200 \pm 1.356^{\text{a}}$	$-4\ 529.720 \pm 1.844$
$\text{Mg}^{2+} + \text{CO}_3^{2-} \rightleftharpoons \text{Mg}(\text{CO}_3)(\text{aq})$	-17.010^{c}	2.98	$-1\ 000.285$	11.351^{c}	$-1\ 130.879$
$\text{Mg}(\text{CO}_3)(\text{aq}) + \text{CO}_3^{2-} \rightleftharpoons \text{Mg}(\text{CO}_3)_2^{2-}$	-5.519^{d}	0.97	$-1\ 533.722$	-35.316	$-1\ 841.425$
$\text{Mg}^{2+} + 2\text{CO}_3^{2-} \rightleftharpoons \text{Mg}(\text{CO}_3)_2^{2-}$	-22.547	3.95		-23.965	
$\text{Mg}^{2+} + \text{CO}_3^{2-} + \text{H}^+ \rightleftharpoons \text{MgHCO}_3^+$	-65.05^{b}	11.4	$-1\ 048.328$	-11.395^{c}	$-1\ 153.625$
$\text{Ca}^{2+} + \text{CO}_3^{2-} \rightleftharpoons \text{Ca}(\text{CO}_3)(\text{aq})$	$-18.380 \pm 0.248^{\text{e}}$	3.22 ± 0.04	$-1\ 099.086 \pm 1.376$	15.790^{c}	$-1\ 202.440$
$\text{Ca}^{2+} + \text{CO}_3^{2-} + \text{H}^+ \rightleftharpoons \text{CaHCO}_3^+$	-65.258 ± 0.204	11.43 ± 0.04	$-1\ 145.964 \pm 1.151$	-3.45^{c}	$-1\ 221.680$
$\text{Sr}^{2+} + \text{CO}_3^{2-} \rightleftharpoons \text{Sr}(\text{CO}_3)(\text{aq})$	-16.04^{f}	2.81		21.83	
$\text{Sr}^{2+} + \text{CO}_3^{2-} + \text{H}^+ \rightleftharpoons \text{SrHCO}_3^+$	-65.68	11.51		10.60	

Table 3.9-7. Continued.

Reaction	$\Delta_r G_m^\circ$ (kJ mol ⁻¹)	$\log_{10} \beta^\circ$	$\Delta_f G_m^\circ$ (kJ mol ⁻¹)	$\Delta_r H_m^\circ$ (kJ mol ⁻¹)	$\Delta_f H_m^\circ$ (kJ mol ⁻¹)
$\text{Ba}^{2+} + \text{CO}_3^{2-} \rightleftharpoons \text{Ba}(\text{CO}_3)(\text{aq})$	-15.49 ^g	2.71		14.84	
$\text{Ba}^{2+} + \text{CO}_3^{2-} + \text{H}^+ \rightleftharpoons \text{BaHCO}_3^+$	-64.55	11.31		8.56	

a [1995ROB/HEM]; b [1990NOR/PLU]; c [1997aSHO/SAS; 1997SVE/SHO]; d [1999KÖN/KÖN]; e [1982PLU/BUS]; f [1984BUS/PLU]; g [1986BUS/PLU].

* calculated $\Delta_f G_m^\circ$ or $\Delta_f H_m^\circ$ in [2003GUI/FAN]

3.9.10. Silicate Compounds

Function of reaction of chrysotile ($\text{Mg}_3\text{Si}_2\text{O}_5(\text{OH})_4$) is available from Robie and Hemingway [1995ROB/HEM].

Functions of reaction of wollastonite and pseudo-wollastonite (CaSiO_3) are available from Wagman *et al.* [1982WAG/EVA] and Robie and Hemingway [1995ROB/HEM]. The ones for larnite ($\alpha - \text{Ca}_2\text{SiO}_4$) are from Robie and Hemingway [1995ROB/HEM]. Calcio-olivine ($\gamma - \text{Ca}_2\text{SiO}_4$) are available in Wagman *et al.* [1982WAG/EVA] and Robie and Hemingway [1995ROB/HEM]. $\beta - (\text{Ca}_2\text{SiO}_4)_2$ and $(\text{CaO})_3:\text{SiO}_2(\text{cr})$ are available in Wagman *et al.* [1982WAG/EVA]. Rankinite ($\text{Ca}_3\text{Si}_2\text{O}_7$) is available in Wagman *et al.* [1982WAG/EVA] and Robie and Hemingway [1995ROB/HEM].

$\text{SrSiO}_3(\text{cr})$ and $\text{Sr}_2\text{SiO}_4(\text{cr})$ are available in Wagman *et al.* [1982WAG/EVA].

The formation functions of barium silicate $\text{BaO}: \text{SiO}_2(\text{cr})$, $\text{BaO}: 2\text{SiO}_2(\text{cr})$, and $(\text{BaO})_2: 3\text{SiO}_2(\text{cr})$ are available in Wagman *et al.* [1982WAG/EVA].

Table 3.9-8. Thermodynamic functions and constants for Si compounds of alkaline earth(II) metals.

Reaction	$\Delta_r G_m^\circ$ (kJ mol ⁻¹)	$\log_{10} \beta^\circ$	$\Delta_f G_m^\circ$ (kJ mol ⁻¹)	$\Delta_r H_m^\circ$ (kJ mol ⁻¹)	$\Delta_f H_m^\circ$ (kJ mol ⁻¹)
$\text{Mg}_3\text{Si}_2\text{O}_5(\text{OH})_4 + 6\text{H}^+ \rightleftharpoons 3\text{Mg}^{2+} + 2\text{Si}(\text{OH})_4(\text{aq}) + \text{H}_2\text{O}$	-185.900 ± 3.432^a	32.57 ± 0.60	$-4\ 032.835 \pm 3.100$	-246.400 ± 5.853^a	$-4\ 354.350 \pm 3.000$
Wollastonite $\text{CaSiO}_3 + \text{H}_2\text{O} + 2\text{H}^+ \rightleftharpoons \text{Ca}^{2+} + \text{Si}(\text{OH})_4(\text{aq})$	-75.000 ± 0.691^a	13.14 ± 0.12	$-1\ 548.401 \pm 1.400$	-82.400 ± 3.007^a	$-1\ 631.730 \pm 1.400$
pseudo-Wollastonite $\text{CaSiO}_3 + \text{H}_2\text{O} + 2\text{H}^+ \rightleftharpoons \text{Ca}^{2+} + \text{Si}(\text{OH})_4(\text{aq})$	-80.500 ± 0.691^a	14.10 ± 0.12	$-1\ 542.901 \pm 1.400$	-89.600 ± 3.007^a	$-1\ 624.530 \pm 1.400$
Larnite $\text{Ca}_2\text{SiO}_4 + 4\text{H}^+ \rightleftharpoons 2\text{Ca}^{2+} + \text{Si}(\text{OH})_4(\text{aq})$	-223.500 ± 2.309^a	39.16 ± 0.40	$-2\ 189.847 \pm 0.643$	-239.300 ± 2.154^a	$-2\ 303.660 \pm 3.060$
Calcio-olivine $\text{Ca}_2\text{SiO}_4 + 4\text{H}^+ \rightleftharpoons 2\text{Ca}^{2+} + \text{Si}(\text{OH})_4(\text{aq})$	-215.800 ± 1.470^a	37.81 ± 0.26	$-2\ 197.547 \pm 1.894$	-229.500 ± 0.800^a	$-2\ 313.460 \pm 3.656$
$(\text{CaO})_2:\text{SiO}_2-\beta + 4\text{H}^+ \rightleftharpoons 2\text{Ca}^{2+} + \text{Si}(\text{OH})_4(\text{aq})$	-230.960 ± 2.009^b	40.46 ± 0.35	$-2\ 182.387 \pm 1.308$	-246.760 ± 1.642^b	$-2\ 296.200 \pm 3.363$
$(\text{CaO})_2:\text{SiO}_2-\gamma + 4\text{H}^+ \rightleftharpoons 2\text{Ca}^{2+} + \text{Si}(\text{OH})_4(\text{aq})$	-222.660 ± 2.214^b	39.01 ± 0.39	$-2\ 190.687 \pm 0.918$	-236.360 ± 2.312^b	$-2\ 306.600 \pm 2.943$
$(\text{CaO})_3:\text{SiO}_2(\text{cr}) + 6\text{H}^+ \rightleftharpoons 3\text{Ca}^{2+} + \text{Si}(\text{OH})_4(\text{aq}) + \text{H}_2\text{O}$	-430.469 ± 2.229^b	75.41 ± 0.39	$-2\ 772.824 \pm 2.509$	-453.720 ± 2.135^b	$-2\ 918.070 \pm 3.801$
Rankinite $\text{Ca}_3\text{Si}_2\text{O}_7 + \text{H}_2\text{O} + 6\text{H}^+ \rightleftharpoons 3\text{Ca}^{2+} + 2\text{Si}(\text{OH})_4(\text{aq})$	-290.600 ± 6.545^a	50.91 ± 1.15	$-3\ 746.148 \pm 7.623$	-314.200 ± 4.311^a	$-3\ 942.890 \pm 5.517$
$(\text{CaO})_3:2\text{SiO}_2(\text{cr}) + \text{H}_2\text{O} + 6\text{H}^+ \rightleftharpoons 3\text{Ca}^{2+} + 2\text{Si}(\text{OH})_4(\text{aq})$	-295.511 ± 2.085^b	51.77 ± 0.37	$-3\ 741.237 \pm 3.304$	-318.860 ± 2.180^b	$-3\ 938.230 \pm 6.653$
$\text{SrSiO}_3(\text{cr}) + \text{H}_2\text{O} + 2\text{H}^+ \rightleftharpoons \text{Sr}^{2+} + \text{Si}(\text{OH})_4(\text{aq})$	-89.251 ± 5.424^b	15.64 ± 0.95	$-1\ 545.208 \pm 5.600$	-94.670 ± 6.449^b	$-1\ 627.360 \pm 7.200$
$\text{Sr}_2\text{SiO}_4(\text{cr}) + 4\text{H}^+ \rightleftharpoons 2\text{Sr}^{2+} + \text{Si}(\text{OH})_4(\text{aq})$	-244.460 ± 1.771^b	42.83 ± 0.31	$-2\ 191.003 \pm 0.800$	-255.700 ± 2.235^b	$-2\ 303.060 \pm 4.000$

Table 3.9-8. Continued.

Reaction	$\Delta_r G_m^\circ$ (kJ mol ⁻¹)	$\log_{10} \beta^\circ$	$\Delta_f G_m^\circ$ * (kJ mol ⁻¹)	$\Delta_r H_m^\circ$ (kJ mol ⁻¹)	$\Delta_f H_m^\circ$ * (kJ mol ⁻¹)
BaO: SiO ₂ (cr) + H ₂ O + 2H ⁺ ⇌ Ba ²⁺ + Si(OH) ₄ (aq)	-100.031 ± 4.832 ^b	17.52 ± 0.85	-1 528.220 ± 5.599	-96.810 ± 4.804 ^b	-1 609.120 ± 6.272
BaO: 2SiO ₂ (cr) + 3H ₂ O + 2H ⁺ ⇌ Ba ²⁺ + 2Si(OH) ₄ (aq)	-71.883 ± 7.816 ^b	12.59 ± 1.37	-2 389.823 ± 8.550	-69.250 ± 9.546 ^b	-2 521.980 ± 11.721
(BaO) ₂ : SiO ₂ (cr) + 4H ⁺ ⇌ 2Ba ²⁺ + Si(OH) ₄ (aq)	-263.340 ± 3.600 ^b	46.13 ± 0.63	-2 159.707 ± 6.400	-256.080 ± 2.440 ^b	-2 270.480 ± 6.400
(BaO) ₂ : 3SiO ₂ (cr) + 4H ₂ O + 4H ⁺ ⇌ 2Ba ²⁺ + 3Si(OH) ₄ (aq)	-159.824 ± 14.418 ^b	28.00 ± 2.53	-3 930.133 ± 15.704	-152.96 ± 12.88 ^b	-4 144.200 ± 16.762

a [1995ROB/HEM]; b [1982WAG/EVA].

* calculated from $\Delta_r G_m^\circ$ or $\Delta_r H_m^\circ$ using $\Delta_f G_m^\circ$ in [2003GUI/FAN]

3.9.11. Estimation of Specific Ion Interaction Parameters

In chloride and nitrate media, only $\varepsilon(\text{Mg}^{2+}, \text{X}^-)$, $\varepsilon(\text{Ca}^{2+}, \text{X}^-)$, and $\varepsilon(\text{Ba}^{2+}, \text{X}^-)$ are given in Guillaumont *et al.* [2003GUI/FAN]. The dependence of the $\varepsilon(\text{M}^{2+}, \text{X}^-)$ values with the inverse of ionic radii, which has been exemplified in Grenthe *et al.* [1997GRE/PLY], could help estimating the missing values for Sr²⁺ and Ra²⁺. These dependences are plotted in a typical manner in Figure 3.9-2a for Cl⁻ and Figure 3.9-2b for NO₃⁻, using the IR values for Mg²⁺, Ca²⁺, and Ba²⁺ taken from Shannon [1976SHA]. Nevertheless, the linear regression are calculated as $\varepsilon(\text{M}^{2+}, \text{X}^-) = f(1/\text{IR})$ in order to calculate the uncertainty of an unknown ε values from the 1/IR value for a particular M²⁺ cation. Using the IR values for Sr²⁺ and Ra²⁺ [1976SHA] allow estimating the $\varepsilon(\text{Sr}^{2+}, \text{X}^-)$ and $\varepsilon(\text{Ra}^{2+}, \text{Cl}^-)$ in Table 3.9-9.

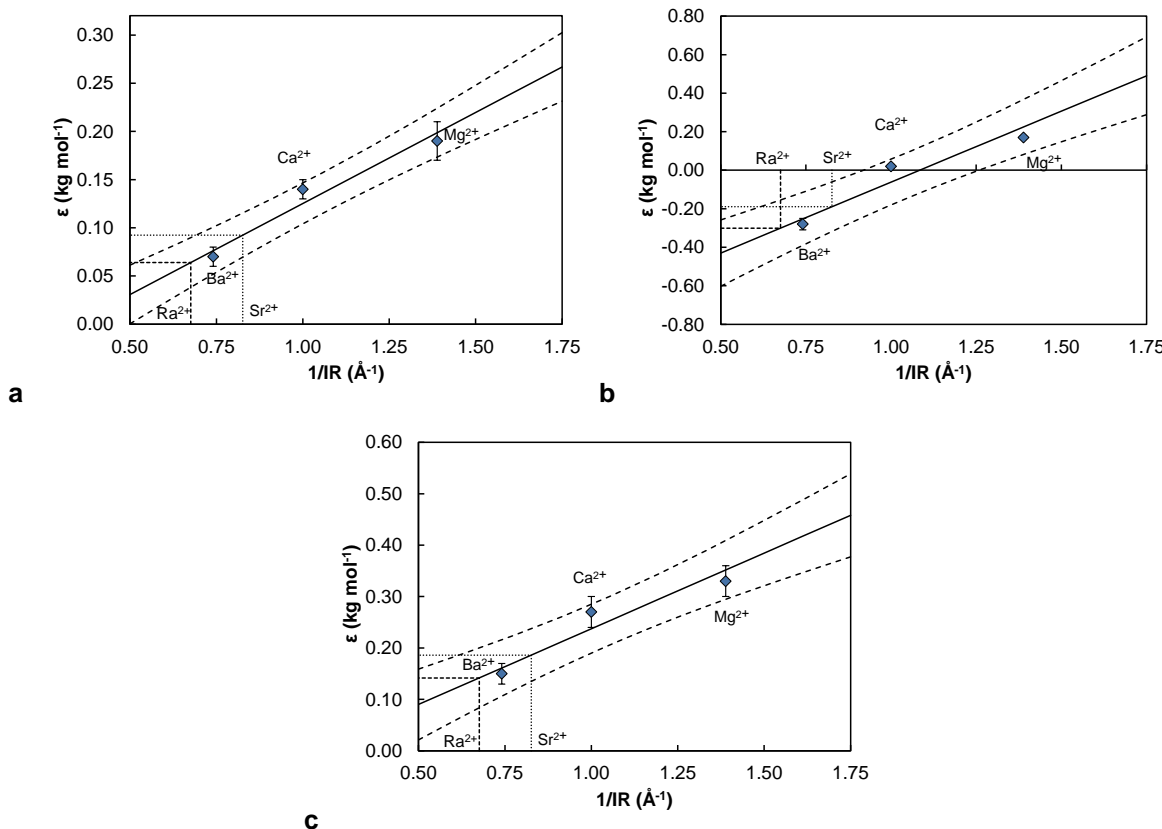


Figure 3.9-2. Dependence of $\epsilon(\text{M}^{2+}, \text{Cl}^-)$ (a), $\epsilon(\text{M}^{2+}, \text{NO}_3^-)$ (b), and $\epsilon(\text{M}^{2+}, \text{ClO}_4^-)$ (c) for the alkaline earth metals from Guillaumont *et al.* [2003GUI/FAN] with the $1/\text{IR}$ value from Shannon [1976SHA]: linear regression (plain line) is calculated as $1/\text{IR} = f(\epsilon)$ even plotted otherwise in a typical manner; the dashed lines represent the 95% confidence interval; dotted line represents the $\epsilon(\text{Sr}^{2+}, \text{X}^-)$ calculated values; the short dotted line represent the $\epsilon(\text{Ra}^{2+}, \text{X}^-)$ values.

Table 3.9-9. Specific ion interaction coefficients between alkaline earth metals (Mg^{2+} , Ca^{2+} , and Ba^{2+}) and anions (Cl^- , ClO_4^- , and NO_3^-) from NEA-OECD reviews and values for Sr^{2+} and Ra^{2+} obtained after regression $1/\text{IR}$ vs. $\epsilon(\text{M}^{2+}, \text{X}^-)$.

Specific ion interaction coefficient	Value $\pm \sigma$	Reference
$\epsilon(\text{Mg}^{2+}, \text{Cl}^-)$	0.19 ± 0.02	[1992GRE/FUG]
$\epsilon(\text{Ca}^{2+}, \text{Cl}^-)$	0.14 ± 0.01	[1992GRE/FUG]
$\epsilon(\text{Sr}^{2+}, \text{Cl}^-)$	0.09 ± 0.02	
$\epsilon(\text{Ba}^{2+}, \text{Cl}^-)$	0.07 ± 0.01	[1992GRE/FUG]
$\epsilon(\text{Ra}^{2+}, \text{Cl}^-)$	0.06 ± 0.03	
$\epsilon(\text{Mg}^{2+}, \text{ClO}_4^-)$	0.33 ± 0.03	[1992GRE/FUG]
$\epsilon(\text{Ca}^{2+}, \text{ClO}_4^-)$	0.27 ± 0.03	[1992GRE/FUG]
$\epsilon(\text{Sr}^{2+}, \text{ClO}_4^-)$	0.19 ± 0.05	
$\epsilon(\text{Ba}^{2+}, \text{ClO}_4^-)$	0.15 ± 0.02	[1992GRE/FUG]
$\epsilon(\text{Ra}^{2+}, \text{ClO}_4^-)$	0.14 ± 0.06	
$\epsilon(\text{Mg}^{2+}, \text{NO}_3^-)$	0.17 ± 0.01	[1992GRE/FUG]
$\epsilon(\text{Ca}^{2+}, \text{NO}_3^-)$	0.02 ± 0.01	[1992GRE/FUG]
$\epsilon(\text{Sr}^{2+}, \text{NO}_3^-)$	-0.19 ± 0.13	
$\epsilon(\text{Ba}^{2+}, \text{NO}_3^-)$	-0.28 ± 0.03	[1992GRE/FUG]
$\epsilon(\text{Ra}^{2+}, \text{NO}_3^-)$	-0.30 ± 0.15	

3.10. Alkali Metals

Alkali metals comprises two of the major cations in the environment (Na^+ , K^+) and one of the major daughter of the ^{235}U fission, *i.e.* ^{137}Cs [1993ENG/RID]. They will be treated all together, as mostly phases will be included. The use of the SIT is including the interactions of anions with the cation from the electrolyte.

3.10.1. Native Metals and Free Ions

The functions of formations for native metals and free cations are taken from Guillaumont *et al.* [2003GUI/FAN]. The common master species are Li^+ , Na^+ , K^+ , Rb^+ , and Cs^+ .

3.10.2. Oxide and Hydroxide Compounds

The functions of formation for $\text{Li}_2\text{O}(\text{cr})$, $\text{Na}_2\text{O}(\text{cr})$, $\text{K}_2\text{O}(\text{cr})$, $\text{Cs}_2\text{O}(\text{cr})$ are taken from Robie and Hemingway [1995ROB/HEM], as well as those for $\text{NaOH}(\text{cr})$ and $\text{KOH}(\text{cr})$.

3.10.3. Halogen Compounds

The functions of formation of $\text{NaF}(\text{cr})$ are available in Guillaumont *et al.* [2003GUI/FAN]. The solubility of halite (NaCl) and $\text{CsCl}(\text{cr})$ are calculated from the functions of formation from Guillaumont *et al.* [2003GUI/FAN]. The solubility of sylvite (KCl) is obtained from Wagman *et al.* [1982WAG/EVA]. The functions of formation of $\text{CsBr}(\text{cr})$ are available in Guillaumont *et al.* [2003GUI/FAN].

3.10.4. Sulphur Compounds

$\text{Na}_2\text{S}(\text{cr})$ is taken from Pankratz *et al.* [1987PAN/MAH], and $\text{Na}_2\text{S}_2(\text{cr})$ from Wagman *et al.* [1982WAG/EVA].

Thenardite (Na_2SO_4) and mirabilite $\text{Na}_2\text{SO}_4 \cdot 10\text{H}_2\text{O}(\text{cr})$ are available in Wagman *et al.* [1982WAG/EVA]. Arcanite (K_2SO_4) and langbeinite ($\text{K}_2\text{Mg}_2(\text{SO}_4)_3$) are available in Robie and Hemingway [1995ROB/HEM].

Mirabilite and aphthitalite ($\text{NaK}_3(\text{SO}_4)_2$) are also treated in the Pitzer model, in Harvie *et al.* [1984HAR/MØL]

3.10.5. Group 15

The solubility of $\text{NaNO}_3(\text{cr})$ and $\text{KNO}_3(\text{cr})$ are so important that it needs the use of the Pitzer model. They are then not included in PRODATA.

3.10.6. Carbon Compounds

$(\text{Na}_2\text{CO}_3)(\text{NaHCO}_3)_3$ can be taken from Robie and Hemingway [1995ROB/HEM].

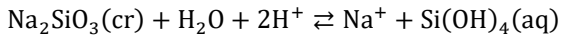
$\text{Na}_2\text{CO}_3(\text{cr})$, Natron ($\text{Na}_2\text{CO}_3 \cdot 10\text{H}_2\text{O}$), $\text{Na}_2\text{CO}_3 \cdot 7\text{H}_2\text{O}(\text{cr})$, Thermonatrite ($\text{Na}_2\text{CO}_3 \cdot \text{H}_2\text{O}$), and Nahcolite (NaHCO_3) are available from Wagman *et al.* [1982WAG/EVA].

Trona ($(\text{Na}_2\text{CO}_3)(\text{NaHCO}_3) \cdot 2\text{H}_2\text{O}$) and $\text{K}_2\text{CO}_3 \cdot 1.5\text{H}_2\text{O}(\text{s})$ are taken from Harvie *et al.* [1984HAR/MØL].

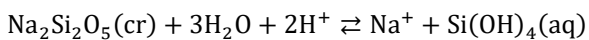
Eitelite ($\text{NaMg}_{0.5}\text{CO}_3$) is taken from Königsberger *et al.* [1992KÖN/SCH].

3.10.7. Silicate Compounds

Functions of reaction for



and,



which are available from Wagman *et al.* [1982WAG/EVA], are used to calculate the solubility and functions of formation of these phases.

3.10.8. Estimation of Specific Interaction Theory for Cs⁺

The correlation between $\varepsilon(M^+, Cl^-)$ and $\varepsilon(M^{2+}, ClO_4^-)$ have been shown — *e.g.* Figure IX.7 in Grenthe *et al.* [1997GRE/PLY] —, as well as the ε vs. $1/IR$ relationships. As the $\varepsilon(Cs^+, Cl^-)$ value is missing in Guillaumont *et al.* [2003GUI/FAN], the $1/IR = f(\varepsilon)$ can be obtained to estimate the missing values — plotted as a typical $\varepsilon = f(1/IR)$ in Figure 3.10-1 —, from which the value of $\varepsilon(Cs^+, Cl^-) = -(0.03 \pm 0.02) \text{ kg}_w \text{ mol}^{-1}$ is obtained. Spahiu [2002SPA] proposed the $\varepsilon(Cs^+, Cl^-) = -(0.05 \pm 0.02) \text{ kg}_w \text{ mol}^{-1}$, which is in agreement with this value.

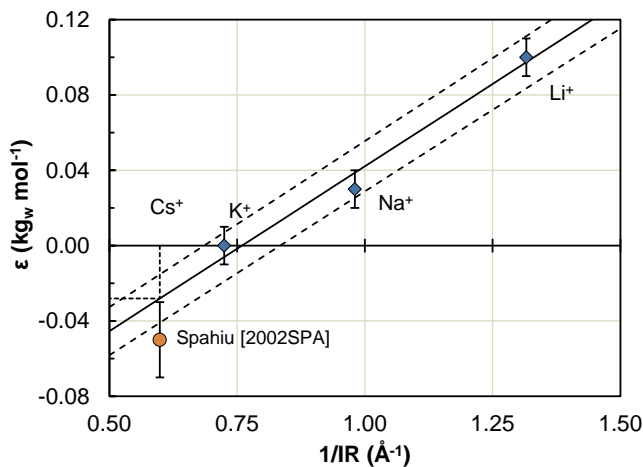


Figure 3.10-1. Dependence of $\varepsilon(M^+, Cl^-)$ for the alkaline metals from Guillaumont *et al.* [2003GUI/FAN] (diamonds) with the $1/IR$ value from Shannon [1976SHA]: linear regression (plain line) is calculated as $1/IR = f(\varepsilon)$ even plotted otherwise in a typical manner; the dashed lines represent the 95% confidence interval; the short dotted line represent the $\varepsilon(Cs^+, Cl^-)$ value; the value estimated in Spahiu [2002SPA] is shown as a circle.

3.11. Aluminosilicate Compounds

The aluminosilicate are treated separately, as they are the basis of clay minerals. The thermodynamic description of clays is not straightforward. Nevertheless, as for oxides, they will bear surface sites, the amount of which can be submitted to the solubility equilibrium of the phases. They also participate to the buffering capacity of a soil or a geologic medium. It is then important to include them as much as possible.

3.11.1. Ortho and Ring Structure, and Chain and Band Structure Silicate Minerals

The function of reaction of zoisite ($Ca_2Al_3Si_3O_{12}(OH)$) and jadeite ($NaAlSi_2O_6$) are taken from Robie and Hemingway [1995ROB/HEM].

3.11.2. Framework Structure Silicate Minerals

Nephelite ($NaAlSiO_4$), analcime ($NaAlSi_2O_6 \cdot H_2O$), dehydrated analcime ($NaAlSi_2O_6$), kaliophilite ($KAlSiO_4$), albite and analbite ($NaAlSi_3O_8$), and sanidine and microcline ($KAlSi_3O_8$) are calculated from Robie and Hemingway [1995ROB/HEM]. The solubility for albite and microcline from LLNL database are included as is after ORANO Mining demand. These latter phases will be eventually cancelled after testing the phases from Robie and Hemingway [1995ROB/HEM].

3.11.3. Sheet Structure Silicate Minerals

This family of mineral includes a lot of important clay minerals that participate strongly in adsorption phenomena.

Functions of reaction of kaolinite and dickite ($\text{Al}_2\text{Si}_2\text{O}_5(\text{OH})_4$) can be calculated from Robie and Hemingway [1995ROB/HEM].

The functions of reaction for ordered and disordered muscovite ($\text{KAl}_3\text{Si}_3\text{O}_{10}(\text{OH})_2$) can be calculated from Robie and Hemingway [1995ROB/HEM]. Within the PHREEQC database from LLNL, a value of $\log_{10} K_s$ — with a temperature analytic dependence — can be found. This value is incorporated within PRODATA, but is not exported by default.

The beidellite family are present in the PHREEQC database from LLNL: beidellite-H ($\text{H}_{0.33}\text{Al}_{2.33}\text{Si}_{3.67}\text{O}_{10}(\text{OH})_2$), beidellite-Ca ($\text{Ca}_{0.165}\text{Al}_{2.33}\text{Si}_{3.67}\text{O}_{10}(\text{OH})_2$), beidellite-Mg ($\text{Mg}_{0.165}\text{Al}_{2.33}\text{Si}_{3.67}\text{O}_{10}(\text{OH})_2$), beidellite-Na ($\text{Na}_{0.33}\text{Al}_{2.33}\text{Si}_{3.67}\text{O}_{10}(\text{OH})_2$), beidellite-K ($\text{K}_{0.33}\text{Al}_{2.33}\text{Si}_{3.67}\text{O}_{10}(\text{OH})_2$), and beidellite-Cs ($\text{Cs}_{0.33}\text{Al}_{2.33}\text{Si}_{3.67}\text{O}_{10}(\text{OH})_2$). The solubility constants are included as is in PRODATA with thermodynamic functions. Conversely, the thermodynamic functions for beidellite_SBld-1 ($\text{Ca}_{0.185}\text{K}_{0.104}\text{Si}_{3.574}\text{Al}_{2.238}\text{Mg}_{0.090}\text{Fe}_{0.112}\text{O}_{10}(\text{OH})_2$), and beidellite_SBld-1:4.5H2O ($\text{Ca}_{0.185}\text{K}_{0.104}\text{Si}_{3.574}\text{Al}_{2.238}\text{Mg}_{0.090}\text{Fe}_{0.112}\text{O}_{10}(\text{OH})_2 \cdot 4.576\text{H}_2\text{O}$) from Gailhanou *et al.* [2012GAI/BLA] are recalculated accounting for the differences between the functions of formation for Al^{3+} and Fe^{3+} in NEA-OECD and the ones chosen in Gailhanou *et al.* [2012GAI/BLA] and Blanc *et al.* [2015bBLA/VIE].

The solubility at 25°C of illite ($\text{K}_{0.6}\text{Mg}_{0.25}\text{Al}_{2.3}\text{Si}_{3.5}\text{O}_{10}(\text{OH})_2$), given in the database from Geochemist's WorkBench, is added as is in PRODATA on demand from ORANO-Mining. No functions of formation are recalculated for the sake of traceability. Conversely the functions of formation for illite_IMt-2 ($(\text{Na}_{0.044}\text{K}_{0.762})(\text{Si}_{3.387}\text{Al}_{0.613})(\text{Al}_{1.427}\text{Fe}_{0.292}\text{Fe}_{0.084}\text{Mg}_{0.241})\text{O}_{10}(\text{OH})_2$) from Gailhanou *et al.* [2012GAI/BLA] are recalculated as for the beidellite from the same authors.

The functions of reaction for ordered and disordered phlogopite ($\text{KAlMg}_3\text{Si}_3\text{O}_{10}(\text{OH})_2$) are calculated from Robie and Hemingway [1995ROB/HEM].

The solubility for the montmorillonite family in LLNL PHREEQC database are added as is: montmorillonite-Mg ($\text{Mg}_{0.495}\text{Al}_{1.67}\text{Si}_4\text{O}_{10}(\text{OH})_2$), montmorillonite-Ca ($\text{Ca}_{0.165}\text{Mg}_{0.33}\text{Al}_{1.67}\text{Si}_4\text{O}_{10}(\text{OH})_2$), montmorillonite-Na ($\text{Na}_{0.33}\text{Mg}_{0.33}\text{Al}_{1.67}\text{Si}_4\text{O}_{10}(\text{OH})_2$), and montmorillonite-K ($\text{K}_{0.33}\text{Mg}_{0.33}\text{Al}_{1.67}\text{Si}_4\text{O}_{10}(\text{OH})_2$).

The functions of formation of nontronite family are recalculated accounting for the differences between the functions of formation for Al^{3+} and Fe^{3+} in NEA-OECD and the ones chosen in Blanc *et al.* [2015bBLA/VIE], nontronite-Mg ($\text{Mg}_{0.17}\text{Fe}_{1.67}\text{Al}_{0.67}\text{Si}_{3.66}\text{O}_{10}(\text{OH})_2$), nontronite-Ca ($\text{Ca}_{0.17}\text{Fe}_{1.67}\text{Al}_{0.67}\text{Si}_{3.66}\text{O}_{10}(\text{OH})_2$), nontronite-Na ($\text{Na}_{0.34}\text{Fe}_{1.67}\text{Al}_{0.67}\text{Si}_{3.66}\text{O}_{10}(\text{OH})_2$), nontronite-K ($\text{K}_{0.34}\text{Fe}_{1.67}\text{Al}_{0.67}\text{Si}_{3.66}\text{O}_{10}(\text{OH})_2$).

The functions of formation of the smectite from Gailhanou *et al.* [2012GAI/BLA] and Gailhanou *et al.* [2017GAI/VIE] are recalculated accounting for the differences between the functions of formation for Al^{3+} and Fe^{3+} in NEA-OECD and the ones chosen by the authors: Na-smectite-MX80 ($\text{Na}_{0.409}\text{K}_{0.024}\text{Ca}_{0.009}(\text{Si}_{3.738}\text{Al}_{0.262})(\text{Al}_{1.598}\text{Mg}_{0.214}\text{Fe}_{0.173}\text{Fe}_{0.035})\text{O}_{10}(\text{OH})_2$), Na-smectite-MX80-3.25H2O ($\text{Na}_{0.409}\text{K}_{0.024}\text{Ca}_{0.009}(\text{Si}_{3.738}\text{Al}_{0.262})(\text{Al}_{1.598}\text{Mg}_{0.214}\text{Fe}_{0.173}\text{Fe}_{0.035})\text{O}_{10}(\text{OH})_2 \cdot 3.25\text{H}_2\text{O}$), Na-smectite-MX80-4H2O

$(Na_{0.409}K_{0.024}Ca_{0.009}(Si_{3.738}Al_{0.262})(Al_{1.598}Mg_{0.214}Fe_{0.173}Fe_{0.035})O_{10}(OH)_2 \cdot 3.989H_2O)$, Na-smectite-MX80-5H2O
 $(Na_{0.409}K_{0.024}Ca_{0.009}(Si_{3.738}Al_{0.262})(Al_{1.598}Mg_{0.214}Fe_{0.173}Fe_{0.035})O_{10}(OH)_2 \cdot 5.189H_2O)$.

Finally the vermiculite family from Blanc *et al.* [2015aBLA/VIE] is also modified accounting for the differences between the functions of formation for Al³⁺ and Fe³⁺ in NEA-OECD and the ones chosen by the authors: vermiculite-Mg ($Mg_{0.43}Mg_{3.00}Si_{3.14}Al_{0.86}O_{10}(OH)_2$), vermiculite-Ca ($Ca_{0.43}Mg_{3.00}Si_{3.14}Al_{0.86}O_{10}(OH)_2$), vermiculite-Na ($Na_{0.86}Mg_{3.00}Si_{3.14}Al_{0.86}O_{10}(OH)_2$), vermiculite-K ($K_{0.86}Mg_{3.00}Si_{3.14}Al_{0.86}O_{10}(OH)_2$).

3.12. Rationale on the Choice of Data

At this point of the development of the PRODATA database, a large part of the included and selected data can be traced to either original publication or selection. It must be reminded that this project is not a complete reappraisal of available thermodynamic data. As noted elsewhere [2019HUM/FIL], some thermodynamic constants or functions of formation are difficult to trace further, particularly in the case of *e.g.* National Bureau of Standard [1982WAG/EVA]. Nevertheless, some data have been included and are still not traced and are still needing further effort.

This database is strongly linked to the selections of commissioned reviews from the NEA-OECD [1992GRE/FUG; 2003GUI/FAN; 2005BRO/CUR; 2005GAM/BUG; 2005OLI/NOL; 2009RAN/FUG; 2013LEM/BER; 2020GRE/GAO; 2020LEM/PAL]. Some other reviews are currently on-going that will be included when available, *e.g.* ancillary data and molybdenum. A continuous effort in maintaining the database is foreseen in the next future. A reflexion on the applicability to other domains of mining activities of ORANO Mining is also on-going.

4. Speciation

4.1. General Conditions

Examples of speciation calculations using PRODATA are presented in this section. The initial solution contains the 38 elements at 10^{-4} mol kg_w⁻¹ in a hypothetical 0.1 mol kg_w⁻¹ indifferent electrolyte Cation⁺ (22.9898 g mol⁻¹)-Anion⁻ (99.4506 g mol⁻¹). The initial pH = 2 is equilibrated by the Anion⁻, and pH values are increased by the base CationOH. All the possible phases are allowed to precipitate, meaning that the phase(s) with the higher saturation index(indices) relative to the stoichiometry of the phase will be precipitated — see Figure 4.1-1 for the ionic strength variation at P(O₂) = 0.21 atm. In order to accelerate the calculation, the ionic strength correction is done using the Davies [1962DAV] equation. Pourbaix diagrams — *i.e.*, E_h vs. pH, pe vs. pH, or log₁₀ fO₂(g) vs. pH predominance diagrams — are first calculated with PHREEPLOT using the PHREEQC database export file for the Davies equation. Then speciation diagram — *i.e.* percentage of species vs. pH — at P(O₂) = 0.21 atm and P(H₂) = 1 atm are presented.

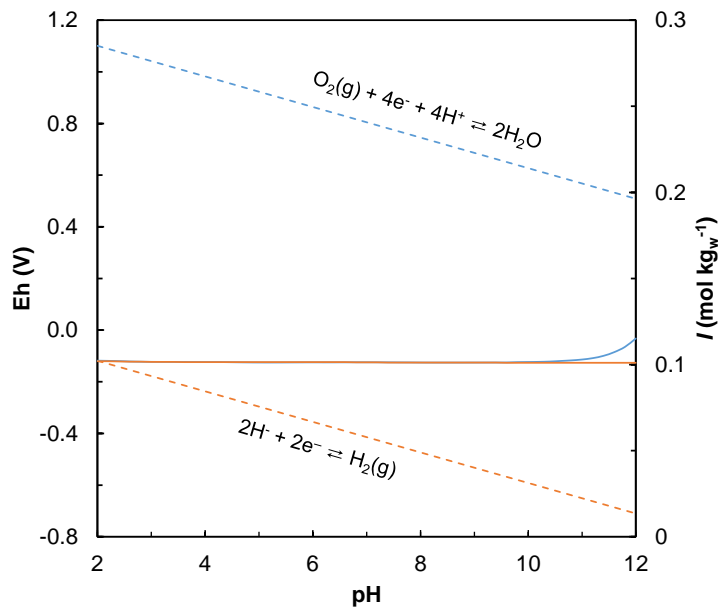


Figure 4.1-1. Potential (dashed lines) and ionic strength (plain lines) evolution during speciation at P(O₂) = 0.21 atm (blue lines) and P(H₂) = 1 atm (orange lines) in a solution containing all elements included in PRODATA at 10⁻⁴ mol kg_w⁻¹; the ionic strength is maintained at 0.1 mol kg_w⁻¹ by a solution containing a hypothetical indifferent Cation/Anion electrolyte; all possible phases are allowed to precipitate; the Davies extraction of the database is used.

4.2. Pourbaix Diagrams

The Pourbaix diagrams can be calculated either using PHREEPLOT, CHESS 3.0, or GWB.

Phreeplot is using two strategies that are described in Kinniburgh and Cooper [2004KIN/COO] and Kinniburgh and Cooper [2011KIN/COO]: the hunt and track approach, which is looking for change in the dominant species or phase along domain boundaries — see Kinniburgh and Cooper [2004KIN/COO] for further details —, and the grid method, which calculate the speciation at each point of a matrix of n points defined by the keyword resolution. The hunt and track method is faster but has the drawback of ignoring potential islands of stability that the grid

method do not ignore. Kinniburgh and Cooper [2011KIN/COO] recommend to use hunt and track in comparison to the grid method. The boundaries of the stability domains are defined as the equality of concentrations. Another algorithm named `minstab` allows to define the stability domain of phases, *i.e.* the domain where the phase precipitates whether the phase is major or not.

4.2.1. Complete Database

4.2.1.1. Halogens

The Pourbaix diagrams of the halogens — F, Cl, Br, and I — are presented in Figure 4.2-1. For fluorine (Figure 4.2-1a), the speciation of the dominant species does not depend on the redox potential of the medium, and consists of F^- and its complexes, mainly linked to non-redox active Al and Th. For chlorine (Figure 4.2-1b), the speciation is mainly linked to the redox chemistry of Hg. The speciation of bromine (Figure 4.2-1c) is dominated by Br^- and the redox chemistry of Ag. The speciation of iodine (Figure 4.2-1d) is distributed between the I(-I), I(0), and I(III) redox state, and the redox chemistry of Ag.

4.2.1.2. Non-metals

The Pourbaix diagrams of the non-metals are plotted in Figure 4.2-2. They are calculated using the hunt and track approach, except for As, which is failing and is calculated using the grid approach. The chemistry of sulphur (Figure 4.2-2a) is mainly dominated by S(-II) and S(VI) phases, and mainly linked to Co(II), Ba(II), and Ra(II). The chemistry of selenium (Figure 4.2-2b) is fixed by Se(-II) phases, Se(V), and Se(VI), and is mainly linked to Pb(II), Cd(II), and Hg(II). The speciation of N (Figure 4.2-2c) — excluding N(0) — is fixed by N(-III) and N(V). The speciation of phosphor (Figure 4.2-2d) is exclusively the one of P(V), and is mainly linked to Cl(-I), Pb(II), Mn(II), and Zr(IV). The chemistry of arsenic (Figure 4.2-2e) is fixed by As(-II), As(0), As(III), and As(V), and is mainly linked to Ni(II), Co(II), Fe(III), U(VI), and Ba(II). The chemistry of carbon (Figure 4.2-2f) is fixed by C(-IV) and C(IV), and is mainly linked to Cd(II).

4.2.1.3. Metalloids

The Pourbaix diagrams of metalloids Si, Pb, and Al are plotted in Figure 4.2-3. The chemistry of silicium (Figure 4.2-3a) is exclusively fixed by Si(IV), and is mainly linked to a Zr(IV)-Ca(II) synthetic phase. The chemistry of lead (Figure 4.2-3b) is fixed by Pb(0), Pb(II), and Pb(IV), and mainly linked to Cl(-I), Se(-II), P(V), and Mo(VI). The chemistry of aluminium (Figure 4.2-3c) is fixed by Al(III), and mainly linked to F(-I) and Mg(II).

4.2.1.4. d-transition metal series

The 13 metals from the d-transition series included in PRODATA are presented in three groups of Figure. The Pourbaix diagrams of Zn, Cd, Hg, Cu, and Ag are plotted in Figure 4.2-4. The chemistry of Zn (Figure 4.2-4a) is fixed by Zn(II), and is mainly linked to As(V), Fe(III), Mn(III), and Ti(IV). The chemistry of cadmium (Figure 4.2-4b) is fixed by Cd(II), and is mainly linked to Se(-II) and C(IV). The chemistry of mercury (Figure 4.2-4c) is fixed by Hg(0) and Hg(II), and mainly linked to Cl(-I), Se(-II) and Se(III). The chemistry of copper (Figure 4.2-4d) is fixed by Cu(0) and Cu(II), and mainly linked to Se(-II), and Fe(II) and Fe(III). The chemistry of silver (Figure 4.2-4e) is fixed by Ag(0) and Ag(I), and mainly linked to Br(-I) and I(-I).

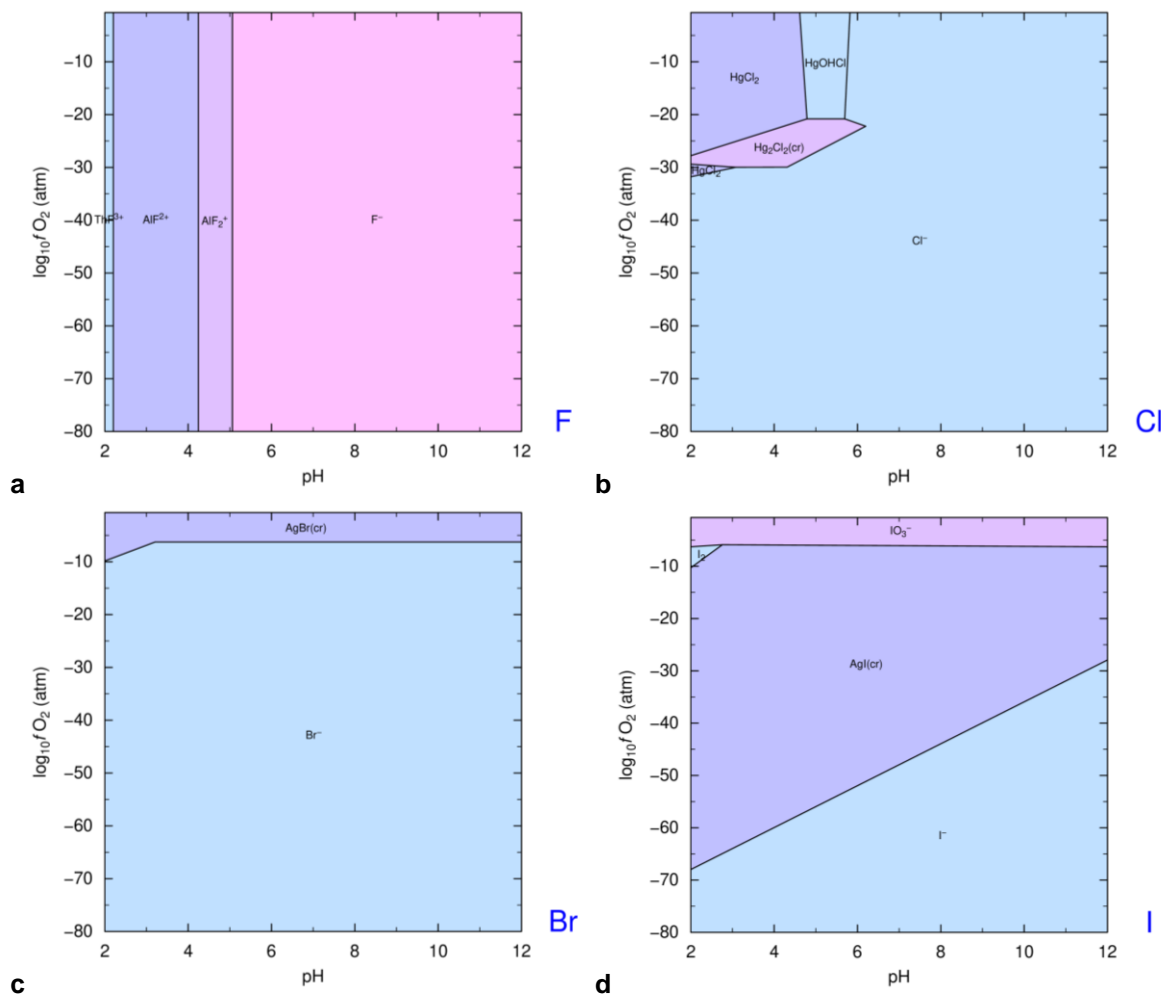


Figure 4.2-1. Pourbaix diagrams (PHREEPLOT) of halogens — F(a), Cl (b), Br (c), and I (d) — in a solution containing all elements included in PRODATA at 10^{-4} mol kg_w⁻¹; the ionic strength is maintained at 0.1 mol kg_w⁻¹ by a solution containing a hypothetical indifferent Cation/Anion electrolyte; all possible phases are allowed to precipitate; the Davies PHREEQC extraction of the database is used.

The Pourbaix diagram of Ni, Co, Fe, and Mn are plotted in Figure 4.2-5. The chemistry of nickel (Figure 4.2-5a) — calculated using the grid method, as the hunt and track method is failing — is fixed by Ni(-II), and linked to As(-II). The chemistry of cobalt (Figure 4.2-5b) is fixed by Co(II) and Co(III), and mainly linked to S(-II). The chemistry of iron (Figure 4.2-5c) is fixed by Fe(II) and Fe(III), and mainly linked to As(III), Zn(II) and Cu(II). The chemistry of Mn (Figure 4.2-5d) is fixed by Mn(II) and Mn(III), and mainly linked to P(V), C(IV), Zn(II), and Ti(IV).

The Pourbaix diagrams of Mo, V, Ti, and Zr are plotted in Figure 4.2-6. The chemistry of molybdenum (Figure 4.2-6a) is fixed by Mo(IV) and Mo(VI), and mainly linked to Pb(II). The chemistry of vanadium (Figure 4.2-6b) is fixed by V(III), V(IV), and V(V), and mainly linked to U(VI) and Sr(II). The chemistry of titanium (Figure 4.2-6c) is fixed by Ti(IV), and mainly linked to Mn(II), Zn(II) and U(IV). The chemistry of zirconium (Figure 4.2-6d) is fixed by Zr(IV) is mainly linked to P, but should be linked to Si(IV) and Ca(II), through the precipitation of $\text{Ca}_2\text{ZrSi}_3\text{O}_{12}(\text{cr})$ — see the Pourbaix diagram of Si in Figure 4.2-3a.

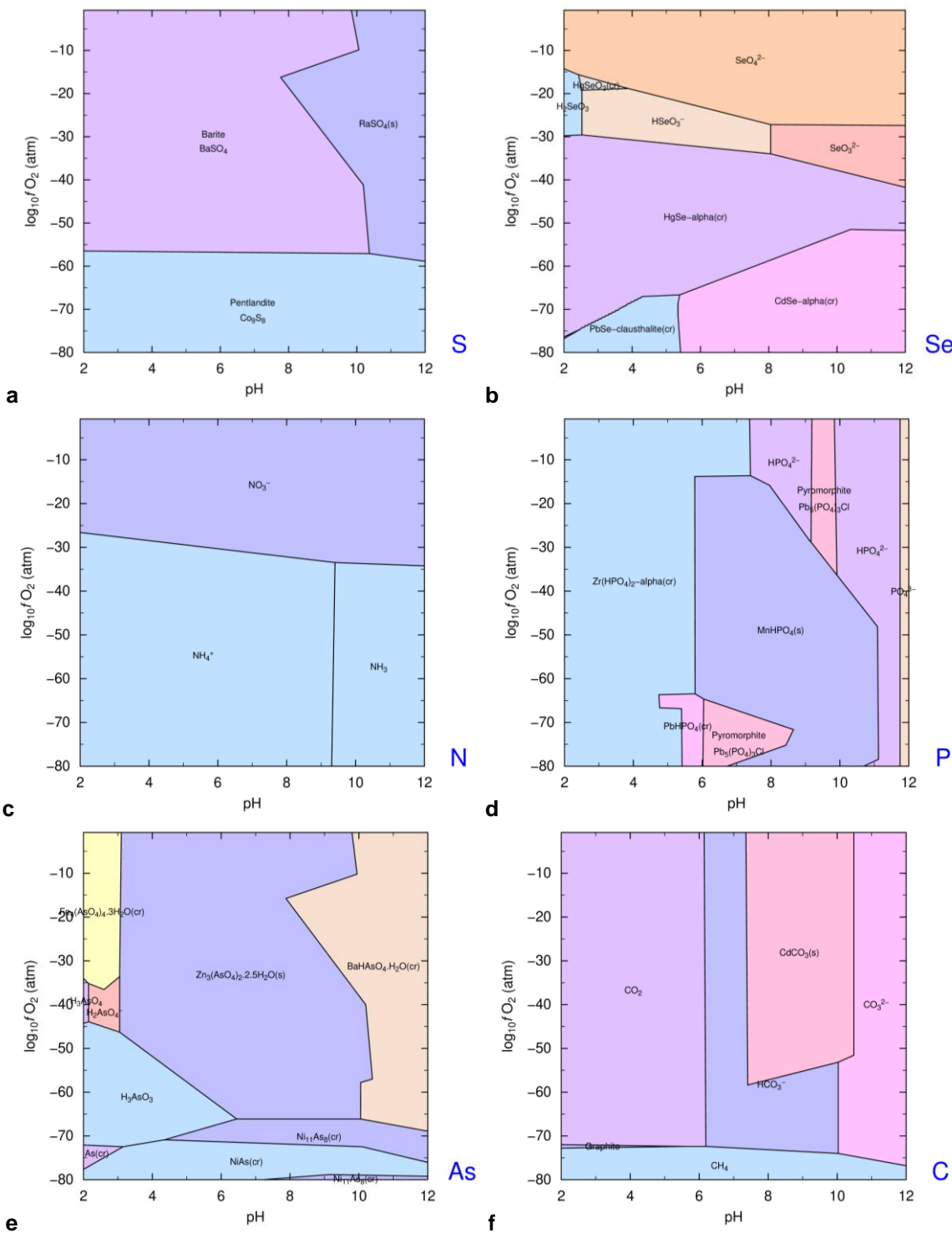


Figure 4.2-2. Pourbaix diagrams (PHREEPLOT) of non-metals — S (a), Se (b), N (c), P (d), As (e), and C (f) — in a solution containing all elements included in PRODATA at 10^{-4} mol kg_w⁻¹; the ionic strength is maintained at 0.1 mol kg_w⁻¹ by a solution containing a hypothetical indifferent Cation/Anion electrolyte; all possible phases are allowed to precipitate; the Davies PHREEQC extraction of the database is used.

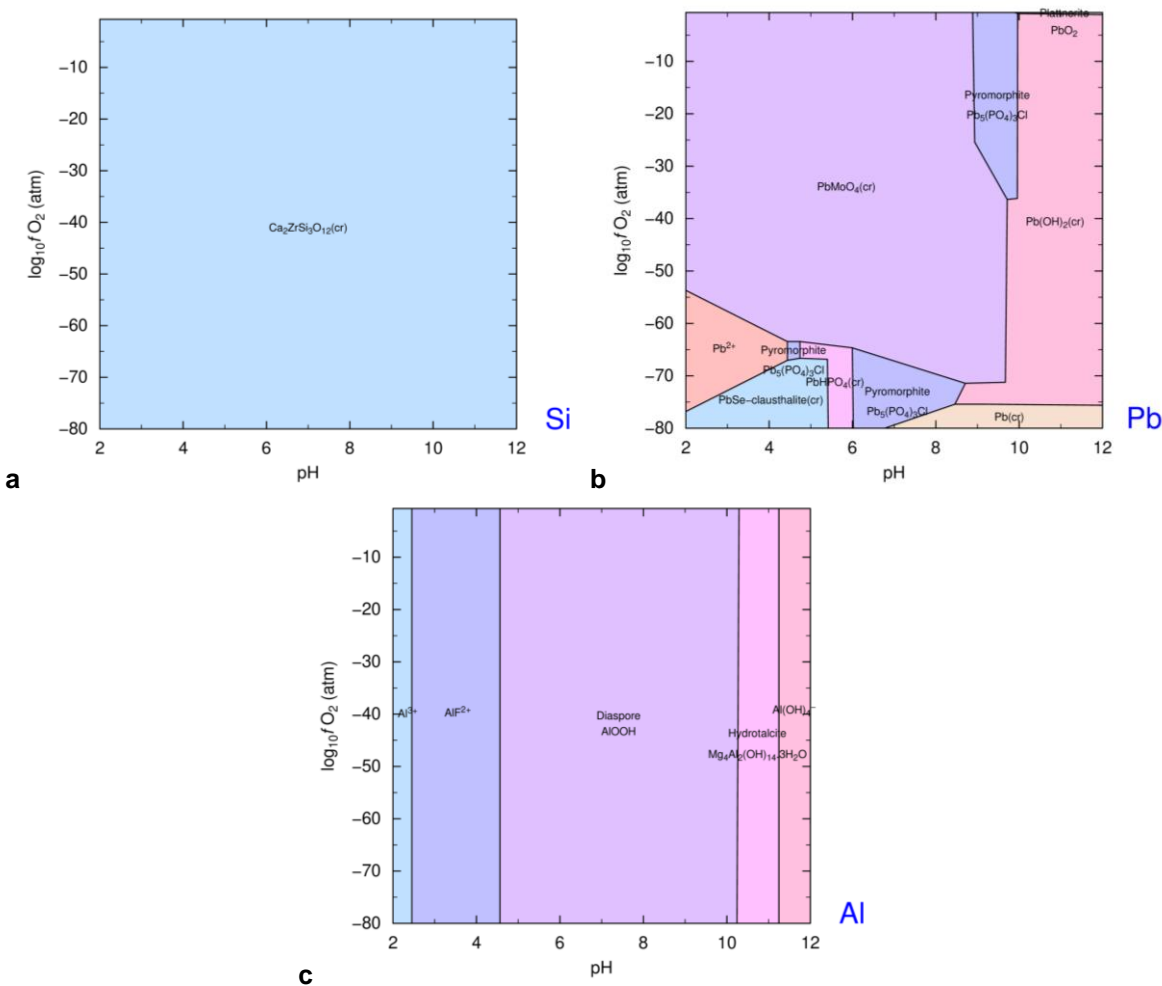


Figure 4.2-3. Pourbaix diagrams (PHREEPLOT) of metalloids — Si (a), Pb (b), and Al (c) — in a solution containing all elements included in PRODATA at $10^{-4} \text{ mol kg}^{-1}$; the ionic strength is maintained at 0.1 mol kg^{-1} by a solution containing a hypothetical indifferent Cation/Anion electrolyte; all possible phases are allowed to precipitate; the Davies PHREEQC extraction of the database is used.

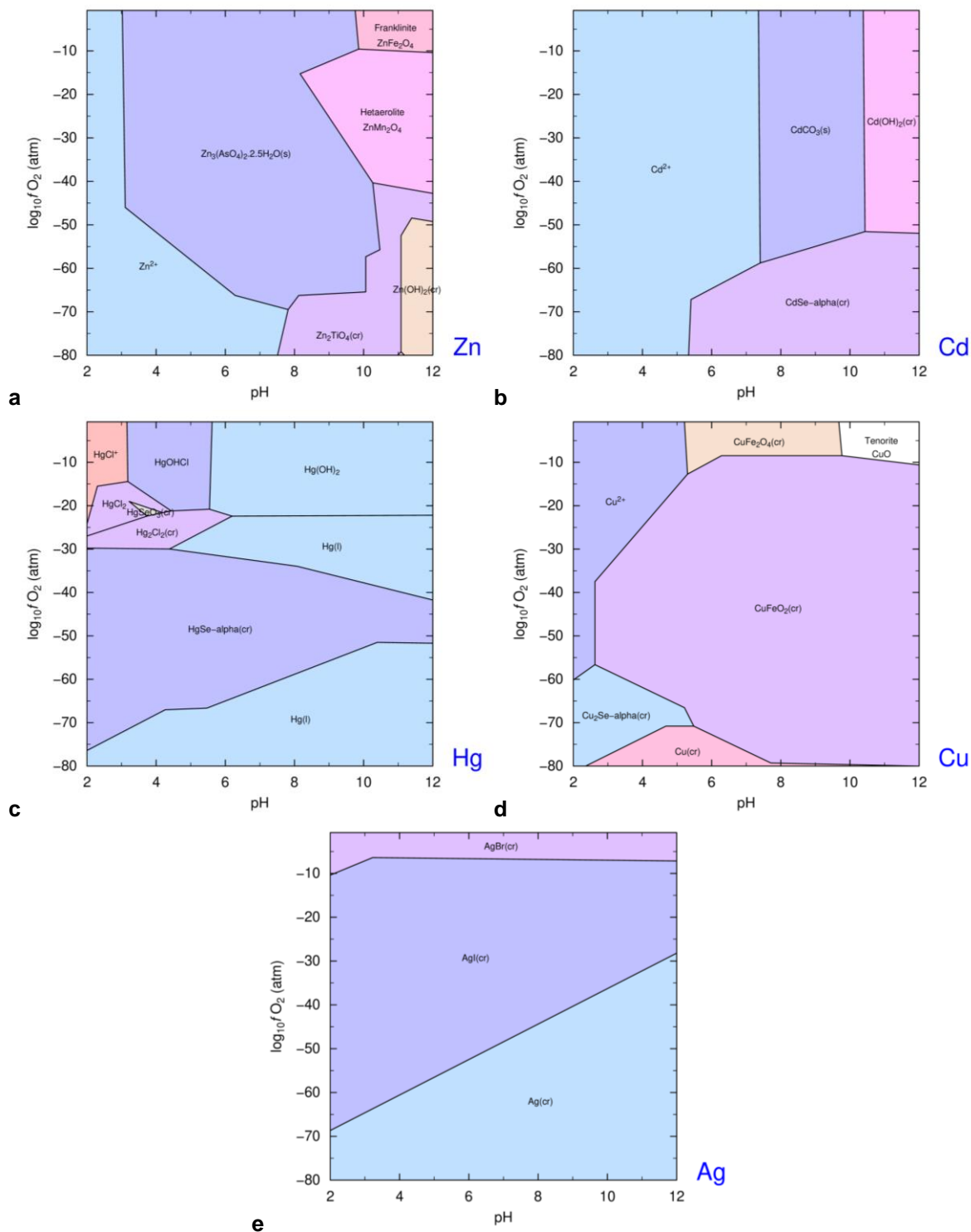


Figure 4.2-4. Pourbaix diagrams (PHREEPLOT) of d-transition metal series — Zn (a), Cd (b), Hg (c), Cu (d), and Ag (e) — in a solution containing all elements included in PRODATA at 10^{-4} mol kg_w⁻¹; the ionic strength is maintained at 0.1 mol kg_w⁻¹ by a solution containing a hypothetical indifferent Cation/Anion electrolyte; all possible phases are allowed to precipitate; the Davies PHREEQC extraction of the database is used.

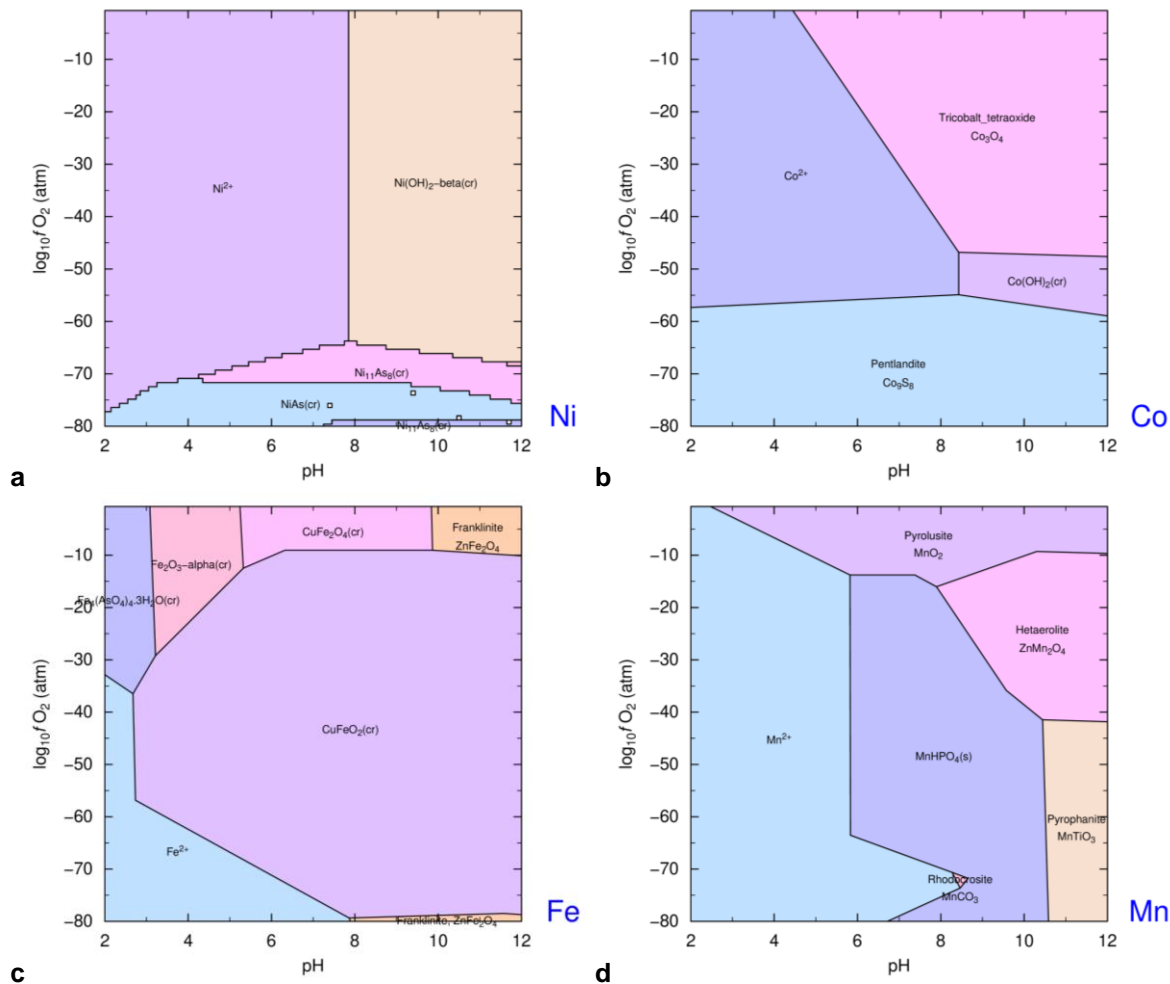


Figure 4.2-5. Pourbaix diagrams (PHREEPLOT) of d-transition metal series — Ni (a), Co (b), Fe (c), and Mn (d) — in a solution containing all elements included in PRODATA at 10^{-4} mol kg $^{-1}$; the ionic strength is maintained at 0.1 mol kg $^{-1}$ by a solution containing a hypothetical indifferent Cation/Anion electrolyte; all possible phases are allowed to precipitate; the Davies PHREEQC extraction of the database is used.

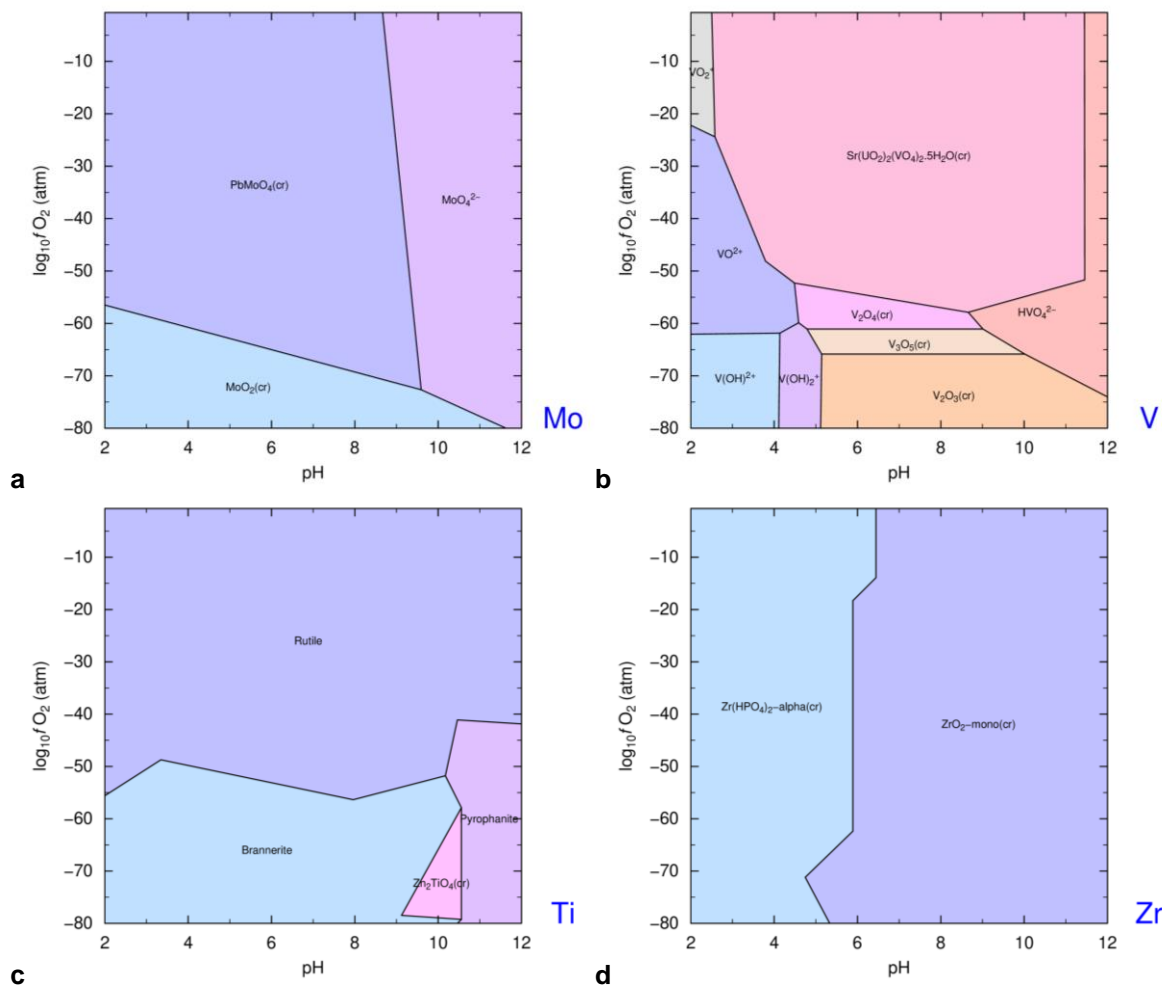


Figure 4.2-6. Pourbaix diagrams (PHREEPLOT) of d-transition metal series — Mo (a), V (b), Ti (c), and Zr (d) — in a solution containing all elements included in PRODATA at 10^{-4} mol kg_w⁻¹; the ionic strength is maintained at 0.1 mol kg_w⁻¹ by a solution containing a hypothetical indifferent Cation/Anion electrolyte; all possible phases are allowed to precipitate; the Davies PHREEQC extraction of the database is used.

4.2.1.5. Actinides

The Pourbaix diagrams of actinides U and Th are plotted in Figure 4.2-6. The diagram of uranium (Figure 4.2-6a) is calculated using the grid approach because of the number of failure in the calculation. The chemistry of uranium is fixed by U(IV) and U(VI), and mainly linked to V(V), Ti(IV), and Sr(II). It can be noted that as in the case of Co (Figure 4.2-5b), Co(UO₂)₂(AsO₄)₂·8H₂O(cr) in Figure 4.2-2e is not appearing. The chemistry of Th (Figure 4.2-6b) is fixed by Th(IV), and mainly linked to F.

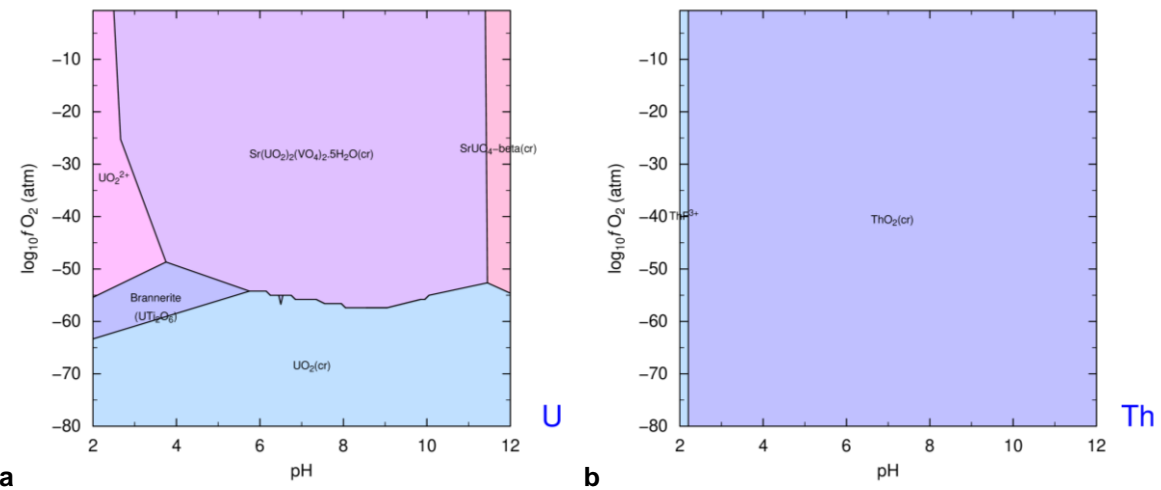


Figure 4.2-7. Pourbaix diagrams (PHREEPLOT) of actinides — U (a), and Th (b) — in a solution containing all elements included in PRODATA at 10^{-4} mol kg_w⁻¹; the ionic strength is maintained at 0.1 mol kg_w⁻¹ by a solution containing a hypothetical indifferent Cation/Anion electrolyte; all possible phases are allowed to precipitate; the Davies PHREEQC extraction of the database is used.

4.2.1.6. Alkaline earth metals

The Pourbaix diagram of alkaline earth metals are plotted in Figure 4.2-8. The chemistry of magnesium (Figure 4.2-8a) is fixed by Mg(II), and mainly linked to Al(III). The chemistry of calcium (Figure 4.2-8b) is fixed by Ca(II), and mainly linked to Si(IV) and Zr(IV) through the precipitation of synthetic $Ca_2ZrSi_3O_{12}(cr)$. The chemistry of strontium (Figure 4.2-8c) is fixed by Sr(II), and mainly linked to V(V) and U(VI). The chemistry of barium (Figure 4.2-8d) is fixed by Ba(II), and mainly linked to S(VI) and As(V). The chemistry of radium (Figure 4.2-8e) is fixed by Ra(II), and mainly linked to S(VI).

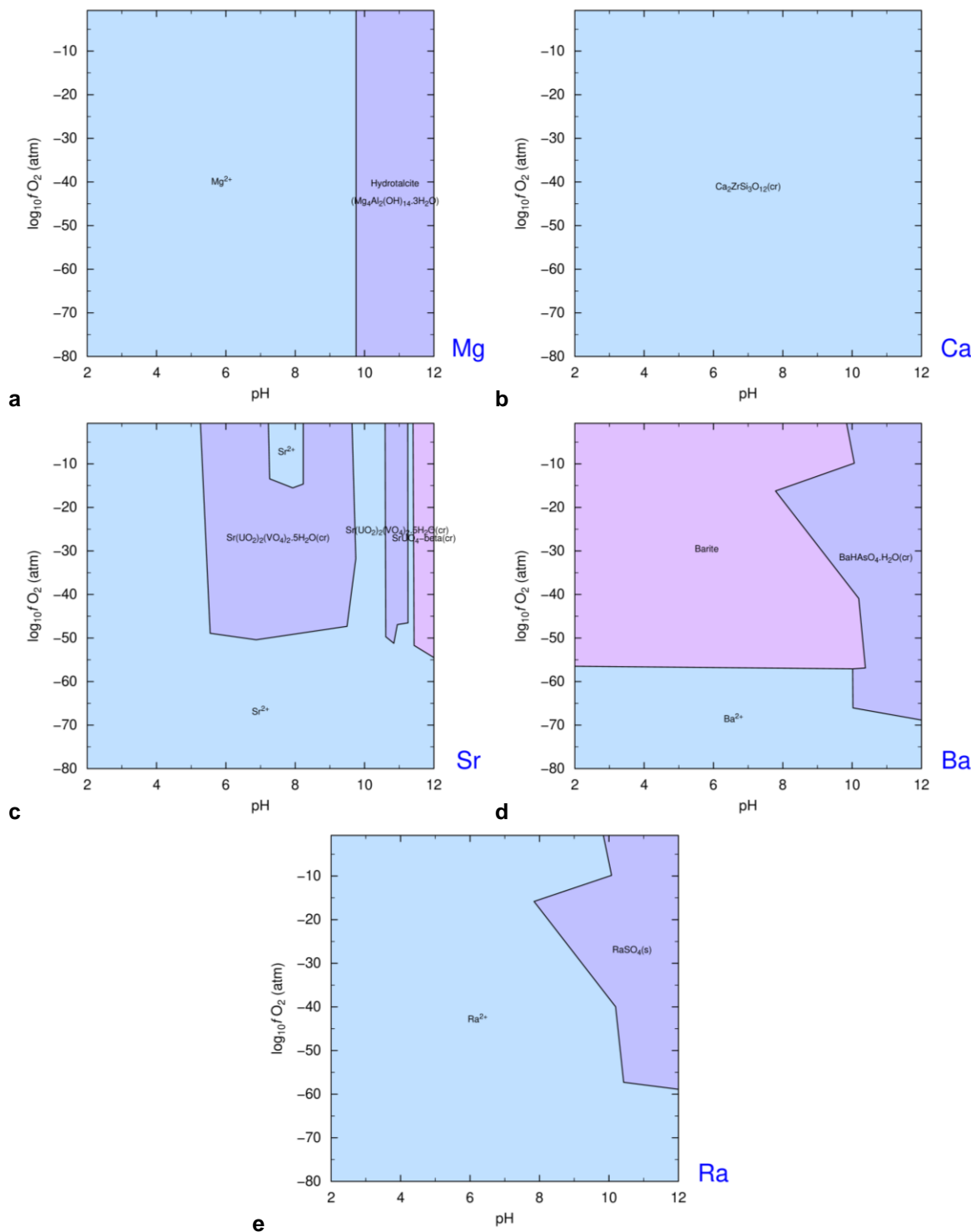


Figure 4.2-8. Pourbaix diagrams (PHREEPLOT) of alkaline earth metals — Mg (a), Ca (b), Sr (c), Ba (d), and Ra (e) — in a solution containing all elements included in PRODATA at 10^{-4} mol kg^w⁻¹; the ionic strength is maintained at 0.1 mol kg^w⁻¹ by a solution containing a hypothetical indifferent Cation/Anion electrolyte; all possible phases are allowed to precipitate; the Davies PHREEQC extraction of the database is used.

4.2.1.7. Alkaline metals

The Pourbaix diagrams of alkaline metals (Figure 4.2-9) are all fixed by M(I), and the chemistry does not seem to be linked to any other elements under these conditions.

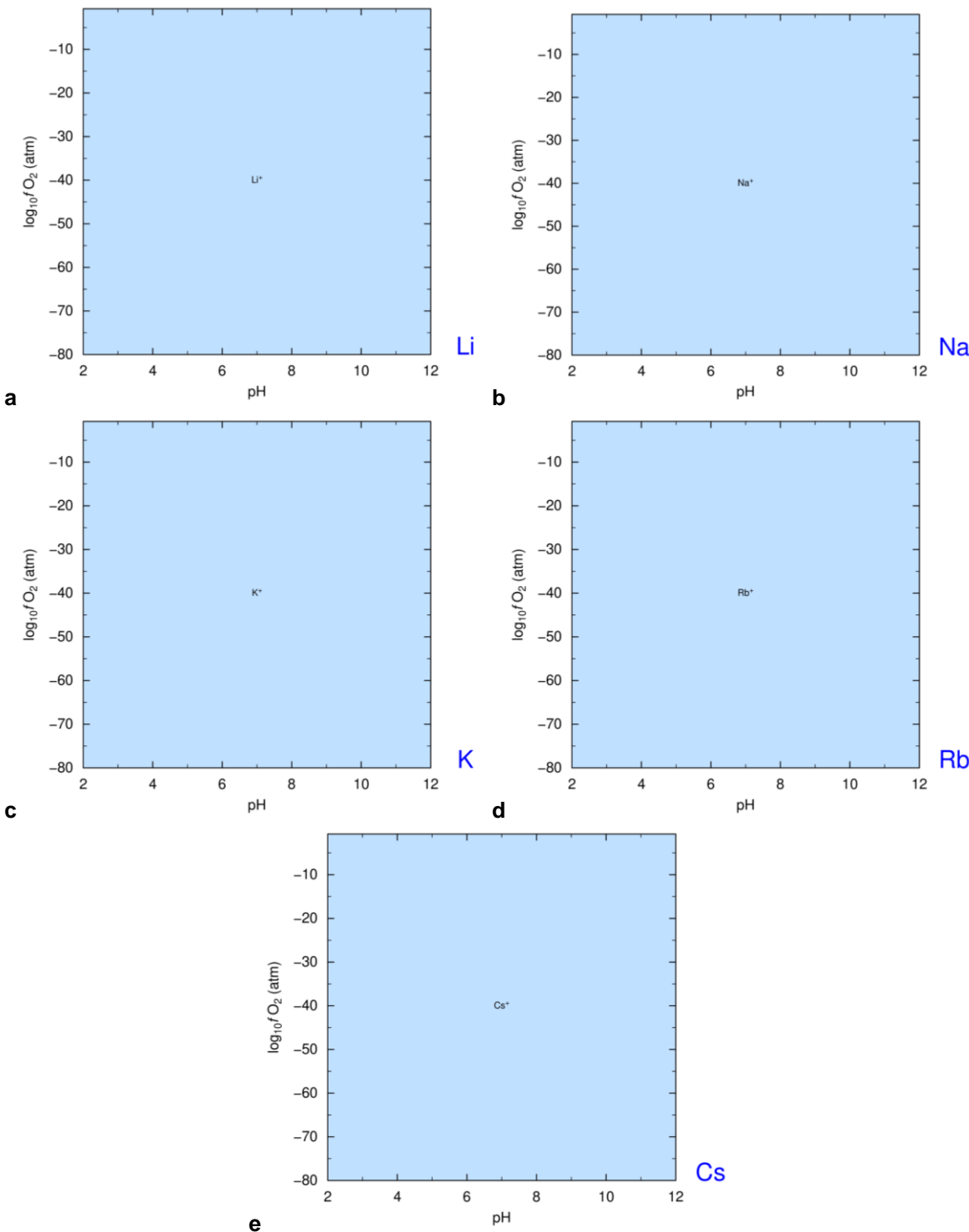


Figure 4.2-9. Pourbaix diagrams (PHREEPLOT) of alkaline metals — Li (a), Na (b), K (c), Rb (d), and Cs (e) — in a solution containing all elements included in PRODATA at 10^{-4} mol kg_w⁻¹; the ionic strength is maintained at 0.1 mol kg_w⁻¹ by a solution containing a hypothetical indifferent Cation/Anion electrolyte; all possible phases are allowed to precipitate; the Davies PHREEQC extraction of the database is used.

4.2.2. Pourbaix Diagrams Excluding $\text{Ca}_2\text{ZrSi}_3\text{O}_{12}(\text{cr})$

The important precipitation of synthetic $\text{Ca}_2\text{ZrSi}_3\text{O}_{12}(\text{cr})$ can be questioned for the chemistry of Si, Zr, and Ca — and linked elements — when the objective of this database is the application to mining operation, which is mainly addressing natural phenomena. Another set of calculation has been performed excluding $\text{Ca}_2\text{ZrSi}_3\text{O}_{12}(\text{cr})$ from the calculation in the Phreeplot input files.

4.2.2.1. Halogens

The Pourbaix diagrams excluding $\text{Ca}_2\text{ZrSi}_3\text{O}_{12}(\text{cr})$ for halogens are plotted in Figure 4.2-10. There are only marginal changes in the Pourbaix diagrams. The boundaries in fluorine diagram (Figure 4.2-10a) are slightly moved to higher pH values; the stability domain of $\text{Hg}_2\text{Cl}_2(\text{cr})$ is slightly increased at the expenses of $\text{HgCl}_2(\text{aq})$ (Figure 4.2-10b); the stability domain of $\text{AgBr}(\text{cr})$ is slightly reduced in acidic pH at the benefit of Br^- (Figure 4.2-10c); the boundaries of iodine species and phases are unchanged (Figure 4.2-10d).

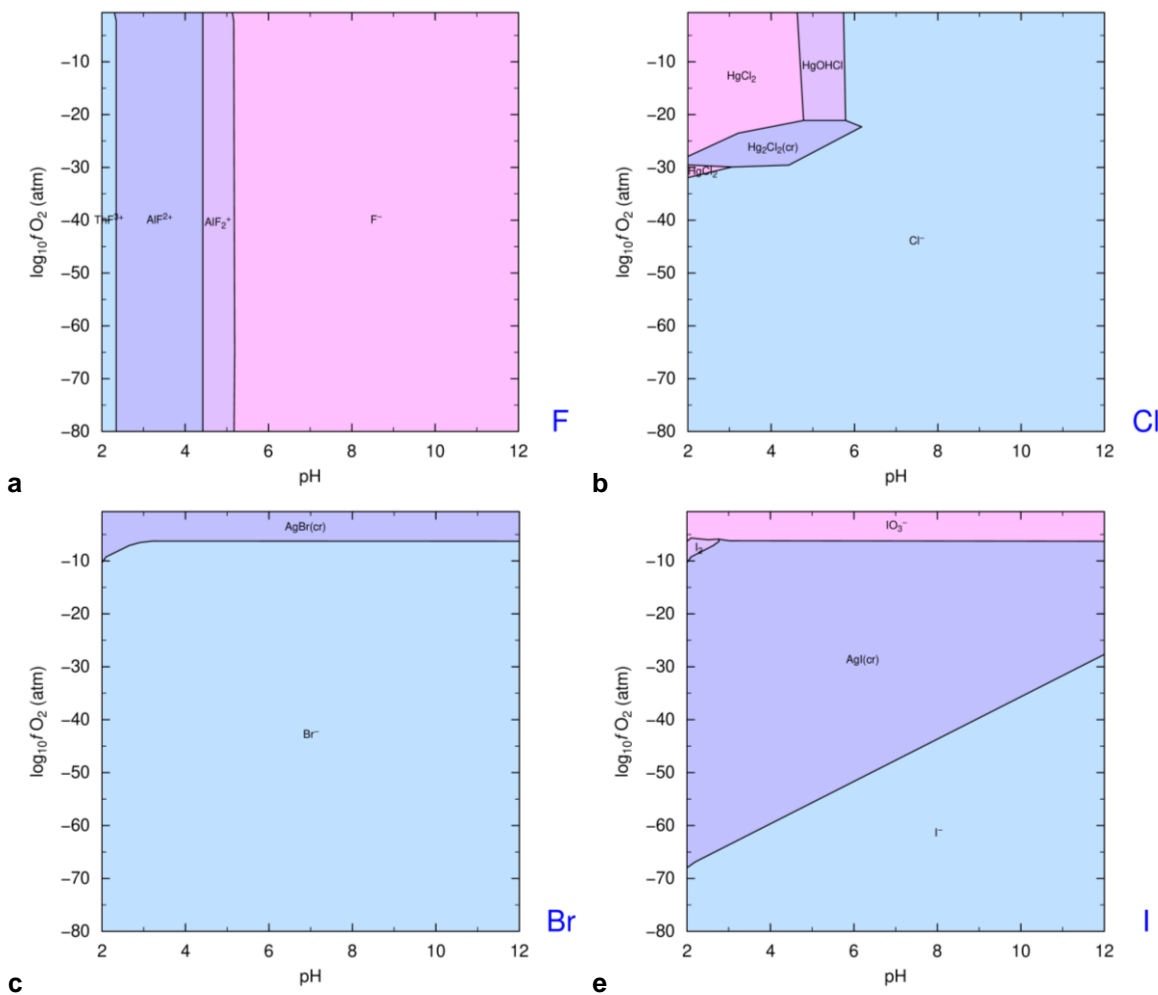


Figure 4.2-10. Pourbaix diagrams (PHREEPLOT) of halogens — F (a), Cl (b), Br (c), and I (d) — in a solution containing all elements included in PRODATA at 10^{-4} mol kg_w⁻¹; the ionic strength is maintained at 0.1 mol kg_w⁻¹ by a solution containing a hypothetical indifferent Cation/Anion electrolyte; all possible phases are allowed to precipitate; the Davies PHREEQC extraction of the database is used, excluding $\text{Ca}_2\text{ZrSi}_3\text{O}_{12}(\text{cr})$ in the input file.

4.2.2.2. Non-metals

The Pourbaix diagrams of non-metals excluding $\text{Ca}_2\text{ZrSi}_3\text{O}_{12}(\text{cr})$ are plotted in Figure 4.2-11. For sulphur (Figure 4.2-11a), the domain of $\text{RaSO}_4(\text{s})$ is increased at the expenses of barite (BaSO_4); for selenium (Figure 4.2-11b) the domain of clausthalite (PbSe) is reduced at the benefit of $\text{HgSe}\text{-alpha}(\text{cr})$, $\text{CdSe}\text{-alpha}(\text{cr})$, and $\text{Cu}_2\text{Se}\text{-alpha}(\text{cr})$ become apparent; the boundaries for nitrogen are mostly unchanged (Figure 4.2-11c); for phosphorus (Figure 4.2-11d), the impeded precipitation of $\text{Ca}_2\text{ZrSi}_3\text{O}_{12}(\text{cr})$ is promoting the precipitation of fluorapatite ($\text{Ca}_5(\text{PO}_4)_3\text{F}$), and the precipitation of $\text{PbHPO}_4(\text{cr})$ occurs at lower pH values; for arsenic (Figure 4.2-11e), the domain of $\text{BaHAsO}_4\text{:H}_2\text{O}(\text{cr})$ is increased at the expenses of $\text{Zn}_3(\text{AsO}_4)_2\text{:2.5H}_2\text{O}(\text{cr})$; for carbon (Figure 4.2-11f), the precipitation of rhodocrocite (MnCO_3) becomes apparent, and other boundaries are unchanged.

4.2.2.3. Metalloids

The Pourbaix diagrams of the metalloids excluding ($\text{Ca}_2\text{ZrSi}_3\text{O}_{12}(\text{cr})$) are plotted in Figure 4.2-12. The Si diagram (Figure 4.2-12a) is modified as $\text{ZrSiO}_4(\text{cr})$ and ordered phlogopite ($\text{KAlMg}_3\text{Si}_3\text{O}_{10}(\text{OH})_2$) are the main phases present; for lead (Figure 4.2-12b), the precipitation of pyromorphite ($\text{Pb}_5(\text{PO}_4)_3\text{Cl}$) is strongly limited at the benefit of $\text{PbMoO}_4(\text{cr})$ in oxidized media, and of $\text{PbHPO}_4(\text{cr})$ in reduced media; for aluminium (Figure 4.2-12c), the precipitation of hydrotalcite ($\text{Mg}_4\text{Al}_2(\text{OH})_{14}\text{:3H}_2\text{O}$) is limited at the benefit of diapore ($\gamma\text{-AlOOH}$); it can be noted that the precipitation of ordered phlogopite ($\text{KAlMg}_3\text{Si}_3\text{O}_{10}(\text{OH})_2$) is not apparent in Figure 4.2-12c but should be nevertheless significant.

4.2.2.4. d-transition metals

As in § 4.2.1.4, the 13 metals from the d-transition series included in PRODATA are presented in three groups of Figure. For zinc (Figure 4.2-13a), the precipitation of willemite (Zn_2SiO_4), takes over the domain of $\text{Zn}(\text{OH})_2(\text{cr})$, and reduces the domain of $\text{Zn}_2\text{TiO}_4(\text{cr})$; for cadmium (Figure 4.2-13b), the modification of selenium induces a modification of the boundaries of $\text{CdSe}\text{-alpha}(\text{cr})$; for mercury (Figure 4.2-13c), only slight modifications of the boundaries could be noticed; for copper (Figure 4.2-13d), the slight increase of the domain of $\text{Cu}_2\text{Se}\text{-alpha}(\text{cr})$ — already noticed for Se in Figure 4.2-11b — at the expenses of $\text{Cu}(\text{cr})$ is the only evident change. There are only limited changes in diagram for Ag (Figure 4.2-13e).

The diagram of nickel (Figure 4.2-14a), cobalt (Figure 4.2-14b), and iron (Figure 4.2-14c) are mostly unchanged; for manganese (Figure 4.2-14d), the impeded formation of $\text{Ca}_2\text{ZrSi}_3\text{O}_{12}(\text{cr})$ allows the precipitation of braunite ($\text{Mn}_7\text{SiO}_{12}$) at the expenses of hetaerolite (ZnMn_2O_4), the increase of the rhodocrocite (MnCO_3) and pyrophanite (MnTiO_3) domains, and the decrease of the domain of $\text{MnHPO}_4(\text{s})$.

For molybdenum (Figure 4.2-15a), the domain of $\text{PbMoO}_4(\text{cr})$ is increased at the expenses of MoO_4^{2-} , and $\text{MoO}_2(\text{cr})$; the diagram of vanadium (Figure 4.2-15b) is mostly unchanged. For titanium (Figure 4.2-15c), the domain of $\text{Zn}_2\text{TiO}_4(\text{cr})$ is decreased at the benefit of pyrophanite (MnTiO_3); for zirconium (Figure 4.2-15d), $\text{ZrSiO}_4(\text{cr})$ is now dominating the Pourbaix diagram at $\text{pH} < 10.5$, where $\text{ZrO}_2\text{-mono}(\text{cr})$ becomes dominant.

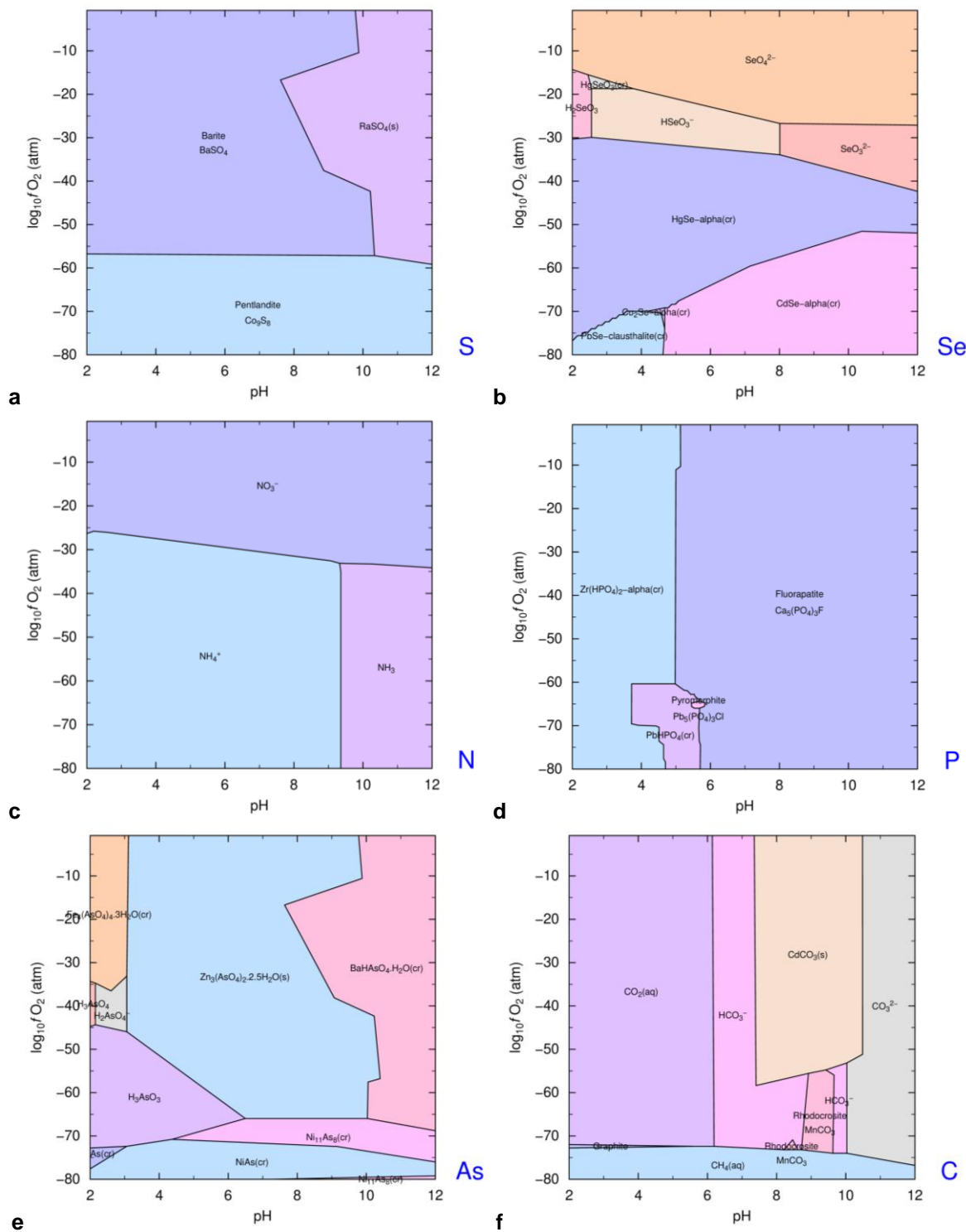


Figure 4.2-11. Pourbaix diagrams (PHREEPLOT) of non-metals — S (a), Se (b), N (c), P (d), As (e), and C (f) — in a solution containing all elements included in PRODATA at 10^{-4} mol kg_w⁻¹; the ionic strength is maintained at 0.1 mol kg_w⁻¹ by a solution containing a hypothetical indifferent Cation/Anion electrolyte; all possible phases are allowed to precipitate; the Davies PHREEQC extraction of the database is used, excluding Ca₂ZrSi₃O₁₂(cr) in the input file.

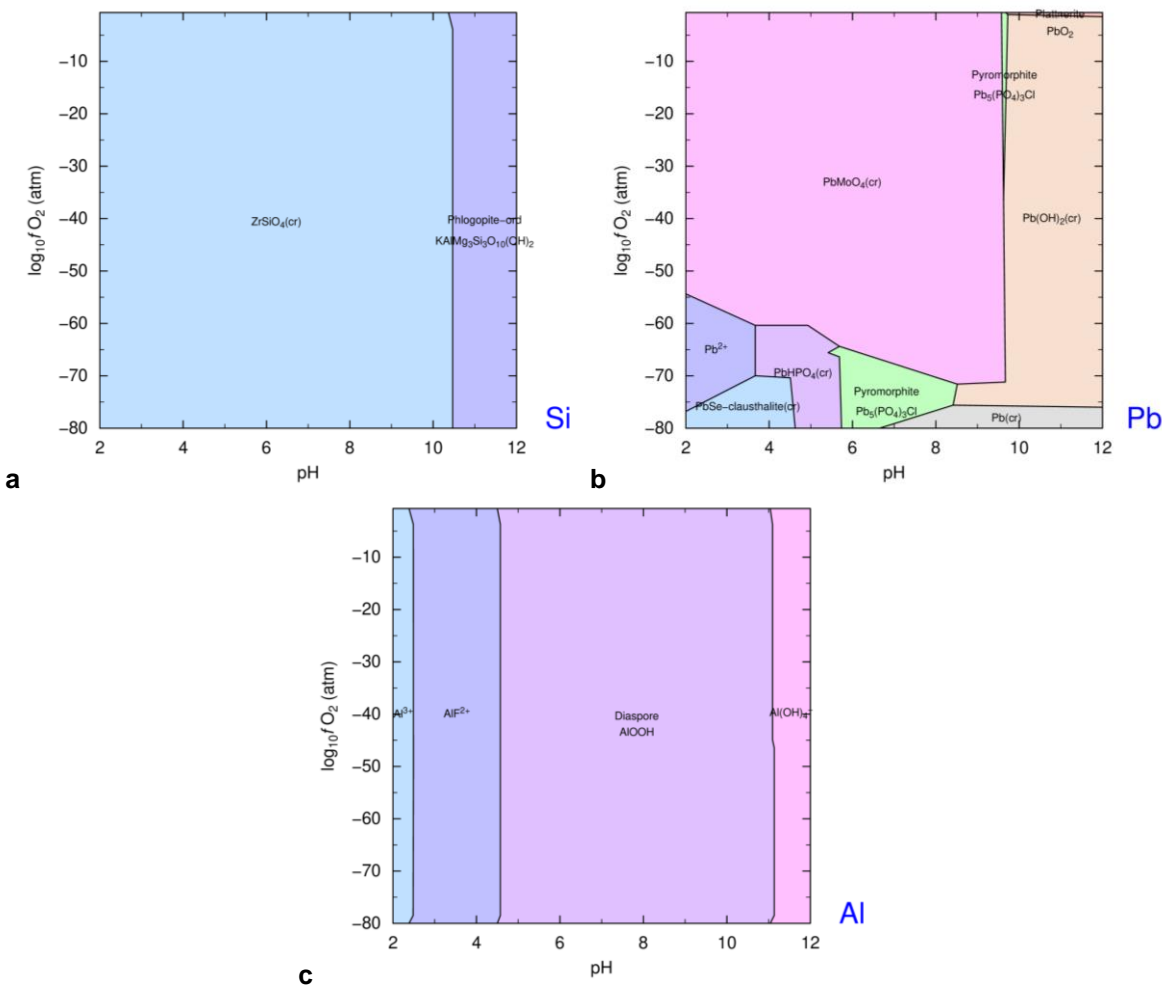


Figure 4.2-12. Pourbaix diagrams (PHREEPLOT) of metalloids — Si (a), Pb (b), and Al (c) — in a solution containing all elements included in PRODATA at 10^{-4} mol kg_w⁻¹; the ionic strength is maintained at 0.1 mol kg_w⁻¹ by a solution containing a hypothetical indifferent Cation/Anion electrolyte; all possible phases are allowed to precipitate; the Davies PHREEQC extraction of the database is used, excluding Ca₂ZrSi₃O₁₂(cr) in the input file.

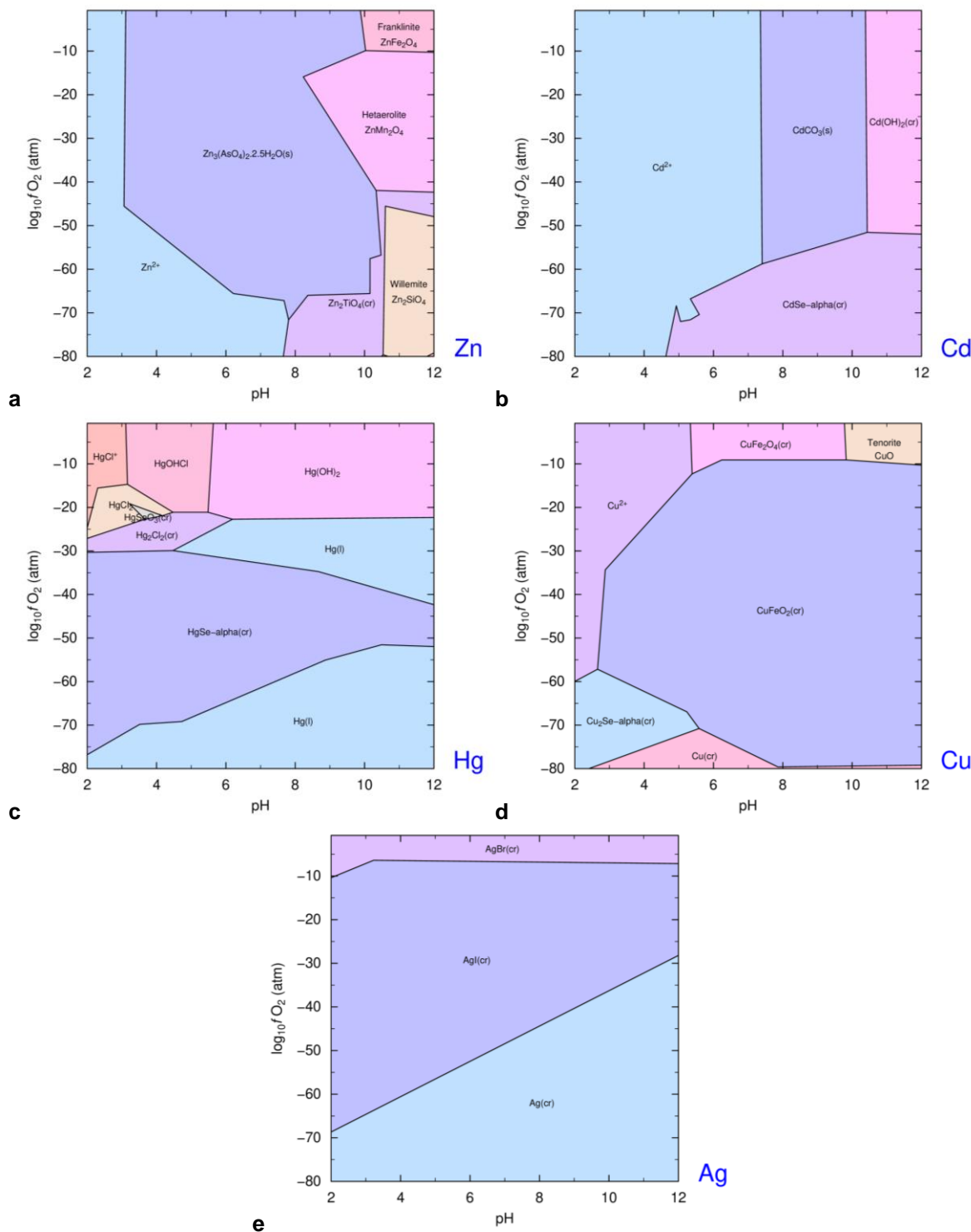


Figure 4.2-13. Pourbaix diagrams (PHREEPLOT) of d-transition metals — Zn (a), Cd (b), Hg (c), Cu (d), and Ag (e) — in a solution containing all elements included in PRODATA at 10^{-4} mol kg⁻¹; the ionic strength is maintained at 0.1 mol kg⁻¹ by a solution containing a hypothetical indifferent Cation/Anion electrolyte; all possible phases are allowed to precipitate; the Davies PHREEQC extraction of the database is used, excluding Ca₂ZrSi₃O₁₂(cr) in the input file.

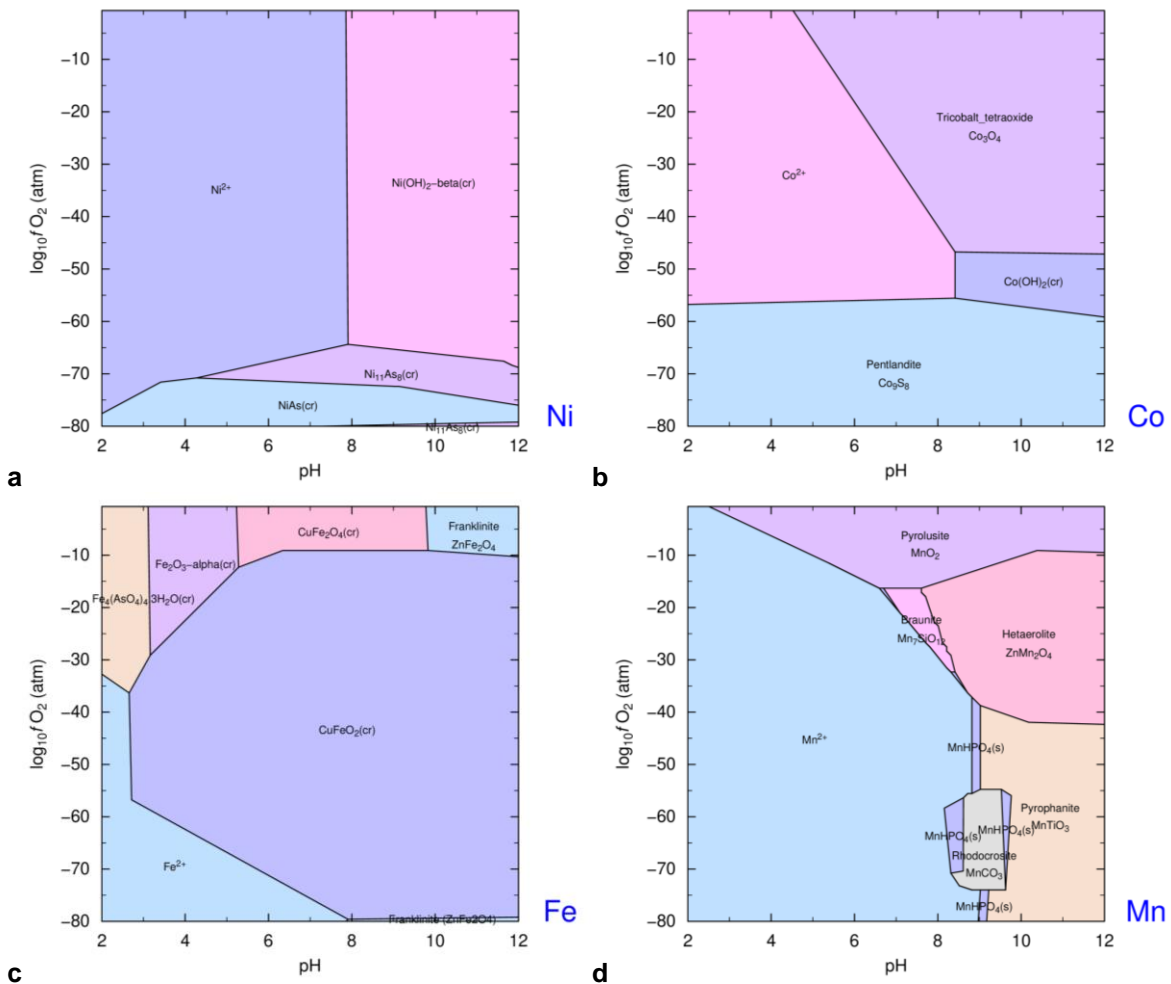


Figure 4.2-14. Pourbaix diagrams (PHREEPLOT) of d-transition metals — Ni (a), Co (b), Fe (c), and Mn(d) — in a solution containing all elements included in PRODATA at 10^{-4} mol kg_w⁻¹; the ionic strength is maintained at 0.1 mol kg_w⁻¹ by a solution containing a hypothetical indifferent Cation/Anion electrolyte; all possible phases are allowed to precipitate; the Davies PHREEQC extraction of the database is used, excluding $Ca_2ZrSi_3O_{12}(cr)$ in the input file.

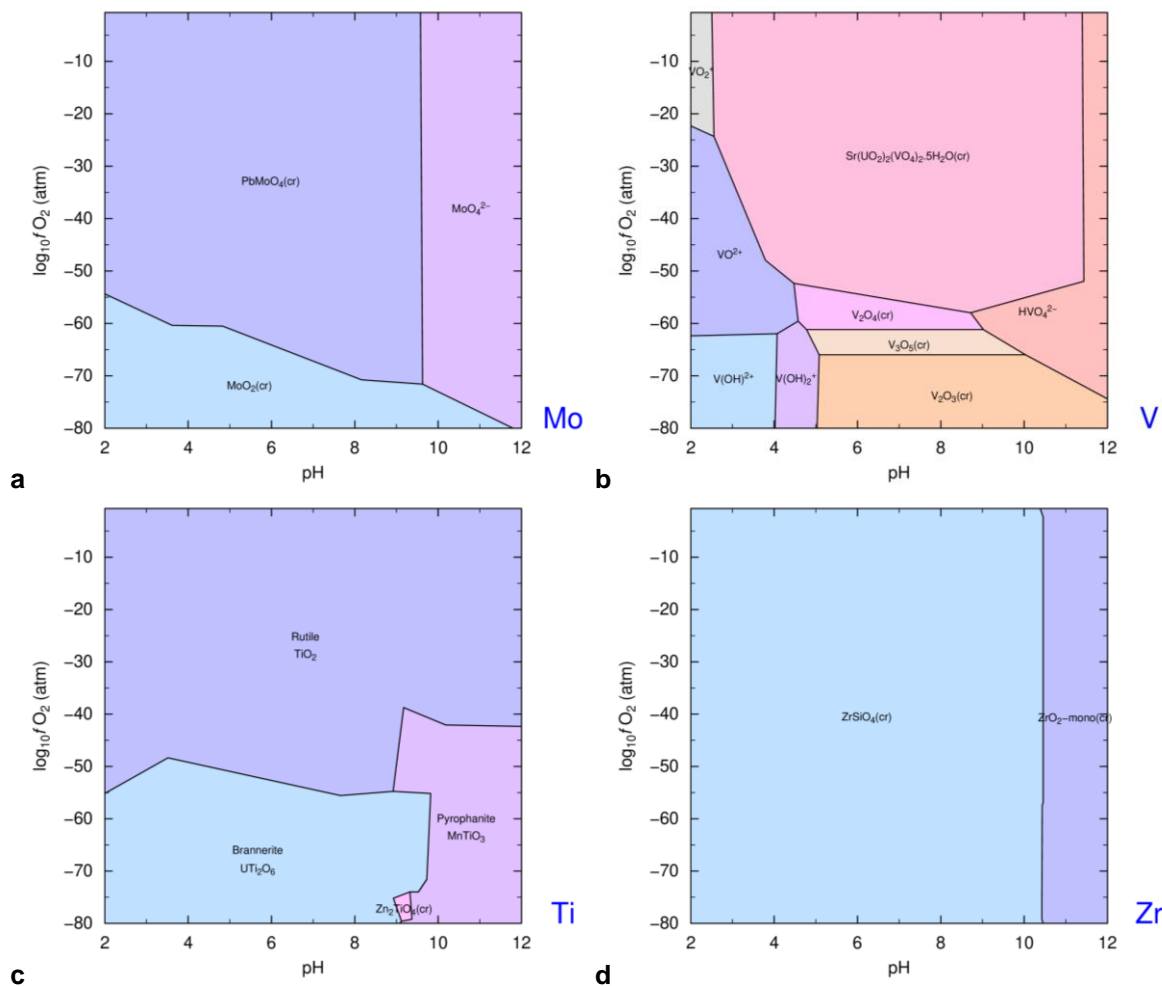


Figure 4.2-15. Pourbaix diagrams (PHREEPLOT) of d-transition metals — Mo (a), V (b), Ti (c), and Zr (d) — in a solution containing all elements included in PRODATA at 10^{-4} mol kg_w⁻¹; the ionic strength is maintained at 0.1 mol kg_w⁻¹ by a solution containing a hypothetical indifferent Cation/Anion electrolyte; all possible phases are allowed to precipitate; the Davies PHREEQC extraction of the database is used, excluding $\text{Ca}_2\text{ZrSi}_3\text{O}_{12}(\text{cr})$ in the input file.

4.2.2.5. Actinides

The Pourbaix diagrams of actinides are plotted in Figure 4.2-16, and seem unchanged for both uranium (Figure 4.2-16a) and thorium (Figure 4.2-16b). It seems that the boundaries of brannerite (UTi_2O_6) are reduced at the benefit of $\text{UO}_2(\text{cr})$.

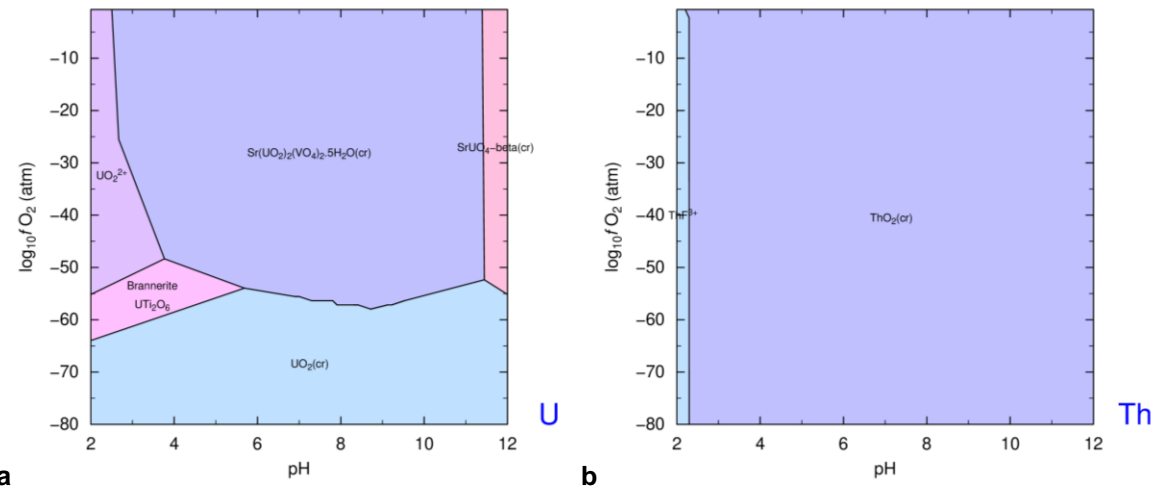


Figure 4.2-16. Pourbaix diagrams (PHREEPLOT) of actinides — U (a), and Th (b) — in a solution containing all elements included in PRODATA at 10^{-4} mol kg_w^{-1} ; the ionic strength is maintained at 0.1 mol kg_w^{-1} by a solution containing a hypothetical indifferent Cation/Anion electrolyte; all possible phases are allowed to precipitate; the Davies PHREEQC extraction of the database is used, excluding $\text{Ca}_2\text{ZrSi}_3\text{O}_{12}(\text{cr})$ in the input file.

4.2.2.6. Alkaline earth metals

The Pourbaix diagram of alkaline earth metals are plotted in Figure 4.2-17. For magnesium (Figure 4.2-17a) the impeded precipitation of $\text{Ca}_2\text{ZrSi}_3\text{O}_{12}(\text{cr})$ allows the formation of ordoned phlogopite ($\text{KAlMg}_3\text{Si}_3\text{O}_{10}(\text{OH})_2$); for calcium (Figure 4.2-17b), the precipitation of fluorapatite ($\text{Ca}_5(\text{PO}_4)_3\text{F}$) is now dominant at $\text{pH}>5$; for strontium (Figure 4.2-17c), the boundaries are almost unchanged; for barium (Figure 4.2-17d), the domain of $\text{BaHAsO}_4 \cdot \text{H}_2\text{O}(\text{cr})$ is increase at the expenses of barite (BaSO_4); for radium (Figure 4.2-17e), the domain of $\text{RaSO}_4(\text{s})$ is increased at the expenses of Ra^{2+} .

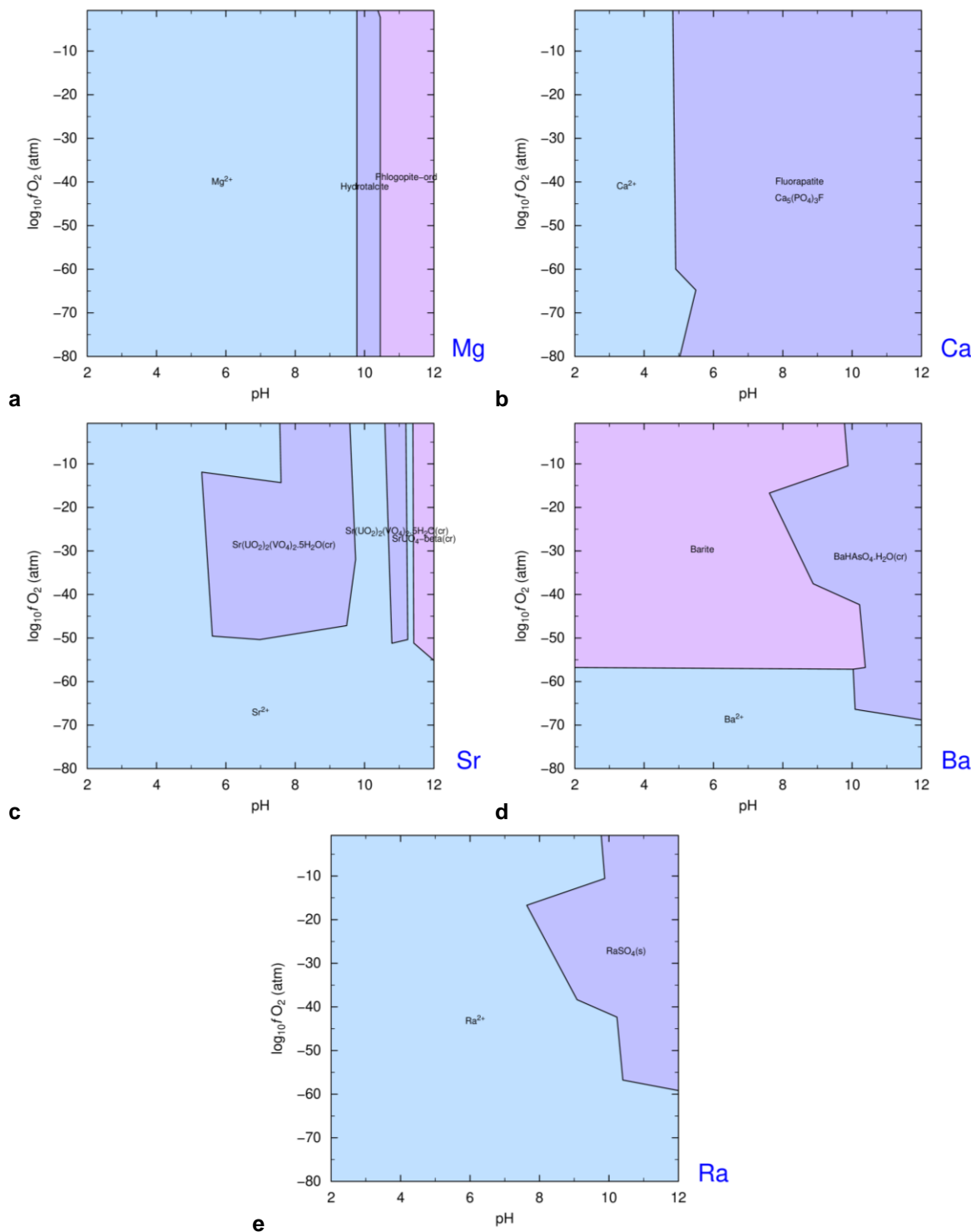


Figure 4.2-17. Pourbaix diagrams (PHREEPLOT) of alkaline earth metals — Mg (a), Ca (b), Sr (c), Ba (d), and Ra (e) — in a solution containing all elements included in PRODATA at 10^{-4} mol kg^{-1} ; the ionic strength is maintained at 0.1 mol kg^{-1} by a solution containing a hypothetical indifferent Cation/Anion electrolyte; all possible phases are allowed to precipitate; the Davies PHREEQC extraction of the database is used, excluding $\text{Ca}_2\text{ZrSi}_3\text{O}_{12}(\text{cr})$ in the input file.

4.2.2.7. Alkaline metals

The Pourbaix diagrams of alkaline metals (not shown) are not different from the one obtained when $\text{Ca}_2\text{ZrSi}_3\text{O}_{12}(\text{cr})$ is allowed to precipitate (Figure 4.2-9). The precipitation of ordered phlogopite

($\text{KAlMg}_3\text{Si}_3\text{O}_{10}(\text{OH})_2$) in Figure 4.2-12a and Figure 4.2-17a should nevertheless induce a significant proportion of this mineral in the general speciation of K.

4.3. Species Repartitions Under Atmospheric Oxygen

Due to the number of elements in the database, different solid phases can coexist depending on the E_h -pH conditions. The speciation diagrams — *i.e.* percentage of species vs. pH — of all the elements included in PRODATA can be calculated at atmospheric $P(\text{O}_2)$ using PHREEPLOT [2011KIN/COO], CHESS 3.0 release 3 (with the Java interface 2.0 release 1), or GWB. The conditions of the calculations are the same as for the predominance Pourbaix diagrams.

4.3.1. Complete Database

4.3.1.1. Halogens

The chemistry of halogens in Figure 4.3-1 is not homogeneous under these particular conditions. Fluorine (Figure 4.3-1a) is dominated by ThF_n^{4-n} at low pH, and AlF_n^{3-n} complexes at pH < 5, when F^- is major at higher pH values and fluoapatite ($\text{Ca}_5(\text{PO}_4)_3\text{F}$) precipitates as a minor phase at pH > 5.5. Chlorine chemistry (Figure 4.3-1b) is dominated by Hg complexes at pH < 6, and Cl^- at higher pH values; pyromorphite ($\text{Pb}_5(\text{PO}_4)_3\text{Cl}$) is precipitating as a minor phase. $\text{AgBr}(\text{cr})$ dominates the chemistry of bromine (Figure 4.3-1c). IO_3^- is the major species of iodine (Figure 4.3-1d).

4.3.1.2. Non-metals

The chemistry of non-metals (S, Se, N, P, As, and C) is contrasted (Figure 4.3-2). The sulphur chemistry (Figure 4.3-2a) is dominated by barite (BaSO_4) at pH < 10 and $\text{RaSO}_4(\text{s})$ at higher pH with SO_4^{2-} as minor species. The selenium chemistry (Figure 4.3-2b) is dominated by selenite (SeO_4^{2-}), with minor U(VI), Ni(II) and Co(II) complexes. The chemistry of nitrogen (Figure 4.3-2c) is dominated by NO_3^- . The chemistry of phosphorus (Figure 4.3-2d) is dominated by $\alpha\text{-Zr}(\text{HPO}_4)_2(\text{cr})$ at pH < 7.5 with fluorapatite ($\text{Ca}_5(\text{PO}_4)_3\text{F}$) as minor phase; hydrogenophosphate ion (HPO_4^{2-}) is major at 7.5 < pH < 9.5 with $\text{PbHPO}_4(\text{cr})$ and fluorapatite ($\text{Ca}_5(\text{PO}_4)_3\text{F}$) as minor phases; at higher pH, pyromorphite ($\text{Pb}_5(\text{PO}_4)_3\text{Cl}$) is the major phase with fluorapatite ($\text{Ca}_5(\text{PO}_4)_3\text{F}$) as minor phase. The analysis of the output file reveals the minor precipitation (less than 2%) of $\text{Cu}(\text{UO}_2)_2(\text{PO}_4)_2 \cdot 8\text{H}_2\text{O}(\text{cr})$ — pH ca. 6 to pH ca. 6.9 —, and $\text{Sr}(\text{UO}_2)_2(\text{PO}_4)_2 \cdot 6\text{H}_2\text{O}(\text{cr})$ — pH ca. 6.9 to pH ca. 9.1. $\text{Fe}_4(\text{AsO}_4)_4 \cdot 3\text{H}_2\text{O}(\text{cr})$ dominates arsenic at pH < 3, with arsenic acid ($\text{H}_3\text{AsO}_4(\text{aq})$) and dihydrogenoarsenate (H_2AsO_4^-) as minor species; $\text{Zn}_3(\text{AsO}_4)_2 \cdot 2.5\text{H}_2\text{O}(\text{cr})$ is the major phase up to pH 9.5, from where $\text{BaHAsO}_4 \cdot \text{H}_2\text{O}(\text{cr})$ is the major phase at higher pH value with AsO_4^{3-} as minor species. The chemistry of carbon is dominated by carbonic acid ($\text{CO}_2(\text{aq})$) and hydrogenocarbonate (HCO_3^-) at pH < 7; otavite ($\text{CdCO}_3(\text{cr})$) is major at pH values up to 11.5; carbonate ion (CO_3^{2-}) is major at higher pH values.

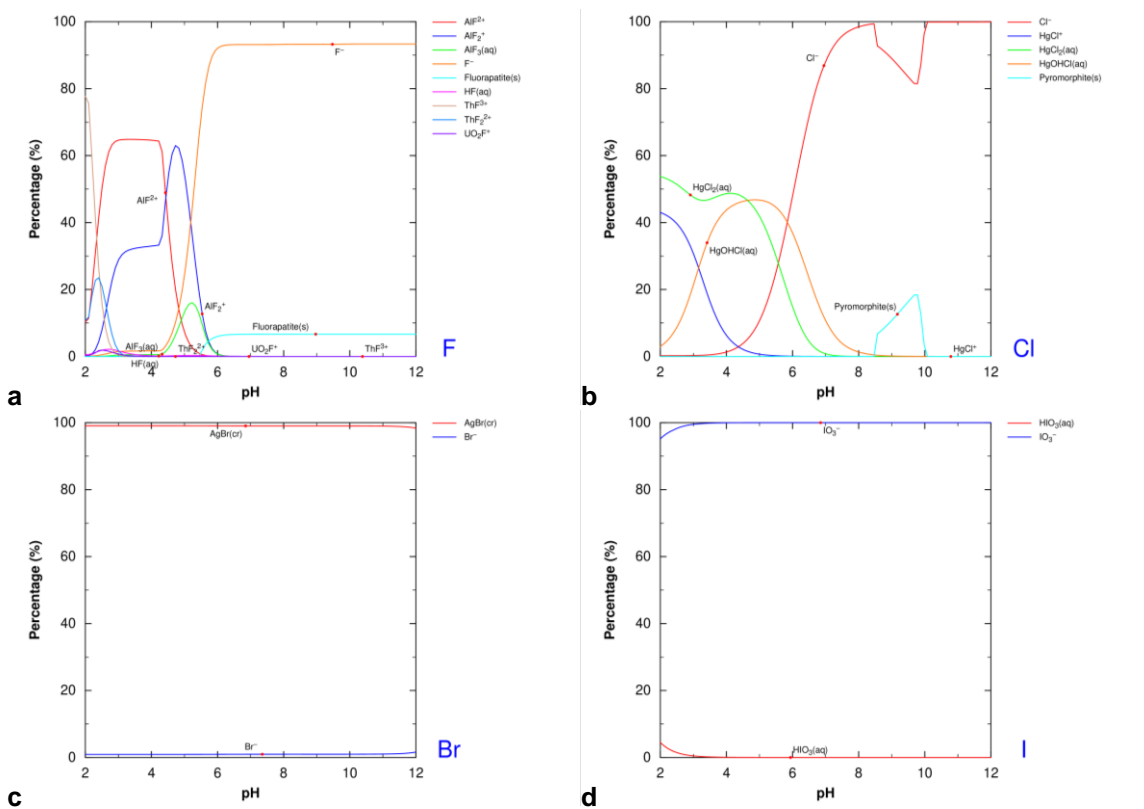


Figure 4.3-1. Speciation at $P(O_2) = 0.21 \text{ atm}$ (PHREEPLOT) of halogens — F (a), Cl (b), Br (c), and I (d) — in a solution containing all elements included in PRODATA at $10^{-4} \text{ mol kg}_w^{-1}$; the ionic strength is maintained at $0.1 \text{ mol kg}_w^{-1}$ by a solution containing a hypothetical indifferent Cation/Anion electrolyte; all possible phases are allowed to precipitate; species less than 2% are not plotted; the Davies PHREEQC extraction of the database is used.

4.3.1.3. Metalloids

The chemistry of metalloids Si, Pb, and Al is described in Figure 4.3-3. Si is completely dominated by highly insoluble $\text{Ca}_2\text{ZrSi}_3\text{O}_{12}(\text{cr})$ (Figure 4.3-3a) — this phase is not known in nature. Pb is occurring under the form of $\text{PbMoO}_4(\text{cr})$ up to pH 9 (Figure 4.3-3b), with $\text{PbHPO}_4(\text{cr})$ as minor phase at pH > 7; pyromorphite ($\text{Pb}_5(\text{PO}_4)_3\text{Cl}$) dominates at higher pH with plattnerite (PbO_2) as minor phases; plattnerite dominates at pH > 9.9. CHESS and GWB are showing $\text{Pb}(\text{OH})_2(\text{cr})$ instead of plattnerite ($\text{PbO}_2(\text{cr})$). The reason of this difference has not been elucidated up to now. One can remind that the default ionic strength correction calculation for PHREEQC is Davies [1962DAV], when it is simplified Debye-Hückel for CHESS, and b-dot for GWB. Free aluminium ion (Al^{3+}) and fluoride complexes — $\text{AlF}_n^{(3-n)+}$, $n = \{1; 2; 3\}$ — dominate at pH < 4.5 (Figure 4.3-3c); diasporite ($\gamma\text{-AlO}(\text{OH})$) is the major phase at pH < 10; hydrotalcite ($\text{Mg}_4\text{Al}_2(\text{OH})_{14} \cdot 3\text{H}_2\text{O}$) shares dominance with $\text{Al}(\text{OH})_4^-$ at pH > 10.

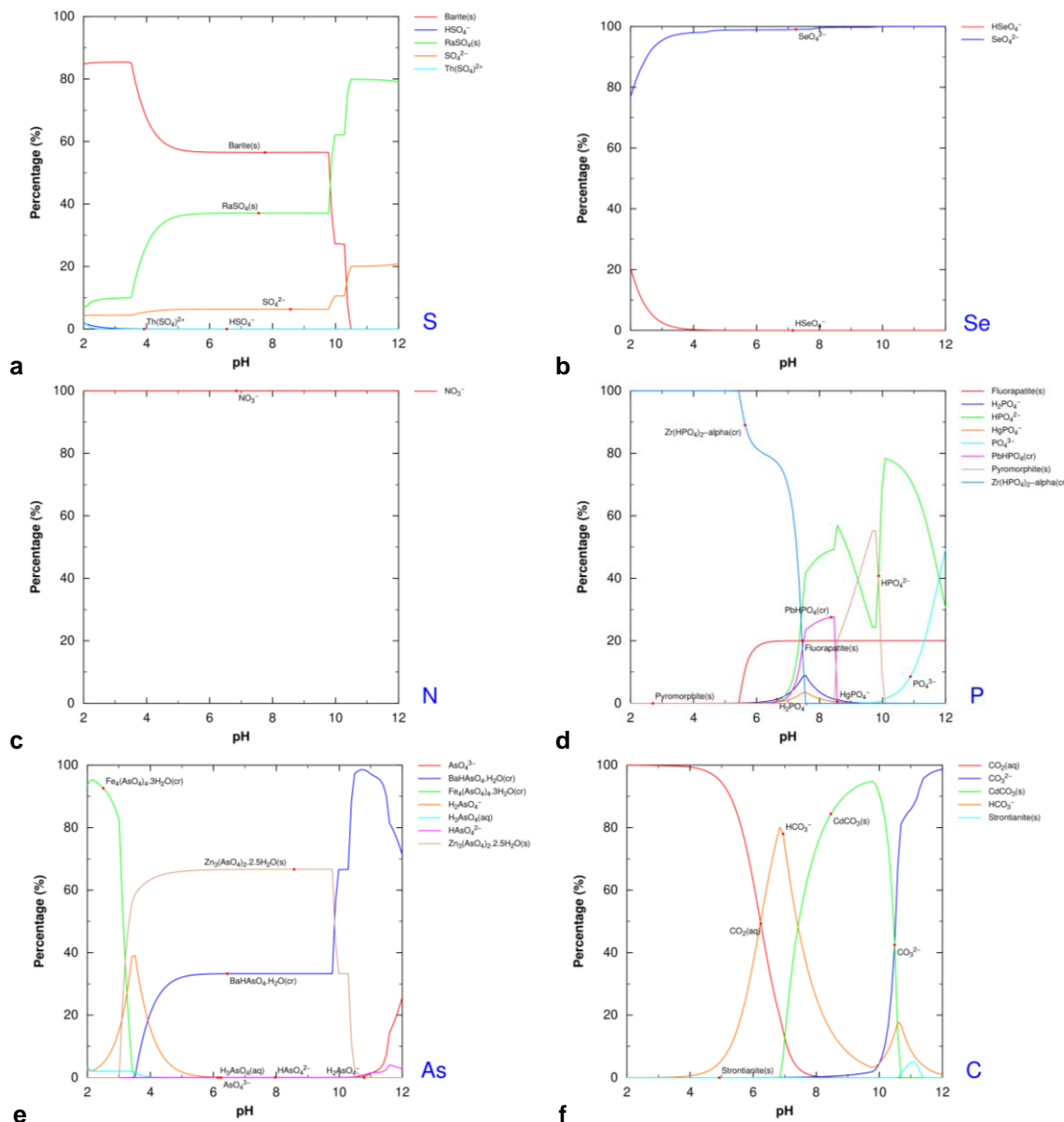


Figure 4.3-2. Speciation at $\text{P(O}_2\text{)} = 0.21 \text{ atm (PHREEPLOT)}$ of non-metals — S (a), Se (b), N (c), P(d), As (e), and C (f) — in a solution containing all elements included in PRODATA at $10^{-4} \text{ mol kg}^{-1}$; the ionic strength is maintained at 0.1 mol kg^{-1} by a solution containing a hypothetical indifferent Cation/Anion electrolyte; all possible phases are allowed to precipitate; species less than 2% are not plotted; the Davies PHREEQC extraction of the database is used.

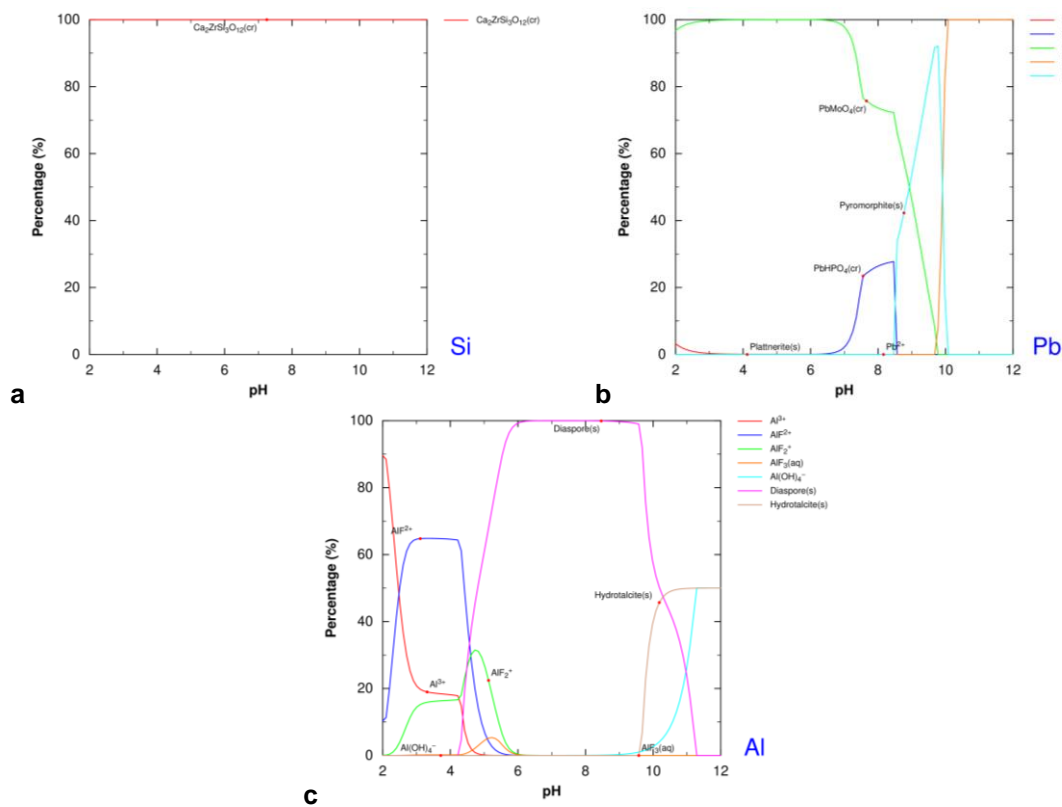


Figure 4.3-3. Speciation at $P(\text{O}_2) = 0.21 \text{ atm}$ (PHREEPLOT) of Si (a), Pb (b), and Al (c) in a solution containing all elements included in PRODATA at $10^{-4} \text{ mol kg}_w^{-1}$; the ionic strength is maintained at $0.1 \text{ mol kg}_w^{-1}$ by a solution containing a hypothetical indifferent Cation/Anion electrolyte; all possible phases are allowed to precipitate; species less than 2% are not plotted; the Davies PHREEQC extraction of the database is used.

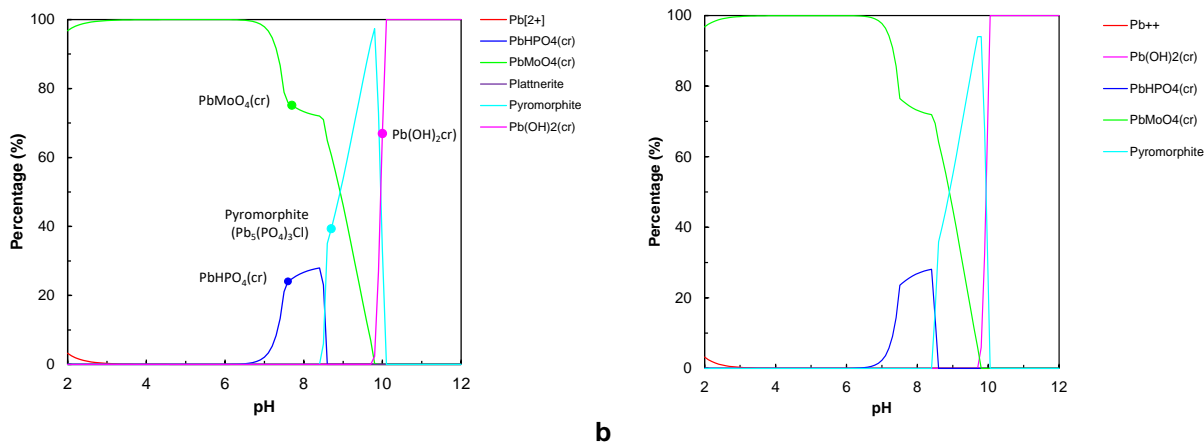


Figure 4.3-4. Speciation at $P(\text{O}_2) = 0.21 \text{ atm}$ of Pb in a solution containing all elements included in PRODATA at $10^{-4} \text{ mol kg}_w^{-1}$; the ionic strength is maintained at $0.1 \text{ mol kg}_w^{-1}$ by a solution containing a hypothetical indifferent Cation/Anion electrolyte; all possible phases are allowed to precipitate; species less than 2% are not plotted; the CHESS (a) and GWB (b) extraction of the database is used.

4.3.1.4. d-transition metal series

The d-transition metals speciation from Zn to Ag obtained with PHREEPLOT are presented in Figure 4.3-5. Zn^{2+} dominates the speciation up to pH 3.2, where $Zn_3(AsO_4)_2 \cdot 2.5H_2O(cr)$ is dominating up to pH 10; from there $Zn_2TiO_4(cr)$ and franklinite ($ZnFe_2O_4$) are sharing predominance. The free Cd^{2+} ion dominates at pH < 7, and otavite ($CdCO_3(cr)$) is major at higher pH values, with minor phases (less than 2%) $Cd_3(PO_4)_2(cr)$ and $Cd(OH)_2(cr)$. The free ion Hg^{2+} and chloride complexes are major at pH < 6, and $Hg(OH)_2(aq)$ at higher pH values. Copper(II) free ion (Cu^{2+}), is major at pH < 6 and tenorite ($CuO(cr)$) and $CuFe_2O_4(cr)$ (cuprospinel) at higher pH. As noted for P, analysis of output file reveals the minor precipitation of $Cu(UO_2)_2(PO_4)_2 \cdot 8H_2O(cr)$ — pH ca. 6 to pH ca. 6.9. $AgBr(cr)$ dominates the silver chemistry.

The d-transition metals speciation from Ni to Mn are shown in Figure 4.3-6. The free Ni^{2+} ion is dominant at pH < 8 and $\beta-Ni(OH)_2(cr)$ at higher pH values (Figure 4.3-6a). The free Co^{2+} ion is dominant at pH < 4.5, and the highly insoluble tricobalt_tetraoxide (Co_3O_4) dominates at higher pH (Figure 4.3-6b). One can remind that the formation of this latter phase occurs under particular conditions [2013ALR/JOS; 2016ZYL/SMO]. The chemistry of iron is dominated by the arseniate phase $Fe_4(AsO_4)_4 \cdot 3H_2O(cr)$ at pH < 3.5, then by Fe_2O_3 -alpha(*cr*) up to pH 5.3, by the cuprospinel $CuFe_2O_4(cr)$ at up to pH ca. 10, and franklinite ($ZnFe_2O_4$) at higher pH values (Figure 4.3-6c). Mn(II) free ion (Mn^{2+}) is major at pH < 2.5 and Mn(IV) phase pyrolusite (MnO_2) at higher pH values (Figure 4.3-6d).

The chemistry of the d-series metals from Mo to Zr are shown in Figure 4.3-7. Molybdenum chemistry is dominated by $PbMoO_4(cr)$ at pH < 9, and molybdate ion (MoO_4^{2-}) at higher pH values (Figure 4.3-7a). Vanadium chemistry is dominated by vanadyl ion at pH < 2.75 and uranylvanadate of strontium at higher pH (Figure 4.3-7b). Rutile is the major phase of titanium with $Zn_2TiO_4(cr)$ at pH > 10 (Figure 4.3-7c). Zirconium is dominated solid phases by $\alpha-Zr(HPO_4)_2(cr)$; with $Ca_2ZrSi_3O_{12}(cr)$ and monoclinic-ZrO₂ as minor phases up to pH *ca.* 7; at higher pH values monoclinic-ZrO₂ dominates with $Ca_2ZrSi_3O_{12}(cr)$ as minor phases (Figure 4.3-7d).

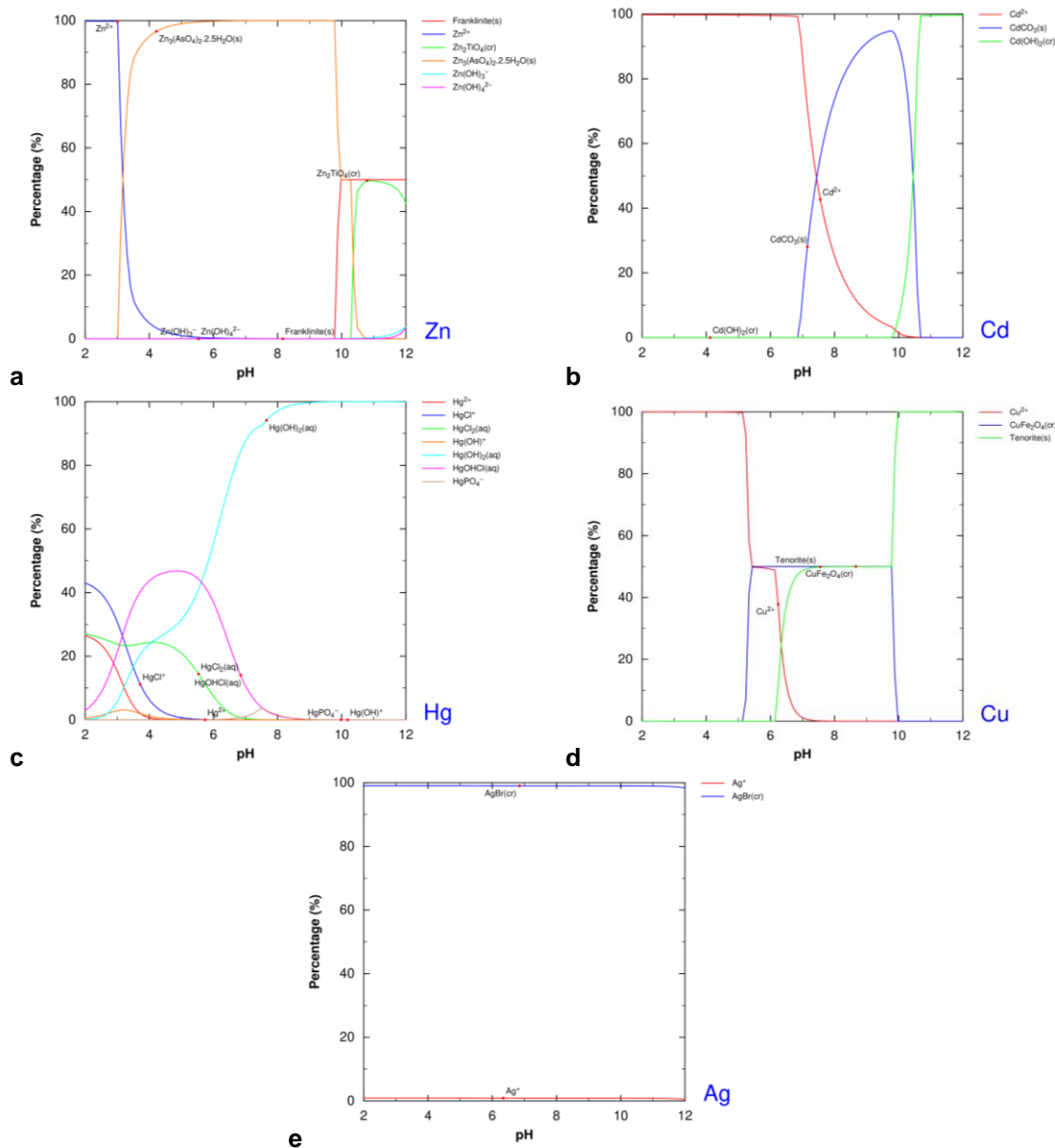


Figure 4.3-5. Speciation at $P(\text{O}_2) = 0.21 \text{ atm}$ (PHREEPLOT) of d-series elements Zn (a), Cd (b), Hg (c), Cu (d), and Ag (e) in a solution containing all elements included in PRODATA at $10^{-4} \text{ mol kg}_w^{-1}$; the ionic strength is maintained at $0.1 \text{ mol kg}_w^{-1}$ by a solution containing a hypothetical indifferent Cation/Anion electrolyte; all possible phases are allowed to precipitate; species less than 2% are not plotted; the Davies PHREEQC extraction of the database is used.

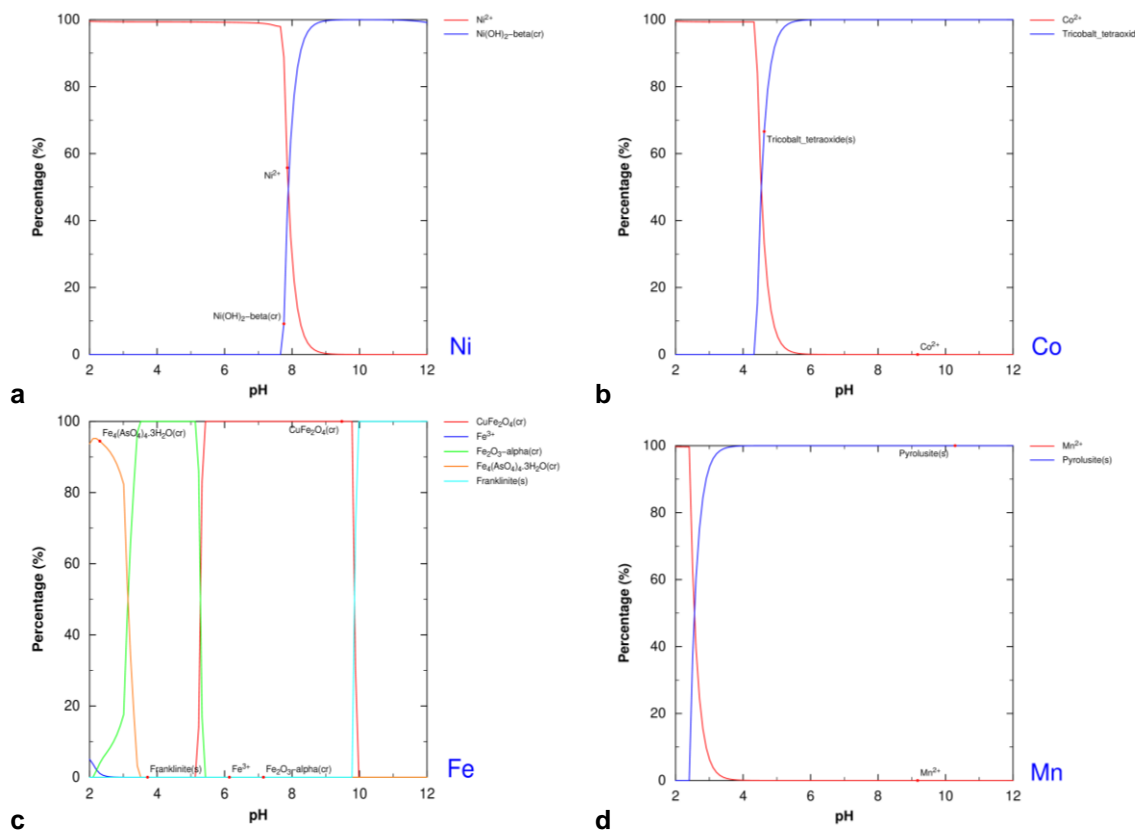


Figure 4.3-6. Speciation at $P(\text{O}_2) = 0.21 \text{ atm}$ (PHREEPLOT) of d-series elements Ni (a), Co (b), Fe (c), and Mn (d) in a solution containing all elements included in PRODATA at $10^{-4} \text{ mol kg}_w^{-1}$; the ionic strength is maintained at $0.1 \text{ mol kg}_w^{-1}$ by a solution containing a hypothetical indifferent Cation/Anion electrolyte; all possible phases are allowed to precipitate; species less than 2% are not plotted; the Davies PHREEQC extraction of the database is used.

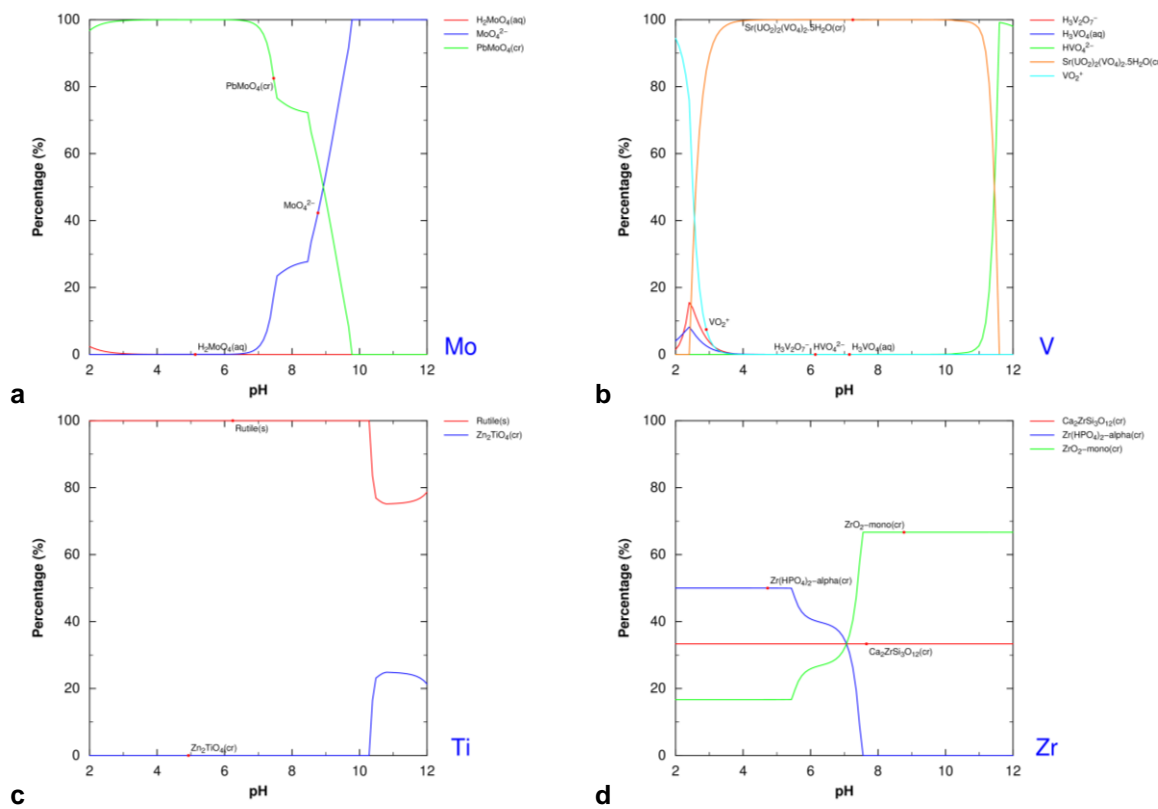


Figure 4.3-7. Speciation at $\text{P}(\text{O}_2) = 0.21 \text{ atm}$ (PHREEPLOT) of d-series elements Mo (a), V (b), Ti (c), and Zr (d) in a solution containing all elements included in PRODATA at $10^{-4} \text{ mol kg}^{-1}$; the ionic strength is maintained at 0.1 mol kg^{-1} by a solution containing a hypothetical indifferent Cation/Anion electrolyte; all possible phases are allowed to precipitate; species less than 2% are not plotted; the Davies PHREEQC extraction of the database is used.

4.3.1.5. Actinides

The two actinides included in PRODATA, U and Th are presented in Figure 4.3-8. UO_2^{2+} dominates the uranium chemistry up to pH 2.75. The uranylvanadate of strontium is the dominant phase at higher pH values (Figure 4.3-8a). The analysis of the total output file reveals the minor precipitation of clarkeite — $\text{Na}(\text{UO}_2)\text{O}(\text{OH})$ ca. pH 10.6 —, $\text{Cu}(\text{UO}_2)_2(\text{PO}_4)_2 \cdot 8\text{H}_2\text{O}(\text{cr})$ — ca. pH 6 to ca. pH 6.75 —, and $\text{Sr}(\text{UO}_2)_2(\text{PO}_4)_2 \cdot 6\text{H}_2\text{O}(\text{cr})$ — ca. pH 6.9 to ca. pH 9.1. The free ion ThF^{3+} dominates the thorium chemistry, with minor proportion of Th^{4+} and ThF_2^{2+} , up to pH 2.5; $\text{ThO}_2(\text{cr})$ is the only phase present at higher pH values (Figure 4.3-8b).

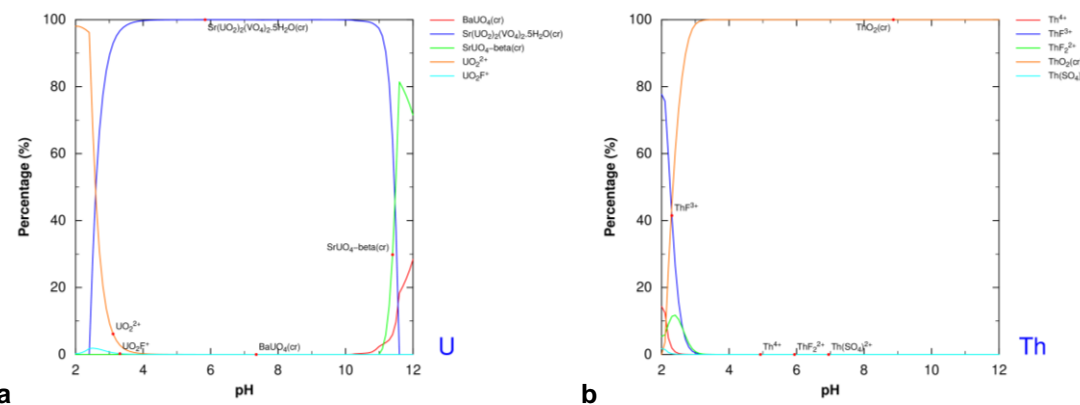


Figure 4.3-8. Speciation at $P(O_2) = 0.21 \text{ atm}$ (PHREEPLOT) of actinides U (a) and Th (b) in a solution containing all elements included in PRODATA at $10^{-4} \text{ mol kg}^{-1}$; the ionic strength is maintained at 0.1 mol kg^{-1} by a solution containing a hypothetical indifferent Cation/Anion electrolyte; all possible phases are allowed to precipitate; species less than 2% are not plotted; the Davies PHREEQC extraction of the database is used.

4.3.1.6. Alkaline earth metals

Alkaline earth metals Mg, Ca, Sr, Ba, and Ra are shown in Figure 4.3-9. The free Mg^{2+} ion dominates the chemistry up to pH 9.8, where hydrotalcite ($Mg_4Al_2(OH)_{14} \cdot 3H_2O$) becomes dominant. The solid $Ca_2ZrSi_3O_{12}(cr)$ is major at all pH values, with free Ca^{2+} ion as minor soluble species up to pH < 5.5, and fluorapatite ($Ca_5(PO_4)_3F$) at higher pH values. The free Sr^{2+} ion is major up to pH 3.5, and strontium uranylvanadate shares the dominance at higher pH values. As already signalled for U, the analysis of the output file reveals the minor precipitation of $Sr(UO_2)_2(PO_4)_2 \cdot 6H_2O(cr)$ — pH ca. 6.9 to pH ca. 9.1. Barium is mostly present under solid barite ($BaSO_4$) up to pH 10, with Ba^{2+} and $BaHPO_4 \cdot H_2O(cr)$ as minor species; $BaHPO_4 \cdot H_2O(cr)$ is major at higher pH values with $BaUO_4(cr)$ as minor phase. Radium is under the free Ra^{2+} ion form up to pH ca. 7.5 and as solid $RaSO_4(s)$ at higher pH values. The link between sulphate chemistry of Ba and Ra, which was clear in Figure 4.3-2a is also apparent here.

4.3.1.7. Alkaline metals

The chemistry of alkaline metals is dominated by their free ions (Figure 4.3-10).

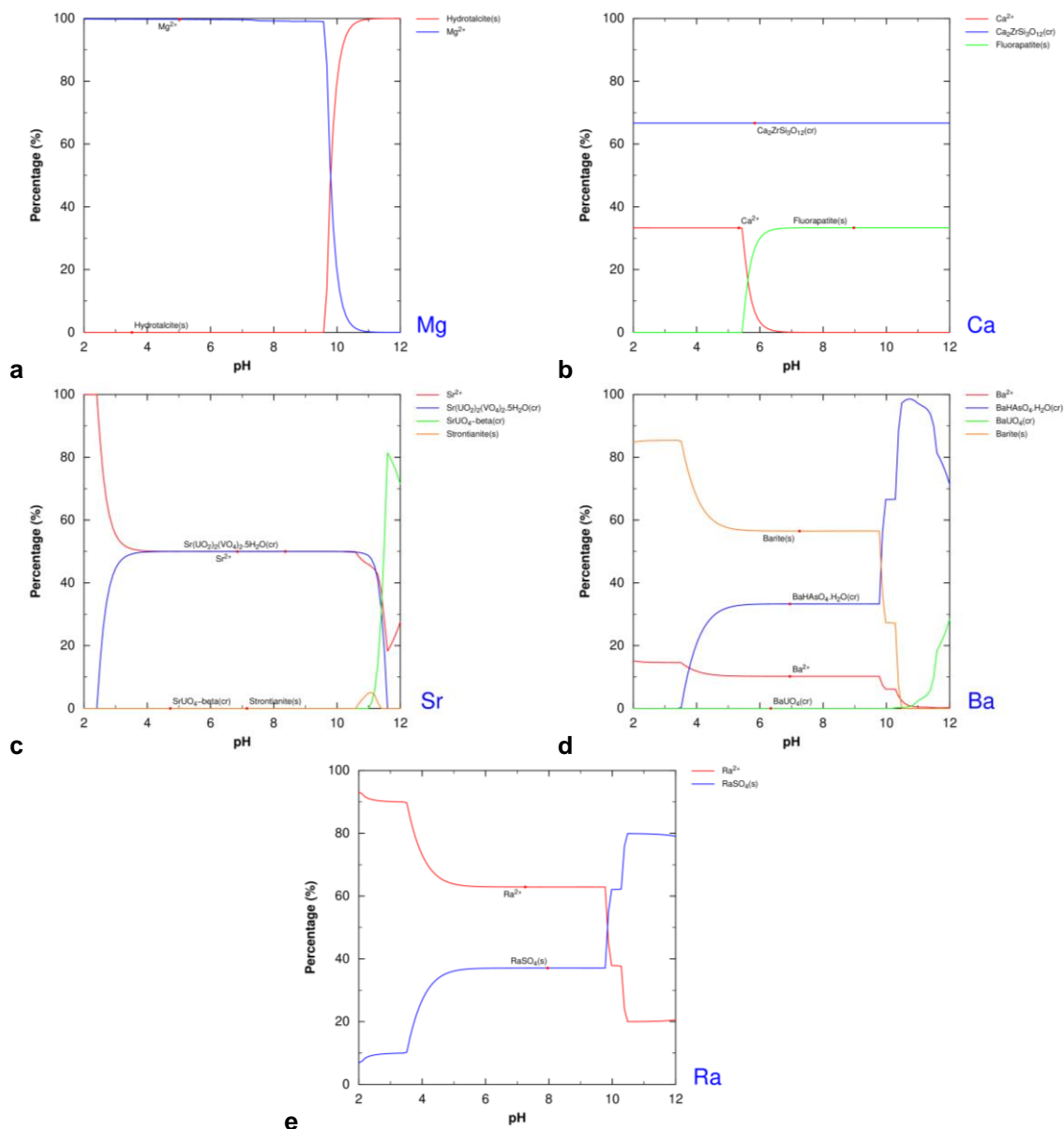


Figure 4.3-9. Speciation at $P(O_2) = 0.21 \text{ atm}$ (PHREEPLOT) of alkaline earth metals Mg (a), Ca (b), Sr (c), Ba (d), and Ra (e) in a solution containing all elements included in PRODATA at $10^{-4} \text{ mol kg}^{-1}$; the ionic strength is maintained at 0.1 mol kg^{-1} by a solution containing a hypothetical indifferent Cation/Anion electrolyte; all possible phases are allowed to precipitate; species less than 2% are not plotted; the Davies PHREEQC extraction of the database is used.

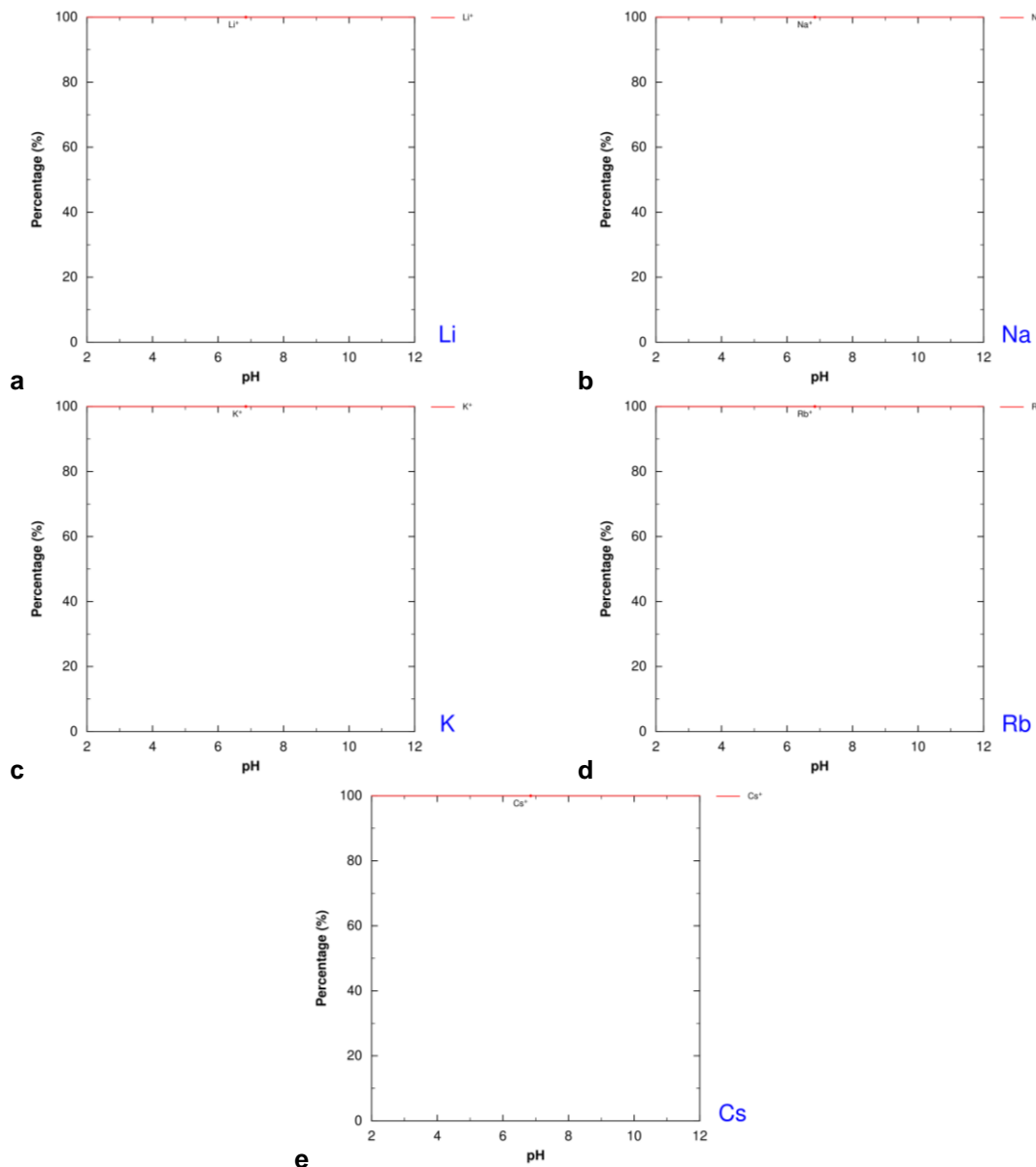


Figure 4.3-10. Speciation at $P(O_2) = 0.21 \text{ atm}$ (PHREEPLOT) of alkaline metals Li (a), Na (b), K (c), Rb (d) and Cd (e) in a solution containing all elements included in PRODATA at $10^{-4} \text{ mol kg}_w^{-1}$; the ionic strength is maintained at $0.1 \text{ mol kg}_w^{-1}$ by a solution containing a hypothetical indifferent Cation/Anion electrolyte; all possible phases are allowed to precipitate; species less than 2% are not plotted; the Davies PHREEQC extraction of the database is used.

4.3.2. Species Repartition Excluding $\text{Ca}_2\text{ZrSi}_3\text{O}_{12}(\text{cr})$

The formation of highly insoluble and synthetic $\text{Ca}_2\text{ZrSi}_3\text{O}_{12}(\text{cr})$ has a direct impact on the chemistry of Ca, Zr, and Si. Through these elements, it should also have an impact on P and F — precipitation of Ca under the form of fluorapatite ($\text{Ca}_5(\text{PO}_4)_3\text{F}$) —, Pb and Cl — precipitation of pyromorphite ($\text{Pb}_5(\text{PO}_4)_3\text{Cl}$). In the following section these impacts on speciation of the different elements will be quantified through the impeded precipitation of $\text{Ca}_2\text{ZrSi}_3\text{O}_{12}(\text{cr})$ in the input file.

4.3.2.1. Halogens

As anticipated, the main impact of the impeded precipitation of $\text{Ca}_2\text{ZrSi}_3\text{O}_{12}(\text{cr})$ is on F and Cl: the increase of the percentage of fluorapatite ($\text{Ca}_5(\text{PO}_4)_3\text{F}$) in Figure 4.3-11a (20%) in comparison to Figure 4.3-1a (6.7%); the

decrease of the percentage of pyromorphite ($\text{Pb}_5(\text{PO}_4)_3\text{Cl}$) in Figure 4.3-11a (9.8%) in comparison to Figure 4.3-1a (18.4%).

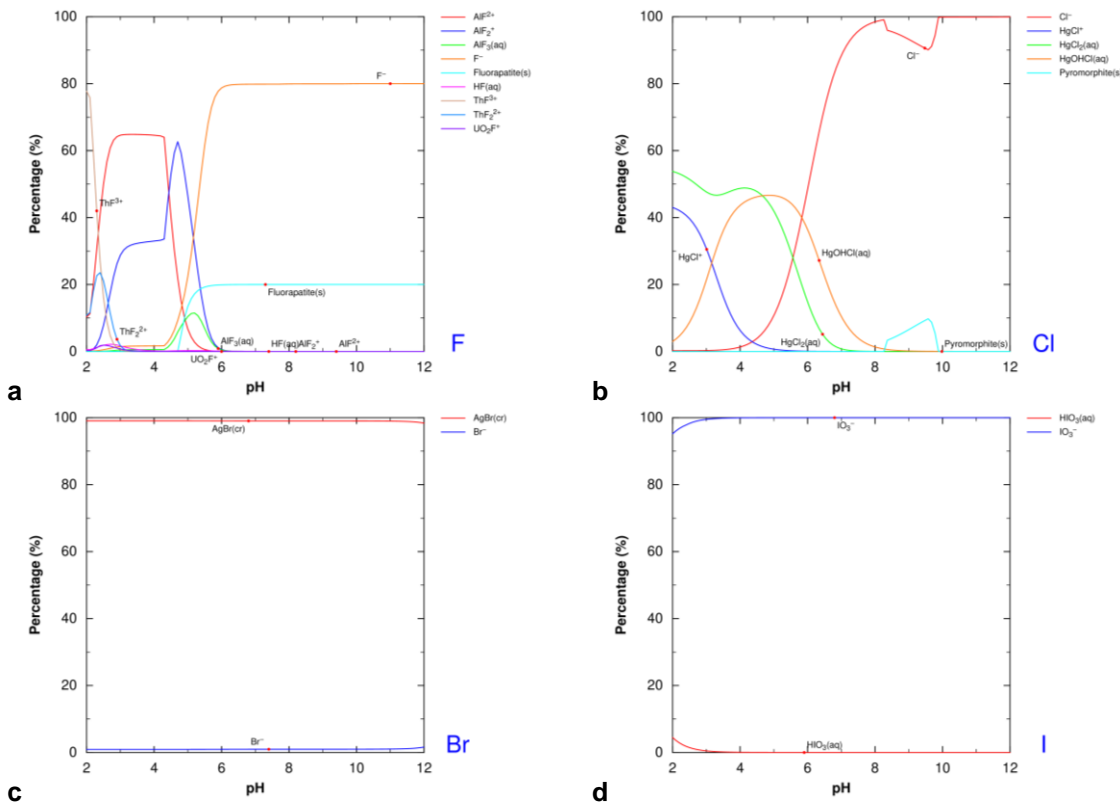


Figure 4.3-11. Speciation at $P(\text{O}_2) = 0.21 \text{ atm (PHREEPLOT)}$ of halogens — F (a), Cl (b), Br (c), and I (d) — in a solution containing all elements included in PRODATA at $10^{-4} \text{ mol kg}^{-1}$; the ionic strength is maintained at 0.1 mol kg^{-1} by a solution containing a hypothetical indifferent Cation/Anion electrolyte; all possible phases are allowed to precipitate; species less than 2% are not plotted; the Davies PHREEQC extraction of the database is used, excluding $\text{Ca}_2\text{ZrSi}_3\text{O}_{12}(\text{cr})$ in the input file.

4.3.2.2. Non-metals

Under these conditions, the impact of $\text{Ca}_2\text{ZrSi}_3\text{O}_{12}(\text{cr})$ is limited on S, Se, N, As and C. Here again the influence is mainly on the increased precipitation of fluorapatite ($\text{Ca}_5(\text{PO}_4)_3\text{F}$) and decreased precipitation of pyromorphite ($\text{Pb}_5(\text{PO}_4)_3\text{Cl}$). The precipitation of fluorapatite occurs also at the expenses of $\text{Zr}(\text{HPO}_4)_2$ -alpha(cr) in the pH range 4-6, and the predominance of HPO_4^{2-} and PO_4^{3-} at pH > 6.

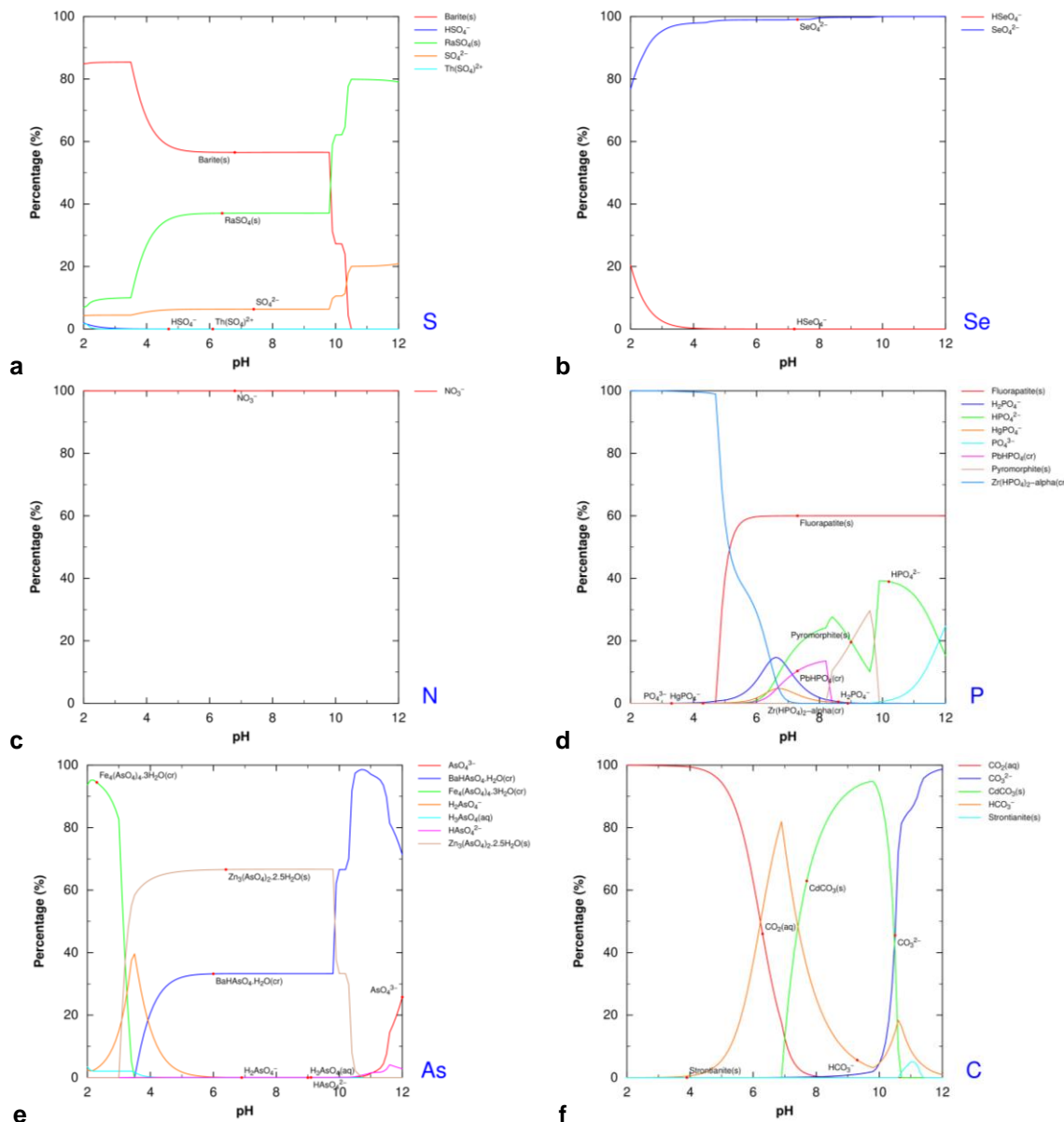


Figure 4.3-12. Speciation at $P(\text{O}_2) = 0.21 \text{ atm}$ (PHREEPLOT) of non-metals — S (a), Se (b), N (c), P (d), As (e), and C (f) — in a solution containing all the elements included in PRODATA at $10^{-4} \text{ mol kg}^{-1}$; the ionic strength is maintained at 0.1 mol kg^{-1} by a solution containing a hypothetical indifferent Cation/Anion electrolyte; all possible phases are allowed to precipitate; species less than 2% are not plotted; the Davies PHREEQC extraction of the database is used, excluding $\text{Ca}_2\text{ZrSi}_3\text{O}_{12}(\text{cr})$ in the input file.

4.3.2.3. Metalloids

The three metalloids are impacted to different degrees by the impeded precipitation of $\text{Ca}_2\text{ZrSi}_3\text{O}_{12}(\text{cr})$. The silicium chemistry is now controlled both by $\text{ZrSiO}_4(\text{cr})$ as shown in the Pourbaix diagram (Figure 4.2-12a), but $\text{Si}(\text{OH})_4(\text{aq})$ share the predominance up to pH 4.7. Ordained phlogopite ($\text{KAlMg}_3\text{Si}_3\text{O}_{10}(\text{OH})_2$) is mostly exclusively dominant at pH > 10.5. For lead, the decreased precipitation of both pyromorphite ($\text{Pb}_5(\text{PO}_4)_3\text{Cl}$) and $\text{PbHPO}_4(\text{cr})$, is inducing an increase precipitation of $\text{PbMoO}_4(\text{cr})$. For aluminium, the precipitation of ordained phlogopite, which was not apparent on Figure 4.2-12c, is changing the speciation at pH > 10.

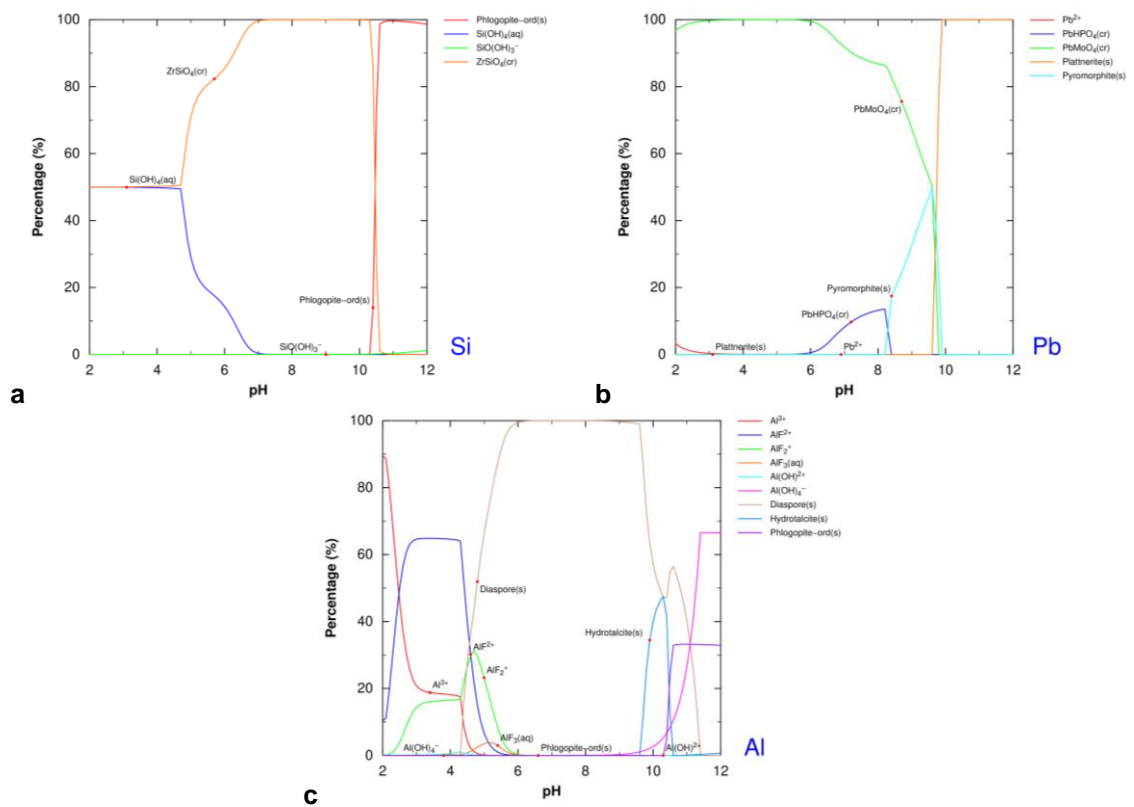


Figure 4.3-13. Speciation at $P(\text{O}_2) = 0.21 \text{ atm}$ (PHREEPLOT) of metalloids — Si (a), Pb (b), and Al (c) — in a solution containing all elements included in PRODATA at $10^{-4} \text{ mol kg}^{-1}$; the ionic strength is maintained at 0.1 mol kg^{-1} by a solution containing a hypothetical indifferent Cation/Anion electrolyte; all possible phases are allowed to precipitate; species less than 2% are not plotted; the Davies PHREEQC extraction of the database is used, excluding $\text{Ca}_2\text{ZrSi}_3\text{O}_{12}(\text{cr})$ in the input file.

4.3.2.4. d-transitions metals

The chemistry of Zn, Cd, Hg, Cu, and Ag are mostly unaffected (Figure 4.3-14), with the exception of the minor formation of HgPO_4^- complex. The influence of the Ni, Co, Fe, and Mn is marginal (Figure 4.3-15). The influence of Mo and precipitation of $\text{PbMoO}_4(\text{cr})$ is a consequence of the increase precipitation of fluorapatite ($\text{Ca}_5(\text{PO}_4)_3\text{F}$). The chemistry of V and Ti is unaffected. As it was the case for Si (Figure 4.2-12a), $\text{ZrSiO}_4(\text{cr})$ is sharing predominance with $\text{Zr}(\text{HPO}_4)_2-\text{alpha}(\text{cr})$ up to pH 5; $\text{ZrO}_2-\text{mono}(\text{cr})$ is exclusively dominating at pH > 10.5.

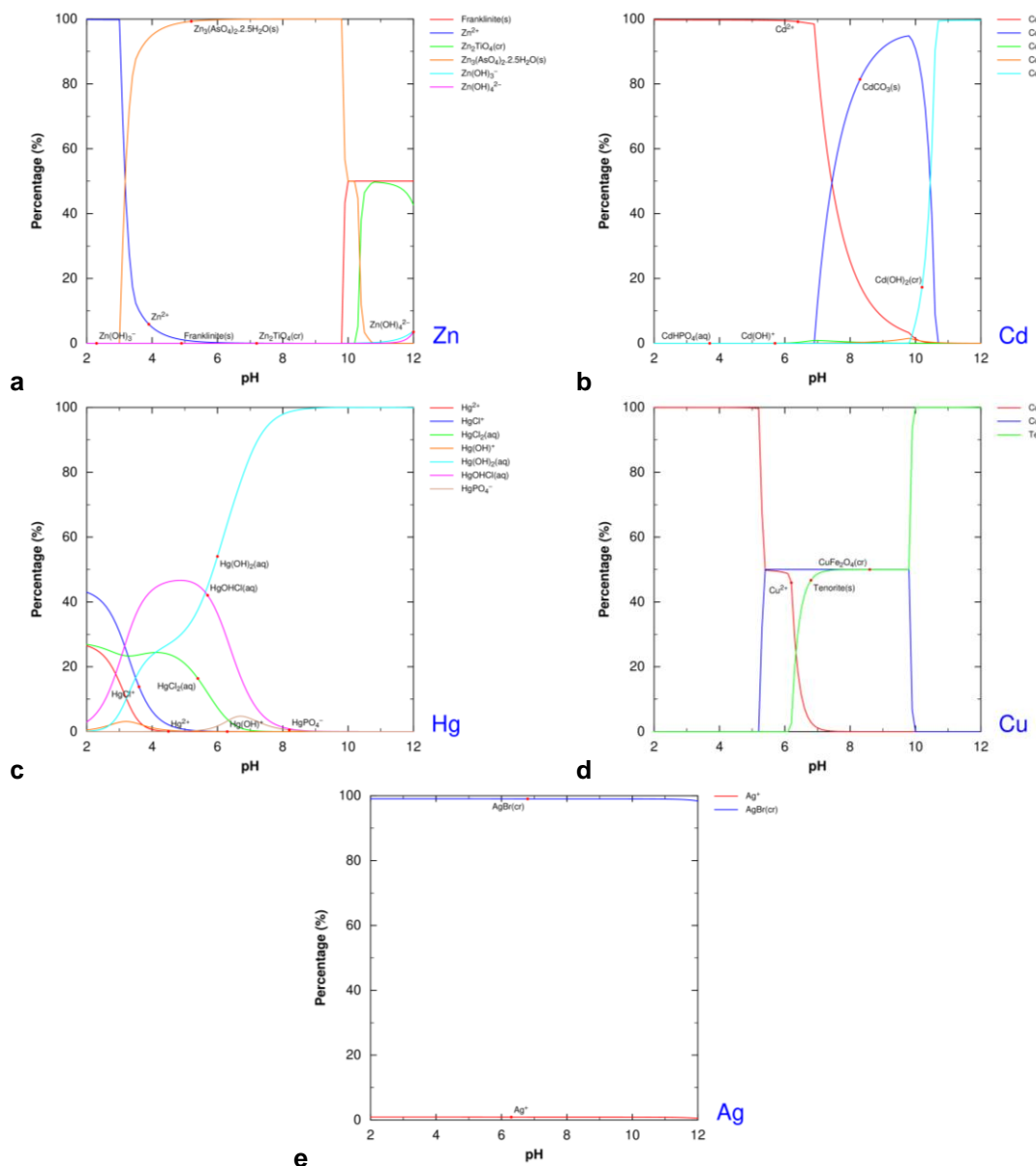


Figure 4.3-14. Speciation at $P(O_2) = 0.21 \text{ atm}$ (PHREEPLOT) of d-transition metals — Zn (a), Cd (b), Hg (c), Cu (d), and Ag (e) — in a solution containing all elements included in PRODATA at $10^{-4} \text{ mol kg}^{-1}$; the ionic strength is maintained at 0.1 mol kg^{-1} by a solution containing a hypothetical indifferent Cation/Anion electrolyte; all possible phases are allowed to precipitate; species less than 2% are not plotted; the Davies PHREEQC extraction of the database is used, excluding $\text{Ca}_2\text{ZrSi}_3\text{O}_{12}(cr)$ in the input file.

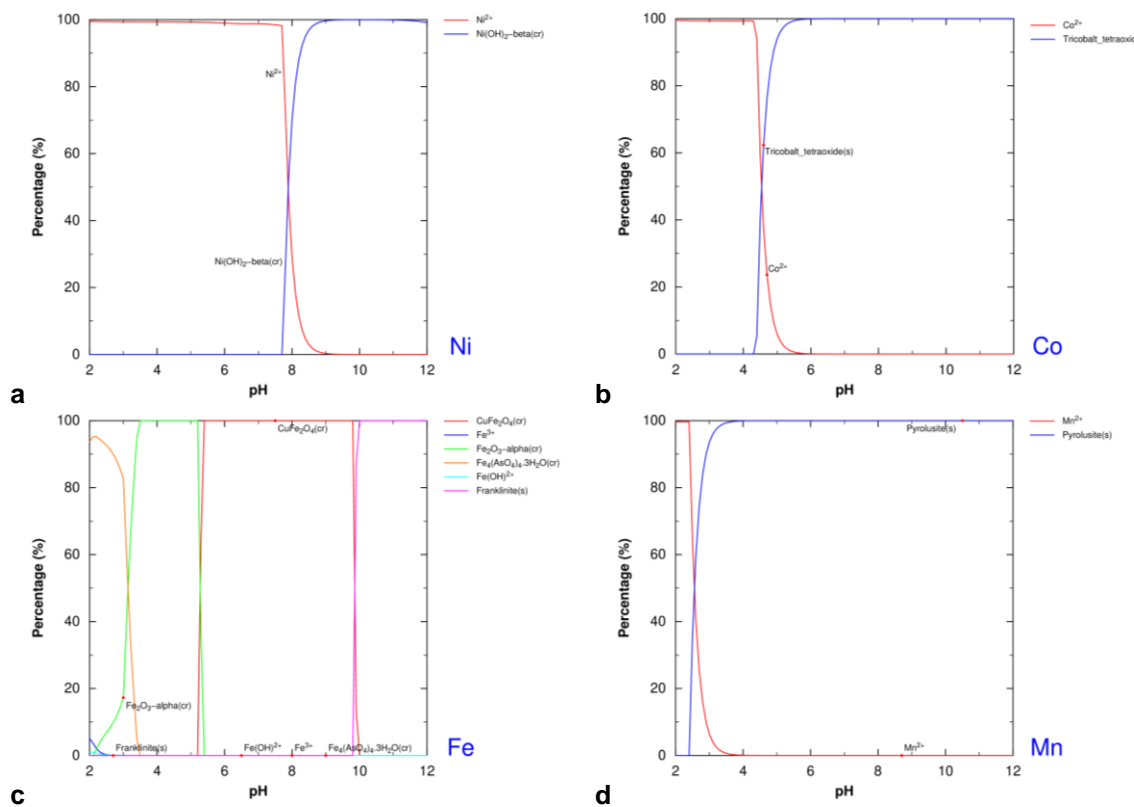


Figure 4.3-15. Speciation at $P(\text{O}_2) = 0.21 \text{ atm}$ (PHREEPLOT) of d-transition metals — Ni (a), Co (b), Fe (c), and Mn (d) — in a solution containing all elements included in PRODATA at $10^{-4} \text{ mol kg}^{-1}$; the ionic strength is maintained at 0.1 mol kg^{-1} by a solution containing a hypothetical indifferent Cation/Anion electrolyte; all possible phases are allowed to precipitate; species less than 2% are not plotted; the Davies PHREEQC extraction of the database is used, excluding $\text{Ca}_2\text{ZrSi}_3\text{O}_{12}(\text{cr})$ in the input file.

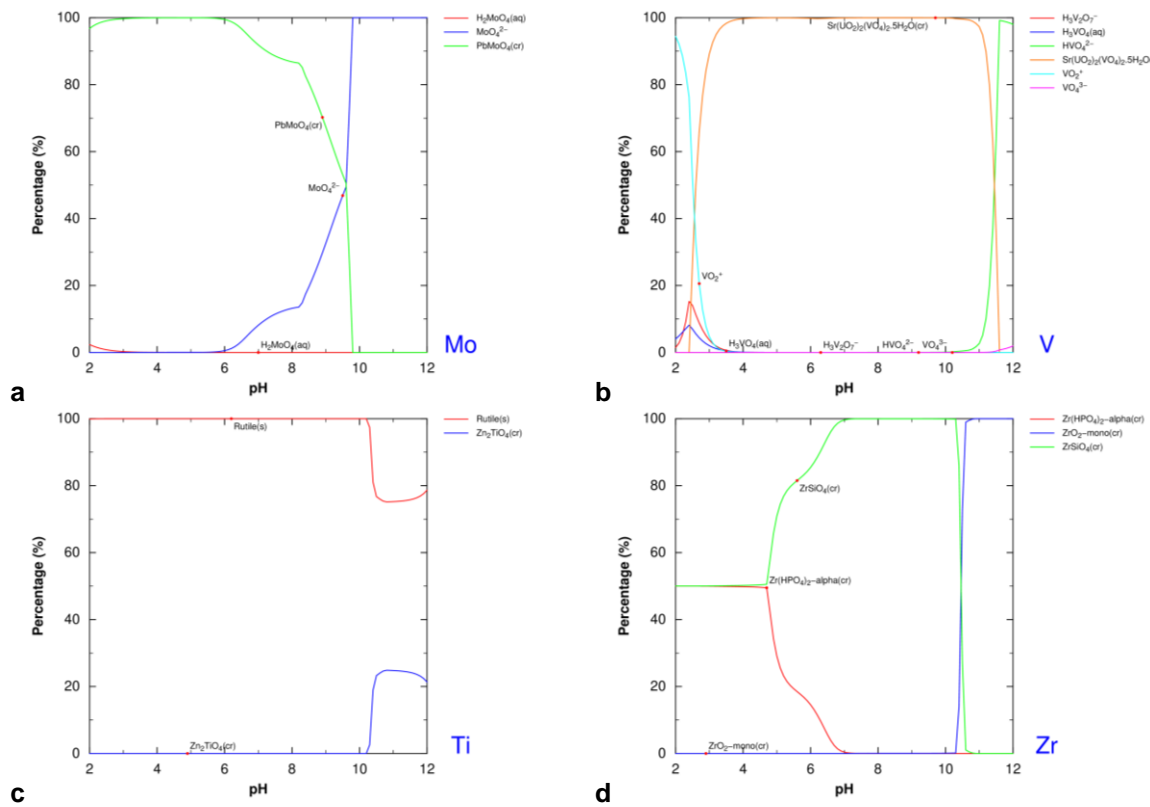


Figure 4.3-16. Speciation at $P(\text{O}_2) = 0.21 \text{ atm}$ (PHREEPLOT) of d-transition metals — Mo (a), V (b), Ti (c), and Zr (d) — in a solution containing all elements included in PRODATA at $10^{-4} \text{ mol kg}_w^{-1}$; the ionic strength is maintained at $0.1 \text{ mol kg}_w^{-1}$ by a solution containing a hypothetical indifferent Cation/Anion electrolyte; all possible phases are allowed to precipitate; species less than 2% are not plotted; the Davies PHREEQC extraction of the database is used, excluding $\text{Ca}_2\text{ZrSi}_3\text{O}_{12}(\text{cr})$ in the input file.

4.3.2.5. Actinides

The impact of the impeded precipitation of $\text{Ca}_2\text{ZrSi}_3\text{O}_{12}(\text{cr})$ on actinides under these conditions is not apparent.

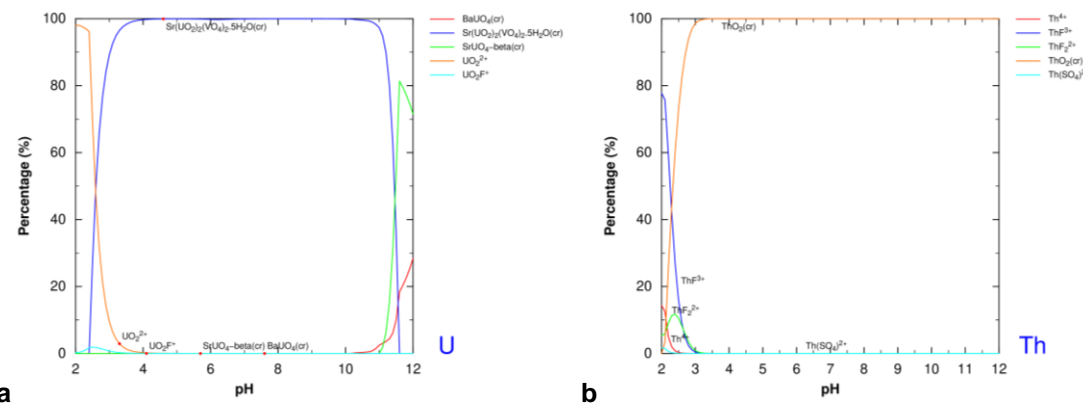


Figure 4.3-17. Speciation at $P(\text{O}_2) = 0.21 \text{ atm}$ (PHREEPLOT) of actinides — U (a), and Th (b) — in a solution containing all elements included in PRODATA at $10^{-4} \text{ mol kg}_w^{-1}$; the ionic strength is maintained at $0.1 \text{ mol kg}_w^{-1}$ by a solution containing a hypothetical indifferent Cation/Anion electrolyte; all possible phases are allowed to precipitate; species less than 2% are not plotted; the Davies PHREEQC extraction of the database is used, excluding $\text{Ca}_2\text{ZrSi}_3\text{O}_{12}(\text{cr})$ in the input file.

4.3.2.6. Alkaline earth metals

The alkaline earth metals are affected to different degrees. For magnesium, the increased precipitation of ordered phlogopite ($\text{KAlMg}_3\text{Si}_3\text{O}_{10}(\text{OH})_2$) at $\text{pH} > 10.5$ is limiting the dominance of hydrotalcite ($\text{Mg}_4\text{Al}_2(\text{OH})_{14} \cdot 3\text{H}_2\text{O}$). For calcium, only Ca^{2+} and fluorapatite ($\text{Ca}_5(\text{PO}_4)_3\text{F}$) are present. The chemistry of Sr, Ba, and Ra are unaffected under these conditions.

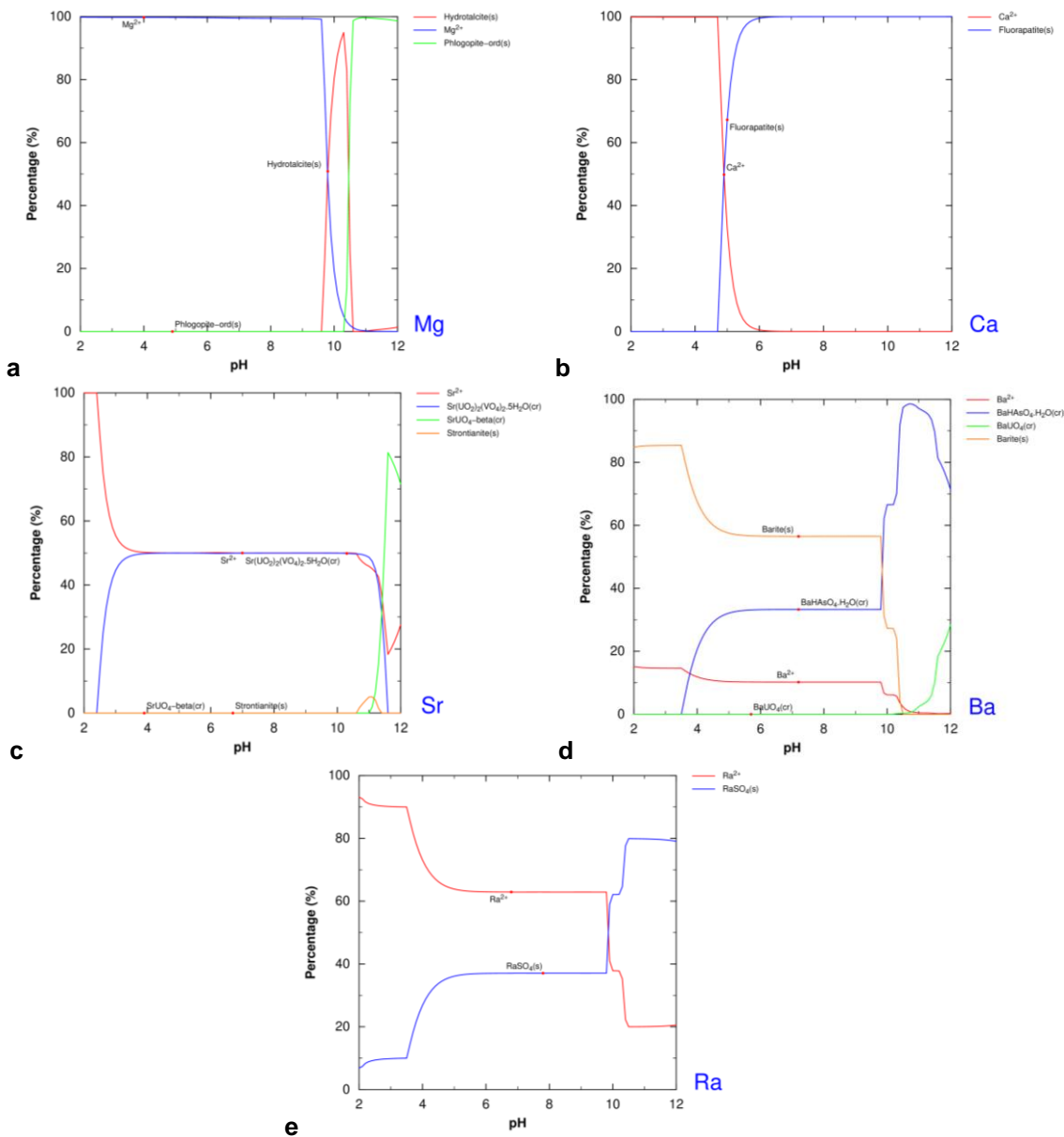


Figure 4.3-18. Speciation at $\text{P}(\text{O}_2) = 0.21 \text{ atm}$ (PHREEPLOT) of alkaline earth metals — Mg (a), Ca (b), Sr (c), Ba (d), and Ra (e) — in a solution containing all elements included in PRODATA at $10^{-4} \text{ mol kg}_w^{-1}$; the ionic strength is maintained at $0.1 \text{ mol kg}_w^{-1}$ by a solution containing a hypothetical indifferent Cation/Anion electrolyte; all possible phases are allowed to precipitate; species less than 2% are not plotted; the Davies PHREEQC extraction of the database is used, excluding $\text{Ca}_2\text{ZrSi}_3\text{O}_{12}(\text{cr})$ in the input file.

4.3.2.7. Alkaline metals

The species distribution of Li, Na, Rb, and Cs is unchanged (not shown). Even if the predominance diagrams of K are not affected (Figure 4.2-9c, and § 4.2.2.7), ordered phlogopite ($\text{KAlMg}_3\text{Si}_3\text{O}_{10}(\text{OH})_2$) is significantly present (33% at $\text{pH} > 10.7$) under these conditions (Figure 4.3-19).

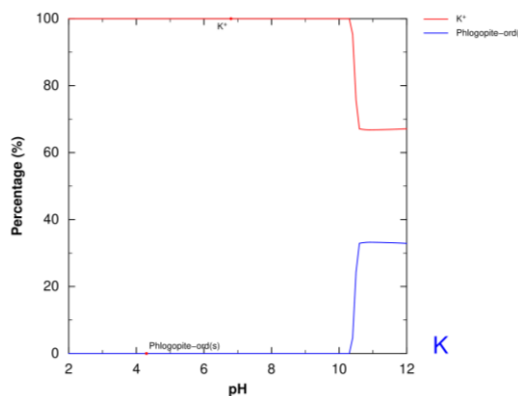


Figure 4.3-19. Speciation at $P(O_2) = 0.21$ atm (PHREEPLOT) of K in a solution containing all elements included in PRODATA at 10^{-4} mol kg_w⁻¹; the ionic strength is maintained at 0.1 mol kg_w⁻¹ by a solution containing a hypothetical indifferent Cation/Anion electrolyte; all possible phases are allowed to precipitate; species less than 2% are not plotted; the Davies PHREEQC extraction of the database is used, excluding Ca₂ZrSi₃O₁₂(cr) in the input file.

4.4. Species Repartition at 1 atm Hydrogen

The speciation diagrams — *i.e.* percentage of species vs. pH — of all the elements included in PRODATA can be calculated at $P(H_2) = 1$ atm using PHREEPLOT [2011KIN/COO]. The conditions of the calculations are the same as for the predominance Pourbaix diagrams.

4.4.1. Complete Database

4.4.1.1. Halogens

As anticipated in the Pourbaix diagram in Figure 4.2-1a, the fluorine speciation diagram at $P(H_2) = 1$ atm is not different from the one at atmospheric $P(O_2)$ (Figure 4.3-1a). The other halogens speciation is dominated by halide anions.

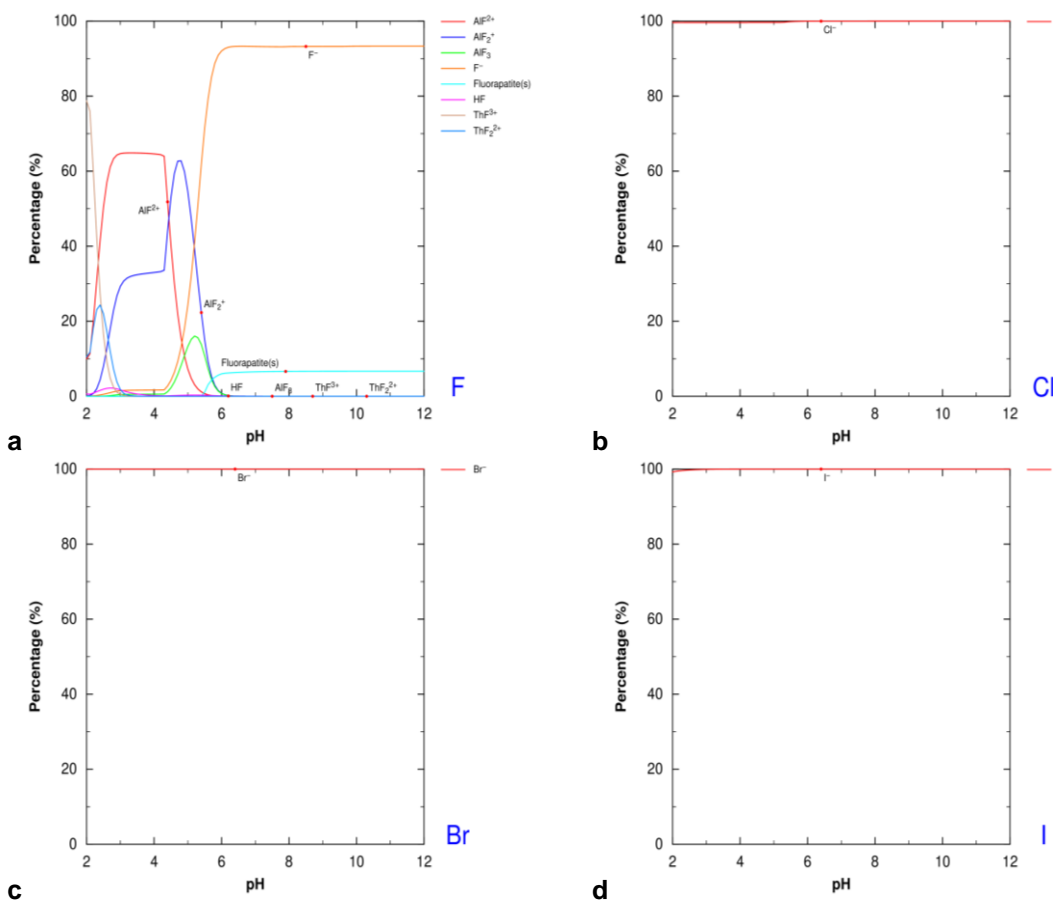


Figure 4.4-1. Speciation at $P(\text{H}_2) = 1 \text{ atm}$ (PHREEPLOT) of halogens — F (a), Cl (b), Br (c), and I (d) — in a solution containing all elements included in PRODATA at $10^{-4} \text{ mol kg}^{-1}$; the ionic strength is maintained at 0.1 mol kg^{-1} by a solution containing a hypothetical indifferent Cation/Anion electrolyte; all possible phases are allowed to precipitate; species less than 2% are not plotted; the Davies PHREEQC extraction of the database is used.

4.4.1.2. Non-metals

Sulfur is dominated by sulfide phases, pentlandite (Co_9S_8), and ca. 11% of molybdenite ($\text{MoS}_2(\text{cr})$) at $\text{pH} < 4$, and $\text{CdS}(\text{cr})$ at $\text{pH} < 8$, and sphalerite (ZnS) at $\text{pH} > 8$. Selenium is also dominated by selenide phases: clausthalite (PbSe) at $\text{pH} < 5.5$ with $\text{Cu}_2\text{Se}(\text{cr})$ as a minor phase at $\text{pH} < 2$; and $\text{CdSe}(\text{cr})$ at higher pH value with clausthalite still present up to $\text{pH} 8$. Nitrogen is present under ammonium/ammoniac acid-base equilibrium. Phosphorus is mainly present under solid phosphates of Zr, Pb, and Mn, with fluorapatite ($\text{Ca}_5(\text{PO}_4)_3\text{F}$) as a significantly present minor phase at $\text{pH} > 6$, HPO_4^{2-} and PO_4^{3-} are major at $\text{pH} > 11$. Arsenic is predominantly present as nickel arsenide phases NiAs and $\text{Ni}_{11}\text{As}_8(\text{cr})$, with the iron diarsenide loellingite (FeAs_2) as significantly present minor phase at $\text{pH} > 6.4$. Carbon is only present as $\text{CH}_4(\text{aq})$.

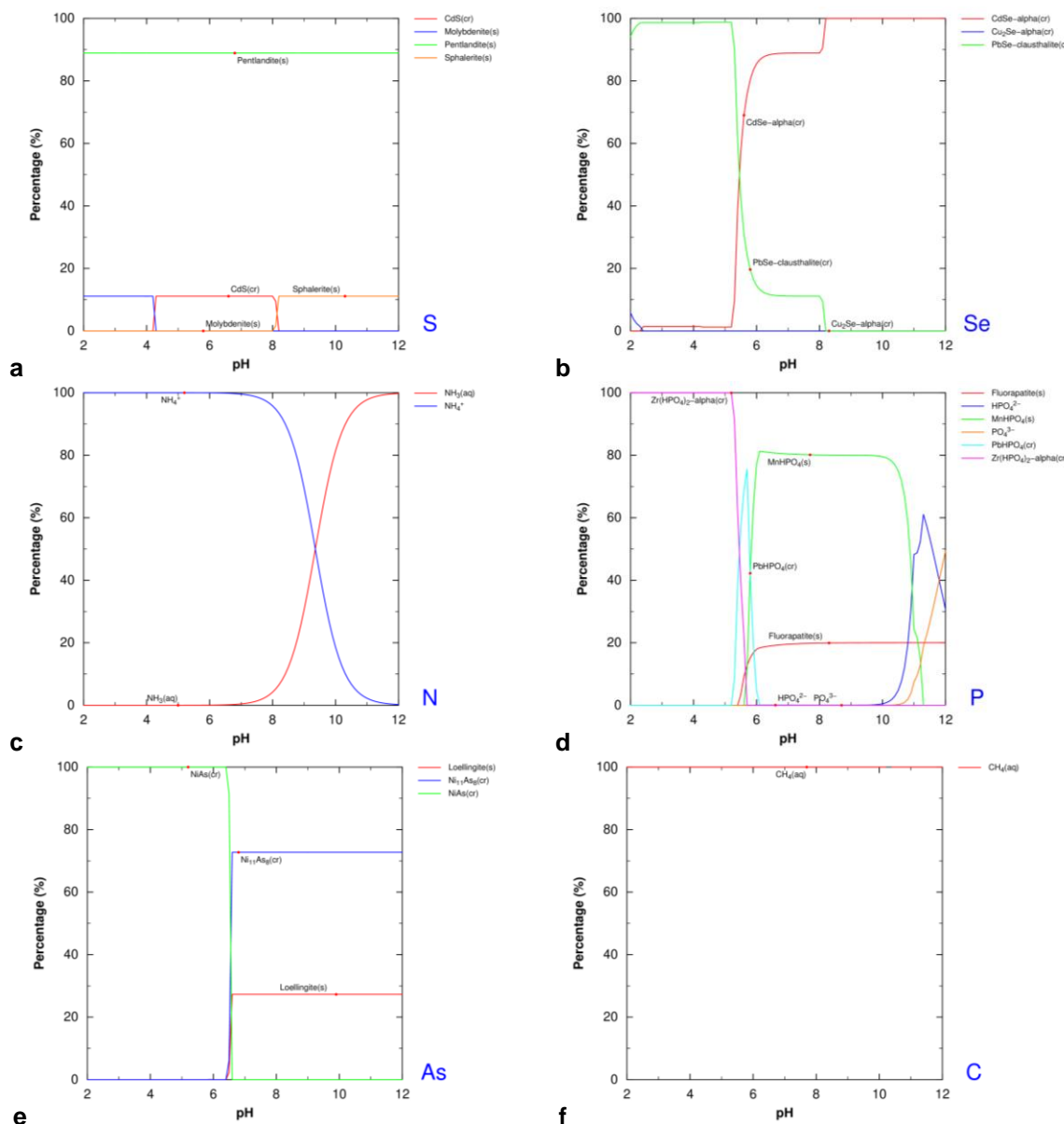


Figure 4.4-2. Speciation at $P(H_2) = 1 \text{ atm}$ (PHREEPLOT) of non-metals S (a), Se (b), N (c), P(d), As (e), and C (f) in a solution containing all elements included in PRODATA at $10^{-4} \text{ mol kg}^{-1}$; the ionic strength is maintained at 0.1 mol kg^{-1} by a solution containing a hypothetical indifferent Cation/Anion electrolyte; all possible phases are allowed to precipitate; species less than 2% are not plotted; the Davies PHREEQC extraction of the database is used.

4.4.1.3. Metalloids

As in Figure 4.2-3a, silicon is only present as $\text{Ca}_2\text{ZrSi}_3\text{O}_{12}(\text{cr})$ as no redox sensitive element is directly linked to the chemistry of Si. This particularly insoluble synthetic phase is not known to occur in natural environments. Lead is present as selenide clausthalite ($\text{PbSe}(\text{cr})$) at all pH and major at pH < 5.5, $\text{PbHPO}_4(\text{cr})$, and metallic $\text{Pb}(\text{cr})$ at higher pH. Speciation of aluminium in Figure 4.4-3c is not changed compared to Figure 4.3-3c as anticipated from Figure 4.2-3c.

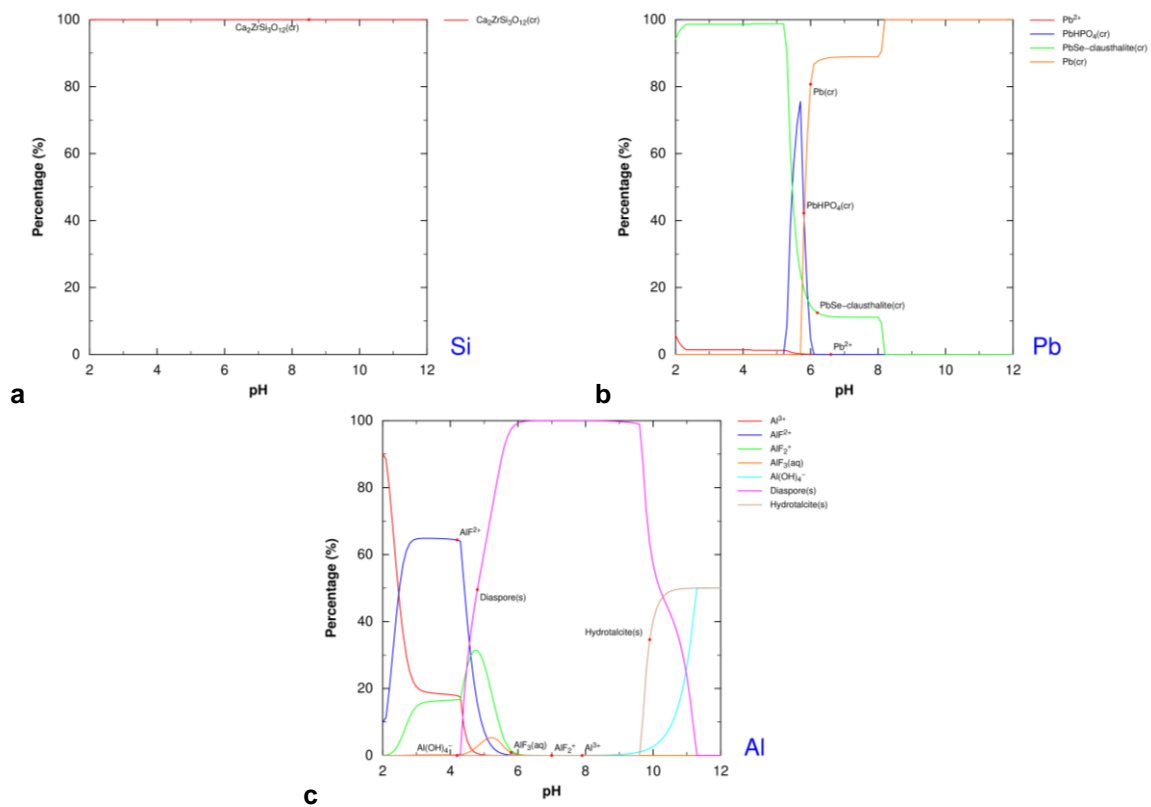


Figure 4.4-3. Speciation at $P(\text{H}_2) = 1 \text{ atm}$ (PHREEPLOT) of Si (a), Pb (b), and Al (c) in a solution containing all elements included in PRODATA at $10^{-4} \text{ mol kg}^{-1}$; the ionic strength is maintained at 0.1 mol kg^{-1} by a solution containing a hypothetical indifferent Cation/Anion electrolyte; all possible phases are allowed to precipitate; species less than 2% are not plotted; the Davies PHREEQC extraction of the database is used.

4.4.1.4. d-transition metal series

The zinc speciation dominated by Zn^{2+} at $\text{pH} < 7.8$, by $\text{Zn}_2\text{TiO}_4(\text{cr})$ up to $\text{pH} 11$, and franklinite (ZnFe_2O_4) at higher pH; sphalerite (ZnS) — from $\text{pH} 8$ — and $\text{Zn(OH)}_2(\text{cr})$ — at $\text{pH} > 11$ — are minor phases; Zn(OH)_3^- and Zn(OH)_4^{2-} are minor species. The cadmium is dominated by Cd^{2+} at $\text{pH} < 5.5$, and $\text{CdSe}(\text{cr})$ at higher pH value, with sulfide $\text{CdS}(\text{cr})$ at $\text{pH} > 4.1$ as a minor phase up to $\text{pH} 8$. Mercury is only present under its native liquid metal form. Copper is mainly present under native metallic form with a minor amount of $\alpha-\text{Cu}_2\text{Se}(\text{cr})$ at $\text{pH} < 2.2$. Silver is only present under its native metallic form.

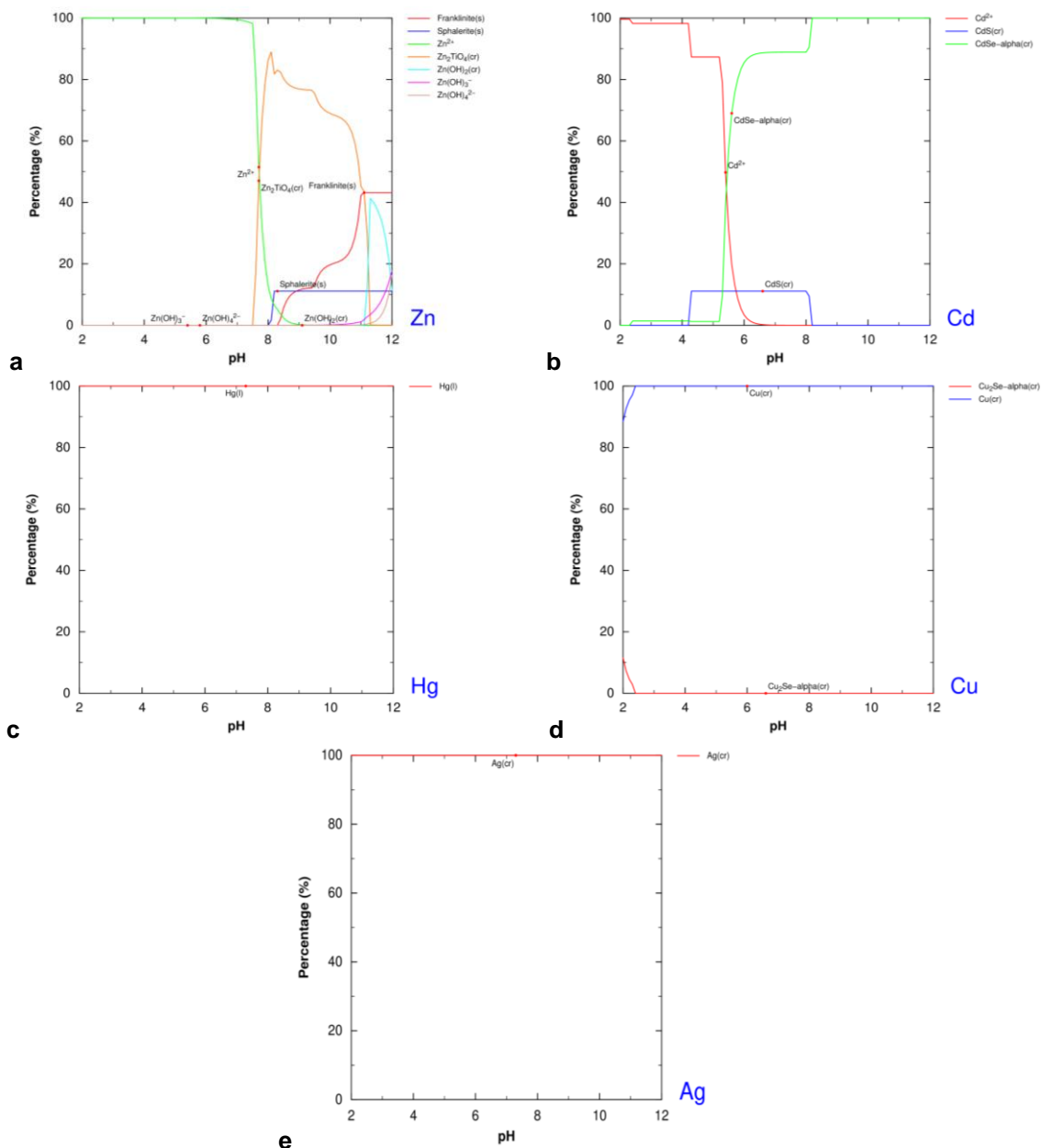


Figure 4.4-4. Speciation at $P(\text{H}_2) = 1 \text{ atm}$ (PHREEPLOT) of d-series elements Zn (a), Cd(b), (c), Cu (d), and Ag (e) in a solution containing all elements included in PRODATA at $10^{-4} \text{ mol kg}^{-1}$; the ionic strength is maintained at 0.1 mol kg^{-1} by a solution containing a hypothetical indifferent Cation/Anion electrolyte; all possible phases are allowed to precipitate; species less than 2% are not plotted; the Davies PHREEQC extraction of the database is used.

Nickel is only present under the solid arsenide forms $\text{NiAs}(\text{cr})$ at $\text{pH} < 6.4$ and $\text{Ni}_{11}\text{As}_8(\text{cr})$ at higher pH values (Figure 4.4-5a). Cobalt is only present under the form of pentlandite (Co_9S_8) (Figure 4.4-5b). Iron is present under Fe^{2+} free ion up to pH 8, ilmenite (FeTiO_3) at $8 \leq \text{pH} \leq 10.5$, and magnetite ($\alpha-\text{Fe}_3\text{O}_4$) at higher pH values; loellingite (FeAs_2) is minor but significant at $\text{pH} > 6.4$ (Figure 4.4-5c). Manganese is present as Mn^{2+} free ion at $\text{pH} < 6$, as $\text{MnHPO}_4(\text{cr})$ at $6 < \text{pH} < 11$, and pyrophanite (MnTiO_3) at higher pH values (Figure 4.4-5d).

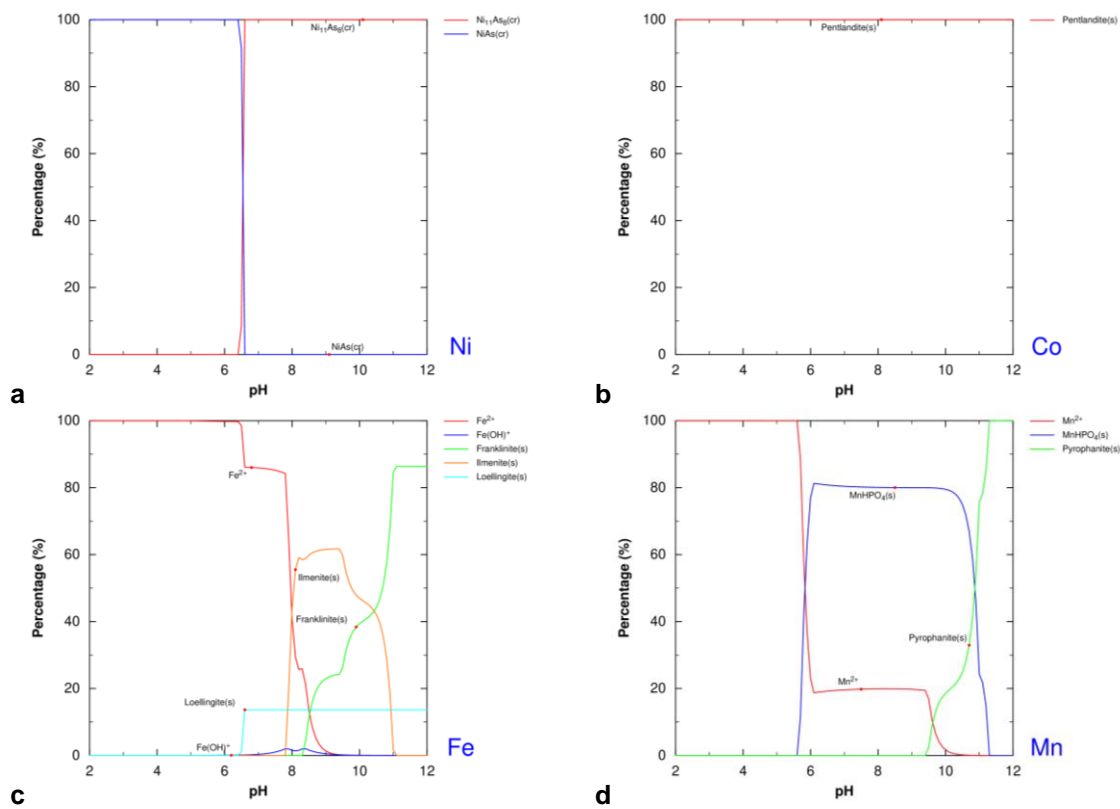


Figure 4.4-5. Speciation at $P(H_2) = 1 \text{ atm}$ (PHREEPLOT) of d-series elements Ni (a), Co(b), Fe(c), and Mn (d) in a solution containing all elements included in PRODATA at $10^{-4} \text{ mol kg}^{-1}$; the ionic strength is maintained at 0.1 mol kg^{-1} by a solution containing a hypothetical indifferent Cation/Anion electrolyte; all possible phases are allowed to precipitate; species less than 2% are not plotted; the Davies PHREEQC extraction of the database is used.

Molybdenum is mainly present under $\text{MoO}_2(\text{cr})$, and as disulphide solid molydbenite ($\text{MoS}_2(\text{cr})$) at $\text{pH} < 4.2$. Vanadium is present under V(III) aqueous species V^{3+} , $\text{V}(\text{OH})^{2+}$, and $\text{V}(\text{OH})^+$ and solid $\text{V}_2\text{O}_3(\text{cr})$ at $\text{pH} > 5.2$. Titanium is mainly brannerite (UTi_2O_6) at $\text{pH} < 8$, ilmenite (FeTiO_3) and $\text{Zn}_2\text{TiO}_4(\text{cr})$ at $8 < \text{pH} < 11$, and pyrophanite (MnTiO_3) at higher pH values. Zirconium is majorly present under α - $\text{Zr}(\text{HPO}_4)_2(\text{cr})$ at $\text{pH} < 5.5$ and monoclinic- ZrO_2 at higher pH; the insoluble synthetic $\text{Ca}_2\text{ZrSi}_3\text{O}_{12}(\text{cr})$ is constantly significantly present.

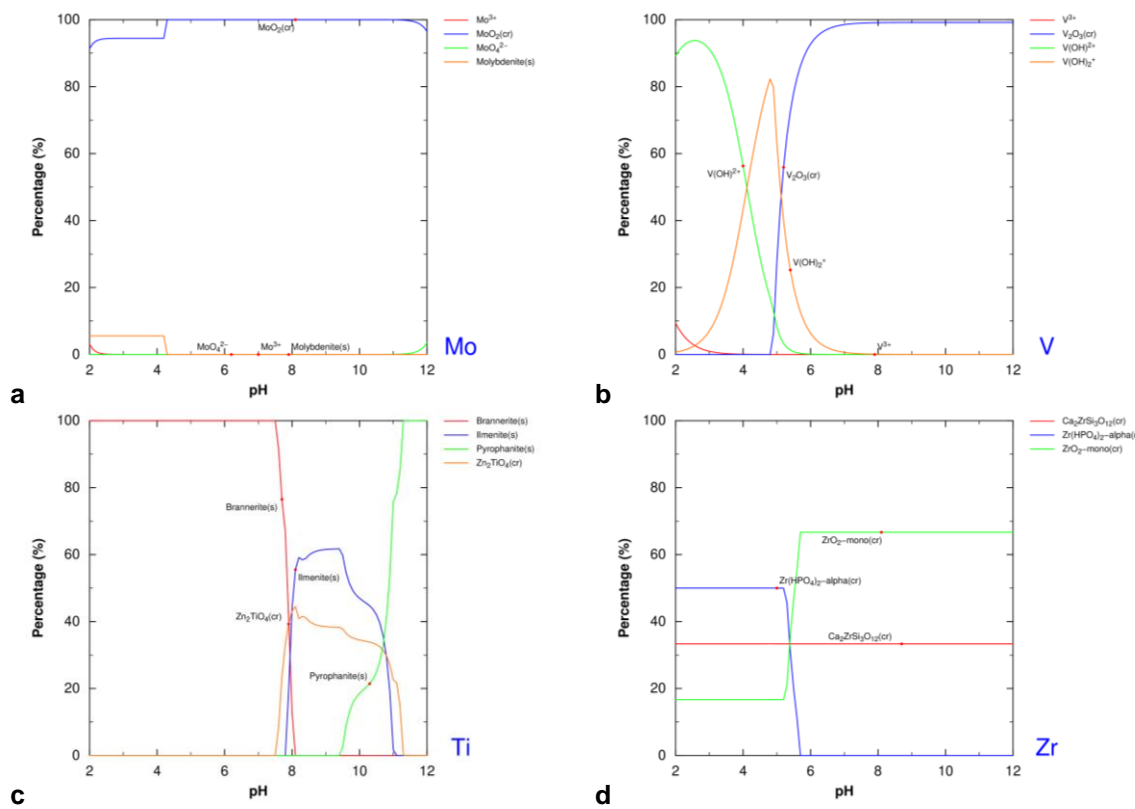


Figure 4.4-6. Speciation at $\text{P}(\text{H}_2) = 1 \text{ atm}$ (PHREEPLOT) of d-series elements Mo (a), V (b), Ti (c), and Zr (d) in a solution containing all elements included in PRODATA at $10^{-4} \text{ mol kg}^{-1}$; the ionic strength is maintained at 0.1 mol kg^{-1} by a solution containing a hypothetical indifferent Cation/Anion electrolyte; all possible phases are allowed to precipitate; species less than 2% are not plotted; the Davies PHREEQC extraction of the database is used.

4.4.1.5. Actinides

Uranium is mainly present as $\text{UO}_2(\text{cr})$ with significant proportion of brannerite (UTi_2O_6) up to pH 8 (Figure 4.4-7a). Speciation of Th is not changed compared to Figure 4.3-8b (not shown).

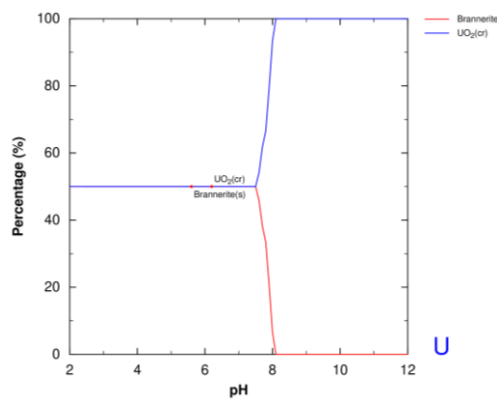


Figure 4.4-7. Speciation at $\text{P}(\text{H}_2) = 1 \text{ atm}$ (PHREEPLOT) of U in a solution containing all elements included in PRODATA at $10^{-4} \text{ mol kg}^{-1}$; the ionic strength is maintained at 0.1 mol kg^{-1} by a solution containing a hypothetical indifferent Cation/Anion electrolyte; all possible phases are allowed to precipitate; species less than 2% are not plotted; the Davies PHREEQC extraction of the database is used.

4.4.1.6. Alkaline earth metals

The magnesium and calcium speciation is not changed compared to Figure 4.3-9ab, as the elements that are redox sensitive are not amongst the major elements linked to the Mg and Ca chemistry under these conditions. The strontium, barium, and radium speciation is dominated by the free ions contrary to Figure 4.3-9cde, because of the reduction of S (Ba, Ra), As (Ba), C , V, and U (Sr).

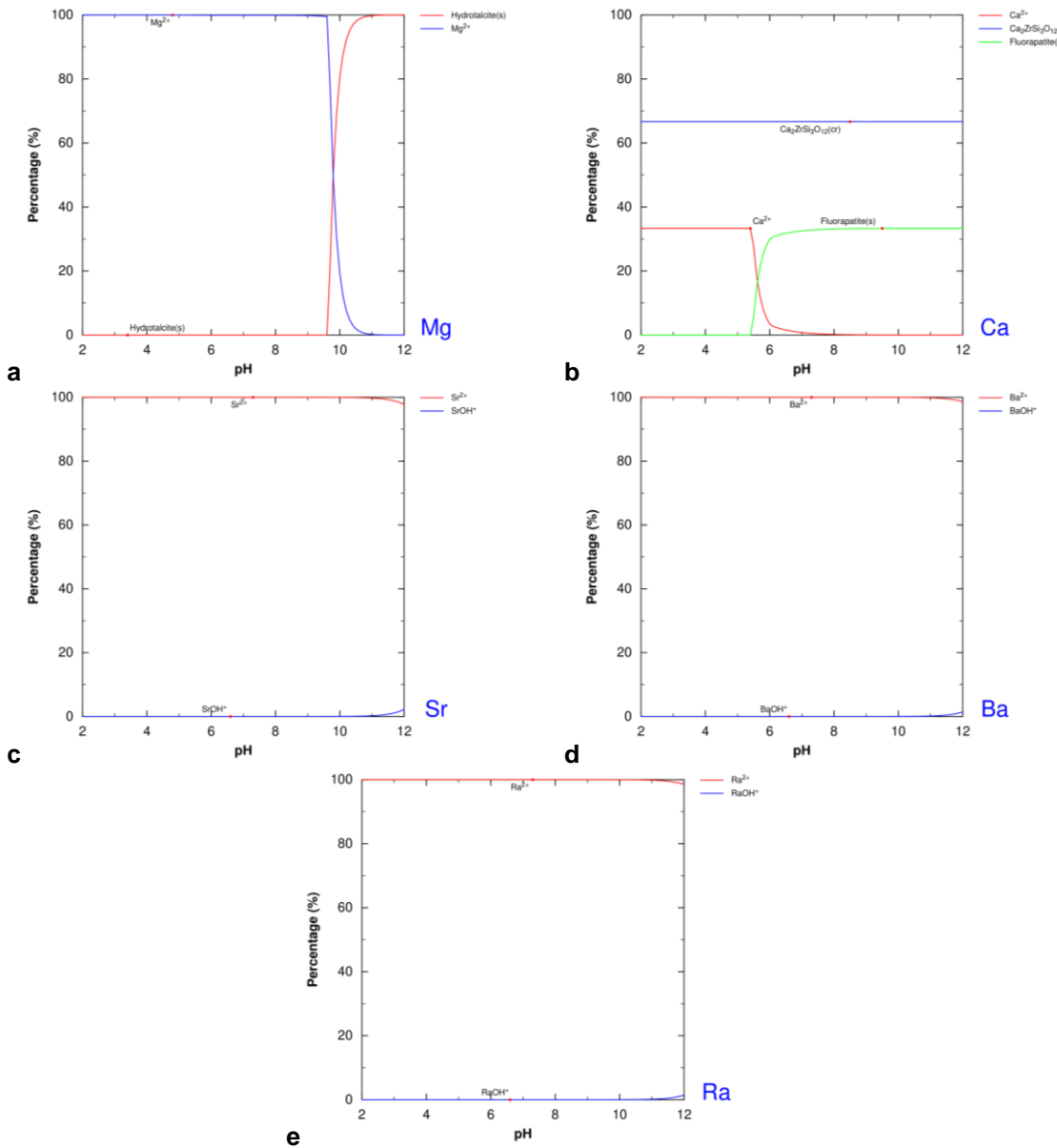


Figure 4.4-8. Speciation at $P(H_2) = 1 \text{ atm}$ (PHREEPLOT) of alkaline earth metals in a solution containing all elements included in PRODATA at $10^{-4} \text{ mol kg}^{-1}$; the ionic strength is maintained at 0.1 mol kg^{-1} by a solution containing a hypothetical indifferent Cation/Anion electrolyte; all possible phases are allowed to precipitate; species less than 1% are not plotted; the Davies PHREEQC extraction of the database is used.

4.4.1.7. Alkaline metals

As awaited, no modification of speciation is obtained for alkaline metals (not shown) compared to Figure 4.3-9.

4.4.2. Species Repartition Excluding Ca₂ZrSi₃O₁₂(cr)

4.4.2.1. Halogens

Speciation of fluorine is slightly changed as the proportion of fluorapatite (Ca₅(PO₄)₃F) is increased to 20%. The speciation of Cl, Br, and I is not changed.

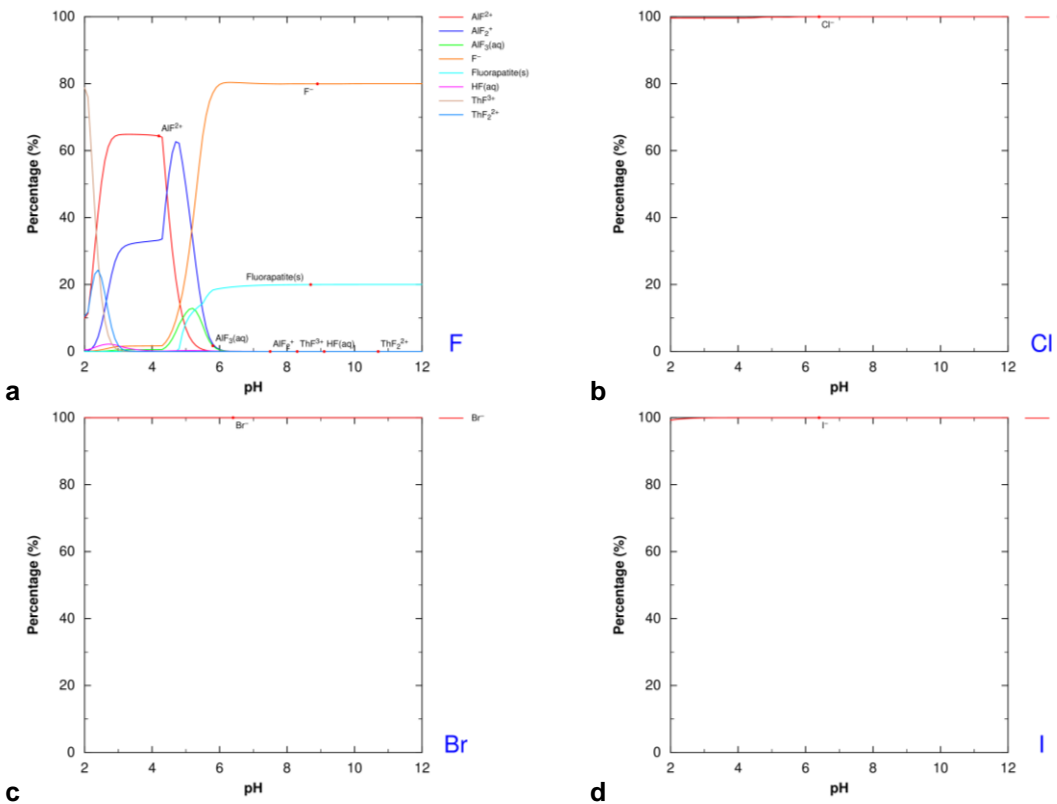


Figure 4.4-9. Speciation at P(H₂) = 1 atm (PHREEPLOT) of halogens — F (a), Cl (b), Br (c), and I (d) — in a solution containing all elements included in PRODATA at 10⁻⁴ mol kg⁻¹; the ionic strength is maintained at 0.1 mol kg⁻¹ by a solution containing a hypothetical indifferent Cation/Anion electrolyte; all possible phases are allowed to precipitate; species less than 2% are not plotted; the Davies PHREEQC extraction of the database is used, excluding Ca₂ZrSi₃O₁₂(cr) in the input file.

4.4.2.2. Non-metals

The speciation of S, N, As, and C is not changed. The speciation of Se sees a slight modification of the proportion of clauthalite (PbSe(cr)) and CdSe(cr). Fluorapatite (Ca₅(PO₄)₃F) is now dominating the speciation of P at pH > 6.

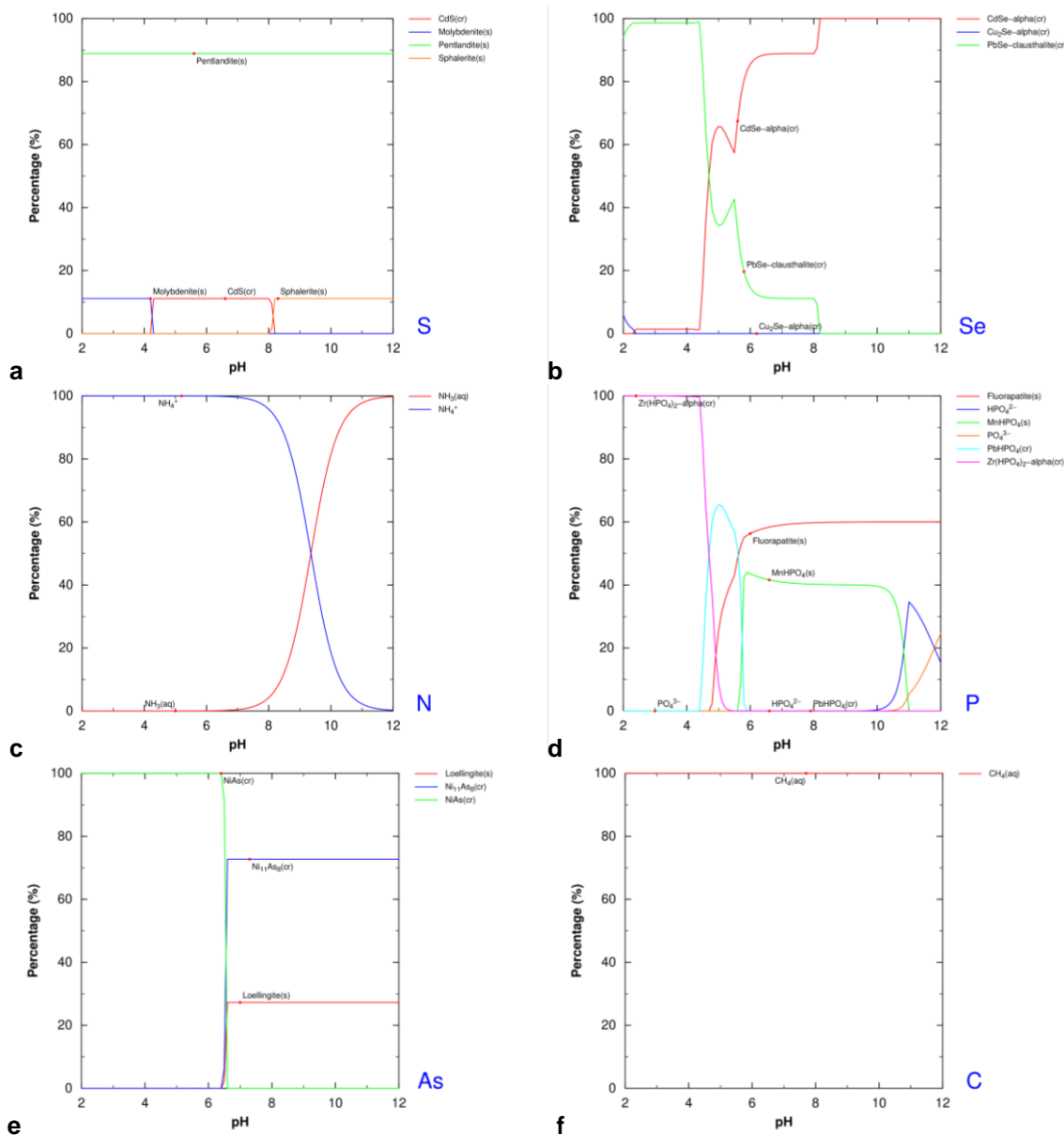


Figure 4.4-10. Speciation at $P(H_2) = 1 \text{ atm}$ (PHREEPLOT) of non-metals S (a), Se (b), N (c), P(d), As (e), and C (f) in a solution containing all elements included in PRODATA at $10^{-4} \text{ mol kg}^{-1}$; the ionic strength is maintained at 0.1 mol kg^{-1} by a solution containing a hypothetical indifferent Cation/Anion electrolyte; all possible phases are allowed to precipitate; species less than 2% are not plotted; the Davies PHREEQC extraction of the database is used excluding $\text{Ca}_2\text{ZrSi}_3\text{O}_{12}(\text{cr})$.

4.4.2.3. Metalloids

The speciation of Si is totally changed, as $\text{ZrSiO}_4(\text{cr})$ and $\text{Si(OH)}_4(\text{aq})$ are sharing dominance at $\text{pH} < 5$. $\text{ZrSiO}_4(\text{cr})$ is dominant up to $\text{pH} 10.5$, with $\text{Si(OH)}_4(\text{aq})$, willemite (Zn_2SiO_4); ordained phlogopite ($\text{KAlMg}_3\text{Si}_3\text{O}_{10}(\text{OH})_2$) is dominant at $\text{pH} > 10.5$. The speciation of Pb allows explaining the modification of Se speciation, as clausthalite (PbSe), $\text{PbHPO}_4(\text{cr})$, and $\text{Pb}(\text{cr})$ are in greater competition at $\text{pH} < 8$ than in Figure 4.4-3b. The precipitation of ordered phlogopite ($\text{KAlMg}_3\text{Si}_3\text{O}_{10}(\text{OH})_2$) is changing the speciation of Al at $\text{pH} > 8.5$.

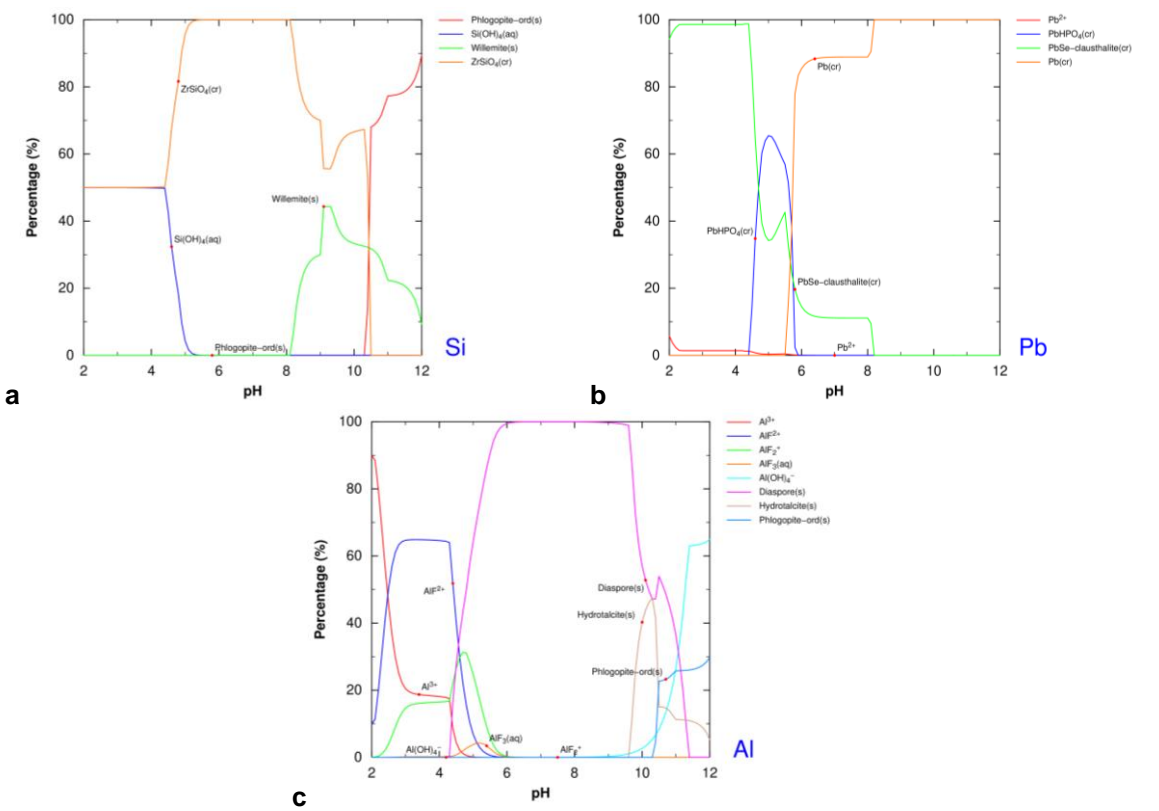


Figure 4.4-11. Speciation at $P(H_2) = 1 \text{ atm}$ (PHREEPLOT) of metalloids — Si (a), Pb (b), and Al (c) — in a solution containing all elements included in PRODATA at $10^{-4} \text{ mol kg}^{-1}$; the ionic strength is maintained at 0.1 mol kg^{-1} by a solution containing a hypothetical indifferent Cation/Anion electrolyte; all possible phases are allowed to precipitate; species less than 2% are not plotted; the Davies PHREEQC extraction of the database is used, excluding $\text{Ca}_2\text{ZrSi}_3\text{O}_{12}(\text{cr})$ in the input file.

4.4.2.4. d-transition metals

The precipitation of willemite (Zn_2SiO_4) changes the speciation of Zn at $8.5 < \text{pH} < 11$ at the expenses of $\text{Zn}_2\text{TiO}_4(\text{cr})$. The effect of Pb-Se-P speciation is also affecting the Cd-Se speciation as already seen in Figure 4.4-10b. the speciation of Hg, Cu, and Ag is not changed.

The speciation of Ni and Co are not changed. The higher precipitation of willemite (Figure 4.4-12) is limiting the precipitation of $\text{Zn}_2\text{TiO}_4(\text{cr})$ and promote precipitation of ilmenite (FeTiO_3). The change in P speciation is limiting the precipitation of $\text{MnHPO}_4(\text{cr})$.

There is no change in the Mo and V speciation. As for Fe, the higher precipitation of willemite — Zn_2SiO_4 , see Figure 4.4-12 — is limiting the precipitation of $\text{Zn}_2\text{TiO}_4(\text{cr})$ and promoting the precipitation of ilmenite (FeTiO_3). $\text{ZrSiO}_4(\text{cr})$ and $\alpha\text{-Zr}(\text{HPO}_4)_2(\text{cr})$ are now sharing predominance up to pH 5, where $\text{ZrSiO}_4(\text{cr})$ becomes dominant with $\alpha\text{-Zr}(\text{HPO}_4)_2(\text{cr})$ and mono-ZrO₂ up to pH 10.5; mono-ZrO₂ is dominant at higher pH values.

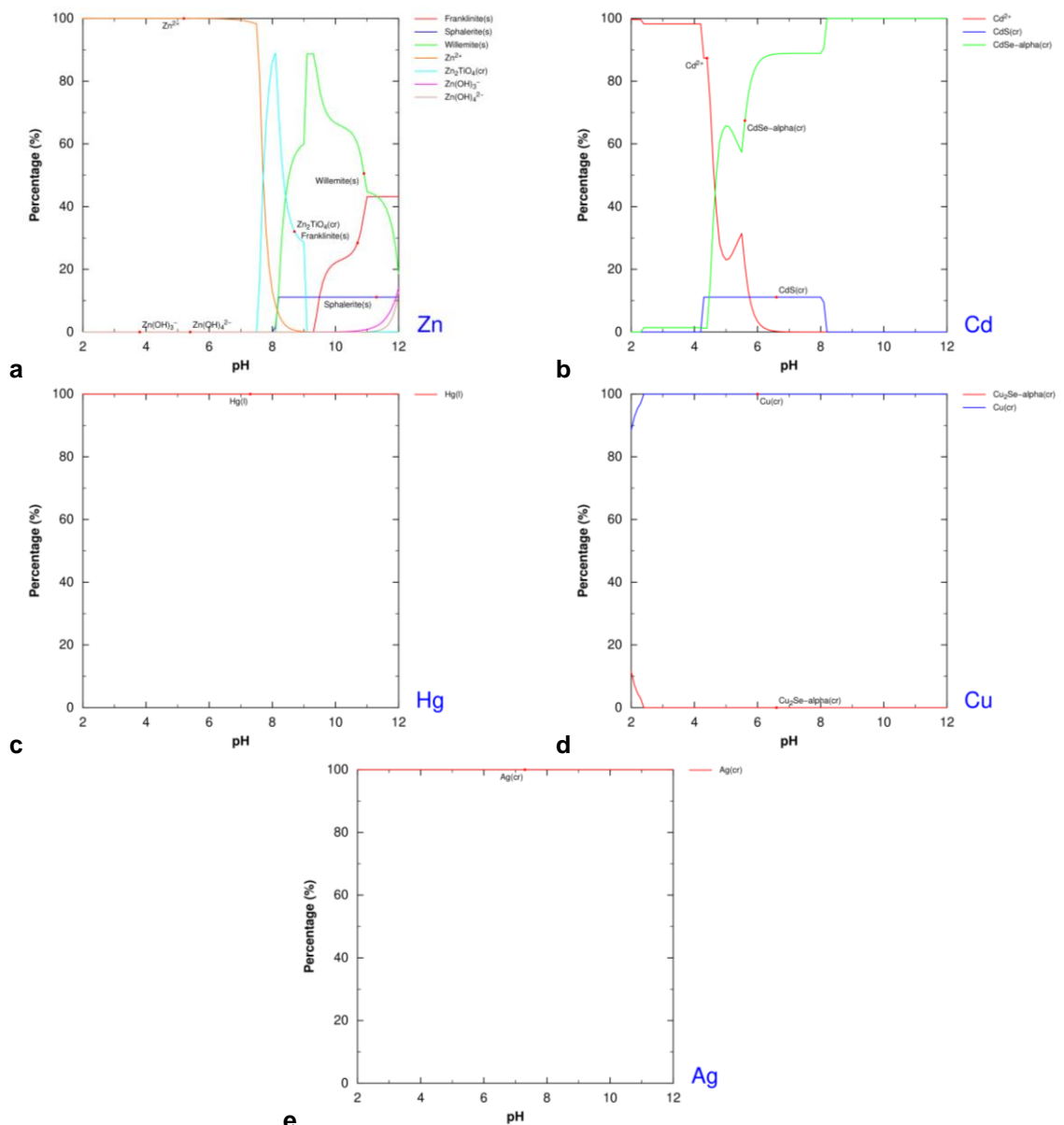


Figure 4.4-12. Speciation at $P(\text{H}_2) = 1 \text{ atm}$ (PHREEPLOT) of d-transition metals Zn (a), Cd (b), Hg (c), Cu(d), and Ag (e) in a solution containing all elements included in PRODATA at $10^{-4} \text{ mol kg}_w^{-1}$; the ionic strength is maintained at $0.1 \text{ mol kg}_w^{-1}$ by a solution containing a hypothetical indifferent Cation/Anion electrolyte; all possible phases are allowed to precipitate; species less than 2% are not plotted; the Davies PHREEQC extraction of the database is used excluding $\text{Ca}_2\text{ZrSi}_3\text{O}_{12}(\text{cr})$.

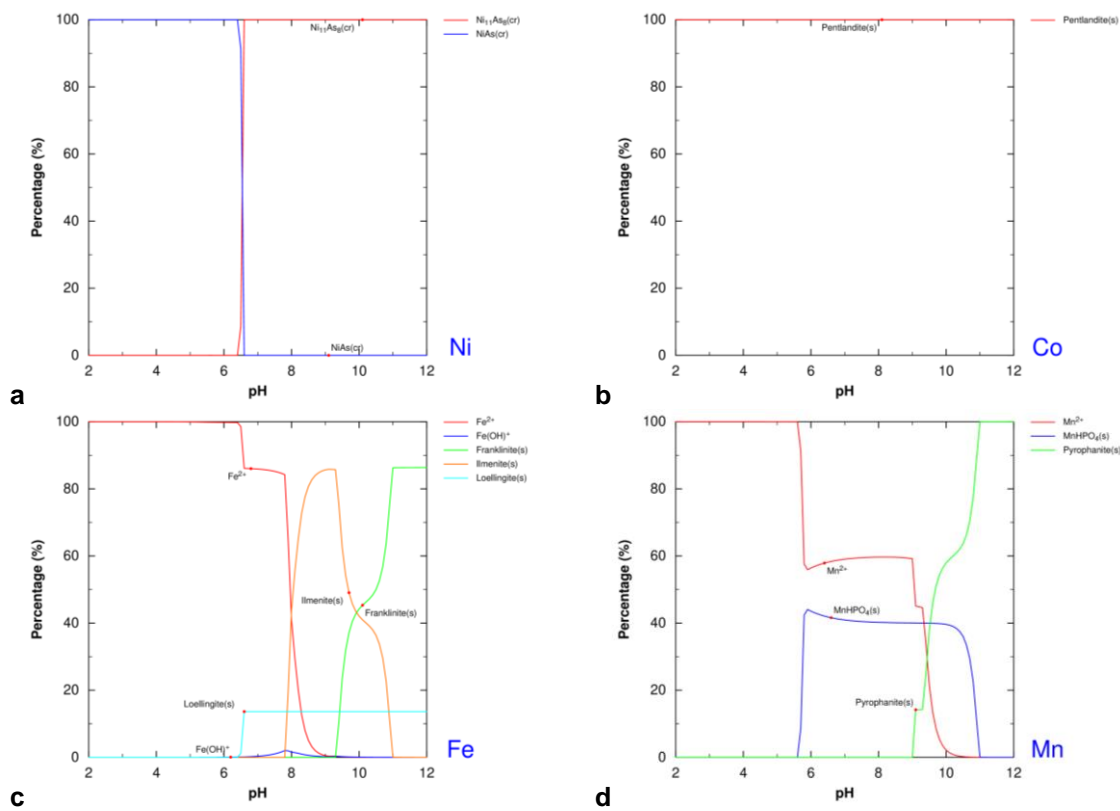


Figure 4.4-13. Speciation at $P(H_2) = 1 \text{ atm}$ (PHREEPLOT) of d-transition metals Ni (a), Co (b), Fe (c), and Mn (d) in a solution containing all elements included in PRODATA at $10^{-4} \text{ mol kg}_w^{-1}$; the ionic strength is maintained at $0.1 \text{ mol kg}_w^{-1}$ by a solution containing a hypothetical indifferent Cation/Anion electrolyte; all possible phases are allowed to precipitate; species less than 2% are not plotted; the Davies PHREEQC extraction of the database is used excluding Ca₂ZrSi₃O₁₂(cr).

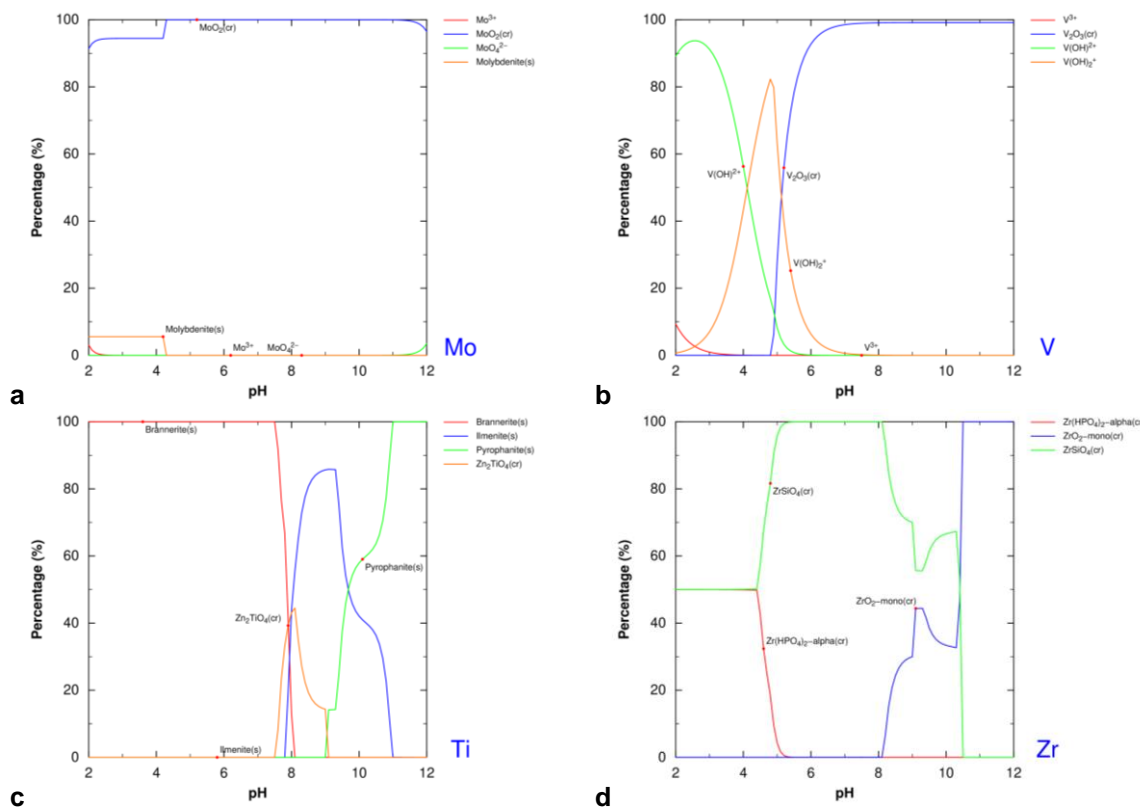


Figure 4.4-14. Speciation at $P(H_2) = 1 \text{ atm}$ (PHREEPLOT) of d-transition metals Mo (a), V (b), Ti (c), and Zr (d) in a solution containing all elements included in PRODATA at $10^{-4} \text{ mol kg}_w^{-1}$; the ionic strength is maintained at $0.1 \text{ mol kg}_w^{-1}$ by a solution containing a hypothetical indifferent Cation/Anion electrolyte; all possible phases are allowed to precipitate; species less than 2% are not plotted; the Davies PHREEQC extraction of the database is used excluding $\text{Ca}_2\text{ZrSi}_3\text{O}_{12}(\text{cr})$.

4.4.2.5. Actinides

The speciation of U and Th is not modified (not shown).

4.4.2.6. Alkaline earth metals

The precipitation of ordered phlogopite ($\text{KAlMg}_3\text{Si}_3\text{O}_{10}(\text{OH})_2$) is changing the speciation of Mg at $\text{pH} > 10.5$. The exclusion of synthetic $\text{Ca}_2\text{ZrSi}_3\text{O}_{12}(\text{cr})$ is leaving only Ca^{2+} and fluorapatite ($\text{Ca}_5(\text{PO}_4)_3\text{F}$) as major species. There is no change in the speciation of Sr, Ba and Ra.

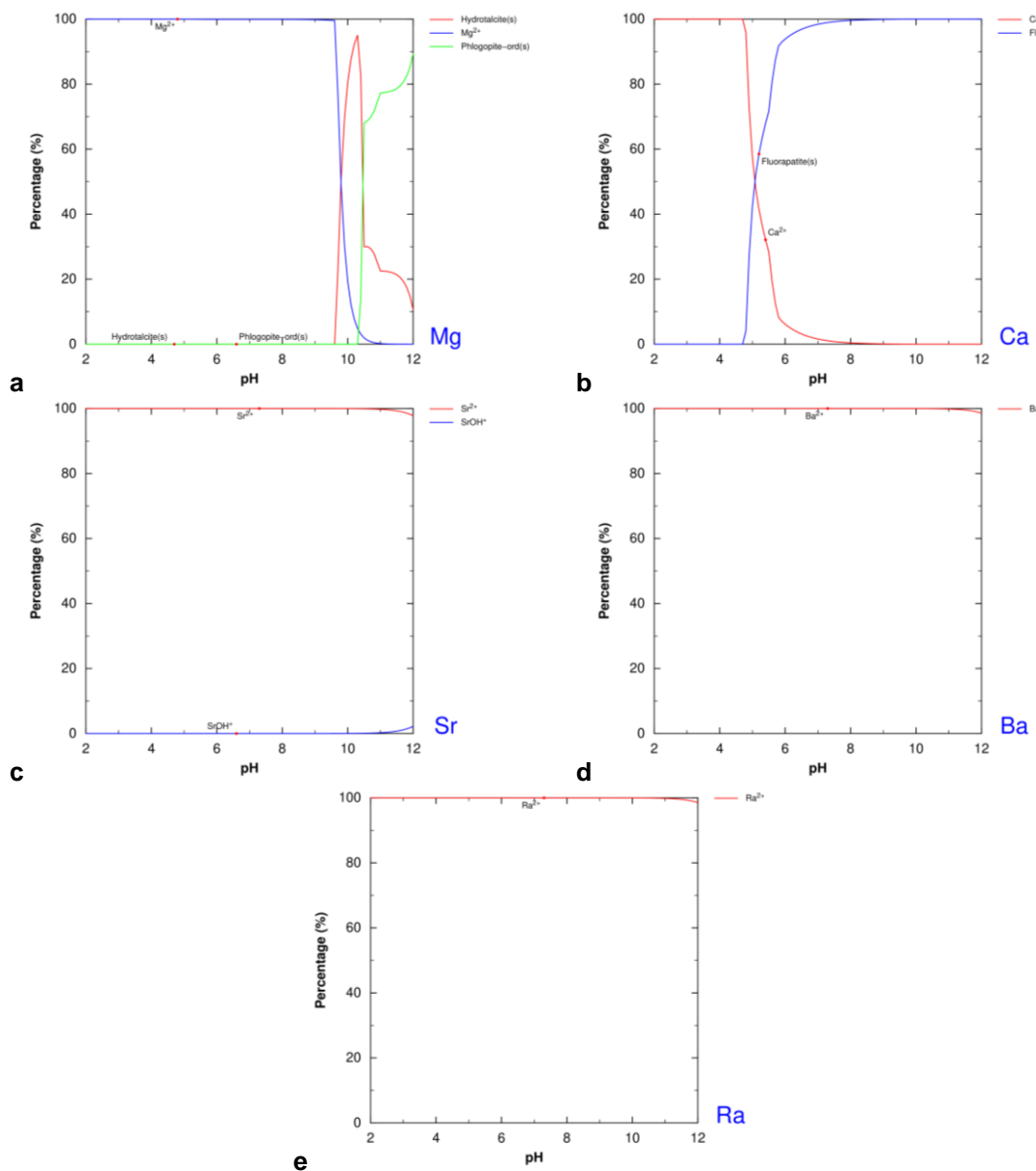


Figure 4.4-15. Speciation at $P(H_2) = 1 \text{ atm}$ (PHREEPLOT) of alkaline earth metals Mg (a), Ca (b), Sr (c), Ba (d), and Ra (e) in a solution containing all elements included in PRODATA at $10^{-4} \text{ mol kg}^{-1}$; the ionic strength is maintained at 0.1 mol kg^{-1} by a solution containing a hypothetical indifferent Cation/Anion electrolyte; all possible phases are allowed to precipitate; species less than 2% are not plotted; the Davies PHREEQC extraction of the database is used excluding Ca₂ZrSi₃O₁₂(cr).

4.4.2.7. Alkaline metals

The precipitation of ordered phlogopite ($\text{KAlMg}_3\text{Si}_3\text{O}_{10}(\text{OH})_2$) is modifying the K speciation above pH 10, even if K⁺ is still major. There is no change in Li, Na, Rb, and Cs speciation (not shown).

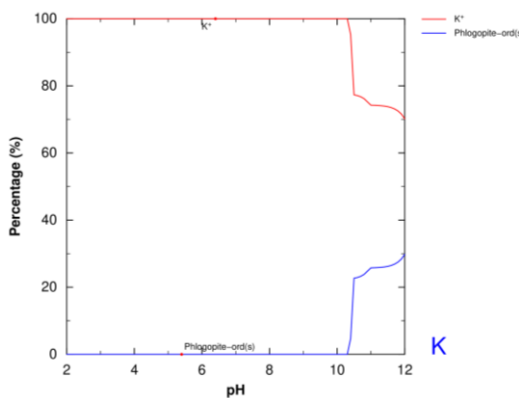


Figure 4.4-16. Speciation at $P(H_2) = 1 \text{ atm}$ (PHREEPLOT) of K in a solution containing all elements included in PRODATA at $10^{-4} \text{ mol kg}_w^{-1}$; the ionic strength is maintained at $0.1 \text{ mol kg}_w^{-1}$ by a solution containing a hypothetical indifferent Cation/Anion electrolyte; all possible phases are allowed to precipitate; species less than 2% are not plotted; the Davies PHREEQC extraction of the database is used excluding $\text{Ca}_2\text{ZrSi}_3\text{O}_{12}(\text{cr})$.

4.5. Predominance in Sulphate-Carbonate media

Reiller and Descotes [2020REI/DES] proposed predominance plots of uranium in an $a(\text{SO}_4^{2-})$ -pH space at varying pCO_2 ($-\log_{10} P(\text{CO}_2)$) to represent the speciation evolution, from ISR process to environmental monitoring. In the following section, we will build the corresponding predominance plots for metals that are sensible to both of these parameters, *i.e.*, Pb, Fe, U, Ba, and Ra. In view of the ionic strength variations, the SIT extraction of PRODATA will be used.

4.5.1. Lead and Iron

The predominance diagram of Pb (Figure 4.5-1) and Fe (Figure 4.5-2) at $\text{pCO}_2 = 2.64, 2.4$, and 1.8 are plotted using Phreeplot. The repartition of the predominant species is not strongly affected by the variation, with the exception of $\text{Pb}(\text{CO}_3)_n^{(2-n)+}$ and $\text{Fe(OH)}_n(\text{CO}_3)_m^{(3-n-2m)+}$ species, which are occurring at lower pH value with decreasing pCO_2 .

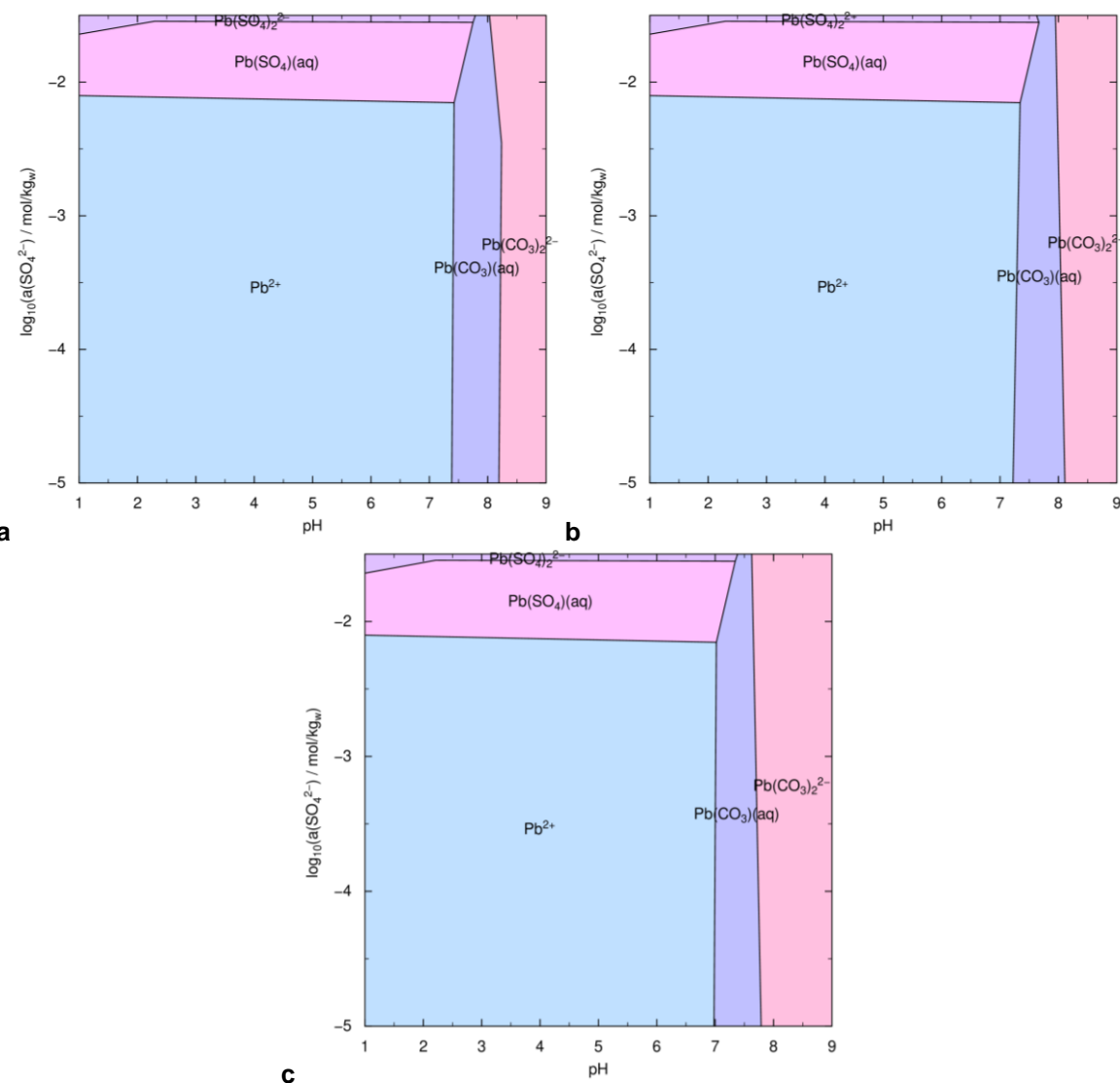


Figure 4.5-1. Predominance plot (PHREEPLOT) of $1 \mu\text{mol kg}^{-1}$ Pb, in a 0.1 mol kg^{-1} HClO_4 solution with increasing $a(\text{SO}_4^{2-})$ and pH, and fixed total carbonate defined in Reiller and Descostes [2020REI/DES]: $p\text{CO}_2 = 2.6$ (a), 2.4 (b), and 1.8 (c); the SIT PHREEQC extraction of the database is used.

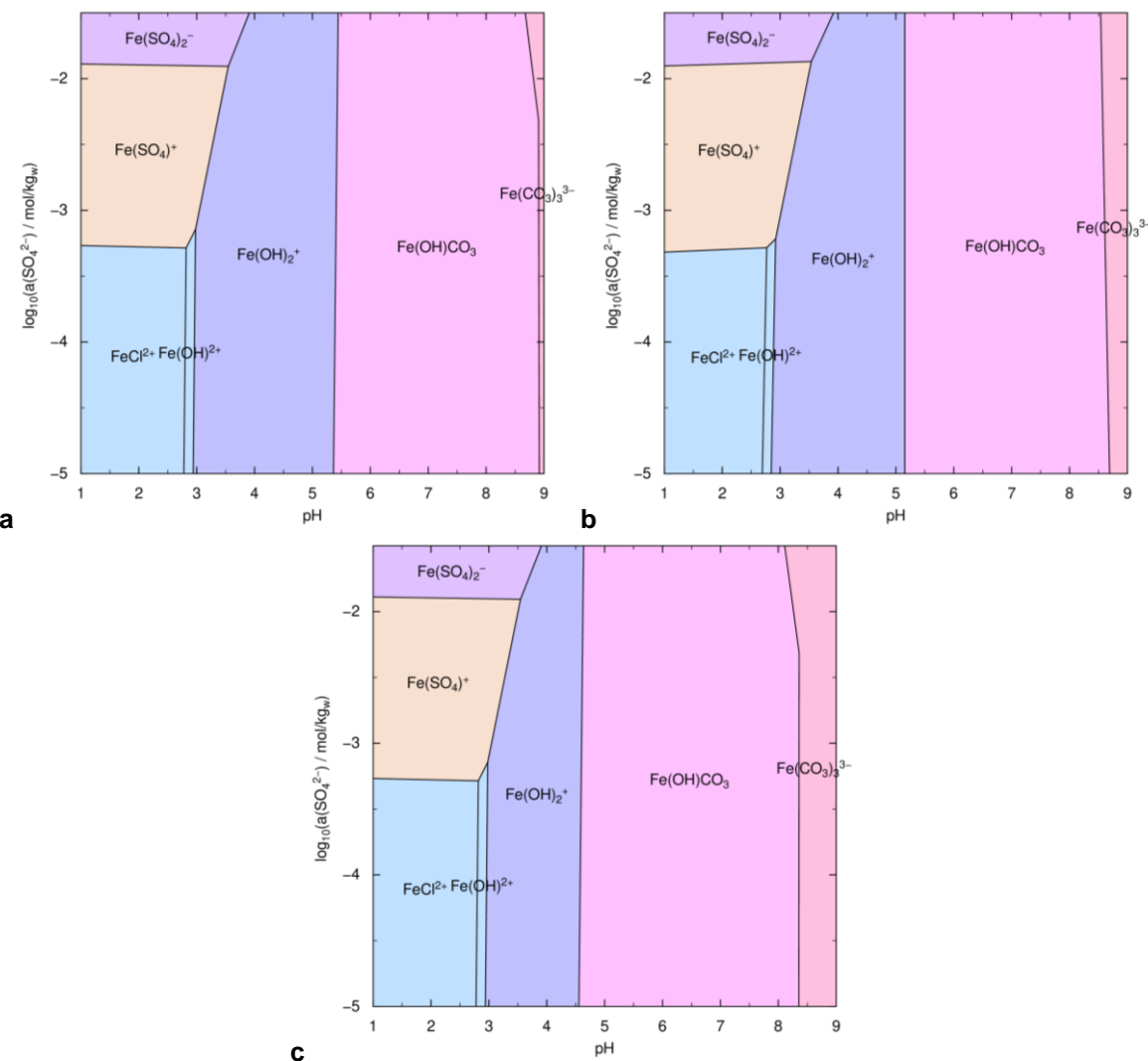


Figure 4.5-2. Predominance plot (PHREEPLOT) of 1 $\mu\text{mol kg}_w^{-1}$ Fe at $P(\text{O}_2) = 0.21 \text{ atm}$, in a $0.1 \text{ mol kg}_w^{-1}$ HClO_4 solution with increasing $a(\text{SO}_4^{2-})$ and pH, and fixed total carbonate defined in Reiller and Descostes [2020REI/DES]: $p\text{CO}_2 = 2.6$ (a), 2.4 (b), and 1.8 (c); the SIT PHREEQC extraction of the database is used.

4.5.2. Uranium

In Reiller and Descostes [2020REI/DES], the relative importance of the $\text{MgUO}_2(\text{CO}_3)_3^{2-}$ complex was due to the high specific ion interaction coefficient $\epsilon(\text{Na}^+, \text{MgUO}_2(\text{CO}_3)_3^{2-})$ value from Dong and Brooks [2008DON/BRO]. In view of the recent determination of the thermodynamic constants and specific ion interaction coefficient from Shang et al. [2020aSHA/REI; 2020bSHA/REI; 2021aSHA/REI], these predominance plots can be redrawn in Figure 4.5-3. As shown in Shang and Reiller [2021aSHA/REI], the predominance of $\text{MgUO}_2(\text{CO}_3)_3^{2-}$ is not likely under these conditions. This complex can nevertheless occur in seawater [2021aSHA/REI].

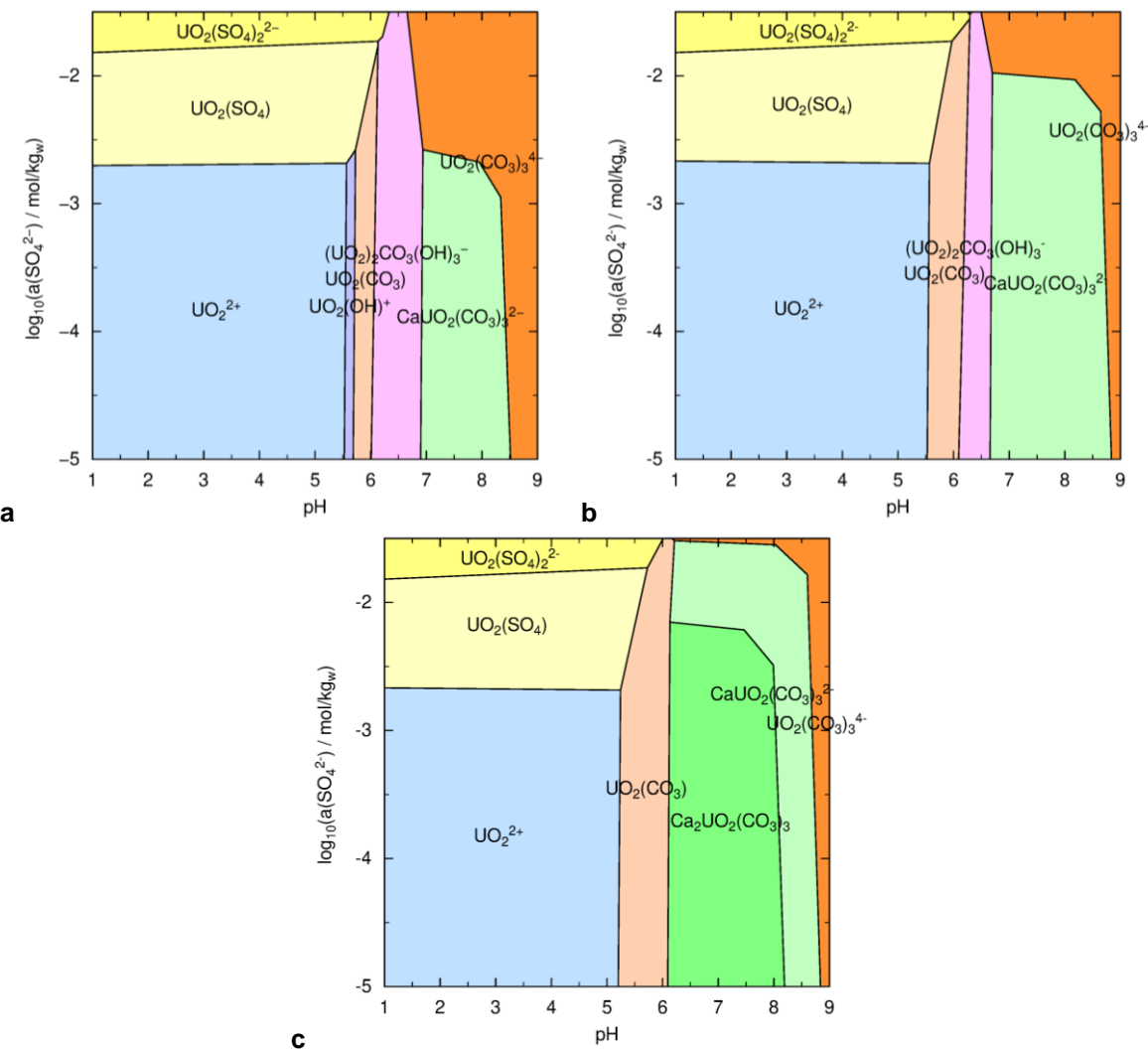


Figure 4.5-3. Predominance plot (PHREEPLOT) of 10^{-6} mol kg_w⁻¹ U at P(O₂) = 0,2095 atm in a 0.1 mol kg_w⁻¹ HClO₄ solution with increasing a(SO₄²⁻) and pH, and fixed total concentration of Ca, Mg, and total carbonate defined in Reiller and Descostes [2020REI/DES]: pCa = pMg = 3.2, pCO₂ = 2.6 (a); pCa = pMg = 2.8, pCO₂ = 2.4 (b); and pCa = 2.0, pMg = 2.2, pCO₂ = 1.8 (c); no phases were allowed to precipitate; the SIT PHREEQC extraction of the database is used.

4.5.3. Barium and Radium

The predominance plots from barium (Figure 4.5-4) and radium (Figure 4.5-5) are showing comparable evolutions. The decrease in $p\text{CO}_2$ is slightly limiting the predominance of barite (BaSO_4) and $\text{RaSO}_4(\text{s})$ at high pH, because of the formation of $\text{BaCO}_3(\text{aq})$ and $\text{RaCO}_3(\text{aq})$

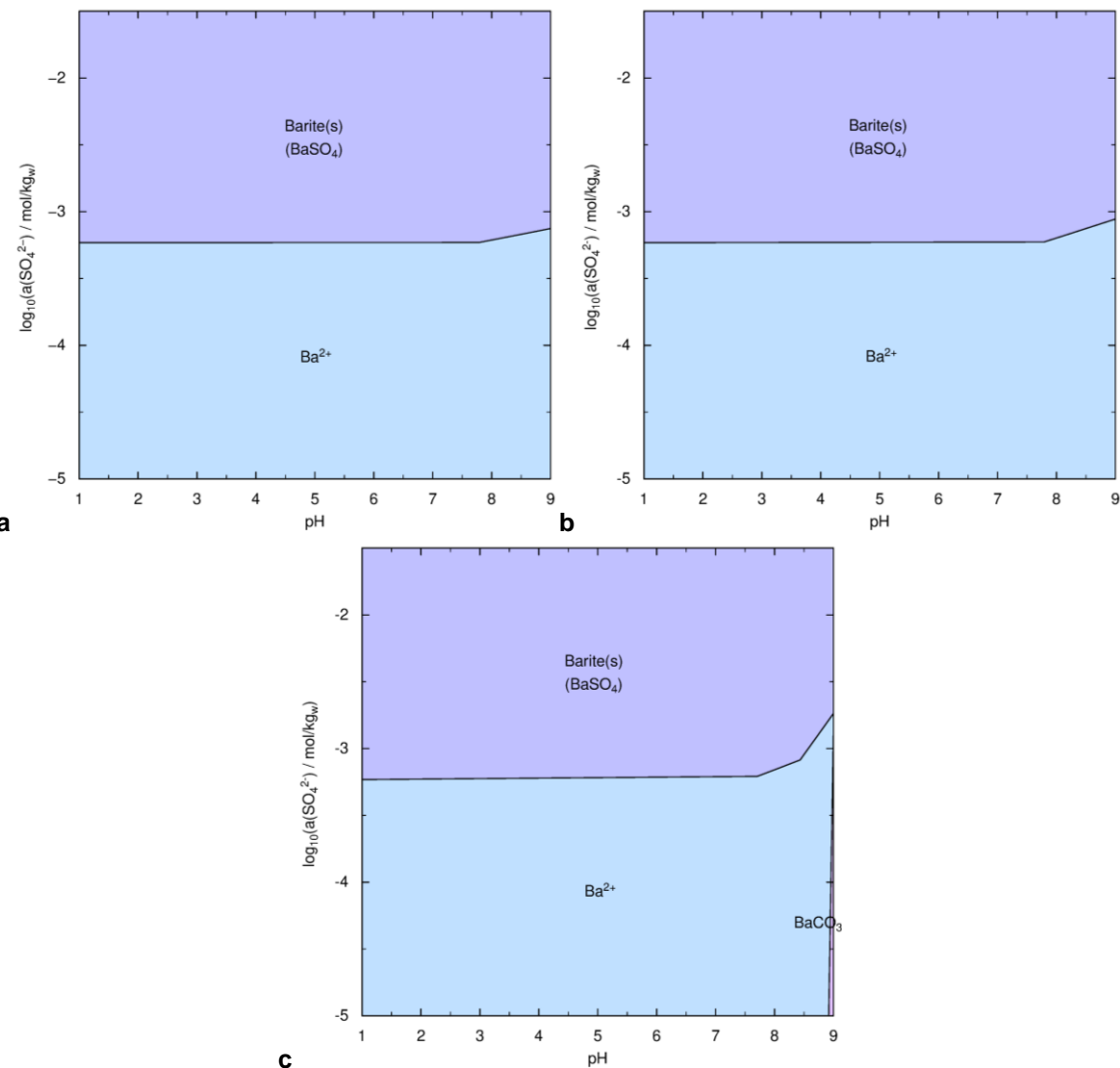


Figure 4.5-4. Activity predominance plot (PHREEPLOT) of 10^{-7} mol kg $_{\text{w}}^{-1}$ Ba, in a 0.1 mol kg $_{\text{w}}^{-1}$ HClO₄ solution with increasing $a(\text{SO}_4^{2-})$ and pH, and fixed total carbonate defined in Reiller and Descotes [2020REI/DES]: $p\text{CO}_2 = 2.6$ (a), 2.4 (b), and 1.8 (c); the Davies PHREEQC extraction of the database is used.

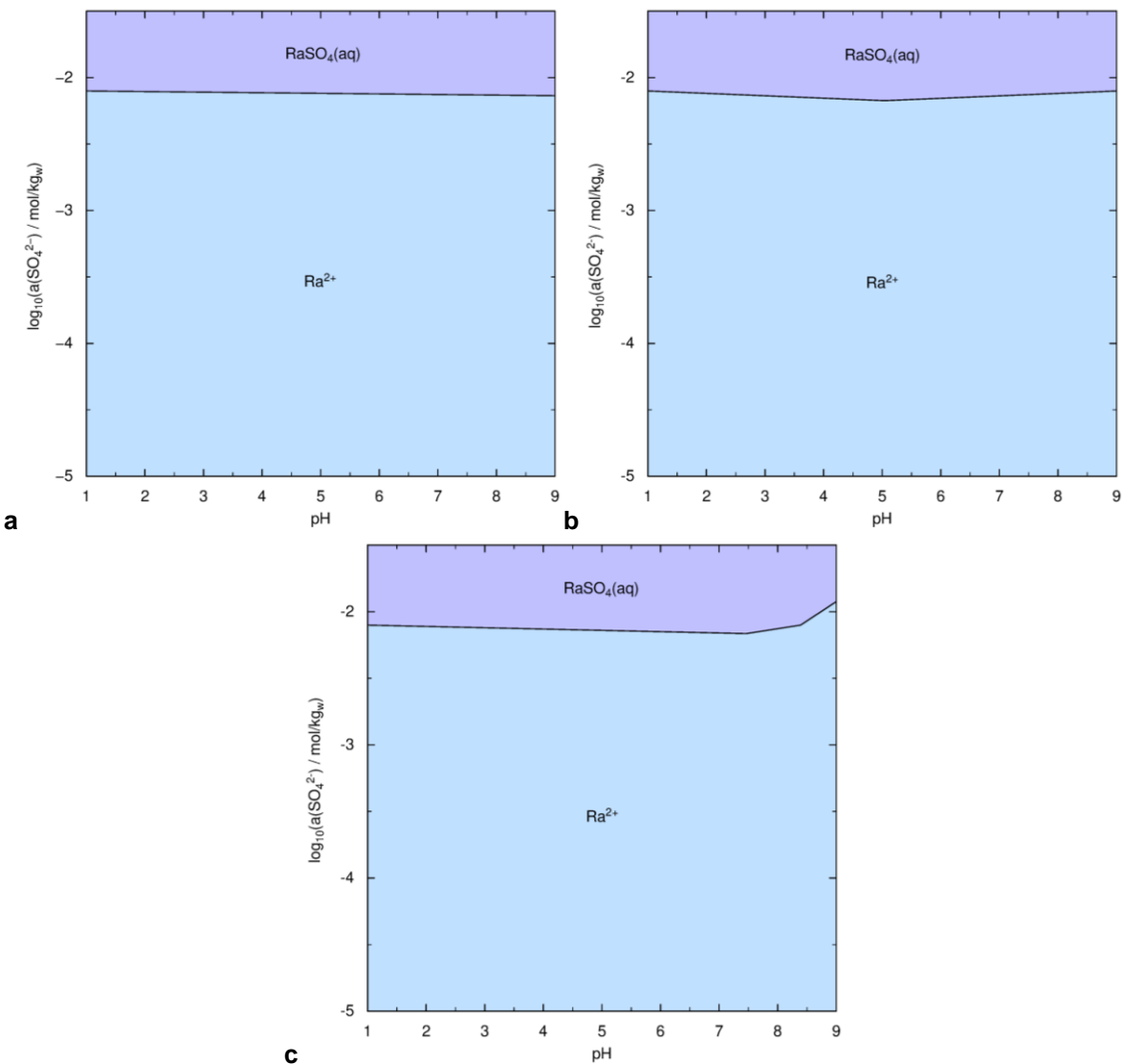


Figure 4.5-5. Predominance plot (PHREEPLOT) of 10^{-10} mol kg_w⁻¹ Ra, in a 0.1 mol kg_w⁻¹ HClO₄ solution with increasing a(SO₄²⁻) and pH, and fixed total carbonate defined in Reiller and Descotes [2020REI/DES]: pCO₂ = 2.6 (a), 2.4 (b) and 1.8 (c); the Davies PHREEQC extraction of the database is used.

4.6. Predominance of Uranium in Na-Mg-Ca-OH-HCO₃-H domains

The repartition of the $M_n\text{UO}_2(\text{CO}_3)^{(4-2n)-}$ species depends on several activity values — *i.e.*, Ca^{2+} , Mg^{2+} , CO_3^{2-} or HCO_3^- , and H^+ — and specific ion interaction coefficients $\varepsilon(M_n\text{UO}_2(\text{CO}_3)^{(4-2n)-}, \text{Na}^+\text{X}^-)$. These representations can be reduced to $\log_{10}(a(\text{HCO}_3^+) a(\text{H}^+))$ vs. $\log_{10}(a(\text{M}^{2+})/a(\text{H}^+)^2)$ at total NaX concentration, and $\log_{10}(a(\text{Na}^+)/a(\text{Na}^+))$ vs. $\log_{10}(a(\text{M}^{2+})/a(\text{H}^+)^2)$ at fixed $\log_{10}(a(\text{HCO}_3^+) a(\text{H}^+))$. These representations will be presented in the following.

4.6.1. Mg-Ca-HCO₃-H domain

The first representation is showing the variations of $\log_{10} a(\text{HCO}_3^+) + \log_{10} a(\text{H}^+)$ vs. four different Mg/Ca activity ratios, *i.e.* $a(\text{Mg}^{2+})/(a(\text{Mg}^{2+}) + a(\text{Ca}^{2+})) = \{10^{-4}; 1; 6.3; 10^4\}$ using the thermodynamic constants and ε values from Shang and Reiller [2020aSHA/REI] for $\text{Ca}_n\text{UO}_2(\text{CO}_3)^{(4-2n)-}$ in NaCl, and Shang and Reiller [2021aSHA/REI] for $\text{MgUO}_2(\text{CO}_3)^2-$ in NaCl. The total NaCl concentration is fixed to 0.5 mol kg_w⁻¹, *i.e.* close to the one of seawater, to minimize the influence of ionic strength variations in these kinds of plots.

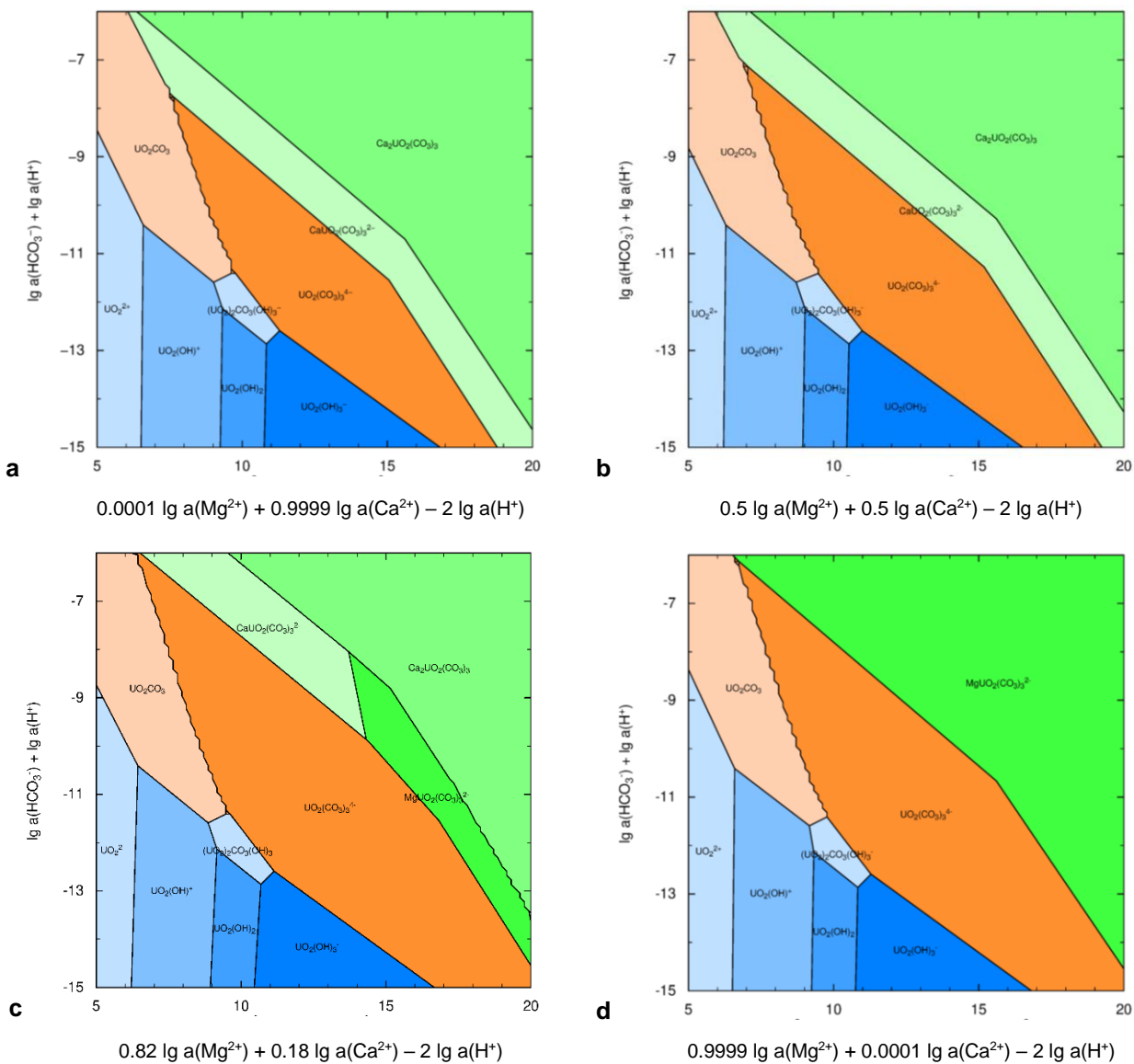


Figure 4.6-1. Activity predominance plots (PHREEPLOT) of 10^{-6} mol kg_w⁻¹ U at P(O₂) = 0.21 atm and [NaCl] = 0.5 mol kg_w⁻¹; the SIT PHREEQC extraction of the database is used.

4.6.2. Na-Cl influence

Using the specific ion interaction coefficients from Shang and Reiller [2020aSHA/REI] for Ca_nUO₂(CO₃)₃⁽⁴⁻²ⁿ⁾⁻ in NaCl, and Shang and Reiller [2021aSHA/REI] for MgUO₂(CO₃)₃²⁻ in NaCl, the predominance activity plots in Figure 4.6-2 can be drawn. The progressive predominance of the successive UO₂(CO₃)_n⁽²⁻²ⁿ⁾⁺ with increasing ionic strength is represented in the ordinates of the plots. The progressive predominance of Ca₂UO₂(CO₃)₃(aq) relative to CaUO₂(CO₃)₃²⁻ is well noticed in the abscise. This could appear counter intuitive as ionic strength should favour the charged species. But the character of the apparent non-charged species should not be forgotten and is reflected in values of $\varepsilon(\text{CaUO}_2(\text{CO}_3)_3^{2-}, \text{Na}^+)$ and $\varepsilon(\text{CaUO}_2(\text{CO}_3)_3(\text{aq}), \text{Na}^+\text{Cl}^-)$.

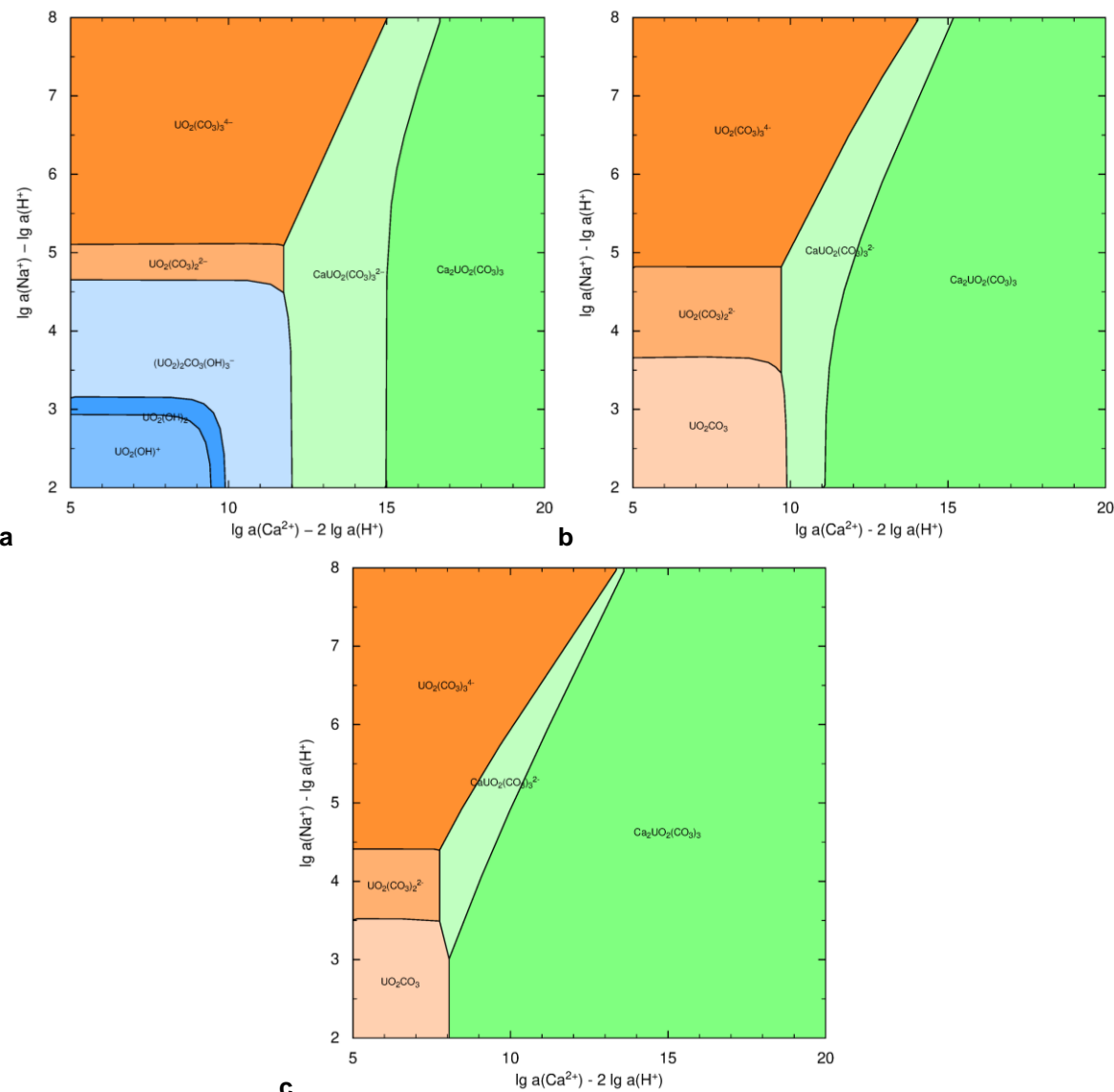


Figure 4.6-2. Activity predominance plots (PHREEPLOT) of 10^{-6} mol kg_w⁻¹ U at $P(\text{O}_2) = 0.21$ atm, $\log_{10}a(\text{HCO}_3^-) + \log_{10}a(\text{H}^+)$ values of -12 (a), -10 (b), and -8 (c); the SIT PHREEQC extraction of the database is used.

4.7. Rationale on the Speciation Exercise

The speciation exercise hereby, and the one in Reiller and Descotes [2020REI/DES], has shown that the database extraction files can be used with confidence with the three software packages PHREEQC, CHESS, and GWB, to obtain comparable results. Nevertheless, it must be emphasized here that the use of an adequate activity correction model should be a central choice before any attempt to model a geochemical system. This would be particularly important under conditions of high salinity or during an ISR process.

For the future, generic cases will be developed in order to test the database under realistic conditions for exploration, exploitation, and remediation of uranium mining activities. Doing so, the coherency will be tested in cases of implementation of new data in the database.

5. References

- [1848SMI] Smith J L; Art. XXXV.—Two new minerals,—Medjidite (sulphate of uranium and lime)—Liebigite (carbonate of uranium and lime), *American Journal of Science* **5**, 336-338.
- [1851SMI] Smith J L; Liebigite, *American Journal of Science* **11**, 259.
- [1889SET] Setschenow J; Über die Konstitution der Salzlösungen auf Grund ihres Verhaltens zu Kohlensäure, *Zeitschrift für physikalische Chemie* **4U** (1), 117-125. In German. <http://doi.org/10.1515/zpch-1889-0409>
- [1923DEB/HÜC] Debye P and Hückel E; Zur Theorie der Elektrolyte, *Physikalische Zeitschrift* **24** (9), 185-206. In German.
- [1937KIE] Kielland J; Individual activity coefficients of ions in aqueous solutions, *Journal of the American Chemical Society* **59** (9), 1675-1678. <http://doi.org/10.1021/ja01288a032>
- [1938DAV] Davies C W; 397. The extent of dissociation of salts in water. Part VIII. An equation for the mean ionic activity coefficient of an electrolyte in water, and a revision of the dissociation constants of some sulphates, *Journal of the Chemical Society (Resumed)*, 2093-2098. <http://doi.org/10.1039/IR9380002093>
- [1944JON/COL] Jones G and Colvin J H; Electrochemical studies on vanadium salts. III. The vanadic-vanadous oxidation-reduction potential, *Journal of the American Chemical Society* **66** (9), 1573-1579. <http://doi.org/10.1021/ja01237a047>
- [1952ROS/WAG] Rossini F D, Wagman D D, Evans W H, Levine S, and Jaffe I; Selected Values of Chemical Thermodynamic Properties, Circular of the National Bureau of Standards 500, U.S. Department of Commerce, Washington, D. C., USA. pp. 1268. <http://archive.org/details/circularchecklistofselectedvaluesofchemicalthermodynamicproperties>
- [1960GAR/THO] Garrels R M, Thompson M E, and Siever R; Stability of some carbonates at 25°C and one atmosphere total pressure, *American Journal of Science* **258** (6), 402-418. <http://doi.org/10.2475/ajs.258.6.402>
- [1962DAV] Davies C W; Ion Association, Butterworths, London, UK. pp. 190.
- [1965MUT] Muto T; Thermochemical stability of ningyoite, *Mineralogical Journal* **4** (4), 245-274. <http://doi.org/10.2465/minerj1953.4.245>
- [1965RAM/SAN] Ramette R W and Sandford R W, Jr.; Thermodynamics of iodine solubility and triiodide ion formation in water and in deuterium oxide, *Journal of the American Chemical Society* **87**, 5001-5005. <http://doi.org/10.1021/ja00950a005>
- [1965VES/PEK] Vesely V, Pekarek V, and Abbrecht M; A study of uranyl phosphates—III. Solubility products of uranyl hydrogen phosphate uranyl orthophosphate and some alkali uranyl phosphates, *Journal of Inorganic and Nuclear Chemistry* **27** (5), 1159-1166. [http://doi.org/10.1016/0022-1902\(65\)80428-6](http://doi.org/10.1016/0022-1902(65)80428-6)
- [1965WAG/EVA] Wagman D D, Evans W H, Halow I, Parker V B, Bailey S M, and Schumm R H; Selected Values of Chemical Thermodynamic Properties. Part 1. Table of the First Twenty-Three Elements in the Standard Order of Arrangement, Institute for Basic Standards. National Bureau of Standards, Washington, D.C., USA, Technical Note 270-1. p. 132. http://nvlpubs.nist.gov/nistpubs/Legacy/TN/nbstchnote270_1.pdf
- [1966KHO] Khodakovsky I L; *Geokhimiya* **7**, 960.
- [1966WAG/EVA] Wagman D D, Evans W H, Halow I, Parker V B, Bailey S M, and Schumm R H; Selected Values of Chemical Thermodynamic Properties. Part 2. Table for the Elements Twenty-Three Through Thirty-Two in the Standard Order of Arrangement, Institute for Basic Standards. National Bureau of Standards, Washington, D.C., USA, Technical Note 270-2. p. 72. http://nvlpubs.nist.gov/nistpubs/Legacy/TN/nbstchnote270_2.pdf
- [1968MOR/GRE] Moreno E C, Gregory T M, and Brown W E; Preparation and solubility of hydroxyapatite, *Journal of Research of the National Bureau of Standards - A Physics and Chemistry* **72A** (6), 773-782. <http://doi.org/10.6028/jres.072A.052>
- [1968WAG/EVA] Wagman D D, Evans W H, Parker V B, Halow I, Bailey S M, and Schumm R H; Selected Values of Chemical Thermodynamic Properties. Table of the First Thirty-Four Elements in the Standard Order of Arrangement, Institute for Materials Research. National Bureau of Standards, Washington, D.C., USA, Technical Note 270-3. p. 264. http://nvlpubs.nist.gov/nistpubs/Legacy/TN/nbstchnote270_3.pdf
- [1969WAG/EVA] Wagman D D, Evans W H, Parker V B, Halow I, Bailey S M, and Schumm R H; Selected Values of Chemical Thermodynamic Properties. Table for Elements 35 Through 53 in the Standard Order of Arrangement, Institute for Materials Research. National Bureau of Standards, Washington, D.C., USA, Technical Note 270-4. p. 164. http://nvlpubs.nist.gov/nistpubs/Legacy/TN/nbstchnote270_4.pdf
- [1971ADA] Adams F; Ionic concentrations and activities in soil solutions, *Soil Science Society of America Journal* **35** (3), 420-426. <http://doi.org/10.2136/sssaj1971.03615995003500030028x>
- [1971HIL/WOR] Hill J O, Worsley I G, and Hepler L G; Thermochemistry and oxidation potentials of vanadium, niobium, and tantalum, *Chemical Reviews* **71** (1), 127-137. <http://doi.org/10.1021/cr60269a006>
- [1971PAR/WAG] Parker V B, Wagman D D, and Evans W H; Selected Values of Chemical Thermodynamic Properties. Table for Elements 92 Through 97 in the Standard Order of Arrangement, Institute for Materials Research. National Bureau of Standards, Washington, D.C., USA, Technical Note 270-6. p. 106. http://nvlpubs.nist.gov/nistpubs/Legacy/TN/nbstchnote270_6.pdf
- [1972FER/GAV] Ferguson J F and Gavis J; Review of arsenic cycle in natural waters, *Water Research* **6** (11), 1259-1274. [http://doi.org/10.1016/0043-1354\(72\)90052-8](http://doi.org/10.1016/0043-1354(72)90052-8)
- [1974aHEL/KIR] Helgeson H C and Kirkham D H; Theoretical prediction of thermodynamic behavior of aqueous electrolytes at high pressures and temperatures: I. Summary of thermodynamic electrostatic properties of solvent, *American Journal of Science* **274** (10), 1089-1198. <http://doi.org/10.2475/ajs.274.10.1089>
- [1974bHEL/KIR] Helgeson H C and Kirkham D H; Theoretical prediction of thermodynamic behavior of aqueous electrolytes at high pressures and temperatures: II. Debye-Hückel parameters for activity coefficients and relative partial molal properties, *American Journal of Science* **274** (10), 1199-1261. <http://doi.org/10.2475/ajs.274.10.1199>
- [1974NAU/RYZ] Naumov G B, Ryzhenko B N, and Khodakovsky I L; Handbook of Thermodynamic Data, U.S. Geological Survey, Menlo Park, CA, USA, USGS-WRD-74-001. p. 328. <http://ntr.usgs.gov/>
- [1974NRI] Nriagu J O; Lead orthophosphates—IV. Formation and stability in the environment, *Geochimica et Cosmochimica Acta* **38** (6), 887-898. [http://doi.org/10.1016/0016-7037\(74\)90062-3](http://doi.org/10.1016/0016-7037(74)90062-3)
- [1974OHA] O'Hare P A G; Thermochemistry of molybdates III. Standard enthalpy of formation of barium molybdate, and standard entropy and standard gibbs energy of formation of aqueous molybdate ion, *Journal of Chemical Thermodynamics* **6** (5), 425-434. [http://doi.org/10.1016/0021-9614\(74\)90003-2](http://doi.org/10.1016/0021-9614(74)90003-2)
- [1975CRU/ROH] Cruywagen J J and Rohwer E F C H; Coordination number of molybdenum(VI) in monomeric molybdic acid, *Inorganic Chemistry* **14** (12), 3136-3137. <http://doi.org/10.1021/ic50154a061>
- [1976BAE/MES] Baes C F, Jr. and Mesmer R E; The hydrolysis of cations, Wiley Interscience Publication, New-York. pp. 489.
- [1976CRU/HEY] Cruywagen J J, Heyns J B B, and Rohwer E F C H; Spectrophotometric investigation of the protonation of monomeric molybdic acid in sodium perchlorate medium, *Journal of Inorganic and Nuclear Chemistry* **38** (11), 2033-2036. [http://doi.org/10.1016/0022-1902\(76\)80463-0](http://doi.org/10.1016/0022-1902(76)80463-0)

- [1976SHA] Shannon R D; Revised effective ionic radii and systematic studies of interatomic distances in halides and chalcogenides, *Acta Crystallographica Section A* **32** (5), 751-767. <http://doi.org/10.1107/S0567739476001551>
- [1977ADA/RAW] Adams F and Rawajfih Z; Basaluminite and alunite: a possible cause of sulfate retention by acid soils, *Soil Science Society of America Journal* **41** (4), 686-692. <http://doi.org/10.2136/sssaj1977.03615995004100040013x>
- [1977McD/GRE] McDowell H, Gregory T M, and Brown W E; Solubility of $\text{Ca}_5(\text{PO}_4)_3\text{OH}$ in the system $\text{Ca}(\text{OH})_2\text{-H}_3\text{PO}_4\text{-H}_2\text{O}$ at 5, 15, 25, and 37 °C, *Journal of Research of the National Bureau of Standards - A Physics and Chemistry* **81A** (2-3), 273-281. <http://doi.org/10.6028/jres.081A.017>
- [1978BAR/SCH] Barner H E and Scheuerman R V; Handbook of Thermochemical Data for Compounds and Aqueous Species, John Wiley & Sons, New York, NY, USA. (ISBN 0-471-03238-7). pp. 156.
- [1978LAN] Langmuir D; Uranium solution-mineral equilibria at low temperatures with applications to sedimentary ore deposits, *Geochimica et Cosmochimica Acta* **42** (6), 547-569. [http://doi.org/10.1016/0016-7037\(78\)90001-7](http://doi.org/10.1016/0016-7037(78)90001-7)
- [1979ROB/HEM] Robie R A, Hemingway B S, and Fisher J R; Thermodynamic Properties of Minerals and Related Substances at 298.15 K and 1 Bar (10^5 Pascals) Pressure and at High Temperature, US Geological Survey, US Geological Survey Bulletin 1452. p. 456. <http://pubs.usgs.gov/bul/1452/report.pdf>
- [1980ALW] Alwan A K; The Chemistry of Formation of Some Mineral Species, PhD Thesis, University of Wales, Cardiff, Wales. pp. 116.
- [1980ALW/WIL] Alwan A K and Williams P A; Aqueous chemistry of uranium minerals. Part 2. Minerals of the liebigite group, *Mineralogical Magazine* **43** (329), 665-667. <http://doi.org/10.1180/minmag.1980.043.329.17>
- [1980CIA] Ciavatta L; The specific interaction theory in evaluating ionic equilibria, *Annali di Chimica Roma* **70** (11-1), 551-567.
- [1981TUR/WHI] Turner D R, Whitfield M, and Dickson A G; The equilibrium speciation of dissolved components in freshwater and sea water at 25°C and 1 atm pressure, *Geochimica et Cosmochimica Acta* **45** (6), 855-881. [http://doi.org/10.1016/0016-7037\(81\)90115-0](http://doi.org/10.1016/0016-7037(81)90115-0)
- [1981WAG/EVA] Wagman D D, Evans W H, Parker V B, Schumm R H, and Nuttall R L; Selected Values of Chemical Thermodynamic Properties. Compounds of Uranium, Protactinium, Thorium, and the Alkali Metals, Center for Thermodynamics and Molecular Science. National Measurement Laboratory. National Bureau of Standards, Washington, D.C., USA, Technical Note 270-8. p. 156. <http://nvlpubs.nist.gov/nistpubs/Legacy/TN/nbstchnicalnote270-8.pdf>
- [1982NOR] Nordstrom D K; The effect of sulfate on aluminum concentrations in natural waters: some stability relations in the system $\text{Al}_2\text{O}_3\text{-SO}_3\text{-H}_2\text{O}$ at 298 K, *Geochimica et Cosmochimica Acta* **46** (4), 681-692. [http://doi.org/10.1016/0016-7037\(82\)90168-5](http://doi.org/10.1016/0016-7037(82)90168-5)
- [1982PLU/BUS] Plummer L N and Busenberg E; The solubilities of calcite, aragonite and vaterite in $\text{CO}_2\text{-H}_2\text{O}$ solutions between 0 and 90°C, and an evaluation of the aqueous model for the system $\text{CaCO}_3\text{-CO}_2\text{-H}_2\text{O}$, *Geochimica et Cosmochimica Acta* **46** (6), 1011-1040. [http://doi.org/10.1016/0016-7037\(82\)90056-4](http://doi.org/10.1016/0016-7037(82)90056-4)
- [1982WAG/EVA] Wagman D D, Evans W H, Parker V B, Schumm R H, Halow I, Bailey S M, Churney K L, and Nuttall R L; The NBS Tables of chemical thermodynamic properties. Selected values for inorganic and C_1 and C_2 organic substances in SI units, *Journal of Chemical Reference Data* **11** (Supplement No. 2), 392.
- [1983AGG/KAD] Aggett J and Kadwani R; Anion-exchange method for speciation of arsenic and its application to some environmental analyses, *Analyst* **108** (1293), 1495-1499. <http://doi.org/10.1039/An9830801495>
- [1983OBR/WIL] O'Brien T J and Williams P A; The aqueous chemistry of uranium minerals. 4. Schröckingerite, grimselite, and related alkali uranyl carbonates, *Mineralogical Magazine* **47** (342), 69-73. <http://doi.org/10.1180/minmag.1983.047.342.12>
- [1983SPA] Spahiu K; Carbonate Complex Formation in Lanthanoid and Actinoid Systems, PhD Thesis, The Royal Institute of Technology, Stockholm, Sweden.
- [1984BUS/PLU] Busenberg E, Plummer L N, and Parker V B; The solubility of strontianite (SrCO_3) in $\text{CO}_2\text{-H}_2\text{O}$ solutions between 2 and 91 °C, the association constants of SrHCO_3^+ (aq) and SrCO_3^0 (aq) between 5 and 80 °C, and an evaluation of the thermodynamic properties of Sr^{2+} (aq) and SrCO_3 (cr) at 25 °C and 1 atm total pressure, *Geochimica et Cosmochimica Acta* **48** (10), 2021-2035. [http://doi.org/10.1016/0016-7037\(84\)90383-1](http://doi.org/10.1016/0016-7037(84)90383-1)
- [1984HAR/MØL] Harvie C E, Møller N, and Weare J H; The prediction of mineral solubilities in natural waters: The Na-K-Mg-Ca-H-Cl-SO₄-OH-HCO₃-CO₃-CO₂-H₂O system to high ionic strengths at 25°C, *Geochimica et Cosmochimica Acta* **48** (4), 723-751. [http://doi.org/10.1016/0016-7037\(84\)90098-x](http://doi.org/10.1016/0016-7037(84)90098-x)
- [1984NRI] Nriagu J O; Formation and stability of base metal phosphates in soils and sediments, in *Phosphate Minerals* (Nriagu J.O. and Moore P.B., Eds.), Springer Berlin Heidelberg, Berlin, Germany, pp. 318-329. http://doi.org/10.1007/978-3-642-61736-2_10
- [1984TAY/LOP] Taylor P and Lopata V J; Stability and solubility relationships between some solids in the system PbO-CO₂-H₂O, *Canadian Journal of Chemistry - Revue Canadienne de Chimie* **62** (3), 395-402. <http://doi.org/10.1139/v84-070>
- [1985BAR/PAR] Bard A J, Parsons R, and Jordan J; Standard Potentials in Aqueous Solution, IUPAC, Marcel Dekker, New York, NY, USA, pp. 834.
- [1985FER/GRE] Ferri D, Grenthe I, Hietanen S, Neher-Néumann E, and Salvatore F; Studies on metal carbonate equilibria. 12. Zinc(II) carbonate complexes in acid solutions, *Acta Chemica Scandinavica Series A: Physical and Inorganic Chemistry* **39** (5), 347-353. <http://doi.org/10.3891/acta.chem.scand.39a-0347>
- [1985LAN/RIE] Langmuir D and Riese A C; The thermodynamic properties of radium, *Geochimica et Cosmochimica Acta* **49** (7), 1593-1601. [http://doi.org/10.1016/0016-7037\(85\)90264-9](http://doi.org/10.1016/0016-7037(85)90264-9)
- [1985ROB] Robins R G; The solubility of barium arsenate - Sherritt barium arsenate process, *Metallurgical Transactions B-Process Metallurgy* **16** (2), 404-406. <http://doi.org/10.1007/bf02679734>
- [1986BUS/PLU] Busenberg E and Plummer L N; The solubility of BaCO_3 (cr) (witherite) in $\text{CO}_2\text{-H}_2\text{O}$ solutions between 0 and 90 °C, evaluation of the association constants of BaHCO_3^+ (aq) and BaCO_3^0 (aq) between 5 and 80 °C, and a preliminary evaluation of the thermodynamic properties of Ba^{2+} (aq), *Geochimica et Cosmochimica Acta* **50** (10), 2225-2233. [http://doi.org/10.1016/0016-7037\(86\)90077-3](http://doi.org/10.1016/0016-7037(86)90077-3)
- [1987GAR/PAR] Garvin D, Parker V B, and White H J; CODATA Thermodynamic Tables. Selections for Some Compounds of Calcium and Related Mixtures: A Prototype Set of Tables, Hemisphere Publishing Corporation, Washington, D. C., USA. (ISBN 08911-67307). pp. 356.
- [1987PAN/MAH] Pankratz L B, Mah A D, and Watson S W; Thermodynamic Properties of Sulfides, U.S. Bureau of Mines, USA, Bulletin 689. p. 427. http://digital.library.unt.edu/ark:/67531/metadc38801/m2/1/high_res_d/metadc38801.pdf
- [1988CHA/NEW] Chandratillake M R, Newton G W A, and Robinson V J; Project Chemval: Comparison of Thermodynamic Databases Used in Geochemical Modelling, Department of the Environment, UK, DOE Report No. DOE/RW/83 074. p. 76.
- [1988ESS] Essington M E; Solubility of barium arsenate, *Soil Science Society of America Journal* **52** (6), 1566-1570. <http://doi.org/10.2136/sssaj1988.03615995005200060008x>
- [1988NOV/SOH] Novotny P and Sohnle O; Densities of binary aqueous solutions of 306 inorganic substances, *Journal of Chemical & Engineering Data* **33** (1), 49-55. <http://doi.org/10.1021/je00051a018>
- [1988SHO/HEL] Shock E L and Helgeson H C; Calculation of the thermodynamic and transport properties of aqueous species at high-pressure and temperatures: correlation algorithms for ionic species and equation of state predictions to 5 kb and 1000°C, *Geochimica et Cosmochimica Acta* **52** (8), 2009-2036. [http://doi.org/10.1016/0016-7037\(88\)90181-0](http://doi.org/10.1016/0016-7037(88)90181-0)

References

- [1988TAR/KLE] Taras Bryndzia L and Kleppa O J; Standard molar enthalpies of formation of realgar (α -AsS) and orpiment (As₂S₃) by high-temperature direct-synthesis calorimetry, *Journal of Chemical Thermodynamics* **20** (6), 755-764. [http://doi.org/10.1016/0021-9614\(88\)90028-6](http://doi.org/10.1016/0021-9614(88)90028-6)
- [1988WAN] Wanner H; The NEA thermochemical data-base project, *Radiochimica Acta* **44-45** (2), 325-329. <http://doi.org/10.1524/ract.1988.4445.2.325>
- [1989COX/WAG] Cox J D, Wagman D D, and Medvedev V A; CODATA Key Values for Thermodynamics, Hemisphere Publishing Corp., New York, USA. pp. 271.
- [1989PAN/SUS] Pan P and Susak N J; Co(II) chloride and Co(II) bromide complexes in aqueous solutions up to 5 m NaX and 90°C: spectrophotometric study and geological implications, *Geochimica et Cosmochimica Acta* **53** (2), 327-341. [http://doi.org/10.1016/0016-7037\(89\)90385-2](http://doi.org/10.1016/0016-7037(89)90385-2)
- [1989SHO/HEL] Shock E L, Helgeson H C, and Sverjensky D A; Calculation of the thermodynamic and transport-properties of aqueous species at high-pressure and temperatures - standard partial molal properties of inorganic neutral species, *Geochimica et Cosmochimica Acta* **53** (9), 2157-2183. [http://doi.org/10.1016/0016-7037\(89\)90341-4](http://doi.org/10.1016/0016-7037(89)90341-4)
- [1989SMI/MAR] Smith R M and Martell A E; Critical Stability Constants. Volume 6: Second Supplement, Springer Science + Business Media, LLC, New York, NY, USA. (ISBN 978-1-4615-6764-6). pp. 643. <http://doi.org/10.1007/978-1-4615-6764-6>
- [1989SPY/REE] Spycher N F and Reed M H; Evolution of a broadlands-type epithermal ore fluid along alternative P-T paths; implications for the transport and deposition of base, precious, and volatile metals, *Economic Geology* **84** (2), 328-359. <http://doi.org/10.2113/gsecongeo.84.2.328>
- [1989TAR/KLE] Taras Bryndzia L and Kleppa O J; Standard molar enthalpies of formation of sulfosalts in the Ag-As-S system and thermochemistry of the sulfosalts of Ag with As, Sb, and Bi, *American Mineralogist* **74** (1-2), 243-249.
- [1990CIA] Ciavatta L; The specific interaction theory in equilibrium analysis. Some empirical rules for estimating interaction coefficients of metal ion complexes, *Annali di Chimica Roma* **80** (5-6), 255-263.
- [1990DYR/KRE] Dyrssen D and Kremling K; Increasing hydrogen sulfide concentration and trace metal behavior in the anoxic Baltic waters, *Marine Chemistry* **30** (1-3), 193-204. [http://doi.org/10.1016/0304-4203\(90\)90070-s](http://doi.org/10.1016/0304-4203(90)90070-s)
- [1990NOR/PLU] Nordstrom D K, Plummer L N, Langmuir D, Busenberg E, May H M, Jones B F, and Parkhurst D L; Revised chemical equilibrium data for major water-mineral reactions and their limitations, in *Chemical Modeling of Aqueous Systems II* (Melchior D.C. and Bassett R.L., Eds.). Chapter 31. ACS Symposium Series, American Chemical Society, Washington, DC, USA, pp. 398-413. <http://doi.org/10.1021/bk-1990-0416.ch031>
- [1990SHO/HEL] Shock E L and Helgeson H C; Calculation of the thermodynamic and transport properties of aqueous species at high-pressure and temperatures: standard partial molal properties of organic species, *Geochimica et Cosmochimica Acta* **54** (4), 915-945. [http://doi.org/10.1016/0016-7037\(90\)90429-o](http://doi.org/10.1016/0016-7037(90)90429-o)
- [1990VOC/HAV] Vochten R and Van Haverbeke L; Transformation of schoepite into the uranyl oxide hydrates: becquerelite, billietite and wölsendorfite, *Mineralogy and Petrology* **43** (1), 65-72. <http://doi.org/10.1007/bf01164222>
- [1990WOL/JAC] Wolery T J, Jackson K J, Bourcier W L, Bruton C J, Viani B E, Knauss K G, and Delany J M; Current status of the EQ3/6 software package for geochemical modeling, in *Chemical Modeling of Aqueous Systems II*. Chapter 8. ACS Symposium Series, Vol. 416, American Chemical Society, pp. 104-116. <http://doi.org/10.1021/bk-1990-0416.ch008>
- [1991BAL/NOR] Ball J W and Nordstrom D K; User's Manual for WATEQ4F, with Revised Thermodynamic Data Base and Text Cases for Calculating Speciation of Major, Trace, and Redox Elements in Natural Waters, US Geological Survey, Menlo Park, CA, USA, Report 91-183. p. 195. <http://pubs.er.usgs.gov/publication/ofr91183>
- [1991PIT] Pitzer K S; Ion interaction approach: theory and data correlation, in *Activity Coefficients in Electrolyte Solution, 2nd Edition* (Pitzer K.S., Ed.), CRC Press, Boca Raton, FL, USA, pp. 75-153.
- [1991WAT/DUF] Waters M, Duffield J R, Griffiths P J F, and Williams D R; Chemval Project. Application and validation of predictive computer programs describing the chemistry of radionuclides in the geosphere, Commission of the European Communities, Brussels, Belgium, Report EUR 13315 EN. p. 138. <https://op.europa.eu/en/publication-detail/-/publication/089896b0-a016-4c88-8149-11a6b86adae0/language-en/format-PDF/source-245332173#>
- [1992GRE/FUG] Grenthe I, Fuger L, Konings R G M, Lemire R J, Muller A B, Nguyen-Trung C, and Wanner H; Chemical Thermodynamics 1. Chemical Thermodynamics of Uranium, Chemical Thermodynamics Series 1, North Holland Elsevier Science Publishers B. V., Amsterdam, The Netherlands. pp. 715. <http://www.oecd-nea.org/dbtdb/pubs/uranium.pdf>
- [1992KÖN/SCH] Königsberger E, Schmidt P, and Gamsjäger H; Solid-solute phase equilibria in aqueous solution. VI. Solubilities, complex formation, and ion-interaction parameters for the system Na⁺ - Mg²⁺ - ClO₄⁻ - CO₂ - H₂O at 25°C, *Journal of Solution Chemistry* **21** (12), 1195-1216. <http://doi.org/10.1007/Bf00667217>
- [1992VER/GOU] Verdes G, Gout R, and Castet S; Thermodynamic properties of the aluminate ion and of bayerite, boehmite, diasporite and gibbsite, *European Journal of Mineralogy* **4** (4), 767-792.
- [1993ENG/RID] England T R and Rider B F; ENDF-349 Evaluation and Compilation of Fission Product Yields, Lawrence Berkeley National Laboratory, Report LA-UR-3106. p. 173. <http://t2.lanl.gov/nis/publications/endf349.pdf>
- [1993SHO/KOR] Shock E L and Koretsky C M; Metal-organic complexes in geochemical processes: calculation of standard partial molal thermodynamic properties of aqueous acetate complexes at high pressures and temperatures, *Geochimica et Cosmochimica Acta* **57** (20), 4899-4922. [http://doi.org/10.1016/0016-7037\(93\)90128-I](http://doi.org/10.1016/0016-7037(93)90128-I)
- [1995CHEN/ZEN] Chen Q Y, Zeng W M, Chen X M, Gu S Q, Yang G Q, Zhou H F, and Yin Z L; Investigation of the thermodynamic properties of γ -Al₂O₃, *Thermochimica Acta* **253**, 33-39. [http://doi.org/10.1016/0040-6031\(94\)01969-n](http://doi.org/10.1016/0040-6031(94)01969-n)
- [1995ROB/HEM] Robie R A and Hemingway B S; Thermodynamic Properties of Minerals and Related Substances at 298.15 K and 1 bar (10⁵ Pascal) Pressure and at Higher Temperatures, US Geological Survey, Denver, CO, USA, US Geological Survey Bulletin 2131. p. 461. <http://pubs.usgs.gov/bul/2131/report.pdf>
- [1995SHO] Shock E L; Organic acids in hydrothermal solutions: standard molal thermodynamic properties of carboxylic acids and estimates of dissociation constants at high temperatures and pressures, *American Journal of Science* **295** (5), 496-580. <http://doi.org/10.2475/ajs.295.5.496>
- [1995SHO/KOR] Shock E L and Koretsky C M; Metal-organic complexes in geochemical processes: estimation of standard partial molal thermodynamic properties of aqueous complexes between metal-cations and monovalent organic acid ligands at high pressures and temperatures, *Geochimica et Cosmochimica Acta* **59** (8), 1497-1532. [http://doi.org/10.1016/0016-7037\(95\)00058-8](http://doi.org/10.1016/0016-7037(95)00058-8)
- [1995SIL/BID] Silva R J, Bidoglio G, Rand M, Robouch P, Wanner H, and Puigdomènech I; Chemical Thermodynamics 2. Chemical Thermodynamics of Americium with an Appendix on Chemical Thermodynamics of Uranium (Grenthe, I., Sandino, M. C. A., Puigdomènech, I., Rand, M. H., Eds.), Chemical Thermodynamics Series 2, North Holland Elsevier Science Publishers B. V., Amsterdam, The Netherlands. pp. 374. <http://www.oecd-nea.org/dbtdb/pubs/americium.pdf>
- [1996BER/GEI] Bernhard G, Geipel G, Brendler V, and Nitsche H; Speciation of uranium in seepage waters of a mine tailing pile studied by time-resolved laser-induced fluorescence spectroscopy (TRLFS), *Radiochimica Acta* **74** (S1), 87-91. <http://doi.org/10.1524/ract.1996.74.special-issue.87>
- [1996FAL/REA] Falck W E, Read D, and Thomas B; Chemval 2: Thermodynamic Database – Final Report, European Commission – Directorate-General for Research, Brussels, Belgium, EUR 16897 EN. p. 164. <https://op.europa.eu/en/publication-detail/-/publication/6a8d8470-c91e-11e6-ad7c-01aa75ed71a1>

- [1996NOR] Nordstrom D K; Trace metal speciation in natural waters: computational vs. analytical, *Water, Air, and Soil Pollution* **90** (1-2), 257-267. <http://doi.org/10.1007/bf00619286>
- [1996HAV/VOC] Van Haverbeke L, Vochten R, and Van Springel K; Solubility and spectrochemical characteristics of synthetic chernikovite and meta-ankoleite, *Mineralogical Magazine* **60** (402), 759-766. <http://doi.org/10.1180/minmag.1996.060.402.05>
- [1997GOO] Goodgame V R; The distribution and origin of arsenic and platinum group element mineralization in the Mariners nickel deposit, Widgiemooltha, Western Australia, PhD Thesis, University of Oregon, pp. 274.
- [1997GRE/PLY] Grenthe I, Plyasunov A V, and Spahiu K; Chapter IX. Estimations of medium effects on thermodynamic data, in *Modelling in Aquatic Chemistry* (Grenthe I. and Puigdomènec I., Eds.). Chapter IX, OECD, Paris, France, pp. 325-426. <http://www.oecd-nea.org/dbtdb/pubs/book-pdf/325-426.pdf>
- [1997MEY/SCH] Meyer B and Scholz F; Redetermination of the transformation enthalpies of the xanthoconite-proustite, pyrostilpnite-pyrargyrite and trechmannite-smithite phase transitions, *Physics and Chemistry of Minerals* **24** (1), 50-52. <http://doi.org/10.1007/s002690050016>
- [1997PAL/WES] Palmer D A and Wesolowski D J; Potentiometric measurements of the first hydrolysis quotient of magnesium(II) to 250°C and 5 molal ionic strength (NaCl), *Journal of Solution Chemistry* **26** (2), 217-232. <http://doi.org/10.1007/bf02767923>
- [1997PLY/WAN] Plyasunova N V, Wang M S, Zhang Y, and Muhammed M; Critical evaluation of thermodynamics of complex formation of metal ions in aqueous solutions. II. Hydrolysis and hydroxo-complexes of Cu²⁺ at 298.15 K, *Hydrometallurgy* **45** (1-2), 37-51. [http://doi.org/10.1016/s0304-386x\(96\)00073-4](http://doi.org/10.1016/s0304-386x(96)00073-4)
- [1997PUI/PLY] Puigdomènec I, Plyasunov A V, Rard J A, and Grenthe I; Chapter X. Temperature correction to thermodynamic data and enthalpy calculations, in *Modelling in Aquatic Chemistry* (Grenthe I. and Puigdomènec I., Eds.), OECD, Paris, pp. 427-493. <http://www.oecd-nea.org/dbtdb/pubs/book-pdf/427-494.pdf>
- [1997RIM] Rimstidt J D; Quartz solubility at low temperatures, *Geochimica et Cosmochimica Acta* **61** (13), 2553-2558. [http://doi.org/10.1016/S0016-7037\(97\)00103-8](http://doi.org/10.1016/S0016-7037(97)00103-8)
- [1997aSHO/SAS] Shock E L, Sassani D C, Willis M, and Sverjensky D A; Inorganic species in geologic fluids: correlations among standard molal thermodynamic properties of aqueous ions and hydroxide complexes, *Geochimica et Cosmochimica Acta* **61** (5), 907-950. [http://doi.org/10.1016/s0016-7037\(96\)00339-0](http://doi.org/10.1016/s0016-7037(96)00339-0)
- [1997bSHO/SAS] Shock E L, Sassani D C, and Betz H; Uranium in geologic fluids: estimates of standard partial molal properties, oxidation potentials, and hydrolysis constants at high temperatures and pressures, *Geochimica et Cosmochimica Acta* **61** (20), 4245-4266. [http://doi.org/10.1016/S0016-7037\(97\)00240-8](http://doi.org/10.1016/S0016-7037(97)00240-8)
- [1997SVE/SHO] Sverjensky D A, Shock E L, and Helgeson H C; Prediction of the thermodynamic properties of aqueous metal complexes to 1000°C and 5 kb, *Geochimica et Cosmochimica Acta* **61** (7), 1359-1412. [http://doi.org/10.1016/s0016-7037\(97\)00009-4](http://doi.org/10.1016/s0016-7037(97)00009-4)
- [1997WAN/ZHA] Wang M, Zhang Y, and Muhammed M; Critical evaluation of thermodynamics of complex formation of metal ions in aqueous solutions III. The system Cu(I,II) -Cl⁻ -e at 298.15 K, *Hydrometallurgy* **45** (1-2), 53-72. [http://doi.org/10.1016/S0304-386X\(96\)00074-6](http://doi.org/10.1016/S0304-386X(96)00074-6)
- [1998CHA] Chase M W; NIST-JANAF Thermochemical Tables - Fourth Edition. Part I, Al-Co, *Journal of Physical and Chemical Reference Data Monograph* **9**, 1951.
- [1998EPA] EPA; MINTEQA2/PRODEFA2, A Geochemical Assessment Model for Environmental Systems: User Manual Supplement for Version 4.0, U.S. Environmental Protection Agency, Athens, GA, USA. p. 81. <http://www.epa.gov/sites/production/files/documents/SUPPLE1.PDF>
- [1998FEL/DIX] Felmy A R, Dixon D A, Rustad J R, Mason M J, and Onishi L M; The hydrolysis and carbonate complexation of strontium and calcium in aqueous solution. Use of molecular modeling calculations in the development of aqueous thermodynamic models, *Journal of Chemical Thermodynamics* **30** (9), 1103-1120. <http://doi.org/10.1006/jcht.1998.0376>
- [1998PLY/ZHA] Plyasunova N V, Zhang Y, and Muhammed M; Critical evaluation of thermodynamics of complex formation of metal ions in aqueous solutions. V. Hydrolysis and hydroxo-complexes of Co²⁺ at 298.15 K, *Hydrometallurgy* **48** (2), 153-169. [http://doi.org/10.1016/S0304-386X\(97\)00078-9](http://doi.org/10.1016/S0304-386X(97)00078-9)
- [1999CHE/EWI] Chen F R, Ewing R C, and Clark S B; The Gibbs free energies and enthalpies of formation of U⁶⁺ phases: an empirical method of prediction, *The American Mineralogist* **84** (4), 650-664. <http://doi.org/10.2138/am-1999-0418>
- [1999EMR/ART] Emrén A T, Arthur R, Glynn P D, and McMurry J; The modeler's influence on calculated solubilities for performance assessments at the Äspö Hard-Rock Laboratory, *Material Research Society Symposium Proceedings* **556**, 559-566. 559. <http://doi.org/10.1557/PROC-556-559>
- [1999KÖN/KÖN] Königsberger E, Königsberger L C, and Gamsjäger H; Low-temperature thermodynamic model for the system Na₂CO₃-MgCO₃-CaCO₃-H₂O, *Geochimica et Cosmochimica Acta* **63** (19-20), 3105-3119. [http://doi.org/10.1016/S0016-7037\(99\)00238-0](http://doi.org/10.1016/S0016-7037(99)00238-0)
- [1999PAR/APP] Parkhurst D L and Appelo C A J; User's Guide to PHREEQC (Version 2) — A Computer Program for Speciation, Batch-Reaction, One-Dimensional Transport, and Inverse Geochemical Calculations, U.S. Geological Survey, Water-Resources Investigations, Lakewood, Colorado, USA, 99-4259 http://www.brr.cr.usgs.gov/projects/GWC_coupled/phreeqc/
- [1999PRA/SHO] Prapaipong P, Shock E L, and Koretsky C M; Metal-organic complexes in geochemical processes: temperature dependence of the standard thermodynamic properties of aqueous complexes between metal cations and dicarboxylate ligands, *Geochimica et Cosmochimica Acta* **63** (17), 2547-2577. [http://doi.org/10.1016/s0016-7037\(99\)00146-5](http://doi.org/10.1016/s0016-7037(99)00146-5)
- [2000DUR/ARC] Duro L, Arcos D, and Bruno J; Blind predictive modelling exercise in Oklo 2nd stage : Uranium in Okélobondo, in Oklo Working Groups. Proceedings of the Second EC-CEA Workshop on Oklo-Phase II, Helsinki, 16 to 18 June 1998 (Eds Louvat D., Michaud V., and von Maravic H.), European Economic Communities, Luxembourg, EUR 19116 EN. pp 399-409. <http://publications.europa.eu/en/publication-detail/-/publication/b8ef3f7d-c345-4597-b779-cf7c00edb895>
- [2000GLA/HUM] Glaus M A, Hummel W, and Van Loon L R; Trace metal-humate interactions. I. Experimental determination of conditional stability constants, *Applied Geochemistry* **15** (7), 953-973. [http://doi.org/10.1016/S0883-2927\(99\)00099-2](http://doi.org/10.1016/S0883-2927(99)00099-2)
- [2000KAL/CHO] Kalmykov S N and Choppin G R; Mixed Ca²⁺/UO₂²⁺/CO₃²⁻ complex formation at different ionic strengths, *Radiochimica Acta* **88** (9-11), 603-606. <http://doi.org/10.1524/ract.2000.88.9-11.603>
- [2001BEN/PAL] Bénézeth P, Palmer D A, and Wesolowski D J; Aqueous high-temperature solubility studies. II. The solubility of boehmite at 0.03 m ionic strength as a function of temperature and pH as determined by in situ measurements, *Geochimica et Cosmochimica Acta* **65** (13), 2097-2111. [http://doi.org/10.1016/S0016-7037\(01\)00585-3](http://doi.org/10.1016/S0016-7037(01)00585-3)
- [2001LEM/FUG] Lemire R J, Fuger J, Nitsche H, Potter P, Rand M, Rydberg J, Spahiu K, Sullivan J C, Ullman W J, Vitorge P, and Wanner H; Chemical Thermodynamics 4. Chemical Thermodynamics of Neptunium and Plutonium, Chemical Thermodynamics, North Holland Elsevier Science Publishers B. V., Amsterdam, The Netherlands. pp. 836. <http://www.oecd-nea.org/dbtdb/pubs/vol4-neptunium-plutonium.pdf>
- [2001NEC/KIM] Neck V and Kim J I; Solubility and hydrolysis of tetravalent actinides, *Radiochimica Acta* **89** (1), 1-16. <http://doi.org/10.1524/ract.2001.89.1.001>
- [2001SCH/SHO] Schulte M D, Shock E L, and Wood R H; The temperature dependence of the standard-state thermodynamic properties of aqueous nonelectrolytes, *Geochimica et Cosmochimica Acta* **65** (21), 3919-3930. [http://doi.org/10.1016/s0016-7037\(01\)00717-7](http://doi.org/10.1016/s0016-7037(01)00717-7)
- [2001TAG/SCH] Tagirov B and Schott J; Aluminum speciation in crustal fluids revisited, *Geochimica et Cosmochimica Acta* **65** (21), 3965-3992. [http://doi.org/10.1016/S0016-7037\(01\)00705-0](http://doi.org/10.1016/S0016-7037(01)00705-0)

References

- [2001ZHA/MUH] Zhang Y and Muhammed M; Critical evaluation of thermodynamics of complex formation of metal ions in aqueous solutions: VI. Hydrolysis and hydroxo-complexes of Zn^{2+} at 298.15 K, *Hydrometallurgy* **60** (3), 215-236. [http://doi.org/10.1016/S0304-386X\(01\)00148-7](http://doi.org/10.1016/S0304-386X(01)00148-7)
- [2001ZHU/HU] Zhu C, Hu F Q, and Burden D S; Multi-component reactive transport modeling of natural attenuation of an acid groundwater plume at a uranium mill tailings site, *Journal of Contaminant Hydrology* **52** (1-4), 85-108. [http://doi.org/10.1016/S0169-7722\(01\)00154-1](http://doi.org/10.1016/S0169-7722(01)00154-1)
- [2002CHEN/YIA] Chen J P and Yiakoumi S; Modeling of depleted uranium transport in subsurface systems, *Water Air and Soil Pollution* **140** (1-4), 173-201. <http://doi.org/10.1023/A:1020123006120>
- [2002CHE/KAR] Chernorukov N G, Karyakin N V, Suleimanov E V, Knyazev A V, and Feoktistova O V; Thermochemistry of $A^{II}(VUO_6)_2 \cdot nH_2O$ compounds ($A^{II} = Mn, Fe, Co, Ni, Cu, Zn, Cd$), *Russian Journal of General Chemistry* **72** (2), 178-182. <http://doi.org/10.1023/a:1015405130748>
- [2002HUM/BER] Hummel W, Berner U, Curti E, Pearson F J, and Thoenen T; Nagra/PSI Chemical Thermodynamic Data Base 01/01, NAGRA, Wettingen, Switzerland, Technical Report NTB 02-06. p. 564. [http://www.nagra.ch/data/documents/database/dokumente/\\$default/Default%20Folder/Publikationen/NTBs%202001-2010/e_ntb02-16.pdf](http://www.nagra.ch/data/documents/database/dokumente/$default/Default%20Folder/Publikationen/NTBs%202001-2010/e_ntb02-16.pdf)
- [2002PRE/GAM] Preis W and Gamsjäger H; Solid-solute phase equilibria in aqueous solution. XVI. Thermodynamic properties of malachite and azurite—predominance diagrams for the system $Cu^{2+}\text{-H}_2\text{O}\text{-CO}_2$, *Journal of Chemical Thermodynamics* **34** (5), 631-650. <http://doi.org/10.1006/jcht.2002.0928>
- [2002SME/KIN] Smedley P L and Kinniburgh D G; A review of the source, behaviour and distribution of arsenic in natural waters, *Applied Geochemistry* **17** (5), 517-568. [http://doi.org/10.1016/s0883-2927\(02\)00018-5](http://doi.org/10.1016/s0883-2927(02)00018-5)
- [2002SPA] Spahiu K; The use of SIT in the NEA TDB Project - Advantages, drawbacks and comparison with the approaches used in some geochemical codes, in *The Use of Thermodynamic Databases in Performance Assessment, Workshop Proceedings, Barcelona, Spain, 29-30 May 2001* (NEA, Ed.), Organization for Economic Cooperation and Development, Nuclear Energy Agency, Paris, pp. 61-68. <http://www.oecd-nea.org/science/pubs/2002/3055-use-thermodynamic-databases.pdf>
- [2003ALT/MET] Altmaier M, Metz V, Neck V, Müller R, and Fanghänel T; Solid-liquid equilibria of $Mg(OH)_2(\text{cr})$ and $Mg_2(OH)_3Cl\cdot 4H_2O(\text{cr})$ in the system $Mg\text{-Na}\text{-H}\text{-OH}\text{-O}\text{-Cl}\text{-H}_2O$ at 25°C, *Geochimica et Cosmochimica Acta* **67** (19), 3595-3601. [http://doi.org/10.1016/s0016-7037\(03\)00165-0](http://doi.org/10.1016/s0016-7037(03)00165-0)
- [2003BAE/BRA] Baeyens B, Bradbury M H, and Hummel W; Determination of aqueous nickel-carbonate and nickel-oxalate complexation constants, *Journal of Solution Chemistry* **32** (4), 319-339. <http://doi.org/10.1023/a:1023753704426>
- [2003GUI/FAN] Guillaumont R, Fanghänel T, Fuger J, Grenthe I, Neck V, Palmer D A, and Rand M; Chemical Thermodynamics 5. Update on the Chemical Thermodynamics of Uranium, Neptunium, Plutonium, Americium and Technetium, Chemical Thermodynamics, North Holland Elsevier Science Publishers B. V., Amsterdam, The Netherlands. pp. 918. <http://www.oecd-nea.org/dbtdb/pubs/vol5-update-combo.pdf>; http://www.oecd-nea.org/dbtdb/pubs/Errata_Update.pdf
- [2003MIT/ELE] Mitsakou C, Eleftheriadis K, Housiadas C, and Lazaridis M; Modeling of the dispersion of depleted uranium aerosol, *Health Physics* **84** (4), 538-544. <http://doi.org/10.1097/00004032-200304000-00014>
- [2003MON/WAN] Mompeán F J and Wanner H; The OECD Nuclear Energy Agency Thermochemical Database Project, *Radiochimica Acta* **91** (11), 617-621. <http://doi.org/10.1524/ract.91.11.617.23468>
- [2003LEE/WIN] van der Lee J, de Windt L, Lagneau V, and Goblet P; Module-oriented modeling of reactive transport with HYTEC, *Computers & Geosciences* **29** (3), 265-275. [http://doi.org/10.1016/s0098-3004\(03\)00004-9](http://doi.org/10.1016/s0098-3004(03)00004-9)
- [2003ZHE/TOK] Zheng Z P, Tokunaga T K, and Wan J M; Influence of calcium carbonate on U(VI) sorption to soils, *Environmental Science & Technology* **37** (24), 5603-5608. <http://doi.org/10.1021/es0304897>
- [2004BRE/FOT] Brett C, Foti C, and Sammartano S; A new approach in the use of SIT in determining the dependence on ionic strength of activity coefficients. Application to some chloride salts of interest in the speciation of natural fluids, *Chemical Speciation & Bioavailability* **16**, 105-110. <http://doi.org/10.3184/095422904782775036>
- [2004CHI] Chivot J; Thermodynamique des Produits de Corrosion - Fonctions Thermodynamiques, Diagrammes de Solubilité, Diagrammes E-pH des Systèmes $Fe\text{-H}_2O$, $Fe\text{-CO}_2\text{-H}_2O$, $Fe\text{-S}\text{-H}_2O$, $Cr\text{-H}_2O$ et $Ni\text{-H}_2O$ en Fonction de la Température, ANDRA, Chatenay-Malabry, France. pp. 141.
- [2004CRE/ROB] Crea F, De Robertis A, and Sammartano S; Medium and alkyl chain effects on the protonation of dicarboxylates in $NaCl_{(\text{aq})}$ and $Et_4NI_{(\text{aq})}$ at 25°C, *Journal of Solution Chemistry* **33** (5), 499-528. <http://doi.org/10.1023/B:IOSL.0000037773.15363.1f>
- [2004FAB/SAX] Fabrichnaya O B, Saxena S K, Richet P, and Westrum E F; Thermodynamic Data, Models, and Phase Diagrams in Multicomponent Oxide Systems. An Assessment for Materials and Planetary Scientists Based on Calorimetric, Volumetric and Phase Equilibrium Data, Data and Knowledge in a Changing World, Springer-Verlag, Berlin, Germany. (ISBN 978-3-662-10504-7). pp. 198. <http://doi.org/10.1007/978-3-662-10504-7>
- [2004KAR/HUB] Karbowiak M, Hubert S, Fourest B, and Moulin C; Complex formation of uranium(VI) in periodate solutions, *Radiochimica Acta* **92** (8), 489-494. <http://doi.org/10.1524/ract.92.8.489.39277>
- [2004KIN/COO] Kinniburgh D G and Cooper D M; Predominance and mineral stability diagrams revisited, *Environmental Science & Technology* **38** (13), 3641-3648. <http://doi.org/10.1021/es0349271>
- [2004POI/LAN] Pointea I, Landesman C, Giffaut E, and Reiller P; Reproducibility of the uptake of U(VI) onto degraded cement pastes and calcium silicate hydrate phases, *Radiochimica Acta* **92** (9-11), 645-650. <http://doi.org/10.1524/ract.92.9.645.55008>
- [2004SMI/MAR] Smith R M, Martell A E, and Motekaitis R J; NIST Standard Reference Database 46. NIST critically selected stability constants of metal complexes database. Version 8.0, National Institute of Standards and Technology, Gaithersburg, MD, USA. http://www.nist.gov/srd/upload/46_8.htm
- [2005BRO/CUR] Brown P, Curti E, Grambow B, and Ekberg C; Chemical Thermodynamics 8. Chemical Thermodynamics of Zirconium, Chemical Thermodynamics Series 8, North Holland Elsevier Science Publishers B. V., Amsterdam, The Netherlands. pp. 512. <http://www.oecd-nea.org/dbtdb/pubs/vol8-zirconium.pdf>
- [2005DON/STE] Donaldson M H, Stevens R, Lang B E, Boerio-Goates J, Woodfield B F, Putnam R L, and Navrotsky A; Heat capacities and absolute entropies of UTi_2O_6 and $CeTi_2O_6$, *Journal of Thermal Analysis and Calorimetry* **81** (3), 617-625. <http://doi.org/10.1007/s10973-005-0833-0>
- [2005GAM/BUG] Gamsjäger H, Bugajski J, Gajda T, Lemire R J, and Preis W; Chemical Thermodynamics 6. Chemical Thermodynamics of Nickel, Chemical Thermodynamics Series 6, North Holland Elsevier Science Publishers B. V., Amsterdam, The Netherlands. pp. 617. <http://www.oecd-nea.org/dbtdb/pubs/vol6-nickel.pdf>
- [2005HUM/AND] Hummel W, Anderegg G, Rao L F, Puigdomènech I, and Tochiyama O; Chemical Thermodynamics 9. Chemical Thermodynamics of Compounds and Complexes of U, Np, Pu, Am, Tc, Se, Ni and Zr with Selected Organic Ligands, Chemical Thermodynamics Series 9, North Holland Elsevier Science Publishers B. V., Amsterdam, The Netherlands. pp. 1088. <http://www.oecd-nea.org/dbtdb/pubs/vol9-organic-ligands.pdf>
- [2005KUB/HEL] Kubatko K-A, Helean K B, Navrotsky A, and Burns P C; Thermodynamics of uranyl minerals: enthalpies of formation of rutherfordine, UO_2CO_3 , andersonite, $Na_2CaUO_2(CO_3)_3(H_2O)_5$, and grimselite, $K_3NaUO_2(CO_3)_3H_2O$, *The American Mineralogist* **90** (8-9), 1284-1290. <http://doi.org/10.2138/am.2005.1821>
- [2005OLI/NOL] Olin Å, Noläng B, Osadchii E G, Öhman L-O, and Rosén E; Chemical Thermodynamics 7. Chemical Thermodynamics of Selenium, Chemical Thermodynamics Series 7, North Holland Elsevier Science Publishers B. V., Amsterdam, The Netherlands. pp. 851. <http://www.oecd-nea.org/dbtdb/pubs/vol7-selenium.pdf>

- [2005PAT/CHO] Pathak P N and Choppin G R; Complexation studies of Co^{2+} ion with orthosilicic acid, *Journal of Radioanalytical and Nuclear Chemistry* **267** (1), 175-182.
<http://doi.org/10.1007/s10967-006-0025-9>
- [2005POW/BRO] Powell K J, Brown P L, Byrne R H, Gajda T, Heftner G, Sjöberg S, and Wanner H; Chemical speciation of environmentally significant heavy metals with inorganic ligands - Part 1: The $\text{Hg}^{2+}-\text{Cl}^-$, OH^- , CO_3^{2-} , SO_4^{2-} , and PO_4^{3-} aqueous systems - (IUPAC technical report), *Pure and Applied Chemistry* **77** (4), 739-800.
<http://doi.org/10.1351/pac200577040739>
- [2005RAI/XIA] Rai D, Xia Y X, Rao L F, Hess N J, Felmy A R, Moore D A, and McCready D E; Solubility of $(\text{UO}_2)_3(\text{PO}_4)_{2.4}\text{H}_2\text{O}$ in $\text{H}^+-\text{Na}^+-\text{OH}^-$ - $\text{H}_2\text{PO}_4^{2-}$ - HPO_4^{2-} - H_2O and its comparison to the analogous PuO_2^{2+} system, *Journal of Solution Chemistry* **34** (4), 469-498.
<http://doi.org/10.1007/s10953-005-5216-4>
- [2006BRE/FOT] Brett C, Foti C, Porcino N, and Sammartano S; SIT parameters for 1:1 electrolytes and correlation with Pitzer coefficients, *Journal of Solution Chemistry* **35**, 1401-1415.
<http://doi.org/10.1007/s10953-006-9068-3>
- [2006CUR/DAV] Curtis G P, Davis J A, and Naftz D L; Simulation of reactive transport of uranium(VI) in groundwater with variable chemical conditions, *Water Resources Research* **42** (4), W04404.
<http://doi.org/10.1029/2005wr003979>
- [2006DON/BRO] Dong W and Brooks S C; Determination of the formation constants of ternary complexes of uranyl and carbonate with alkaline earth metals (Mg^{2+} , Ca^{2+} , Sr^{2+} , and Ba^{2+}) using anion exchange method, *Environmental Science & Technology* **40** (15), 4689-4695. <http://doi.org/10.1021/es0606327>
- [2006PAT/CHO] Pathak P N and Choppin G R;
Complexation/speciation studies of Ni^{2+} ion with ortho silicic acid in perchlorate media, *Journal of Radioanalytical and Nuclear Chemistry* **267** (2), 309-314. <http://doi.org/10.1007/s10967-006-0049-1>
- [2007DAV/CUR] Davis J A and Curtis G P; Consideration of Geochemical Issues in Groundwater Restoration at Uranium In-Situ Leach Mining Facilities, U.S. Geological Survey, Washington, DC, USA, Report NUREG/CR-6870. p. 164.
<http://www.nrc.gov/docs/ML0706/ML070600405.pdf>
- [2007GOR/MAZ] Gorman-Lewis D, Mazeina L, Fein J B, Szymanowski J E S, Burns P C, and Navrotsky A; Thermodynamic properties of soddyite from solubility and calorimetry measurements, *Journal of Chemical Thermodynamics* **39** (4), 568-575. <http://doi.org/10.1016/j.jct.2006.09.005>
- [2007MON/MÜG] Montarnal P, Mügler C, Colin J, Descotes M, Dimier A, and Jacquot E; Presentation and use of a reactive transport code in porous media, *Physics and Chemistry of the Earth, Parts A/B/C* **32** (1), 507-517.
<http://doi.org/https://doi.org/10.1016/j.pce.2006.01.009>
- [2007POW/BRO] Powell K J, Brown P L, Byrne R H, Gajda T, Heftner G, Sjöberg S, and Wanner H; Chemical speciation of environmentally significant metals with inorganic ligands - Part 2: The $\text{Cu}^{2+}-\text{OH}^-$, Cl^- , CO_3^{2-} , SO_4^{2-} , and PO_4^{3-} systems - (IUPAC technical report), *Pure and Applied Chemistry* **79** (5), 895-950.
<http://doi.org/10.1351/pac200779050895>
- [2007YAB/FAN] Yabusaki S B, Fang Y, Long P E, Resch C T, Peacock A D, Komlos J, Jaffe P R, Morrison S J, Dayvault R D, White D C, and Anderson R T; Uranium removal from groundwater via in situ biostimulation: field-scale modeling of transport and biological processes, *Journal of Contaminant Hydrology* **93** (1-4), 216-235.
<http://doi.org/10.1016/j.jconhyd.2007.02.005>
- [2008ALT/NEC] Altmairer M, Neck V, and Fanghänel T; Solubility of $\text{Zr}(\text{IV})$, $\text{Th}(\text{IV})$ and $\text{Pu}(\text{IV})$ hydrous oxides in CaCl_2 solutions and the formation of ternary $\text{Ca}-\text{M}(\text{IV})-\text{OH}$ complexes, *Radiochimica Acta* **96** (9-11), 541-550. <http://doi.org/10.1524/ract.2008.1535>
- [2008BAC/PLA] Bachmaf S, Planer-Friedrich B, and Merkel B J; Effect of sulfate, carbonate, and phosphate on the uranium(VI) sorption behavior onto bentonite, *Radiochimica Acta* **96** (6), 359-366. <http://doi.org/10.1524/ract.2008.1496>
- [2008BON/COT] Bonin L, Cote G, and Moisy P; Speciation of An(IV) (Pu, Np, U and Th) in citrate media, *Radiochimica Acta* **96** (3), 145-152. <http://doi.org/10.1524/ract.2008.1476>
- [2008DON/BRO] Dong W and Brooks S C; Formation of aqueous $\text{Mg}\text{UO}_2(\text{CO}_3)_{32-}$ complex and uranium anion exchange mechanism onto an exchange resin, *Environmental Science & Technology* **42** (6), 1979-1983. <http://doi.org/10.1021/es0711563>
- [2008GEI/AMA] Geipel G, Amayri S, and Bernhard G; Mixed complexes of alkaline earth uranyl carbonates: a laser-induced time-resolved fluorescence spectroscopic study, *Spectrochimica Acta Part A: Molecular and Biomolecular Spectroscopy* **71** (1), 53-58.
<http://doi.org/10.1016/j.saa.2007.11.007>
- [2008GOR/BUR] Gorman-Lewis D, Burns P C, and Fein J B; Review of uranyl mineral solubility measurements, *Journal of Chemical Thermodynamics* **40** (3), 335-352.
<http://doi.org/10.1016/j.jct.2007.12.004>
- [2008GOR/FEI] Gorman-Lewis D, Fein J B, Burns P C, Szymanowski J E S, and Converse J; Solubility measurements of the uranyl oxide hydrate phases metaschoepite, compreignacite, Na-compreignacite, bequerelite, and clarkeite, *Journal of Chemical Thermodynamics* **40** (6), 980-990. <http://doi.org/10.1016/j.jct.2008.02.006>
- [2009GOR/SHV] Gorman-Lewis D, Shvareva T, Kubatko K-A, Burns P C, Wellman D M, McNamara B, Szymanowski J E S, Navrotsky A, and Fein J B; Thermodynamic properties of autunite, uranyl hydrogen phosphate, and uranyl orthophosphate from solubility and calorimetric measurements, *Environmental Science & Technology* **43** (19), 7416-7422.
<http://doi.org/10.1021/es9012933>
- [2009MEL/AZE] Meleshyn A, Azeroual M, Reeck T, Houben G, Riebe B, and Bunnenberg C; Influence of (Calcium-)Uranyl-Carbonate Complexation on U(VI) Sorption on Ca- and Na-Bentonites, *Environmental Science & Technology* **43** (13), 4896-4901.
<http://doi.org/10.1021/es900123s>
- [2009POW/BRO] Powell K J, Brown P L, Byrne R H, Gajda T, Heftner G, Leuz A-K, Sjöberg S, and Wanner H; Chemical speciation of environmentally significant metals with inorganic ligands. Part 3: The $\text{Pb}^{2+} + \text{OH}^-$, Cl^- , CO_3^{2-} , SO_4^{2-} , and PO_4^{3-} systems (IUPAC Technical Report), *Pure and Applied Chemistry* **81** (12), 2425-2476.
<http://doi.org/10.1351/pac-rep-09-03-05>
- [2009RAN/FUG] Rand M, Fuger J, Grenthe I, Neck V, and Rai D; Chemical Thermodynamics 11. Chemical Thermodynamics of Thorium, Chemical Thermodynamics Series 11, OECD Nuclear Energy Agency Data Bank Eds., OECD Publications, Paris, France. pp. 900. <http://www.oecd-nea.org/science/pubs/2007/6254-DB-chemical-thermodyn-11.pdf>
- [2010CUR/FUJ] Curti E, Fujiwara K, Iijima K, Tits J, Cuesta C, Kitamura A, Glaus M A, and Muller W; Radium uptake during barite recrystallization at 23 ± 2 °C as a function of solution composition: an experimental ^{133}Ba and ^{226}Ra tracer study, *Geochimica et Cosmochimica Acta* **74** (12), 3553-3570.
<http://doi.org/10.1016/j.gca.2010.03.018>
- [2010STE/MAY] Stewart B D, Mayes M A, and Fendorf S; Impact of uranyl-calcium-carbonato complexes on uranium(VI) adsorption to synthetic and natural sediments, *Environmental Science & Technology* **44** (3), 928-934. <http://doi.org/10.1021/es902194x>
- [2011BRA/BAE] Bradbury M H and Baeyens B; Predictive sorption modelling of Ni(II), Co(II), Eu(III), Th(IV) and U(VI) on MX-80 bentonite and Opalinus Clay: a "bottom-up" approach, *Applied Clay Science* **52** (1-2), 27-33.
<http://doi.org/10.1016/j.clay.2011.01.022>
- [2011EKB/ODE] Ekberg C and Ödegaard-Jensen A; Uncertainties in chemical modelling of solubility, speciation and sorption, *Accreditation and Quality Assurance* **16** (4), 207-214.
<http://doi.org/10.1007/s00769-010-0723-4>
- [2011EKB/KNU] Ekberg C, Knutsson A, Albinsson Y, and Brown P L; Complexation of thorium with phosphate, *Radiochimica Acta* **99** (1), 31-35. <http://doi.org/10.1524/ract.2011.1793>
- [2011JON/BUT] Jones M J, Butchins L J, Charnock J M, Patrick R A D, Small J S, Vaughan D J, Wincott P L, and Livens F R; Reactions of radium and barium with the surfaces of carbonate minerals, *Applied Geochemistry* **26** (7), 1231-1238.
<http://doi.org/10.1016/j.apgeochem.2011.04.012>

References

- [2011JOS/SCH] Joseph C, Schmeide K, Sachs S, Brendler V, Geipel G, and Bernhard G; Sorption of uranium(VI) onto Opalinus Clay in the absence and presence of humic acid in Opalinus Clay pore water, *Chemical Geology* **284** (3-4), 240-250.
<http://doi.org/10.1016/j.chemgeo.2011.03.001>
- [2011KIN/COO] Kinniburgh D G and Cooper D M; Creating Graphical Output with PHREEQC, <http://www.phreeplot.org>
- [2011MAY/FIL] May P M and Filella M; Chemical modelling of multicomponent mixtures: quality assurance is more than just equilibrium data quality assessment, *Accreditation and Quality Assurance* **16** (4), 179-184. <http://doi.org/10.1007/s00769-010-0701-x>
- [2011POW/BRO] Powell K J, Brown P L, Byrne R H, Gajda T, Heftner G, Leuz A-K, Sjöberg S, and Wanner H; Chemical speciation of environmentally significant metals with inorganic ligands. Part 4: The Cd²⁺ + OH⁻, Cl⁻, CO₃²⁻, SO₄²⁻, and PO₄³⁻ systems (IUPAC Technical Report), *Pure and Applied Chemistry* **83** (5), 1163-1214.
<http://doi.org/10.1351/pac-rep-10-08-09>
- [2012GAI/BLA] Gailhanou H, Blanc P, Rogez J, Mikaelian G, Kawaji H, Olives J, Amouric M, Denoyel R, Bourrelly S, Montouillout V, Vieillard P, Fialips C I, Michau N, and Gaucher E C; Thermodynamic properties of illite, smectite and beidellite by calorimetric methods: enthalpies of formation, heat capacities, entropies and Gibbs free energies of formation, *Geochimica et Cosmochimica Acta* **89**, 279-301. <http://doi.org/10.1016/j.gca.2012.04.048>
- [2012GAM/GAJ] Gamsjäger H, Gajda T, Sangster J, Saxena S K, and Voigt W; Chemical Thermodynamics 12. Chemical Thermodynamics of Tin, Chemical Thermodynamics Series 12, OECD Nuclear Energy Agency Data Bank, Eds., OECD Publications, Paris, France. pp. 609. <https://www.oecd-nea.org/dbtdb/pubs/tin.pdf>
- [2012REI/VER] Reiller P E, Vercouter T, Duro L, and Ekberg C; Thermodynamic data provided through the FUNMIG project: analyses and prospective, *Applied Geochemistry* **27** (2), 414-426. <http://doi.org/10.1016/j.apgeochem.2011.09.011>
- [2013ALR/JOS] Alreħaili L M, Joseph J M, Biesinger M C, Guzonas D A, and Wren J C; Gamma-radiolysis-assisted cobalt oxide nanoparticle formation, *Physical Chemistry Chemical Physics* **15** (3), 1014-1024. <http://doi.org/10.1039/C2CP43094K>
- [2013CRE/SZE] Cretaz F, Szenknect S, Clavier N, Vitorge P, Mesbah A, Descotes M, Poinsot C, and Dacheux N; Solubility properties of synthetic and natural meta-torbernite, *Journal of Nuclear Materials* **442** (1-3), 195-207. <http://doi.org/10.1016/j.jnucmat.2013.08.037>
- [2013LEE/YUN] Lee J-Y and Yun J-I; Formation of ternary CaUO₂(CO₃)₃²⁻ and Ca₂UO₂(CO₃)₃(aq) complexes under neutral to weakly alkaline conditions, *Dalton Transactions* **42** (27), 9862-9869. <http://doi.org/10.1039/c3dt50863c>
- [2013LEM/BER] Lemire R J, Berner U, Musikas C, Palmer D A, Taylor P, and Tochiyama O; Chemical Thermodynamics 13a. Chemical Thermodynamics of Iron. Part 1, Chemical Thermodynamics Series, OECD Nuclear Energy Agency Data Bank, Eds., OECD Publications, Paris, France. pp. 1082. <https://www.oecd-nea.org/dbtdb/pubs/6355-vol13a-iron.pdf>
- [2013PAR/APP] Parkhurst D L and Appelo C A J; Description of Input and Examples for PHREEQC Version 3 — A Computer Program for Speciation, Batch-Reaction, One-Dimensional Transport, and Inverse Geochemical Calculations. Chapter 43 of Section A, Groundwater Book 6, Modeling Techniques, U.S. Geological Survey, Denver, Colorado, USA. p. 497.
<http://pubs.usgs.gov/tm/06/a43/pdf/tm6-A43.pdf>
- [2013POW/BRO] Powell K J, Brown P L, Byrne R H, Gajda T, Heftner G, Leuz A-K, Sjöberg S, and Wanner H; Chemical speciation of environmentally significant metals with inorganic ligands. Part 5: The Zn²⁺ + OH⁻, Cl⁻, CO₃²⁻, SO₄²⁻, and PO₄³⁻ systems (IUPAC Technical Report), *Pure and Applied Chemistry* **85** (12), 2249-2311.
<http://doi.org/10.1351/pac-rep-13-06-03>
- [2014END/RAO] Endrizzi F and Rao L; Chemical speciation of uranium(VI) in marine environments: complexation of calcium and magnesium ions with [(UO₂)(CO₃)₃⁴⁻] and the effect on the extraction of uranium from seawater, *Chemistry-A European Journal* **20** (44), 14499-14506. <http://doi.org/10.1002/chem.201403262>
- [2014SAJ/BRY] Sajih M, Bryan N D, Livens F R, Vaughan D J, Descotes M, Phrommavanh V, Nos J, and Morris K; Adsorption of radium and barium on goethite and ferrihydrite: a kinetic and surface complexation modelling study, *Geochimica et Cosmochimica Acta* **146**, 150-163. <http://doi.org/10.1016/j.gca.2014.10.008>
- [2014THO/HUM] Thoenen T, Hummel W, Berner U, and Curti E; The PSI/Nagra Chemical Thermodynamic Database 12/07, Paul Scherrer Institute, Villigen, Switzerland, PSI Bericht Nr 14-04 (ISSN 1019-0643). p. 416. <http://www.psi.ch/les/database>
- [2015aBLA/VIE] Blanc P, Vieillard P, Gailhanou H, Gaboreau S, Gaucher E, Fialips C I, Made B, and Giffaut E; A generalized model for predicting the thermodynamic properties of clay minerals, *The American Journal of Science* **315** (8), 734-780.
<http://doi.org/10.2475/08.2015.02>
- [2015bBLA/VIE] Blanc P, Vieillard P, Gailhanou H, Gaboreau S, Marty N, Claret F, Madé B, and Giffaut E; ThermoChimie database developments in the framework of cement/clay interactions, *Applied Geochemistry* **55**, 95-107.
<http://doi.org/10.1016/j.apgeochem.2014.12.006>
- [2015MAR/VER] Marques Fernandes M, Vér N, and Baeyens B; Predicting the uptake of Cs, Co, Ni, Eu, Th and U on argillaceous rocks using sorption models for illite, *Applied Geochemistry* **59**, 189-199. <http://doi.org/10.1016/j.apgeochem.2015.05.006>
- [2015PAL] Palandri J, SOLTHERM Thermodynamic Database for Geochemical Modeling.
- [2015RAG/BRA] Ragoussi M E and Brassinnes S; The NEA Thermochemical Database Project: 30 years of accomplishments, *Radiochimica Acta* **103** (10), 679-685. <http://doi.org/10.1515/ract-2015-2392>
- [2015SMI/BRY] Smith K F, Bryan N D, Swinburne A N, Bots P, Shaw S, Natrajan L S, Mosselmans J F W, Livens F R, and Morris K; U(VI) behaviour in hyperalkaline calcite systems, *Geochimica et Cosmochimica Acta* **148**, 343-359.
<http://doi.org/10.1016/j.gca.2014.09.043>
- [2015STE/APP] Steefel C I, Appelo C A J, Arora B, Jacques D, Kalbacher T, Kolditz O, Lagneau V, Lichtner P C, Mayer K U, Meeussen J C L, Molins S, Moulton D, Shao H, Simunek J, Spycher N, Yabusaki S B, and Yeh G T; Reactive transport codes for subsurface environmental simulation, *Computational Geosciences* **19** (3), 445-478. <http://doi.org/10.1007/s10596-014-9443-x>
- [2016AMA/FRO] Amayri S, Frohlich D R, Kaplan U, Trautmann N, and Reich T; Distribution coefficients for the sorption of Th, U, Np, Pu, and Am on Opalinus Clay, *Radiochimica Acta* **104** (1), 33-40. <http://doi.org/10.1515/ract-2015-2409>
- [2016BRO/EKB] Brown P L and Ekberg C; Hydrolysis of Metal Ions, Wiley-VCH Verlag GmbH & Co., Weinheim, Germany. pp. 918. <http://doi.org/10.1002/97835272765189>
- [2016DZO/LEE] Drozdak J, Leermakers M, Gao Y, Elskens M, Phrommavanh V, and Descotes M; Uranium aqueous speciation in the vicinity of the former uranium mining sites using the diffusive gradients in thin films and ultrafiltration techniques, *Analytica Chimica Acta* **913**, 94-103.
<http://doi.org/10.1016/j.aca.2016.01.052>
- [2016END/LEG] Endrizzi F, Leggett C J, and Rao L; Scientific basis for efficient extraction of uranium from seawater. I: understanding the chemical speciation of uranium under seawater conditions, *Industrial & Engineering Chemistry Research* **55** (15), 4249-4256. <http://doi.org/10.1021/acs.iecr.5b03679>
- [2016JOH/TUT] Johnson R H and Tutu H; Predictive reactive transport modeling at a proposed uranium in situ recovery site with a general data collection guide, *Mine Water and the Environment* **35** (3), 369-380. <http://doi.org/10.1007/s10230-015-0376-y>
- [2016PAR/AVA] Paredes E, Avazeri E, Malard V, Vidaud C, Reiller P E, Ortega R, Nonell A, Isnard H, Chartier F, and Bresson C; Evidence of isotopic fractionation of natural uranium in cultured human cells, *Proceedings of the National Academy of Sciences of the United States of America* **113** (49), 14007-14012.
<http://doi.org/10.1073/pnas.1610885113>

- [2016REE/SPY] Reed M H, Spycher N F, and Palandri J; SOLVEQ-XPT : A Computer Program for Computing Aqueous-Mineral-Gas Equilibria. Version 2.2.3, Department of Geological Sciences, University of Oregon, Eugene, OR, USA. p. 42. <http://pages.uoregon.edu/palandri/data/solveq-xpt%20guide%20v.2.23.pdf>
- [2016REI/LY] Reinoso-Maset E and Ly J; Study of uranium(VI) and radium(II) sorption at trace level on kaolinite using a multisite ion exchange model, *Journal of Environmental Radioactivity* **157**, 136-148. <http://doi.org/10.1016/j.jenrad.2016.03.014>
- [2016SAN] Sander R, Base de données standard de référence NIST numéro 69. <http://webbook.nist.gov/chemistry/>
- [2016ZYL/SMO] Źyła M, Smoła G, Knapik A, Rysz J, Sitarz M, and Grzesik Z; The formation of the Co_3O_4 cobalt oxide within CoO substrate, *Corrosion Science* **112**, 536-541. <http://doi.org/10.1016/j.corsci.2016.08.016>
- [2017BEC/MAT] Beccia M R, Matara-Aho M, Reeves B, Rogues J, Solari P L, Monfort M, Moulin C, and Den Auwer C; New insight into the ternary complexes of uranyl carbonate in seawater, *Journal of Environmental Radioactivity* **178-179**, 343-348. <http://doi.org/10.1016/j.jenrad.2017.08.008>
- [2017BRE/CIG] Brett C, Cigala R M, Crea F, De Stefano C, Gattuso G, Irto A, Lando G, Milea D, and Sammartano S; Thermodynamic properties of O-donor polyelectrolytes: determination of the acid-base and complexing parameters in different ionic media at different temperatures, *Journal of Chemical and Engineering Data* **62** (9), 2676-2688. <http://doi.org/10.1021/acs.jced.7b00101>
- [2017GAI/VIE] Gailhanou H, Vieillard P, Blanc P, Lassin A, Denoyel R, Bloch E, De Weireld G, Gaboreau S, Fialips C I, Made B, and Giffaut E; Methodology for determining the thermodynamic properties of smectite hydration, *Applied Geochemistry* **82**, 146-163. <http://doi.org/10.1016/j.apgeochem.2017.04.015>
- [2017LEE/VES] Lee J-Y, Vespa M, Gaona X, Dardenne K, Rothe J, Rabung T, Altmaier M, and Yun J-I; Formation, stability and structural characterization of ternary $\text{MgUO}_2(\text{CO}_3)_3^{2-}$ and $\text{Mg}_2\text{UO}_2(\text{CO}_3)_3(\text{aq})$ complexes, *Radiochimica Acta* **105** (3), 171-185. <http://doi.org/10.1515/ract-2016-2643>
- [2017ROB/TER] Robin V, Tertre E, Beaucaire C, Regnault O, and Descotes M; Experimental data and assessment of predictive modeling for radium ion-exchange on beidellite, a swelling clay mineral with a tetrahedral charge, *Applied Geochemistry* **85**, 1-9. <http://doi.org/10.1016/j.apgeochem.2017.07.009>
- [2018BOR/BEA] Bordelet G, Beaucaire C, Phrommavanh V, and Descotes M; Chemical reactivity of natural peat towards U and Ra, *Chemosphere* **202**, 651-660. <http://doi.org/10.1016/j.chemosphere.2018.03.140>
- [2018CLA/MAR] Claret F, Marty N, and Tournassat C; Modeling the long-term stability of multi-barrier systems for nuclear waste disposal in geological clay formations, in *Reactive Transport Modeling* (Xiao Y., Whitaker F., Xu T., and Steefel C., Eds.). Chapter 8, John Wiley & Sons Ltd., Oxford, UK, pp. 395-451. <http://doi.org/10.1002/9781119060031.ch8>
- [2018JOR/DEM] Jordan N, Demnitz M, Losch H, Starke S, Brendler V, and Huittinen N; Complexation of trivalent lanthanides (Eu) and actinides (Cm) with aqueous phosphates at elevated temperatures, *Inorganic Chemistry* **57** (12), 7015-7024. <http://doi.org/10.1021/acs.inorgchem.8b00647>
- [2018PAR/AVA] Paredes E, Avazeri E, Malard V, Vidaud C, Reiller P E, Ortega R, Nonell A, Isnard H, Chartier F, and Bresson C; Impact of uranium uptake on isotopic fractionation and endogenous element homeostasis in human neuron-like cells, *Scientific Reports* **8** (1), 17163. <http://doi.org/10.1038/s41598-018-35413-4>
- [2018TRA/TEU] Tran E L, Teutsch N, Klein-BenDavid O, Kersting A B, Zavrin M, and Weisbrod N; Radionuclide transport in brackish water through chalk fractures, *Water Research* **163**, 114886. <http://doi.org/10.1016/j.watres.2019.114886>
- [2019WAN/SHI] Wang X, Shi Z, Kinniburgh D G, Zhao L, Ni S, Wang R, Hou Y, Cheng K, and Zhu B; Effect of thermodynamic database selection on the estimated aqueous uranium speciation, *Journal of Geochemical Exploration* **204**, 33-42. <http://doi.org/10.1016/j.gexplo.2019.05.001>
- [2020GRE/GAO] Grenthe I, Gaona X, Plyasunov A V, Rao L, Runde W H, Grambow B, Koning R J M, Smith A L, and Moore E E; Chemical Thermodynamics 14. Second Update on the Chemical Thermodynamics of Uranium, Neptunium, Plutonium, Americium and Technetium, Chemical Thermodynamics Series, OECD Nuclear Energy Agency Data Bank, Eds., OECD Publications, Paris, France. pp. 1572. http://www.oecd-nea.org/jcms/pl_46643/second-update-of-u-np-pu-am-and-tc
- [2020LAR/CHA] Lartigue J E, Charrasse B, Reile B, and Descotes M; Aqueous inorganic uranium speciation in European stream waters from the FOREGS dataset using geochemical modelling and determination of U bioavailability baseline, *Chemosphere* **251**, 126302. <http://doi.org/10.1016/j.chemosphere.2020.126302>
- [2020LEM/PAJ] Lemire R J, Palmer D A, Taylor P, and Schlenz H; Chemical Thermodynamics 13b. Chemical Thermodynamics of Iron. Part 2, Chemical Thermodynamics Series, OECD Nuclear Energy Agency Data Bank, Eds., OECD Publications, Paris, France. pp. 882. <http://www.oecd-nea.org/dbtdb/pubs/7499-vol13b-iron.pdf>
- [2020OHE/VER] Oher H, Vercouter T, Réal F, Shang C, Reiller P E, and Vallet V; Influence of alkaline earth metal ions (Mg^{2+} and Ca^{2+}) on structures and luminescent properties of $\text{UO}_2(\text{CO}_3)_3^{4-}$ complex: theoretical and experimental study, *Inorganic Chemistry* **59** (20), 15036-15049. <http://doi.org/10.1021/acs.inorgchem.0c01986>
- [2019ALL/STA] Allevato E, Stazi S R, Marabottini R, and D'Annibale A; Mechanisms of arsenic assimilation by plants and countermeasures to attenuate its accumulation in crops other than rice, *Ecotoxicology and Environmental Safety* **185** <http://doi.org/10.1016/j.ecoenv.2019.109701>
- [2019HUM/FIL] Hummel W, Filella M, and Rowland D; Where to find equilibrium constants?, *Science of the Total Environment* **692**, 49-59. <http://doi.org/10.1016/j.scitotenv.2019.07.161>
- [2019HUS/LEE] Husson A, Leermakers M, Descotes M, and Lagneau V; Environmental geochemistry and bioaccumulation/bioavailability of uranium in post-mining context – Bois-Noirs Limouzat mine, *Chemosphere* **236**, 124341. <http://doi.org/10.1016/j.chemosphere.2019.124341>
- [2019JO/KIR] Jo Y, Kirishima A, Kimuro S, Kim H-K, and Yun J-I; Formation of $\text{CaUO}_2(\text{CO}_3)_3^{2-}$ and $\text{Ca}_2\text{UO}_2(\text{CO}_3)_3(\text{aq})$ complexes at variable temperatures (10 – 70 °C), *Dalton Transactions* **48** (20), 6942-6950. <http://doi.org/10.1039/c9dt01174a>
- [2019JO/KIM] Jo Y, Kim H-K, and Yun J-I; Complexation of $\text{UO}_2(\text{CO}_3)_3^{4-}$ with Mg^{2+} at varying temperatures and its effect on U(VI) speciation in groundwater and seawater, *Dalton Transactions* **48** (39), 14769-14776. <http://doi.org/10.1039/c9dt03313k>
- [2019LAG/REG] Lagneau V, Regnault O, and Descotes M; Industrial deployment of reactive transport simulation: an application to uranium in situ recovery, *Reviews in Mineralogy and Geochemistry* **85** (1), 499-528. <http://doi.org/10.2138/rmg.2019.85.16>
- [2019LEE/AMA] Lee J Y, Amayri S, Montoya V, Fellhauer D, Gaona X, and Altmaier M; Solubility and stability of liebigite, $\text{Ca}_2\text{UO}_2(\text{CO}_3)_3 \cdot 10\text{H}_2\text{O}(\text{cr})$, in dilute to concentrated NaCl and NaClO_4 solutions at T=22–80 °C, *Applied Geochemistry* **111**, 104374. <http://doi.org/10.1016/j.apgeochem.2019.104374>
- [2019LES/BEA] Lestini L, Beaucaire C, Vercouter T, Ballini M, and Descotes M; Role of trace elements in the 226-radium incorporation in sulfate minerals (gypsum and celestite), *ACS Earth and Space Chemistry* **3** (2), 295-304. <http://doi.org/10.1021/acsearthspacechem.8b00150>
- [2019MAR/SAN] Martinez J S, Santillan E-F, Bossant M, Costa D, and Ragoussi M-E; The new electronic database of the NEA Thermochemical Database Project, *Applied Geochemistry* **107**, 159-170. <http://doi.org/10.1016/j.apgeochem.2019.05.007>
- [2019MUR/WAG] Mühr-Ebert E L, Wagner F, and Walther C; Speciation of uranium: compilation of a thermodynamic database and its experimental evaluation using different analytical techniques, *Applied Geochemistry* <http://doi.org/10.1016/j.apgeochem.2018.10.006>
- [2019TRA/TEU] Tran E L, Teutsch N, Klein-BenDavid O, Kersting A B, Zavrin M, and Weisbrod N; Radionuclide transport in brackish water through chalk fractures, *Water Research* **163**, 114886. <http://doi.org/10.1016/j.watres.2019.114886>
- [2019WAN/SHI] Wang X, Shi Z, Kinniburgh D G, Zhao L, Ni S, Wang R, Hou Y, Cheng K, and Zhu B; Effect of thermodynamic database selection on the estimated aqueous uranium speciation, *Journal of Geochemical Exploration* **204**, 33-42. <http://doi.org/10.1016/j.gexplo.2019.05.001>

References

- [2020REI/DES] Reiller P E and Descotes M; Development and application of the thermodynamic database PRODATA dedicated to the monitoring of mining activities from exploration to remediation, *Chemosphere* **251**, 126301.
<http://doi.org/10.1016/j.chemosphere.2020.126301>
- [2020aSHA/REI] Shang C and Reiller P E; Determination of formation constants and specific ion interaction coefficients for $\text{Ca}_n\text{UO}_2(\text{CO}_3)_{3(4-2n)}^-$ complexes in NaCl solution by time-resolved laser-induced luminescence spectroscopy, *Dalton Transactions* **49** (2), 466-481. <http://doi.org/10.1039/C9DT03543E>
- [2020bSHA/REI] Shang C, Reiller P E, and Vercouter T; Spectroluminescence measurements of stability constants of $\text{Ca}_n\text{UO}_2(\text{CO}_3)_{3(4-2n)}^-$ complexes in NaClO_4 medium and investigation of interaction effects, *Dalton Transactions* **49** (43), 15443-15460. <http://doi.org/10.1039/D0DT03164I>
- [2021MAI/RIB] Maia F M S, Ribet S, Bailly C, Grivé M, Madé B, and Montavon G; Evaluation of thermodynamic data for aqueous Ca-U(VI)- CO_3 species under conditions characteristic of geological clay formation, *Applied Geochemistry* **124**, 104844. <http://doi.org/10.1016/j.apgeochem.2020.104844>
- [2021aSHA/REI] Shang C and Reiller P E; Thermodynamic constant of $\text{MgUO}_2(\text{CO}_3)_3^{2-}$ complex in NaClO_4 and NaCl media using time-resolved luminescence spectroscopy, and applications to different geochemical contexts, *Dalton Transactions* **50** (12), 4363-4379. <http://doi.org/10.1039/d0dt04124f>
- [2021bSHA/REI] Shang C and Reiller P E; Effect of temperature on the complexation of triscarbonatouranyl(VI) with calcium and magnesium in NaCl aqueous solution, *Dalton Transactions* **50**, 17165-17180. <http://doi.org/10.1039/D1DT03204F>